UNIVERSITÉ DU QUÉBEC À MONTRÉAL

MULTIVALENT GLYCODENDRIMERS DESIGNED AS THERAPEUTIC STRATEGIES IN DRUG DELIVERY TARGETING URINARY TRACT INFECTIONS

DISSERTATION

PRESENTED

AS PARTIAL FULFILLMENT

OF THE DOCTORATE IN CHEMISTRY

BY

LAMYAA SALLAM

FEBRUARY 2023

UNIVERSITÉ DU QUÉBEC À MONTRÉAL

CONCEPTION DE GLYCODENDRIMÈRES MULTIVALENTS COMME STRATÉGIES THÉRAPEUTIQUES DANS L'ADMINISTRATION DE MÉDICAMENTS CIBLANT LES INFECTIONS DES VOIES URINAIRES

THÈSE

PRÉSENTÉE

COMME EXIGENCE PARTIELLE

DU DOCTORAT EN CHIMIE

PAR

LAMYAA SALLAM

FÉVRIER 2023

ACKNOWLEDGMENTS

Over the journey of my research as a Ph.D. candidate in chemistry, it has now finally culminated in the completion of this thesis. I have been immeasurably fortunate to have not only spent years performing research in the design of organic macromolecules but to have stumbled into many valuable relationships, and friendships. There are many individuals that have made my experience at UQAM what it is today, but several deserve special mention. Dr. Rene Roy. Also, thanks to all my committee members, Dr. Ali Nazemi, Dr. Abdelkrim Azzouz, Chemistry Department (UQAM), and Dr. Ashok Kakkar, Chemistry Department (McGill University), for sparing their time to evaluate my work and paramount notes. Their feedback, critique, and expertise opened my mind in many aspects. Many thanks to Alexandre Arnold, who was always quick to lend in the NMR facility. Also, thanks to the group at the Research Institute of the McGill University Health Center (MUHC) for carrying out all the high-resolution mass spectrometry (MALDI) tests of my synthesized big molecules.

When I started to pursue my Ph.D. program at UQAM, I had the opportunity to study courses at McGill University; during that time, I had the chance to meet incredible mentors, and I am grateful to them for igniting my passion for science and research and for continuing to serve an advisor, and I believe it has helped me reach my full potential as a graduate student.

I am grateful to all who offered their time and energy to help me. I fear that I will miss out on many names. However, I would like to take this opportunity to extend my appreciation to Mr. Jasmin Roy, (Directeur des Services à la vie étudiante, UQAM), and Dr. Normand Séguin (Doyen- Faculté des sciences- UQAM) for their support. I would like to thank Mr. Jean-Jacques Rondeau (Bibliothèque des sciences) for his guidance on thesis formatting. Special thanks go to my family, for encouraging a love of science and inquiry. In my highest and lowest times, they have been there with an open ear and words of encouragement. They provided ongoing emotional and spiritual assistance.

Once more, I would like to extend my sincere and heartfelt gratitude to all my colleagues who were a continuous source of cooperation and encouragement.

TABLE OF CONTENTS

LIST OF FIGURES

LIST OF SCHEMES

LIST OF TABLES

LIST OF ABREVIATIONS

Ac	Acetyl
Ac_2O	Acetic anhydride
AcOH	Acetic acid
Å	Angstrom
$BF_3.Et_2O$	Boron trifluoride diethyl etherate
Boc	*tert*-Butyloxycarbonyl
Cbz	Benzyloxycarbonyl
CH_3CN	Acetonitrile
$CHCl_3$	Chloroform
COSY	Correlation Spectroscopy
CRDs	Carbohydrate Recognition Domains
CuAAC	Cu(I) catalyzed azide alkyne cycloaddtion
DCM	Dichloromethane
DIC	*N,N*'-diisopropylcarbodiimide
DIPEA	*N,N*-Diisopropylethylamine
DMF	Dimethyl formamide
DOX	Doxorubicin
E. Coli	*Escherichia coli*
EDTA	Ethylene diamine tetraacetate disodium

ELISA	Enzyme-linked immunosorbent assay
ELLA	Enzyme-linked lectin assays
ESI	Electron Spectrometry ionization
EtOAc	Ethyl acetate
Fuc	Fucose
G	Generation
Glc	Glucose
GlcNAc	N-Acetylglucosamine
Glycotopes	Sets of glycan recognition motifs
HCCP	Hexachlorocyclophosphazene
HOBt	Hydroxybenzotriazole
HPLC	High performance liquid chromatography
HSQC	Heteronuclear single quantum coherence
Hz	Hertz
IC_{50}	Concentration of inhibitor resulting in 50% inhibition of binding
ITC	Isothermal titration calorimetry
Kd	Dissociation constatnt
Lectin	Protein receptors
LiHMDS	Lithium bis(trimethylsilyl)amide
MALDI-TOF	Matrix assisted laser desorption inonization spectroscopy time of flight
Man	Mannose

MeOH	Methanol
$MgSO_4$	Magnesium Sulfate
MPS	Mononuclear phagocyte
MS	Mass Spectrometry
NaH	Sodium hydride
$NaHCO_3$	Sodium bicarbonate
NaN_3	Sodium azide
NaOH	Sodium hydroxide
NaOMe	Sodium methoxide
n-BuOH	1-Butanol
NHS	N-Hydroxysuccinimide
NPhth	Phthalimide group
P.A	*Pseudomonas aeruginosa*
PDC	Pyridinium dichromate
PEG	Polyethylene glycol
PPh_3	Triphenylphosphine
PyBOP	Benzotriazole-1-yl-oxytripyrrolidinophosphonium hexafluorophosphate
RES	Reticuloendothelial system
SPR	Surface plasmon resonance
TBAF	tetra-*n*-butyl ammonium floride
TBDMS	*tert*-butyldimethylsilyl

TBTA	Tris[(1-benzyl-1*H*-1,2,3-triazol]-4-yl) methyl]amine
TEG	Triethyelene glycol
TFA	Trifloroacetic acid
THF	Tetrahydrofuran
TMS	Trimethylsilyl

RÉSUMÉ

Les infections urinaires (IU) sont l'une des maladies les plus répandues au monde et sont causées le plus souvent par Escherichia coli uropathogène (UPEC) et par Pseudomonas aeruginosa (P. A.). De plus, P. A. est l'une des principales causes d'infections nosocomiales. La liaison des agents pathogènes aux cellules hôtes se fait par reconnaissance protéine-glycane (CRD). Escherichia coli se fixe aux cellules urothéliales de l'hôte par FimH, une adhésine présente à l'extrémité des pili bactériens de type 1 et se liant au mannose, tandis que la bactérie opportuniste P. aeruginosa produit la lectine LecB, qui se lie fortement au L-fucose de Lewisa (Lea) d'une glycoprotéine présente à la surface des globules rouges, première étape des infections qui en découlent. Il est bien connu que les interactions multivalentes entre ces deux lectines bactériennes et les récepteurs des cellules hôtes jouent un rôle crucial dans l'établissement des infections urinaires. Les fluoroquinolones sont des antibiotiques efficaces ; toutefois, elles ont été associées à des effets secondaires indésirables. La ciprofloxacine (Cip) est l'antibiotique le plus fréquemment utilisé pour traiter les infections urinaires. Elle peut être administrée par voie orale ou intraveineuse. La Cip cible les enzymes bactériennes ADN gyrase et ADN topoisomérase IV, où elle stabilise un complexe covalent enzyme-ADN dans lequel les deux brins de l'ADN sont clivés. Cela entraîne la mort cellulaire et s'avère être un moyen très efficace de tuer les bactéries. Cependant, l'utilisation excessive de cet antibiotique entraîne le développement d'une résistance bactérienne qui conduit à l'échec du traitement. Par conséquent, d'autres approches thérapeutiques sont nécessaires pour traiter efficacement les infections urinaires et remédier à la résistance aux antibiotiques. Compte tenu de l'importance des glycanes en tant que molécules de ciblage, nous pensons que la conception et la synthèse d'oligomères de glycoclusters à l'aide de réactions courantes pourraient se révéler importantes dans le développement d'inhibiteurs plus efficaces, spécifiques et ciblés dans le domaine des systèmes d'administration de médicaments. Dans la présente thèse, la ciprofloxacine a été modifiée pour être conjuguée à un dendrimère par un lieur (acyloxy) alkylester clivable afin d'obtenir des promédicaments dirigés par des glycodendrimères ciblant les lectines bactériennes. Ce type de conjugué reste donc non toxique lors de sa distribution et traversera la membrane cellulaire bactérienne, où il pourra ensuite être transformé en une molécule antibiotique bioactive via un mécanisme intracellulaire, tel que l'hydrolyse enzymatique ou un environnement cellulaire spécifique (pH acide). Dans cette étude, une série de glycodendrimères hexavalents ou trivalents a été développée avec succès selon une méthode permettant de modifier les propriétés du squelette et l'architecture ainsi que d'introduire des groupes liants bioactifs spécifiques dans la chaîne latérale. Les glucides sont particulièrement intéressants en tant que ligands, car ils permettent la synthèse de glycomimétiques bien définis pour l'étude des interactions glucide-lectine. En outre, la ciprofloxacine conjuguée à l'ester méthylique (acyloxy) a été synthétisée. D'autres études impliquant des analyses MALDI-TOF, RMN 1H et RMN 19F ont confirmé ces structures globales. Le glycodendrimère est composé de trois « générations » ou couches principales (G) : le noyau du dendrimère (G1), l'échafaudage du promédicament (G2) et le sucre ciblé par la lectine (G3). Le développement clé de la complexité a été accompli par une approche convergente en deux étapes utilisant la cycloaddition azide-alcyne médiée par le cuivre(I) (CuAAC). Pour réaliser cette étude, nous avons utilisé deux échafaudages G2 distincts, dérivés de formes clivables du promédicament basées sur l'ester β-D-glucuronique ou sur la β-D-glucosamine, respectivement. La sélectivité de ces échafaudages était déterminée par un dérivé thiol du sucre G3 ciblé par la lectine. La première partie de la thèse présente une synthèse détaillée de l'échafaudage de l'ester 1-azidoethanol-2,3,4-tri-allyl-β-D-glucuronique. La première étape est la glycosylation du D-glucose-pentaacétate afin d'obtenir le 1-azidoethanol-D-glucopyranoside, dont le β-isomère a été isolé avec un rendement élevé. La silylation régiosélective d'un groupe OH primaire en position C-6 suivie de l'allylation en trois positions à *O*-2, *O*-3 et *O*-4 a permis la synthèse du dérivé tri-allyl-β-D-glucopyranoside. Enfin, la désilylation suivie par une oxydation/estérification en une étape en position C-6 a permis d'obtenir l'ester tert-butyl-β-D-glucuronique. Ce nouvel échafaudage contient des groupes azide, ester tert-butyl-carboxylique et alcène terminal, ce dernier étant le résidu actif de la réaction radicalaire thiol-ène photo-induite (TEC). Par la suite, une méthode a été développée pour la synthèse avec un haut rendement de α-L-

fucose thiol portant un lieur triazole rigide. Puis, deux glycomonomères différents dérivés de l'ester β-D-glucuronique, et de l'α-L-fucose thiol ou de l'α-D-mannose thiol respectivement, ont été couplés par TEC en utilisant la 2,2-Diméthoxy-2-phénylacétophénone comme initiateur radicalaire, formant ainsi deux branches dendritiques trithioglyco différentes (dendrons). L'étape suivante a été la synthèse des glycodendrimères finaux en utilisant un couplage CuAAC. Malheureusement, les dendrons et le noyau du dendrimère n'ont pas interagi, et aucun produit souhaité n'a été obtenu. Le groupe azide s'est avéré sensible à la réduction sous les conditions des réactions photolytiques. Par conséquent, des stratégies de synthèse alternatives ont été employées. La réduction du groupe azide a été évitée par l'introduction d'une amine protégée par le Fmoc. Par la suite, la réaction TEC de cette nouvelle molécule a permis d'obtenir des dendrons NH-Fomc trimannoside-β-D-glucuronique et NH-Fomc trifucoside-β-D-glucuronique, respectivement, avec un bon rendement. Les dendrons finaux mannoside et/ou fucoside protégés par Fmoc ont été soumis à une approche en deux étapes, en éliminant d'abord le groupe protecteur et en libérant ainsi la partie amine réactive, puis en effectuant un diazotransfert en utilisant le sulfate de 1H-imidazole -1-sulfonyle azide. Ces nouveaux dendrons synthétiques ont été couplés à plusieurs noyaux de dendrimères en utilisant le couplage CuAAC. À cette fin, un certain nombre de méthodes alternatives ont été utilisées pour créer divers noyaux dendritiques contenant des fragments d'alcynes terminaux, notamment le PEG_3-cyclotriphosphazène et le benzène-1,3,5-tricarbodimide (BTA-PEG_3). Un noyau rigide centré sur le dipentaérythritol a également été étudié. Une série de quatre glycodendrimères avec différents sucres ciblés par les lectines, dont le D-Glu-α-Man ou le D-Glu-α-Fuc, ont été synthétisés par couplage click. Ces nouveaux glycodendrimères ont été soumis à deux étapes de déprotection, d'abord celle des groupes acétyles par la réaction de Zemplin, suivie de celle du groupe tert-butyle en utilisant le TFA/toluène. La deuxième partie de la recherche a été axée sur la synthèse de conjugués multivalents de D-glucosamine. Plusieurs voies ont été empruntées pour la synthèse totale de l'échafaudage du promédicament β-D-glucosamine fonctionnalisé, notamment la glycosylation de la D-glucosamine avec le lieur PEG_3-N_3 en position C-1, suivie par une allylation en positions *O*-3, *O*-4 et *O*-6, puis d'un amido-couplage du butanoate de méthyle au -NH_2 en position C-2, et enfin d'une réduction de Staudinger, suivie de la stratégie de protection NH-Boc. Ce nouvel échafaudage NH-Boc triallyl β-D-glucosamine a été lié au α-D-mannose thiol par réaction TEC pour obtenir un nouveau bloc trithiomannoside β-D-glucosamine. Afin de déterminer si l'espacement a un impact sur l'interaction du dendrimère avec la lectine, nous avons choisi d'allonger le connecteur PEG3-N3 avec une chaîne de trois carbones. Par la suite, le dendron trithiomannoside β-D-glucosamine a été soumis à trois réactions consécutives : le retrait des groupes protecteurs -OAc et Boc pour libérer les amines, suivi du couplage de ces dernières avec l'acide azido butanoïque en utilisant PyBOP. L'étape finale de la synthèse du dendrimère a été réalisée en fixant le dendron sur le noyau de dipentaerythritol à l'aide d'un couplage CuAAC. La troisième partie de ce projet s'est centrée sur la synthèse d'un conjugué d'ester d'alkyle (acyloxy) lié à l'amine secondaire de Cip. Cet agent de couplage Cip terminé par un groupe fonctionnel amine libre, qui est sélectif, peut être lié au groupe carboxylique libre du dendrimère en utilisant le réactif de couplage amide standard (PyBOP). Dans cette étude, nous avons proposé deux méthodes alternatives pour lier le médicament au squelette du dendrimère.

Notre recherche sur le système d'administration de médicament par dendrimère peut améliorer l'activité antibiotique par rapport à la ciprofloxacine sous forme libre. De plus, les problèmes de toxicité peuvent être atténués en modifiant les dendrimères avec différents ligands permettant de diriger le médicament vers sa cible thérapeutique.

Mots-clés : promédicaments dendrimères ; inhibition bactérienne ; infections urinaires ; résistance aux antibiotiques ; E. coli ; P. aeruginosa ; lectines bactériennes ; α-L-fucose, α-D-mannose ; glycosylation ; ester D-glucuronique ; D-glucosamine ; branches dendritiques ; noyau dendritique ; multivalence ; reconnaissance moléculaire; glycodendrimères ; chimie click ; réactions photolytiques thiol-ène ; administration de médicaments.

ABSTRACT

Urinary tract infections (UTIs) is one of the most infectious diseases all over the world and are caused by a range of pathogens, most commonly uropathogenic *Escherichia coli* (UPEC) and *Pseudomonas aeruginosa* (*P.A*). Moreover, *P.A* one of the leading causes of nosocomial infections. The adhesion of pathogens to host cells occurs through protein-glycan recognition (CRD). The attachment of *Escherichia coli* to the host urothelial cells is mediated by FimH, a mannose-binding adhesin at the tip of bacterial type 1 pili, while the opportunistic bacterium *P. aeruginosa* produces lectin LecB, that strongly binds to L-fucose of lewis^{a} (Le^{a}) from a glycoprotein found on red blood cells, subsequently allowing the bacteria to trigger the infections. It is well known that the multivalent interactions between these two bacterial lectins and the host cell receptors play a crucial role in the establishment of UTIs. Fluoroquinolones (FQs) are effective antibiotics; however, they have been associated with negative side effects. Ciprofloxacin (Cip) is the most antibiotics drugs frequently used to treat UTIs. It can be administered orally and intravenously. Cip target the bacterial enzymes DNA gyrase and DNA topoisomerase IV, where they stabilize a covalent enzyme-DNA complex in which the DNA is cleaved in both strands. This leads to cell death and turns out to be a very effective way of killing bacteria. However, overuse of the antibiotic resulted in developing bacterial resistance which resulted in treatment failure. Therefore, other therapeutic approaches are needed for the effective treatment of UTIs and to combat antibiotic resistance. In view of the importance of glycans as targeting molecules, we believe that the design and synthesis of glycocluster oligomers using standard reactions has substantial significance in the development of more efficient, specific, and targeted inhibitors in the field of drug delivery systems. In the present thesis, ciprofloxacin was modified to be conjugated to the dendrimer by a cleavable (acyloxy) alkyl ester linker to yield glycodendrimer lectin-targeted prodrugs. This conjugate therefore remains non-toxic in the system distribution and will be carried across the bacterial cell membrane, where can be transform into a bioactive antibiotic molecule *via* an internal mechanism, such as enzyme hydrolysis or a specific cellular environment (acidic pH). In this study, a series of hexa-, tri-valent glycodendrimers were successfully developed, allowing for the ability to modify the backbone properties, the architecture as well as to introduce specific bioactive binding moieties in the side chain. As binding moieties, especially carbohydrates are of interest, allowing for the synthesis of well-defined glycomimetics for the investigation of carbohydrate-lectin interactions. Furthermore, ciprofloxacin conjugated with (acyloxy) methyl ester, was synthesized. More studies involving MALDI-TOF and ^{1}H NMR, ^{19}F NMR analysis, supported these overall structures. The glycodendrimer is composed of three major generations (G); dendrimer core (G1); prodrug scaffold (G2); and lectin-targeted sugar (G3), The key buildup of complexity was accomplished *via* double-stage convergent approach using copper(I) mediated azide-alkyne cycloaddition (CuAAC). To conduct this study, we used two distinct scaffolds, each representing G2 and derived from β-D-glucuronic ester and β-D-glucosamine cleavable prodrug, respectively. These scaffolds selectivity was linked to the lectin targeted G3 sugar thiol. In the first part of the thesis started with a detailed synthesis of the scaffold of 1-azidoethanol-2,3,4-tri-*allyl*-β-D-glucuronic ester. In this regard, the first step is the glycosylation of D-glucosepentaacetate to obtain 1-azidoethanol-β-D-glucopyranoside, which was separated as a single β-isomer in a high yield. Regioselective silylation of a primary OH group at C-6 position followed by the allylation at three positions at *O*-2, *O*-3, and *O*-4 afforded tri-allyl-β-D-glucopyranoside derivative, which after desilylation followed by one step oxidation/esterification at C-6 position, accomplished *tert*-butyl-*β*-D-glucuronic ester. This new scaffold contains azide, *tert*-butyl carboxylic ester, and terminal alkene groups, the latter is the active moiety in radical photoinduced thiol-ene reaction (TEC). A successful method was then established for the synthesis of α-L-fucose thiol containing a rigid triazole linker, which obtained in good yield. Next, two different sequence glycomonomers produced from β-D-glucuronic ester, and α-L-fucose thiol or α-D-mannose thiol, were coupled by TEC using 2,2-Dimethoxy-2-phenylacetophenone as a radical initiator, therefore forming two different trithioglyco dendritic wedges (dendrons). The following step is the final glycodendrimers construction using CuAAC. Unfortunately, the dendritic wedges and dendrimer core did not interact, and

no desired products were obtained. It is found that the azide group is vulnerable to reduction during photolytic reactions. As a result, an alternative synthetic strategy was applied. The reduction of azide group was prevented by the introduction of Fmoc-protected amine. Subsequently, TEC reaction of this new molecule afforded NH-Fomc trimannoside-*β*-D-glucuronic and NH-Fomc trifucoside-*β*-D-glucuronic dendritic wedges, respectively, in a good yield. The final Fmoc-protected dendrons mannoside and/or fucoside were subjected to a two-steps approach, first removing the protecting group and thereby liberating the reactive amine moiety followed by diazo transfer using 1H-imidazole-1-sulfonyl azide sulfate. These new synthetic dendrons were coupled to several dendrimer cores using CuAAC. In this regard, a number of alternative methods were used to create various dendritic cores containing terminal alkyne moieties, including PEG_3-cyclotriphosphazene and benzene-1,3,5-tricarbodimide (BTA-PEG_3). Also, a rigid dipentaerythritol centred core was applied. After conducting the click coupling conditions, a series of four different glycodendrimers with different lectin-targeted, including D-Glu-α-Man, or D-Glu-α-Fuc, were synthesized. These new glycodendrimers were subjected to two different steps of deprotection, first the deprotection of Acetyl groups under Zemplén reaction, followed by the deprotection of *tert*-butyl group using TFA/ toluene. The second part of the research was focused on the synthesis of D-glucosamine multivalent conjugates. A complete total synthesis of functionalized β-D-glucosamine prodrug scaffold was achieved by several synthetic routes including glycosylation of D-glucosamine with PEG_3-N_3 linker at C-1 position, followed by allylation at *O*-3, *O*-4, *O*-6 positions. Subsequent, amide coupling with butanoic methyl ester at -NH_2 of C-2 position, finally Staudinger reduction, followed by NH-Boc protection strategy. The new NH-Boc triallyl β-D-glucosamine scaffold was coupled to α-D-mannose thiol by TEC to obtain a novel trithiomannoside β-D-glucosamine building block. To determine whether the introduced spacing has any impact on the dendrimer interaction towards lectin, we choose to extend PEG_3-N_3 linker with an extra three-carbon chain. Therefore, trithiomannoside β-D-glucosamine building block was subjected to three continuous steps, removal of -OAc and Boc groups to liberate free amine, which is subsequently coupled with azido butanoic acid by using PyBOP to obtain the desired dendron. The final step of the dendrimer synthesis was achieved by coupling the dendron with dipentaerythritol core using CuAAc. The third part of this project was focused on the synthesis of Cip-(acyloxy) alkyl ester conjugates carrying terminal amine group, which is selectivity can be linked to the free carboxylic group of the dendrimer using the standard amide coupling reagent (PyBOP). In this study, we suggested two alternative methods for linking the drug to the dendrimer backbone.

Our research on the dendrimer-drug delivery system may enhance antibiotic activity compared to free ciprofloxacin, moreover, the toxicity problems may be solved by modifying dendrimers with targeting ligands.

Keywords: Dendrimers prodrugs; Bacterial inhibition; UTIs; Drug resistance; *E. coli*; *P. aeruginosa*; Bacterial lectins; α-L-fucose, α-D-mannose; Glycosylation; D- glucuronic ester; D-glucosamine; Dendritic wedges; Dendritic core; Multivalency; Molecular recognition; Glycodendrimers; Click chemistry, Thiol-ene photolytic reactions; Drug delivery

CHAPTER 1
BACKGROUND AND INTRODUCTION

1.1 Bacterial infections overview

Bacterial infections have a large impact on public health. Drug-resistant bacteria, viruses, parasites, and fungi cause 700,000 deaths every year worldwide (**Figure 1.1**). The World Health Organization (WHO) published research on global health in 2016, estimating that infectious and parasitic diseases represent 9.7% of the whole deaths worldwide. Although the human body coexists in an advantageous symbiosis with its own microbiota, there are numerous bacterial pathogens that can infect and colonize the human body and cause serious diseases. Bacteria can be transmitted to humans through food, water, air, or living things. [1]

Figure 1.1 Most common human bacterial infections[1]

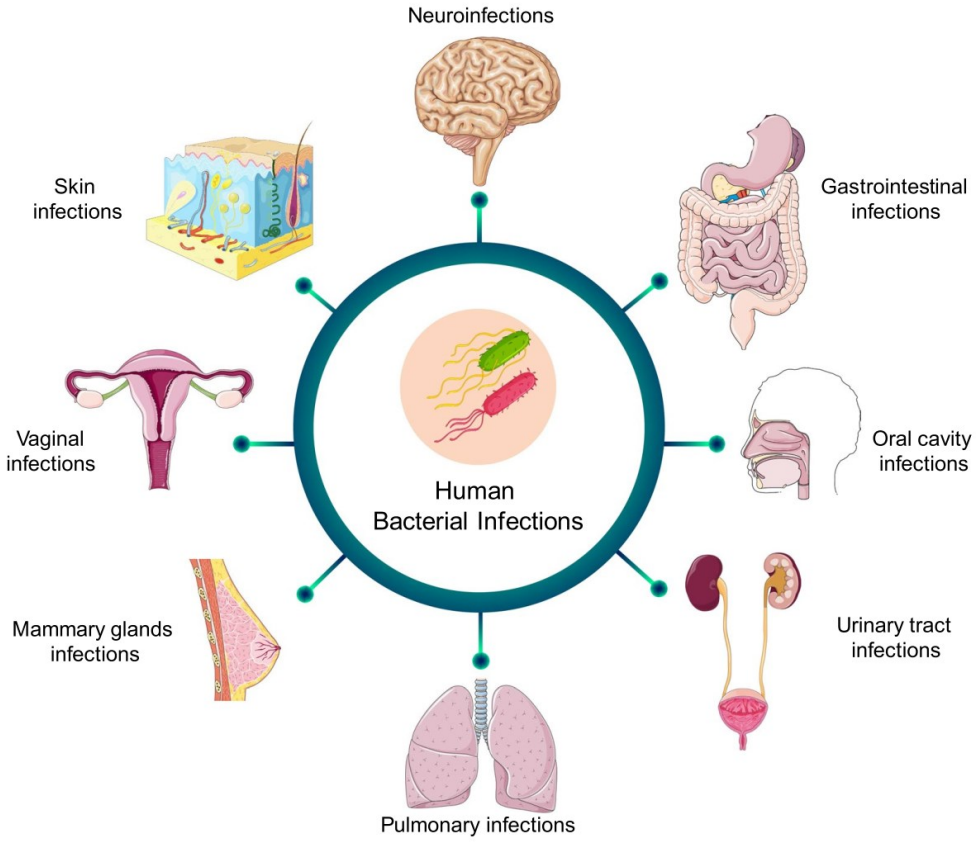

This chapter aims to describe urinary tract infections (UTIs), and bacterial causes, with particular emphasis on the mechanism of antibiotic resistance mechanism. Further focus will be on the development of dendrimers and their applications in the area of drug delivery. Since this study is directed toward the design and the synthesis of novel glycodendrimers, bacterial lectins and their role in UTIs will be also reviewed.

1.2 Urinary tract infections

Urinary tract infections (UTIs) are a severe public health problem and are caused by a range of pathogens, but most commonly by *Escherichia coli, P. aeuroginosa*, *Klebsiella pneumoniae*, *proteus mirabilis*, *Enterococcus faecalis*, and *staphylococcus saprophyticus*. High recurrence rates and increasing antimicrobial resistance among uropathogenic threaten to greatly increase the economic burden of these infections. [2-4] UTIs is clinically divided into major infections, characterized by the localization of the bacteria in the urinary tract, cystitis, and pyelonephritis. Cystitis, or lower UTIs, is an infection of the bladder. Once in the bladder, bacteria can ascend the ureters and colonize the kidneys, causing pyelonephritis or upper UTIs. While the incidence of pyelonephritis is low (0.3%-0.6%) it is particularly dangerous as uncontrolled bacterial infection can spread to the bloodstream, causing sepsis (which occurs in 2% of pyelonephritis cases). [5, 6] UTIs are also categorized as uncomplicated or complicated infections. Complicated UTIs occur in patients with: (i) functional or structural urinary tract abnormalities; (ii) renal failure; (iii) immunosuppression; (iv) pregnancy; and /or (v) foreign bodies, such as indwelling catheters, placed within their urinary tract. [7-9] Catheter-associated UTIs (CAUTI), make up 70%-80% of all complicated UTIs and are the most common type of nosocomial infection. [5] CAUTI are of particular concern as they result in high morbidity, increased mortality and are the most common causes of secondary sepsis in hospital patients. While complicated UTIs affects individuals of both genders, uncomplicated UTIs primarily affect otherwise healthy women. Pyelonephritis often occurs in a healthy, non-pregnant woman but can be categorized as a complicated UTIs because of the potential of developing a bloodstream infection.

1.3 Current treatment of UTIs

1.3.1 Antibiotics

Traditionally, broad-spectrum antibiotics have been the drug of choice to combat both community-acquired and hospital-associated UTIs (**Figure 1.2**). Usually, UTIs are treated with antibiotics. Through inhibition of pivotal enzymes or disturbing membrane integrity, these antibiotics induce bacterial growth retardation or cell death. [10] Antibiotics that are in current use for the treatment of UTIs include aminoglycosides (e.g., Tobramycin), fluoroquinolones (e.g. ciprofloxacin), and β-lactam antibiotics cephalosporins (e.g., ceftazidime). [11]

Figure 1.2 Example of antibiotic used for the treatment of UTIs

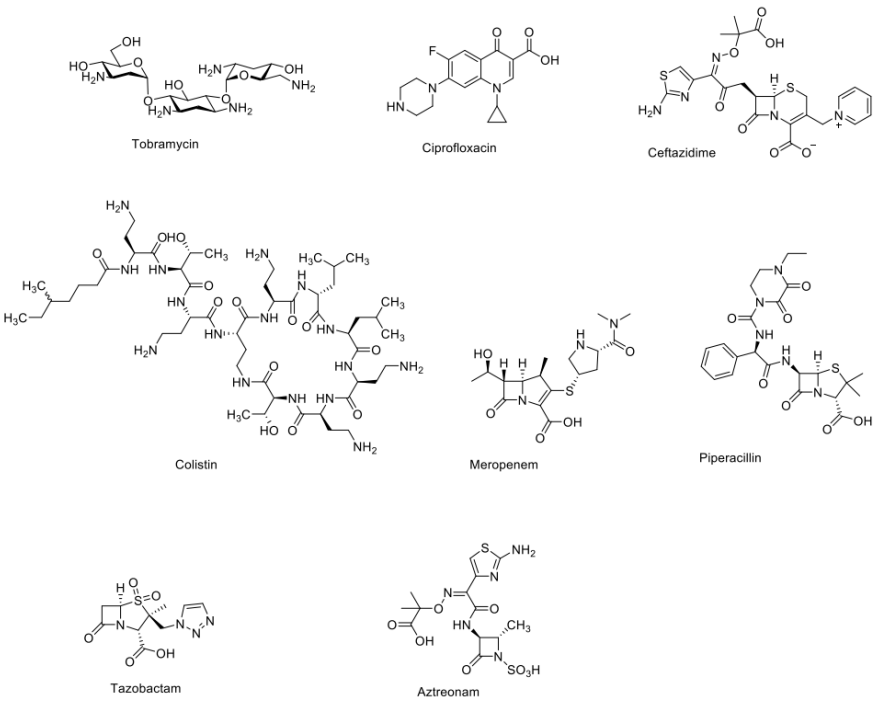

1.3.2 Combination therapies

Combinations of antibiotics are often used to take advantage of different mechanisms of action and/or toxicity profiles. Disadvantages of combination therapy include: (a) increase expense, (b) increased risk of adverse effects, and (c) superinfection. [12]

As clinically used antibiotics expose bacteria to extensive selective pressure, bacteria exhibit multiple resistance mechanisms to antibiotics. This antibiotic resistance affects the major classes of antibiotics such as β-lactams, aminoglycosides, and quinolones. An overview of the mode of action of the different antibiotics (**Figure 1.3**). All exhibit a bactericidal effect, resulting in selection pressure for bacterial survival. [13]

1.4 Antibiotic resistance mechanism

Despite huge successes in the field of antibiotic discovery seen in the previous century, infectious diseases have remained a serious cause of death. Specifically, pathogenic Gram-negative bacteria have become a global danger due to their extraordinary to acquire resistance against any clinically available antibiotic, thus urging for the discovery of novel antibacterial agents. While the pharmaceutical companies have been unsuccessful in bringing new classes of antibiotics to the market, the overuse of the current antibiotics has

increased multidrug resistance (MDR) in clinical pathogens. In fact, very recently global concerns in clinics have risen when several bacteria, e.g., carbapenem resistant Enterobacteria, acquired resistance against colistin, an antibiotic also known as polymyxin E. Facing this thread, several global initiatives started to fight antimicrobial resistance (AMR). These actions were also triggered by the fact that the so-called ESKAPE pathogens[14, 15] (*Enterococcus faecium*, Staphylococcus aureus, *Klebsiella pneumoniae*, *Acinetobacter baumanii*, *Pseudomonas aeruginosa*, and *Enterobacter spp*) but also other pathogens causing nosocomial infections are acquiring resistances to most antibiotics at a tremendous rate, (**Figure 1.3)**. Therefore, the need to understand the mechanism of AMR and to find new therapeutic approaches is greater than ever. AMR in microbes can be intrinsic, acquired, and adaptive. [16] There are many mechanisms of resistance in bacteria. Of these, five are the most frequently observed, showing high prevalence in clinical isolates. They are enzymatic inhibition, penicillin-binding protein (PBP) modifications, porin mutations, efflux pumps, and target changes. [17-22]

Figure 1.3 The common mechanism of bacteria resistance in Gram-negative bacteria. [23]

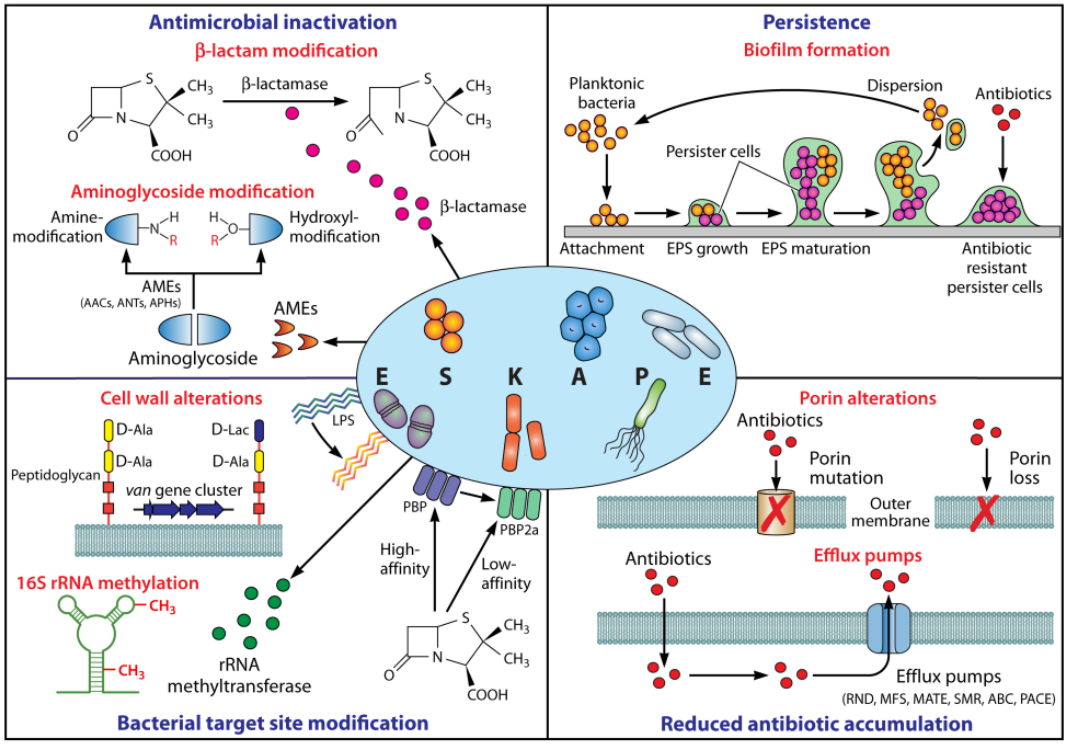

1.4.1 Enzymatic Inhibition

The most common mechanism of resistance in bacteria is enzymatic inhibition. This mechanism is based on several strategies for modifying the structure of antibacterial compounds: with hydrolysis, a type of reaction that occurs mainly with β-lactam agents; transference of functional groups (acyl, phosphoryl, thiol,

nucleotide, ADP-ribosyl, glycosyl), which occurs with a lot of antibacterial, such as aminoglycoside, chloramphenicol, rifamycin, and lincosamide; and other chemical modifications (redox, lyase), which occur with tetracycline, rifamycin, and streptogramin. Among the vast abundance of enzymes that can modify antibacterial compounds, β-lactamases are a major problem in the treatment of Gram-negative bacteria. [24, 25] These include penicillinases, which confer resistance against penicillin, AmpC cephalosporinases (eg., MOXs, MIR, FOX family CMI family, and others), and which are also able to hydrolyze penicillin's and many cephalosporins that avoid clinical β-lactamase inhibitors (eg., SHV-1, TEM-1, TEM-2, CTX-Ms, and others), which are able to hydrolyze penicillins and all cephalosporins. This group of enzymes confers resistance against penicillin and all cephalosporins, including cefotaxime and ceftazidime; many producers of TEM and SHV display resistance to tetracyclines, sulfonamides, and aminoglycosides. The majority of CTX-M producers are also resistant to fluoroquinolones. Finally, the carbapenemases (e.g, IMP family, VIM family, KPCs, OXAs, and others), which are enzymes capables of inactivating all β-lactam agents. [25, 26]

1.4.2 Efflux across a double membrane, Multidrug efflux pumps

Bacterial efflux pumps are an important source of multidrug resistance. [27] The majority of gram-negative bacterial multidrug efflux pumps are entirely different in their construction. Four multidrug efflux pump systems have been identified in *P. aeruginosa*: "MexA-MexB-OprM, MexC-MexD-OprJ, MexE-MexF-OprN and MexX-MexY-OprM". The primary multidrug resistance efflux in *E. coli* is AcrAB- ToIC. Three different proteins make up this pump that span the inner and outer cell membrane: a periplasmic linker protein AcrA, the inner membrane efflux transport AcrB, and the outer membrane channel ToIC. These efflux pumps have different substrate specificities and can expel a vast of molecules from both the cytoplasm and periplasm of the bacterial cell, including secondary metabolites and nearly all clinically available antibiotics. All of the efflux pumps systems are energy dependent (*i.e*. protein motive force driven) and consist of three components: a resistance-nodulation-division (RND) exporter protein (located in the cytoplasmic membrane), a gated outer membrane protein (located in the outer membrane), and a membrane fusion protein (MFP) that links RND exporter protein with the gated outer membrane protein. [28] A schematic of the proposed structure and function of these efflux pump systems is depicted in (**Figure 1.4)**.

Figure 1.4 Structure and function of RND efflux pumps in *P. aeruginosa*.

RND pumps typically exist in a tripartite system consisting of an RND cytoplasmic membrane transporter (RND), a membrane fusion protein (MFP), and an outer membrane factor (OMF). Fluoroquinolones (general structure) enter into the RND transporter through openings known as vestibules and are exported through the channel to the extracellular milieu using proton-motive force. [29]

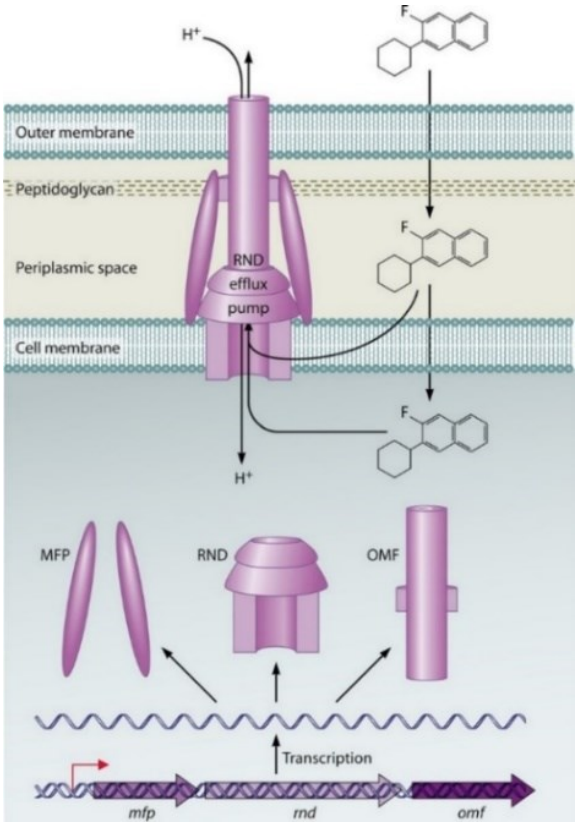

1.4.3 Permeation barrier and protein alteration (Porin modification)

Gram-negative bacteria have a multifaceted cell envelope comprising an outer membrane that limits access to the periplasm by acting as a molecular filter, and therefore forming an efficient selective permeation barrier. [30] This outer membrane is mainly made up of a bilayer of lipids. Because of this, most of the hydrophilic molecules cannot permeate the lipid bilayer membrane. The intake of hydrophilic molecules, it is mainly controlled by specific water-filled open channels called outer membrane proteins (Omps) or porins **(Figure 1.5)**.

Figure 1.5 Antibiotic resistance mechanism associated with Omps modification.

Antibiotic molecules are represented by green balls, and Omps as trimmers by grey cylinders. The curved arrows exemplify the uptake failure/ reduced uptake occurring with the following: B. decrease in the level of wild-type Omps, C. expression of restricted-channel Omps, D. mutation or modification of the functional properties of a porin channel, and E. synthesis of modified Omps with significant construction. [31]

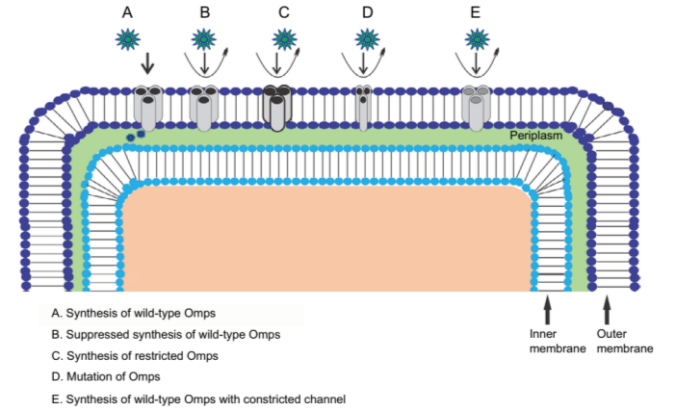

Bacterial adaptation to reduce influx through these Omps is an increasing problem that contributes, in addition to the efflux system, to antibiotic resistance. Like other hydrophilic molecules, polar antibiotics including β-lactam antibiotics and fluoroquinolones often enter Gram-negative bacteria by using these Omps. [32] Any slight modification in the responsible Omps can significantly affect the intake of the drug, and thus reduce the effectiveness of the antibiotic.

1.4.4 Resistance due to modified target sites

The function they play in microbial growth and survival is a crucial aspect of the target areas for antimicrobial drugs. If their function is disrupted, the cells either die or are inhibitory to cell growth. The peptidoglycan component of the bacterial cell wall provides an excellent example of a selective target. The resistance to β-lactamase, also partly results from the modification of the target site of the Penicillin-Binding Proteins (PBPs). Compared with panel A (**Figure 1.6**), The β-lactams cannot bind with the modified PBP. This renders the β-lactams in panel B. an altered PBP with low affinity was reported after 7 imipenem treatment, as well as after administration of high doses of piperacillin in patients suffering from cystic fibrosis. [33] one of the major mechanisms, besides active efflux, that accounts for fluoroquinolone resistance in *Pseudomonas aeruginosa* is through structural modifications in target enzymes. Fluoroquinolones act by inhibiting DNA gyrase and topoisomerase IV, two enzymes involved in bacterial DNA synthesis. [34] point mutations in the *gyrA/ gyrB* genes within the QQRDR (quinolone resistance- determine- active region) motif, which is considered as the enzyme's active site, allow the modification of the primary target for fluoroquinolones (DNA gyrase, also known as topoisomerase II) to occur. Therefore, the amino acid sequence of A and B subunits alters, which leads to the synthesis of modified topoisomerase II with low

affinity to quinolone molecules. Modification of a second target (topoisomerase IV) occurs as a result of mutations in *par C* and *par E* genes encoding parCc and parE enzyme subunits, respectively. [35]

Figure 1.6 Antibiotic resistance of *P. aeruginosa* due to target modification.

Panel A: interaction of β-lactams. β-lactams molecules penetrate the periplasmic spacer either by passing directly through the outer membrane or entering through specific porins. Once they entered the periplasmic space, β-lactams can interact with their target binding proteins (PBP) located on the outside of the cytoplasmic membrane. Panel B: β-lactams cannot bind to the mutated PBP, and Fluoroquinolones cannot bind to Topo IV and DNA gyrase. [29]

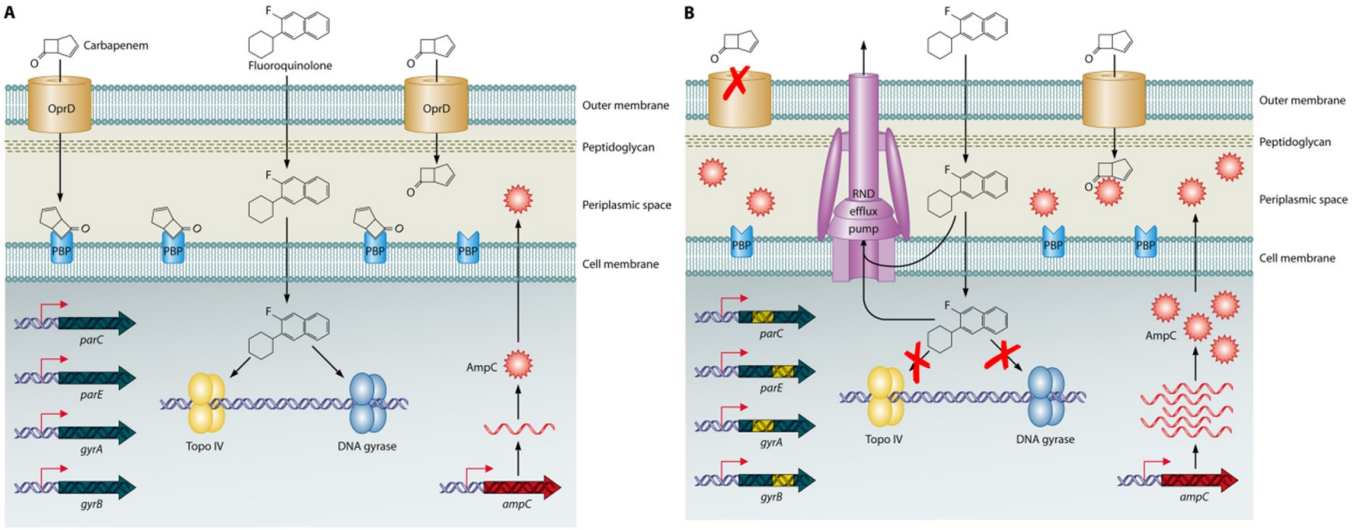

Increasing resistance rates are a worldwide threat and include the majority of available antibiotics. Accordingly, resistance UTI pathogens were confirmed for several antibiotic classes like β-lactams, quinolones, aminoglycosides, and tetracyclines.

1.5 Fluoroquinolone (Ciprofloxacin)

Fluoroquinolones (FQs) represent a major class of antibacterial with great therapeutic potential and are active against a wide range of Gram-negative and Gram-positive pathogens. Over the years, several structure-activity and side-effect relationships have been developed, covering thousands of analogues, in an effort to improve antimicrobial efficacy while reducing undesirable side effects. [36] Ciprofloxacin, is one of the most commonly recommended therapeutics for UTIs. [37] additionally, the clinical applications of these antibiotics have been extended to the treatment of lower respiratory tract infections, skin and soft tissue infections. [38-41] However, due to the extensive use of these drugs in human and veterinary medicine, the number of fluoroquinolones -resistant strains has been growing steadily. [40-43]

1.5.1 Ciprofloxacin structure-function

As shown in (**Figure 1.7)**, carboxylic acid at positions C-3 and carbonyl at C-4 are known to be essential for antibacterial activity, because they mediate binding to the DNA-gyrase complex. These groups are involved in the formation of the Mg^{2+} water bridge for tight complex binding. If these groups are chemically modified or removed, the activity is reduced. The fluorine at C-7 (the basis for the name fluoroquinolones) is also essential for high potency. The substituent C-8 greatly influences potency, spectrum, and pharmacokinetics. [44] The optimal groups have been 5- and 6- membered nitrogen heterocycles containing peripheral basic nitrogens with the most common being piperazines. The substituents attached to N-1, control antibacterial potency. The optimal groups are cyclopropyl. [45]

Figure 1.7 (A) The observed structure-activity relationships (SARs) of quinolone core substitutions. [36] (B) The pharmacophore and potential multiple drug-target interactions of ciprofloxacin[46]

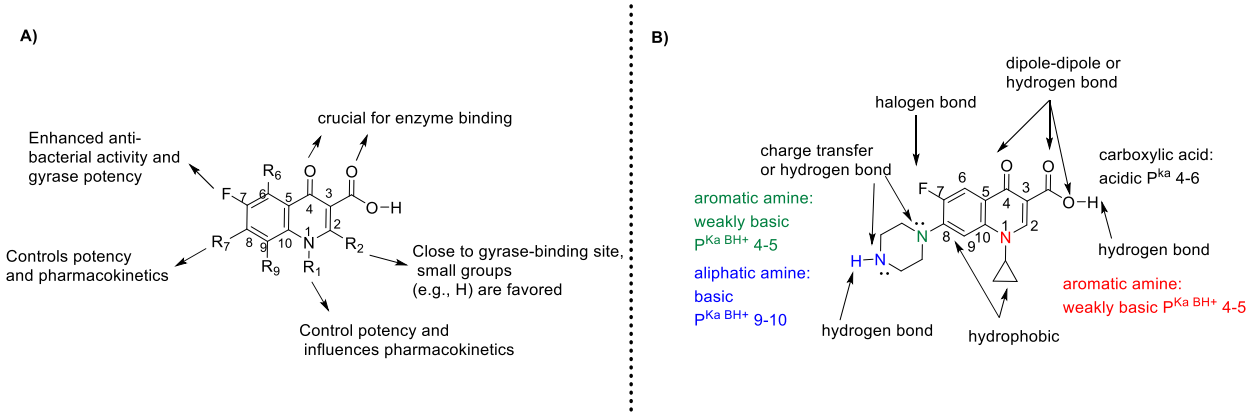

1.5.2 Ciprofloxacin uptake

Ciprofloxacin has two protonation sites. In water, the carboxylic acid has a pK_a of 6.5 and the terminal nitrogen on the piperazine has a pK_{aH} of 7.5. Ciprofloxacin is also known to coordinate Mg^{2+} ions, this causes the complex to acquire a positive charge. Once the molecule is charged, it is removed from the lipid bilayer, [47] nevertheless it is known that porins in the bacterial outer membrane have a preference to transport cations. [48] The porin OmpF is widely known to be the primary ciprofloxacin transport in the *E. coli* bacterial membrane. [47-50] As the modifications would mask the ionizable groups, it was hypothesized that by masking the ionizable groups, the rate of diffusion through the bacterial plasma membrane would be accelerated.

1.5.3 Fluoroquinolones inhibition mechanism

Gyrase appears to be the primary cellular target for quinolone antibacterial in multiple pathogenic bacteria. Given the significance of this type II topoisomerase as a drug target, it is critical to understand how quinolones interact with gyrase and how specific mutations lead to resistance. The carboxylic acid group at

position 3 and the carbonyl at position 4 seem to be essential for the activity of the quinolones. Quinolone's antibiotics inhibit DNA synthesis by targeting two essential type II topoisomerases, DNA gyrase and topoisomerase IV (topo IV), two enzymes essential for bacteria viability, (**Figure 1.8**).

Figure 1.8 Fluoroquinolones bind to Topoisomerase (II and/ or IV) and stabilize the complex of topisomerase and the recently cleaved DNA strands. This results in double-strand DNA breaks. [51, 52]

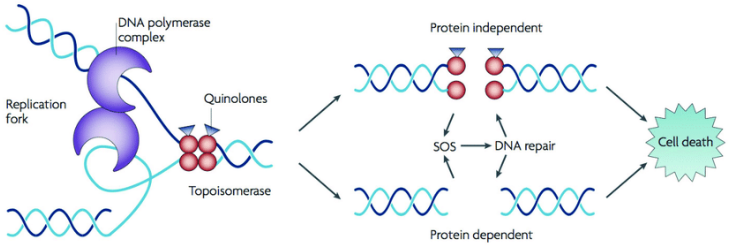

Fluoroquinolones antibiotics bind to DNA gyrase in the midst of the catalytic cycle, when the duplex DNA has been cut. The stoichiometry is two fluoroquinolones per tetrad of the gyrase subunit. Antibiotic binding in this way is DNA dependent and the molecules have a low affinity for free gyrase. Gyrase itself forms a binding pocket for the fluoroquinolone in a relaxed DNA substrate in the presence of adenylate triphosphate ATP. The drug intercalates into nicks in the DNA created by the enzyme. The binding complex involves the carboxylic acids and carbonyl of the quinolone to form a Mg^{2+} water bridge to an aspartic/ glutamic acid residue and serine in helix IV of a GyrA subunit. (**Figure 1.9)**, shows the proposed water-metal ion bridge that mediates critical interactions between quinolones and topoisomerase IV. A generic quinolone structure is depicted in black, water molecules are in blue, Mg^{2+} is in orange and the coordinating serine and glutamic acid residues are in red and green, respectively. Blue dashed lines indicate the octahedral coordination sphere of the divalent metal ion interacting with four water molecules and the C3/C4 keto acid of the quinolone. The red dashed lines represent hydrogen bonds between the serine side chain hydroxyl group and two of the water molecules. The green dashed line represents a hydrogen bond between the glutamic acid side chain carboxyl group and one of the water molecules.

Figure 1.9 Diagram of the proposed water-metal ion bridge that mediates critical interactions between quinolones and topoisomerase IV. [53]

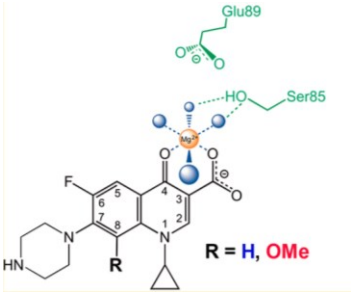

1.6 Resistance to fluoroquinolones

Quinolone resistance is acquired by a variety of different resistance mechanisms, including target site mutations, enzymatic inactivation, and target protection and efflux systems.

1.6.1 Target site mutations

Specific target alteration of the DNA Gyrase GyreA subunit and Topoisomerase IV ParC subunit is a common mechanism of resistance and may be the most significant one clinically. The most common mutations are identified at the Serine82 and acidic residues of gyrA and parC that are critical for binding of Quinolones via the water-metal-ion bridge. Other mutations leading to resistance are within discrete regions of the enzyme, called quinolone resistance-determining regions (QRDRs). Mutations typically involve replacing a hydroxyl group with a bulky hydrophobic residue which leads to an altered active site geometry. This region is the binding pocket for DNA Gyrase onto DNA and as fluoroquinolones bind on the DNA Gyrase-DNA complex any changes here can lower the binding affinity. Overcoming this kind of resistance is extremely difficult and no such examples have reached clinical use.

There are more chromosome-based resistance mechanisms. Fluoroquinolones cross the bacterial membrane mainly making use of porins, though they can diffuse across. The cellular concentration of quinolones is regulated by opening actions of diffusion-mediated drug uptake and pump-mediated efflux. The outer membrane of Gram-negative bacteria poses an additional barrier that drugs must cross to enter the cell. Therefore, drug influx in Gram-negative species is facilitated by protein channels called porins. If the expression of porins is downregulated, it led to low-level resistance to quinolones.

1.6.2 Fluoroquinolones resistance due to mutations at non-target sites

Quinolone-resistant bacteria frequently exhibit a variety of distinct non-target site alterations. Including, harmful mutations in acrR and multiple-antibiotic-resistance (Mar) phenotype marR, a factor that both directly and indirectly inhibits the expression of the endogenous AcrAB-To1C efflux system in *E. coli,* [54] resulting in increased quinolone efflux levels. MarR works by suppressing marA expression, a global transcriptional activator, that activates expression of acrAB. In addition, MarA also activates transcription of micF, encoding and antisense RNA that post- transcriptionally inhibits the outer membrane porin, OmpF. OmpF is important for quinolone entry into the cell in *E. coli* and its inhibition lead to decreased quinolone susceptibility. [55] Other Gram-negative bacteria have similar efflux systems. For example, *Pseudomonas aeruginosa* express the MexAB-OprM efflux system that is repressed by MexR. Quinolone resistant clinical isolates of *P. aeruginosa* often have mutations in mexR leading to overexpression of the MexAB-OprM efflux pump. [56]

1.6.3 Plasmid-mediated Fluoroquinolones resistance

Three families of genes are associated with plasmid-mediated quinolone resistance. The first is the Qnr proteins are part of a small of pentapeptide repeat proteins and share homology with DNA mimics. These bind to DNA Gyrase and topoisomerase IV both in the cytoplasm and while complexed to DNA to reduce the number of enzyme target sites for fluoroquinolones and hence their efficacy. The second one is QepA and OqxAB efflux pumps. QepA and OqxAB are the primary efflux pump types responsible for plasmid-mediated quinolone resistance (PMQR). QepA is able to actively pump out hydrophilic fluoroquinolones, especially norfloxacin and ciprofloxacin. The increase in MIC conferred by QepA varies from 2- 64 fold, this large range is probably caused by most likely contributed to differences in QepA expression. The OqxAB efflux system is a member of the resistance-nodulation-cell division family of transporters and is able to pump out a range of different antibiotics, including quinolones, chloramphenicol and trimethroprim. [53, 57-60]

The third one is inactivation by AAC(6´)-lb-cr mediated acetylation. The AAC(6´)-lb protein family consists of 6´-*N*-acetyltranferases that can deactivate several aminoglycoside antibiotics by acetylation. [61]
Therefore, it came as a surprise when a clinical strain of *E. coli* disrupted AAC(6')-lb gene on a multiple resistance plasmid, resulting in an increase in ciprofloxacin susceptibility. An acetylation assay showed that this novel member of the AAC(6´)-lb family was able to *N*-acetylate ciprofloxacin at the amino nitrogen on its piperazinyl substituent (**Figure 1.10**). So the enzyme was given the name AAC(6´)-Ib-cr, where "cr" stands for ciprofloxacin resistance.
A number of other efflux systems in Gram-neative bacteria have linked to quinolone resistance, [62] but these will not be discussed here.

Figure 1.10 AAC(6´)-Ib-cr acetylation of the amino nitrogen of the piperazine ring

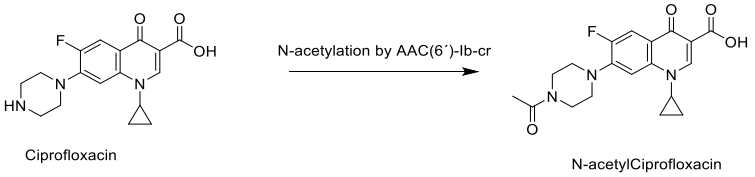

In an effort to overcome the current crisis with treating infections caused by multi-drug resistant bacteria, many different treatment strategies have been studied.

1.7 Fluoroquinolone-based conjugate therapies

The evolution of the various fluoroquinolone generations has demonstrated that they provide a great target for additional modifications. Extensive work has been carried out investigating the effects of modifying the piperazine ring of ciprofloxacin. In 2012, S. Wang *et al*. discovered that ciprofloxacin was up to eight times more effective than ciprofloxacin against Gram-positive bacteria when modified with an *N*-terminal 4-methoxybenzene. They explain improve fluoroquinolone activity is due to increases in lipophilicity. [63]

Figure 1.11 Synthesis of ciprofloxacin dimers using various linkers

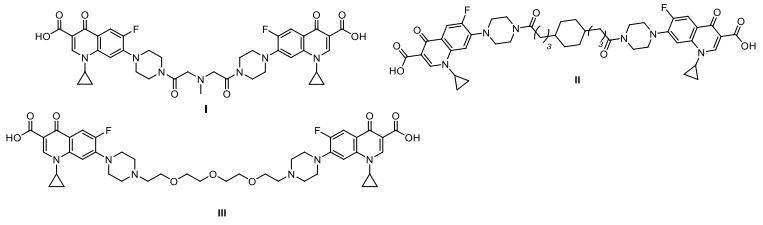

Several fluoroquinolone dimers with the same fluoroquinolone core or two different fluoroquinolones tethered by a number of linkers at the piperazine ring were screened for their in vitro antibacterial activities against a panel of clinically relevant pathogens including drug-resistant strains. [64, 65]

In 2015, Ross *et al*. carried out further ciprofloxacin dimer analysis, (**Figure 1.11)**. Amide links, **I** and **II**, were synthesized with the aim of improving interactions with DNA and the solubility profile. [66] However the dimerization resulted in a significantly increased MIC (32 μM) against *E. coli* compared to ciprofloxacin (<0.03 μM). The MIC was decreased when tested against an outer membrane permeability mutant, indicating that one of the problems was with diffusion past the membrane, however, direct DNA Gyrase assays indicated a three-fold decrease in IC_{50}. In another study, Ross and co-workers also synthesized PEG dimers of ciprofloxacin **III**, (**Figure 1.11)**. Interestingly, their studying proved that DNA Gyrase's IC_{50} was significantly greater for the new ciprofloxacin in-conjugate. This indicates that PEGylation is enhancing membrane permeability while decreasing DNA Gyrase binding. It is hypothesized that the PEG linker can stretch across the phospholipid bilayer without rupturing the membrane. [66]

1.7.1 Cleavable linker

Chemical modification of drugs into labile derivatives (prodrugs) with improved physicochemical properties that enable better transport through biological barriers is an effective method for improving drug delivery. This type of transformation occurs more frequently on ionizable molecules such as carboxylic acids and amines in order to modify their ionization at physiological pH and to render desirable partition

and solubility properties. A necessary requirement of this approach is the capability of the prodrug to return to the parent drug in the body by enzymatic or chemical action, at the desirable rate.

1.7.1.1 Disulfide Based Prodrugs

The disulfide bridge has the benefit of resisting the oxidizing extracellular fluid environment while being susceptible to breakdown in the reducing intracellular environment, (**Figure 1.12**).

Figure 1.12 The general structure for the disulfide bridge

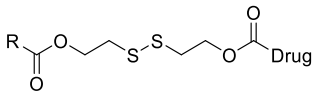

However, the previous information from the literature indicates that disulfide linkers have limited activity and may not be generally applicable for conjugation strategies of antibiotics. [67]

1.7.1.2 (Acy1oxy) alkyl carbamates as novel labil Prodrugs

(Acy1oxy) carbamates of the type R_1R_2N-CO-O-CH_2-OCO-R_4 are described as novel bio reversible prodrugs for primary and secondary amines. Enzymatic hydrolysis of the ester bond in these ester carbamate leads to a cascade reaction resulting in rapid regeneration of the parent drug. The benefits of a carbamate are as follows: (a) carbamylated amines do not ionize and hence are more compatible with organic and lipoidal systems, (b) the modification is applicable to primary and secondary amines essentially irrespective of basicity, (c) there is potential for chemical selectivity in the presence of competing functionalities such as hydroxyl, and (d) they are chemically stable. [68] For example, Rivault *et al.* [69] synthesized pyochelin–norfloxacin conjugates **IV** and **V** (**Figure 1.13)**. The linker was expected to be stable in the extracellular assay conditions but would be cleaved by intracellular esterases upon entry into the cell. The connection of the linker would enhance the retention of the conjugate in cells.

Figure 1.13 Ciprofloxacin conjugated with ester linker

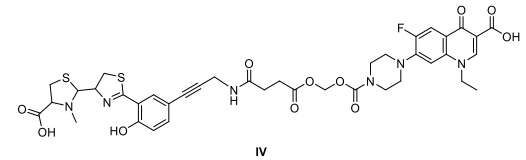

IV

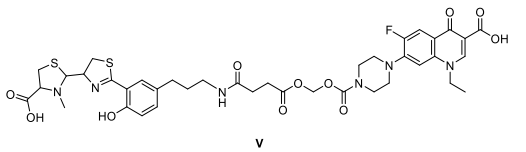

V

The properties of related linkers (**Figure 1.14**, R=Me) were studied by Gogate and co-workers, who discovered that under optimal conditions it remained stable for many years. [70] The hydrolysis of a secondary amine prodrug is dependent on the ester hydrolysis rate, therefore the cleavage rate can be tuned by changing the R group between the ester and amide. [71, 72] The *N*-(acetoxyethoxycarbonyl) (R = Me) linkers have been shown to be cleaved by esterase at a faster rate than the buffer, and thus show promise in prodrugs. [73] Therefore, ciprofloxacin payload from the conjugates in our study was hence hopeful they would permit intracellular release.

Figure 1.14 The cleavable linker intended for use in this study

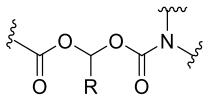

Overall, these examples show that fluoroquinolone-based conjugate therapies are a promising strategy to deliver antibiotics across the bacterial membrane, but it is important to note that conjugation of antibiotics may lead to loss of activity. There is therefore increasing interest in treatments that would not quickly lead to the emergence of resistance. These treatments frequently target bacterial virulence, rather than killing bacteria completely. One important target is bacterial virulence factors, lectins, (sec. 1.15.3 and 1.16.3).

The second strategy in novel antibiotic discovery is to enhance or regain the activity of known antibiotics by avoiding a resistance mechanism. For example, antibiotics are often excluded from cells due to membrane impermeability or efflux. This may be overcome by attaching the antibiotic to a molecule with which the cell membrane has a strong affinity. The most well-known example of this strategy is nanoparticle (NPs) drug conjugation. Nanoscale materials are similar in size to biological molecules and systems (**Figure 1.15**) and possess unique properties, such as high surface area-to-volume ratio, and tunable electronic, and biological properties. In addition, they can be engineered for desired physical properties (sizes, shapes), and chemical characteristics (composition, surface chemistry). [74] Their unique properties present opportunities in therapeutic applications.

Nanotechnology has exploited the enhanced permeability and retention effects for “passive targeting”. [75] “Active targeting” further improves the targeting specificity by conjugating these nanocarriers to ligands that bind to specific receptors on the surface of the cells. [76]

Figure 1.15 Schematic represenation of a variety of nanocarriers used to transport drugs (the image adopted with permission from ref). [77]

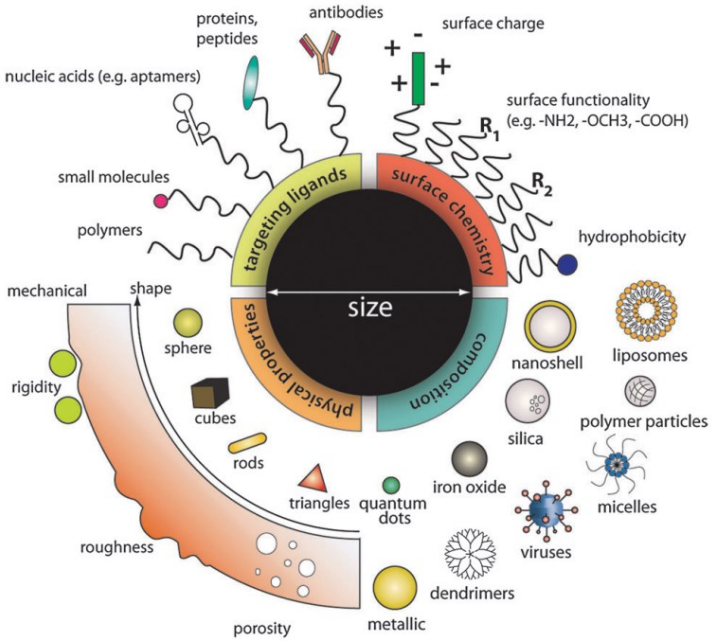

1.8 Antibiotics encapsulation delivery system

Nanoencapsulation of drug molecules in nanocarriers (NCs) is a very promising strategy for nanomedicine development. Modern drug encapsulation methods allow the effective loading of drug molecules inside the NCs thereby reducing systemic toxicity associated with drugs. Targeting of NCs can be improved by the accumulation of nanoencapsulated drugs at the infected site. [78] The use of encapsulation delivery systems (such liposomes, polymer, and dendrimers) as potential drug carriers for a range of active substances, such as small molecule medicines and biologics, therapeutic protein and vaccines, have been studied.

1.8.1 Liposomes for antibiotics delivery

Liposomes are colloidal systems, usually 0.05-5 μm in diameter primarily composed of a combination of natural synthetic or lipids (phospho- and sphingolipids) and other bilayer constituents such as cholesterol and hydrophilic polymer-lipid conjugates. Because of the lipid relative polarity and hydrophilic head groups and thermodynamic influences from the hydrophobic effect, liposomes can undergo spontaneous self-assembly under hydrated aqueous conditions to form unilamellar and multilamellar vesicles. Drugs with widely varying lipophilicities can subsequently be encapsulated in these constructs, either in the lipid bilayer or entrapped in the aqueous core of the liposome. Many techniques have been developed to prepare liposomal drug delivery systems. (e.g., reverse-phase evaporation, freeze-thaw, extrusion) and depend strongly on the co-solvents used and the physiochemical properties of the encapsulated drug. [79] These

approaches oftentimes yield difficulty in reproducibility and manufacturing scalability, and result in poor drug encapsulation efficiencies. In addition to the difficult formulation process, liposomes can also suffer from incomplete and burst drug release kinetics which may limit control over individual medication dose and efficacy. The clinical applications of liposomes are well known, and the initial success achieved with many liposome-based drugs has stimulated additional clinical research. For example, an inhalable liposomal ciprofloxacin (Aradigm) formulation is currently undergoing pre-clinical trials for localized treatment and prevention against pulmonary anthrax infections. Wang and co-workers established the utility of ciprofloxacin and colistin liposomes formulations which resulted in enhanced antibacterial activity against multiresistant *P.A*.[80] Also, in a recent study it was found that the use of liposomes loaded a combination of colistin and ciprofloxacin is a promising approach for the treatment of (MDR) *P. aeruginosa* infections, particularly in pulmonary delivery for lung infections.[81, 82] Ciprofloxacin was also loaded on liposomes with 45% loading efficiency. The release rate of encapsulated ciprofloxacin was modulated by the addition of cysteine to the dithiobenzyl urethane linkage between the lipid and the PEG in liposomes.[83]

1.8.2 Antibiotic encapsulation on dendrimer

Due to the highly variable and oftentimes poor physiological stability properties of liposomal systems, polymer drug encapsulation carriers offer an alternative approach to better control the delivery and release of drugs and minimize daily drug dosing. periphery.[84] The drug molecule can be coordinated to the outer functional groups of the dendrimer with ionic interactions. The second method describes that the dendrimer function as a unimolecular micelle comprising a hydrophobic core and a polar surface by encapsulating a drug molecule through the formation of a dendrimer-drug (host-guest) interaction. The encapsulation ability of dendrimers increases with the increase in dendritic generation and with the increase in size and molecular weight of the functional groups attached.[78] Sulfamethoxazole (SMZ) is an antibiotic widely used for bacteriostatic and urinary tract infections with trimethoprim. But its poor aqueous solubility and bioavailability limited its clinical applications. Wen and co-workers reported the encapsulation of SMZ into G3 Polyamidoamine (PAMAM) dendrimer. They investigated the potential of ethylenediamine (EDA) core polyamidoamine (PAMAM) dendrimers as drug carriers of SMZ by aqueous solubility, in *vitro* release as well as anti-bacterial activity studies. The *in vitro* release behavior and anti-bacterial activity studies indicated that PAMAM dendrimers might be considered potential drug carriers of sulfonamides with a sustained release behavior under suitable conditions.[85] In 2006 Kumar *et al* Published an example of dendrimers polyconjugated to both drugs and targeting moieties.[86] accomplished this by noncovalently encapsulating Rifampicin (RIF) (**Figure 1.16**), a hydrophobic antitubercular drug with low macrophage penetration, in mannosylated dendrimers with five generations of polyproyleneimine branches building off an ethylene diamine core (G5 EDA-PPI). This strategy takes advantage of surface-bound mannose-binding

proteins, which then facilitate receptor-mediated endocytosis. The conjugate experienced significantly increased concentrations of RIF in alveolar macrophages in comparison to free RIF, as well as good drug release at pH 5.0 (pH of phagolysosomes). However, the drug has a problem with solubility, the solubilizing propensity of G5 EDA-PPI-mannosylated dendrimer decreases since mannose increases the steric hindrance on the surface of mannosylated dendrimer and reduces the molecular gap present in the dendrimers.

Figure 1.16 Rifampicin drug encapsulation with Mannosylated 5G EDA-PPI dendrimer. [87]

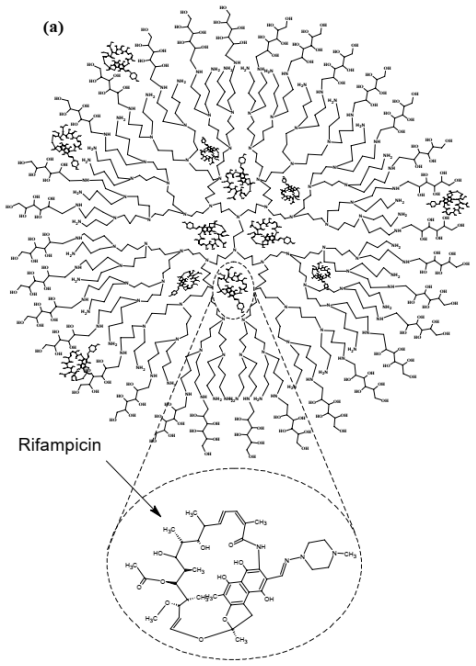

Drug encapsulation techniques have drawbacks as a result of their complexity and difficulty in the preparation methods. Similar to the formulation of liposomal systems, the synthesis and development of polymer derived drug encapsulated particulates is associated with high cost, and slow progress in the development of biologically stable carriers as well as low encapsulation efficiency and failure to control the release of the drug from the dendrimer pockets/cavities due to insufficient interactions between the dendrimer molecules and the drug. Alternative approaches using chemically- labile dendrimer-drug conjugation techniques have been explored to more readily drug delivery systems. [88-92]

1.9 Dendrimers drug conjugates provide advantages over encapsulated drug systems

Drug conjugation to polymer systems (eg., dendrimer) offers various benefits for example, small molecule delivery, including the potential for sustained and controlled release of bioactive, (**Figure 1.17**). Specifically, the drug release rate is modified based on the chemical bonds that link the active drug to the polymer (e.g., ester, hydrazine, acetal, amide), formulation properties of the polymer (e.g., powder,

hydrogel, microspheres) and polymer chemical composition (e.g., nonbioactive polymer backbone or drug-linker molecules). Additionally, by covalently linking the drug, higher drug loading is achieved compared to physical encapsulation methods. [93-94]

Figure 1.17 In *vivo* bioactivation of prodrugs by enzymatic and / or chemical transformation[95]

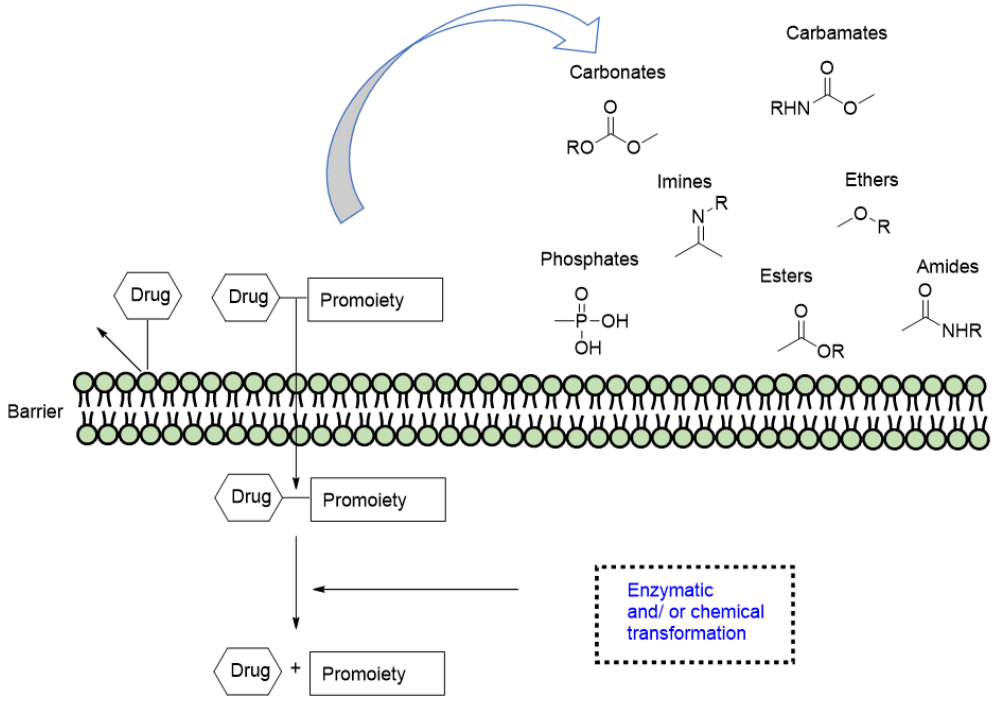

This approach offers improved drug solubility, stability, drug release, and pharmacokinetics. Additionally, it can facilitate the accumulation of a drug at the site of action and improve safety.

1.9.1 Chemical conjugation of antibiotic to dendrimers

The chemical conjugation of a small molecule to a dendrimer, usually results in cleavable covalent bonds linking the antibiotic to the dendrimer backbone. Fluoroquinolones, such as ciprofloxacin and norfloxacin, are among the well-investigated antibiotics for direct chemical conjugation. For example, Cip-dendrimer prodrugs were developed for bacterial targeting drug delivery to inhibit DNA gyrase. In their research, photocaged ciprofloxacin was attached to a lipopolysaccharide (LPS)-binding poly(ammidoamine) (PAMAM) dendrimer nanoconjugate for cell wall targeted delivery (**Figure 1.18A**). The authors demonstrated that the LPS-binding groups direct the conjugate to membranes of Gram-negative bacteria, and then exposure to UV light (365 nm) cleaves the photolabile ortho-nitrobenzyl linker between dendrimer

and Cip. Although antibacterial activity was lower for the conjugate than for free Cip, the lack of UV exposure had a limited effect on bacterial viability, validating the photo-controlled release of antibiotic. [96]

Figure 1.18 (A) Light-controlled targeted delivery of ciprofloxacin (ONB-Cipro) [96],(B) Synthesis of PMOx30-Cip conjugate

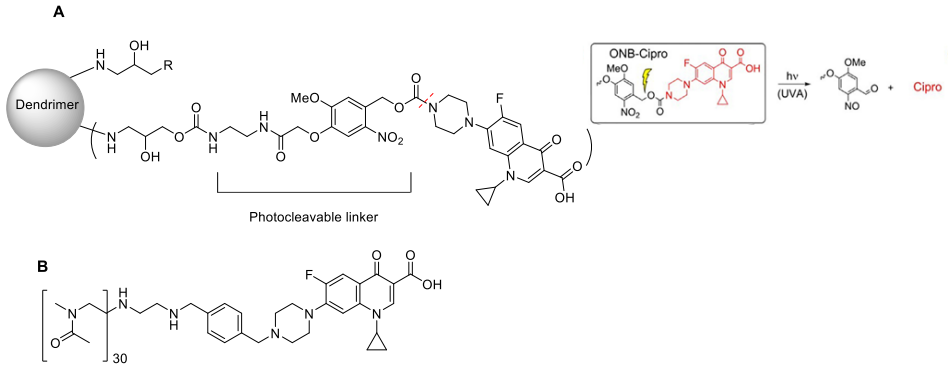

In another study, Tiller and co-worker studied the covalent attachment of the antibiotic ciprofloxacin[97] to the chain end of poly(2-methyloxazoline)(PMOx), poly(2-ethyloxazoline)(PEtOx) (**Figure 1.18 B)**, and polyethylene glycol (PEG), and the antimicrobial activity of these conjugates were tested for *E. coli*, *P. aeruginosa*.

Table 1.1 Summary of dendrimers conjugated with antibiotics

Dendrimers	**Antibiotics conjugates**	**Pathogens tested**	**Mechansim of antibiotic release**
Polyamidoamines (PAMAM)	Ciproflaxacene	*E-coli*	Light-active release[96]
PAMAM	Erythromycin	*S.aureus*	Hydrolysis of ester[98]
Polypropylene imine (PPI)	Amoxicillin	*E.coli* *P.aeruginosa*	NA[99]
PPI	Ceftazidime	*P.aeruginosa*	P^H-active release
Carbohydrate-glyco peptide	Tobramycine	*P.aeruginosa*	Temperature active release[100]
PAMAM	Sulfamethoxazole	*E.coli*	NA[101]

The efficient treatment of urinary infections, reducing drug dose, and reducing cytotoxicity remain priorities. Dendrimers prodrugs as localized, controlled antimicrobial delivery systems allow sufficiently high concentration and extended-release mechanisms to successfully treat infections. The advantage of using prodrug monomer as opposed to direct conjugation of antibiotics stems from the greatly improved

drug loading that is achieved using conjugation of antibacterial-linked delivery systems at the end of dendrimer synthesis. A prodrug is a poorly active or inactive compound containing the parental drug that undergoes some in *vivo* biotransformation through chemical or enzymatic cleavage, enabling the delivery of the active molecule at efficacious levels. Carrier-linked prodrugs are commonly attached by chemical groups such as ester, amide, carbamate, carbonate, ether, imine, and phosphate. [102, 103]

Dendrimers emerge as potential nanocarriers of particular interest given their small size (usually under 10 nm), highest payload capacity by weight material from all nanocarrier systems, and availability of a large number surface groups which can be functionalized with both therapeutic molecules and ligands *via* tunable chemistry bonds allowing for the design of drug carriers that can facilitate the drug permeation into the bacterial cell. Dendrimers are at the center of the work discussed in this dissertation.

1.10 Dendrimers

Dendrimer generations and branching offer controllable attachment points to explore spatial control. The structure of which is determined by three unique components: (1) the interior core, (2) the interior layer, made up of repetitive generations (units) connected with the interior core, and (3) the periphery (surface functionality). Representation of a typical dendrimer is shown in (**Figure 1.19)**, which includes all dendrimer parts, i.e., core, branches, and generations. [104] The term dendrimer was first introduced in 1983. Donald Tomalia and co-workers synthesized and characterized these hyperbranched polymers in 1983 and these molecules were named as dendrimer. [104] Later on dendrimer was synthesized using the convergent method for the first time by Hawker and Fréchet (1990). [105]

Figure 1.19 General representation of the model structure of a dendrimer. [106]

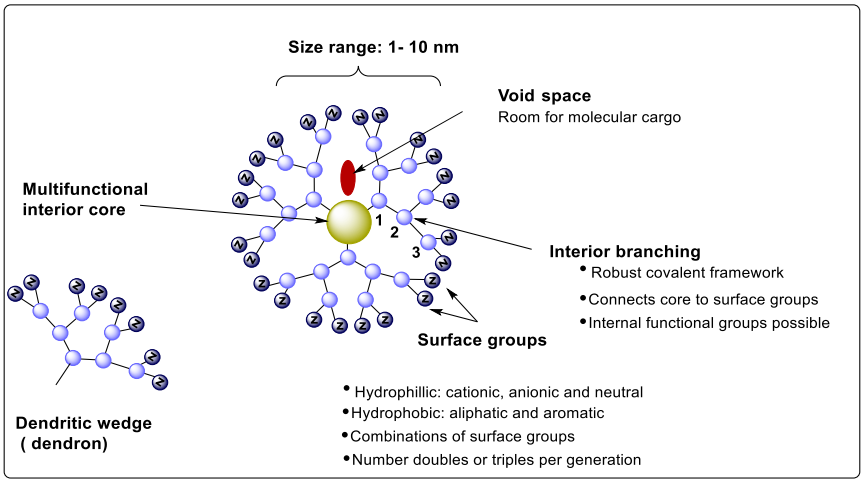

Dendrimers are attractive systems for drug delivery due to their highly defined dispersity, nanometer size range, spheroid-like shape, and multi-functionality. Aside from their ease of preparation, dendrimers have multiple copies of functional groups on the molecular surface which enables derivatization for biological recognition processes. [107] Even so, dendrimers are reported to cause haematological toxicity, [108] especially in the case of non-functionalization. Examples of typical dendrimers are poly(propyleneimine) (PPI), poly(amido amine) (PAMAM), [109, 110] poly(2,2-bis(hydroxymethyl) propionic acid (bis-MPA), poly(glycerol-succinic acid) (PGLSA-OH). [111] Although their high charge density allows easy insertion into membranes, and can facilitate endosomal escape, [112] dendrimers have low water solubility and exhibit elevated cytotoxicity. [113] For example, PAMAM NPs have limited applications in medicine due to their original toxicity. PAMAM is known to induce nephrotoxicity as well as hepatotoxicity, and its cationic charge can cause platelet aggregation by disruption of membrane integrity. [114] Nevertheless, it is possible to reduce cytotoxicity by chemical modification.

1.11 Dendrimer synthesis

1.11.1 Divergent and convergent methods

There are two different strategies have been applied for the dendrimers synthesis, divergent and convergent syntheses. There is a fundamental difference between these two strategies. The divergent method was proposed by Tomalia and co-workers for the synthesis of PAMAM dendrimers. [104] in this strategy, the construction of a dendrimer starts from the core and builds out to the periphery, as shown in (**Figure 1.20**). The first generation dendrimer is produced by the reaction of the core molecule with a monomer molecule (or dendron) containing one reactive and two or more inactive groups. Then the inactive groups on the periphery of the molecule are activated or transformed to create a new reactive surface functionality. These are used to react with monomer molecules to give generation 2. The process is repeated several times and a dendrimer is built layer by layer. There are some disadvantages of the divergent approach. [115] The rapid increase in the number of reactive groups at the periphery in every generation leads to a number of problems as growth is pursued: (1) any incomplete reaction of these terminal groups would lead to structure imperfections, [116] (2) To prevent side reactions and to force reactions to completion, huge amounts of reagents are required in later stages of growth. This led to some difficulties in the purification of the final product. There are some advantages of this approach: (1) it is very easy to modify the full surface of the dendrimer in a single step. Since dendrimers characteristics are mainly determined by the type of terminal groups, (2) The possibility of stopping the reaction at any step as well as the possibility of automating the repetitious steps makes a library of various generation dendrimers easier to create. [117-122]

Figure 1.20 Dendrimer synthesis by divergent method[123]

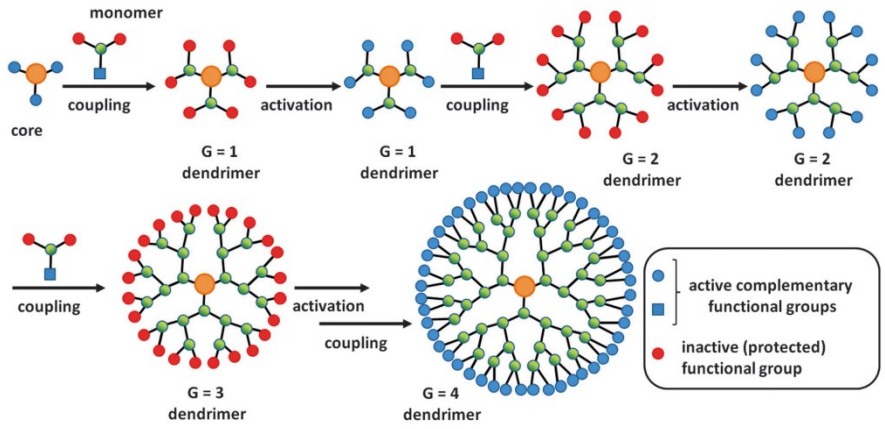

The second strategy, the convergent method, was first reported by Hawker and Fréchet for the preparation of poly(arylether) dendrimers. [105] In this strategy, the dendrimer is constructed starting from end groups, progressing inwards as illustrated in (**Figure 1.21)**. Individual dendritic wedges (i.e., dendrons) are synthesized first and then coupled with a multifunctional core. This method has several advantages over the divergent method: (1) Structural defects are fewer in this approach because of the limited number of reactions done on the same molecule from one generation to the next, and intermediates are more easily purified at successive stages of the synthesis, (2) it is relatively easy to purify the product because the reagents are used in equimolar or slight excess amounts for the reaction progress, (3) forming a library of dendrimers that differ in the nature of core is easy in this approach because the addition of same dendron to different cores gives a new dendrimer in one reaction step. [115, 124]

Figure 1.21 Dendrimer synthesis by convergent method[123]

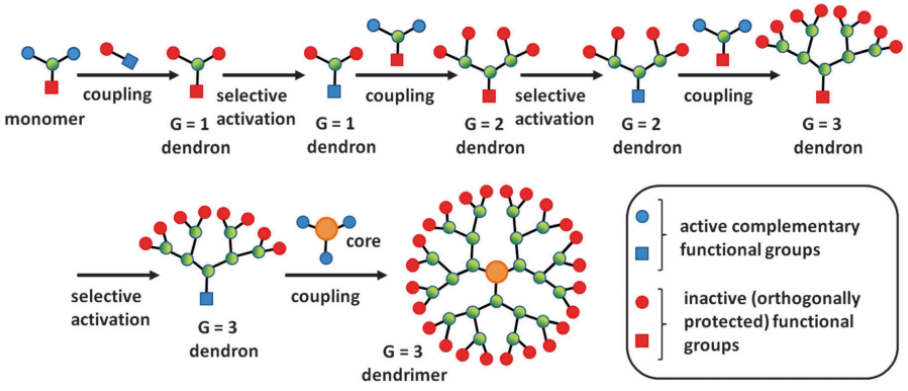

A disadvantage of this method is that it does not allow the formation of higher-generation dendrimers due to steric problems when coupling large dendrons with a core molecule. The reactive group at the point of

the wedge is called the focal point. As the size of the dendron increases, the steric hindrance at the focal point increases.

1.11.2 Accelerated approaches for dendrimer synthesis

Dendrimers are becoming more and more common, and they have a lot of exciting potential for use in a variety of fields, therefore, the need for highly effective alternative synthetic methods protocols for their development is highly required. The last few years have been an exponential increase in the number of publications in the field of dendrimer chemistry, but few dendrimers have successfully reached the clinical trial. The classical approaches used for dendrimer synthesis are very long and time-consuming. In addition, huge excess of reagents makes purification difficult. Therefore, innovative synthetic protocols are desired which can provide the shortest possible route by decreasing the number of reaction steps. There are several strategies of accelerated approaches for the dendrimers synthesis, including, double stage convergent method, hypermonomer strategy, [125] double exponential method, [126] and orthogonal accelerated synthesis. [127] We will explain in this part only one strategy.

In the dendrimer synthesis, the mixing of divergent and convergent approaches is particularly infamous. There are examples of divergently made dendrons being linked together at the focus as a last reaction[128] and convergently made dendrimers going through a reaction on the periphery in the last step. [129, 130]

1.11.2.1 Double stage conversion method

To improve the existing strategies and for rapid synthesis of high-generation dendrimers, the first attempt was made in 1990 by Frechet *et. al*, who created the double-stage convergent approach. [131] To build high generation dendrimers using divergent methodology can lead to imperfect dendrimers due to the presence of a huge number of end groups involved in chemical conjugation, on the other hand, with a convergent approach there are steric influences due to the use of bulkier dendrons. It is known that double stage convergent method is a combination of convergent and divergent methods and in the strategy, the core unit is synthesized divergently followed by a subsequent attachment of the dendritic wedge in a convergent fashion, thereby generating the hypercore containing dendrimer.

Scheme 1.1 CuAAC mediated synthesis of galactose coated dendrimer, double stage convergent approach

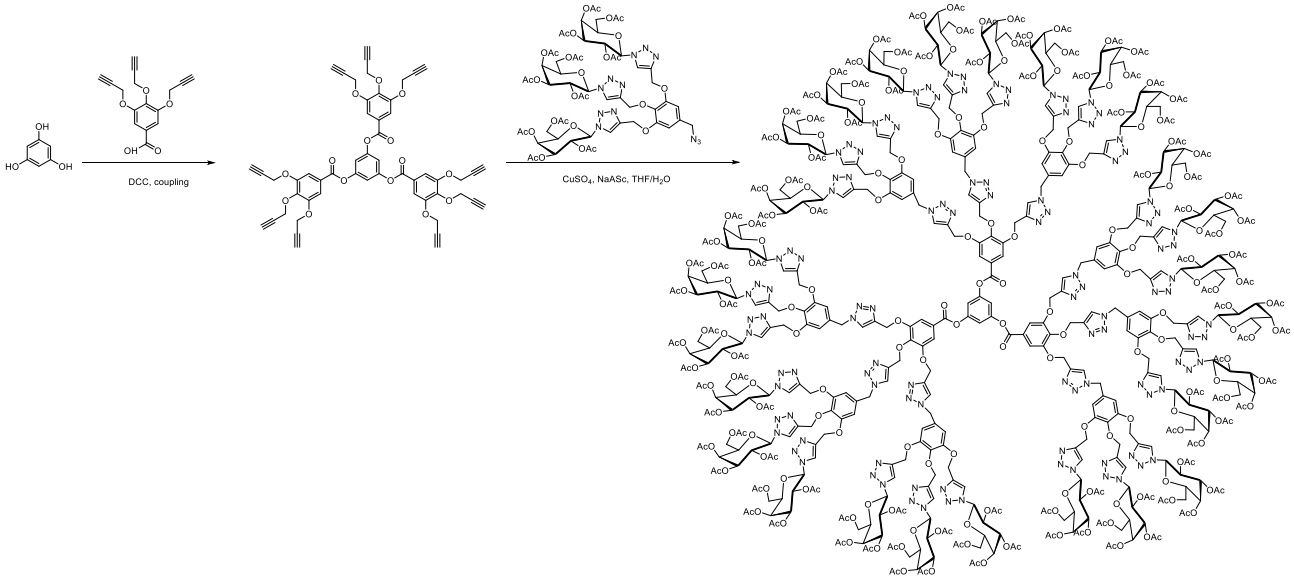

Tiwai and co-workers[132] synthesized a nonavalent dendrimer core carrying nine terminal alkyne groups, (**Scheme 1.1)**. Consequently, this synthetic hypercore unit was used as starting material for CuAAC coupling with a dendritic wedge to afford a series of glycodendrimers. In this context, the dendrimer core unit was conjugated with galactose azide, dendritic wedge using $CuSO_4.5H_2O$, and sodium ascorbate to prepare a glycodendrimer coated with 27 peripheral galactose.

In our synthetic strategy, building the dendrimer at high generation was extremely difficult, therefore, we used the accelerated approach double-stage conversion strategy, aiming to reduce steric hindrance issues during the core coupling step, (details in **Chapter 3**). [133]

1.12 Click reaction, photolytic thiol-ene reactions are highly efficient approaches to develop dendrimer

Regardless of the efforts and significant research, dendrimer-based products have been slow to reach human trials and a lot of the excitement over the potential application of this technology has faded. A significant issue preventing dendrimers from progressing is the polydispersity of their conjugates. Any therapeutic platform conjugated with multiple drugs or targeting moieties through an excess of attachment sites can result in a heterogeneous population that becomes more dispersed as more functionalities are added. Orthogonal pathways to construct multifunctional dendritic provide a higher level of selectivity and flexibility in reaction conditions that may be able to overcome the ligand polydispersity of conventional dendrimer platforms, (**Figure 1.22**). [134-136]

Figure 1.22 Methods of orthogonal coupling

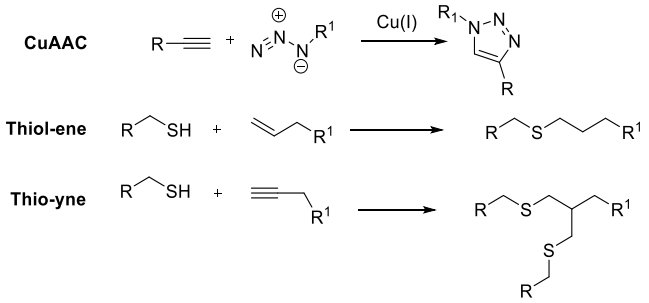

In this thesis research, we looked at how to generate new glycodendrimers by orthogonally coupling dendron focal sites using CuAAC extremely selective nature and thiol-ene click chemistry with well-defined chemical synthesis.

1.12.1 Copper (I) mediated azide-alkyne cycloaddition (CuAAC)

The CuAAC reaction is a copper-catalyzed and stereospecific variety of the (3+2)-cycloaddition reaction of an azide and an alkyne forming a 1,2,3-triazole which was first introduced by Huisgen in 1967. [137]

Figure 1.23 (A) Proposed catalytic cycle for CuAAC, catalyzed the synthesis of 1,4-Substituted 1,2,3-triazole; (B) Proposed catalytic cycle for RuAAC, catalyzed the synthesis of 1,5-Substituted 1,2,3-triazole

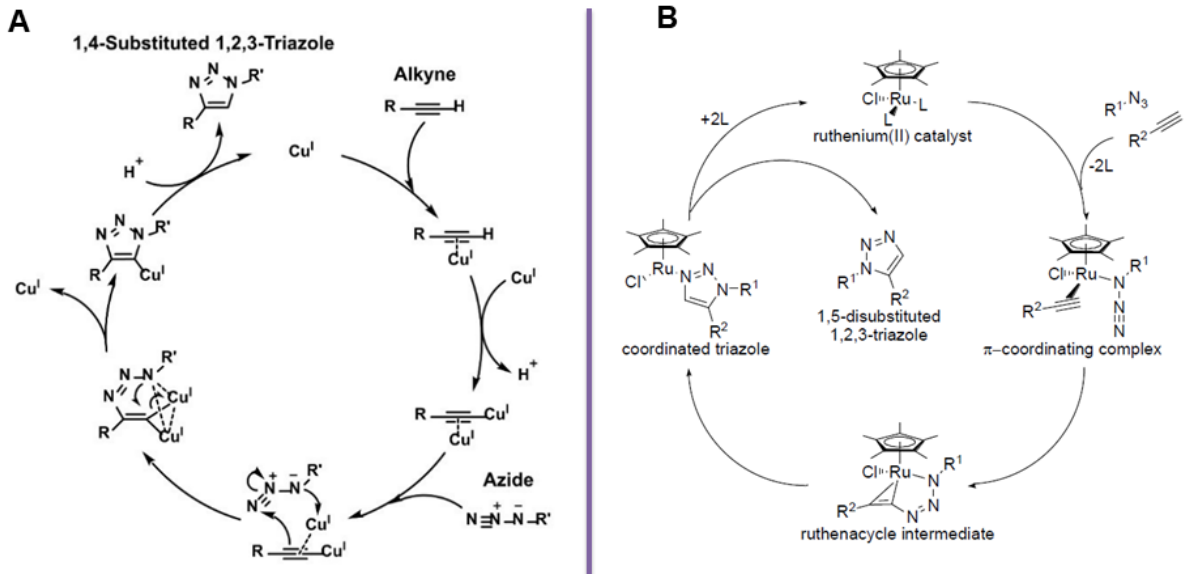

In addition to lacking stereospecificity, Huisgen's reaction was also very slow proceeding reaction and required high temperature. The reaction rate dramatically increased when a copper catalyst was added, with

the reaction almost reaching completion even at room temperature and exclusively forming the 1,4-functionalized traizole. [138]

The stereospecificity can be explained by the proposed reaction mechanism as indicated in (**Figure 1.23 A**). When using a ruthenium (II) catalyst instead of copper (I), exclusively the 1,5-adduct is formed, (**Figure 1.23 B**). [139] since copper (I) is a sensitive catalyst and prone to oxidation, a reducing agent is typically added to the reaction mixture. A reducing agent, sodium ascorbate has been widely used. Generally, cycloaddition proceeds through an associated mechanism. However, according to experimental kinetic data and molecular modeling[140] performed on the Huisgen 1,3-dipolar cycloaddition reaction, it suggested a stepwise reaction pathway. [141] During the reaction two Cu^{I} cations coordinate onto the terminal alkyne moiety under its deprotonation. The π complexation of Cu^{I} lowers the pKa of the terminal alkyne by as much as 9.8 pH units, allowing deprotonation to occur in an aqueous solvent without the addition of a base. [142] If a non-basic solvent such as acetonitrile was to be used, then a base, such as 2,6-lutidine or *N,N′*-diisopropylethylamine (DIPEA), [143] would have to be added. The ring formation with the azide occurs under the release of one of the coordinated transition metals. In the final step, the second Cu (I) which is attached in position 5 of the triazole is substituted by a hydrogen, generating the final 1,4-functionalized 1,2,3-triazole as well as the Cu(I) catalyst which can undergo a second catalytic cycle. [140, 144, 145]

1.12.2 Phosphorous Ligands

One of the important ligands used in the cycloaddition of azides and alkyne was phosphorus-containing ligands, and phosphines in particular, (**Figure 1.24)**. After their discovery, copper(I) species as catalysts for azide-alkyne cycloadditions, $CuBr(PPh_3)_3$ and $CuI[P(OEt)_3]$ complexes, were applied to the synthesis of various glycopolymers in good yields. [146] In some cases, reactions were conducted under microwave irradiation in the presence of an organic base such as DIPEA or DBU for the most difficult substrate reactions. These conditions have been widely used in diverse applications such as macromolecular synthesis. Phosphorus ligands have been considered the catalysts for the preparation of glycopolymers[147-150] and oligomers or biologically active molecules. $CuBr(PPh_3)_3$ was a functioning catalyst when using 0.5 mol% under neat or aqueous conditions at room temperature and in the absence of any other additive. [151] In all cases, the corresponding triazoles were recovered in pure form after simple filtration or extraction, although higher copper loadings (2 mol%) and/ or toluene as solvent were required for the preparation of some glycopolymers,

Figure 1.24 Phosphine-ligand/copper(I)-mediated CuAAC

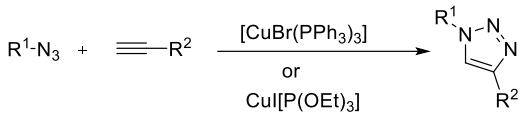

1.12.3 Multivalent glycodendrimer assembly based on “click ” reaction (CuAAC)

Carbohydrates and their derivatives fill numerous roles in the working process of metabolism, cell-cell interaction, cell migration processes, and pathogen defense providing great opportunities for attractive drug discovery. However, Carbohydrate-based drug discovery does not develop quickly. Carbohydrates make poor lead compounds due to their well-known modest affinities for the respective enzymes or receptors, poor pharmacological properties, and difficult synthesis. However, multivalent carbohydrates are attractive synthetic targets since they often bind much stronger to the respective receptors than their monovalent counterparts. Several kinds of linkages of sugars to scaffold molecules have been utilized over the years and impressive affinity increases have been reported. [152] "CuAAC" (**Figure 1.25**) promises to simplify and accelerate the discovery of highly- affinity multivalent carbohydrates as known as it has already been utilized in numerous systems. "CuAAC" reactions have also been utilized to conjugate multiple sugars with a central aromatic platform. [153]

Figure 1.25 . Click reaction in the synthesis of different dendrimers. [154, 155]

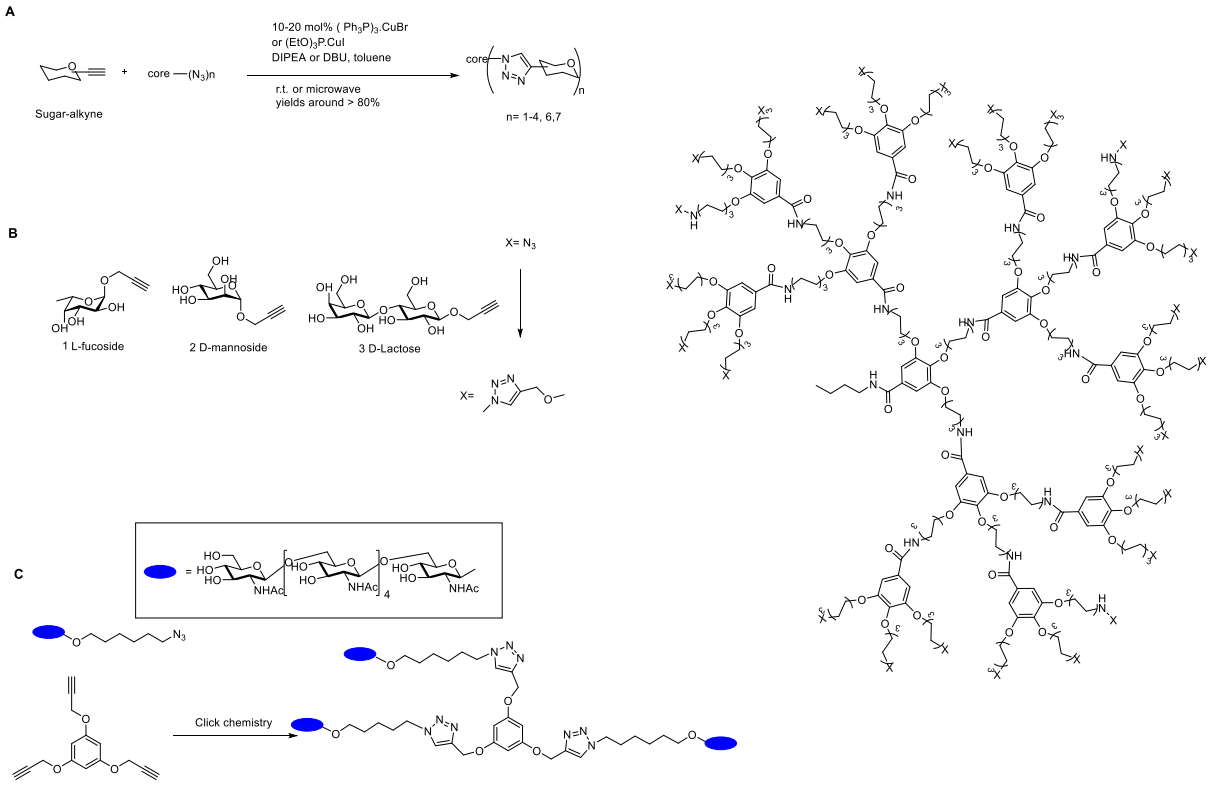

Riguera and colleagues functionalized a larger dendrimer complex using click chemistry, [156] includes the relative 3,4,5-trihydroxy-benzoic acid repeating unit, (**Figure 1.25 B**). They report one case of azide on the periphery of the dendrimer and the alkyne on the carbohydrates. In this case, they decided to place azide and alkyne functional groups on the dendrimer and the carbohydrate partners, respectively. With the use of the click reaction, it allows easy preparation and incorporation of up to 27 unprotected fucose, mannose, and lactose residues to generate large systems in high yield, requiring only catalytic amounts of Cu in a *tert*-BuOH/H_2O mixtures. [130, 157-159] CuAAC reactions have also been utilized to conjugate multiple sugars with a central aromatic core. For example, a C-3 symmetric (1-6)-*N*-acetyl-β-D-glucosamine octadecasaccharide was synthesized through triazole-linkage for the purpose of applying the multivalent concept, (**Figure 1.25 C**). [154, 160]

1.12.4 Thiol-ene coupling

The reaction of thiols with alkene leading to the formation of thioethers (**Figure 1.26**) is a highly efficient and fast-proceeding reaction. Thiol-ene coupling (TEC) has advantages over the widely known CuAAC reaction. Despite its distinctive reaction kinetics and the exclusive synthesis of one product, the use of copper catalysts is a constraint factor when applying CuAAC on biologically relevant structures due to its toxicity for living organisms. Therefore, the CuAAC was replaced by TEC because of the better physiological compatibility. [161] The TEC can proceed through a radical anti-Markovnikov addition. The radical-mediated TEC starts with the formation of a thiyl radical *via* hydrogen abstraction using a suitable initiator reagent. The next reaction step is the addition of the thiyl radical to the present alkene moiety. The addition occurs in an anti-Markovnikov, leading to a higher substitute and therefore more stable carbon-centered radical.

Figure 1.26 Thiol-ene reaction mechanism

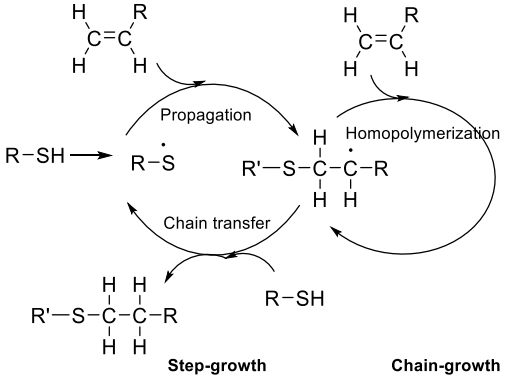

From the carbon radical, two pathways are possible, a step-growth as well as a chain-growth pathway. [162] When proceeding in a step-growth fashion, the following reaction step is the abstraction of a hydrogen atom from a further thiol group generation a new thiyl radical as well as the final thioether which is inactive.
The thiyl radical can then propagate to a further alkene moiety followed again by a chain transfer step. In the chain-growth pathway, the carbon-centered radical undergoes a reaction with another alkene moiety again resulting in a carbon-centered radical with the possibility of following either the step-growth or chain-growth. The reaction rate of the propagation and the chain transfer step determines whether a radical-mediated TEC proceeds in a step-growth or chain-growth manner. For an ideal step-growth TEC reaction the rates of propagation and chain transfer have to be identical thus neither the thiyl nor the carbon-centered radical accumulates during the reaction process. In the case of the chain transfer being the rate-limiting reaction step, a chain-growth polymerization is probably due to the high excess of carbon-centered radicals. A slow propagation reaction is generally due to the low reactivity of the alkene moiety, which would then lead to the accumulation of thiyl radicals and termination the reaction by recombination resulting in the formation of disulfides.

1.12.5 Multivalent thio-glycoclusters

Oligosaccharides, glycoconjugates, and their mimetics are investigated in molecular studies, [163] drug discovery, and vaccine development. [164] Thioglycosides in which the glycosidic oxygen is replaced by a sulfur atom are metabolically stable analogues of the natural *O*-glycosides, justifying their synthesis and application as glycomimetics. [165] Furthermore, due to the similar spatial arrangement of *S*- and *O*-glycosides, many lectins tolerate the *O* to *S* replacement, and some have even stronger affinity toward *S*-glycosides than the corresponding *O*-glycosides. Thioglycoclusters can be prepared by photochemical thiol-ene coupling (TEC reaction) between 1-thiosugars and alkene-functionalized scaffolds (**Figure 1.27**). In this context, the radical-mediated thiol-ene coupling emerged as a powerful method for glycoconjugation[166] which, if unsaturated sugars are applied as the alkene partners, opens the way for the stereoselective synthesis of a broad range of thio-linked glycomimetics. [167]

Figure 1.27 Multivalent photochemical thiol-ene reaction[165]

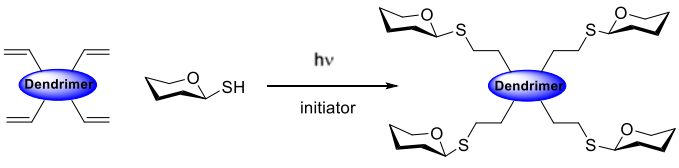

Recently, the photoclick-optimized conditions were applied to various linear and cyclic scaffolds using 1-thio-β-D-glucose and two other thiosugars of interest for lectin recognition: 1-thio- β-D-galactose and 1-

thio-α/β-D-mannose. [168, 169] The binding affinities of selected thioglycoclusters were evaluated towards two soluble lectins produced by *Pseudomonas aeruginosa* LecA (galactose specific lectin) and *Burkholderia cenocepacia* dimeric lectin BC2L-A (mannose-specific lectin, BC2L-A that has two binding sites 40 Å apart) which are pathogenic bacteria involved in opportunistic infection in patients with immunosuppression or in life-threatening lung infection in cystic fibrosis patients. [165, 170]

Roy and co-workers developed an accelerated orthogonal approach by combining thiol-ene chemistry and SN^2 reaction to synthesize multifunctional glycodendrimers. They constructed two different orthogonal monomers (**Scheme 1.2**). First monomer consisted of a chloroacetyl group as a focal point with four allyl groups on the periphery while the other monomer was a thiogalactoside consisting of free thiol (-SH) focal point and four hydoxyl groups on the surface. The synthesis started around hexacetylated core by performing SN^2 reaction using tetraallylated precursor yielding 24 alkene groups at G1 stage. In the next step, thiol-ene reaction between thiogalactoside monomer and G1 dendrimer yielded G2 generation glycodendrimer carrying 24 galactose on the periphery.

Scheme 1.2 Synthesis of glycodendrimer with 24 galactose units at the periphery

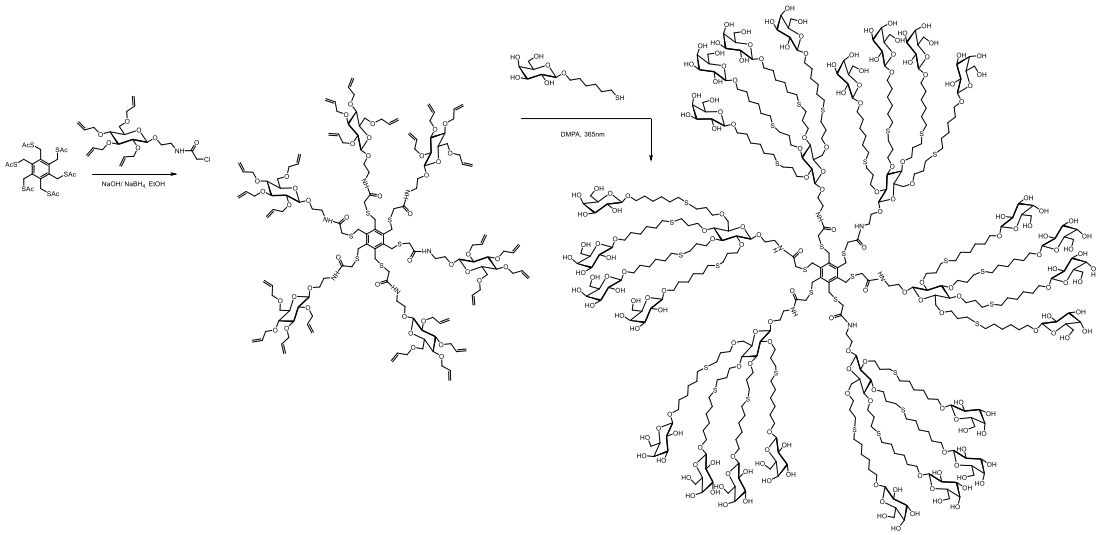

While the majority of dendrimers that have been studied have focused on the treatment of bacterial infections, particularly biofilm infections from *P. aeruginosa*, as reported by Reymond and his coworkers, [171] or different other dendrimers based on lysine-dendrons for the purpose of studying the binding affinity of LecB, as reported by Renaudt and coworkers. [172] Another type of dendrimer with well- defined targeting moieties is also being investigated for its potential to inhibit the adhesion of different strains of *E. coli*. [173]

The unique of our research is to design and synthesize glycodendrimer prodrug that is conjugated to the ciprofloxacin through a cleavable linker. This drug delivery system allows the antibiotic to be carried across the cell membrane, which can be transformed into a bioactive antibiotic molecule *via* internal mechanism, such as enzyme hydrolysis or a specific cellular environment (acidic pH). Since the main objective is to design a new family of glycodendrimer to block the adhesion from both *P. aeruginosa* and *E. coli*. Thus, it is important to study the structure, function, and characterization of bacterial lectins and understand the molecular mechanism of the interactions with their targeting ligands.

1.13 The crucial role of carbohydrates in nature and the key for selectivity

The monomeric units of carbohydrates, are, in addition to lipids, amino acids, and nucleotides, one of the four main building blocks in biology, each one contributing essential properties and functions within a living organism. The field of glycobiology covers the study of carbohydrates in biological processes but also the elucidation of their structures, their biosynthesis as well as their linkage to proteins or lipids. [174] The term was first used by the Dwek group in 1988[175] after it became clear how important carbohydrates were to living things beyond their function in energy production and storage or as a structural component. In addition, the carbohydrates were observed to also take part in a variety of several processes, including cell communication, [176] cell adhesion, storage and delivery of information, signal transduction, and pathogen recognition, such as bacterial or viral infection. Especially due to the contribution in bacterial infection processes, further information about their exact role and mechanism of action becomes extremely important to potentially develop novel antibiotic medications.

Figure 1.28 Structures of the most abundant monosaccharides in mammalian cell surface oligosaccharides relevant in carbohydrate-proteins interactions for cell communication, cell adhesion, signal transduction, and pathogen recognition processes.

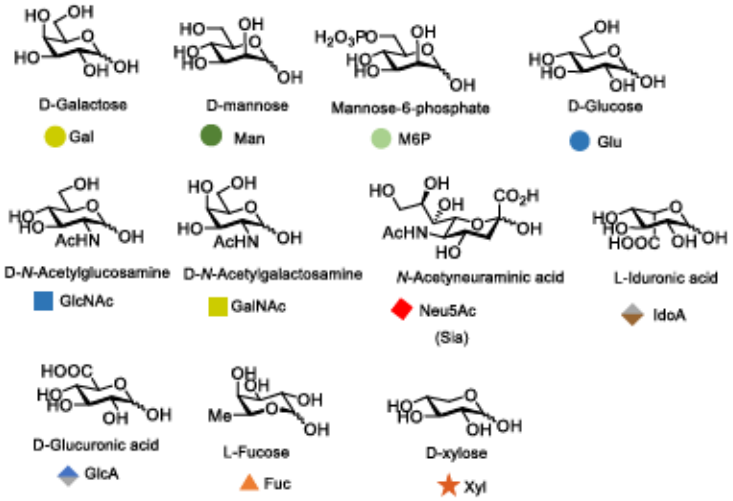

The new information about carbohydrates in biological processes is acquired quite slowly, which is associated with the high structural complexity of carbohydrates in comparison to that of the other main classes of biopolymer. [177] While nucleotides or amino acids only have one possible point of attachment, they are arranged linearly within the biopolymer, two monosaccharides can be connected at various positions each hydroxyl group could be as a glycosidic bond. Besides that, also conformational differences for some linkage positions or different sizes of the formed heterocycle are possible. Overall, the coupling of just two monosaccharides can already result in sixteen different disaccharides. By extending this idea and taking into account that there are twenty relevant monosaccharides in a living organism, three monosaccharides can be coupled to form a large distinct trisaccharide structures. The possibility of linking the same monomeric units in a variety of diverse arrangements provides access to many structures carrying specific information. However, it is quite difficult to synthesize and isolate such oligosaccharides for their research.

Figure 1.29 A) Schematic illustration of a cell membrane out of a phospholipid bilayer and membrane proteins as well as exposed carbohydrates were incorporated into the membrane in terms of glycolipids or glycoproteins which assemble the glycocalyx. The interactions of a virus and a bacteria via cell surface carbohydrates with lectin receptors of the pathogens are also presented. B): Electron microscope image of a stained glycocalyx of an erythrocyte[178, 179]

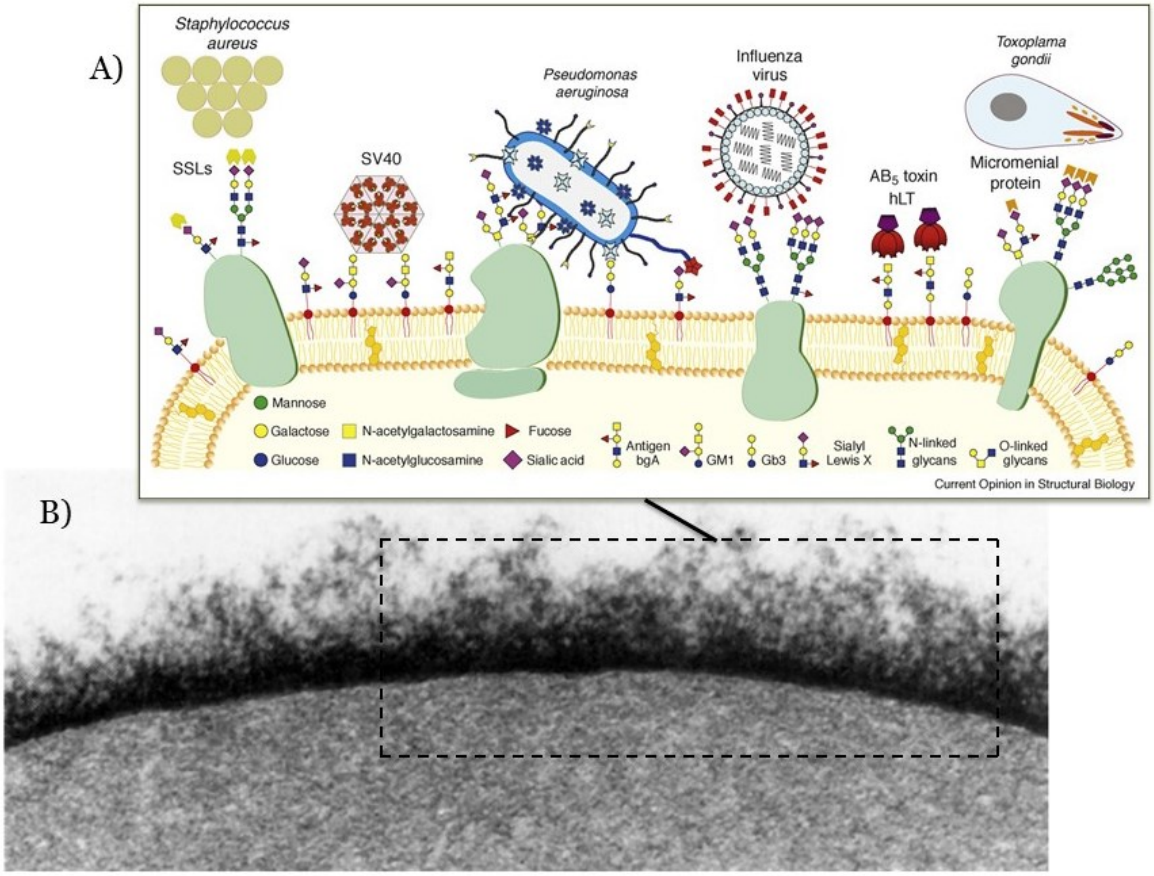

In a living organism, the oligosaccharides are mainly presented on the outside of the cell membrane, generally attached to proteins or lipids as glycoconjugates within the lipid bilayer. Most abundant monosaccharides are *N*-acetylglucosamine (Glc*NAc*), galactose (Gal), and mannose (Man). However, the most exposed monosaccharides and thus the ones that are most likely to be significant in the mentioned biological processes are *N*-acetylneuraminic acid (Neu5Ac), fucose (Fuc), and Gal. The structure, abbreviation, and symbol of the most common monosaccharides in mammalian cell surface oligosaccharides are given in (**Figure 1.28)**.

The oligosaccharide presentation is highly dense, resulting in carbohydrate capsule, referred to as glycocalyx, which surrounds almost every cell. [180] A schematic illustration of a cell membrane containing exposed carbohydrates as well as an electron microscope image of an erythrocyte with its dense glycocalyx are shown in (**Figure 1.29)**. [178] The type of presented carbohydrates is characteristic of each organism but also for the type of cell or its development stage within the same organism. The glycocalyx plays a fundamental role as a mediator between cells and also in the recognition of exogenous compounds or cells. The interactions of the presented carbohydrates are mainly towards carbohydrate recognizing receptor protein, the so-called lectins, which are reversible and of non-covalent nature similar to well-known protein-protein interactions. Unlike the extensively researched protein-protein interactions such as the majority of antibody-antigen recognition processes, carbohydrate-protein interactions are generally much weaker. For most protein-based antibody-antigen interactions, it is possible to attain dissociation constants (K_D) in the nanomolar range. [181] whereas the K_D is within the millimolar range for the interaction of a monosaccharide with its corresponding lectin.

One of many examples of glycoproteins can be mentioned as the blood groups and tissue antigens like ABH(O) and Lewis antigens. [182] where the oligosaccharide chain is attached to proteins or ceramide lipids. The ABH(O) antigens are fucosylated oligosaccharides presented on endothelial cells and red blood cells of all individuals (**Figure 1.30**). The Lewis determinants are structurally related to determinants of the ABO and the H blood group systems and are composed of four major carbohydrate antigens: *Lewis a* (Le^a), *Lewis b* (Le^b), *Lewis X* (Le^X), and *Lewis Y* (Le^Y). Le^a and Le^b are genetically and biochemically related molecules detected on red blood cells and tissues. [183]

Figure 1.30 Schematic representations of H and Lewis determinants[184]

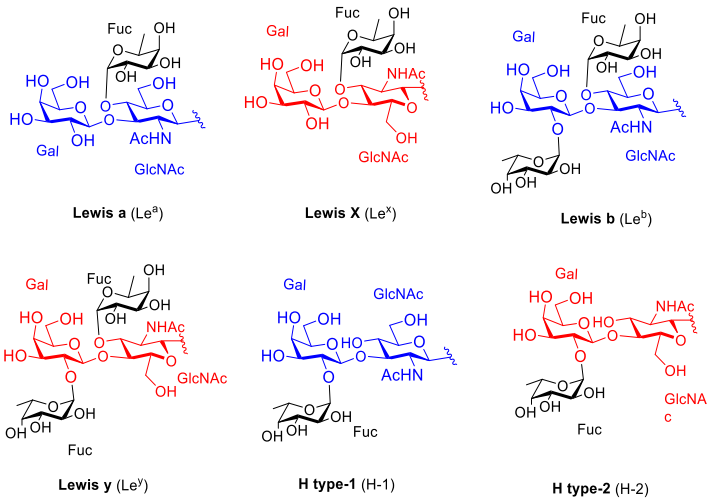

1.14 Strategies of Adhesions and Anti-adhesion

Carbohydrate-protein binding is frequently a part of several biological significant processes, such as the binding of bacterial, viruses, and other pathogens to host cells. These proteins are commonly name are lectins. [174] For *P. aeruginosa,* two soluble lectins, LecA and LecB, have been found to be crucial for this pathogen's attachment to host cells. [185, 186] Both of them have a tetrameric structure, with specificity for galactose and fucose respectively. [187] Studies showed that solution of galactose and fucose have a therapeutic effect against *Pseudomonas aeruginosa,* and cystic fibrosis patients. [188] This motivated researchers to use galactose and fucose derivatives to inhibit the attachment of *P. aeruginosa*, and thus the adhesion and subsequent infection should be inhibited. For *E. coli* (UPEC) expressing type 1 pili. The FimH adhesin at the tip of type 1 pili recognizes terminal mannose units of uroplakin Ia (UPIa), a membrane glycoprotein that is abundantly expressed on superficial epithelial umbrella cells of the urinary tract. For several years, many natural as well as synthetic mannoside ligands of FimH have been designed and tested for their inhibitory potencies. This strategy is called anti-adhesive (**Figure 1.31**). Despite these advantages, the main problem is that lectins and carbohydrates have a weak interaction, usually with a dissociation constant in millimolar range. In nature, the weak binding issue has been overcome by using the "multivalency effect", which works through simultaneous binding of multiples sugars, displayed on the cell surface, to the multivalent proteins. [189-192] By appending carbohydrates on the surface of dendrimers to afford glycodendrimer structures, such multivalency can be achieved to improve binding affinity. [193] Inspired by this, multivalent mannoside and fucosides were synthesized by appending different numbers of mannose and fucose on multivalent scaffolds.

Figure 1.31 The adhesion and the antiadhesion strategy[194]

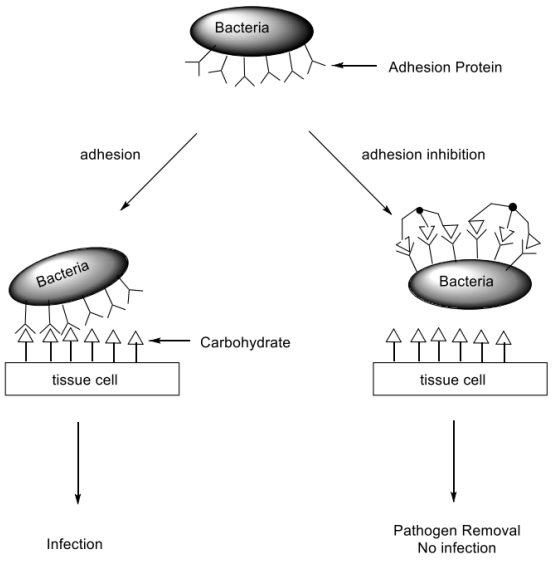

One major advantages of a multivalent system is the set number of defined binding sites that can be chemically controlled. The multivalent effect for dendrimers can be described as a special delivery system with a variety of biomedical characteristics, such as geometric, size, and shape. It has been hypothesized that UTIs treatment using a drug- conjugates with multiple sites could require a much smaller concentration of the drug and therefore it would be more effective in the treatment of UTIs. Having multivalent dendrimers containing an increased number of binding sites will lead to multiple interactions between the bacteria and dendrimer. This interaction is very important because it leads to blocking bacterial adhesions.

1.14.1 The concept of multivalency

Multivalent frameworks can augment binding interactions through several distinct mechanisms. Multivalent ligands present multiple copies of binding epitopes that can bind a receptor upon dissociation of a previous interaction (**Figure 1.32a**). [195] Binding enhancement is a statistical effects resulting from the high localized concentration of epitopes that effectively increase the time that the binding site is engaged (i.e. decreases dissociation kinetics (Koff). [196] Examples of binding affinity enhancement due to the statistical effect can be found with high density receptor displays in which decreased dissociation rate constants are observed. [197, 198] Additionally, as shown in (**Figure 1.32b**), a multivalent ligand can bind an oligomeric receptor by simultaneously interacting with multiple binding sites. [195] This mechanism is known as the chelate effect, and it is entropically favorable compared to the constituent monovalent interactions: translational and rotational entropic costs are paid with the first receptor-ligand contact, and subsequent intermolecular binding interactions proceed without paying these entropic costs (although, conformational entropy still actors in free energy of binding). [195] Furthermore, as shown in (**Figure 1.32c)**, the binding of a multivalent

ligand to multiple cell-surface receptors can result in clustering of the receptors in a microdomain. [195] As shown in (**Figure 1.32d)**, multivalent ligands can interact with auxiliary binding sites on a receptor to enhance binding. In addition to enhancing binding affinity, a synthetic multivalent ligand is bound to multiple receptors on one entity (e.g., cell-surface receptors) and can sterically inhibit interactions with natural ligands (**Figure 1.32e**). In this mechanism, known as steric shielding, the backbone of the multivalent ligand effectively forms a layer on the cell surface that precludes the attachment of the natural ligand to the bound receptor. [199] Steric shielding is a unique mechanism for inhibition that is fundamentally inaccessible by monovalent molecules.

Figure 1.32 Multivalent protein carbohydrate interaction mechanisms.

(a) Chelate effect, in which a multivalent receptor coordinates with a multivalent ligand. (b) Subsite interactions, in which binding affinity is enhanced due to the ability of multivalent ligands to occupy multiple binding sites on a receptor. (c) Steric inhibition, in which a multivalent ligand, once bound to a multivalent receptor, sterically prevents the approach of another ligand. (d) Receptor clustering, in which a multivalent ligand binds to and induces the clustering of independent receptors. (e) Statistical effect, in which a high concentration of ligands on a multivalent scaffold allows for the receptor to be occupied over a longer period. [200]

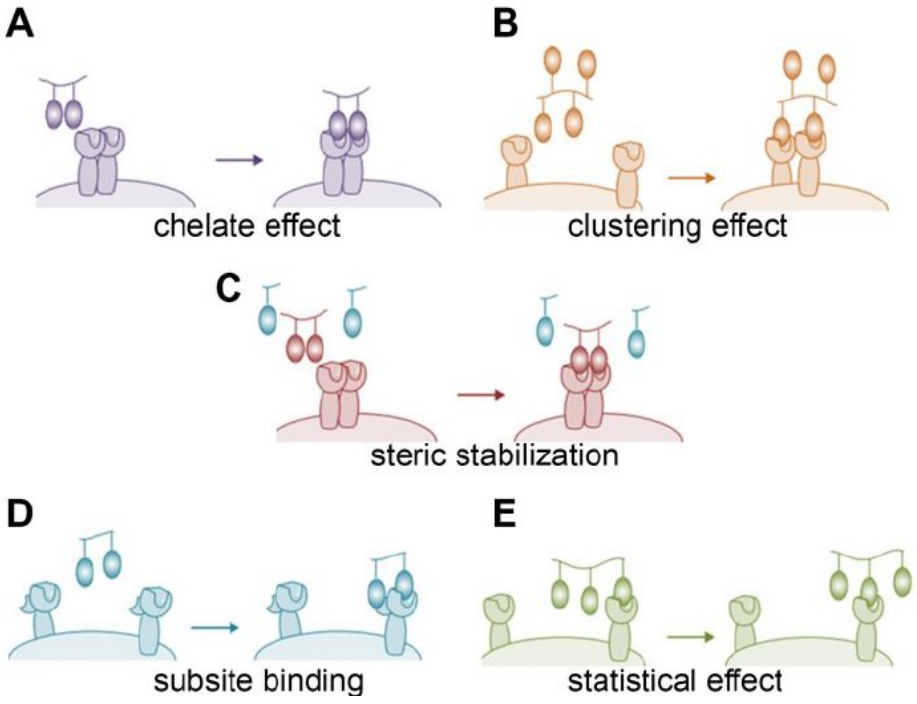

1.14.2 Synthetic multivalent glycomimetics: Glycodendrimers

Synthetic chemists created the idea of carbohydrate-presenting macromolecules that replicate the structural characteristics of their natural counterparts in order to reduce the complexity of studying the interaction between carbohydrates and lectins. They represent novel pharmaceutically active compounds in addition to acting as model compounds in mechanistic studying. [201, 202]

The removal of all unnecessary sugar moieties that do not demonstrate binding to a lectin and replacement with a synthetic scaffold that is less complex than natural oligosaccharides and therefore easier to access during synthesis is one method for reducing the structural complexity of these carbohydrate ligands (**Figure 1.33**). Given this, the synthetic scaffold is fixed with several copies of the smallest binding epitope, which is often a monosaccharide but also a di- or trisaccharide, attached to the synthetic scaffold resulting in a multivalent glycomimetic.

Figure 1.33 The concept of glycomimetics is to replace a natural carbohydrate ligands's complex oligosaccharide scaffold with a synthetic dendrimer scaffold that bears the carbohydrate-binding motif. Here, a glycodendrimer backbone carrying the greater and lower high affinity carbohydrate moieties

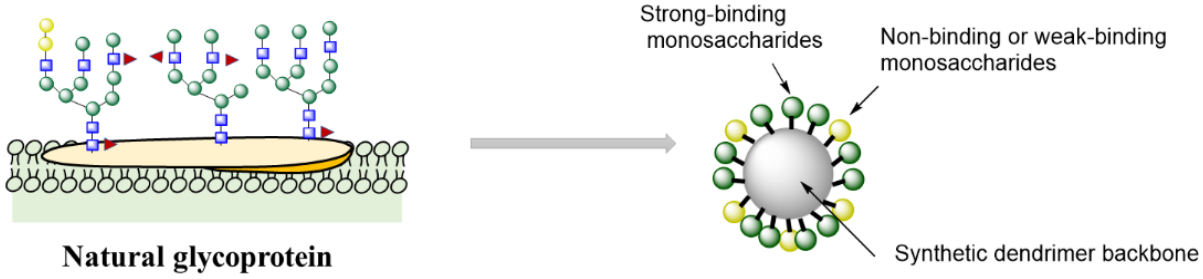

Over the years, numerous different glycomimetics have been developed, specifically varying the architecture to study the effects of sugar presentation and physicochemical characteristics. Their molecular weights range from low-molecular-weight compounds with few copies of binding ligands to high-molecular-weight, multivalent polymers, and surface with extensive functionalization. [203] In terms of architecture, glycodendrimers[204] (**Figure 1.34**) as well as liner, [205] star shaped [206] or brush glycopolymers were synthesized, whereas the scaffold properties were, for example, varied from flexible to more rigid scaffolds but also scaffolds that were hydrophilic and hydrophobic were compared. [207] Another important approach is to connect carbohydrates to nano- or microparticles, mimicking a complete cell with a simplified glycocalyx. [208] Besides, it has been demonstrated that glycolipids, which subsequently self-assemble to supramolecular micelles, are effective mimics of a cell with an exposed carbohydrate shell.

Figure 1.34 Simplified structure of cell oligosaccharides. (A) Glycoprotein and glycolipids of cell membrane with (✹) N-glycan structures and (✦) Type-1 and -2 Lewis determinants. [209] (B) Glycodendrimers showing the most exposed saccharides of a natural oligosaccharide built on an artificial scaffold

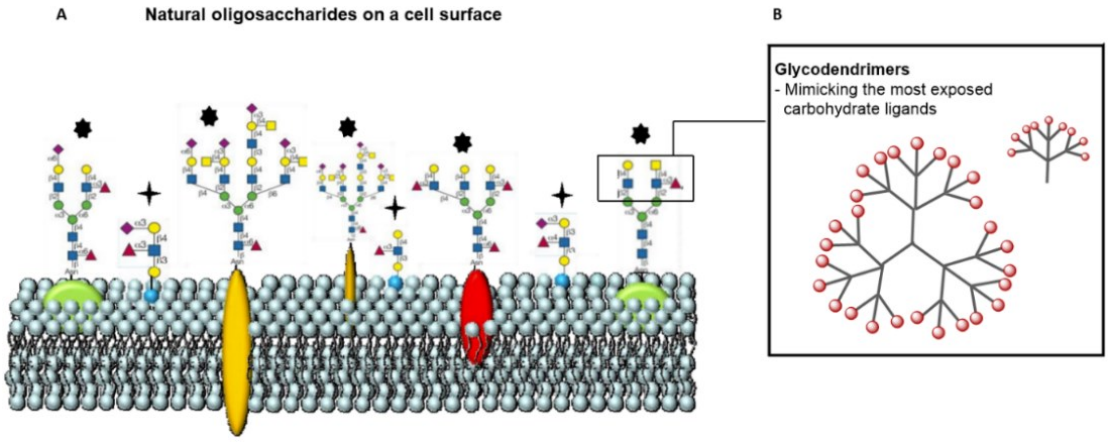

Further elucidating the carbohydrate-lectin binding mechanisms is typically less difficult for glycomimetic compared to the natural constructions because of their simpler form. Additionally, the structure of the glycomimetic can be modified specifically to potentially target one of the different binding pathways as explained before, and then adjust the resulting biological properties. For example, the chelate effect is often targeted as a main binding mechanism, aiming to accurately adjust the distance between two binding sugar moieties using the selected scaffold, spanning two binding sites and thus allowing for simultaneous binding of two CRD of the lectin understudying. Pieters and co-workers were able to demonstrate a significant increase in binding affinity after carefully bridging the gap between two binding sites in LecA and Shiga-like toxins, wheat germ agglutinin (WGA), [210] it could be demonstrated that the backbone properties are crucial for chelate binding. Rigid scaffolds show the best binding if the distance between the two carbohydrate ligands is matches the distance of two CRD since they are entropically more favored over flexible scaffolds which have higher degrees of freedom. If that is not the case, a chelate binding does not occur due to a severe distortion of the backbone, and more flexible scaffold are more suitable. [211]

Studies have revealed that, high-mannose-type N-glycans ranging from $Man_6GlcNAc_2$ to $Man_9GlcNAc_2$ residues (**Figure 1.35 a**), are expressed on urothelial cell. In $Man_9GlcNAc_2$ structures, all terminally exposed mannose residues are α1-2 linked, while in $Man_9GlcNAc_2$ structures the terminal mannose moieties can be additionally α1-3 and α1-6 linked. While Le^a (βGal 1-3(αFuc 1-4) βGlcNac) trisaccharides (**Figure 1.35 b)**, are fucosylated type that exists on red blood cells. $Lewis^a$ oligosaccharides is important recognitions motifs for interactions with LecB of *P.A* (K_d= 212 nM). [212]

Figure 1.35 a) High-mannose type N-glycans presented on FimH receptors. b) Lewis a (Le^a) antigen

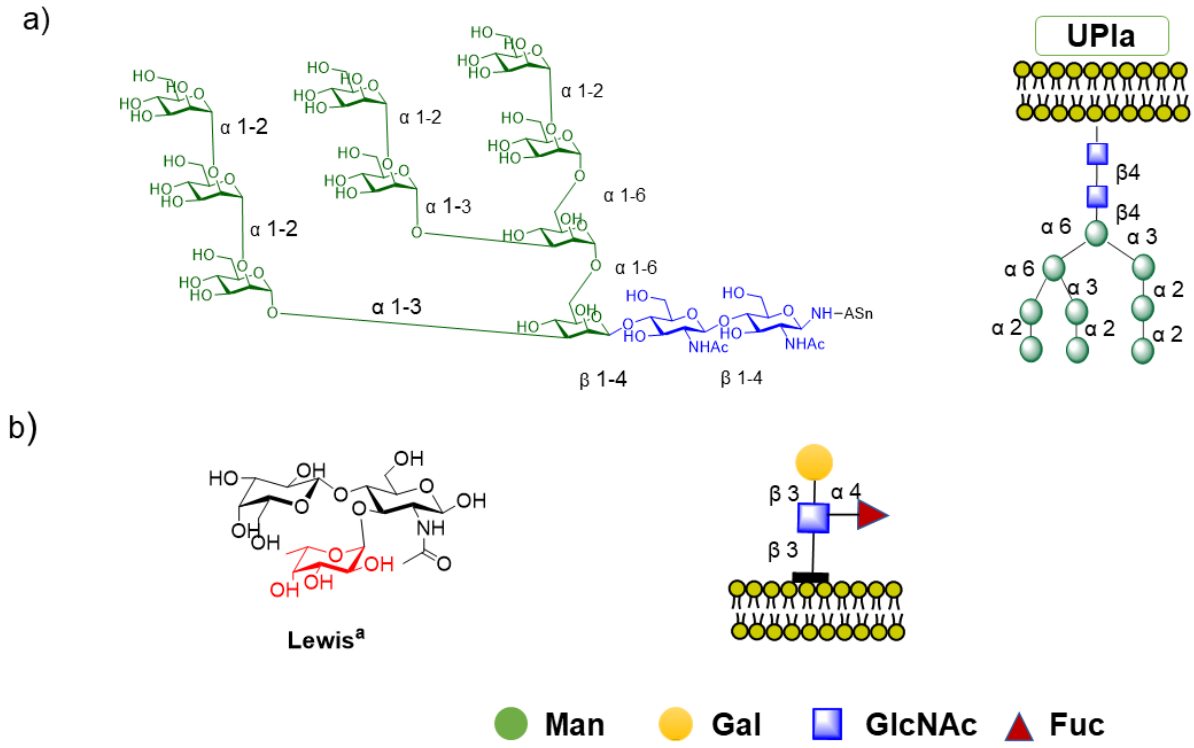

1.15 Uropathogenic *E. coli* (UPEC), type 1-fimbriae adhesion

The binding of UPEC to host cells causes bacterial internalization and the generation of biofilm-like intracellular bacterial communities (IBCs). The toxins released by some *E. coli* bacteria can damage the host cells in the intestine and leads to diarrhea and damage the in kidneys. Pili (or fimbriae) are long proteinaceous filaments that are utilized by Gram-negative bacteria to adhere to host surfaces while maintaining a separation between the cell membranes, preventing the electrostatic repulsion that occurs as a result of the net negative charge found on the surface of both the bacteria and host, (**Figure 1.36)**. Fimbriae of *E. coli* has been shown to facilitate bacterial colonization and invasion of human bladder cells. In the first step of the infection cycle, UPEC attaches to the urothelial glycoprotein uroplakin Ia of the host by means of the bacterial adhesin FimH. The FimH expression of *E. coli* bacteria mediates the mannose sensitive binding to target host cells and it has been demonstrated that a mannose-binding site is located at the top of the protein domain. A wide range of studies have been made on uropathogenic strains of *E. coli* that produce type 1 fimbriae and these indicate that FimH can be a potential vaccine candidate for the prevention of infection in the urinary tract. [213, 214]

Figure 1.36 Structural elements of UPEC. a) Electron micrograph of a type 1-fimbriated uropathogenic *E. coli* (UPEC); b) schematic representation of UPEC binding to oligo mannosylated UPIa. c) illustration of a type I pilus consisting of a helical rod (FimA subunits) and a fibrillar tip (FimF, FimG, and FimH). [215, 216]; d) Crystal structure of full-length FimH consisting of a lectin domain ($FimH_{LD}$), and a pilin domain ($FimH_{PD}$). [217]

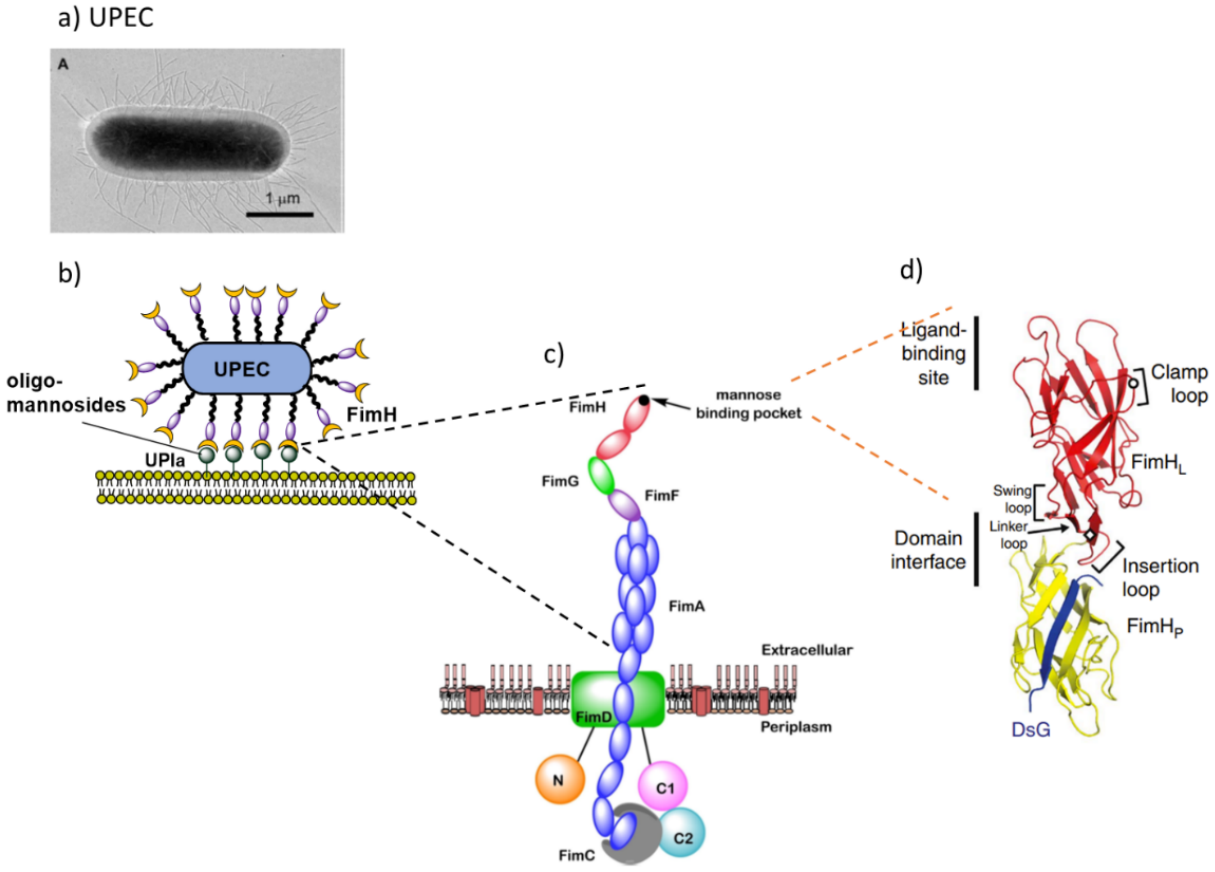

1.15.1 The bacterial lectin FimH and mannose binding site

FimH consists of a β-sandwich-fold containing a mannose specific binding site in a distal position to the rest of the pilus (**Figure 1.36 d)**. FimH exhibits a deep, negatively charged ligand-binding site that selectively binds the α-configuration of D-mannose **(Figure 1.37**). α-D-mannose exhibits a remarkable micromolar affinity with a K_D value of 2.3 µM. The mannopyranose moiety is coordinated by the side chains of (Asp46, Asp54, Gln133, Asn135 and Asp140, and the main chain of Phe1, and Asp46 forming extensive hydrogen bonds. Over the last few years a range of highly potent mono-valent antagonists consisting of a mannose moiety and a lipophilic aglycone was published, (section 1.15.3). The various aglycones provide hydrophobic contacts or π-π stacking interactions to amino acids forming the entrance to the mannose binding pocket. This entrance called 'tyrosine gate' is composed of two tyrosines and one isoleucine (Tyr48, Ile52, and Tyr137) forming the entrance to the mannose-binding pocket. This effect leads to a further improvement of affinity as documented by *n*-heptyl α-D-mannoside, K_D= 22 nM. [218]

Figure 1.37 A) The crystal structure of FimHLD is co-crystallized with n-heptyl-D-mannopyranoside (this image is adopted from ref). [219] B) The carbohydrate recognition domain of isolated FimH lectin domain in complex with n-heptyl α-D-mannopyranoside (HM). [220]

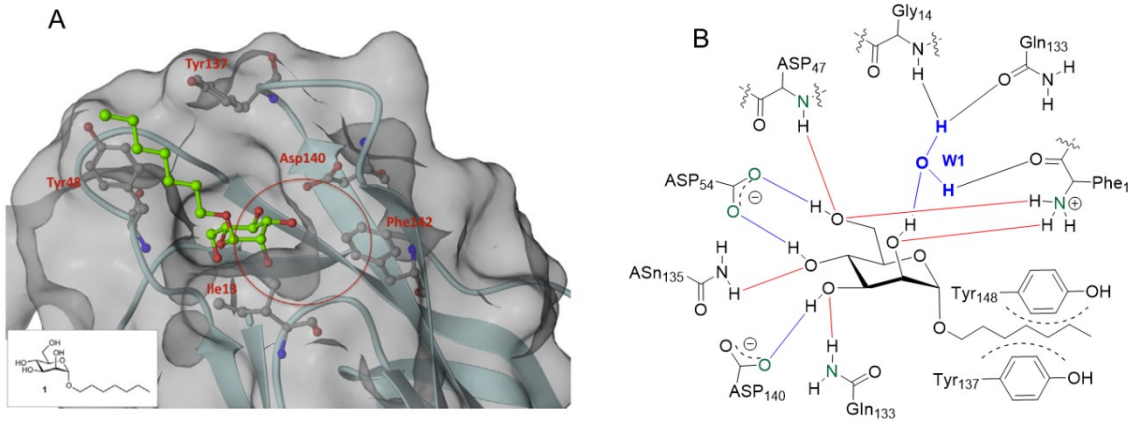

1.15.2 Interactions of FimH with its natural target ligands (FimH-CRD)

The FimH lectin domain contains 157 amino acids, which assemble to form an 11-stranded β-barrel structure encompassed within the β-barrel structure is a polar binding pocket[221] (residues Asn 46, Asp 47, Asp 54, Gln133, Asn135 and Asp140) to which terminal mannose units can engage in a complex network of hydrogen bonding, and electrostatic interactions. [222] The polar binding pocket is surrounded by a hydrophobic region, (residues Phe 1, Ile13, Tyr137, and Phe 142) which contains a tyrosine gate (residues Tyr 48, Ile52, Thr 51, and Tyr137). [222] This region provides support for the binding site through electrostatic interactions with the tyrosine gate, which is shown to be influential in the ability of ligands to enter the binding site. Further interactive features of FimH lectin domain are a small hydrophobic pocket adjacent to the sugar binding pocket (residues IIe52, Tyr137, and ASn138) [222] a salt bridge (residues Arg98, and Glu50) which facilitates further hydrogen bonding, and Tyr48 and Tyr 137 residues, which facilitates further hydrogen bonding, and the Tyr148 and Tyr137 residues, which involved in hydrophobic and ring stacking interactions [223, 224] as well as forming direct and water-mediated hydrogen bonds to ligands. [224] A summary of the main interactions that occur between the FimH lectin domain and mannose-based pentasaccharide is presented in (**Figure 1.38)**. The binding of mannose-based ligands to the extended FimH binding site is the result of a complex network of interactions and hydrogen bonding. [218, 225]

Figure 1.38 High-mannose type N-glycans displayed by the glycoprotein UPIa

A depiction of the main interactions that occur between mannose based pentasaccharide and the extended FimH binding site, red indicates interactions mediated by Van der Waals, aromatic stacking and hydrophobic interactions, blue indicates interactions mediated by hydrogen bonding (adapted from ref.) [226]

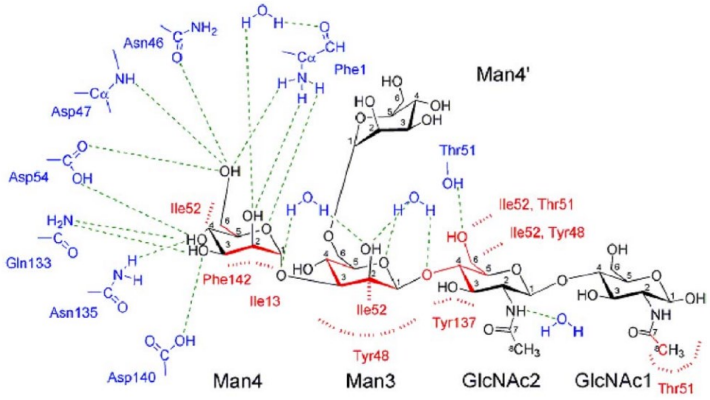

The X-ray crystal structure of the isolated FimHLD with oligomannose-3, provided evidence that the tyrosine gate is involved in hydrophobic interactions with oligomannosides. [227] As a result, many studies focused on the development of mannoside derivatives with hydrophobic aglycones for anti-adhesive therapy of UTIs. Favorable stacking and van der Waals interactions of the aglycone with aromatic side chains of the tyrosine gate leads to continuously improved affinities of synthetic FimH antagonists. However, in contrast to synthetic FimH ligands, different studies have shown a partial or complete removal of the tyrosine gate had no impact on the binding affinity of dimannoside in comparison with wild-type FimH.

1.15.3 The ligands targeting FimH

Several research groups have been involved in discovering potent FimH inhibitors with a view to find non-antimicrobial alternate approaches toward the prevention of recurrent UTIs. A selection of mono valent FimH antagonists are depicted in (**Figure 1.39)**. [228-231] one of the first classes of D-mannopyranoside-based FimH were alkyl mannoside. Studies proved that butyl α-D-mannoside (**2**, K_d= 151 nM) to bind to FimH with 15-30 times greater affinity than α-D-mannose (K_d=2.3 μM). [232] Further studies into the binding affinity of alkyl mannoside found that the binding affinity increases as alkyl chain length increases, for example, hept- α-D-mannoside **(3** K_d = 5 nM). [232] Aromatic α-D-mannoside was reported to be powerful inhibitors of the adherence of type 1 fimbriated *E.coli*. The most potent aromatic α-mannoside inhibitor reported was *p*-nitro-*O*-chlorophenyl-α-mannoside **4** which shows to increase the inhibition. Diamond squarate mannoside **5** was also synthesized and it is structure was shown to be potent inhibitor of FimH (IC_{50}= 6.38 μM). [233] Another well-studied group of FimH analogues are biphenyl mannosides. The most potent analogue was **6 (**IC_{50}= 0.94 μM). Biphenyl mannoside **10** (IC_{50}=0.16 μM) to be a promising lead candidate. [223, 231]

Ernst and co-workers synthesized a series of indolylphenyl α-D-mannoside. The most promising analogue was **11**, achieved (IC_{50}= 20 nM). [234]

Figure 1.39 α-D-mannopyranoside- based inhibitors. The structures of each FimH antagonist contain a crucial for binding mannose moiety and an aliphatic (1-3) or an aromatic (4-11) aglycone

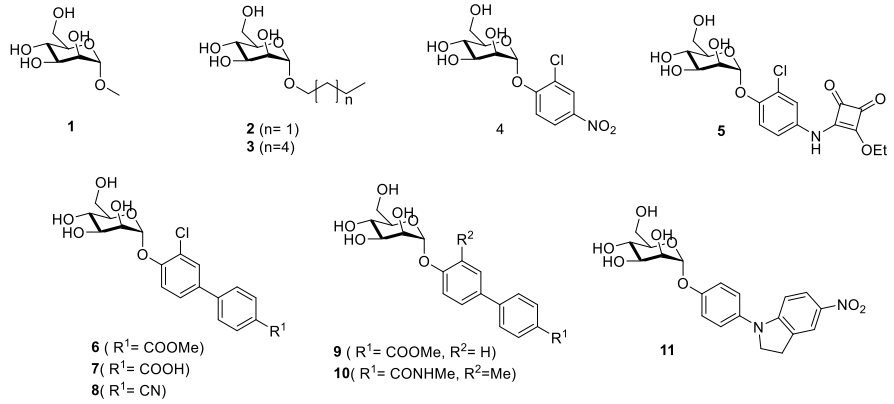

The reported affinities can be explained on the basis of the structure of the CRD that is located on the tip of the FimH protein, (**Figure 1.39**). First, the hydroxyl groups at the C-2, C-3, C-4 and C-6 positions of mannose form an extended hydrogen bond network. Second, the so-called "tyrosine gate" which is the entryway to the binding site formed by two tyrosines and one isoleucine, supports hydrophobic interactions. The aromatic aglycons of antagonists as found in compound **4** for example can establish energetically favorable π–π interactions with this tyrosine gate, resulting in significantly better affinities. The FimH inhibitors have been optimized to contain hydrophobic substituents at their reducing end; these substituents can interact with the tyrosine gate located at the entrance of the FimH binding site. The 'tyrosine gate' is FimH-specific characteristic, which most likely explains the selectivity displayed by these inhibitors. Furthermore, multivalent ligand presentation is known to play a significant role in nature. In nature carbohydrate ligand presentation is mainly multivalent, thus suggesting that the potency of α-D-mannosidepyrnoside based inhibitors may be limited due to only achieving monovalent targeting. The phenomenon describing how many multivalent ligands display greater affinity than their monovalent counterparts has been termed the "cluster glycoside effect". [215]

Figure 1.40 Multivalent Man- dendrimer inhibition of bacterial FimH adhesions

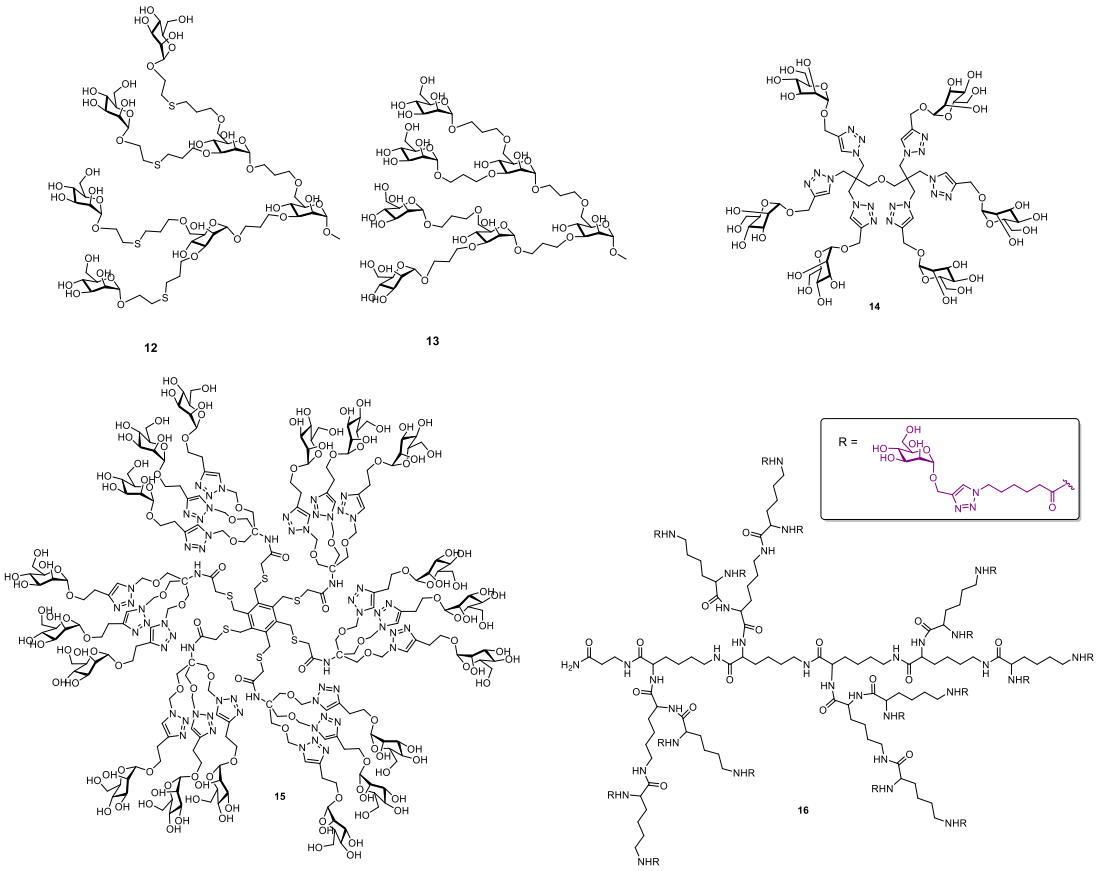

Iterative synthesis of spaced glycodendrons as oligomannoside mimetics was developed using a novel method for synthesizing glycodenrimers, in which a 3,6-diallylated carbohydrate is utilized as a core molecule, hydroboration-oxidation in the activating step, and glycosylation with branched and unbranched sugar trichloroacetamidates is used for dendritic growth. The new hyperbranched glycodendrons were tested for their potential as inhibitors of *E. coli* type 1 fimbriae-mediated bacterial adhesion, (**Figure 1.40**). Heidecke and Lindhorst described the synthesis of thioether-spaced thioether glycodendrone **12**, [235] and glycodendron **13**. [236] Their abilities as inhibitors of the mannospecific adhesion of *E. coli* were measured through ELISA, by using polysaccharide mannose coated plates. Compound **13** showed better inhibitor data with an IC_{50} of 0.03 mM, lower than that obtained for the inhibitor MeMan (IC_{50}= 5.9 mM). Multivalent ligand presentation can further increase lectin binding through crosslinking. Here, several ligands from a multivalent species bind to distinct target unit lectins, crosslinking the target unit and causing the bacteria to aggregate. [237] Due to the complexity of multivalent carbohydrate interactions, it is often an accumulation of multiple factors that cause the "cluster glycoside effect". In the case of FimH it is likely that multivalent mannose-based ligands bind to multiple different FimH units, resulting in the formation of *E. coli* clusters.

Multivalent ligands and their lectin binding studied by several researchers. [238] Gouin *et. al.* successfully applied CuAAC strategies in the synthesis of a great variety of multivalent mannoside dendrimers by using oligo(ethylene glycol) linkers. [239] It is worth mentioning the preparation of hexavalent dendrimer **14** through the CuAAC reaction. [240] Aromatic dendritic scaffolds have been extensively applied in the preparation of antibacterial glycoconjugates. [241] For example, a family of glycodendrimers containing mannopyranosidic units based on the employment of poly-propargylated dendritic core **15** have been successfully synthesized. [242]

Not all interactions can be explained by multivalency or cluster effect. Lindhorst and co-workers proposed that understanding of fimbriae-mediated bacterial adhesion may require at least two distinct viewpoints. [236] One method addresses results obtained from hemagglutination inhibition assays or ELISA. They observed an inhibition of bacterial adhesion that can be neither explained on the basis of the known crystal structure of FimH nor interpreted based on a classical ‘‘multivalency effect’’. The inhibition of bacterial adhesion should be rather explained by a ‘‘macromolecular effect’’. the inhibitory potencies can be related to characteristics that are common for macromolecules and the interactions they form, rather than for distinct molecular epitopes. For example, Lindhorst and co-workers studied the computational docking the surface of the lectin domain of bivalent molecule (**Figure 1.41)**, in an effort to find additional carbohydrate-binding sites in the FimH lectin. [243] Three new carbohydrate binding cavities on the surface of the FimH lectin domain, in addition to the mannose pocket at the tip of the domain, were identified which have a marked preference for the same subset of high-mannose trisaccharides substructures, mainly α-D-Man-(1→3)-[α-D-Man-(1→6)]-D-Man. By employing site-directed mutagenesis, it was found that mutations in one of these cavities significantly reduce binding, indicating that this could be a second carbohydrate binding site, relevant for ligand binding. [244, 245]

Figure 1.41 Connolly surface of FimH in complex with FimC. a) Docking studies were used to estimate the length of a linker that is required to bridge the putative two binding sites. [245] b) The bivalent glycopeptide

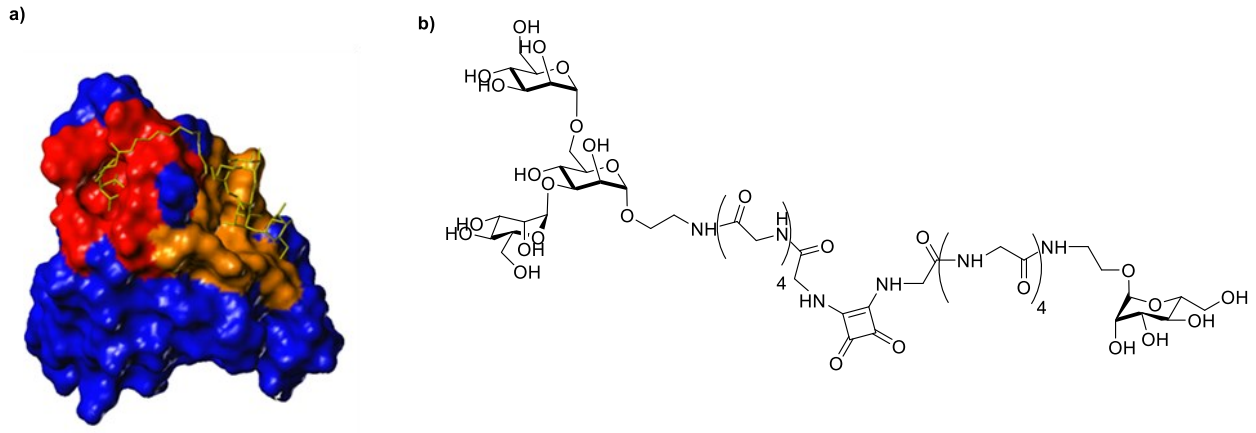

1.16 *Pseudomonas aeruginosa* pathogensis LecB and LecA adhesion

P. aeruginosa is a ubiquitous Gram-negative bacterium. It can cause serious infections predominantly in cystic fibrosis patients and those who are immunocompromised, such as HIV patients, cancer patients, and patients with burn wounds. *P. aeruginosa* infections are difficult to treat because the bacteria have a high natural resistance to antibiotics and rapidly acquire new antibiotic resistance. In addition, the bacterium can change its lifestyles that allow it to evade the immune system as well as antibiotic treatment. When infecting the human body, *P. aeruginosa* typically encounters polarized epithelial cell layers, which function as protective barriers. *P. aeruginosa* has also been shown to have the propensity to enter and colonize wounded epithelia. [246] In addition, it has evolved strategies to alter the polarity of host epithelial cells to facilitate infection. [247-250] However, limited reports are available regarding the role of this bacterium in urinary tract infections. [250]

P. aeruginosa produces two carbohydrate-binding proteins, so-called lectins, LecA and LecB, which are also named PA-IL and PA-IIL, respectively. Whereas LecA is galactophilic, LecB high affinity for Le^a oligosaccharide (**Figure 1.42 e**) and has been demonstrated to recognize L-fucose and its derivatives. [251] LecB is transported to the outer bacterial membrane, where it binds to the porin OprF, resulting in its presentation at the outer surface of the bacteria. [251] Our focus in this research is the inhibition of lectin LecB. Inhibition of the lectin mediated adhesion could be a potential therapeutic strategy. [252] In this section we briefly explain the general features of the structure of LecB and binding sites with L-fucose. [186-185] LecB is a tetramer consisting of four 11.73 kDa subunits, each of them containing two Ca^{2+} ions and each binding sugar ligand. The overall fold of PA-IIL is that of a nine-strand antiparallel β-sandwich, (**Figure 1.42**). In each subunit, strands 1-5 form a Greek-key structural motif extended by strands 6-8 which associate with strands 1 and 4 to form a 5-strand curved β-sheet. Dimerization is a result of a head-to-tail association between two monomers that make contact through the curved five stranded β-sheet. The quaternary structure of PA-IIL is that of a tetramer occurring mainly by the antiparallel association of β- sheet from each dimer with their counterparts in the other dimer. [186] The best monovalent LecB ligand has been identified by Imberty and co-workers using a glycan array, the natural trisaccharide Le^a (**19**, k_d = 212 nM), which forms additional interactions *via N*-acetyl glucosamine moiety (**Figure 1.42 e**).

Figure 1.42 a) LecA tetramer structure, with distances between Ca^{2+} (magenta spheres), and the shortest distance between galactose-binding sites indicated; b) LecA binding-site interactions with D-Gal; c) LecB tetramer structure, with distances between Ca^{2+}, and the shortest distance between fucose-binding sites indicated; d) LecB binding-site interactions with L-fuc.; (e) The best-known monovalent ligand for LecB, trisaccharide Lewis[a] (the image adopted with permission from the ref). [253, 254]

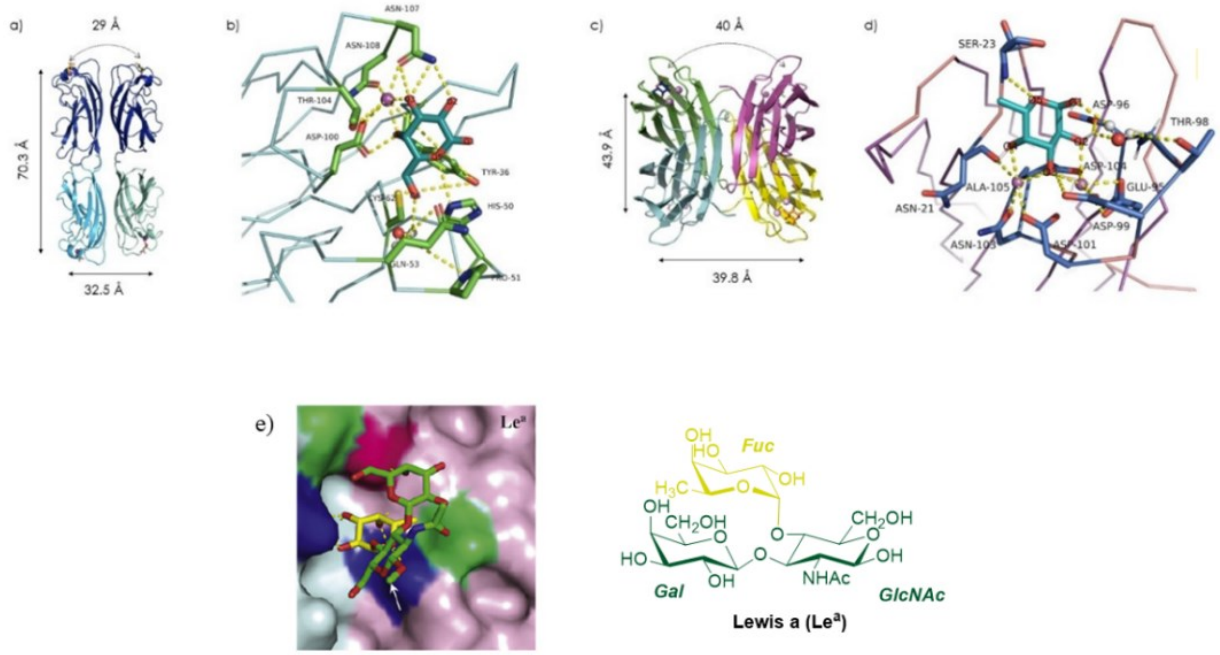

The structure of LecB has a unique binding site with two closely located calcium ions (3.76 Å apart) that are directly involved in the sugar binding through the coordination of three hydroxyl groups of the carbohydrate ligand. Tow protein bound Ca^{2+} ions were used to mediate the binding of one fucose to LecB by coordination with the C(2), C(3) and C(4) OH groups, (**Figure 1.42 d**). [255] The two calcium ions contribute to the receptor specificity since they coordinate monosaccharides with the stereochemistry of two equatorial and one axial hydroxyl group are present in fucose and mannose. These two calcium ions are also believed to play a role in the unusually strong affinity of LecB for fucose, which is in the low micromolar range, as compared to the millimolar affinity usually observed for lectin/monosaccharide interactions. [256] For the design of novel glycodendrimers that reach higher affinity, it is important for a more precise understanding of the protein/sugar/calcium triplet. Imberty and co-workers studied for the first time, the visualization of all hydrogen atoms in the complex in the LecB/fucose complex. [257] Their studies showed that the fucose ring adopts the stable $^1C_4$ chair conformation, with the α- configuration at the anomeric position. The use of perdeuterated fucose provided high-quality neutron density maps, the neutron map clearly shows the hydrophobic contacts between the methyl group on the C-6 position of fucose and the -CH_2 and methyl groups of Ser23 and Thr45, respectively. The deuterium atoms in the -CH_3 group create a

triangular-shaped neutron density and are in the most stable staggered conformation with respect to the aliphatic deuterium atom on C-5.

Also, the studying of the coordination of calcium ions showed that each calcium is hepta-coordinated, with the involvement of three oxygen atoms of the fucose ligand (2 of these for each calcium ion), oxygen atoms from two asparagine residues, and the carboxylate atoms of six acidic amino acids (three aspartates, one glutamate, and the C-terminal group of Gly from the neighboring monomer). The co-cristal LecB/Lewis^a (Galβ 1-3(Fucα 1-4) GlcNAc) showed that all monosaccharides of Lewis^a interact with the surface of LecB. The authors have shown that, in addition to a network of hydrogen bonds between fucose and LecB, the GlcNAc residue makes a hydrogen bond between its *O*-6 atom and the Asp96 of LecB, and that both GlcNAc and Gal residues establish additional interactions with LecB through the bridging of water molecules. [258] Studies show that the GlcNAc moiety does not interact with the binding site and serves solely as a linker that positions the galactose and the fucose moiety in the correct spatial orientation.

In addition to conventional antibiotics, different methods of treating *P.A.* has been reported. Including inhibition of quorum sensing, biofilm-formation, iron-chelation, and interfering with biosynthetic pathways of the bacterium. An emerging anti-*P. aeruginosa* strategy involves targeting these lectins with glycoconjugates. A vast array of monovalent[259] and multivalent[260] LecB inhibitors have been reported, with structural variation significantly affecting the binding affinity and selectivity, among other properties.

1.16.1 Ligand targeting lectin LecB (PA-IIL)

The lectin LecB has been isolated from heat-resistant fractions of *P. aeruginosa* by Gilboae-Garber and coworkers. [261] LecB has a preferable binding affinity for L-fucose over D-mannose and others. [186] Two proteins bound Ca^{2+} ions were used to mediate one fucose to LecB by coordination to the C (2), C (3) and C (4) OH groups. Compared with D-mannose, L-fucose (**17**, K_d = 2.9 μM) [262] and its methyl glycoside (**18**, K_d = 430 nM) [263] showed a stronger binding. This was explained by the additional lipophilic interaction of the C-6 methyl group with the protein (**Figure 1.43**). The distances between the binding sites are around 40-50 Å. due to the large distance, no chelation is possible with relatively small dendrimers. Using a glycan array, Imberty and co-workers identified the best monovalent LecB ligand, the natural trisaccharide Lewis^a (**19,** K_d = 210 nM), which forms additional interactions via its N-acetyl glucosamine moiety. Because the galactose residue has little contact with the protein, Roy and co-workers synthesized truncated disaccharides (**20**, K_d= 290 nM), [264] and oxazole-substituted fucosides (**21**, K_d = 430 nM) with a comparable affinity for LecB to Lewis^a. [265-260]

Figure 1.43 Lewis[a] and selected monovalent inhibitors for *P. aeruginosa* LecB

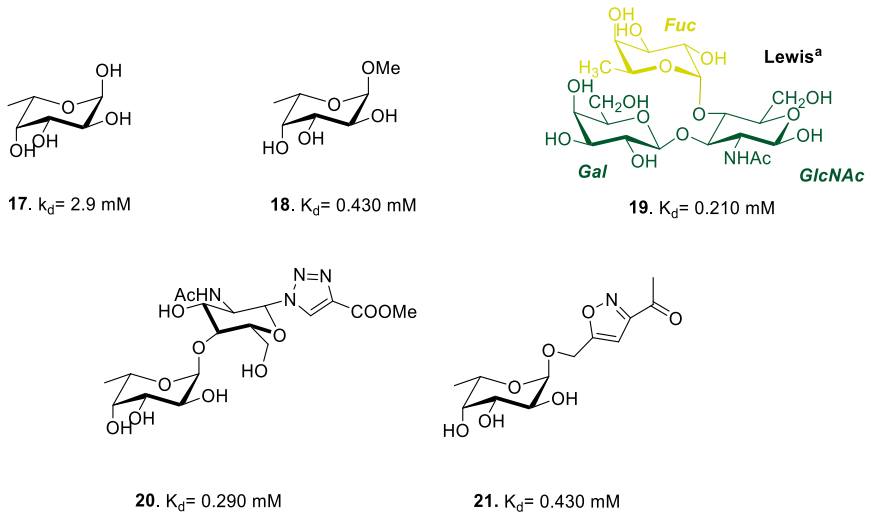

17. k_d= 2.9 mM **18**. K_d= 0.430 mM **19**. K_d= 0.210 mM

20. K_d= 0.290 mM **21.** K_d= 0.430 mM

However, several multivalent inhibitors have been found to bind in the nanomolar range, supporting the utility of a multivalent approach to lectin inhibition. This "multivalent" effect has been exploited in the design of multivalent glycoconjugate inhibitors of the LebB soluble adhesins. These synthetic glycoclusters have utilized a variety of scaffolds including peptides, and modified oligonucleotides. [238] The search for high-affinity ligands for LecB initiated the synthesis of several classes of fucose-containing compounds based on calixarene **22**, [266] pentaerythritol **23**, [267] or peptide dendrimer **24** scaffolds. Several common linker groups utilized in the multivalent systems are defined in **(Figure 1.44)**.

Figure 1.44 Common linkers in *P. aeruginosa* lectin-inhibitor design

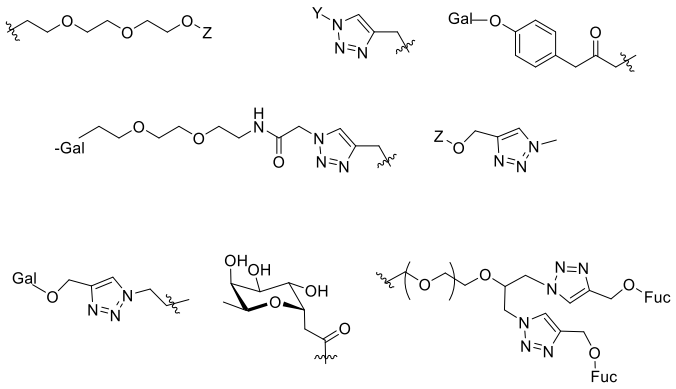

Vidal and co-workers, they construct glycoclusters from building blocks, consisting usually of glycosides (with a linker), phosphoramidate tether, a scaffold, and nucleotides or a short strand of synthetic DNA (**Figure 1.45**). Components are assembled through well-known and reliable reactions; phosphoramidite

chemistry (using DNA-synthesieser) for the pentaerithriyl phosphodiester core, and microwave-assisted CuAAC to conjugate glycosides giving clusters. [267]

Figure 1.45 Molecular structure of multivalent fucosides

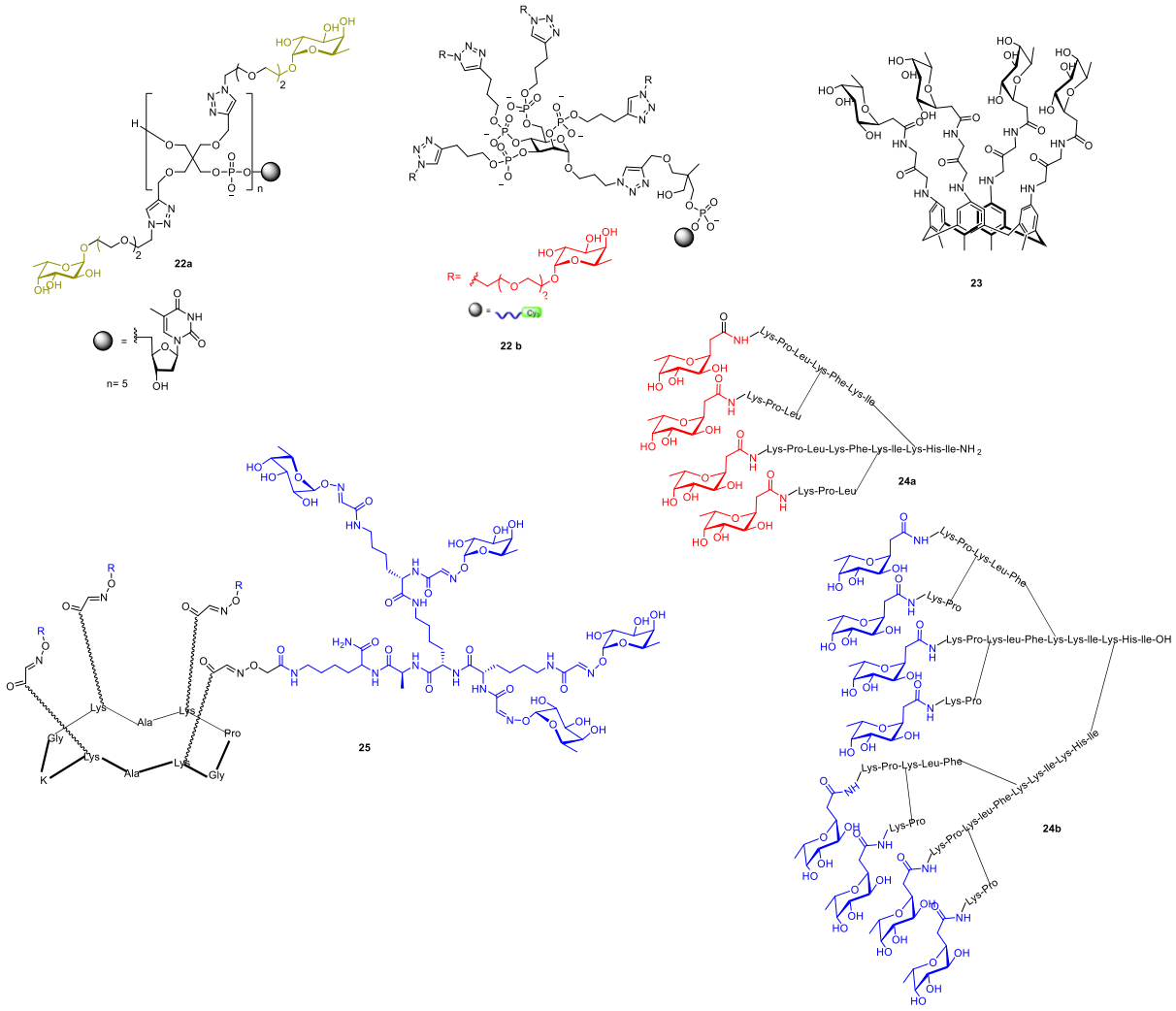

For example, Vidal and co-workers synthesized 16 fucosylated glycoclusters with antenna-like, linear, or crown-like special arrangements. Through a rapid screening method with a carbohydrate microarray, they identified the antenna-like fucomimetic **22a**, bearing four residues demonstrating the best binding properties among these compounds (IC_{50}= 0.70 µM). [267] A variety of glycoclusters were synthesized based on carbohydrate scaffolds. A series of fucosylated ligands was synthesized based on carbohydrate scaffolds for PA lectin targeting. For example, $MAN3_{Fuc}$ **22b,** performed significantly better towards *P.A* lectin binding (IC_{50} = 2 µM). Macrocycles, including calixarenes **23**, are attractive scaffolds for lectin-targeting mainly due to their versatility in achieving varying topologies and valencies, [268] and several glycocluster families based on macrocyclic cores are reported. Imberty and Vidal reported the first series of publications exploring

calix[4] arene scaffolds, CalixA-C, as *P.A* lectin-inhibitors. [269] However, due to the added hydrophobicity and rigidity of the linker, this arm led to major solubility issues when coupled with almost all scaffolds studied, resulting in limited data from biological assays.

The increased binding of the compound is not attributed to a "cluster" effect, since the potency per carbohydrate is only of 2. Instead, the enhancement is more likely to be attributed to the "macromolecular" effect. [236, 270] Glycopeptide dendrimer ligands for LecB were identified by screening combinatorial libraries of peptide dendrimers functionalized with N-terminal C-fucoside residues at the end of the dendrimer branches. Reymond and coworkers discovered a potent dendrimer **24a** by screening combinatorial libraries of multivalent fucosyl-peptide dendrimers, (IC_{50} = 0.14 μM by ELLA). Interestingly, compound **24a** could lead to completely preventing *P. aeruginosa* biofilm formation (IC_{50} ~10 μM). Another example reported from the Reymond's group, octavalent ligands **24b** (IC_{50}= 25 nM) was identified which was up to 30-fold more potent per sugar than a monovalent glycopeptide reference compound in an enzyme-linked lectin assay. Although **24b** could still prevent the formation of biofilm, it is unable to bridge two lectins with fucose binding sites within the same lectin tetramer as derived from the molecular modeling. [271]

A significant number of *P. aeruginosa* lectin-inhibitors based on glycopeptide dendrimer scaffolds are reported, with lysine residues acting as branching points. The LecB ligand with the greatest affinity is the hexadecavalent ligand **25** (K_d= 28 nM, IC_{50}= 0.6 nM), made by Renaudet's and co-workers, the molecular modeling suggested that the high affinity observed might be due to an aggregative chelate binding mode involving four sugar head groups and two lectins. [172]

Despite the fact that several dendrimers have been reported for antiadhesive strategy, in this research, we reported the design of a new family of dendrimers as a prodrug, which has a dual function to treat bacterial infections.

1.17 Selection of spacer, linker for optimal ligand binding

The choice of a scaffold able to provide the best orientation of carbohydrates is an important point in the design of potent inhibitors, (**Figure 1.46**). Given the ease of synthesis of a flexible linker compared to rigid ones and their high adaptability to the protein topology, thus, it is frequently PEG-based spacers are found in the structure of multivalent ligands. However, linker flexibility in such multivalent ligands can decrease the binding affinity due to a high entropic cost during multivalent binding with the protein. Moreover, when utilizing a flexible linker, it's also important that the linker's effective length corresponds to the binding distance. On the other hand, a rigid spacer, is compared with a flexible one.

In theory, the use of a rigid spacer should create stronger binding since it could decrease the loss of conformational entropy which occurs during the multivalent binding. However, the creation of a rigid structure is difficult to realize. The low mobility of rigid systems requires a design that strongly matches the geometry of the protein, which is difficult to achieve, not only because the structure of the protein in solution has to be known but also because of the difficulty to find chemical units that combine to yield a spacer of the desired geometry and length. Another hurdle that must be overcome is the solubility of the spacer which should be sufficient to yield soluble multivalent constructs.

Figure 1.46 Influence of linker length and rigidity on cell binding

(A) While some ligands that are tethered to a nanoparticle via a flexible linker may mediate target cell docking regardless of linker chemistry, in other cases inefficient nanoparticle binding can be caused by a linker that is either too short or overly flexible. (B) for a linker that is too short, surface ligands can become buried within the passivation layer and become inaccessible to cell surface receptors. (C) Even with longer linkers, some ligands may prefer to bury themselves within the passivation layer than extend into the aqueous surroundings. (D) To prevent this tendency, a long rigid spacer can be used to force protrusion of the ligand into the aqueous surroundings. [272]

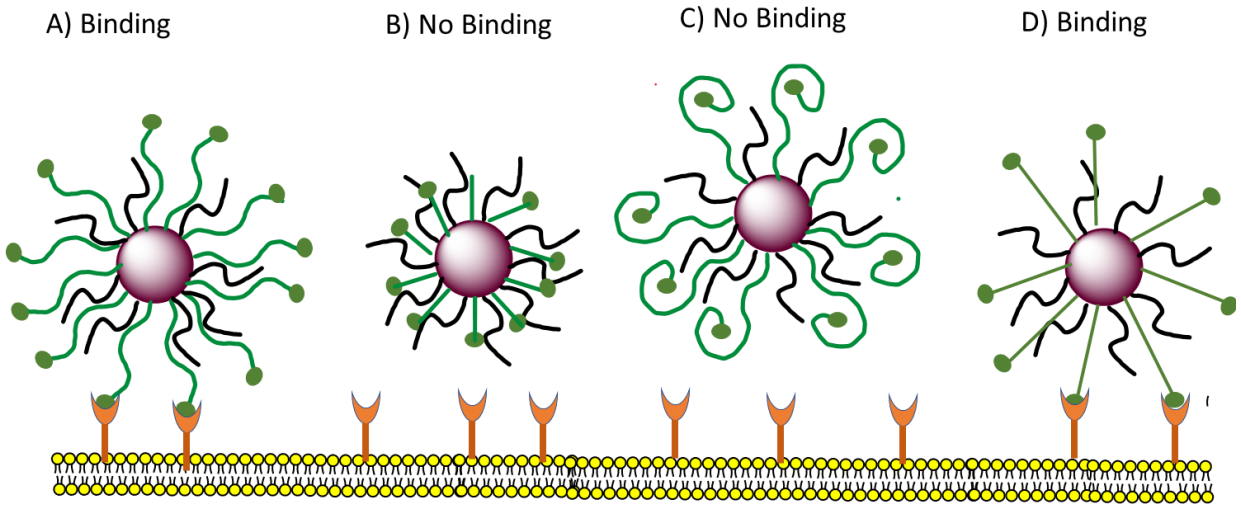

1.17.1 Controlled Drug- release in *vivo*

Controlled drug release processes can be divided into main groups: the ones triggered by internal factors, which are already present in the host organism, and the ones requesting a supplementary external input. Internal triggers comprise the use of physiological agents either influencing only the stability of dendrimer-drug-inclusion complexes, with the preservation of the general chemical integrity (i.e., pH, the presence of compounds having more affinity to the dendrimer than the encapsulated drugs), or leading to its degradation (i.e., achieved by the sensitivity of some dendrimers to carboxylesterases and GSH). It is worth noting, however, besides the efforts to design a system sensitive to the internal parameters mentioned above,

differences in bio-distribution compared to control are usually not significant. Therefore, for a very localized drug release, it is preferred to provide the vector with additional features, such as the ones responsible for adequate targeting of pathological sites. The external triggering can be achieved by localized ultrasounds, temperature, and UV radiation. [273-275]

1.18 Hypothesis and objectives

The aim of this project is to synthesize dendrimer-drug delivery system. In this research, we propose to use generation three (G3) glycodendrimers as drug carriers for the treatment of urinary infections. The glycodendrimer-prodrug system relies on i) ligands-targeted bacterial lectins FimH, and LecB; ii) a corresponding prodrug that is inactive in administered form but is activated by the enzymatic, (or acidic pH) hydrolysis. We hypothesize that the conjugation of ciprofloxacin to PEGylated dendrimer *via* a cleavable linker will prevent any interactions between secondary amine in ciprofloxacin. Additionally, will lead to a greater penetration/improved distribution of the carriers through the cell membrane. Acid cleavable linkers were initially promising but due to the stability requirements imposed by highly potent payloads, their value has been diminished. Accordingly, to overcome the lack of stability and the hurdle in intracellular drug release, in our research project, (Acy1oxy) alkyl ester prodrug strategy was followed. Additionally, employing PEG_3 chains to the backbone of the macromolecule for improving membrane permeability.
We anticipate achieving the following three goals in order to fulfill the project:
Aim 01: **Synthesis and characterize glycodednrimer conjugates with varying surface characteristics**. Synthesis and characterization a family of glycodendrimers as a prodrug conjugate with varying targeting ligands and active functional groups (i.e., carboxylic group) for covalent amide coupling. The Surface group modifications with targeting fucoside and /or mannoside are capable of modulating the interaction between the dendrimers and bacterial outer membrane lectins, allowing an increase of local concentration of antibiotics throughout the bacterial membrane.
Aim 02: **Synthesis of Antibiotic conjugated with a cleavable linker**. Synthesis of an antibiotic linker conjugate. The conjugation of this antibiotic *via* the cleavable bond, will allow enzymatic or pH dependent hydrolysis in the bacteria cytosis.
Aim 03: The biological properties of these newly created dendrimers prodrugs will be investigated by well-established methods like haemagglutination Inhibition Assays (HIA), Enzyme-Linked Lectin Assays (ELLA), Surface Plasmon Resonance (SPR), and Isothermal Titration Calorimetry (ITC).

In meeting these objectives, in our research, we explored the importance of carbohydrate-scaffold topology by the synthesis of D-glucuronic acid (**Chapter 2**) and D-glucosamine (**Chapter 4**) cleavable prodrug

scaffolds. The two scaffolds were prepared in seven steps, respectively, and subsequently were tethered with different synthetic fucoside or mannoside lectin-targeted.

In **Chapters 3, and 4**; a different series of PEGylated glycodednrimers modified with mannoside and /or fucoside (G3(OH)-(COOH)-PEG_3), and non-PEGylated glycodendrimers, were synthesized. The dendrimers were characterized using NMR and MALDI-TOF spectrum. In **Chapter 5**, ciprofloxacin conjugated with a combination of carbamate (acyloxy) linker terminated with amine group was synthesized. The products are fully characterized by ^{1}H NMR, ^{19}F NMR, and ESI-MS.

The synthesis of the glycodendrimers generations and drug conjugates required efforts in designing, efficient multi-step synthesis and conjugation protocols to achieve a controlled assembly of the different modules. Consequently, in my Ph.D. research, the majority of efforts have been devoted to developing synthetic strategies to reach such unprecedented macromolecular structures.

1.19 Outline of this thesis

This thesis describes research focusing on the design, and synthesis of new different multivalent dendrimers for antibiotic drug delivery.

Chapter 1 provides a comprehensive literature study on the clinical treatment for urinary tract infections and the mechanism involved in antibiotic resistance; essential notions of the bacterial lectins and their role in UTIs have been outlined. A description was given of multivalent glycoconjugates, which have emerged as a family of potential anti-infective therapeutics.

Chapter 2 describes the general strategies towards the design of the new library of (G3) multivalent homo-glycodendrimers. Followed the detailed synthesis D-glucuronic ester as a prodrug scaffold. Advances in chemical synthesis techniques enabled us to introduce diverse functional groups including, alkene, azide, and carboxylic group, the key components in the development of our third generation of fully synthetic dendrimers.

Chapter 3 focused on the synthesis of multivalent homo-glycodendrimers. The first part of **Chapter 3** describes the detailed synthesis of fucoside thiol model structure conjugated to the rigid spacer, as the first ligand. Also, mannose thiol has been applied in this research project. In the second part, the multi-component assembly of various monomers into a functionalized trivalent dendritic is presented, D-glucuronic ester is employed to create a trivalent dendritic wedge (dendrons) including: trivalent fucoside and/ or mannoside ligands essential for LecB and FimH binding, respectively. The optimized reactions were

all highly reliable so that the crude product of some steps could be used in the next steps without any further purification. The last part of **Chapter 3** describes the synthesis of a series of multivalent glycodendrimers using mannosylated or fucoside model structures by applying double stage convergent approach *via* copper(I)-catalyzed alkyne-azide cycloaddition, (CuAAC).

Chapter 4 describes the synthesis of D-glucosamine derivatives as a second prodrug. The attempts of spacer optimization were carried out to build a new architecture of a glycodendrimer.

Chapter 5 a study is performed towards the design of a ciprofloxacin-cleavable linker conjugate to modulate the stability of the antibiotic in *vivo*. Furthermore, to achieve optimal effective drug concentrations over time. The attempts made for the final conjugation step of the antibiotic to the dendrimers are described in the concluding section of the same chapter.

Chapter 6 covered the synthesis of a new class of dendritic cores with modified PEG_3 chains for non-toxicity and improve water-solubility.

CHAPTER 2
SYNTHESIS OF D-GLUCURONIC ACID CLEAVABLE PRODRUG SCAFFOLD

2.1 Introduction

One of the biggest challenges in drug development still involves simultaneously enhancing biochemical potency and membrane permeability. A lot of the research for new antibiotics is still focused on developing versions of existing molecules. Some have been developed through logical and systematic changes that make them more efficient or less susceptible to resistance mechanisms. [276] One of the important approaches to efflux-mediated resistance could be a modification of fluoroquinolones so they are not substrates for efflux pumps while maintaining antimicrobial activity, moreover, increasing cellular uptake.

In recent years, progress has been made in developing synthetic, carbohydrate-antibiotic conjugates to improve pharmacokinetics and reduce antibiotic cytotoxicity. For example, ciprofloxacin was conjugated with several monosaccharides (**Figure 2.1**), utilizing glycosidic linkers "Glycosylated ciprofloxacin conjugates" [277] which provide an attractive route by which drug conjugates can be prepared directly on the carbohydrate backbone, with no dendrimer conjugation reactions. In this approach, carbohydrate-modified analogues of ciprofloxacin were synthesized as chemical probes of the uptake pathways. A.Titz *et al*, published the synthesis of the first lectin-targeted antibiotic conjugates and their microbiological and biochemical evaluation. [278] They described the antimicrobial structure-activity relationship of these lectin-binding conjugates. The antibiotic conjugates **26** and **27** (**Figure 2.1**) showed effective lectin binding against LecA and LecB variants from *P. aeruginosa* PAO1 and PA14, which represent a broad range of clinical isolates of *P. aeruginosa*. Their studying proved that conjugation of ciprofloxacin to lectin probes enabled biofilm accumulation in *vitro*, and reduced the antibiotic cytotoxicity, but also resulted in a decreased antibiotic activity.

Figure 2.1 Carbohydrates ciprofloxacin conjugates

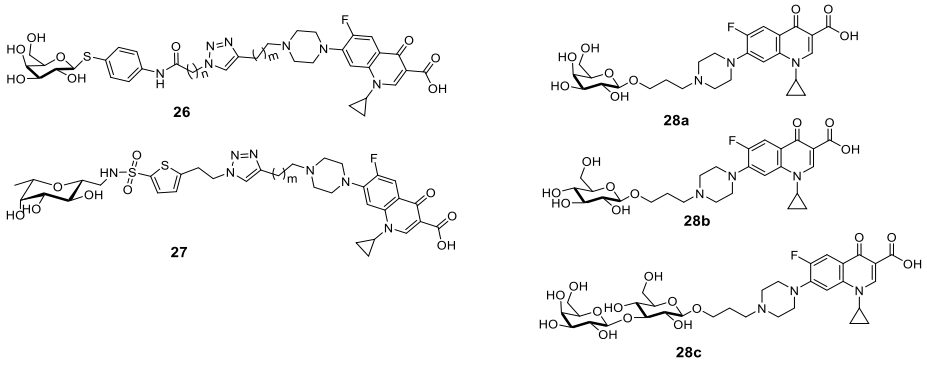

Moreover, carbohydrate modified analogues of ciprofloxacin have been employed by a variety of other groups. Routledge and co-workers, [279] synthesized glycosylated carbohydrate-Cip conjugate (**Figure 2.1, 28a-c**) in order to investigate the potential of exploiting carbohydrate transporters for fluoroquinolone delivery. Their studies have shown that using a high concentration of analogue **28c** has a significant effect on its ability to inhibit the target DNA gyrase, whereas the target glucose **28a** and galactose **28b** made a small difference in the activity of antimicrobial.

In previous studies it has been shown that the attachment of the drug to the monomer ligand via a non-cleavable linker, has an effect on antibiotic activity. In the current research, we developed a glycodendrimer-prodrug system in which ciprofloxacin conjugates to the sugar surface through a cleavable linker, the cleavable linker was designed as acyl(oxy)alkyl ester and were covalently attached to the drug using carbamate linkage. The incorporation of enzymatically cleavable linker in drug-carrying dendrimers will allow selective release at diseased sites only, where the prodrug can be transformed into a bioactive antibiotic molecule via internal mechanism, such as enzyme hydrolysis or a specific cellular environment (acidic pH). This might increase the effectiveness of the drug-delivery device, which is our ultimate goal. A schematic overview over the design of lectin-targeted glycodendrimer drug delivery system is depicted in (**Scheme 2.1**).

2.2 The design of glycodendrimer lectin-targeted drug delivery system

As shown in (**Scheme 2.1**), the general strategy to access the targeted analogues involved the late-stage coupling of dendritic wedges and cores *via* CuAAc reactions to afford glycodendrimers. This approach allowed for the modular synthesis of a variety of different target structures. The synthetic strategy for the preparation of dendrimer-drug conjugates was designed based on several considerations: (1) the introduction of the carboxylic group (-COOH) to the surface of the dendrimer; (2) structure modification for the ciprofloxacin and conjugation to dendrimer *via* labile bond; (3) The new dendrimers were decorated with two different kinds of lectin-targeted ligands for site-selective delivery and blocking bacterial adhesions, α-L-fucose selective for Lec B from *P. aeruginosa* and α-D-mannose selective for FimH from *E. coli*; (4) Aromatic or PEGylation of dendrimer core to achieve hypothesized physical characteristics. In this research, we chose glycodendrimers as a drug carrier due to their lower toxicity and possessing enough surface groups to maintain drug loading capacity (ex. 72 surface hydroxyl groups). However, one of the challenges of constructing dendrimer-drug covalent conjugation is the drug-modified cleavable linker.

Scheme 2.1 Retrosynthetic of glycodendrimer prodrug design and optimization

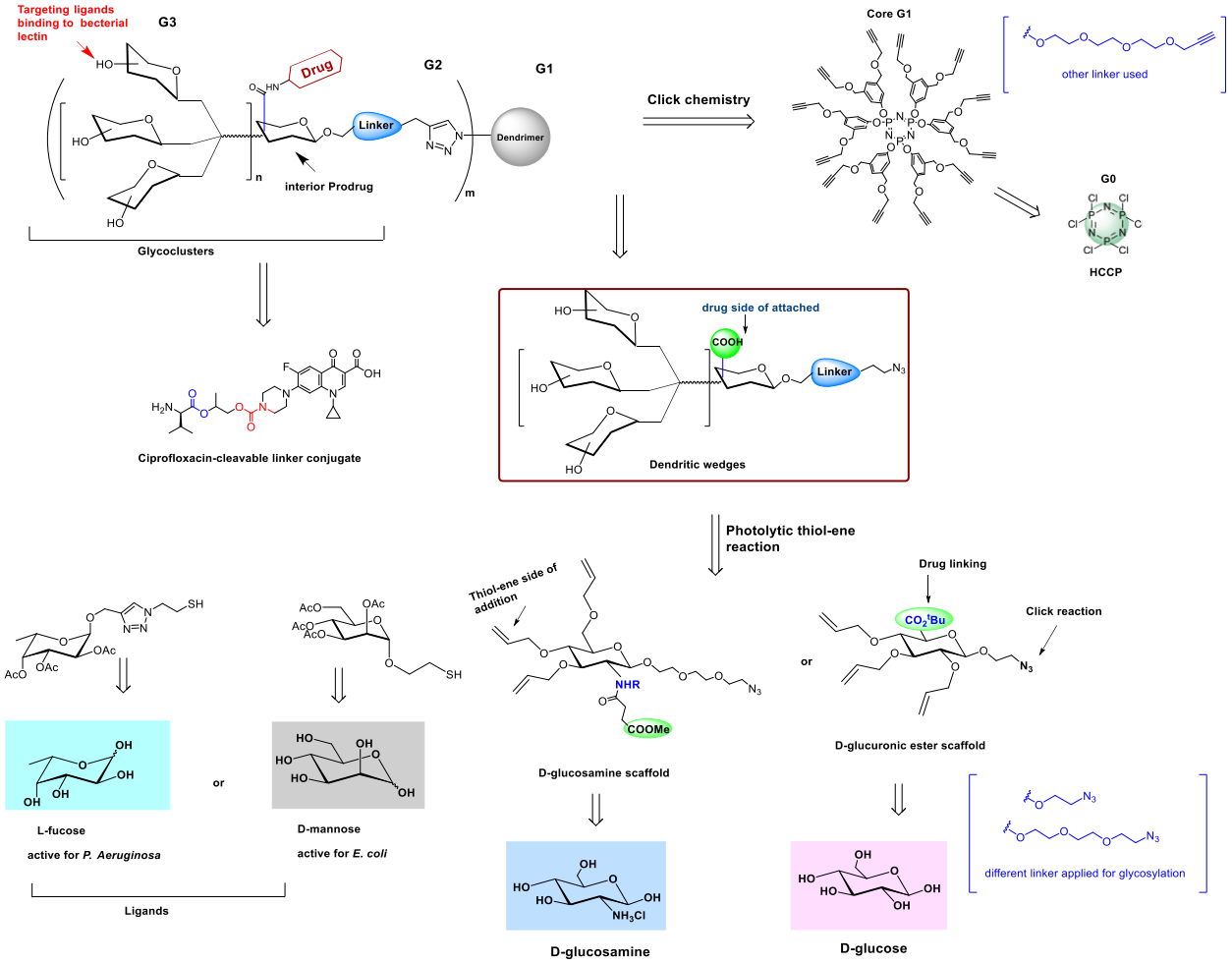

The synthesis plan for the disconnections of glycodendrimer dissecting the target in three generations (**G**), A (**G1**), B (**G2**), and C(**G3**) (**Scheme 2.1**). The central building block starts from different commercial scaffolds including hexachlorocyclotriphosphazene (HCCP), benzene-1,2,5-tricarboxylic acid, and dipentaerythritol which provides the dendrimer first-generation (**G1**). [280-282] The second generation (**G2**) is based on two key prodrug scaffolds; D-glucuronic ester[283] or D-glucosamine, synthetic nature of these sugars platform is designed to achieve scale-up, and provides further opportunities to incorporate targeting ligands to maximize uptake of the drug. [284, 285] Therefore, we initiated the syntheses of two different scaffolds; β-D-glucuronic ester (**Chapter 2**) and β-D-glucosamine (**Chapter 4**) having the two commonly employed linkers functionalities, alkene, and azide groups. These unique sites will be subjected to several chemical reactions including thiol-ene reaction, CuAAC, and drug bio-conjugation to the carboxylic group. The third generation (**G3**) consists of acetyl-protected glycosyl thiols of two different sugars (mannose and

fucose) that have active thiol functional group, (**Scheme 2.1**). The dendrimer-drug conjugate will be prepared by conjugation to the drug through an amide bond, as discussed in (**Chapter 5**).

2.3 Results and discussion

D-glucuronic acid is a prime constituent of many biologically relevant poly- and oligosaccharides and glycoconjugates. [286] D-glucuronic acids are frequently encountered in saponins, a very diverse class of glycosylated steroid- and triterpene-based compounds, forming the active ingredient of many traditional folk medicines. Because of their biological relevance, the synthesis of D-glucuronic acid containing oligosaccharides has received considerable attention. [287-293] In turn, the preferred prodrugs for drug delivery, namely glucuronides are not developed for glycodendrimer for antibacterial agent. Glucuronides are attaractive in that they exhibit stability in human plasma. [294]

2.3.1 Synthetic strategies of β-D-glucuronic ester scaffold

The general retrosynthesis of β-D-glucuronic acid derivative is depicted in (**Scheme 2.2)**. The high degree of functionality of β-D-glucuronic ester represents a challenging synthetic target. The order of the glycosidic bond forming, and the timing of oxidation state adjustment of C-6 all represent important considerations that must be addressed at the onset of any synthetic efforts.

Scheme 2.2 General retrosynthesis of D-glucuronic ester cleavable prodrug scaffold

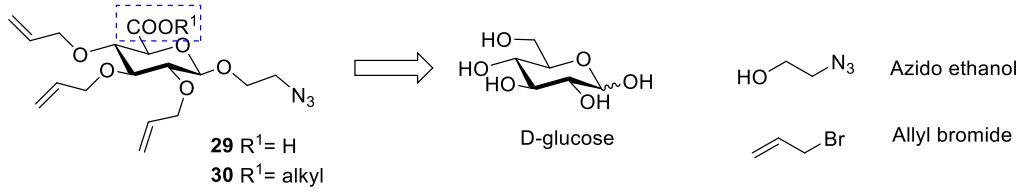

The glycosyl donors derived from D-glucuronic acid (Glc A) often perform poorly in glycosylation due to a low reactivity which is caused by the electron-withdrawing properties of the C-6 ester in the uronic acid derivatives, [295-297] that destabilizes the oxocarbenium ion like transition state of glycosylation. [297-299] Therefore, as a part of this research, we describe a strategy whereby β-D-glucuronic acid is formed at the end of the synthetic sequence by selective oxidation of C-6 hydroxyl, followed by protection with *tertiary*-butyl group in one single step. The target β-D-glucuronic ester **38** was synthesized as described in (**Scheme 2.3**). This approach avoids synthetic problems associated with the use of D-glucuronic acid such as epimerization of C-5, and poor glycosyl-donating properties. [300]

Scheme 2.3 Synthesis of β-D-Glucuronic ester scaffold **38** with two different protection group strategy; A) the protection of primary hydroxyl group using TBDMSCl; B) the protection of primary hydroxyl group using TBDPSCl

A)

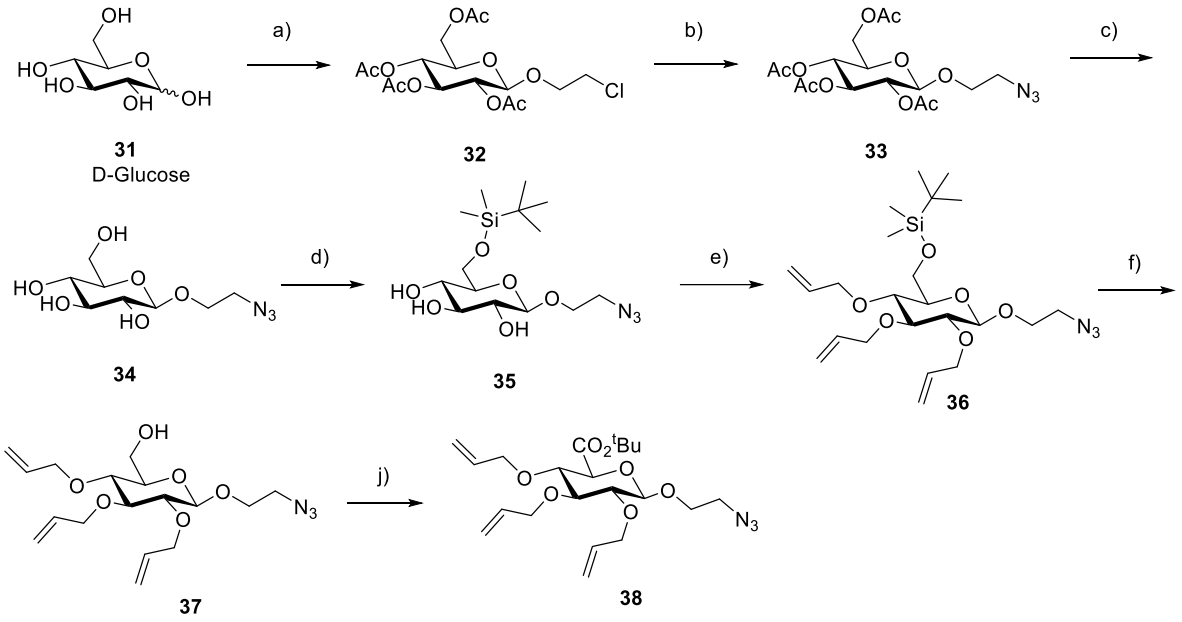

a) (*i*) Ac_2O, Py. 0 °C-rt, (*ii*) HO⁄⁄Cl, DCM, $BF_3.OEt_2$, - 40 °C to -10 °C, 12 h, 70%; b) NaN_3, *n*-Bu_4NI, DMF; 80 °C, 16 h, 80%; c) NaOMe, MeOH, rt, 5h, 95%; d) TBDMSCl, DMF, imidazole, 0 °C, 7h, 70%; e) Allyl Br, NaH, DMF, 0 °C- rt, 2.5 h, 92%; f) TBAF, THF, 12 h, 81%; j) PDC, *t*-BuOH, Ac_2O, DCM, rt, 7h, 74%.

B)

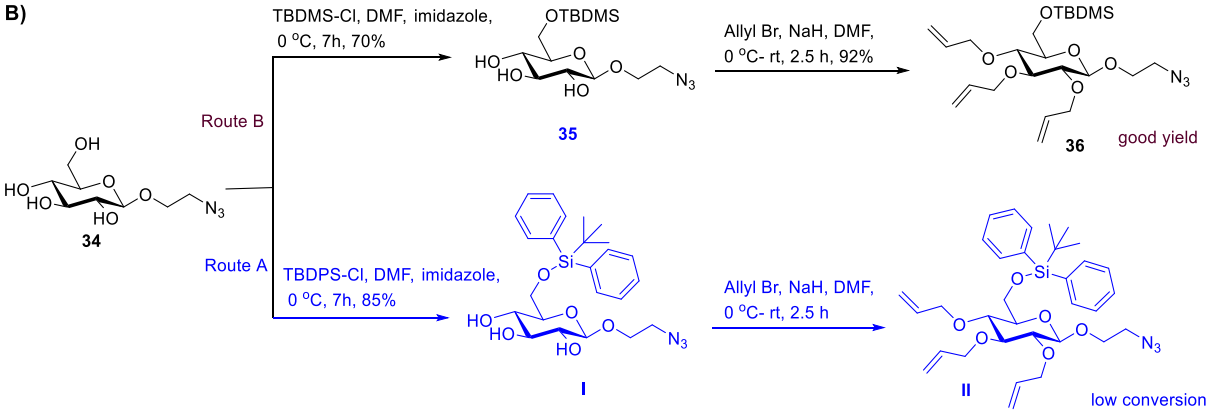

It is known that 2-Haloethyl glycosides are useful intermediates in the preparation of the corresponding 2-azidoethyl and 2-aminoethyl glycosides, and it is often used to generate multivalent displays of glycosides by grafting the azido derivative to alkyne-modified scaffolds by means of Cu-catalyzed azide-alkyne cycloaddition (CuAAC) reaction. Therefore, the synthesis started with glycosylation of common precursor D-glucose pentaacetate donor with 2-chloroethanol[301] in dichloromethane at -40 °C to -10 °C in the presence

of Lewis acid $BF_3.Et_2O$ afforded β-D-chloroethyl glucopyranoside **32** as a major product in 70% and α-form in 14% yield. [302, 303] Boron trifluroide etherate ($BF_3.Et_2O$) in dichloromethane at a temperature of -40 °C to -10 °C has been proved to be very suitable with regard to yield diastereoselectivity of the glycosylation. With the neighboring group participation of 2-*O*Ac the 1,2-*trans* product was obtained. [304, 305] The anomeric configuration of the newly formed β-D-glucopyranosides **32** was determined based on previous reports, based on the chemical shift values of the H-1 signals at δ= 4.58 ppm, and the coupling constant $J_{1,2}$ = 8.0 Hz, respectively, these values are in accordance with the reported data. [306]

One can manage the formation of the kinetical β- or the thermodynamical α-anomer by means of different reaction conditions. Conduct the reaction at a temperature -40 °C to -10 °C yield β-anomer as a major product, while running the reaction at 0 °C to room temperature yield α-anomer as a major product (**Scheme 2.4)**. The observed stereoselectivity, likely arises from the neighboring group participating leading to 1,2-trans glycosides. D-Glucose pentaacetate adopts preferentially chair conformation, where all the acetyloxy substituents are in equatorial positions. Thus, after interaction with the Lewis acid, BF_3.OAc is lost from hemiketals, the pyran oxonium ion maintains this most stable conformation. The carbocation is stabilized by the neighboring oxygen lone pair because of their planar arrangement. In this case, the oxacarbenium ion can be further stabilized *via* a bicyclic acyloxonium intermediate, which becomes the key intermediate on route to glycosylation products. Since the bottom face of the ring is blocked, nucleophilic attack of the glycosyl acceptor would be directed from the opposite, top face. This typically provides access to the 1,2-trans linkage with very high or complete stereoselectivity. [307]

Scheme 2.4 General outline of glycosylation and the key intermediates involves

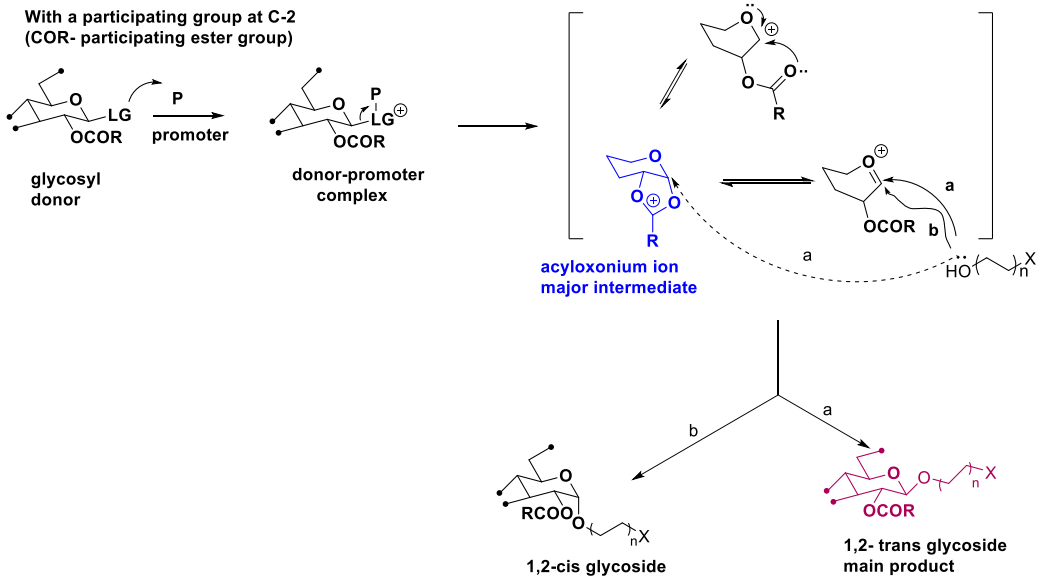

On the other hand, a kinetic anomeric effect is observed when the orbital interaction stabilizes the transition state of a bond-forming or bond-cleavage process. [308, 309] The anomeric effect is a stereoelectronic effect first encountered in carbohydrate chemistry, where it was observed that electronegative anomeric substituent preferred the axial α position. This is explained e.g., with a favorable hyper-conjugative interaction, only possible for the α- anomer, of the nonbonding orbital of the ring oxygen with parallel empty orbital located on the anomeric position.

The subsequent step is the nucleophilic displacement of chloride by the use of sodium azide in the presence of *n*-Bu_4NI and DMF at 80 ºC to afford β-D-glucopyranoside **33** in 90% yield. Followed by removing of acetyl groups according to Zemplén procedure using NaOMe/MeOH to obtain compound **34** in 95% yield. [310] Next, we turned our attention to install allyl moiety at three positions, *O*-2, *O*-3, and *O*-4. In this regard, it is important to selectivity protect OH group at C-6. In a first attempt, we used TBDPS-Cl as protecting silyl group. The reaction was performed using imidazole in DMF to afford TBDPS-protected glucopyranoside **I** in a good yield, (**Scheme 2.3 B**, *pathway A*). Next, allyl bromide was found to be a good reagent to process the allylation reaction in the presence of NaH as a base. In order to achieve full conversion to tri-allyl derivative **II**, 5.9 equiv of allyl bromide and 4.5 equiv NaH (60%) were used, under these conditions the desired product was obtained in low yield. The relatively lower conversion of the product is mainly due to the cleaving of the silyl group. We optimized the conditions for the synthesis of tri-allyl derivative by using *tert*-butyldimethylsilyl chloride (TBDMSCl), (**Scheme 2.3 A)**. Therefore the reaction of compound **34** with TBDMSCl in the presence of imidazole, [311, 312] afforded the desired product **35** in 70% yield after 7 h at 0 ºC. Subsequent reaction of **35** with allyl bromide and sodium hydride in DMF provided compound **36** in 70%, it was observed that TBDMS group survives some rather harsh conditions than TBDPS. The allylation at *O*-2, *O*-3, and *O*-4 positions was confirmed by ^1H NMR (**Figure 2.2**), A significant downfield multiple peaks at 6.12- 5.74 ppm which integrated for three allyl protons H_{10}, H_{17}, H_{21}. Another multiple peak at 5.28- 5.00 ppm are integrated for protons H_{11}, H_{18}, H_{22} and 4.4- 4.14 ppm for protons H_9, H_{16}, H_{20}. A distinct upfield singlet peak of TBDMS at 0.89 ppm that integrated for nine protons and another singlet peak at 0.05 ppm that integrated for six protons. ^{13}C NMR analysis for compound **36** shows peaks at 135.27, 135.14, 135.00 ppm are equivalent to C_{10}, C_{17}, C_{21}. Other peaks at 116.78, 116.76, 116.69 ppm which equivalent to C_{11}, C_{18}, C_{22}.

Figure 2.2 ^{1}H NMR analysis of compound **36** (300 MHz, $CDCl_3$)

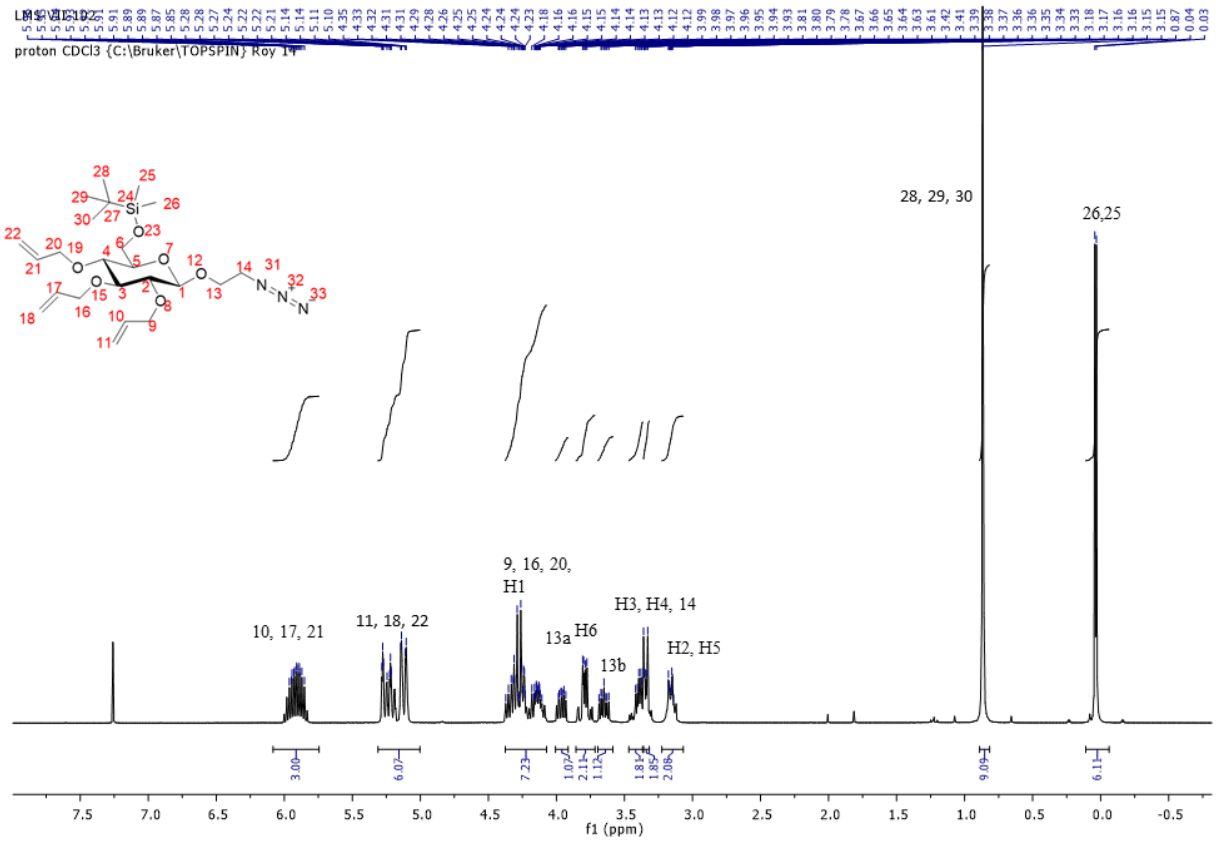

To accomplish the oxidation at C-6 hydroxyl group, compound **36** was subjected to the following two steps reaction sequence; *tert*-Butyldimethylsilyl (TBDMS) protecting group was removed by using tetrabutylammonium fluoride (TBAF). [313] When 5 equiv. TBAF (1.0 M in THF) was used, alcohol **37** was isolated in only 50 % yield. The lower yield was likely caused by the strong basic nature of TBAF as well as the hydroxide present in commercial TBAF. To optimize the yield, we envisioned that it would be helpful to add buffer and to control the reaction concentration. Thus, silyl ether cleavage with less TBAF (2.5 equiv.) and buffered with 20 mol % AcOH, led to cleavage of TBDMS group and provide alcohol **37** in 90% yield. Following Corey modified oxidation, [314] compound **37** was subjected to a one-pot sequence of reaction, consisting of oxidation of the primary hydroxyl group using pyridinium dichromate/ acetic anhydride, and the reaction of intermediate aldehyde with *tert*-butyl alcohol giving rise to *tert*-butyl β-D-glucuronic ester **38** in 74% yield, (**Scheme 2.3 A**). [315] From a mechanistic perspective, we demonstrate that *t*-BuOH acts as a nucleophile in the reaction and that initially formed a *tert*-butyl ester. The scaffold **38** were fully characterized by ^{1}H NMR spectroscopy (**Figure 2.3**). The vicinal of H-1 and H-2 couple to each other with $J_{1,2}$= 7.6 Hz. The reason for a large coupling constant between H-1 and H-2 is because of the axial/equatorial interaction, which clearly indicates the stereochemistry at the anomeric position. ^{1}H NMR yielded a distinct

singlet peak of *tert*-butyl at 1.50 ppm, is integrated for nine protons. the more downfield multiple peaks at 6.03- 5.78 ppm, are equivalent to the three protons from the double bond of allyl linker. Another multiple peaks at 5.35- 4.25 ppm, are equivalent to the remaining protons of allyl moiety. ^{13}C NMR for compound **38** shows a peak at 27.93 ppm, which confirms the presence of *tert*-butyl group. The more downfield peak at 167.63 ppm, is equivalent to the carbonyl group. Also, it is observed from NMR analysis, C_4-H shifted to more downfield at 3.55 ppm upon oxidation of C6.

Figure 2.3 ^{1}H NMR analysis of **38** (600 MHz, $CDCl_3$)

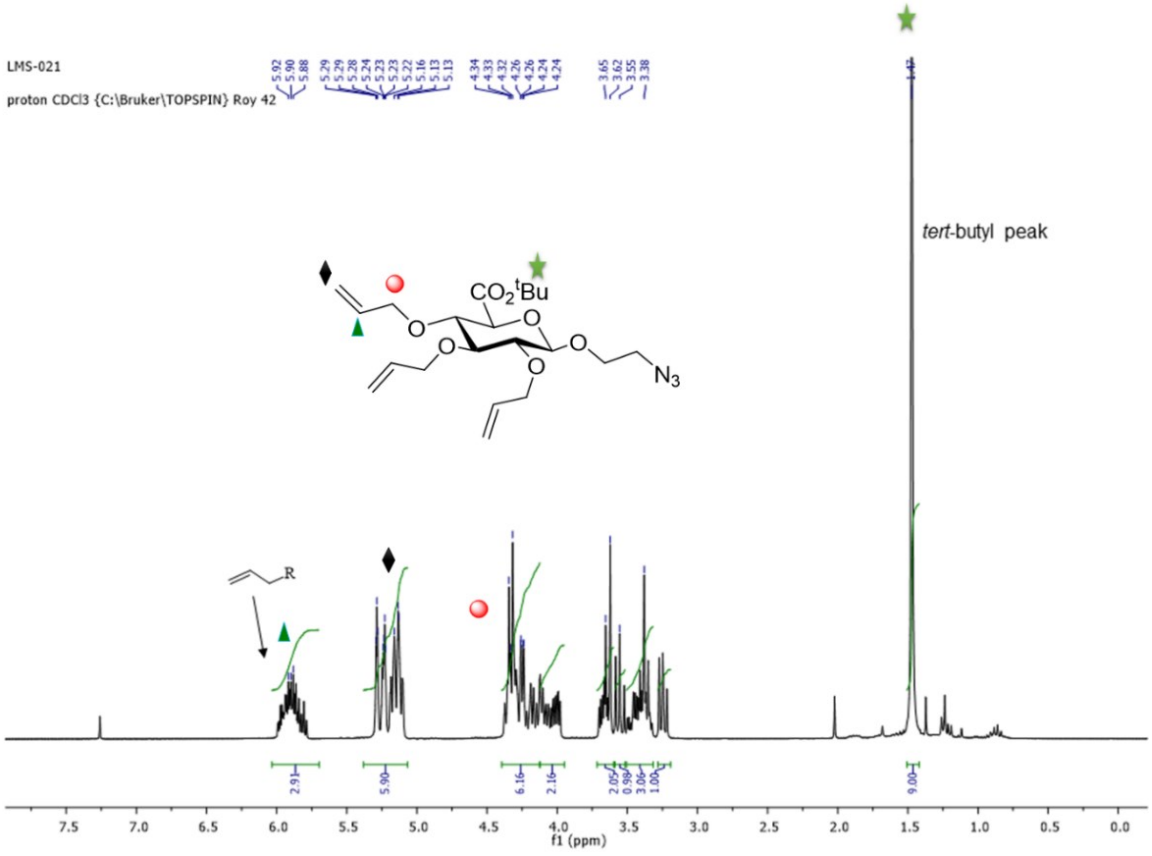

The information from IR spectra in combination with HRMS (see Supporting information), proved key to confirm the structure of **38**. (**Figure 2.4**) shows the specific absorption peak at 2100 cm^{-1} corresponds to azide group stretching vibration peak. The signal at 1738.38 cm^{-1}, shows the C=O stretch, confirming the presence of the carboxyl ester group.

Figure 2.4 IR spectra analysis of compound **38**

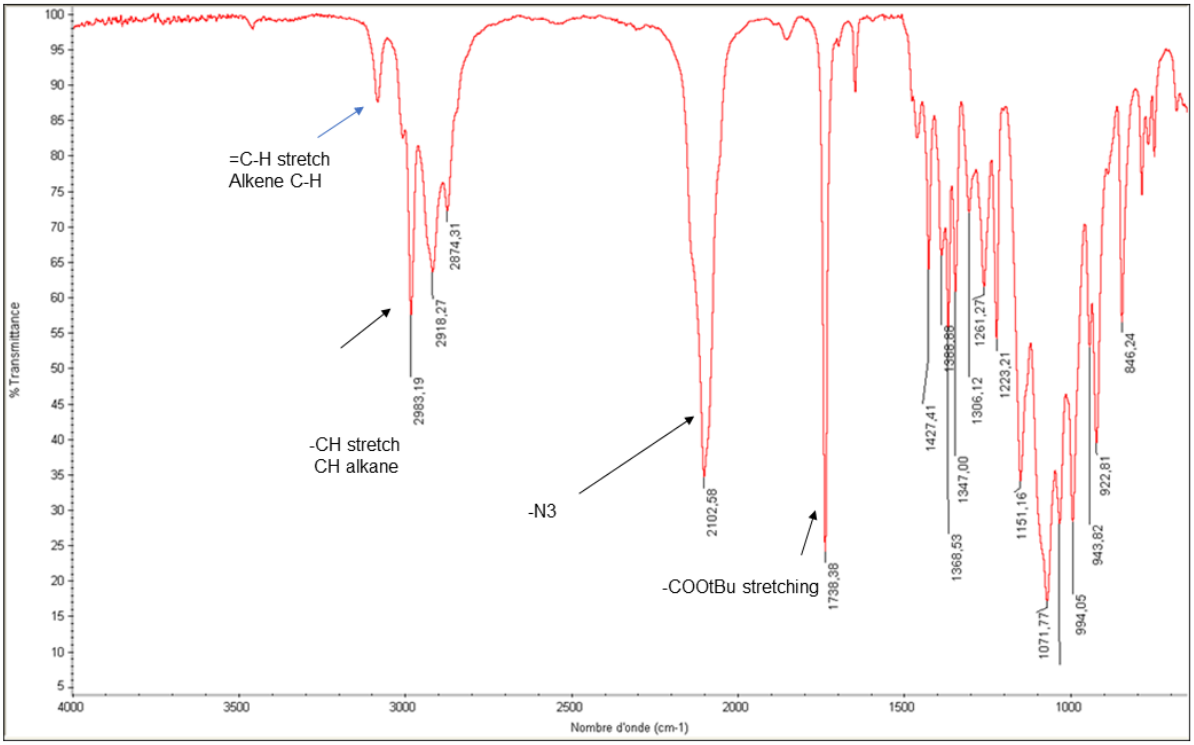

CHAPTER 3
A NOVEL CLASS OF FUCOSIDE AND MANNOSIDE HOMO GLYCODENDRIMERS BASED ON D-GLUCURONIC ESTER SCAFFOLD FOR CIPROFLOXACIN CONJUGATION

3.1 Introduction

The use of synthetic polymers in drug delivery is one such area that has drawn more interest in nanomedicine. The key feature for their success is their multivalence and their structure which can be modified to have suitable biological properties. However, despite all the achievements related to polymeric nanomedicine, there has been increased concern over the balance between efficacy and potential biological risk. This mainly results from a lack of knowledge of their biological interactions, particularly at biological interfaces. Consequently, the development of the next generation of polymeric drug delivery systems should be done along with an understanding of how they interact with the main biological components. In this regard, dendrimers are suitable drug delivery systems due to their precise structure that can be further modified to have specific biophysical characteristics. Furthermore, dendrimers can also be made of biocompatible and biodegradable building blocks. [316] Over several years many scaffold topologies have been explored for targeting LecB, and FimH, which provided us with more insight and information about the importance of scaffolds and linkers, which are important key elements in the field of lectin-targeted drug delivery. The important examples from the literature will be presented in the following sections.

3.1.1 Di-; Tri-; and Tetra- valent fucoside glycodendrimers for lecB (PA-IIL)

A broad variety of potential multivalent inhibitors were designed and tested against PA-IIL, including C-glycosidic glycomimetics, glycopeptide dendrimers, and photoswitchable Janus glycodendrimer micelles. [265, 317-318-321] Divalent ligand **45** was prepared from the disaccharide α-L- Fucα(1-4)-β-D-GlcNAc and dimeric linker using click conditions, $CuSO_4$/sodium ascorbate, (**Scheme 3.1a**), the dissociation constant (K_d) of this divalent ligand was measured, the low dissociation constant K_d= 90 nM was observed. [322] In another study, Roy and coworkers use a convergent procedure to synthesize several glycodendrimers and studied their binding properties to PA-IIL lectins from *P. aeruginosa*. Glycodendrimer **46** was obtained from the coupling of propargyl α-L-fucopyranoside and tetrazido ending dendritic core (**Scheme 3.1b**) using $CuSO_4$ and sod. ascorbate. [323, 324] The design suffered from a drawback, increasing the dendrimer generation did not cause further increase in the kinetics of binding with the lectin. This was explained by an unfavorable steric crowding with the lectin amino acids. [323]

Scheme 3.1 Examples of glycodendrimers inhibitors for *P. aeruginosa* lectin LecB

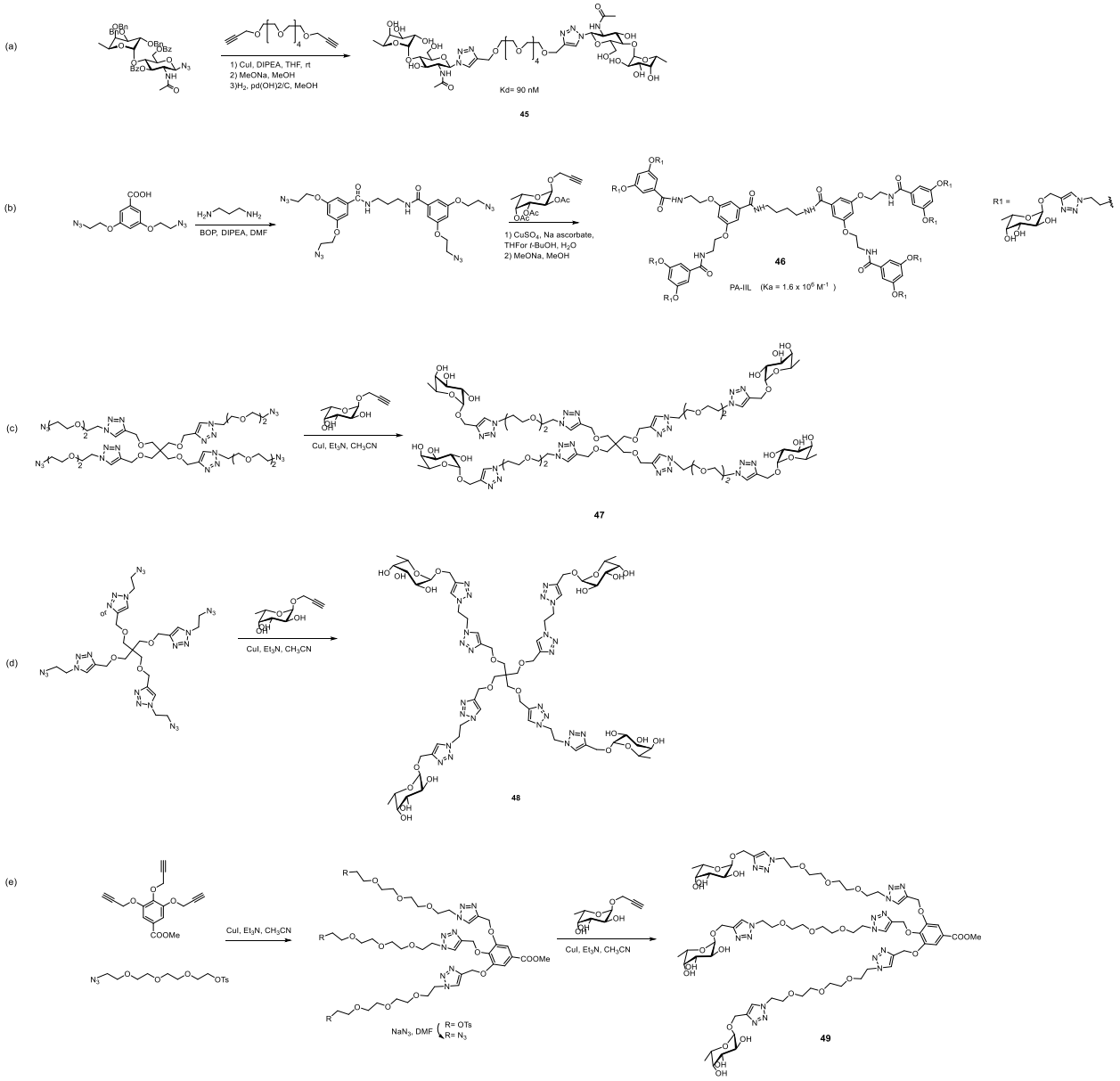

Son Thai le *et al*, synthesized a series of multivalent glycoclusters decorated with various α-L-fucoside. Fucoclusters **47**, **48**, and **49** have been created using a variety of structural components, beginning with the center cores undergoing two sequential 1,3-dipolar azide-alkyne cycloaddition click reactions (**Scheme 3.1**). The hemagglutination assay results from their investigation showed that tri- and tetravalent glycocluster-containing multivalent α-L-fucoside can inhibit *P. aeruginosa* LecB. (HIA), the best inhibitor, however, was determined by HIA to be the tetravalent glycocluster compound **47** (**Scheme 3.1c**), which was exothermic- and enthalpy-driven. Compound **47** had a significant protecting effect against *P. aeruginosa* adhesion, the inhibitor was able to reduce bacterial adhesion to ∼30% when used in the most effective

concentration (0.25 mM). The same group successfully synthesized a series of thio-α/β-1-fucopyranosides which are more stable in *vivo* due to the resistance to the degradative enzymes. The hemagglutination inhibition assays showed that the α-thio-fucopyranosides were generally better inhibitors than α-L-fucose for all lectins. Therefore, the thioglycosides could potentially use in the inhibitors to achieve higher stability towards glycoside hydrolase enzyme. Although the binding affinities increased to varying degrees compared to the monovalent control, none of the binding modes were experimentally verified because the orientation of the binding sites prevents chelation with relatively short multivalent dendrimers and the straight-line distances between the binding sites is long i.e., around 35-50 Å (**Figure 3.1a**). [325-322]

Figure 3.1 (A) The straight distance between the binding sites of LecB. [319, 326]

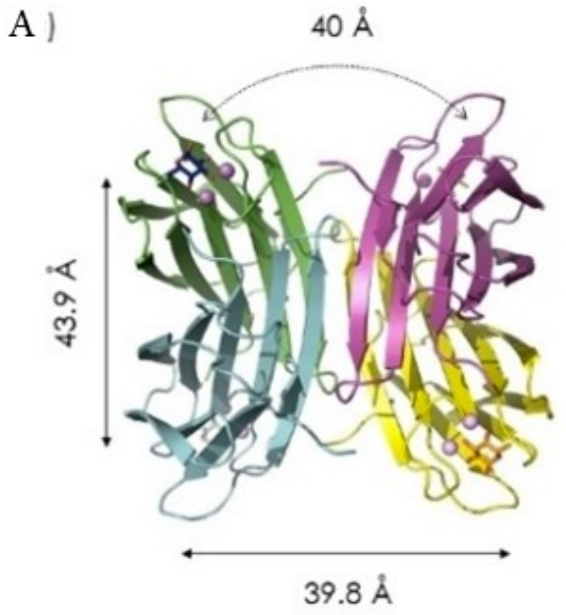

3.1.2 Tetravalent and multivalent glycodendrimers based on mannoside monomer

The development of FimH-targeting polyvalent scaffolds with a variety of mannose aglycones (**50**, **Scheme 3.2a**), with applications in the treatment of UPEC-induced UTIs, has been the subject of much investigation. For example, three of the main polyvalent mannose scaffolds that have been studied include multimeric heptylmannosides, [327] glycoclusters, [216], and dendrimers. Multimeric heptylmannoside is one of the most studied polyvalent scaffolds; these aim to build upon the high-inhibitory potency displayed by heptyl α-D-mannoside. Gouin and co-workers synthesized a series of multivalent glycoconjugates based on a 1,1,1-tris(hydroxymethyl)ethane or pentaerythritol core (**51**, **Scheme 3.2b**), and measured their inhibitory potencies, the data showed a positive correlation between potency and valency. [327]

Scheme 3.2 Important glycodendrimers inhibitors for *E. coli*/FimH with a variety of different aglycones

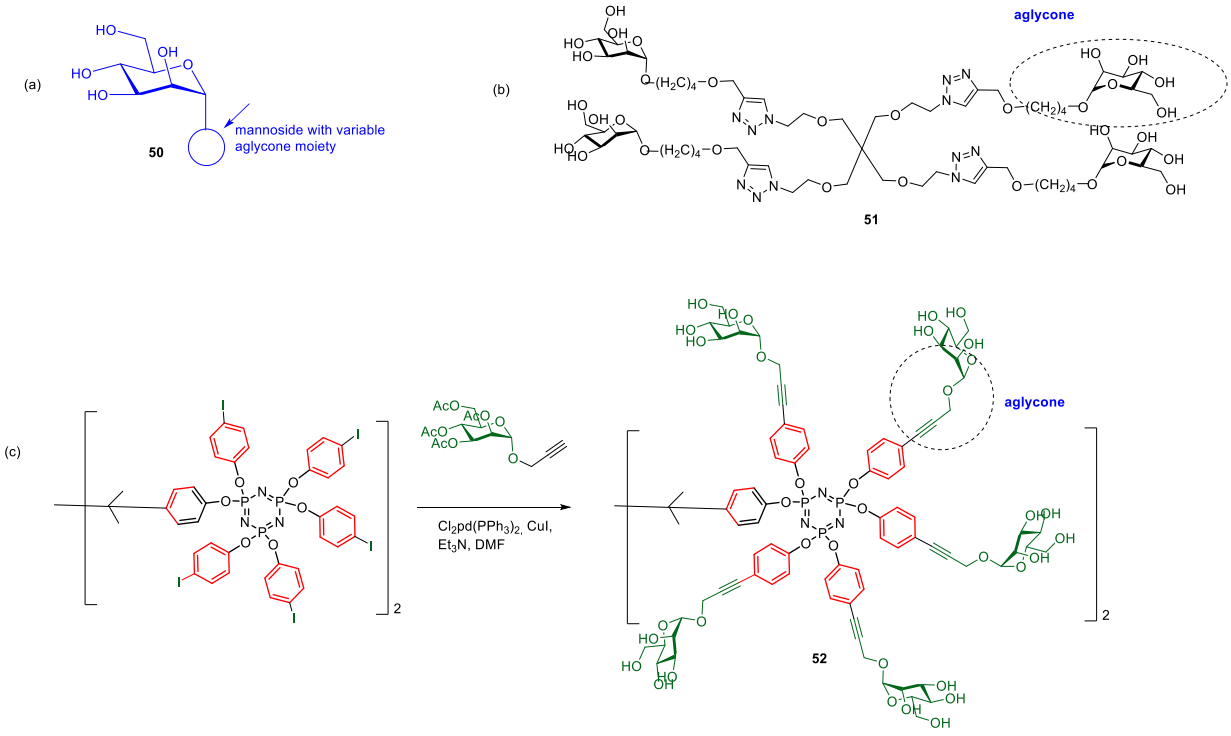

To develop new mannosylated dendrimers as potential drug candidates for gastrointestinal and urinary tract infections caused by *E.coli*, the group of Roy[328] synthesized the first synthesis of ‘‘Majoral-type’’multivalent glycodendrimers bearing covalently bound α-mannopyranosides (containing alkyne spacer) onto a cyclotriphosphazene scaffold, using single-step Sonogashira and click chemistry (**52**, **Scheme 3.2c**).

From these studies, we conclude that both the number and spacing of sugar ligands along with the macromolecular scaffolds strongly influence complex formation with lectins. The drawbacks of these methods, however, are the build-up of the dendritic wedges is time-consuming and the increasing steric hindrance, which occurs at the focal functional group with dendron growth, may inhibit its anchoring to a central core. Therefore, in this research, we present the synthesis of novel glycodendrimers using a double-stage convergent approach (**Scheme 3.3**). [329] In this strategy the core unit is synthesized divergently (see **Chapter 6**), and subsequently attached to dendritic wedges in a convergent method. In this chapter, we provide a details synthesis of trivalent dendrons that are lectins targeted. Finally, The assembly of these dendrons for the ultimate synthesis of glycodendrimers.

Synthetic approaches to macromonomers and their implementation in complex setting relevant to biology require development of mild synthetic methods characterized by chemoselectivity and modularity. A well-

established class of reactions that meets these criteria is click chemistry. Specifically, Cu(I)-catalyzed azide-alkyne cycloadditions (CuAACs) have been widely adopted, and numerous approaches are available for preparation of azides and alkynes. Moreover, diverse approaches, including thiol-ene photolytic reaction (TEC), diazo transfer and protection/deprotection groups strategy, were applied.

3.2 Results and discussion

Specifically, this project was designed to prepare the thiosugar based multivalent sugar clusters to enhance the binding affinity of sugar-lectin recognition. Additionally, the target mannoside or fucoside clusters are not only having specificity for bacterial lectin, but also the presence of sulfur atom in sugar moiety to display potent inhibitory activities toward glycosidases due to the higher specificity of the sulfur-containing sugars with the enzyme. [330] Therefore, the prepared trithiomannoside or trithiofucoside clusters may have significant potential in medicinal chemistry due to the high glycotope density. In this study, we show an interest to synthesize and study the *P. A* inhibition properties using trithiofucoside moieties and *E.coli* inhibition properties using trimannoside moieties with different dendritic cores. The photoinitiated thiol-ene click reaction of tri-*O*-allyl derivative **38** and 2,3,4,6-tetra-*O*-acetyl α-D-mannopyaranose thiol **67** and 2,3,4-tri-*O*-acetyl α-L-fucose thiol **63** are used to synthesize trimeric form of mannoside dendron and fucoside dendron respectively, and the structures of thioglycodendron that are synthesized using click strategy are depicted in the (**Scheme 3.3)**.

3.2.1 Design of a novel thioglycodendrons for lectin-targeted

Two different dendritic wedges (thioglycodendron) **80**, and **83** were synthesized (**Scheme 3.3)**. These molecules are composed of two generations: targeting moiety (G3) (trimeric Man or Fuc) linked to the D-glucuronic ester scaffold (G2). A schematic overview of the molecular structures is shown in (**Scheme 3.3**), which demonstrated that these two target dendrons could be synthesized from three building blocks: monosaccharides **67** and **63**, and β-D-glucuronic ester (**38**). The following sections will introduce the details synthesis of two different thiol monomers, **63** and **67**.

Scheme 3.3 The molecular structures of the newly synthesized dendritic wedges **80**, and **83**

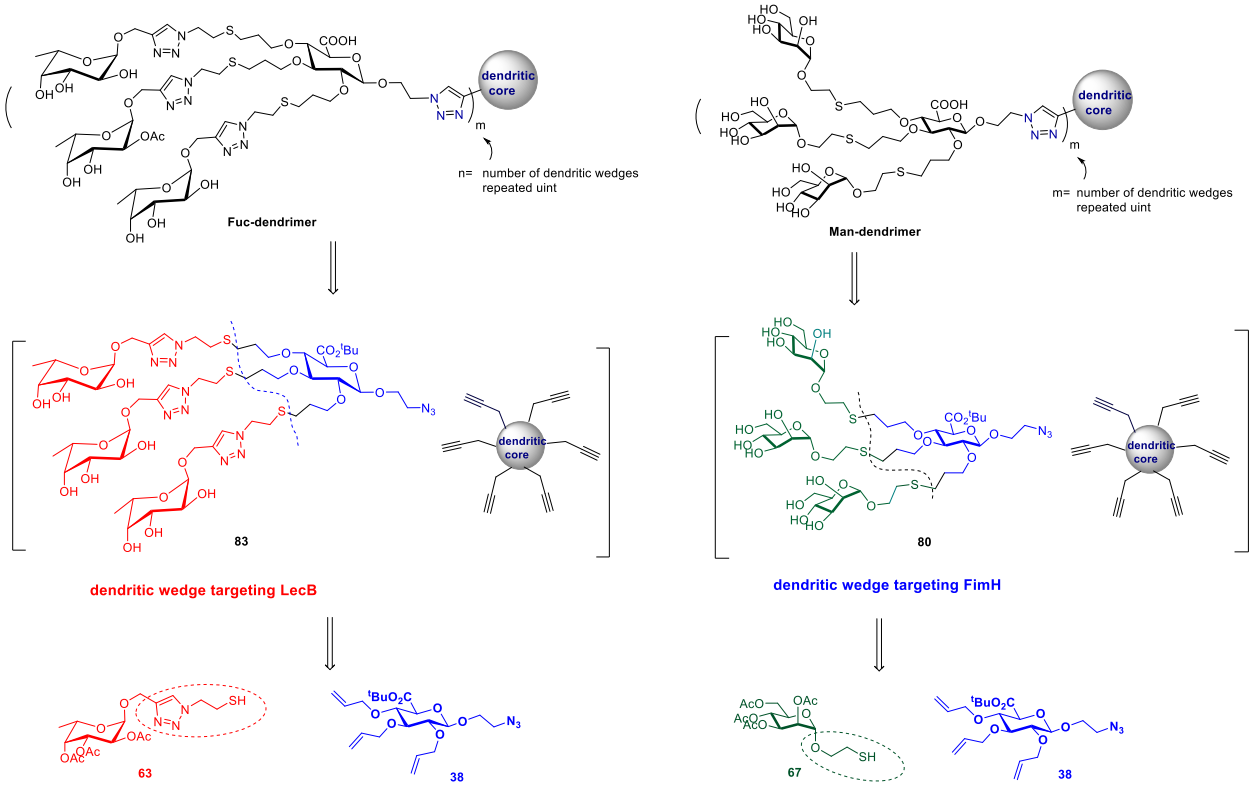

3.2.2 Synthesis of novel 1,4-triazole, and 1,5-triazole α-L-fucoside thiol monomers **63**, and **67**

The structural basis of the great inhibitory potential of 1,5-triazole α-L-fucoside is elucidated in the docking model experiment (**Figure 3.2 A**). The additional interaction of the triazole ring is congruent with the high affinity found for the synthetic inhibitors.

The potential of ligand-based design of the glycodendrimer-drug delivery system is ruled by the structural mimicry of natural ligands and extends into the blocking of bacterial adhesions. Therefore, in our research, we envisioned the design and synthesis of 1,4-triazole α-L-fucopyranoside thiol **54** and its isomer 1,5-triazole α-L-fucopyranoside thiol **55**, (**Figure 3.2 B**).

Figure 3.2 (A) Docking model of the interactions between the terminal 1,5-triazole α-L-fucoside **53** and the protein; (B) the two different analogues 1,4-triazole α-L-fucoside thiol **54**, and 1,5-triazole α-L-fucoside thiol **55**, used in this studying

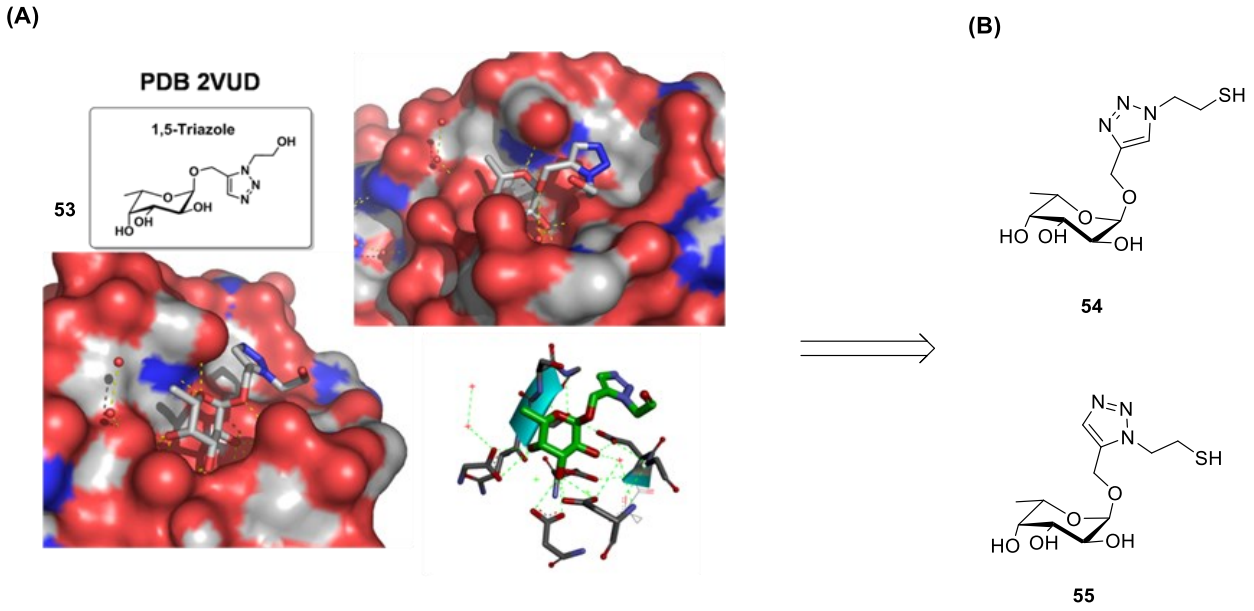

Initially, we set out to identify a site for installing thiol groups to be used in our planned thiol-ene reactions. [331-335] Another explanation for this is that 1,2,3-triazole make an excellent linkers. Many evidences approved that the triazole group displays structural and electric similarities to the amide bind, mimicking a Z or an E-amide bond depending on the patterns of substitution (the 1,4-disubstituted triazole moiety shows similarity with a Z-amide bond, on the other hand, the 1,5-substitution pattern mimics the E-amide bond). Thiol L-fucoside harboring 1,4- or 1,5-triazoles **54** and **55** were synthesized from the same intermediates using CuAAC and RuAAC respectively. The synthesis of propargyl fucoside was reported but the introduction of a longer clickable fucoside thiol has not been reported. The key challenge is the synthesis are α-glycosylation along with the acid lability of L-fucose. [336, 337]

The approach toward the synthesis of α-L-fucose thiol synthesis which bears a triazole chain at the L-fucose alpha position, is depicted in (**Scheme 3.4)**. The synthesis started with the acetylation of L-fucose **56** in a mixture of acetic anhydride and pyridine to obtain 2,3,4-tri-*O*-acetyl-L-fucose **57** as a mixture of α- and β-isomers. Subsequent glycosylation of **57** with propargyl alcohol in presence of $BF_3.Et_2O$ provided 1-propargyl 2,3,4-tri-*O*-acetyl-α-L-fucoside **58** as a major product. [338] In attempts to synthesize **58**, other researchers proposed alternative synthetic strategies. [339] In 2007, Mukhopadhyay *et. al* described the preparation of the alpha anomer of *O*- Propargyl fucoside by Fischer-type glycosylation. [323, 340-342] Sulfuric acid treatment of unprotected fucose in the presence of silica, and propargyl alcohol, afforded the product

as the α/β mixture. Due to the high polarity of the product and difficulty in separation on column chromatography, therefore, this mixture was subjected to acetylation to afford α/β isomers (12:1) in 74%. Despite being useful, the reaction conditions suffer from a number of serious shortcomings such as the use of large excess of alcohols (important concerns for costly alcohols), strong mineral acids or Lewis acids, preparation of catalysts in some cases, longer reaction time, decomposition of the product under reaction conditions, the requirement of special techniques. In this context, in 2011 Kumar Misra *et. al.* described the synthesis of alkyl glycosides using sulfamic acid in the Fischer glycosylation of unprotected reducing sugars under neat reaction conditions. [342] In contrast, our proposed synthetic strategy (**Scheme 3.4**), relies upon using L-fucoside as a glycosyl donor which underwent glycosylation with propargyl alcohol in dichloromethane, using $BF_3.Et_2O$ as a promoter, which afforded a crude product as a mixture of α-, and -β *O*-propargylated fucosides **58** and **59**, these two isomers were successfully separated by using column chromatography to afford the α-isomer **58** in 70% yield. We did not isolate the corresponding β-linked isomer **59** and so we are unable to comment on selectivity with respect to glycosylation. Overall, the experimental setup was much easier than for Fischer glycosylation and the yield of the desired α-*O*-propargylated fucoside **58** was quite high.

Scheme 3.4 Synthesis of 1,4-triazole α-L-fucoside thiol **63**

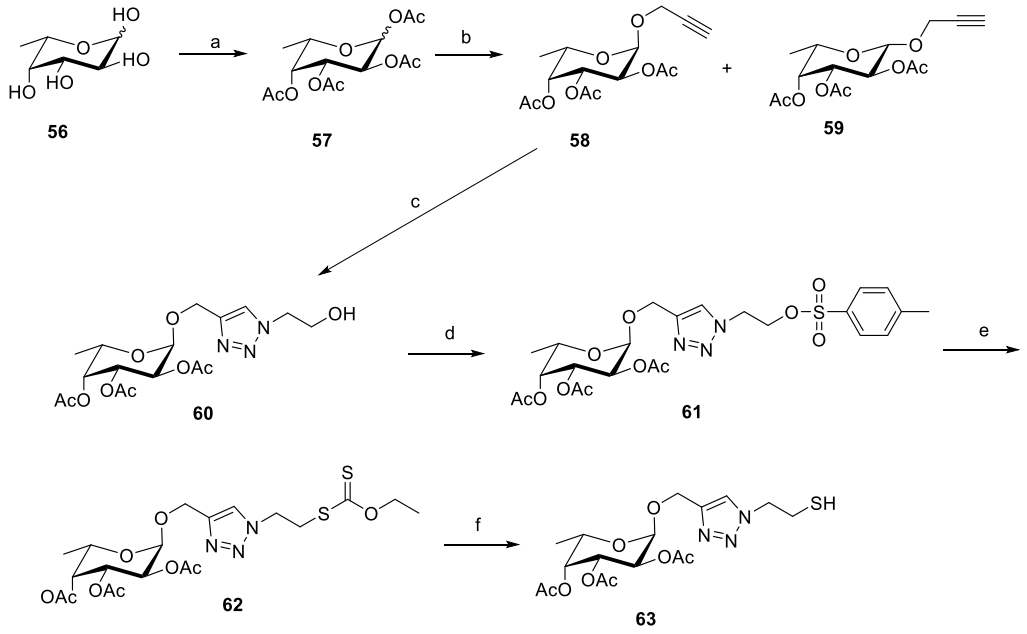

a) Ac_2O, pyridine., 0 °C- rt, 12h; b)  , $BF_3.Et_2O$, DCM, 0 °C- rt, 7h, 73%; c), $CuSO_4.5H_2O$, sod. ascorbate, THF/H_2O, rt, 24 h, 85%; d) *p*-TSCl, NEt_3, DCM, rt, 7 h, 95%; e)  , acetone, rt, 12 h, 90%; f) *n*-$BuNH_2$, THF, rt, 2h, 75%.

^{1}H NMR analysis of **58** (**Figure 3.3** and **Figure 3.4**, respectively), showed the coupling constant between H_1 and H_2 to be J= 3.7 Hz, confirming axial- equatorial coupling between these two protons, which indicated that the anomeric proton has the right configuration.

Figure 3.3 Conformational analysis of **58**. Double-headed arrows indicated coupling between H_1-H_2

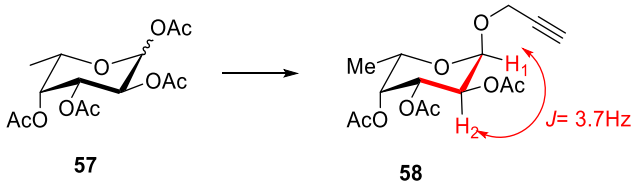

Figure 3.4 ^{1}H NMR analysis of **58** with an enlargement of the area from 1.05 to 1.15 ppm, and the area from 5.10 to 5.35 ppm

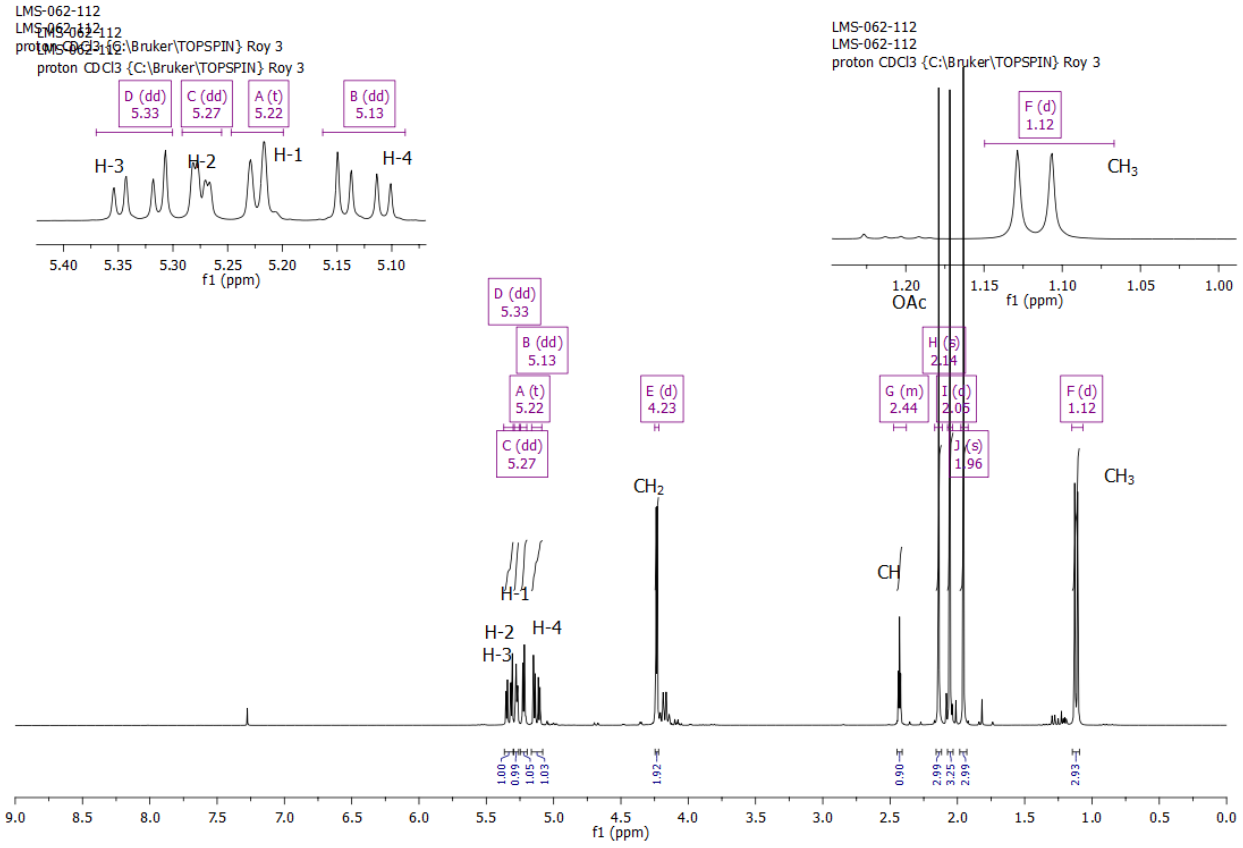

It is known that protective groups in the glycosyl donor influence the stereochemistry of glycosylation. this selectivity may arise from 1,2-trans directing effect of acyl substituents at *O*-2 which is widely employed in oligosaccharides synthesis. [343] However, there is some experimental evidence that acyl groups at other positions may also influence the stereoselectivity of glycosylation. Particularly such effects were observed

for 4-*O*-acylated fucosyl bromides[343-345] and ethylthio galactoside with a non-participating group at *O*-2.[346] The influence of acetyl group at *O*-3 of the fucosyl donor **57** was shown to have a larger effect on the efficiency of α-fucosylation. It is hypothesized that this is a result of the ability of acetyl group at *O*-3 to participate in glycosyl cation stabilization.[347] The acyl group at *O*-3 may share the positive charge in the glycosyl cation **I** by forming a stabilized bicyclic cationic intermediate **II** (**Figure 3.5**). Such intermolecular interaction favors further nucleophilic attach from α-side as compared with the case of glycosyl cation **I** whose interaction with nucleophile is not specifically stereocontrolled from α- or β-sides. The stabilization also involves intermediate **III**.

Figure 3.5 Delocalization of the positive charge in the intial glycosyl cation I via intramolecular participation of acetyl group at *O*-3

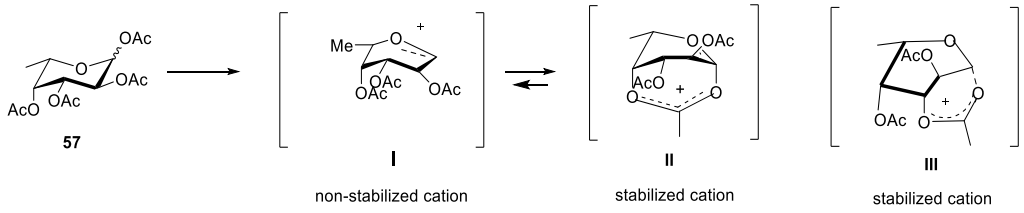

Compound **58** is stabilized by anomeric effect, with an axial alkoxy group, (**Figure 3.6**). In explaining this stereochemical phenomenon, anomeric effect, it is common to rely on an orbital-interaction argument. Thus, the overlap of the nonbonding, occupied n-orbital of the acetal oxygen atoms with unoccupied σ* orbitals from the other C-O bond is accompanied by delocalization of electrons and thus stabilization, (**Figure 3.6 a**). In the α-configuration with axial oxygen, two such interactions are possible, whereas an equatorially oriented oxygen **59** can engage in only a single [n(*O*)- σ*(C-H)] overlap, so the latter is energetically less favorable structure, (**Figure 3.6 b**).

Figure 3.6 Conformation of fucoside; *Exo*- and *Endo*- anomeric effects

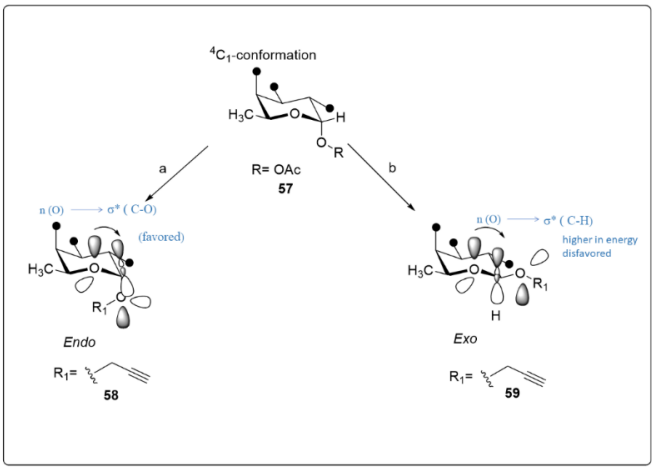

Structure **58** is preferred because it avoids positioning the ether C-O bond in the equatorial arrangement as shown for **59**, wherein its interaction with HOMO-LUMO would lead to a lowering of its energy and thus an increase of the activation energy for glycosylation.

O-propargyl α-L-fucoside **58** was subsequently reacted with azido ethanol in the presence of a copper (II) salt and a reducing agent to obtain precursor **60** in 85% yield (**Scheme 3.4**). [348] ^{1}H NMR analysis of **60** showed proton of triazole ring at δ= 7.63 ppm, (**Figure 3.7**).

Figure 3.7 ^{1}H NMR analysis of compound **60**

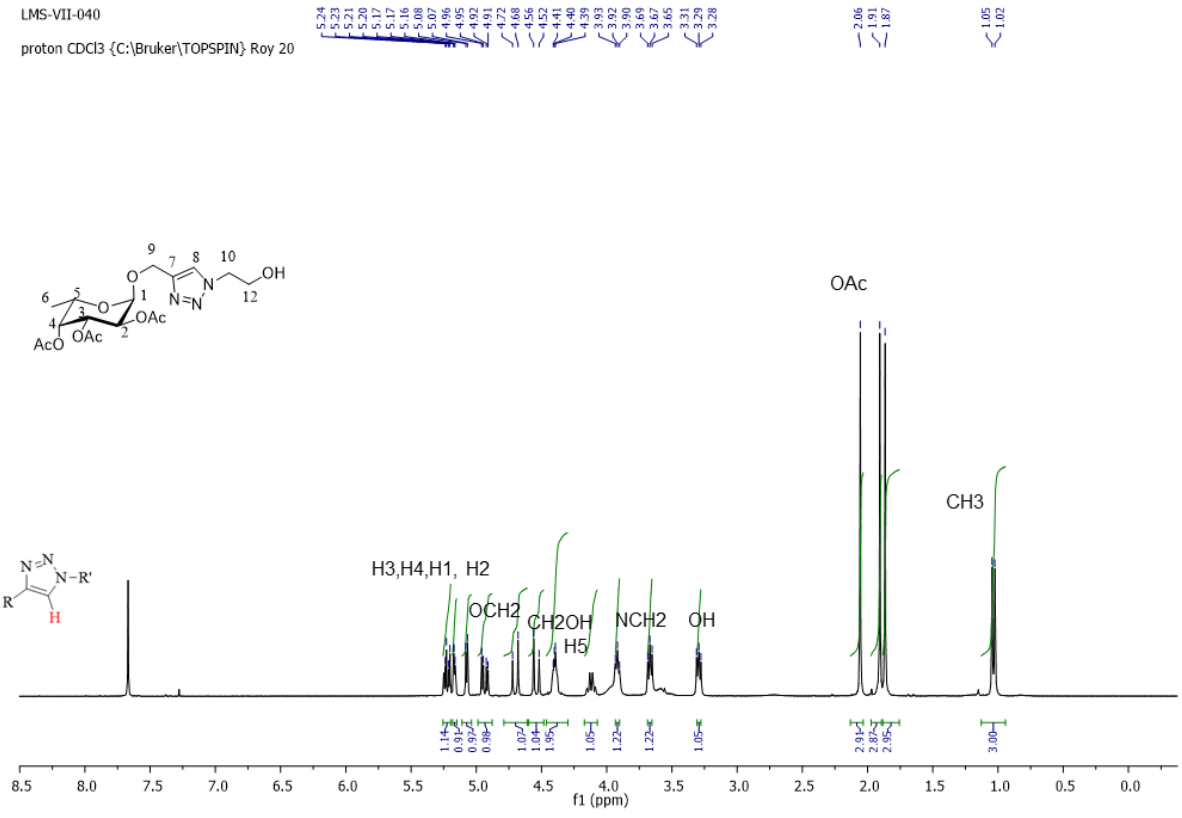

We focused next on the synthesis and characterization of fucoside with a thiol group, which is an active moiety in thiol-ene coupling reaction. As shown in (**Scheme 3.4**), compound **60** was subjected to the following three steps. The first step is to convert the hydroxyl group to a good leaving group for the subsequent step. Thus, the reaction of compound **60** with *p*-toluenesulfonyl chloride (*p*-TSCl) in the presence of Et_3N, provided tosylate **61** in 95%. ^{1}H NMR analysis of **61** shows a distinct peaks of the tosylate group (**Figure 3.8** top). A significant singlet peak from the methyl group appears at 2.5 ppm, and multiple peaks appears at 7.77, and 7.33 ppm which are equivalent to four aromatic protons. Next, the reaction of

compound **61** with potassium ethyl xanthogenate in dry acetone at room temperature, [349, 350] provided α-L-fucoside xanthate **62** in 95% yield. [351] The product was characterized by ^{1}H NMR and ^{13}C NMR analysis.

Figure 3.8 ^{1}H NMR analysis of compounds **61**(top**)** and **62** (bottom)

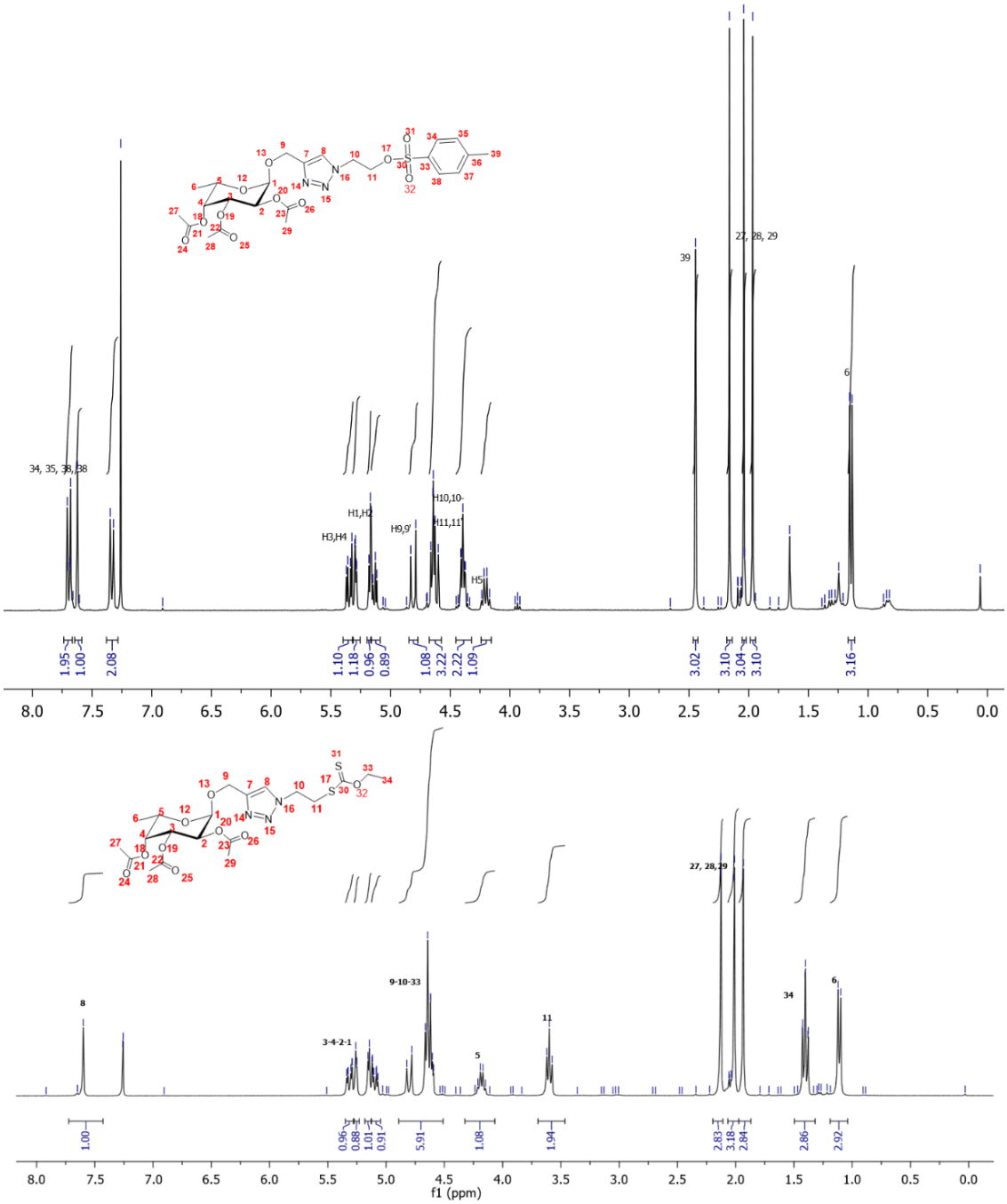

^{1}H NMR spectrum of **62** (**Figure 3.8**, bottom) showed the existence of 5 protons at 4.68 and 1.41 ppm, which correspond to the integration of -CH_2 and -CH_3 xanthate ethyl group. ^{13}C NMR analysis of **62** also showed a significant peak at 213.1 ppm of carbonyl xanthate, (see Supporting information).

The next step is the treatment of **62** with *n*-butylamine for the deprotection of the xanthate group, the reaction proceeded in dry THF to afford α-L-fucoside thiol **63**. [349] Since the reactive thiol end group tend to oxidize, resulting in disulfides which cannot react during the TEC, therefore, it was important to adjust the reaction parameters. The effect of using *n*-butylamine in the reaction mixture was evaluated. The optimal amount was determined to be 1.3 equiv, reaching the highest yield. A second parameter studied was the duration required to liberate free thiol group. Through a series of control experiments, it was determined 2 hours as optimal, enable efficient synthesis of ample quantities of **63** (75%).

Figure 3.9 ^{1}H NMR analysis of compound **63**

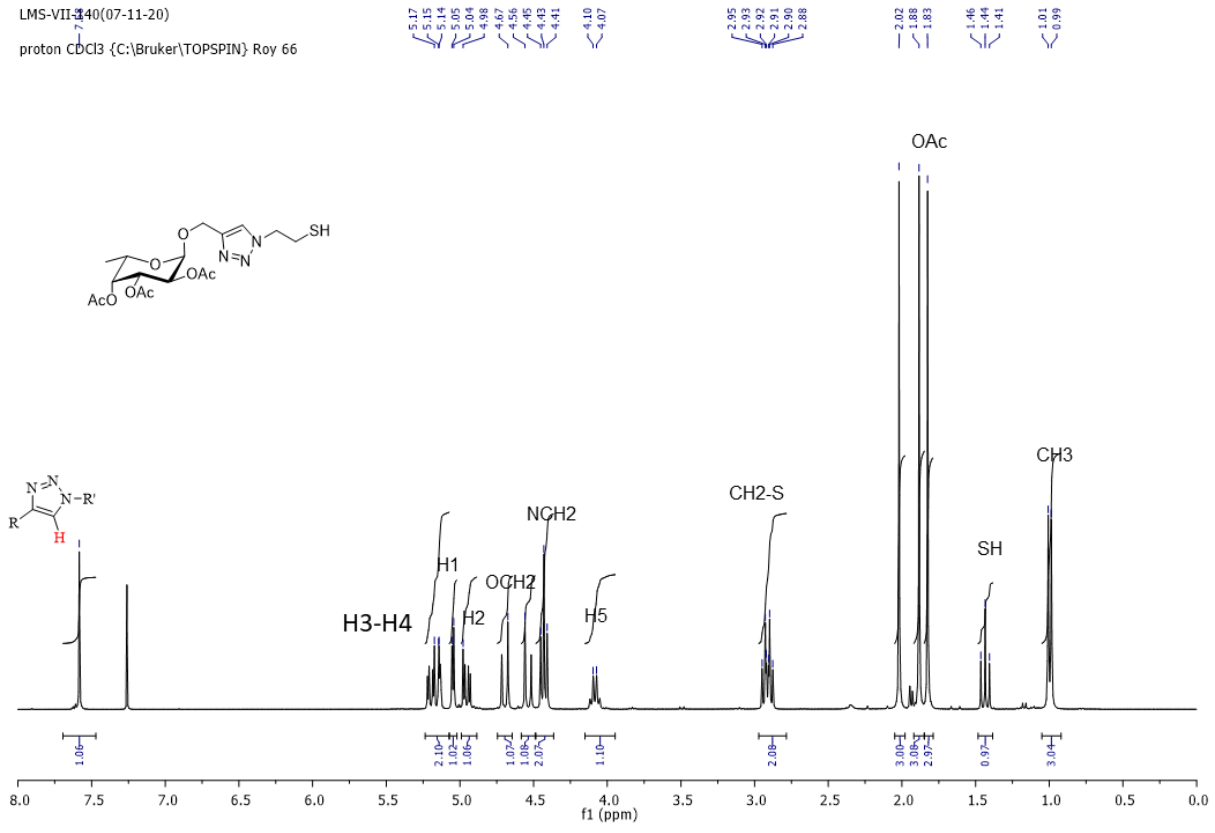

The structure of α-L-fucoside thiol **63** was confirmed by ^{1}H NMR analysis (**Figure 3.9**). The triplet peak at 1.46-1.41 ppm which is the significant peak for -SH group, and a doublet of triplets (dt) at 2.91 ppm is equivalent to -SCH_2. The molecular weight of fucoside thiol **63** was also confirmed by using electron ionization mass spectrometry (ESI-MS). In (**Figure 3.10**), two peaks of free fucoside thiol were detected at

a molecular weight of $[M+H]^+$ 433.0 and $[M+Na]^+$ 455.0 which is consistent with the theoretical molecular weight of α-L-fucoside thiol $C_{17}H_{25}N_3O_8S$ $[M+Na]^+$ 454.46, or $C_{17}H_{25}N_3O_8S$ $[M+H]^+$ 432.46.

Figure 3.10 ESI-MS spectrum of α-L-fucoside thiol **63**

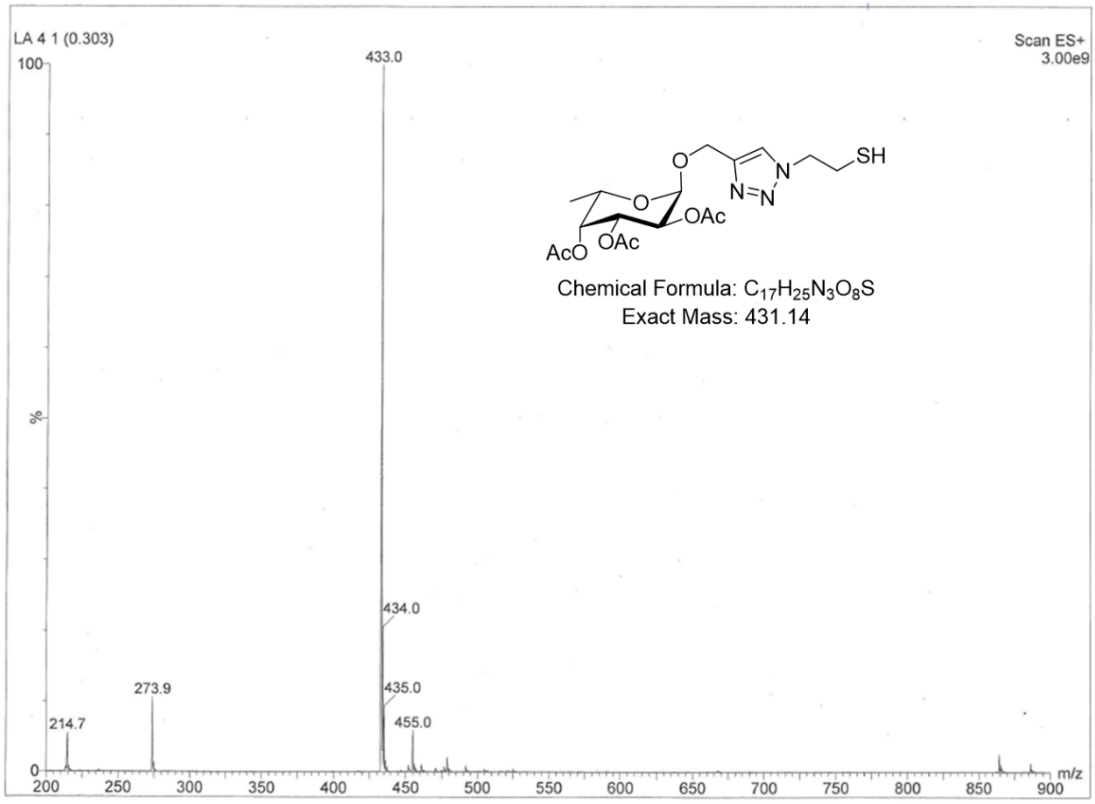

3.2.3 Synthesis of 1,5 α-L-fucoside thiol **64**

A similar strategy has been used to synthesize the 1,5 L-thiofucoside isomer, (**Scheme 3.5**). Early efforts toward the synthesis of 1,5-disubstituted fucoside isomer was carried out under thermal condition. However, 1,3-cycloaddition of 2-azidoethanol and *O*-propargylated fucoside **58** afforded a mixture of 1,4- and 1,5-disubstituted triazole (2:1, 3:4), that were not readily separable by chromatography. Fokin *et al* [352] showed that by using Ru (II) catalyst resulted in an efficient way to access 1,5-triazole regioselectivity. Given the remerkable cycoaddition selectivity observed, we decide to proceed to use Ru catalysts reaction to the synthesis of 1,5 L-fucoside thiol. In this research, the initial experiment was performed in the presence of 2.5 mol % Cp*RuCl $(PPh_3)_2$ at 60 °C in dioxane, wherein only 39% conversion was obtained after 12 h. Increasing the loading of the Ru catalyst to 5 mol% gave full conversion and an 80% isolated yield of **64**.

Scheme 3.5 Synthesis of 1,5-triazole α-L-fucoside thiol **65**

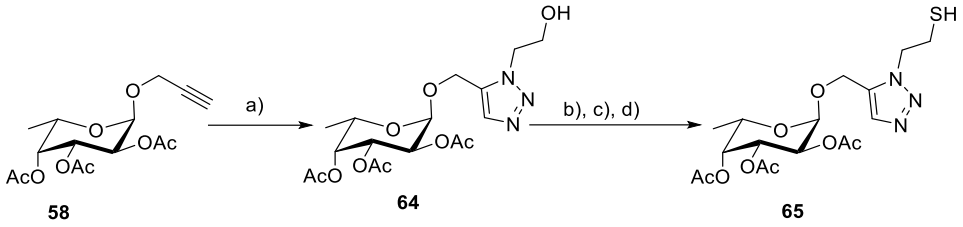

a) N_3⁓OH, Cp*RuCl $(PPh_3)_2$, dioxane, 60 °C, 36h, 80%; b) *p*-TsCl, NEt_3, DMAP, DCM, rt, 7 h, 95%; c) EtO(S)C⁻ SK^+, acetone, rt, 12 h, 90%; d) *n*-$BuNH_2$, THF, rt, 2 h, 70%.

The ^{1}H NMR spectra of 1,4- and 1,5 triazole proton ring, (**Figure 3.11** and **Figure 3.12**, respectively), showed the proton of 1,4-isomer at δ =7.63 ppm, while 1,5-regioisomer showed the triazole proton at δ= 7.67 ppm. Moving forward with 1,5 triazole α-L-fucoside **64** in hand, the desired analogue fucoside thiol **65** was synthesized following the same sequence we previously used.

Figure 3.11 Comparison between fucoside 1,4- and 1,5 triazole ring proton chemical shift

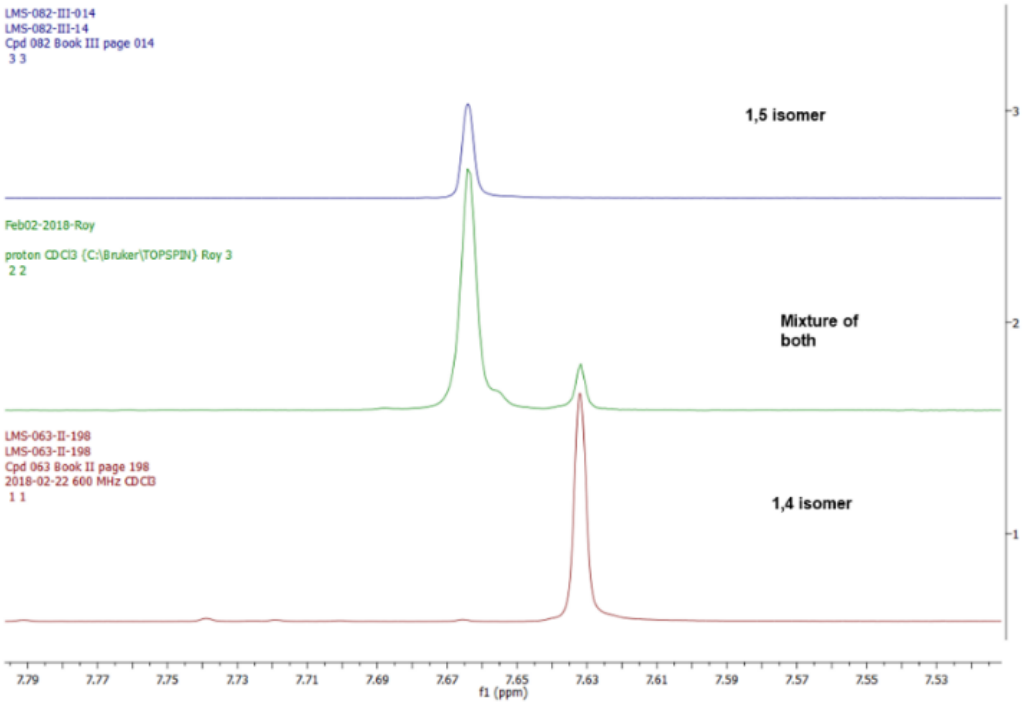

Figure 3.12 ^{1}H NMR analysis of 1,5 triazole α-L-fucoside **64**

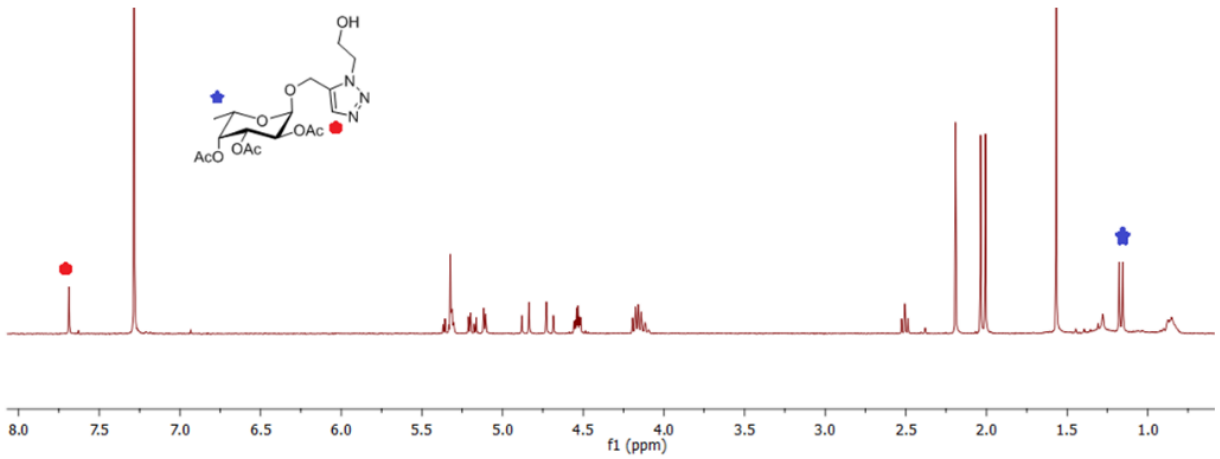

3.2.4 Synthesis of α- D-mannoside thiol **67**

The synthesis of α-D-mannosyl thiol **67** is depicted in (**Scheme 3.6)**. The synthesis started with glycosylation of mannose pentaacetate[353] **66** with 2-bromoethanol in the presence of $BF_3.Et_2O$ to yield 2-bromoethyl α-D-mannopyranoside as a mixture of α- and β-isomers in (85:15) ratio. [354, 355] Both isomers were separated by flash column chromatography to obtain the desired product 2-bromoethyl α-D-mannopyranoside in 60% yield. Next, we focused on α-D-mannose thiol synthesis.

Scheme 3.6 Synthesis of mannoside thiol **67**

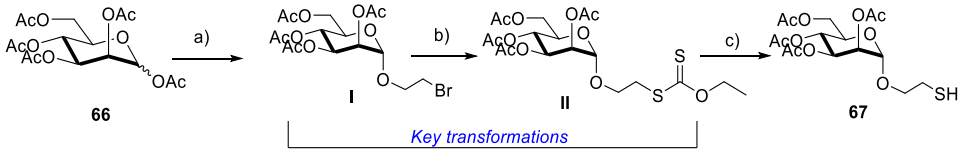

a) HO⁄⁄Br, $BF_3.Et_2O$, DCM, 36 h, 60%; b) KS⁄⁄S⁄O , dry acetone, rt, 7 h, 90%; c) *n*-$BuNH_2$, THF, 5 h, rt, 80%

The preparation of the mannose thiol **67** was previously reported by Roy group. [356] We investigated optimization to their procedure to enable access to large amounts of thiol **67**, because it features prominently early in the synthetic approach (**Scheme 3.6**). To this end, 2-bromoethyl α-D-mannopyranoside **I** was subjected to nucleophilic substitution by potassium ethyl xanthate in dry acetone obtaining **II**, followed by selective xanthate deprotection with 1.3 equiv *n*-butylamine in THF to liberate free thiol **67** in 84% yield The structure of the final mannose thiol was confirmed using ^{1}H NMR, (**Figure 3.13**).

Figure 3.13 ^{1}H NMR analysis of Man thiol **67**

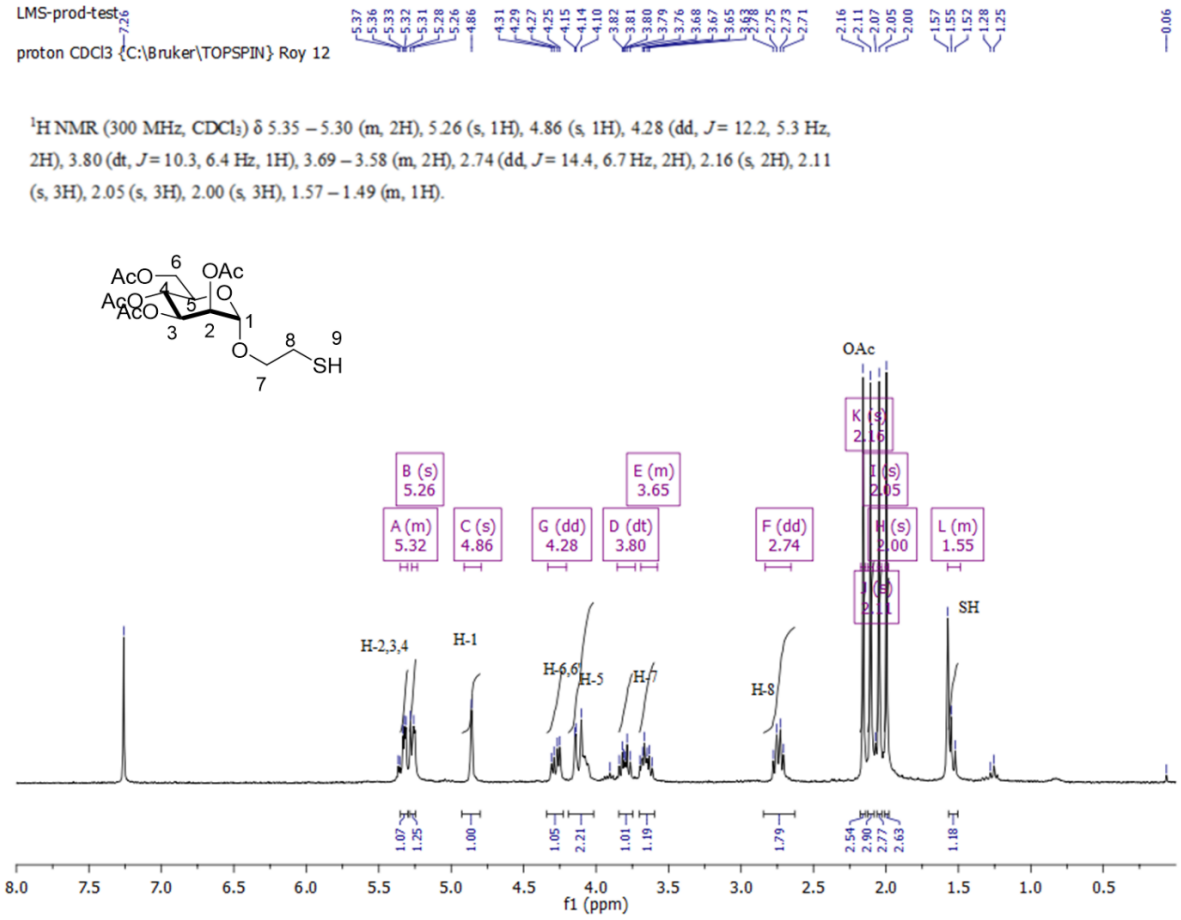

The successful synthesis of α-L-Fuc thiol, and α-D-Man thiol monomers, setting the stage for preparation of trithioglyco dendrons. As a result, several trivalent molecules have been synthesized as explained in the following sections.

3.3 Synthesis of lectin-targeted carbohydrate β-D-glucuronic ester conjugates (G3)

3.3.1 Tri-thiomannoside β-D-Glu ester and tri-thiofucoside β-D-Glu ester dendrons

Thiol-ene reaction is a photolytic technique for establishing a very stable thioether bonds (C-S bond) with minimal disruption to the function of the protein. It is a highly efficient and powerful approach for directly accessing structurally diverse buildings in a single operation. [162, 357, 358] With all building blocks **38** ,**63**, and **67** in hand we began to assemble LecB-targeted fucoside and FimH-targeted mannoside dendrons, respectively, (**Scheme 3.7**).

Scheme 3.7 Reaction overview of the thiol-ene coupling between: (A) α-L-fucoside thiol and tri-allyl β-D-glucuronic ester, resulting in trithiofucoside molecule **68**; (B) α-D-mannoside thiol and tri-allyl of β-D-glucuronic ester, resulting in trithiomannoside molecule **69**

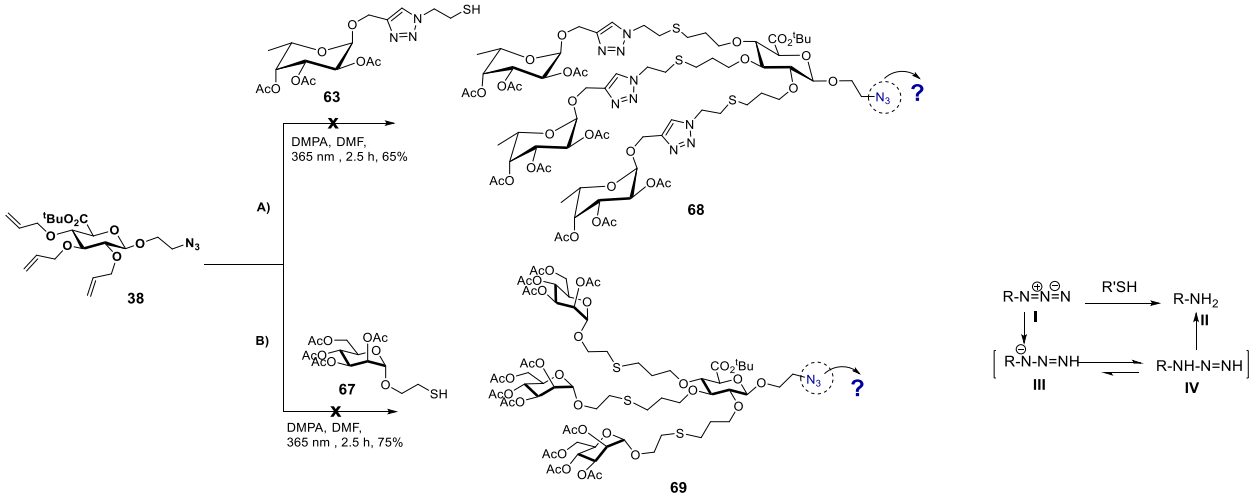

First, we initiated our studies on α-L-fucoside thiol **63** and α-D-mannoside thiol **67** with β-D-glucuronic ester **38**, (**Scheme 3.7**). [359] Besides the ratio of each monomer, different reaction parameters were varied to achieve the best reaction outcome. After using DMF as an adequate solvent ensuring good solubility of the monomers, as well as extra reactants during the entire process of the reaction, the first parameter which was optimized is the photoinitiator. It found that 2,2-Dimethoxy-2-phenylacetophenone (DMPA), the most suitable initiator for photoinduced TEC, with absorption maxima close to the emitted wavelength λ_{max}= 356 nm. During the optimization, it is observed that the equimolar amount of 50 mg (DMPA), provides the best result of TEC reaction. A second parameter investigated was the duration of UV irradiation. The investigation determined 2-3 hours as the optimal yield. Thus, two different experiments were carried out under the optimal TEC reaction resulting in isolation of two different compounds **68** and **69** in 65% and 75%, respectively. [360]

With building blocks **68**, and **69** in hand, different pathways to access the final glycodendrimer synthesis using click reaction (CuAAC), were explored.

3.3.2 Failed attempts of click reaction

The click reaction was studied under several conditions by copper-catalyzed azide-alkyne cycloaddition (CuAAC), (**Scheme 3.8**). Tris[(1-benzyl-1H-1,2,3-triazol-4-yl) methyl] amine (TBTA) was employed as a ligand to facilitate the click reaction (entry **2**, and **8**, **Table 3.1**). However, all the attempts to click reactions failed to give the desired compounds despite using higher catalyst loading and longer reaction times, instead resulting in complex reaction products, as indicated by TLC. ^{1}H NMR did not confirm the formation of the

desired products. These results suggests that the azide group was reduced during the process of photolytic reaction. The analytical HPLC spectrum of the formed products **68**, and **69** revealed multi peaks presumably due to the side products. The susceptibility of alkyl-azide to reduction by thiol under photolytic reaction conditions has been reported, but to my knowledge, there is no detailed mechanistic study has been reported. Knowles *et al* have studied the ability of thiols to reduce azide under photolytic reaction conditions. [361] On the other hand, the initial mechanistic study by Armstrong *et al*. demonstrated that the photochemical reduction of azide by thiol may well involve free radicals. [362] They suggested the reduction of R-N_3 through the formation of intermediate **II** and **I**, as depicted in (**Scheme 3.7**). Thus, we concluded that the azide functional group of compound **38** undergoes reduction under photolytic reaction conditions, thus, rendering them impotent. [361-366] From these results it implies that exist free azide group under thiol- photolytic reaction is unfavorable.

Scheme 3.8 Failed attempts to Click reaction

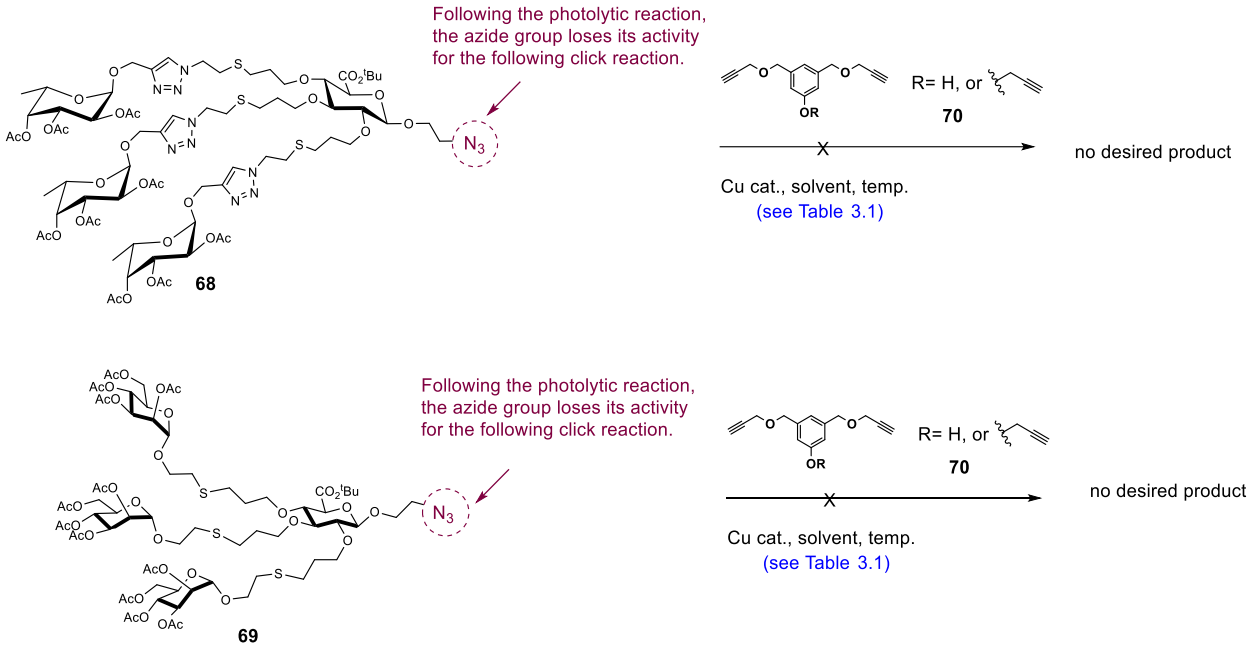

Table 3.1 Screening of different click reactions conditions

Entry	[Cu]	Ligand	Solvent	Temp (°C)
1	$CuSO_4$/NaAsc	-	THF/H_2O	23
2	$CuSO_4$/NaAsc	TBTA	*t*-BuOH/H_2O	23
3	CuI/DIPEA	-	THF	23
4	CuI/DIPEA	-	DMF	Microwave
5	CuI $[P(OEt)]_3$	-	Toluene	80
6	CuI$[P(OEt)]_3$	-	MeOH, THF	80
7	$[Cu(CH_3CN)_4]PF_6$	-	*t*-BuOH/H_2O	23
8	$[Cu(CH_3CN)_4]PF_6$	TBTA	*t*-BuOH/H_2O	23

Subsequent attempts are proposed to overcome this problem. Therefore, to enables the synthetic approaches to conveniently access divergent sets of the desired trithioglyco dendrons, here, we explored the thiol-ene photolytic reactions on the NH-protected molecule followed by the diazo transfer methode. [350, 367, 368]

3.4 Modification of the synthetic approach

In intial attempts, we employed glycosylation of glucose-pentaacetate with linker N(Cbz)(Bn)ethanol using $BF_3.OEt_2$ as promoter in dry DCM, (**Scheme 3.9**, *pathway C*), however due to the poor yield of the desired glycosylated product, we looked into additional synthetic modification.

The inherent stability of the azide group is compatible under a wide range of reaction conditions and can be readily reduced and protected, therefore, a stepwise strategy was pursued starting with Staudinger reduction of the molecule **38** to liberate the free amine group, followed by protection of terminal amine prior to the photolytic reaction, and finally diazo transfer, [369] (**Scheme 3.9**, *pathway A, and B*).

3.4.1 Suitable focal point protecting group

The choice of focal point protecting group was crucial to an effective synthesis since it had to be stable to both the growth/ activation chemistry used during the construction of the dendron scaffold and also be easily removed. Our modified approach is shown in (**Scheme 3.9**). Staudinger reduction on compound **38** was

effected with PPh_3 in aqueous THF, furnishing compound **71** in a good yield. [370] Subsequent step is the protection of the resulting amine, we selected the benzyloxycarbonyl (Cbz) and benzyl (Bn) as protecting groups because both groups can be chemoselectively removed by hydrogenolysis under neutral conditions, thus reaction of **71** with CbzCl and $NaHCO_3$ in EtOAc/H_2O (4 :1) afforded product **72(I)** in 90% yield, followed by the protection with BnBr in the presence of TBAI, DMAP, K_2CO_3 in a refluxed acetonitrile as a solvent, to obtain the product **72(II)** in 70% yield, with which undergoes thiol-ene photolytic reaction with α-D-mannoside thiol **67** to provide product **73A**, (**Scheme 3.9**, *pathway A*).

Scheme 3.9 A synthetic approach to TEC using N(Cbz)(Bn)-tri-allyl β-D-glucuronic ester scaffold

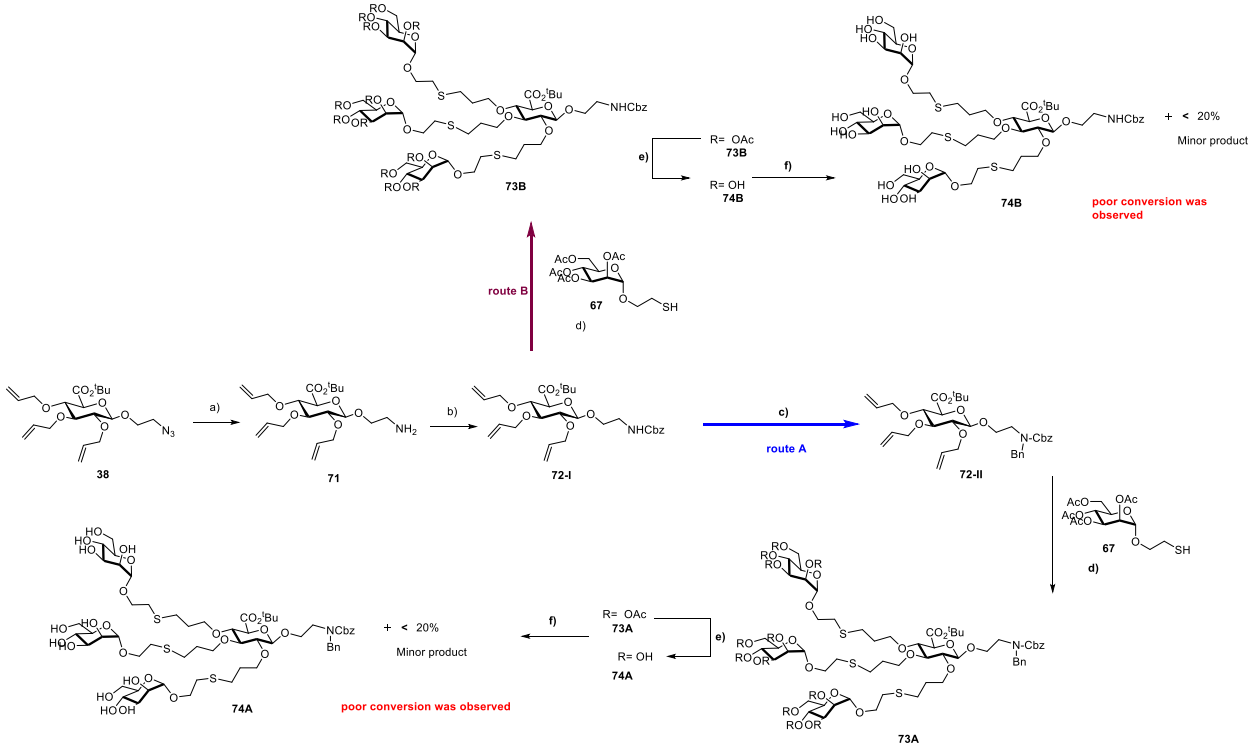

a) PPh_3/H_2O, rt, 12 h, 96%; b) CbzCl, $NaHCO_3$, AcOEt, rt, 12 h, 90%; c) BnBr, TBAI, DMAP, K_2CO_3, ACN, reflux, on, 70%; d) DMPA, DMF, 365 nm, 2.5 h, 80%; e) NaOMe/MeOH, 5 h, rt; f) Pd/C, H_2, MeOH, 36 h.

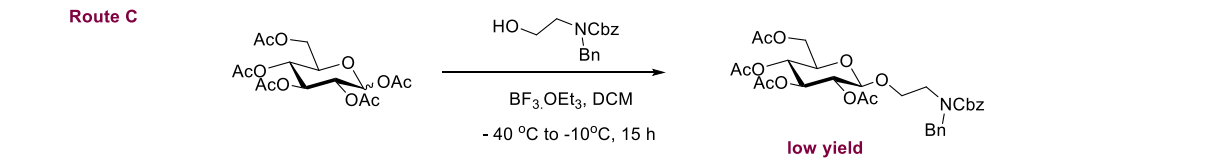

Next, to liberate free amine, the compound **73A** was subjected to two-steps deprotection. The first step is the removal of *O*-Ac groups using Zemplén condition (NaOMe/MeOH), after the product was acidified

using Amberlite IR120 H^+ resin to afford the product **74A** in quantitative yiled. Subsequantly, for the deprotection of (Cbz)(Bn) groups, the dendron **74A** was dissolved in Methanol and palladium on carbon (20%) was added carefully to the reaction vessel. The vessel was backfilled with hydrogen three times and left stirring vigorously under a hydrogen atmosphere for 36 hours at room temperature. Unfortunately, there was low conversion and the deprotection was less than 20% according to TLC analysis, and repeating the reaction using 10% w/w Pd $(OH)_2$/C (10%) catalyst (also known as Pearlman's catalyst) made little difference. Furthermore, the purification of the low amount of the crude product on the column chromatography was not efficient. All attempts to improve the yield of Cbz/Bn deprotection were also unsuccessful, even when the hydrogenolysis was performed upon a gentle heating at 50 °C, the amount of desired product was small (as indicated by TLC), and with changing methanol for another water-miscible solvents (eg., isopropyl alcohol, *tert*-butyl alcohol) using a fresh catalyst, did not change the situation appreciably. We next examined whether direct TEC on compound **71(I)** would improve the yield of the desired product, (**Scheme 3.9**, *pathway B*). Accordingly, photolytic reaction on compound **71(I)** and mannose thiol **67** under the same conditions we previously used, afforded the building block **73 B** in a good yield. Subsequent deprotection of *O*-Ac in NaOM/MeOH followed by deprotection of Cbz under hydrogenolysis using the previous conditions, poor conversion was observed. Our attempts to scale up the final deprotection step indicated that it was capricious (0- 20%). It was concluded that catalytic poisoning through the presence of a divalent sulfur atom (thioether) in the dendron moieties prevented the hydrogenation reaction from occurring. This tenuous result compelled us to choose a new focal point protecting group. The protecting groups for these glycosylated trisaccharides must be carefully chosen and are rather limited, as the *O*-glycoside bond is acid labile. Thus, we selected to use Fmoc N-hydroxysuccinimide ester (Fmoc-OSu) as an alternative to the Cbz protecting group (**Scheme 3.10**). Thus the reaction of **71** with Fmoc-OSu in dry CH_2Cl_2 in the presence of triethylamine, afforded -NHFmoc **75** product in 90% yield.

Scheme 3.10 A synthetic approach to TEC using NHFmoc-tri-allyl β-D-glucuronic ester scaffold

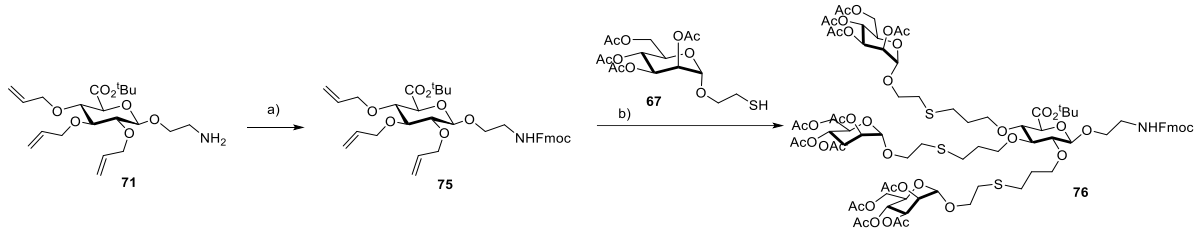

a) Fmoc-OSu, NEt_3, DCM, rt, 12 h, 90%; b) DMPA, DMF, 365 nm, 2.5 h, 79%

The proton ^{1}H NMR analysis for compound **75** (**Figure 3.14**) shows a more downfield peaks which is significant for Fmoc group. The spectrum analysis shows four peaks patterns of the aromatic ring; doublet peaks (d) at 7.76 and 7.60 ppm, that equivalent to four protons from H_{39}- H_{42} and H_{36}- H_{45}, respectively. Another triplet (t) at 7.40, and doublet of triplet (dt) at 7.31 ppm that equivalent to four protons from H_{38}-H_{43} and H_{37}-H_{44}, respectively. ^{13}C NMR shows peak at 127.69, 127.06, 125.11 which are equivalent to C_{38}, C_{44}, C_{37}, C_{41}, and a more upfield peak at 41.18 ppm for C_{34}. Two peaks at 167.67 ppm for carbonyl of the ester group, and 156.48 ppm for carbonyl of Fmoc group, (See supporting information).

Figure 3.14 ^{1}H NMR analysis of NH-Fmoc-tri-allyl β-D-glucuronic ester scaffold **75**

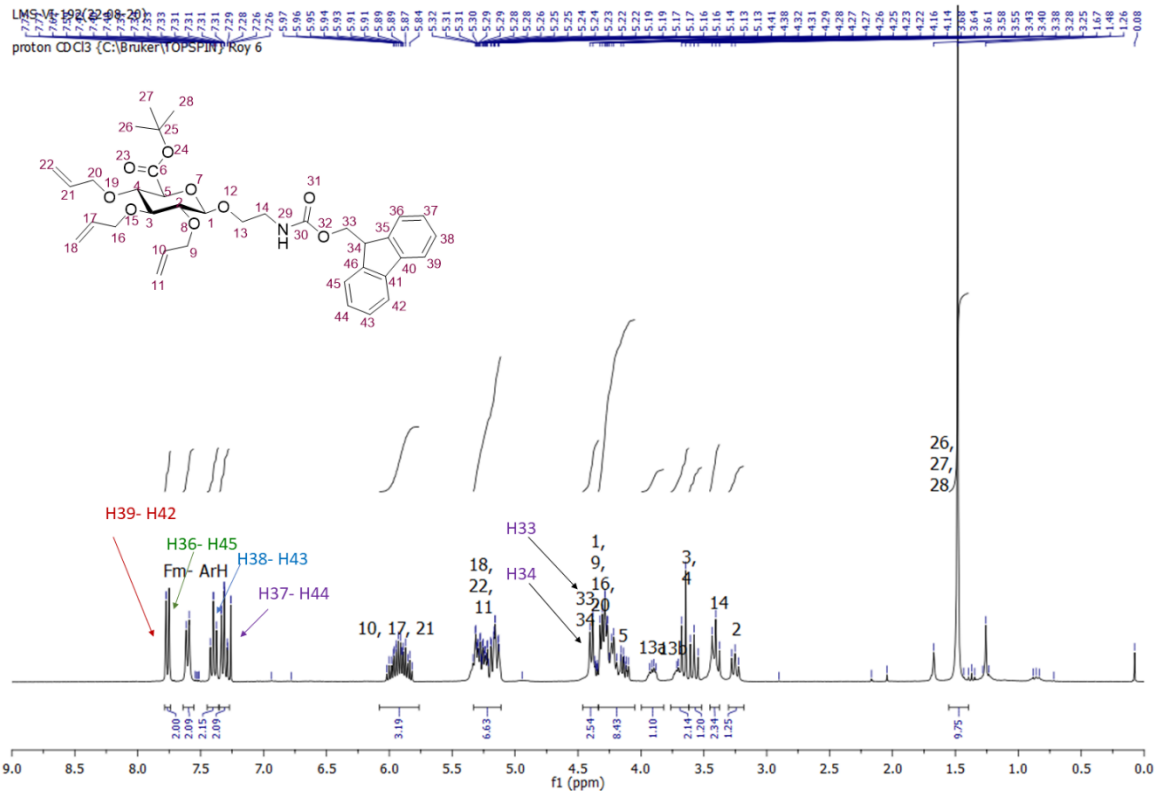

We next turned our attention to the photolytic thiol-ene reaction on NHFmoc tri-allyl β-D-glucuronic ester **75**, (**Scheme 3.10**). When irradiating mannose thiol **67** and molecule **75**, for a molar ratio of (6 :1) for 2.5 hours at 365 nm in the presence of 0.6 equivalent photoinitiator DMPA using a total of 700 µl of a mixture of DMF and water in a ratio of (9:1). The ^{1}H NMR of the crude mixture showed complete conversion to the final product. Also, TEC reaction was tested without the addition of water, reaching a good yield, thereby showing there is no essential to add water to the reaction mixture. However, in addition to the TEC step-growth, a further side-reaction was observed. The side-reaction was identified to be the oxidation of the thiol groups to disulfide. The side-product was successfully removed by performing the purification on

column chromatography to obtain the desired building block NH-Fmoc tri-thiomannoside-β-D-glucuronic scaffold **76** in 79% yield. The ^{1}H NMR spectra (**Figure 3.15**), illustrated the completion of the multiple hydrothiolation process by the entire disappearance of signals belonging to the alkene function at δ 6.12 and 5.49 ppm together with the presence of the characteristic multiplet signal at δ 1.80 ppm corresponding to the newly formed aliphatic -$OCH_2CH_2CH_2S$- moiety.

Figure 3.15 Thiol-ene reaction and comparison spectra between **75** (up), and **76** (bottom)

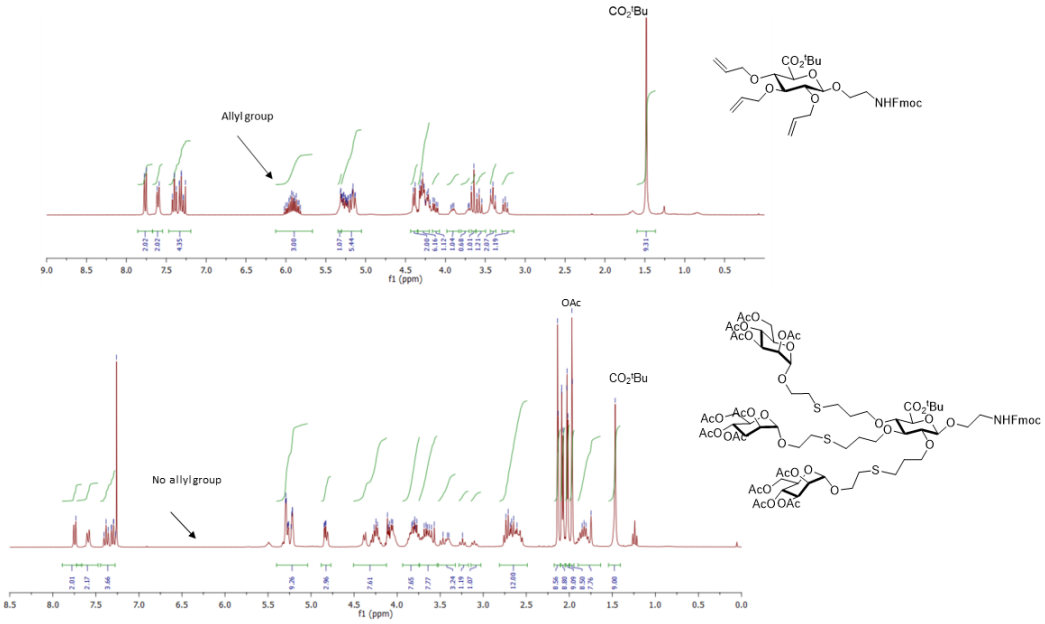

Scheme 3.11, shows the typical reaction mechanism of the addition of thiols to electron-rich alkenes. In general, the UV- initiated thiol-ene process occurs *via* a chain process involving three main steps: Initiation, addition, and chain-transfer. A thiol undergoes a chemical reaction with a photoinitiator DMPA to generate a thiyl radical. This thiyl radical adds across an electron rich double bond forming a carbon-centered radical. This carbon-centered radical subsequently abstracts hydrogen from another thiol producing another thiyl radical. Because of the inherent behavior of the thiol within this system, a free radical step growth reaction occurs. Additionally, termination reactions possible happen involving the coupling of radical-radical species as side products, e.g., thiyl-thiyl radical coupling (thiol dimer). [371] The efficiency of the thiol-ene reactions highly depends on the stability of the carbon-centered radical intermediate **II**, which directly influences both the chain-transfer activation barrier and the reversibility of the propagation step as revealed by recent computational and kinetic studies. [162] The formed carbon radical intermediates existing in a $^{4}C_{1}$ chair conformation, the gluco configured **II** featuring an all equatorial substitution pattern has lower energy. [162, 372]

Scheme 3.11 mechanistic pathway of free-radical addition in thiol-ene coupling

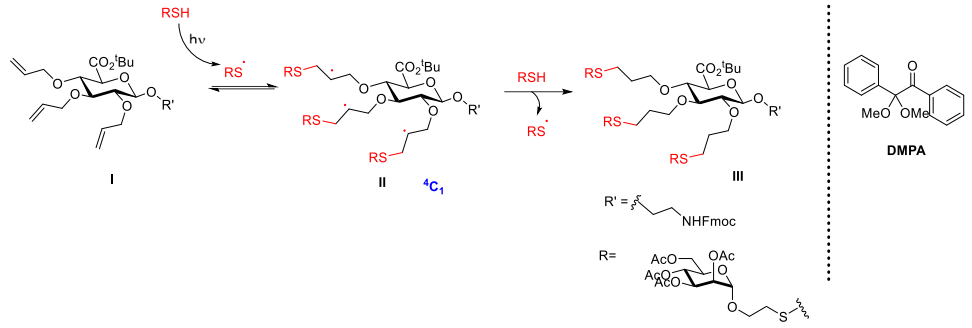

Subsequent deprotection of *O*-Acetyl and N-Fmoc groups (**Scheme 3.12**) was achieved in two continuous steps using NaOMe/ MeOH, followed by 20% piperidine in DMF. [373, 374]

Scheme 3.12 Deprotection of *O*-Actyl and NHFmoc protecting groups

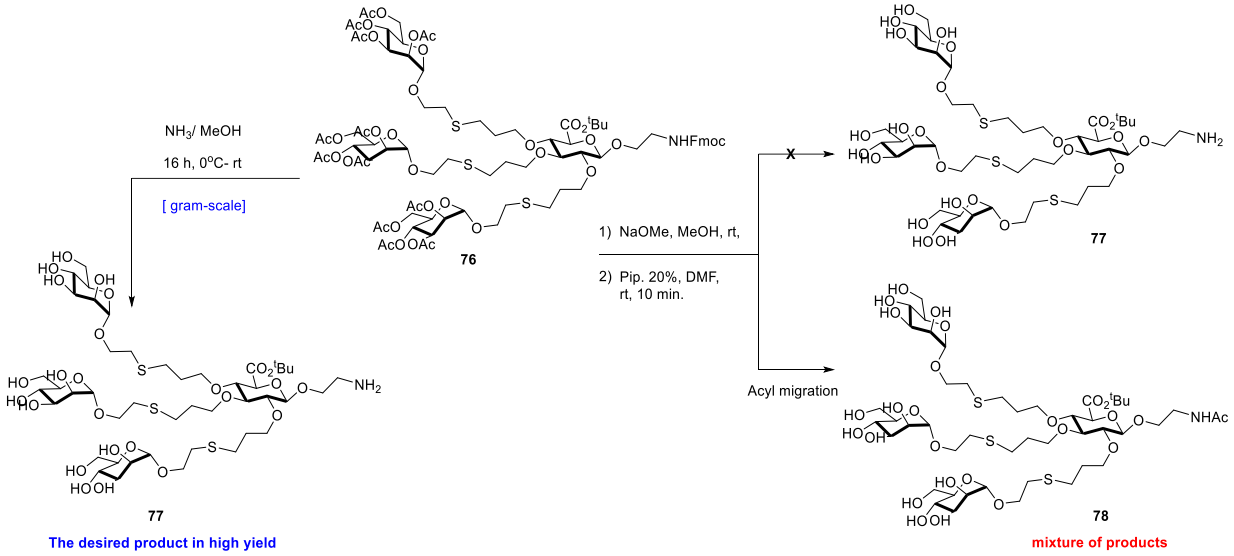

Unfortunately, it gave complex mixtures of undesired products arises from rapid *O*→*N* acetyl migration (data not shown). [375] This tenuous results compelled us to look for an alternative method to remove the protecting groups. Quantitative cleavage of Fmoc, acetyl groups finally proceeded in one-step reaction using 7N solution of ammonia in methanol (pH= 8), (**Scheme 3.12**), to afford the full deprotected product after stirring the reaction mixture at room temperature for 16 h. [376-378] The purification of the product was done by excessive rinsing the crude reaction mixture with chloroform to remove the undesired by-products. ^{1}H NMR (**Figure 3.16**) confirmed the full deprotection of protecting groups. Product **77** was exceptionally clean, resulting in 93% NMR-based yield, which is used for the next step without further purification. Under this condition, no migration of the acetyl group from *O*- to *N*- was observed. [376, 379]

Figure 3.16 Comparison of the ^{1}H NMR spectra of compounds **76** (up) and **77** (bottom)

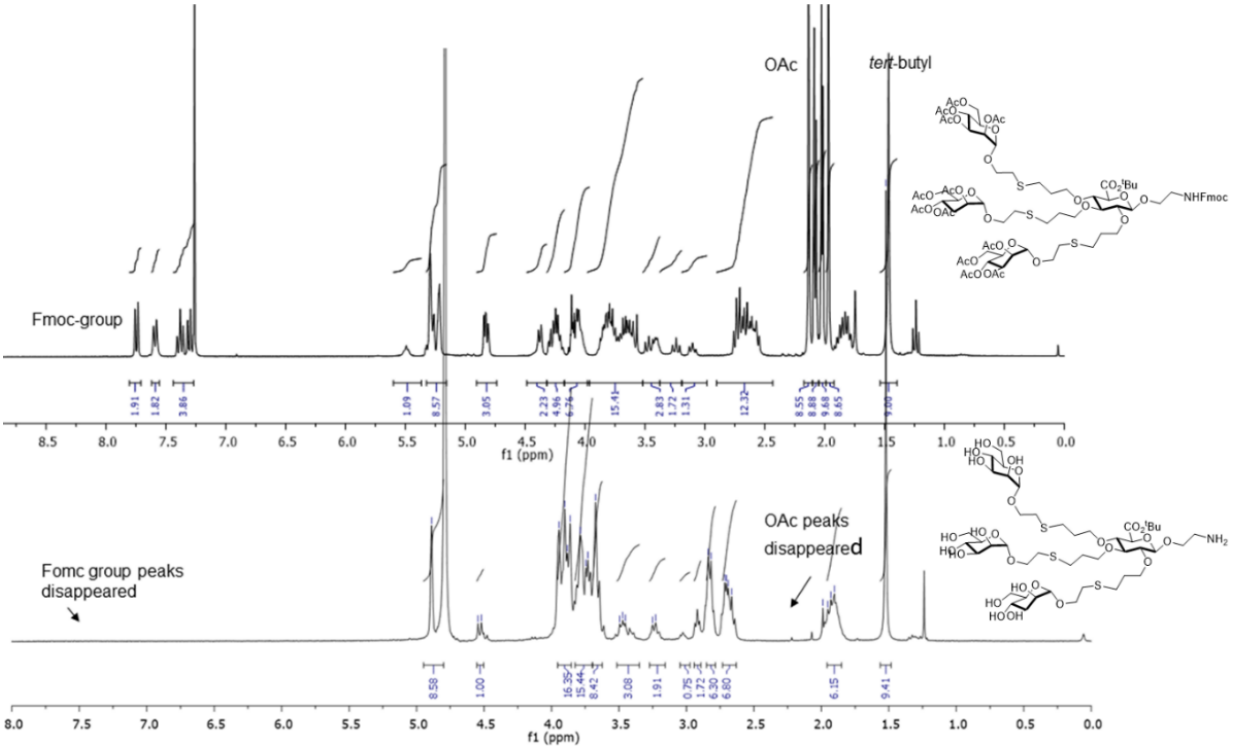

With a scalable route to access building block **77** bearing free amine, efforts were made to explore the conditions for diazo transfer to install the terminal azide group, (**Scheme 3.13**). [380-383] The diazo transfer proceeded admirably with the procedure reported by Valery V. Fokin. [384] After optimizing the reaction conditions, the free amine derivative of **77** was treated with imidazole-1-sulfonyl azide sulfate **79** and catalytic copper sulphate in a mixture of *t*-BuOH/ H_2O to afford the corresponding azide derivative **80** in 90%, complete conversions were typically observed after stirring the reaction mixture for 16 h at room temperature.

Scheme 3.13 Synthesis of azido-tri-man-D-glucuronic ester dendron **80**

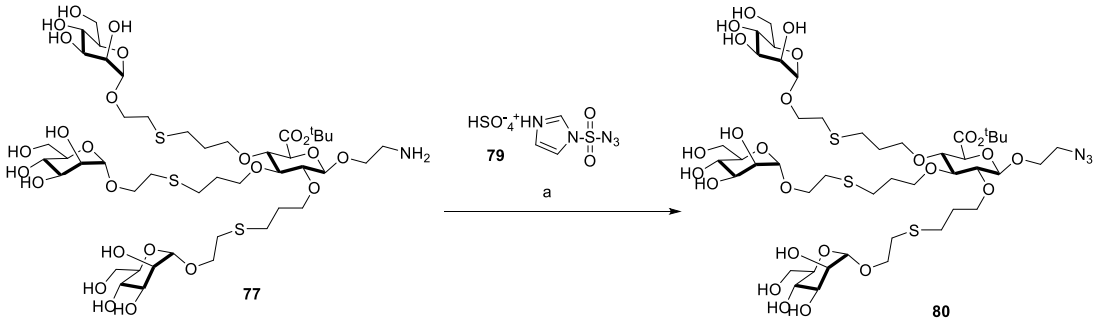

a) $CuSO_4$, $NaHCO_3$, H_2O/*tert*-BuOH, 16 h, rt, 90%

IR spectra are sensitive towards the functional groups of molecule **80**. IR data (**Figure 3.17**), showed the peak corresponding to azide at 2103.39 cm-1, the strong bands around 3300 cm^{-1} were derived from the OH groups.

Figure 3.17 IR analysis of compound **80**

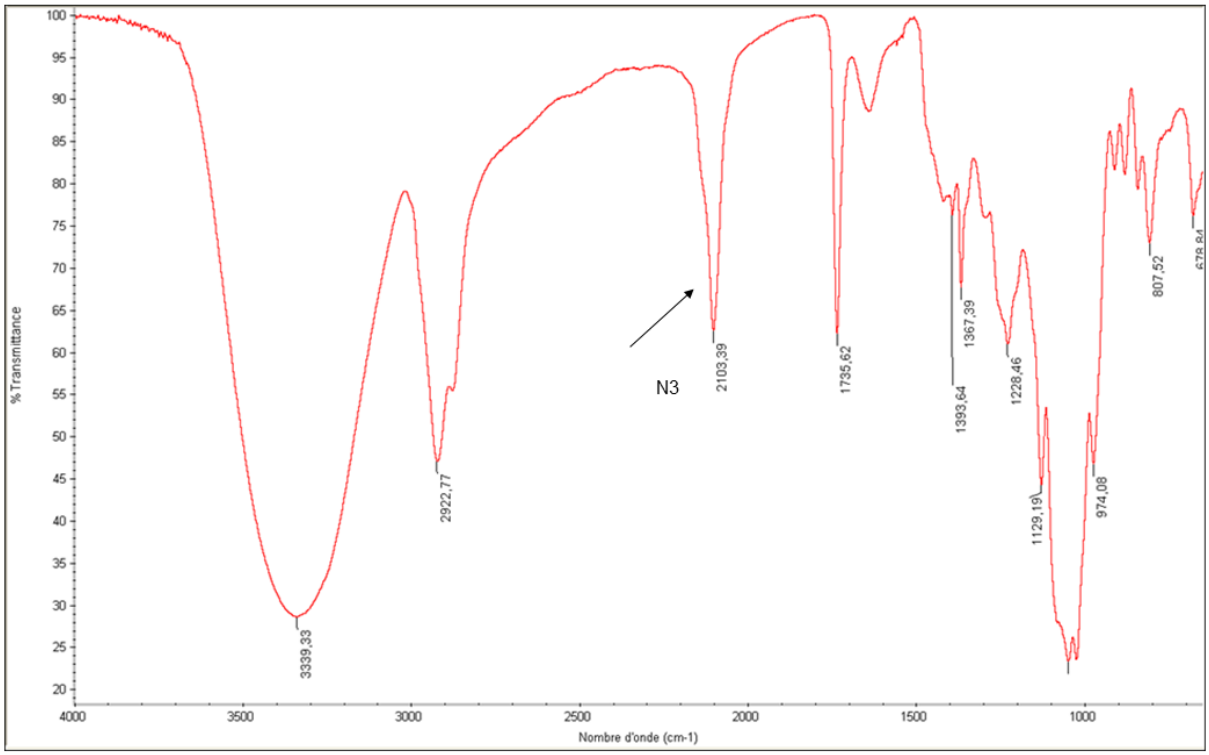

3.4.2 Mechanestic insight of diazo transfer reaction

The mechanistic study of diazo transfer using imidazole-1-sulfonyl azide was published in 2014 by Samuelson and co-workers. [385] Their detailed study provides evidence that the diazo transfer reaction involves the transfer of the two terminal nitrogen atoms of the "azidating" reagent to the amine. This was confirmed by using labeled imidazole-1-sulfonyl azide, (**Scheme 3.14)**. which was in agreement with the proposed mechanistic study by Wong and co-workers[386] as shown in (**Scheme 3.15)**.

Scheme 3.14 Mechanistic study of diazo transfer

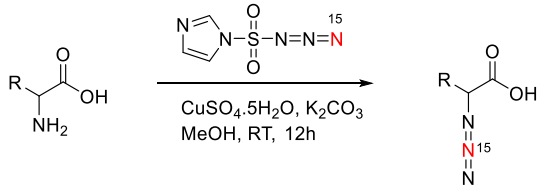

Scheme 3.15 Plausible mechanism of Cu catalyzed diazo transfer reaction illustrated with the terminally labeled isotopomer of TfN_3

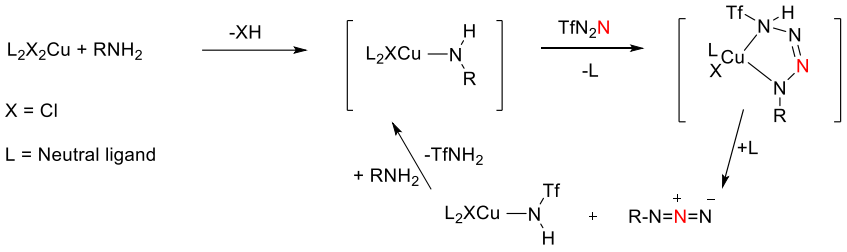

It should be emphasized that this sequence proved considerably more reliable than alternatives pursued, involving TEC reactions between azido triallyl-β-D-glucuronic ester and thiol monomers, whose adduct turned out to be unstable.

We next turn our attention to the synthesis of tri-thiofucoside-β-D-glucuronic building block, which synthesized in accordance with the design approach of tri-thiomannoside β-D-glucuronic

3.4.3 Synthesis of tri-thiofucoside-β-D-glucuronic scaffold **83**

A schematic overview over the total synthesis of target trivalent fucoside ligand G3 is depicted in (**Scheme 3.16**). To the best of our knowledge, thiol-ene photoinitiation represents the first example of α-L-fucoside-thiol as a building block.

Scheme 3.16 Synthesis of azido tri-thiofucoside-β-D-glucuronic scaffold **83** (G3)

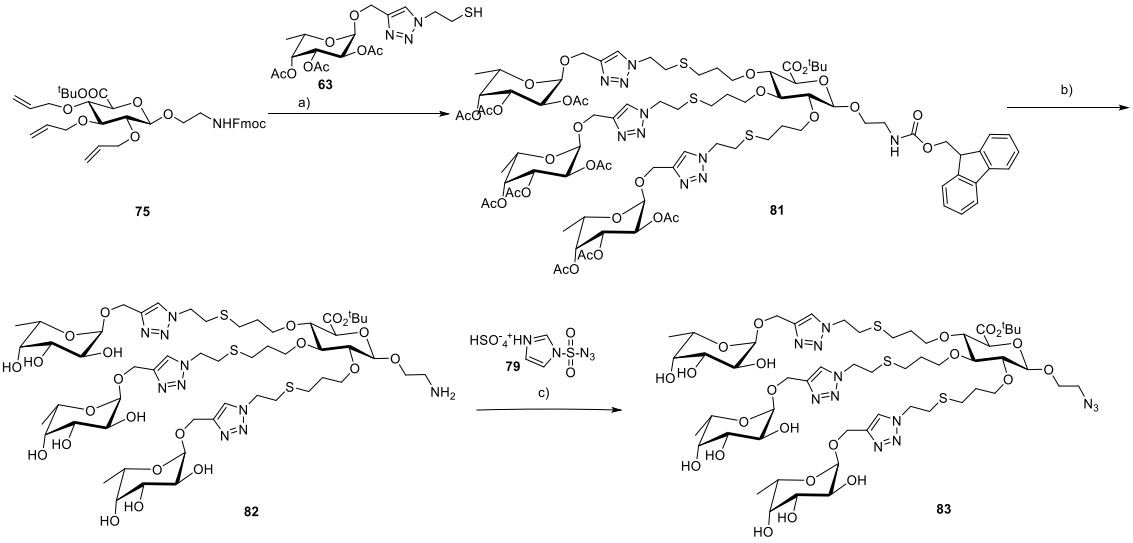

a) DMPA, DMF, 365 nm, 3h, 66%, b) NH_3/MeOH, 12 h, rt, 85%, c) $CuSO_4$, $NaHCO_3$, H_2O/*tert*-BuOH, 16h, rt, 80%

The first step is the photolytic irradiation between β-D- glucuronic ester derivative **75** and α-L-fucoside thiol **63**. It is observed that during the photolytic reaction α-L-fucose thiol has a tendency to oxidize quickly to disulfide, resulted in no completion of the reaction, as confirmed by ^{1}H NMR of the crude product. Therefore, during the optimization it is found that the reactants mixed in a in a molar ratio of 18 :1 (Fucose thiol: alkene), for 2.5 hours in the presence of 0.6 equivalent photoinitiator DMPA using a total of 700 µl of a mixture of DMF and water in a ratio of (9:1), gave the best product outcomes. The reaction afforded NHFmoc tri-thiofucoside-β-D-glucuronic ester **81** in 66%. The product **81** is fully characterized by NMR as shown in (**Figure 3.18)**.

Figure 3.18 ^{1}H NMR analysis of compound **81** with an enlargement of the area from 7.00 to 8.00 ppm

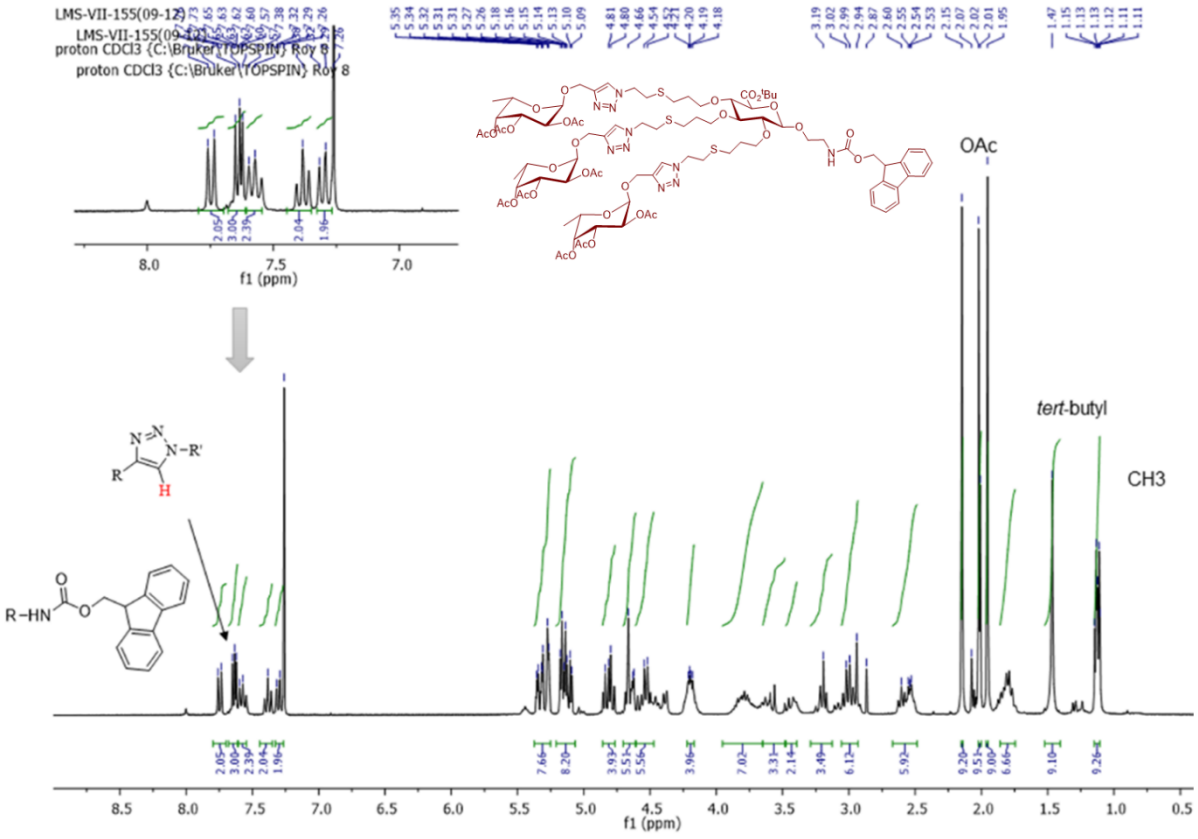

Subsequent deprotection of *O*-acetyl and -NHFmoc protecting groups in a mixture of ammonia in methanol afforded compound **82** in 85% yield (**Scheme 3.16**). The product was pure enough, therefore, it was used for the next step without any further purification. Following similar routes as explained previously, thus, treatment of compound **82** with imidazole-1-sulfonyl azide sulfate **79** in a mixture of *tert*-butanol/water, in the presence of sodium bicarbonate as a base, afforded compound **83** in 80% *via* diazo transfer. The ^{1}H

NMR analysis of **83** (**Figure 3.19**) has shown characteristic signals for triazole protons at 8.08 ppm, and fucose anomeric protons at 4.96 ppm.

Figure 3.19 ^{1}H NMR analysis of compound **83**

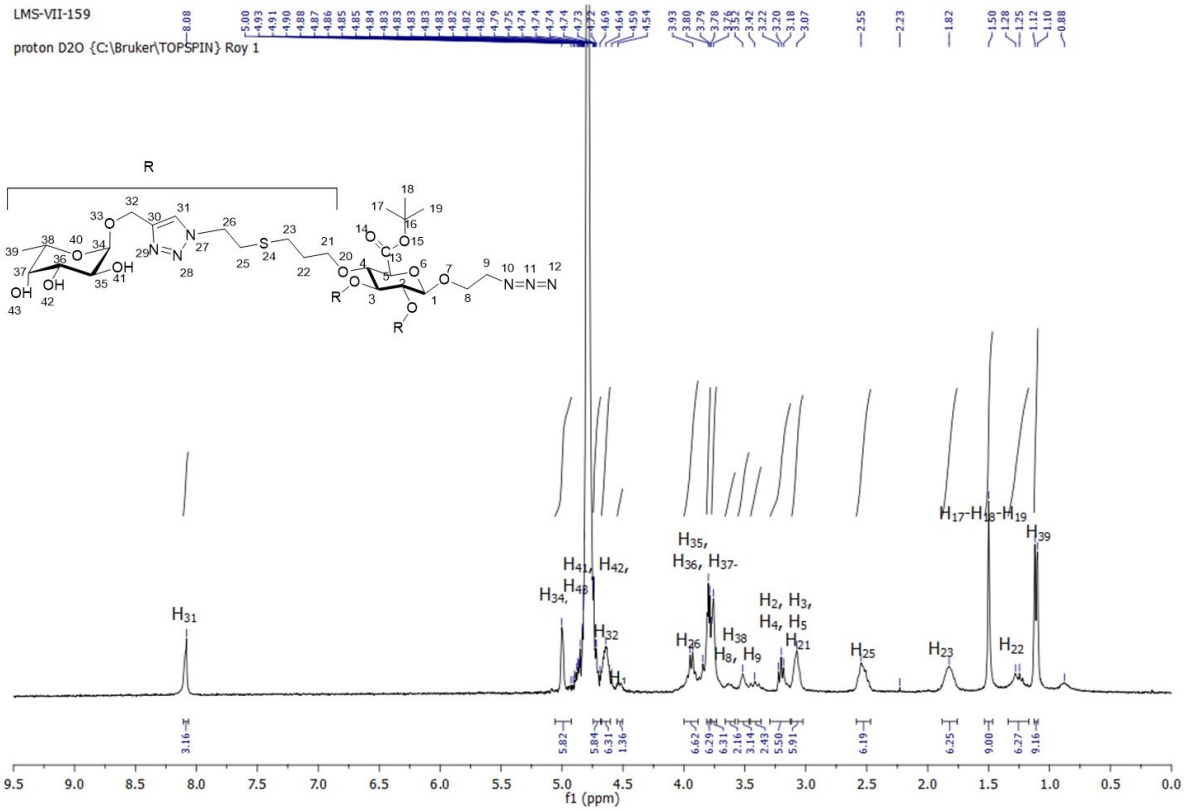

The molecular weight of the compound bearing free amine **82** and the building block **83** after azide transfer, were further confirmed by using electron ionization mass spectrometry (ESI-MS). In (**Figure 3.20**) one peak of the product **82** was detected at a molecular weight of $[M+2H]^{2+}$1330.9 which is in match with the theoretical weight $C_{54}H_{92}N_{10}O_{22}S_3$ $[M+2H]^{2+}$ 1330.55. In (**Figure 3.21**), one peak of product **83** was detected at molecular weight of $[M+Na]^{+}$ 1378.7 which is in match with the theoretical weight $C_{54}H_{90}N_{12}O_{22}S_3$ $[M+Na]^{+}$ 1377.55.

Figure 3.20 ESI-MS spectrum of **82**

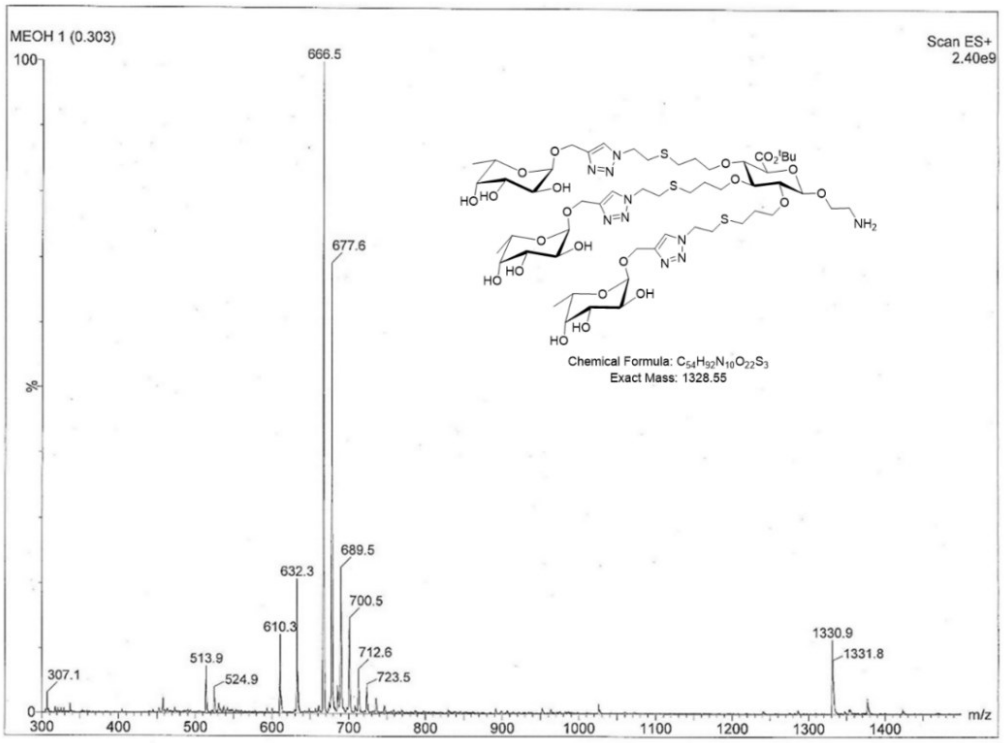

Figure 3.21 ESI-MS spectrum of **83**

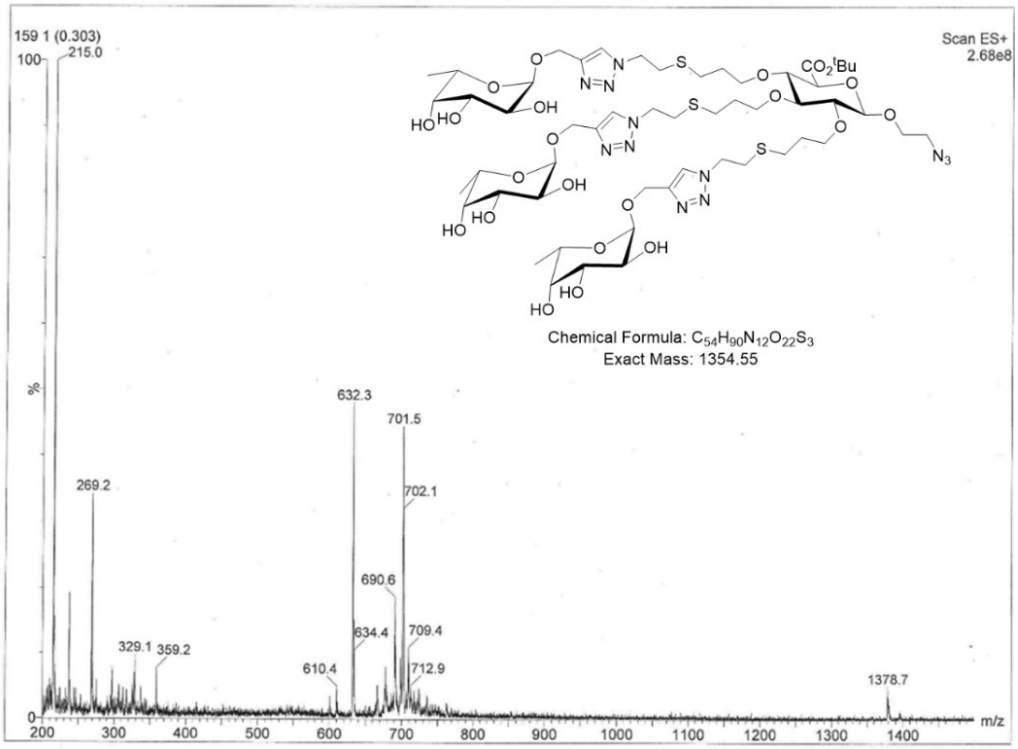

In conclusion, two different trivalent dendrons, azido-trithiomannoside and azido-trithiofucoside, were synthesized in a good yield. With the aim of continuing our research towards the design and synthesis of glycodendrimers with intriguing biological activity, we started a new set of multivalent structure synthesis. A small library of glycodendrimers displays α-L-fucosides dendritic wedge, and α-D-mannoside dendritic wedge, were designed to be carrying active carboxylic group, which is subsequently capable to conjugate to ciprofloxacin drug. [387, 388]

Hexachlorocyclotriphosphazene (HCCP) is an interesting structural unit for the construction of dendrimers due to its distinct advantages like synthetic versatility, high stability on functionalization, and higher yields with up-scalability. [389] Although it has been reported that a number of dendrimers-based HCCP cores have aromatic rings in the dendrimer architecture, in this study we disclose the use of cyclotriphosphazene including PEG_3-linker as a dendritic core, which employs in the synthesis of a new class of dendrimers, (**Figure 3.21**). The tri-ethylene glycol was chosen as they are commercially available and can create enough space for Man and Fuc binding blocks to be readily accessible to the receptor sites.

3.5 Synthesis of fucosylated and mannosylated homodendrimers

A series of new homodendrimers D1, D2, and D3 have been successfully synthesized with active α-L-fucoside dendron (I), and α-D-mannoside dendron (II), having carboxylic ester at the dendrimer periphery. The structures of obtained multivalent dendrimers are depicted in (**Figure 3.22**). The proposed mannosylated multivalent dendrimers have different Man valences of nine and eighteen. Hexavalent eighteen valences mannoside-glycodendrimer structures were reached by the assembly of mannoside dendritic wedge (II), and cyclotriphosphazene-PEG_3 (flexible, long linker), or dipentaerythritol core (rigid, short linker), respectively. Trivalent nine valences mannoside-glycodendrimer was synthesized using Benzene-1,3,5-tricarbodimide (BTA-PEG_3). [390] The model was designed in which the hexavalent binding was achieved by using a flexible tri ethylene glycol (PEG_3) spacer to allow the chelation and drug attachment to proceed without constraints. [390] All of the dendritic cores used had been synthesized with terminal alkyne groups, (see detailed **Chapter 6** supporting information).

The key to the efficient synthesis of the glycodendrimer is the introduction of the dendrons to the dendrimer core (**Figure 3.22**). The introduction reaction should have high reactivity and functional group selectivity to complete the reaction at multiple reaction sites without side reactions. Among various ligation reactions, Cu(I)-catalyzed azide/alkyne cycloaddition (CuAAC) has been commonly used for the introduction of glycodendrimers synthesis. CuAAC has high functional group orthogonality. However, its reactivity is occasionally insufficient, therefore, it is crucial to choose the most effective catalyst and procedures.

Figure 3.22 Structures of tri- and hexa-valent glycodendrimers **85-94**

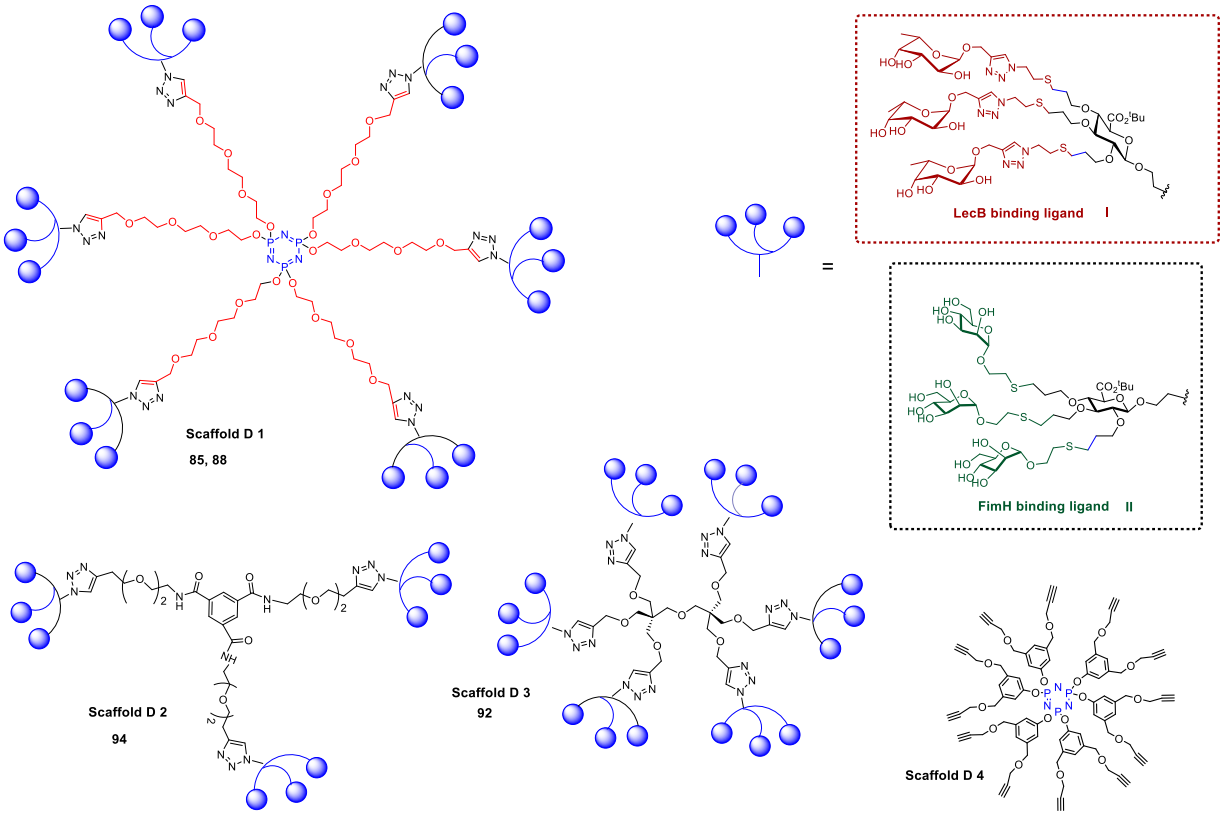

3.5.1 Synthesis of fucoside and mannoside homo-glycodendrimers based cyclotriphosphazene-PEG_3

Chemical Synthesis. In the present study, a novel class of six-valent glycodendrimers was produced *via* copper-catalyzed azide-alkyne cycloaddition (CuAAC) between glycodendrons containing azide **80**, or **83**, and dendritic core **84**, to provide glycodendrimers **85**, **88**, and **92**, respectively, (**Figure 3.22**). The mannoside-dendrimer **85** was synthesized as shown in (**Scheme 3.17**). Initial screening of CuAAC catalysts, was performed using $CuSO_4$/sod.acorbate. Accordingly, 20 mol% sodium ascorbate and 20 mol% copper sulfate per alkyne group were dissolved in 1 mL water and added to 2 equiv of the dendrone **80** per alkyne group and 1 equiv dendrimer core that had been dissolved in 3 mL DMF, the mixture was stirred overnight. Nevertheless, the Sharpless click reaction was not readily performed on the trithiomannoside β-D-Glucuronic ester substrate **80** and dendritic core because copper ion can coordinate strongly to thiomannoside backbone, resulting in the deactivation of the reaction, the reaction never goes to completion. Introducing several molecules of thiomannoside dendron with large and complex structures, *i.e.*, many hydroxyls and molecular weight, make 1,3-dipolar cycloaddition more difficult. To overcome this problem, the click reaction was performed using Iodo (triethyl phosphite) copper(I), CuI [$P(OEt)_3$] catalyst in a mixture of MeOH/acetonitrile at 80 °C for 24 h and DIPEA as a base that lead to a good conversion. Due to the coordination of copper to the sulfur ($S\text{-}CH_2$), besides the high polarity of the crude product, makes it is

more difficult to purify the product using column chromatography. Meanwhile, residual copper is also a harmful reagent for the biological test. Therefore, how to remove the copper becomes a challenge. The resins become one of the most attractive techniques, it has been reported that chelating resin Dowex M4195, resin (Cuprisorb), and chelex® resin (50-100 mesh) have a high copper chelating selectivity. [391] Unfortunately, we could not be able to get any of these chelating resins. An alternative safe route is the acetylation of hydroxyl group in a mixture of Ac_2O/pyridine followed by excessive washing with copper chelating agent, to obtain the full acetylated hexavalent dendrimer **85**, (**Scheme 3.17**).

Scheme 3.17 Synthesis of generation three (G3) Man-glycodendrimer **85** and its structural elements

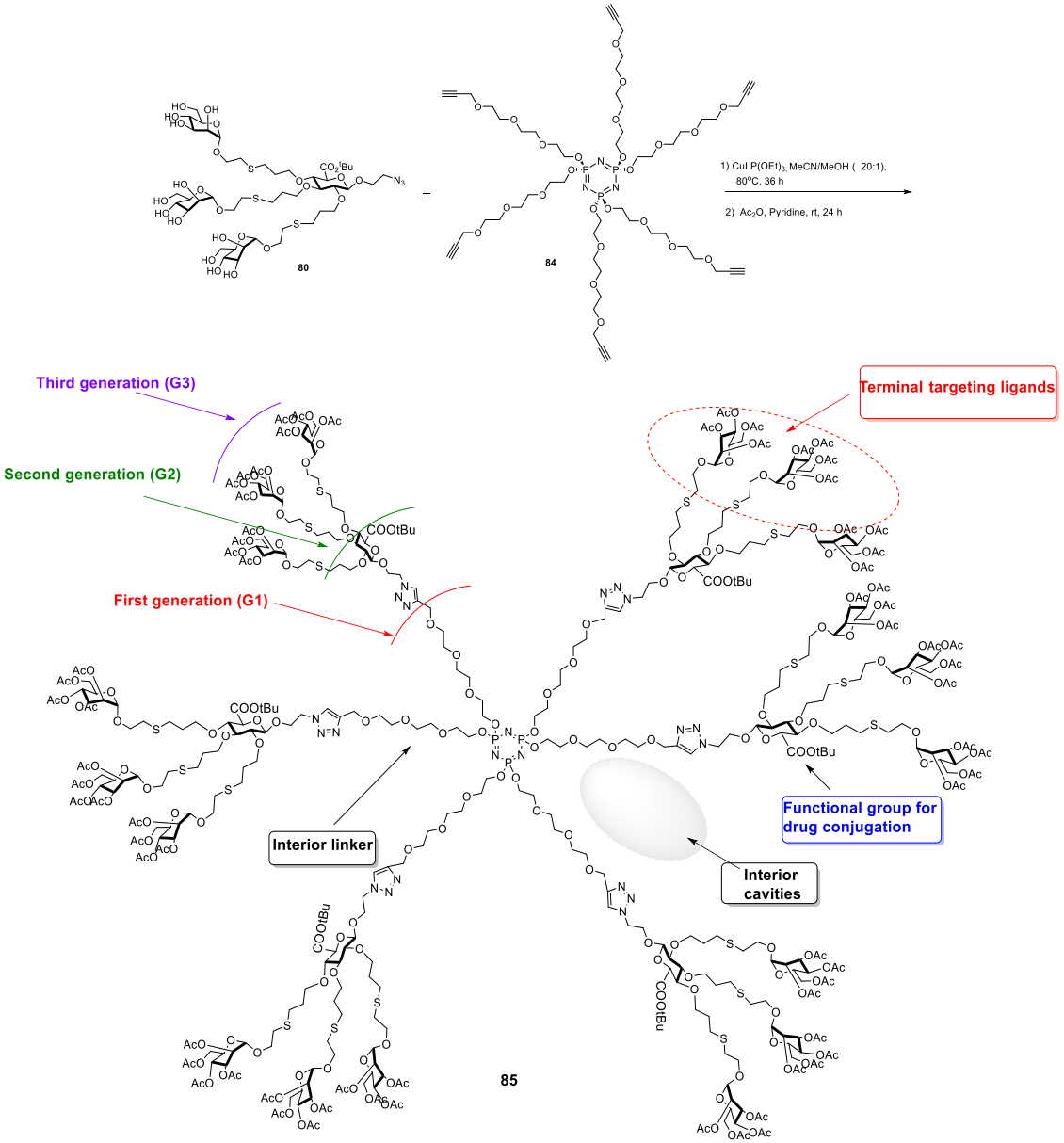

The structure of Man-dendrimer **85** was confirmed using ^{1}H NMR spectrum, ^{31}P NMR spectrum, and MALDI-TOF MS analysis. Due to the large size of the dendrimer, the peaks associated with the PEG_3 core protons, and the sugar backbones become more broadened and overlapping. Therefore, it was difficult to integrate all of the peaks and obtain accurate proton counts, (**Figure 3.23**). The integration ratio between characteristic triazole peak near 7.6 ppm (H= 6), mannose anomeric protons near 4.8 ppm (H=18), and singlet peak *tert*-butyl protons at 1.47 ppm showed to be consistent with target **85**. The methylene protons of the ethylene oxide units of the PEG_3 correspond to the peak at 3.7 ppm. ^{13}C NMR shows two distinct carbonyl peaks, at 170.01, 169.84, 169.83, and 169.72 ppm, which correspond to C=O of acetyl groups, and a peak at 170.61 ppm corresponding to C=O of *tert*-butyl group. The peaks at 20.89, 20.78, 20.73, and 20.68 ppm correspond to the methyl-acetyl. A peak at 28.00 ppm corresponds to *tert*-butyl group (see Supporting information).

Figure 3.23 ^{1}H NMR analysis of dendrimer **85**

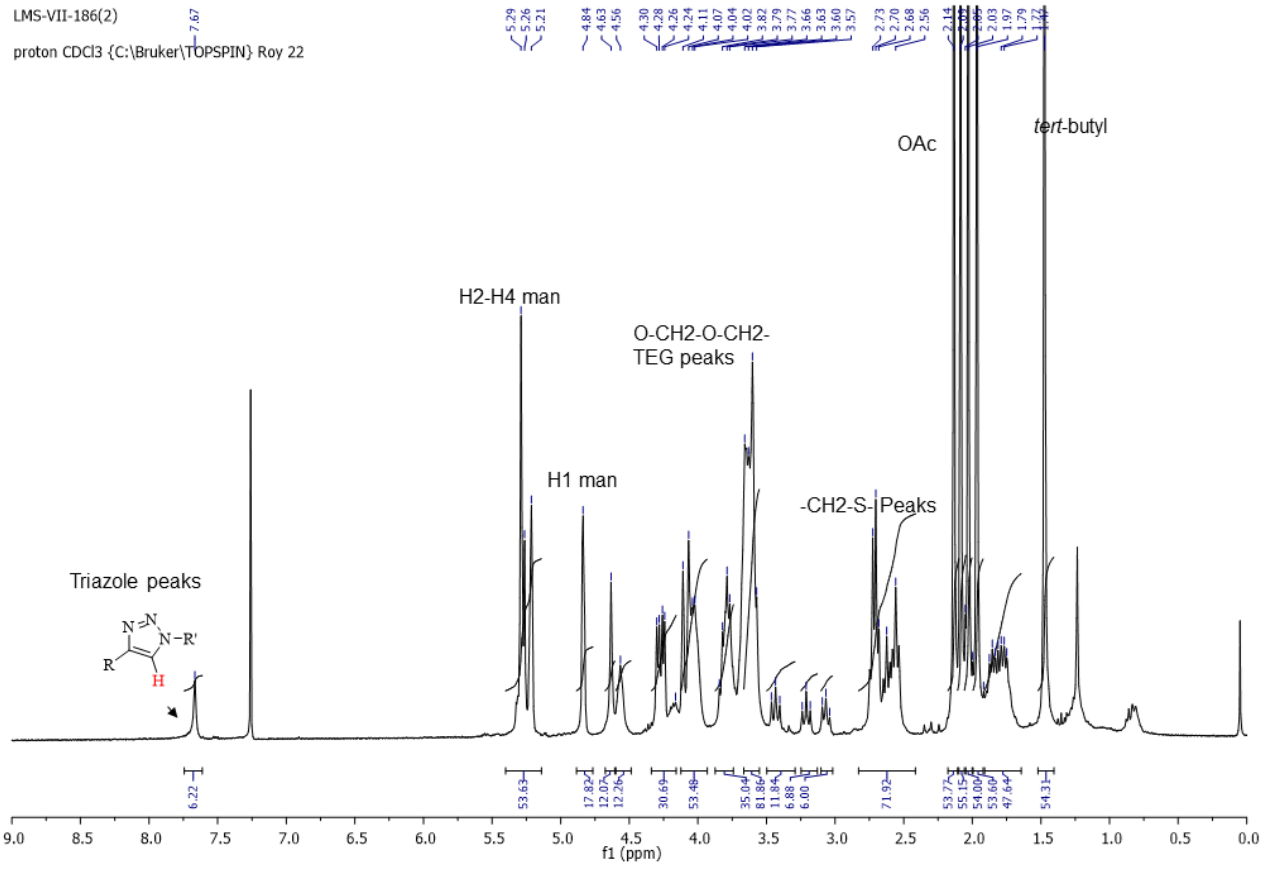

Moreover, the ^{31}P NMR (peak at 17.74 ppm) represents a useful tool to assess the equivalence of the three phosphorus atoms, suggesting a symmetrical functionalization of the core scaffold, (**Figure 3.24)**.

Figure 3.24 ^{31}P NMR analysis of dendrimer **85**

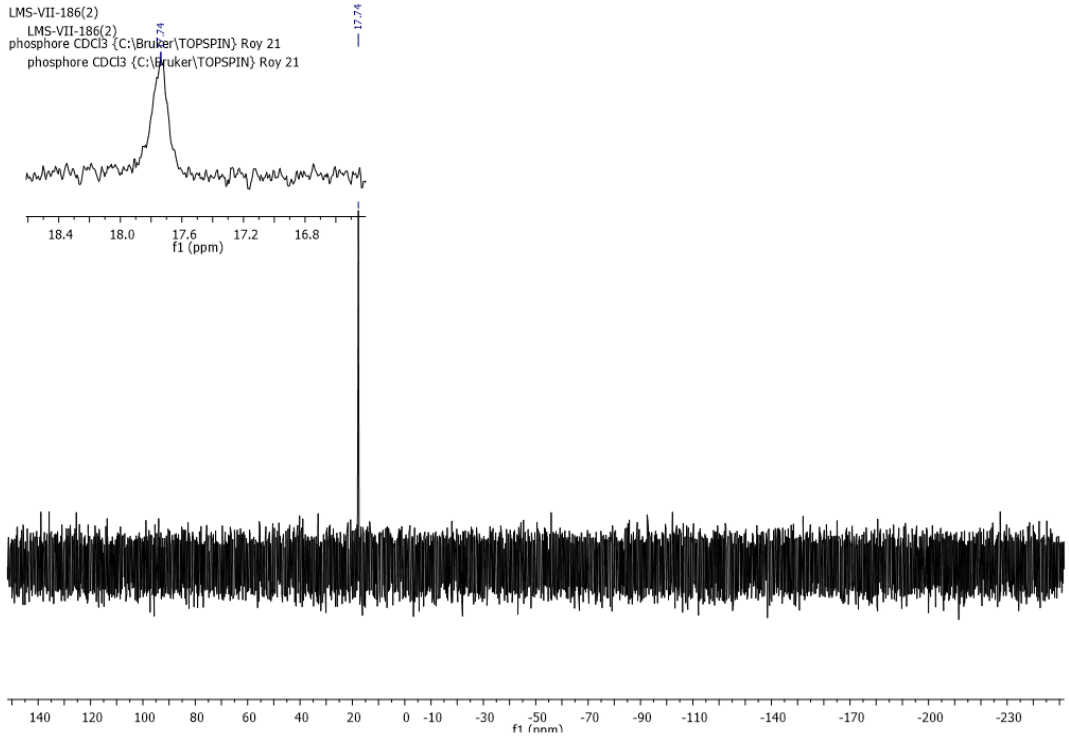

The structure of dendrimer **85** is further confirmed by MALDI-TOF-MS. Peak integration yielded an average of six dendrons attached per dendrimer, in agreement with MW 11246.98 Da in the MALDI-TOF spectra of **85**, (**Figure 3.25**).

Figure 3.25 MALDI-TOF MS spectrum of dendrimer **85**

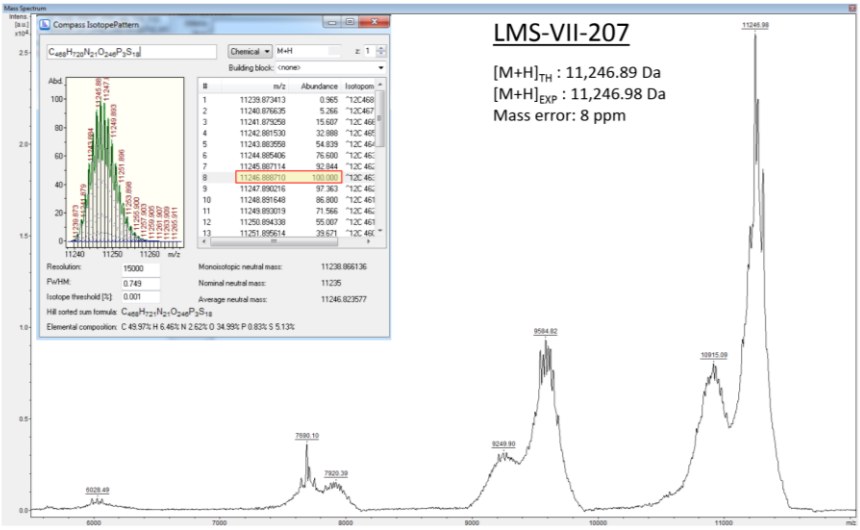

Finally, the dendrimer was deprotected by two steps procedures, a schematic overview of the sequence of deprotection is shown in, (**Scheme 3.18**). The first step involves Zemplén reaction using MeONa/MeOH, resulting in the removal of *O*-acyl groups to afford dendrimer **86** in good quantitative yield. Followed by the removal of *tert*-butyl group, the deprotection was completed in 90% aqueous trifluoroacetic acid (TFA/H_2O 9:1) [392] in one hour, then, the reaction mixture pass through anion exchange resin. Trifluoroacetate was removed according to the described procedure. [393] An anion exchange resin was transferred to a syringe and washed three times with 10 mL of 1.6 N acetic acid and three times with 10 mL of 0.16 N acetic acid. The dendrimer was transferred to a syringe with the anion exchange resin. The syringe was shaken for 15 min, the dendrimer solution was recovered in a flask and the resin was washed with water. The dendrimer was freeze-dried to remove water. ^{1}H NMR and ^{13}C NMR analysis were not powerful enough to reveal as much possible information on the full structure of the dendrimer. To further analyze the expected structure, MALDI-TOF-MS analysis of the dendrimer (**Figure 3.26**) shows little peaks that are close to the molecular weight of the dendrimer, while the intense peaks belong to the branch dendrons. So, we believe that, dendrimers such as **85**, which contain acid-sensitive glycosidic linkages, are not stable to treat under moderately strong acidic conditions.

Figure 3.26 (A) Deprotection of dendrimer **85** in NaOMe/MeOH, followed by deprotection in aqueous TFA/H_2O; (B) MALDI analysis of the resulted dendrimer; blue and red shows analysis from two samples deprotected under the same conditions; (C) Negative and positive modes of the dendrimer

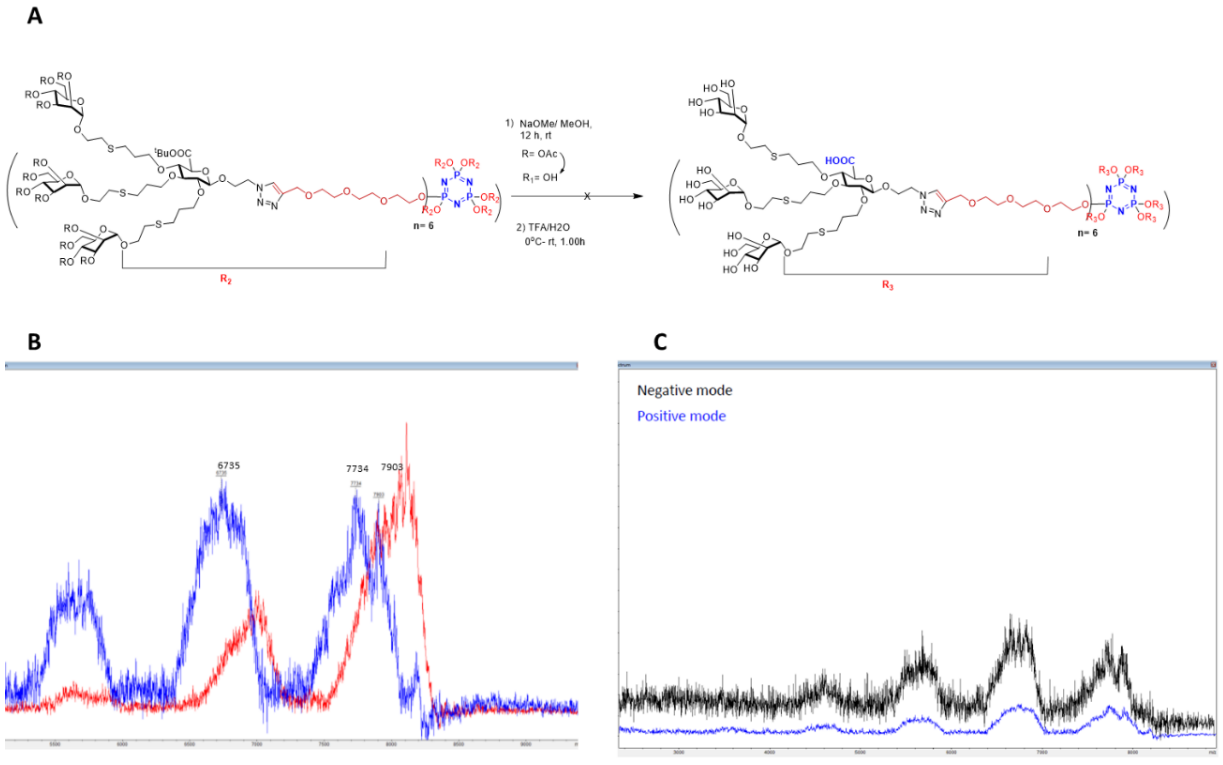

Thus, due to the perception that an oligosaccharides molecule is prone to acid-mediated hydrolysis, [394] we found that using a mixture of TFA in toluene (9:1) led to a clean removal of *tertiary* butyl under ambient conditions in 1.30 hr, which gave the target dendrimer **87**, this methodology represents an improvement over the previously reported one. After evaporation of TFA/toluene under reduced pressure an additional H_2O was added and the mixture was transferred to a dialysis tube of MWCO 3000. Subsequently, the product was freeze-dried to remove water. The desired dendrimer G3-OH- (COOH) **87** was obtained as a solid residue. The resulting dendrimer was fully characterized by NMR spectroscopy. The NMR spectra presented all peaks as expected, which confirm the successful synthesis of the required product. ^{1}H NMR results confirm the successful deprotection of -*O*Ac, and *tert*-butyl protecting groups. The peak shown in the MALDI-TOF spectrum of [G3-OH- (COOH)+Na]$^+$ at 7892 Da further confirms product **87**, (**Figure 3.27)**. The resulting dendrimer **87** has displayed excellent solubility in both water and organic solvents like DMF.

Scheme 3.18 The deprotection of -*O*Ac and *tert*-butyl ester of Man-glycodendrimer

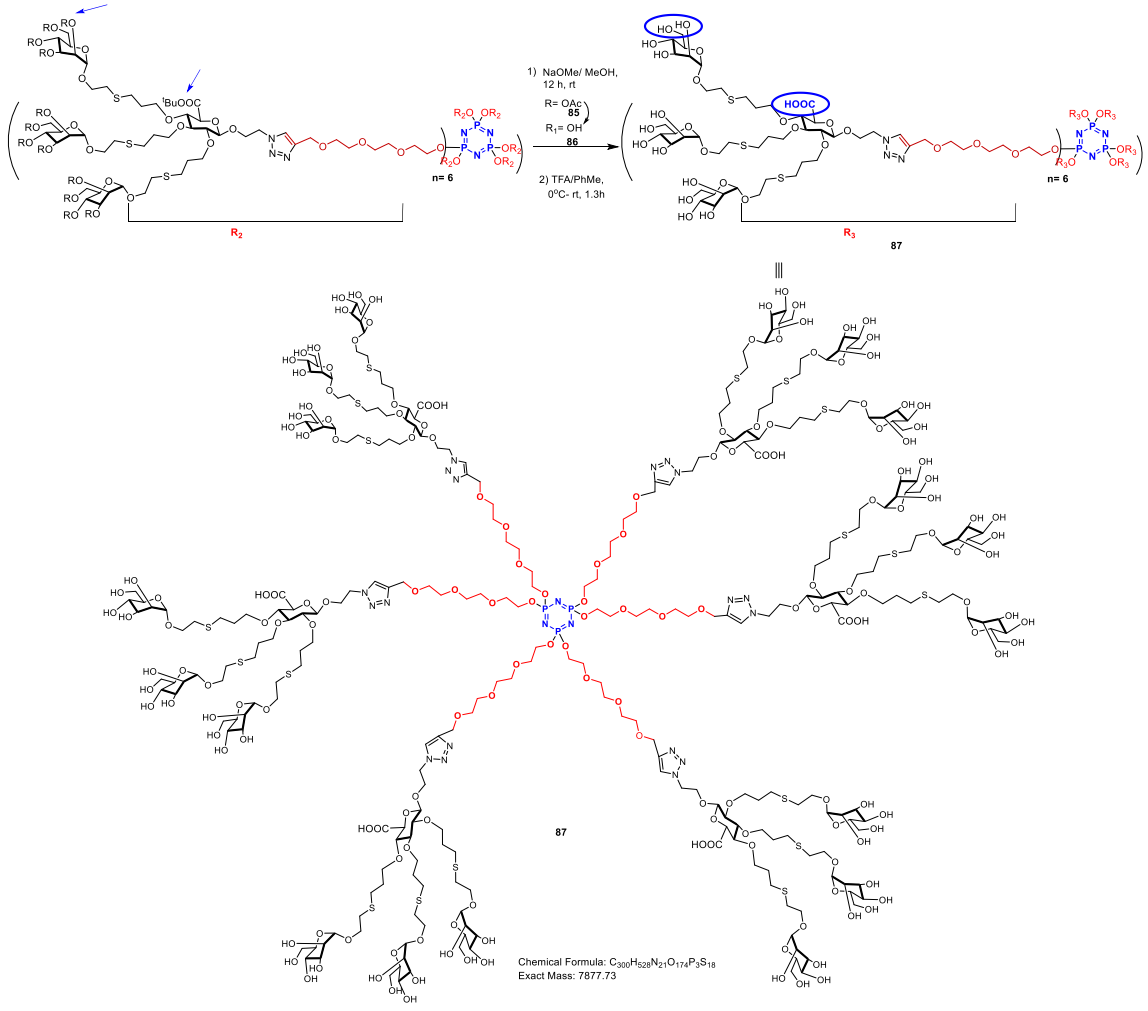

Figure 3.27 MALDI-TOF MS spectrum of dendrimer **87**

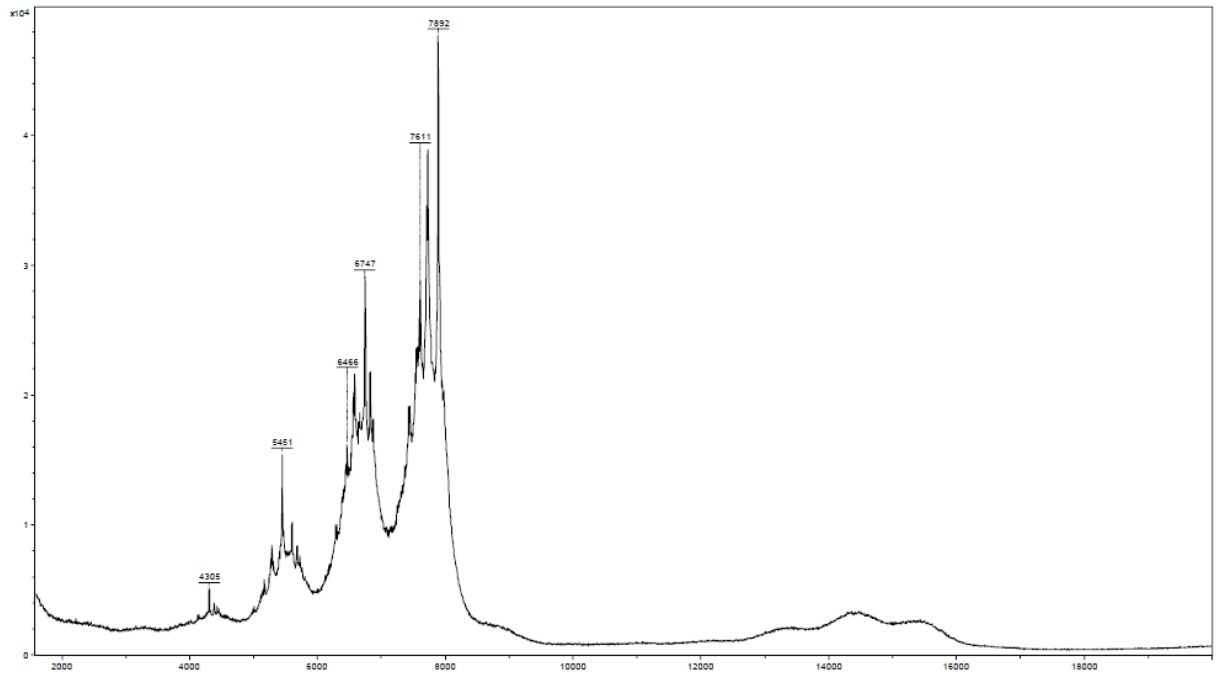

The two compounds **85** and **87** were detected with very good precision (less than 50 ppm), (**Figure 3.28)**. There is a clear positive correlation between the number of mannose units and its ability to bind to bovine erythrocytes. To clarify this speculation more detailed studies will be needed to understand the relationship between the number of mannose units and the effect of these numbers on binding to bacterial lectin in the future.

Figure 3.28 (A) MALDI-TOF analysis high-resolution (internal calibration) of dendrimer **85** and **87**

A

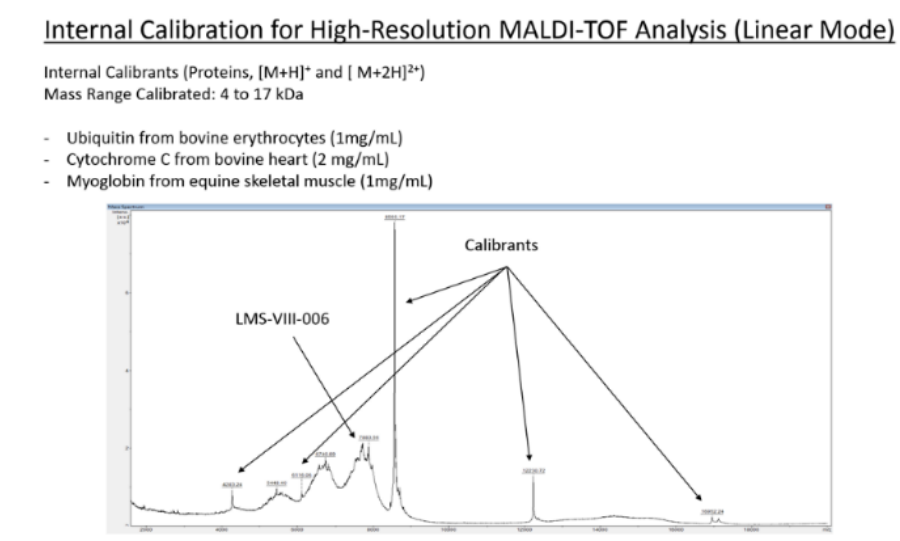

We next turned our attention to the synthesis of G3-fucoside homodendrimer which proceeded following the same procedure we used previously.

Scheme 3.19 Synthesis of fucoside glycodendrimer **88**

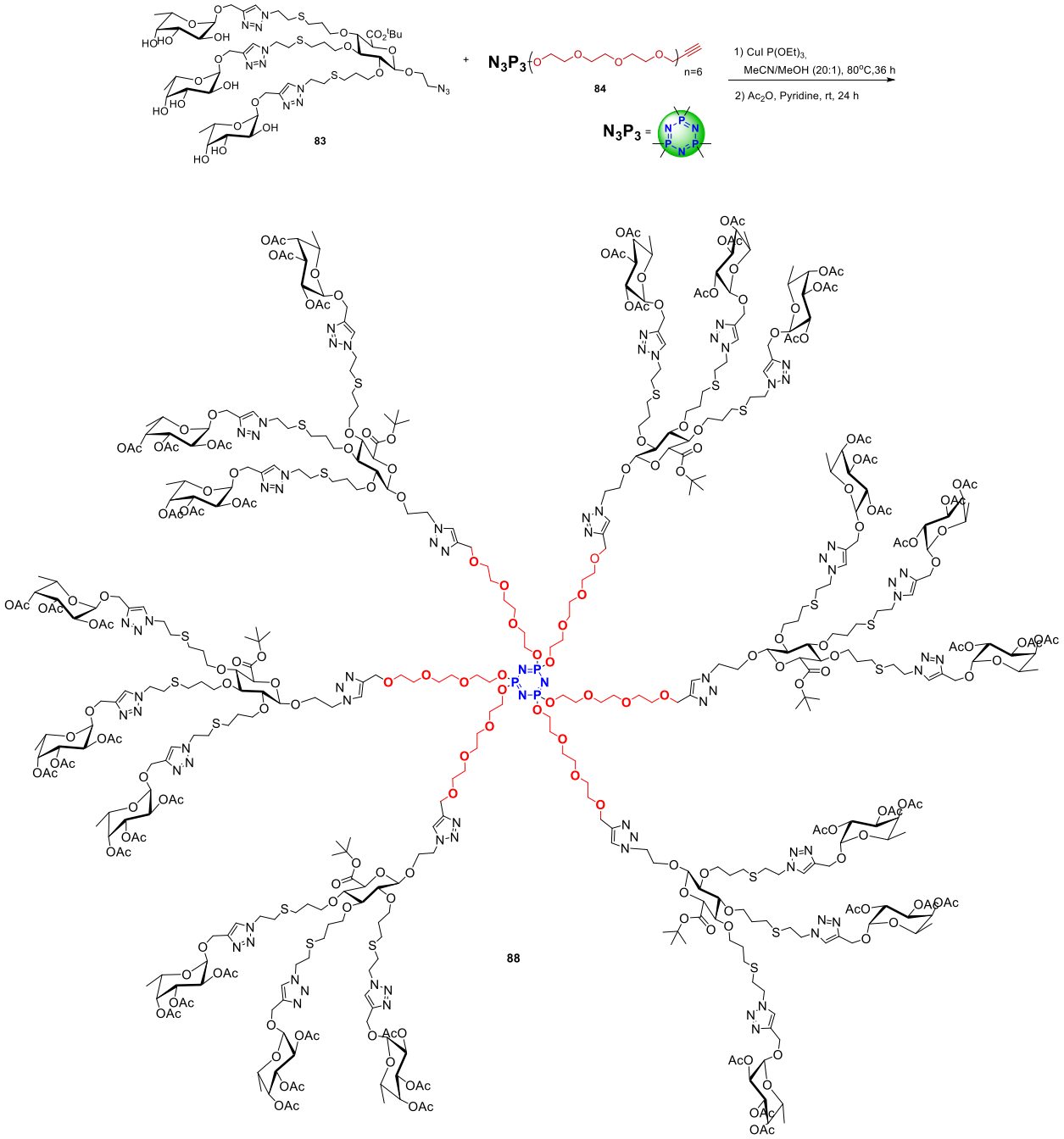

As depicted in (**Scheme 3.19)**, the synthesis was achieved in two sequence steps. First, the click reaction of trithiofucoside β-D-glucuronic ester **83** and dendrimer core **84** was performed using Iodo (triethyl

phosphite) copper(I), CuI[P(OEt)$_3$] catalyst in a mixture of MeOH/acetonitrile at 80 ºC for 24 h and DIPEA as a base, following by removal of the solvent and insitu acetylation in a mixture of acetic anhydride/ pyridine, which after work-up and purification provided of a full acetylated fucoside dendrimer **88**.

MALDI-TOF-MS was employed to further analyze the dendrimer **88**. However, the spectra failed to display molecular ion for the whole dendrimer with six ligands; (11653 Da), it revealed a molecular ion that corresponding to the dendrimer with five ligands attached; (9996 Da), and small signal peak corresponding to the molecular weight of a product (11727 Da), (**Figure 3.29**), which could suggest that complete functionalization of the core structure happened in low yield, Conversely, ^{1}H NMR of **88** (**Figure 3.30**), shows a consistent integration ratio between triazole, Fuc-methyl, *tert*-butyl protons, respectively, which confirmed that six dendrons were attached to the dendrimer core.

Figure 3.29 a) MALDI-TOF- Spectrum (zoom) of compound **88**

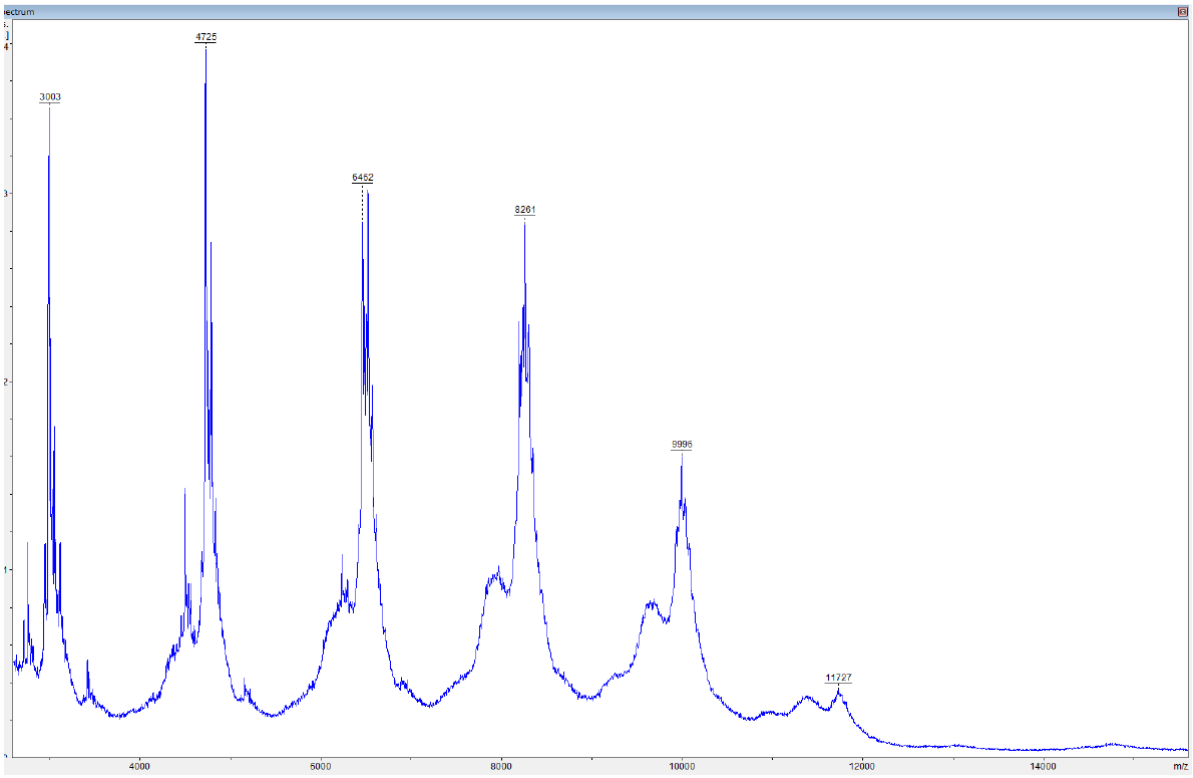

Figure 3.30 ^{1}H NMR spectrum analysis of dendrimer **88**

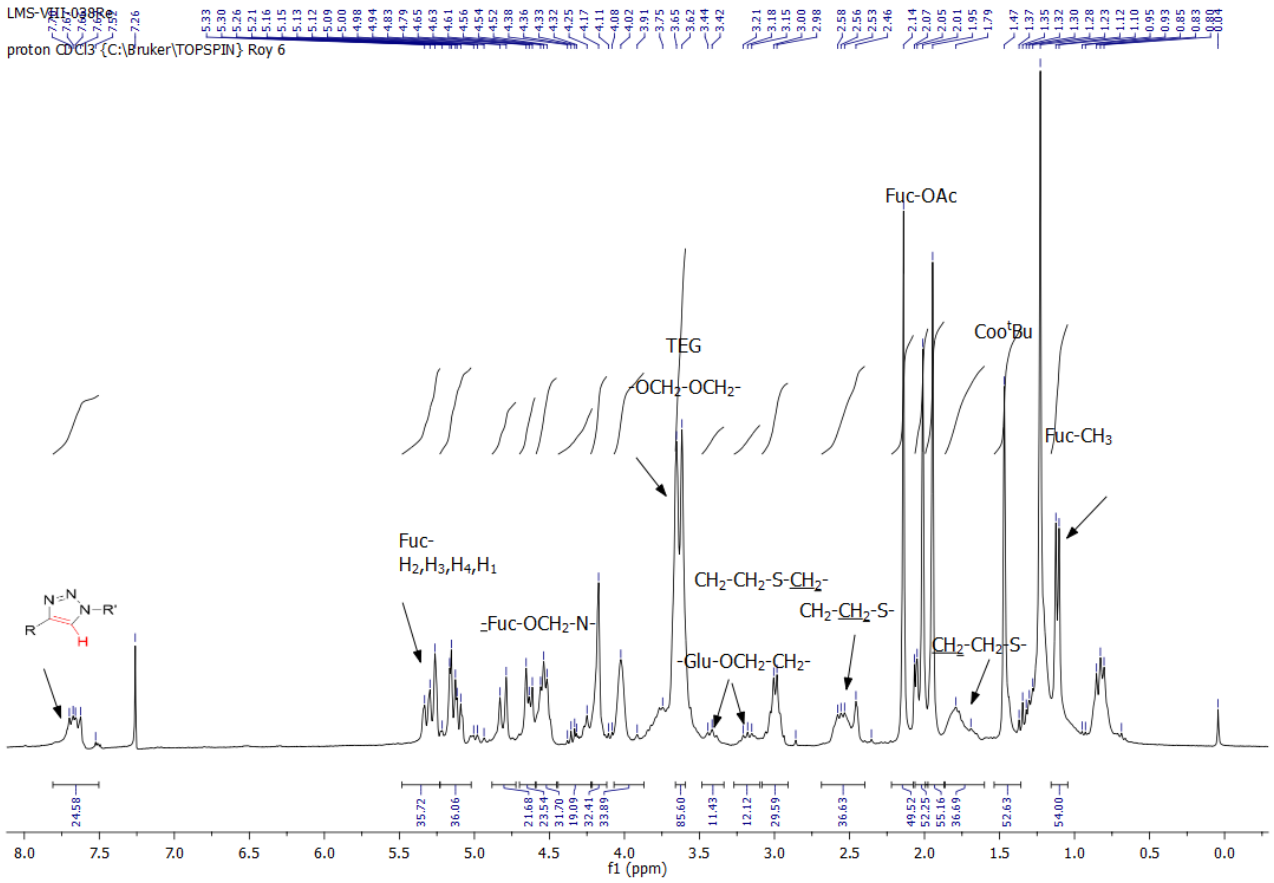

Following the previous procedure, dendrimer **88** was subjected to two continuous steps of deprotection, using NaOMe/MeOH followed by TFA /toluene to afford the desired product G3-OH (COOH) fucoside **90**. A schematic overview of the deprotection methods is shown in (**Scheme 3.20**).

Scheme 3.20 The deprotection of -*O*Ac and *tert*-butyl ester of Fuc glycodendrimer

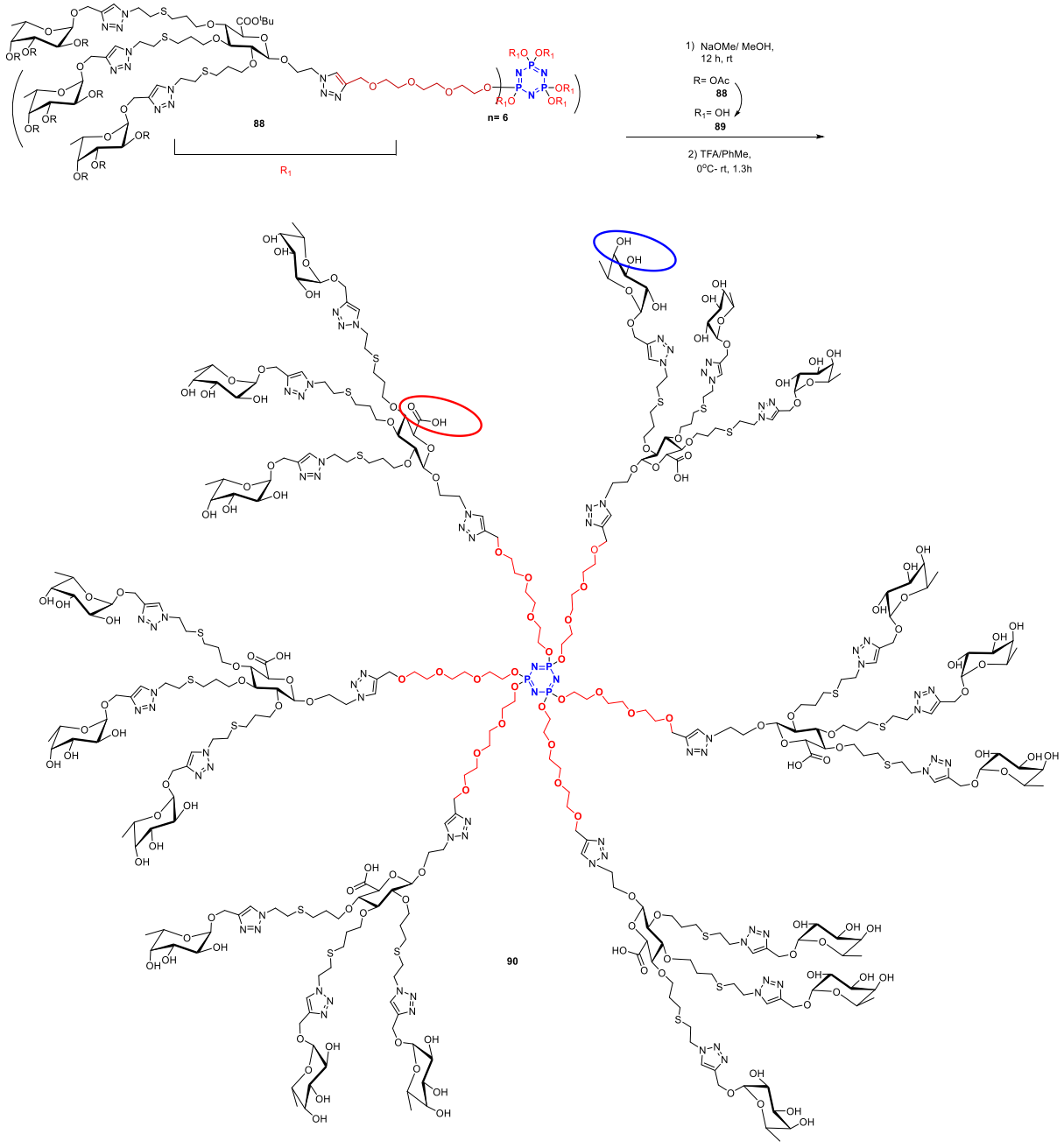

3.5.2 Mannose-dendrimer based on rigid dipentaerythritol core

With the aim of further studying the effect of rigidity, linker length, and valency on the dendrimer-lectin binding, we synthesized another class of glucodendrimers. To this aim, azido-trimannoside dendron **80** was conjugated to the hexa propargylated dipentaerythritol core **91** displays six alkyne functionalities using iodo (triethyl phosphite) copper (I) [CuI.P(OEt)$_3$] Catalyzed alkyne- azide cycloaddition (CuAAc) in a mixture of MeOH, acetonitrile, and DIPEA, followed by complete acetylation of the resulting free hydroxyl groups

in Ac_2O/pyridine afforded the acetylated hexavalent dendrimer **92** (**Scheme 3.21**). The dendrimer is fully characterized by ^1H NMR and ^{13}C NMR spectroscopy. ^1H NMR analysis showed the absence of propargylic signal at δ= 2.50 ppm, and the appearance of H triazole ring signal at δ= 7.69 ppm. The NMR analysis confirmed the attachment of 6 dendrons to the dendrimer core. We did not run MALDI analysis of dendrimer **92**.

Scheme 3.21 Synthesis of hexavalent Man-glycodendrimer **92** based on dipentaerythritol core

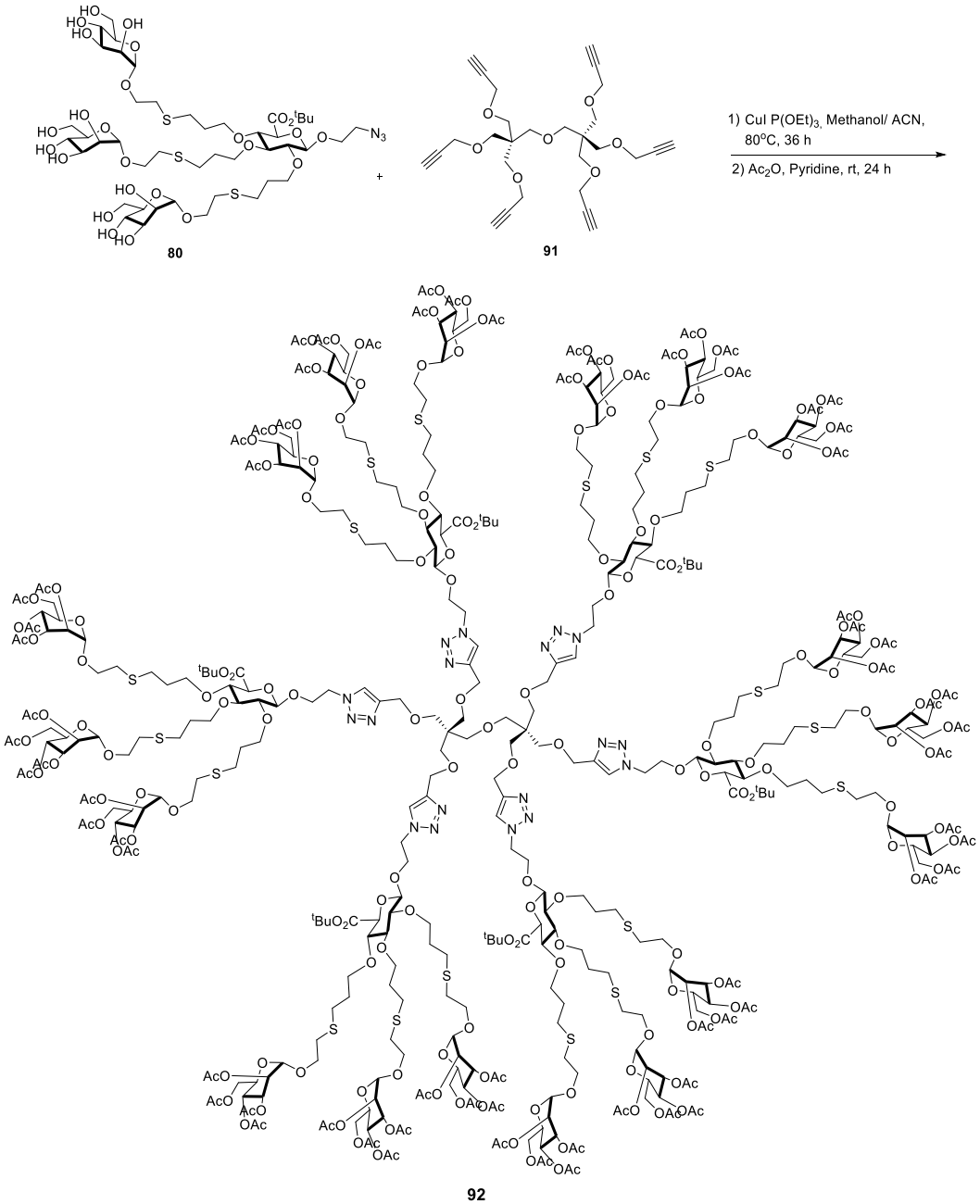

3.5.3 Synthesis of trivalent Man-glycodendrimer based on Benzene-1,3,5-tricarbodimide core

The third class of glycodendrimers is built on benzene-1,3,5-tricarbodimide (BTA-PEG$_3$) core, (**Scheme 3.22**). The trivalent dendritic scaffold **94** was therefore produced by the reaction between tri-mannose-β-D-Glu ester **80** with (BTA-PEG$_3$) **93**, the reaction proceeded as described in our previously reported procedure.

Scheme 3.22 Synthesis of trivalent Man-glycodendrimer based on (BTA-PEG$_3$) dendritic core

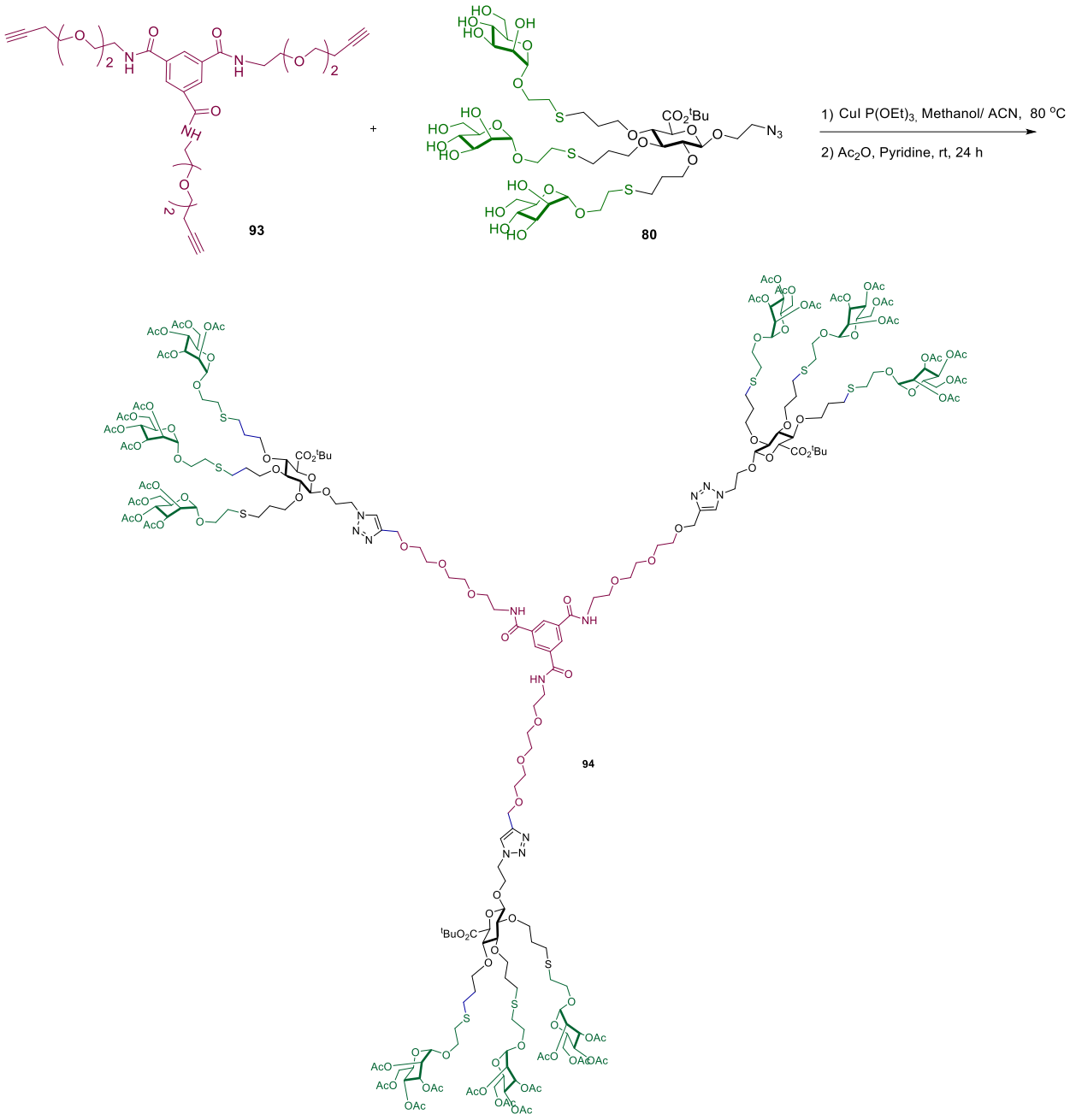

The ^{1}H NMR of **94** (**Figure 3.31**), exhibits several distinct peaks. First, the identification of the aromatic peak at 8.38 ppm as the downfield singlet. Second, the singlet peak at 7.65 ppm which integrated for three protons from the triazole ring, confirms the formation of three arms of glycodendrimer. A broad peak at 7.35 ppm, which is equivalent to -NH amide bond. Multiple peaks at 5.36- 4.55 ppm which is significant to Man. Other multiple peaks at 2.91- 2.36 ppm and 1.97- 1.61 ppm are equivalent to CH_2-S. Finally, four singlet peaks at 2.14- 2.03 are equivalent to acetyl groups, and a singlet peak at 1.47 is equivalent to *tert*-butyl group.

Figure 3.31 ^{1}H NMR analysis of dendrimer **94**

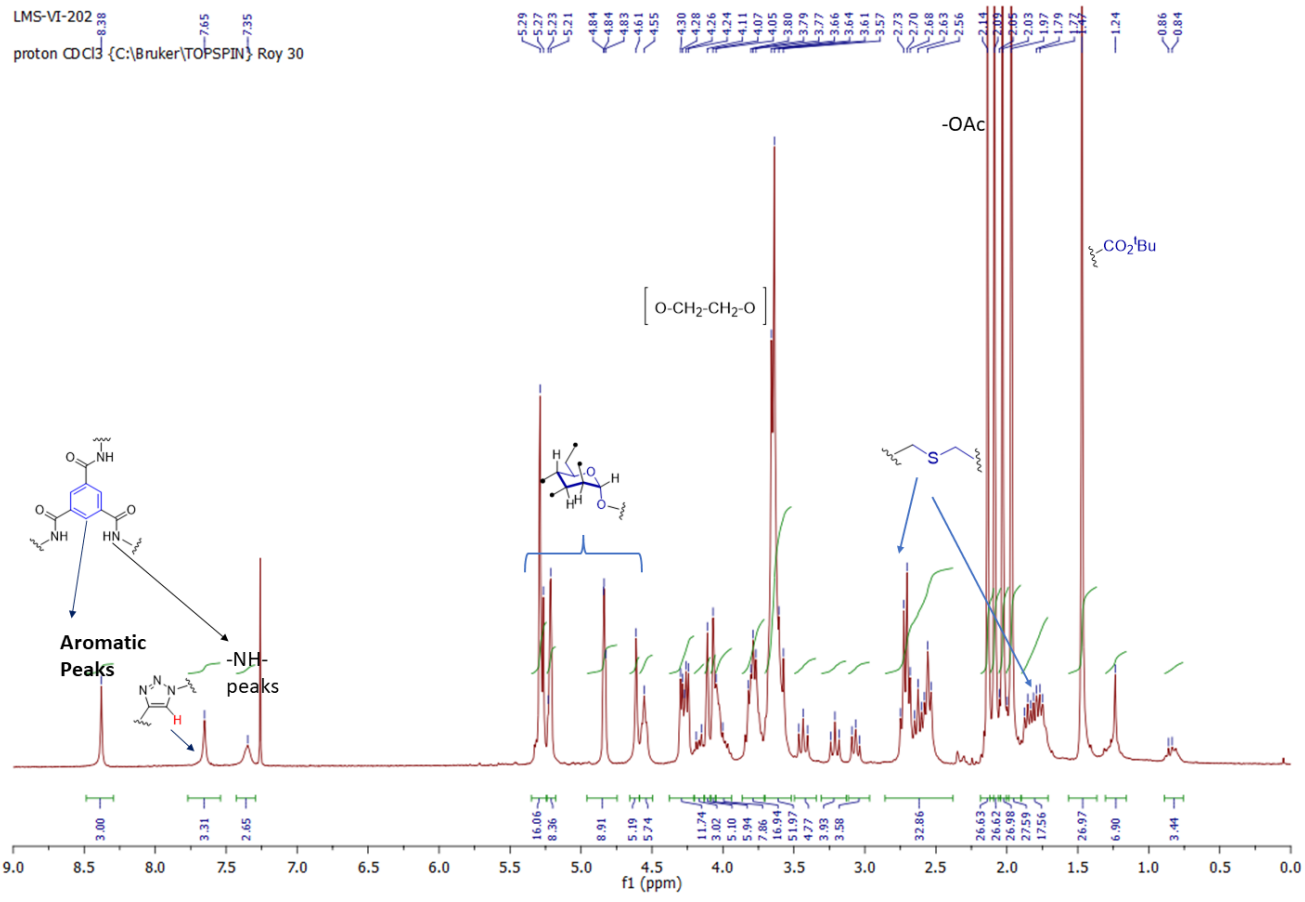

Unfortunately, under the similar reaction conditions, CuAAC did not seem to work properly for core **95**, (**Scheme 3.23)**. Click reaction of dendron **80** with dendritic core **95** using [CuI.P(OEt)$_3$] in a mixture of ACN/MeOH, and DIPEA as a base, leading to incomplete conversion and results of a mixture of low product outcome, (route A, **Scheme 3.23)**. The analysis of the resultant glycoconjugate was found to be very difficult due to a low degree of ligand conjugation. Unlike the spectrum of dendrimer **85 (**see **Figure 3.23)**, all the

peaks were relatively weak, especially the specific signals from 1,2,3-triazole ring and sugar fragment could not be clearly observed in the spectrum. Since the first experiment failed to provide the desired 12-mer glycodendrimer another synthetic pathway was undertaken. Therefore, the polarity of dendron **80** was reduced by full acetylation of hydroxyl groups in a mixture of Ac_2O/ pyridine to obtain a fully acetylated compound **96**. A solution of core **95** and compound **96** in DMF was mixed with an aqueous solution of $CuSO_4$/sodium ascorbate, the reaction was stirred overnight. NMR-based crude analysis showed that the reaction did not give the expected product (route B, **Scheme 3.23**).

Scheme 3.23 Unsuccessful approach to 12-mer glycodendrimer synthesis

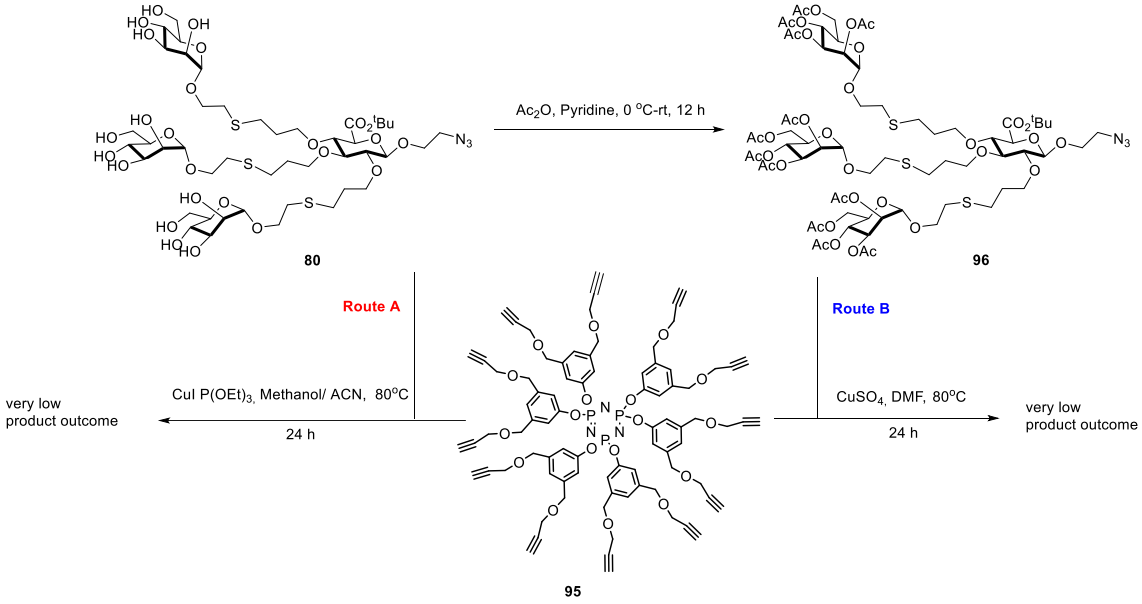

In summary, we have shown that click reaction with CuI [$P(OEt)_3$] is an efficient catalyst in the synthesis of macromolecules in a mixture of polar solvents ACN/MeOH with good conversion. We are currently directing our efforts toward enhancing the high reaction outcomes by screening different solvents.

CHAPTER 4
HOMO GLYCODENDRIMER SYNTHESIS BASED ON D-GLUCOSAMINE PRODRUG SCAFFOLD FOR ANTIBIOTIC CONJUGATION

4.1 Introduction

The second generation of polyvalent glycoclusters built on D-glucosamine is discussed in detail. The design of high-affinity ligands for lectins requires the best possible match between valency and topological display of the carbohydrate epitopes that surround the multivalent core scaffold. Both of these parameters have been extensively examined in the literature, [319, 395] and the influence of the linker arm that connects the carbohydrate to the central core unit has also been previously addressed. [396] The design of spacer arms that present different rigidities with similar lengths would provide the basis for a careful analysis of the parameters that govern multivalent carbohydrate-lectin interactions. Enthalpy improvements would result from modifications of the structure of the carbohydrate epitope through additional stabilizing constants, but increased affinities for lectins can also be obtained with more rigid linker arms, which decrease the entropic cost upon binding. Polyethylene glycols (PEG) are typical spacer arms used for the design of multivalent glycoconjugates; they have the advantage of being water-soluble, of various lengths, and with an alcohol moiety that can be either derivatized to alternative functional groups or even directly involved in a glycosidic bond for connection to the carbohydrate epitope. Triethyleneglycol (TEG) is a very common member of this family, and numerous examples have been previously described in the literature. [269, 397-401] this linker arm is easy to introduce through glycosylation but also provides improved water solubility for the resulting multivalent ligands synthesized. The sp^3 hybrid of carbon and oxygen atoms along its chain provides high freedom of movement for the terminal carbohydrate epitopes.

Figure 4.1 Structure of the designed D-glucosamine linker arms

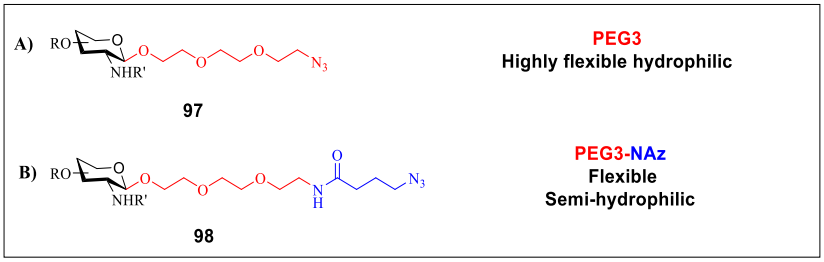

The general formula of the glycoclusters core is presented in (**Figure 4.1**). Linker arms with SP^2-hybridized atoms in a chain analogous to PEG_3 in terms of length can be used to obtain glycoclusters that present more rigidity than the parent PEG_3-based structures. Such glycoconjugates would provide relative entropic gain

and therefore, better binding properties towards lectin. Nevertheless, the introduction of rigidity motifs in the linker arm should be accurately balanced since a too-rigid linker may not allow the second epitope to reach its binding pocket on the multivalent in a chelate binding mode.

4.2 Design and synthetic strategy

In this part of the research, a new class of dendrimer-ciprofloxacin conjugates is designed for bacteria targeting-drug delivery system based on G3 glycodendrimer. This dendrimer generation provides a sufficient number of peripheral functional groups; hydroxyl groups to bind to bacterial lectin; and carboxylic group to be amenable to covalent conjugation with drug molecules, (**Scheme 4.1**).

Scheme 4.1 Retrosynthesis of target dendrimer based on D-glucosamine scaffold

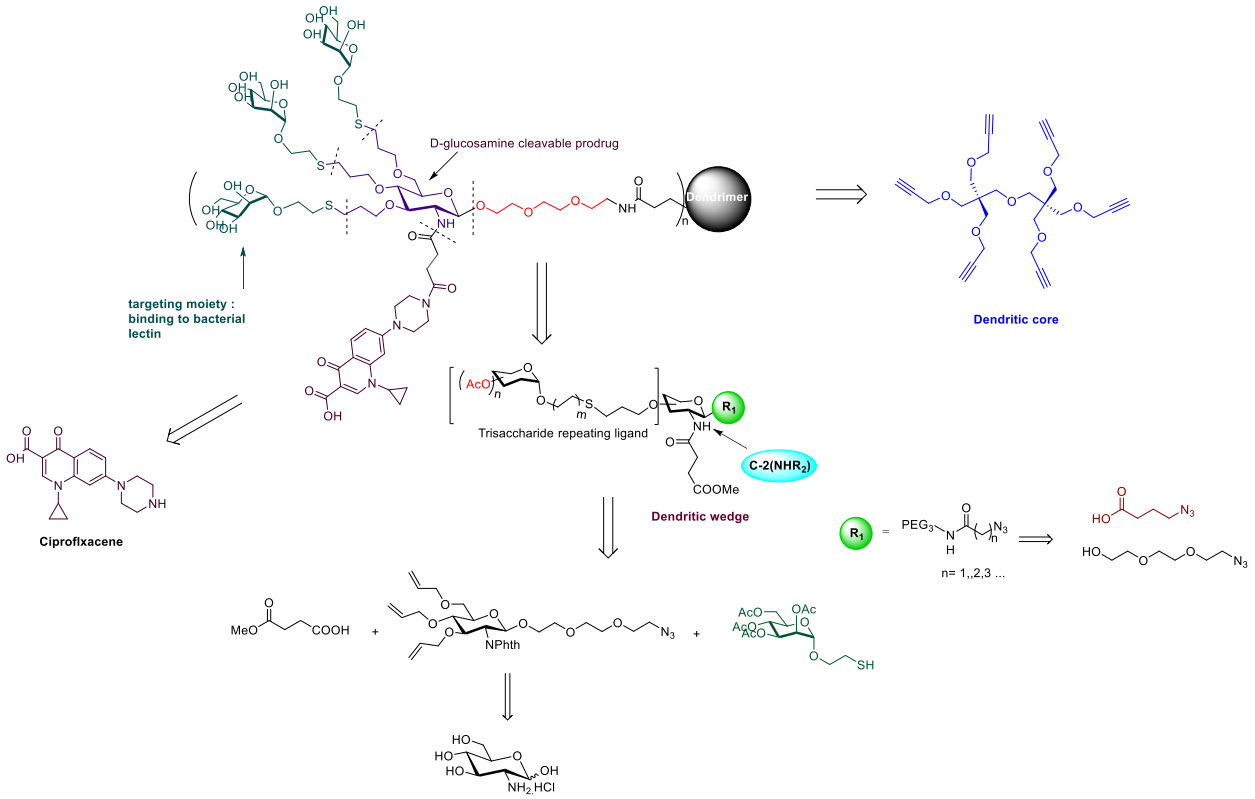

As shown in (**Scheme 4.1)**, the main building blocks of the dendrimer components are hexa-propargylated dipentaerythritol core, α-D-mannose thiol, and *O*-glycosidic β-D-glucosamine, the three building blocks conjugated together *via* thiol-ene photolytic reaction, Cu-catalyzed Azide-Alkyne Cycloaddition (CuAAC).

Our approach in the design of Cip-G3 dendrimer conjugates involves important parameters pertinent to D-glucosamine: (i) C-1 as the position to attach semi-hydrophilic PEG_3 linker with a terminal azide, thereby, spacing between D-glucosamine bearing Man binding bocks was further increased; (ii) modification of -NH_2 group at C-2 position by coupling with methoxy butanoic acid linker; C-2(NHR) which subsequently conjugates to the drug through an amide bond.

4.3 Literature background

In the field of synthetic carbohydrate chemistry, stereocontrol at the anomeric center is one of the most important subjects of chemical glycosylation. [402] Stereoselectivity to produce 1,2-trans glycosides has been achieved through the participation of neighboring acyl- or carbamate-protecting groups located at the 2-position of the glycosyl donor. Recently, various participating groups introduced at the 2-OH of the glycosyl donor have been applied to chemical glycosylation. For example, the dialkylphosphate group, picolinyl group, 2-nitobezyl group, and 2-nirobenzyl group, and 2-cyanobenzyl group have been developed to assist the synthesis of 1,2-trans glycosides. In the case of 2-aminosugars, the phthaloyl group and carbamate groups, such as Troc, are frequently used for β-glycosylation with high selectivity. The 2,4-dinitrophenyl groups were used for the 2-N protection of glucosaminyl donor. [403-405] No neighboring group participation was observed, hence, glycosylation in this case, leads to the formation of an anomeric mixture (2 :1- 3.5 :1 α/β ratio). In some cases, however, the use of any N-protecting groups must be carefully chosen, particularly when approaching a complex carbohydrate because of the difficulty of the removal step.

4.3.1 Synthesis od 2-Deoxy-2-acetamido-glycopyranoside

For 2-(acylamino) -2-deoxyhexoses (e.g., **99**), such electrophilic activation forms a reactive oxocarbenium ion **100** intermediate, which often collapses rapidly to an oxazolinium ion **101** intermediate (**Scheme 4.2**, mechanism A). Intermediate **100** is expected to undergo nucleophilic attack at C-1 selectively from the β-face of the glycosyl donor to yield only 1,2-trans-glycosides, in those cases where an α/β mixture is observed, this is often attributed to reactions of **100**. However, with the 2-amino group acylated, e.g., N-acetyl, the intermediate **101** can be stabilized further through abstraction of the amide proton to form a relatively stable 1,2-oxazolines **102**. [406] However, 1,2-Oxazolines **102** can be used as glycosyl donors although rather harsh glycosylation conditions are required.

Scheme 4.2 Intermediates in Lewis acid activated glycosylation with D-glucosamine

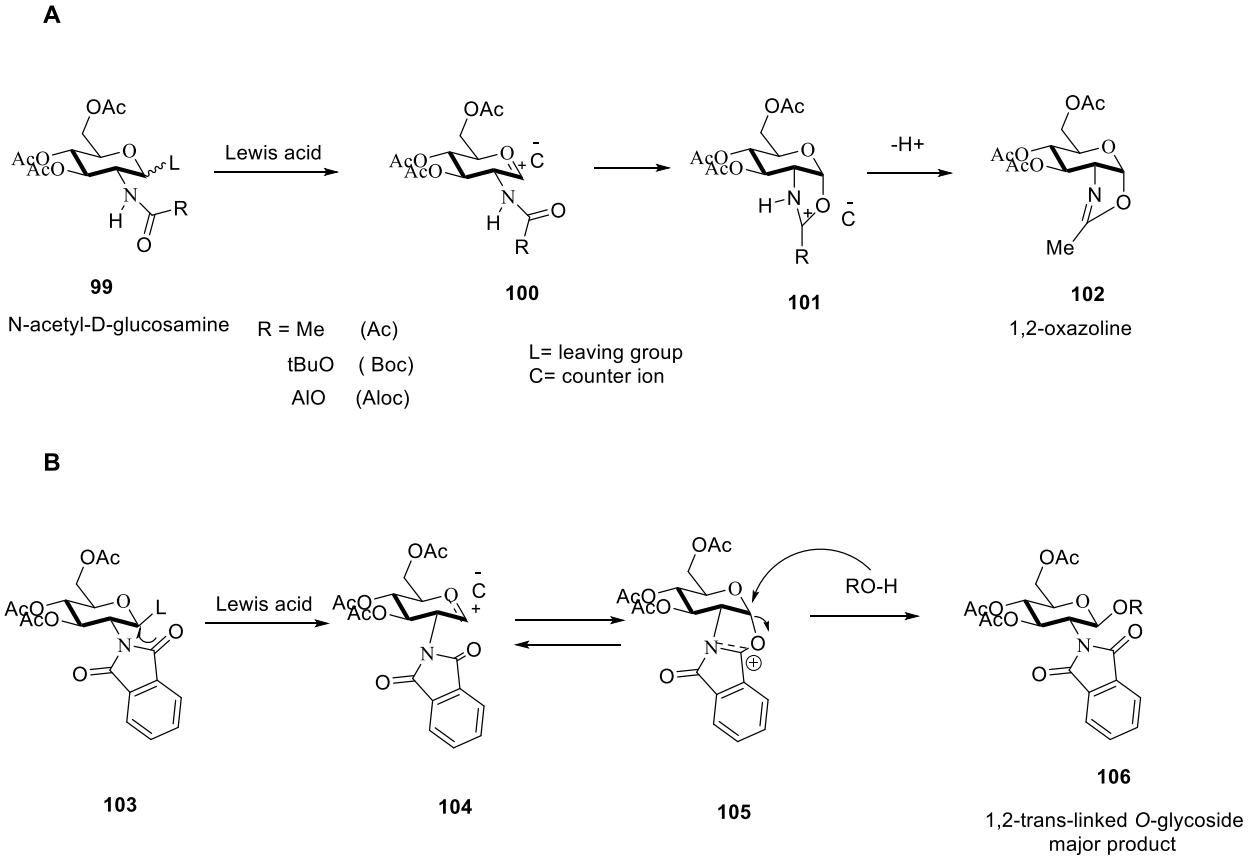

The formation of an oxazoline intermediate **102** upon electrophilic activation may be prevented when the abstraction amide proton is substituted by a protecting group that is not cleaved during the glycosylation step. This can be achieved by blocking the 2-amino group with two monovalent protecting groups, or by application of the bivalent N-phthaloyl (Phth) group (**Scheme 4.2**, mechanism B).[407] Electrophilic activation of the bivalently protected glycosyl donor **103** yields an oxocarbenium ion **104** which can form an oxazolinium ion **105**. The reactive intermediate **105** can only be attacked from the β-face by a nucleophile and cannot form stable oxazoline. Glycosylation with Phth-protected glycosyl donors occurs under mild conditions at low temperatures and gives exclusively 1,2- trans-glycosides **106**. An improved protocol for the introduction of the phthalimido function was reported.[406] Thus, glycosyl bromides, acetates,[408] and trichloroacetimidates,[409] thioglycoosides,[311, 410] all proved to be effective in the synthesis of 2-phthalimido-2-deoxy-β-D-glucopyranosides. Usually, the 2-phthalimido protecting group is maintained until the synthesis of the target oligosaccharides. Therefore, 2-NPhth-D-glucosamine donor (GlcN) **103** was chosen as the monosaccharide unit. This decision was based solely on the assumption that any stereochemical ambiguity could be eliminated by the strong 1,2-trans directing nature of (NPhth) group.[406, 411-414]

4.4 Results and discussion

4.4.1 Synthesis of β-D-glucosamine cleavable prodrug scaffold

Given the success of the previous synthesis of protected D-Glucosamine[407, 415] **108** as a building block, we anticipated that a semi-synthetic approach would be the most viable means to achieve a scalable synthesis for the next step (**Scheme 4.3**). We intend to compare the length at the anomeric position by installing azido-PEG_3 linker. Thus, triethylene glycol (PEG_3) was selected as a model that can be conveniently synthesized and modified. To this end PEG_3-N_3 **109** linker was prepared, (see supporting information**)**.

Scheme 4.3 Synthesis of glycosylated β-D-glucosamine **111**

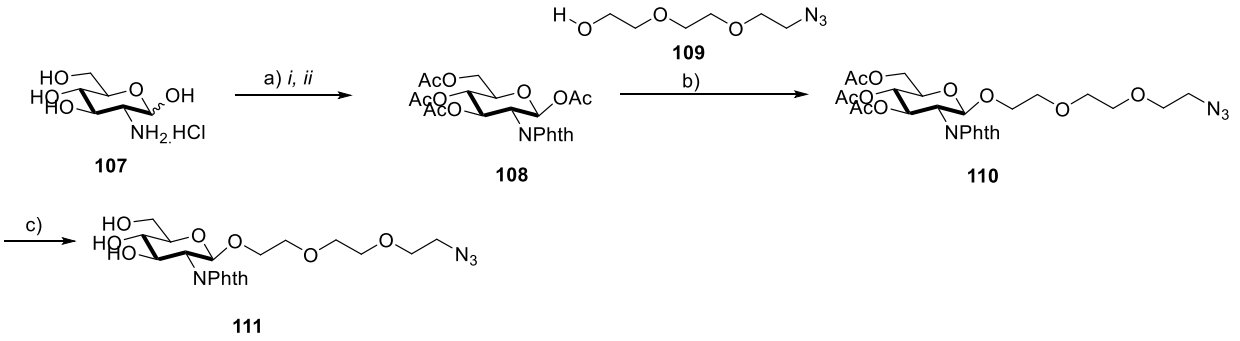

a) *i*) Ac_2O, Pyridine, 0 °C- rt, 12h; *ii*) Phthalic anhydride, NaOMe, MeOH, 0 °C- rt, 12h, 50%; b) $BF_3.Et_2O$, DCM, 0 °C-rt, 20 h; 60%, c) NaOMe/ MeOH, pH= 7, 5h, 95%.

A schematic overview of the glycosylation strategy of 2-phthalimido D-glucosamine, [336, 416, 417] is depicted in (**Scheme 4.3)**. The synthesis started with glycosylation of 1,3,4,5-tetra-*O*-acetyl-2-deoxy-2-phthalimido-2-D-glucopyranose. [407] **108** as a glycosyl donor with azido-PEG_3-OH **109**[418] in dry dichloromethane in the presence of $BF_3.Et_2O$ as a promotor afforded product **110** in 60% yield. The reaction requires the use of excess promotor resulting in the best reaction outcome. ^{1}H NMR analysis of compound **110** is shown in (**Figure 4.2)**. The stereochemistry of the newly installed linker was determined to be β-linked on the basis of the GlcN H-1 and H-2 coupling constant (*J*= 8.5 Hz). PEG_3-related peaks appeared between 3.3 and 3.7 ppm; peak integration produced 12 protons.

Figure 4.2 ^{1}H NMR analysis of compound **110**; with an enlargement of the area from 5.00 to 6.00 ppm. The coupling between H1-H2 indicated by double-headed arrows

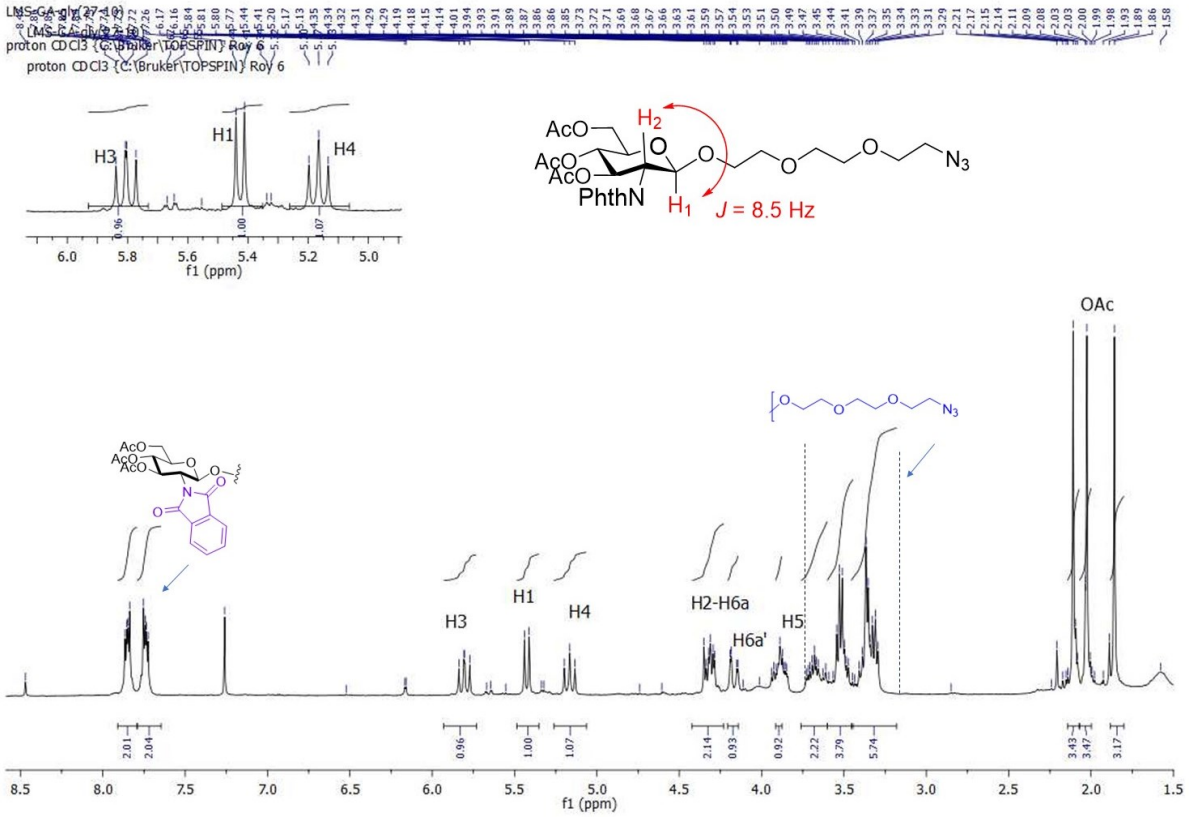

Subsequent removal of *O*-acetyl groups under Zemplén condition with sodium methoxide in methanol at pH= 9, for 7h at room temperature, resulted in a mixture of products as indicated by TLC, and by analysis of ^{1}H NMR, it shows that major products were compound **111**, accompanied by phthalamic acid **112**, (**Scheme 4.4)**, which is obtained as a result of nucleophilic ring opening of the phthalimido group (NPhth), **(**data is not shown), this led to drastically lower the yield of the desired product **111**. To overcome the cleavage of phthalimido group (NPhth), the Zemplén condition had to be adjusted at pH 6-7 for 5 hours at room temperature which afforded the desired product **111** in quantitative yield.

Scheme 4.4 Proposed ring opening of 2-phthalimido-β-D-glucopyranose

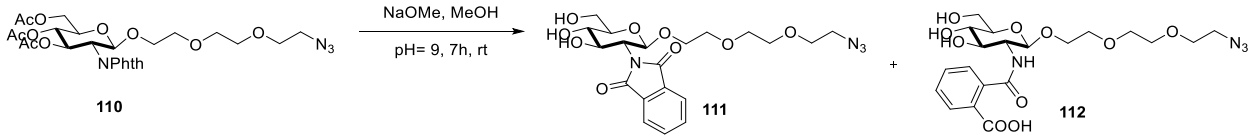

The next step is allylation (**Scheme 4.5**). The reaction of compound **111** with allyl bromide under basic conditions in the presence of 4.5 equivalent of sodium hydride (60%) in DMF as a solvent for 2.5 h at room

temperature, (*pathway A*, **Scheme 4.5**), provided the desired product *O*-2, *O*-4, and *O*-6-triallyl **113** albeit with very low conversion, and accompanied by side products. Di-allylation of β-D-glucosamine **111** and nucleophilic ring opening of the phthalimido group (NPhth), were found to be the predominate reaction pathway, (as indicated by ^{1}H NMR analysis, data are not shown). Therefore, the use of standard conditions involving sodium hydride was incompatible with the base-sensitive (NPhth) group. In order to investigate alternative methodology to optimize the yield, we further explored the allylation under different conditions. Thus, using LiHMDS as a base led to an improvement of the yield to the product **113** (60%), (*pathway B*, **Scheme 4.5**). [419, 420]

Scheme 4.5 Synthesis of triallyl D-glucosamine **113**

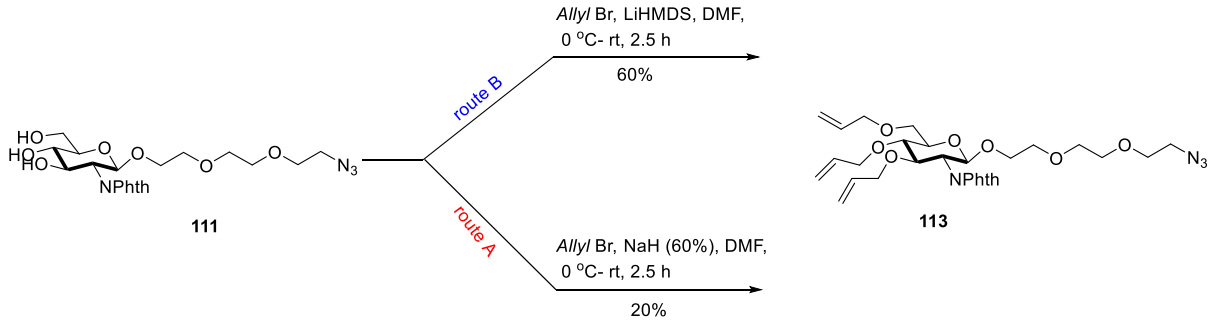

The proton NMR analysis of compound **113** in (**Figure 4.3**) shows the distinct peaks corresponding to allyl protons. The ^{1}H NMR shows a difference between the double bond geometry of allyl bromide. Interestingly, two new different multiplets appeared at 6.09- 5.74 ppm integrates for two protons, and the other multiplet at 5.62-5.47 ppm. We attributed this to the presence of phthalimide ring. More downfield peaks from the phthalimide ring appear multiplet at 7.94-7.75 that integrated to two protons, and another doublet of a doublet at 7.74 ppm integrated to the other two protons. The peaks from PEG_3 appear at a chemical shift between 3.27 and 3.69 ppm.

Figure 4.3 ^{1}H NMR analysis of triallyl β-D-glucosamine scaffold **113**

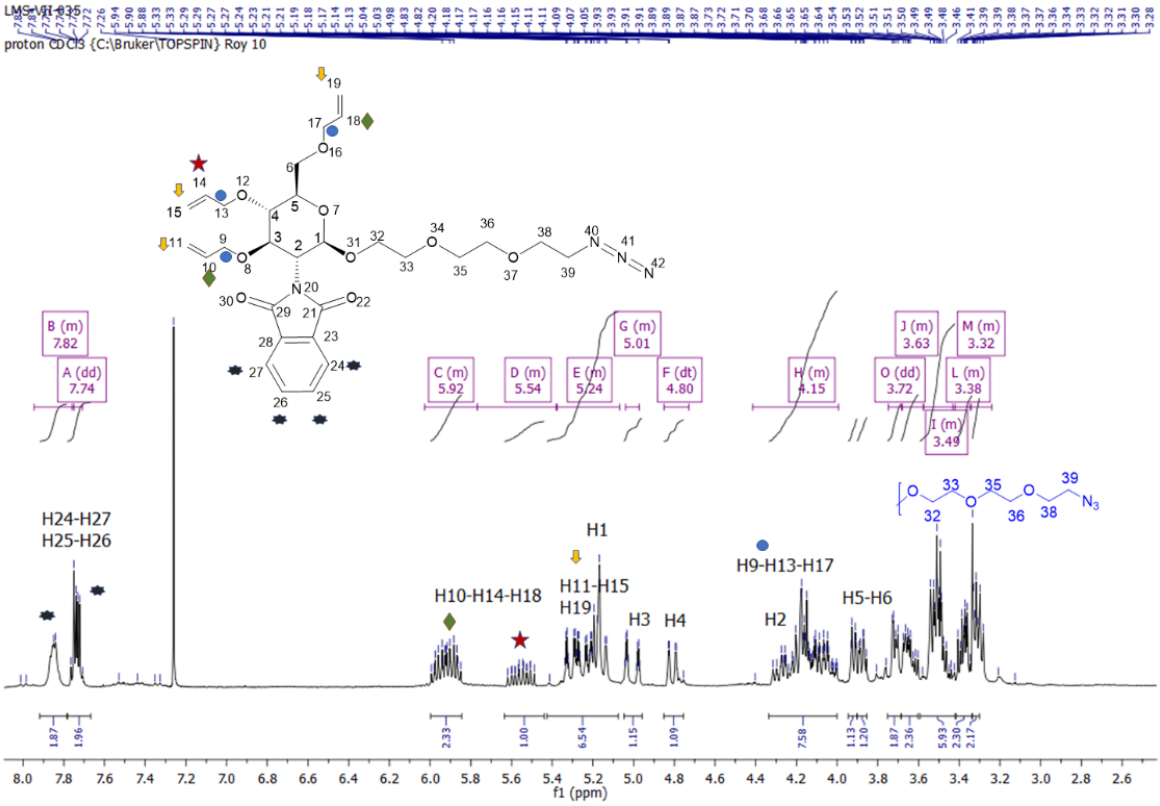

The next step in the synthesis process was to install a linker at -NH_2 of C-2 position that incorporated a terminal ester. Thus, compound **113** was subjected to two separate steps, as shown in (**Scheme 4.6**). The first step is the deprotection of phthalimido group (NPhth). We employed two different conditions, first stirring in hydrazine and methanol at room temperature, there is no product observed even after several days of stirring at room temperature. Second, the reaction is performed in reflux hydrazine and ethanol, unfortunately, we observed an allylic exchange (as indicated by ^{1}H NMR, data are not shown) and we did not observe the desired product. Therefore, we optimized the conditions of one-pot deamination of phthalimido group. We found that the addition of alcohol as a co-solvent was necessary to achieve the best reaction outcome for the step of the deprotection. Using *n*-butanol was optimal because the temperature of the reaction mixture was higher than that with methanol or ethanol, and the higher temperature prompted deamination. Ethylenediamine was selected as the amine for deprotection [421] because it is safer than hydrazine which we used previously. With this optimized condition, compound **113** reacted with ethylene diamine in *n*-BuOH for 2.30 h at 95 °C to liberate free amine **114** with excellent yield (83%).[422-425]

Scheme 4.6 Synthesis of β-D-glucosamine scaffold **117**

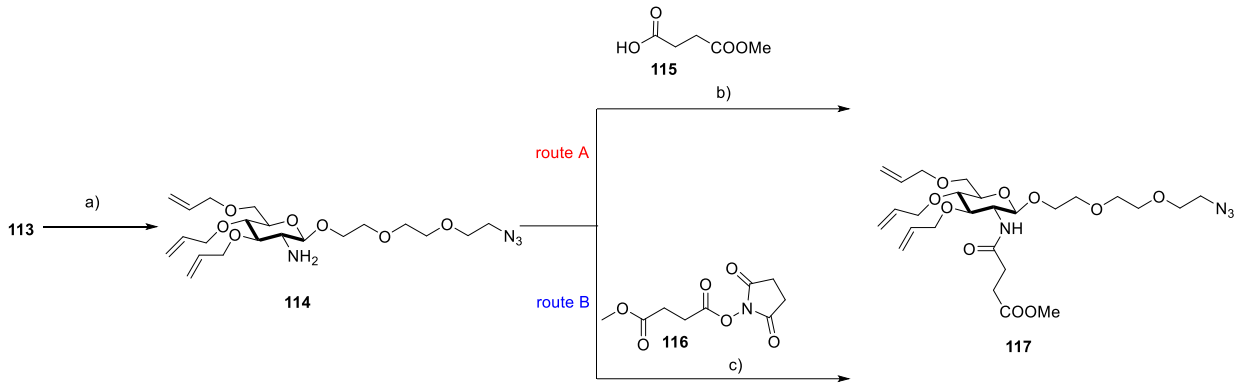

a) $H_2N\sim\sim NH_2$, *n*-BuOH, 95 °C, 2h, 83%; b) DIC, HOBt, Et_3N, 16 h, 72%; c) DMF, DIPEA, rt, 10 h.

^{1}H NMR analysis of compound **114** (**Figure 4.4**) confirmed the complete deprotection of (NPhth).

Figure 4.4 ^{1}H NMR analysis of β-D-glucosamine derivative **114**

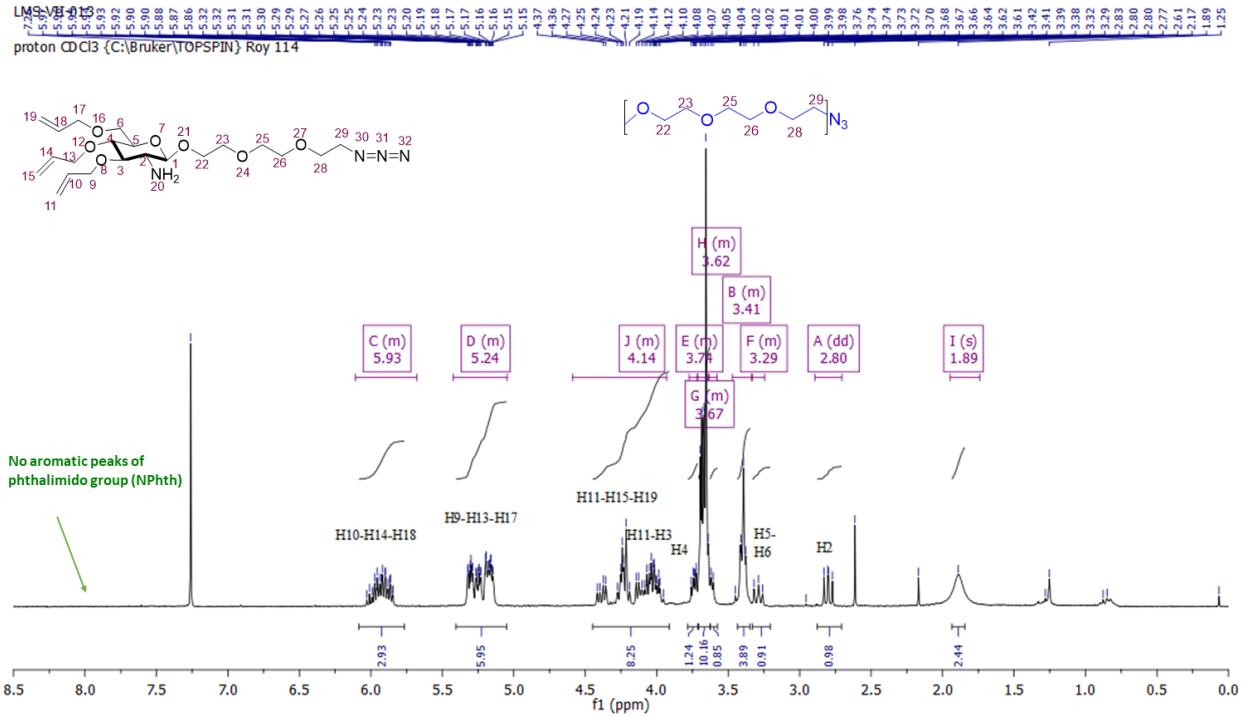

Subsequent step is the coupling of compound **114** with the methoxy butanoic acid **115,** the reaction is performed using *N,N*-diisopropylcarbodimide (DIC), and 1-hydroxybenzotriazol.H_2O (HOBt) in the presence of triethyl amine (NEt_3) to obtain the amide product **117** in 72% yield, (**Scheme 4.6**, *pathway A*).

However, because of the difficulty to remove little impurities eluted with the desired product during the purification on column chromatography, we found that the reaction of compound **114** with 2,5-dioxopyrrolidin-1-yl methyl succinate linker **116** in the presence of DIPEA (**Scheme 4.6**, *pathway B*) gave much pure product **117**. The resulting product was confirmed by ^{1}H NMR, one of the most specific chemical shift protons come from the three protons -COOMe (3.7 ppm) of the newly attached linker. However, the signal from linker PEG_3 and the signal from methyl ester overlap. The appearance of a peak at 2.5 ppm further confirms the butanoic linker (-CH_2-CH_2-), (**Figure 4.5**). The conjugation of this linker to β-D-glucosamine derivative will provide spacing (4 carbon chain) from the dendrimer surface which may lower the steric hindrance as the drug conjugates and release.

Figure 4.5 ^{1}H NMR analysis of compound **117**

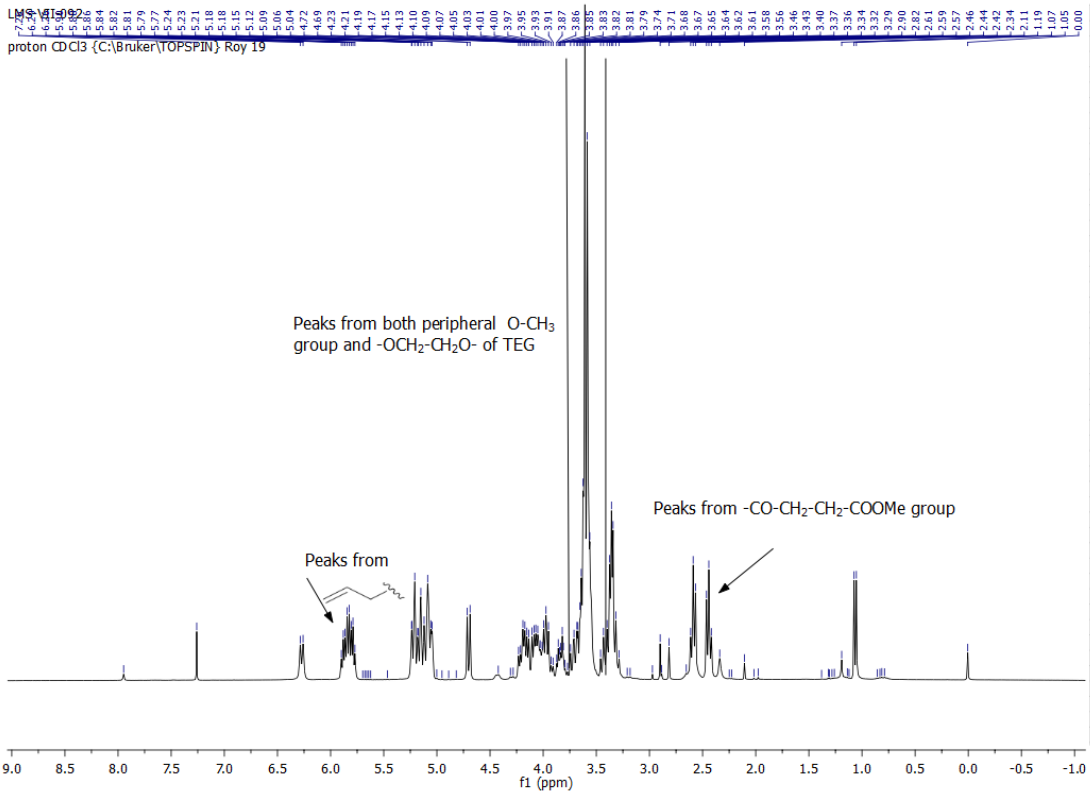

Reduction of the azide **117** with PPh_3 in THF-H_2O at room temperature provided the corresponding free amine **118**. Subsequantely, the amine site protected by Boc group to prevent any undesired side reactions during the chemical process, (**Scheme 4.7**), therefore, reaction of compound **118** with 1.3 equivalent of di-*tert*-butyl dicarbonate $(Boc)_2O$ using triethylamine in dry DCM, afforded NH-Boc protected amine **119** in 72% yield (**Scheme 4.7**). [426]

Scheme 4.7 Synthesis of D-glucosamine building block **119**

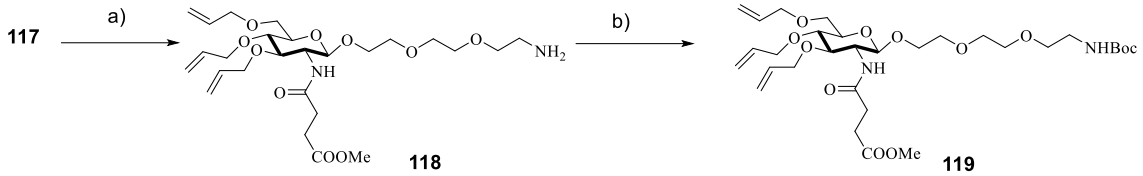

a) PPh_3, THF, H_2O, 12 h, rt, 52%; b) Boc_2O, DCM, NEt_3,12 h, rt, 84%

^{1}H NMR results show a singlet peak at 1.39 ppm integrated for nine protons of Boc group, indicating successful protection of amine group, (**Figure 4.6**). HRMS analysis of compound **119**, the molecular ion detected at *m/z* 667.3397 was found to match with theoretical of $C_{31}H_{52}N_2O_{12}$ [M+Na^+], 667.3412, (see supporting information).

Figure 4.6 ^{1}H NMR of β-D-glucosamine building block **119**

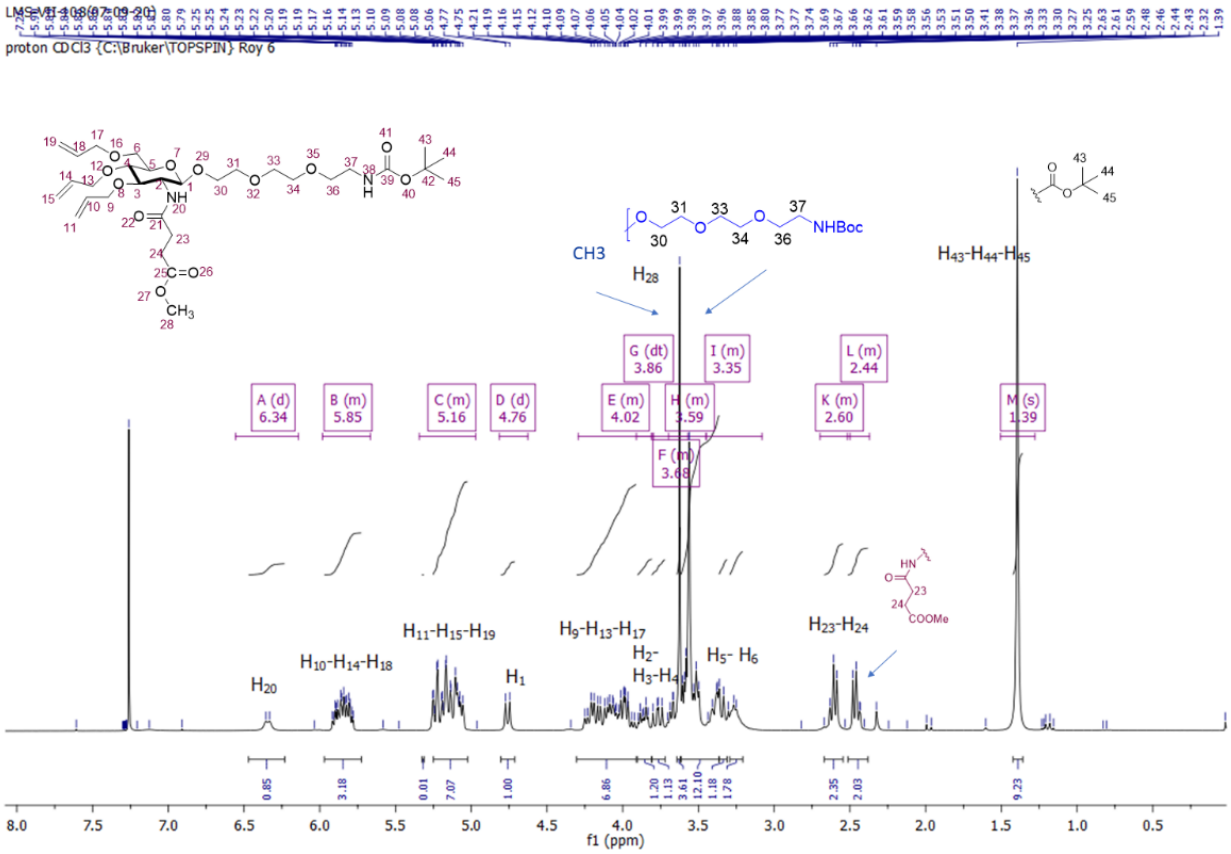

4.4.2 Synthesis of trithiomannoside β-D-glucosamine scaffold **125**

We next turned our attention to the synthesis of the target trivalent mannoside D-glucosamine building block, (**Scheme 4.8**). The exposure of a mixture of NH-Boc tri-allyl compound **119** and 2,3,4,6-tetra-*O*-acetyl-α-D-mannoside thiol **67** in the presence of 2,2-Dimethoxy-2-phenyl acetophenone (DMPA) as the radical initiator in the minimal amount of DMF solvent. For a standard set of conditions, mannose thiol **67** and compound **119** were mixed in a molar ratio of 6:1 (thiol: alkene), and this mixture was irradiated for 3 h at 365 nm, led to the formation of thiol-ene addition product, trithiomannoside dendron (confirmed by the disappearance of olefinic protons of allyl groups in ^{1}H NMR of the crude mixture). After the reaction work-up, the crude product was purified on column chromatography to afford the trithiomannoside β-D-glucosamine **120** in 87% yield. [360] ^{1}H NMR analysis shows the existence of both the PEG_3 backbone at 3.60-3.50 ppm, and the mannoside thioether at 2.5-3 ppm (**Figure 4.7**, bottom). No peaks of alkene protons were observed. The disappearance of the signal reveals the consumption of starting material, and the conversion efficiencies were found to be essentially high yield for the photochemical reaction. The resulting trithiomannoside **120** was isolated in 85%. Purification of the product was done by flash column chromatography. (**Figure 4.7**) displays the results of **119** ^{1}H NMR (top), and ^{1}H NMR **120** (bottom).

Scheme 4.8 Synthesis of targets trivalent thiomannoside β-D-glucosamine building block **125**

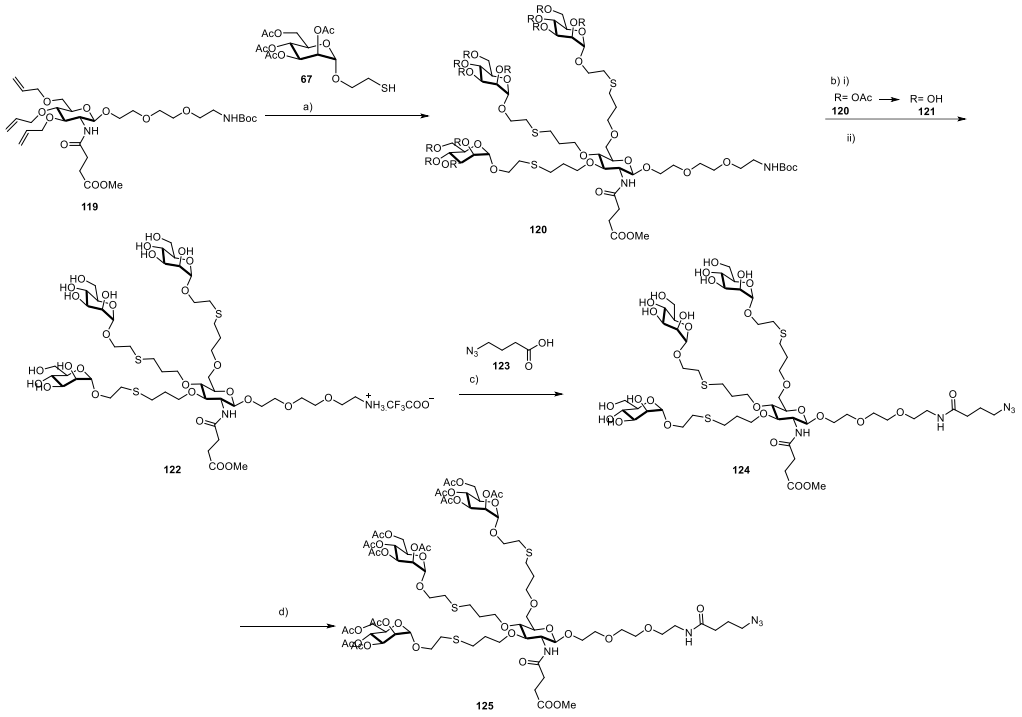

a) DMPA, DMF, 365 nm, 3 h, 85%, b) *i*) NaOMe/MeOH, 12 h, rt; *ii*) 20% TFA/DCM, 2h, 87%, c) PyBop, DIPEA, DMF, 12 h; d) Ac_2O, Pyridine, rt, 12 h

Figure 4.7 ^{1}H NMR analysis of **119** (top), and **120** (bottom)

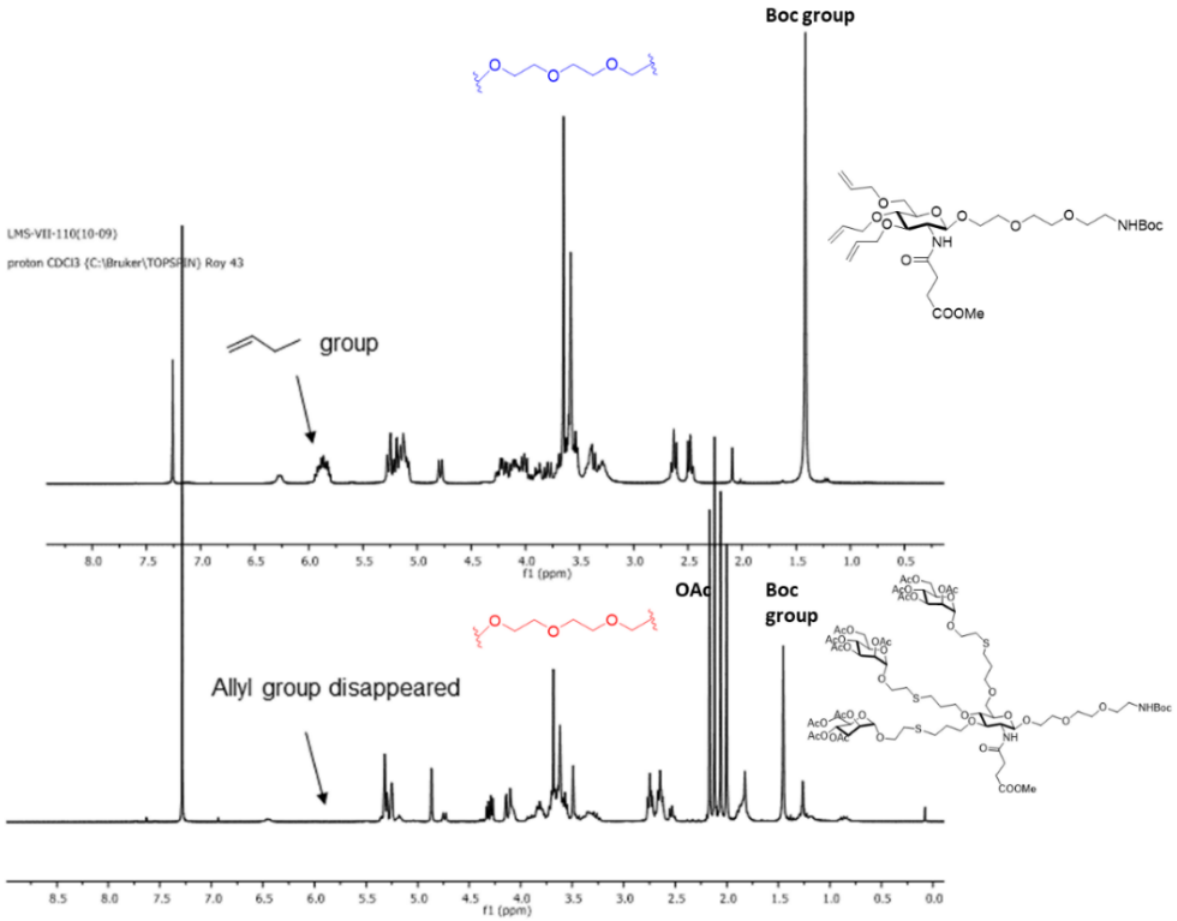

The next step in the synthetic process is to extend the PEG_3 linker with extra four carbon chain. Therfore, compound **120** was further converted to **124** derivative in an effective three step sequence. First, acetyl groups were removed using 1M solution of NaOMe in MeOH followed by acidification using Amberlite IR120 H^+ to afford the free hydroxyl trithiomannoside **121**. Subsequent deprotection of the Boc group with 20% trifluoroacetic acid (TFA) in CH_2Cl_2 to afford compound in TFA salt form **122**, the crude product is pure enough for the next step reaction. HRMS analysis of **122** (**Figure 4.7**), the molecular ion was clearly detected at *m/z* 1266.50, accompanied by a significant fragment ion MeOH at *m/z* 1233.48, indicating the desired structure unambiguously.

Figure 4.8 HRMS-TripleTOF (QTOF) analysis of **122**

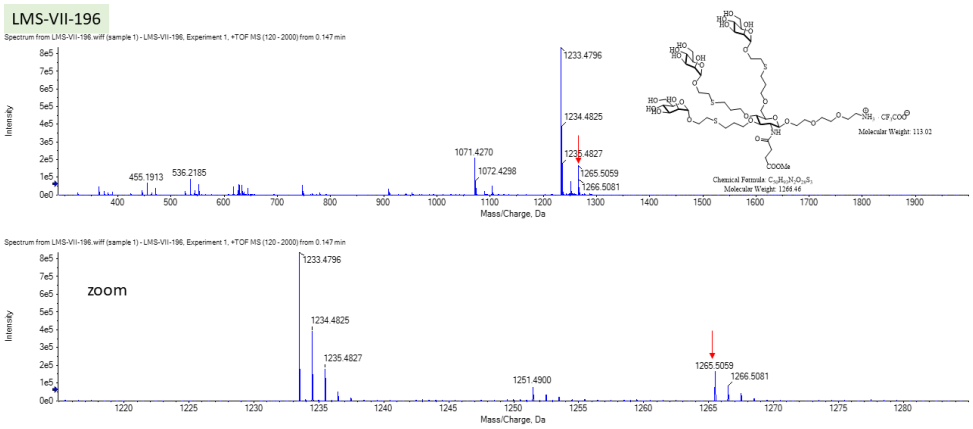

Sample	Formula	Adduct	Neutral mass Da	Calculated *m/z*	Observed *m/z*	PPM	Intensity
LMS-VII-196	C50H93N2O28S3	+	1265.5077	1265.50715	1265.5062	-0.8	683962
LMS-VII-196 -MeOH	C49H89N2O27S3	+	1233.48149	1233.48094	1233.48001	-0.7	3164593
LMS-VII-196 -Me	C49H91N2O28S3	+	1251.49205	1251.4915	1251.49062	-0.7	444481

Finally, trithiomannoside amine **122** coupled with 4-azidobuanoic acid **123** using standard PyBOP coupling reagent and *N,N*-diisopropylethylamine in DMF to afford the desired building block **124** with terminal azide group. [427, 428]

The pluasible mechanism of PyBOP mediated amide synthesis is shown in (**Scheme 4.9**). [429]

Scheme 4.9 Plausible mechanism of PyBOP type coupling reagent

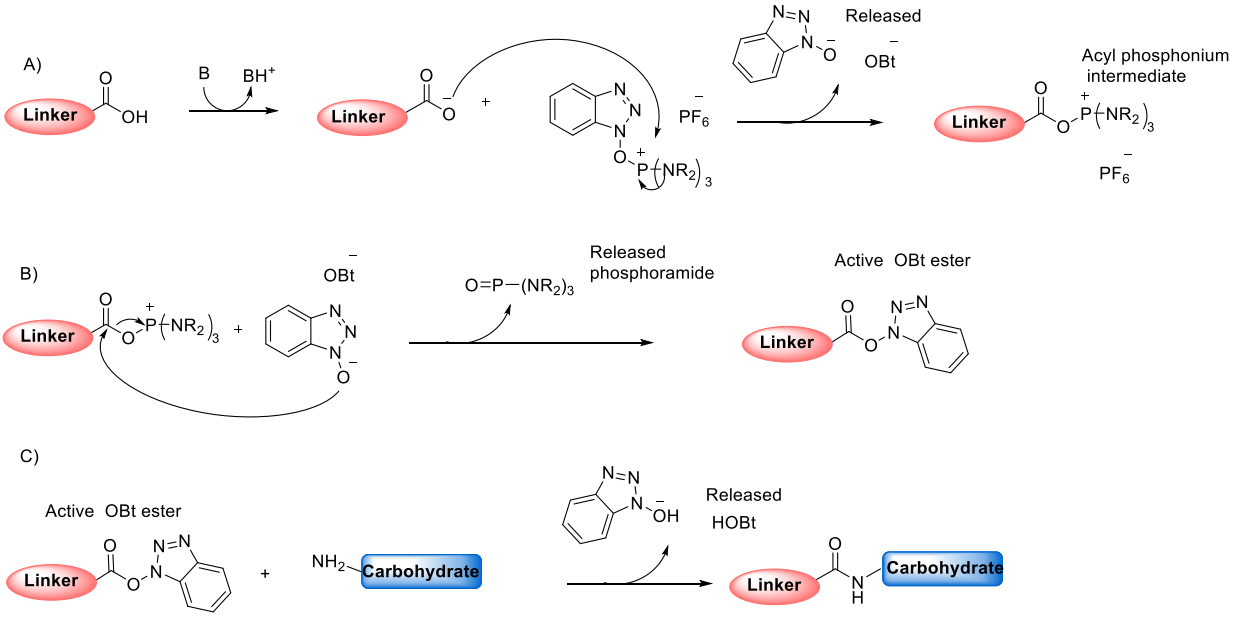

We found that in the case of PyBop coupling reagent, a significant peak overlap of UV-active by-products was observed, which overlap with the final product, Phosphoramide by-product. This compound is not completely removed after chromatography purification (as detected by TLC), but presents no problem, being inert.[430] Subsequent treatment with acetic anhydride pyridine mixture afforded full acetylated product **125**, which allows for easy purification, and set the stage for dendrimer growth. In addition to NMR, IR also plays an important role to confirm the structure. Compound **125** has different functional groups. Stretching vibrations of these bonds produce a strong absorption peak. Acetyl group Its absorption peak is about 1740.7 cm^{-1} and 1704.7 cm^{-1} for an ester group, while in an amide it is about 1652.5 cm^{-1}, the azide group gives a strong absorption peak at 2100 cm^{1}, (**Figure 4.9**).

Figure 4.9 IR analysis of **125**

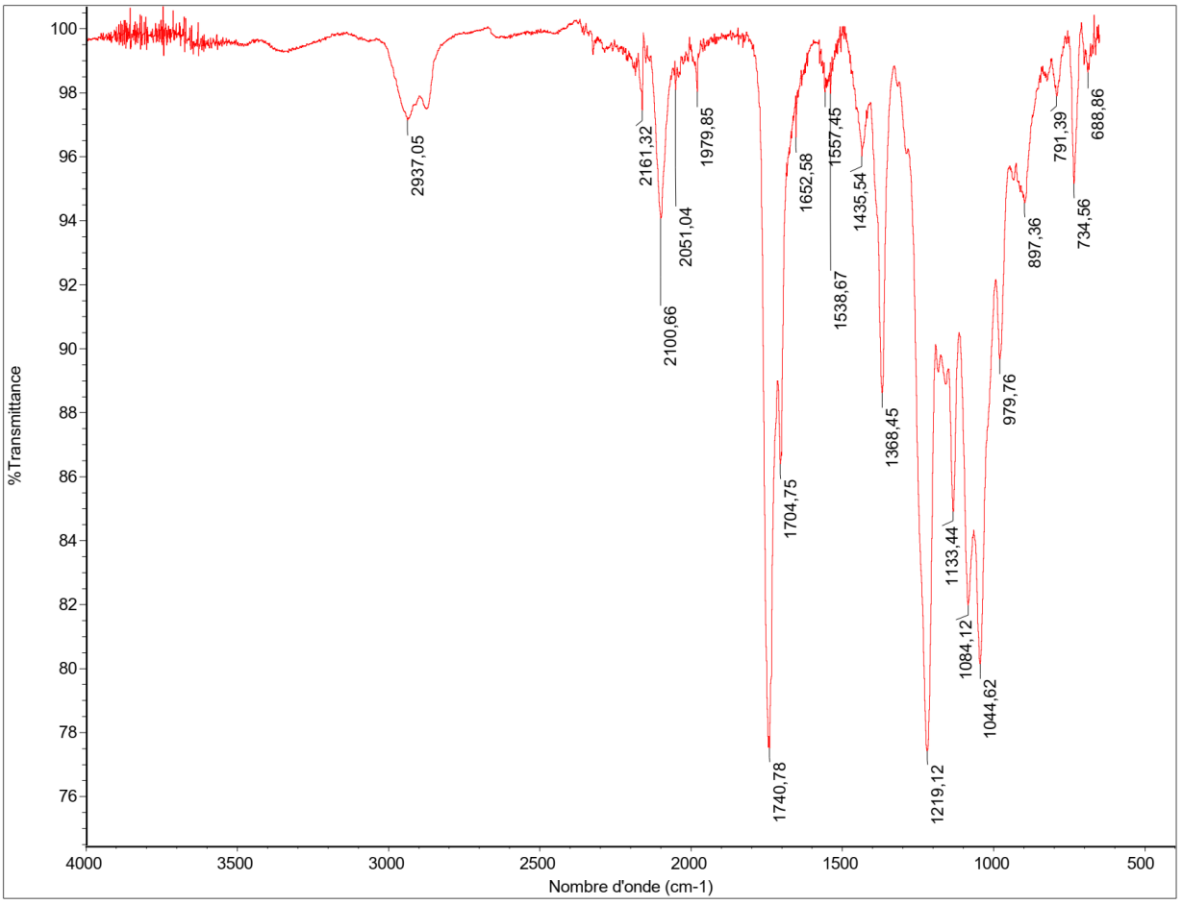

It is noteworthy that this highly modular approach combined with high functional group tolerance gives access to β-D-glucosamine building block. Functionalization of this scaffold gave a number of versatile dendritic wedges including different targeting lectin ligands, thus demonstrating the synthetic utility of this method.

With trimannoside-β-D-glucosamine dendron **125** in hand, setting the stage to the mulivalent dendrimer synthesis.

4.4.3 Growth of multivalent dendrimer

Pentaerythritol resembles a highly symmetrical structure with equivalent hydroxyl groups which have frequently been employed for the synthesis of the multivalent cluster. [431, 432] Thus, with all building blocks in hand, we began to assemble the final dendrimer, (**Scheme 4.10**). Hexavalent valent dendrimer was constructed by the reaction between hexapropargylated dipentaerythritol **91**, [433] and dendron **125** following click reaction strategy using $[CuI(P(OEt)_3]$. Dendrimer core **91** was synthesized by employing a previously reported procedure. [433] Different reaction parameters were conducted to achieve the best reaction outcome, which was reaching the highest degree of dendrons coupling. Therefore, the solvent, the concentration of the reactants as well as the reaction temperature were adapted from the previous protocol (see **chapter 3**). As final reaction conditions we found that using dry toluene as a solvent is suitable to run the click reaction, moreover, the catalyst $[CuI(P(OEt)_3]$ shows better activity in a non-polar solvent. The reaction temperature was set at 80 ºC for 24 h. Residual copper ions were removed by EDTA chelation. Subsequent chromatography purification afforded the dendrimer **126** a molecular weight of 11.600 KDa, (no MALDI data for this dendrimer).

This dendrimer is characterized by ^{1}H NMR, (**Figure 4.10**), ^{1}H NMR confirms the coupling of all six macromonomers with the core. The yield of this click reaction was not as good as expected. Further improvement of the yield of the reaction will be applied in order to study their generations and ligand dependence properties in the coming biological test. We did not run HRMS analysis for this dendrimer.

Scheme 4.10 Synthesis of man-glycodendrimer based on D-glucosamine scaffold

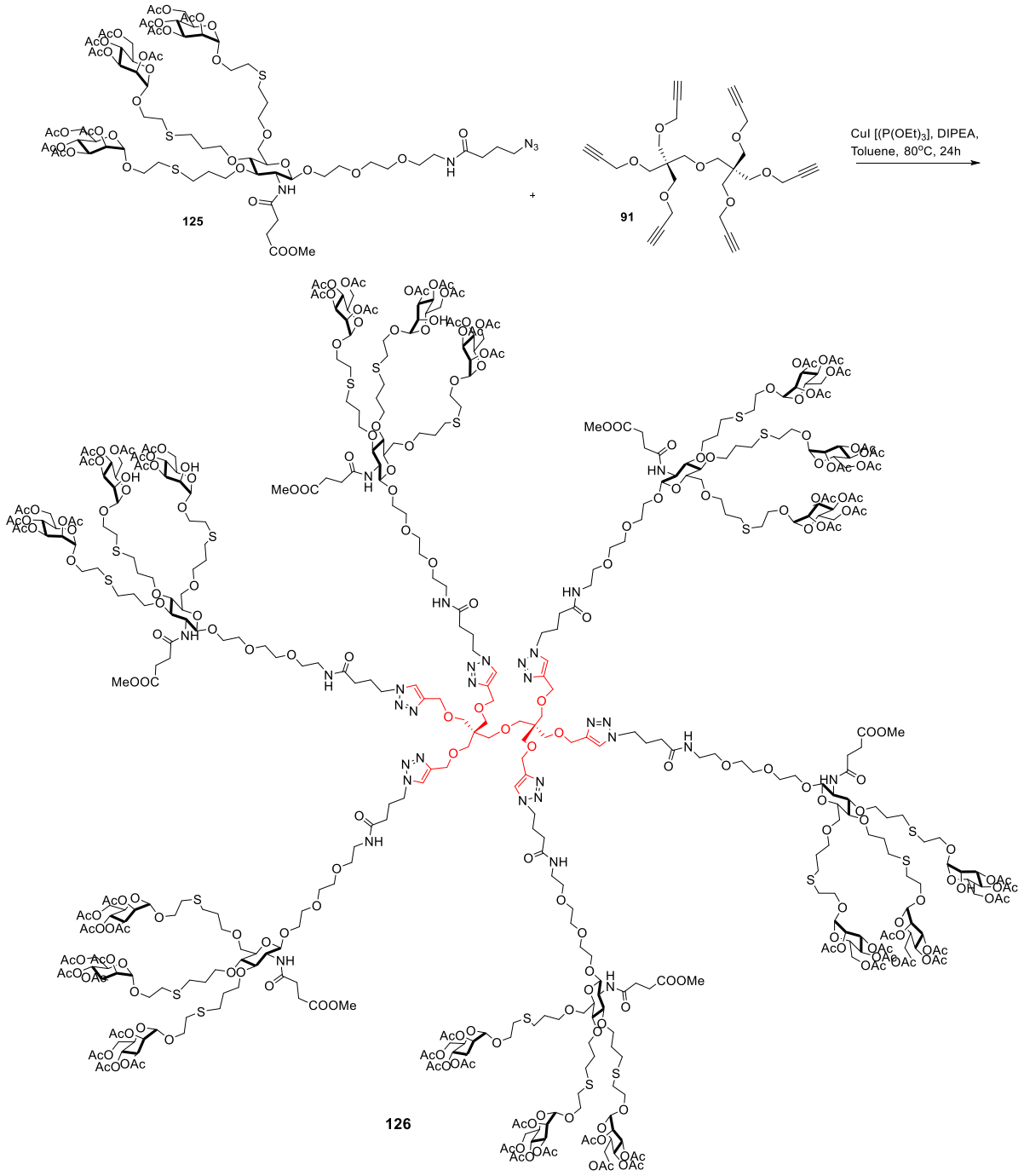

Figure 4.10 ^{1}H NMR analysis of dendrimer **126**

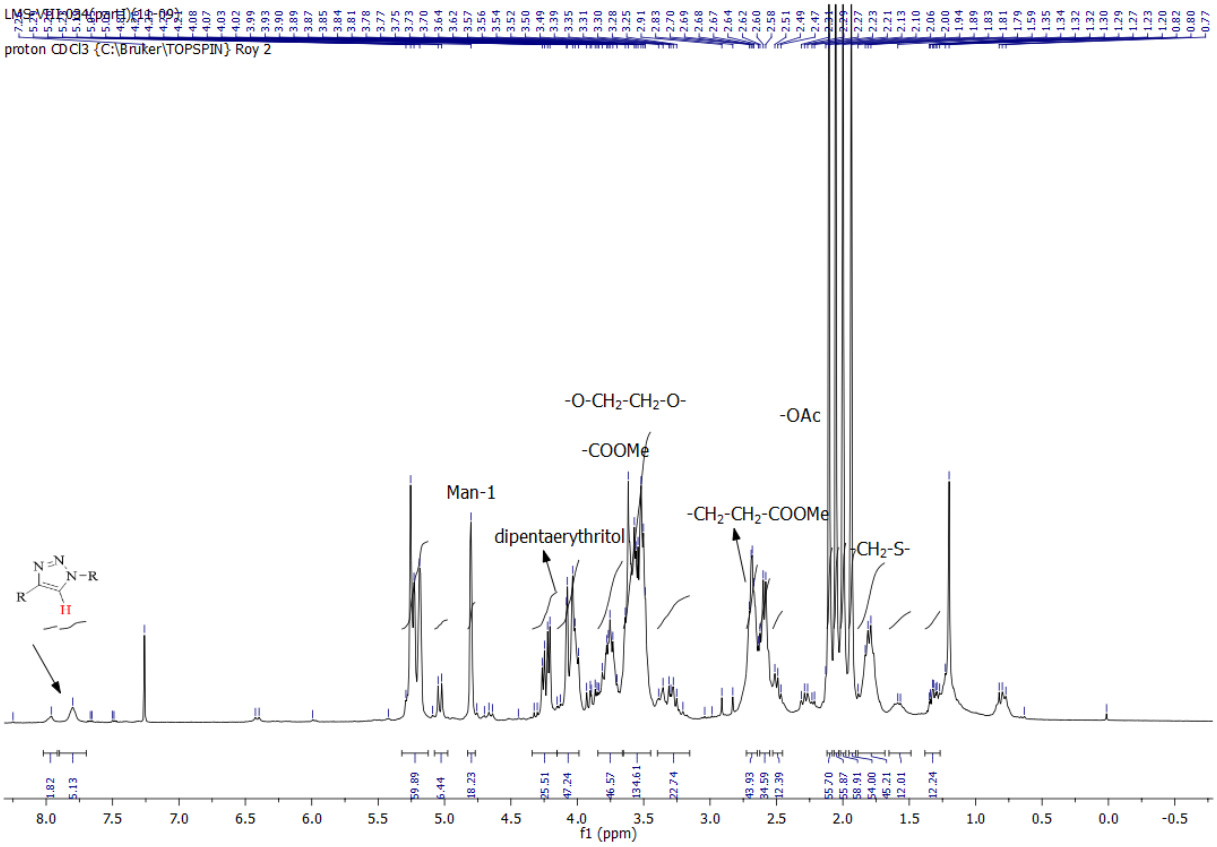

In process:

The final synthetic passway towards the dendrimer **128** will be reached by two sequence steps as shown in (**Scheme 4.11**). The first is the removal of acetyl groups using NaOMe/MeOH, following the treatment with aq. LiOH in a mixture of THF/MeOH at room temperature. [434-439]

Scheme 4.11 The final synthetic passway towards the dendrimer **128** construction

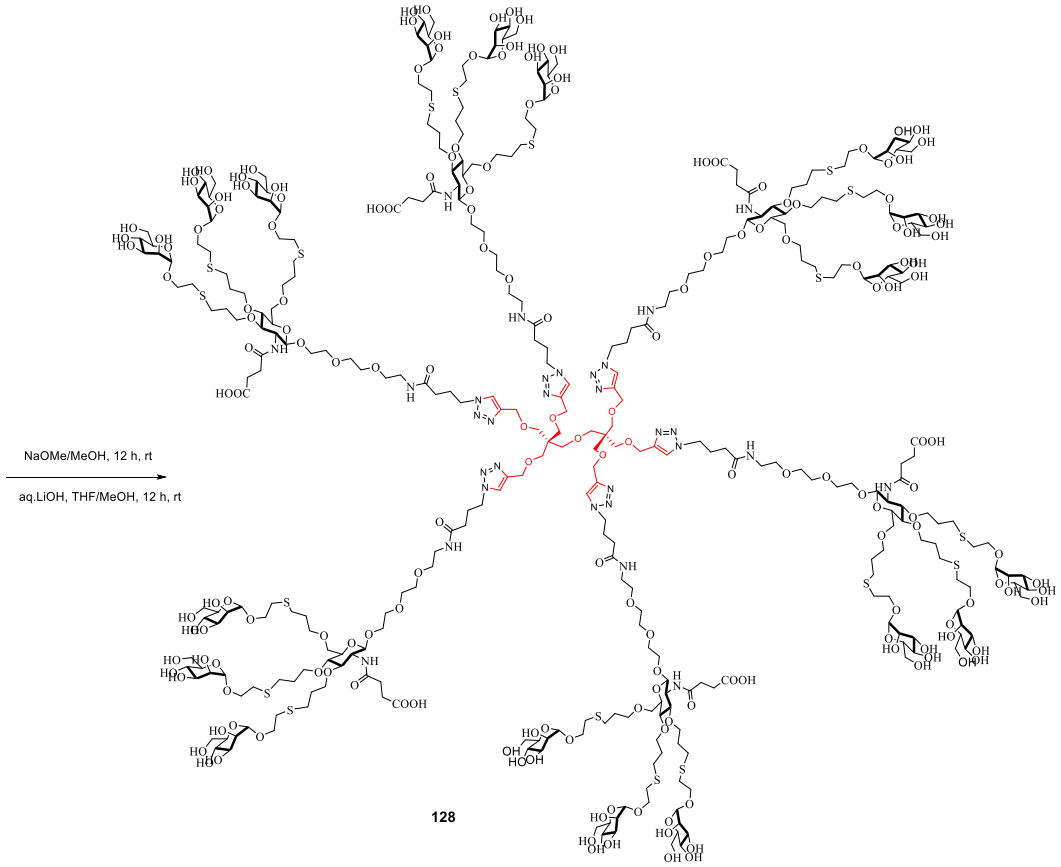

CHAPTER 5
SYNTHESIS OF CIPROFLOXACIN-(ACYLOXY) ALKYL ESTER CONJUGATES

5.1 Introduction

Ciprofloxacin is an antibiotic in the fluoroquinolone class used to treat bacterial infections such as urinary tract infections and pneumonia. Ciprofloxacin has FDA approval to treat urinary tract infections, skin, bone, joint infections, prostatitis, typhoid fever, gastrointestinal infections, lower respiratory tract infections, anthrax, plague, and salmonellosis. Ciprofloxacin is available orally, intravenously, and in topical formulations (ophthalmic and otic). Adverse effects are mild at the therapeutic doses and are mostly limited to gastrointestinal disruptions such as nausea and diarrhea. The serious adverse effects of ciprofloxacin include prolonged QT interval, hyper or hypoglycemia, and photosensitivity. Oral ciprofloxacin therapy is associated with an increased risk of peripheral neurotherapy based on the cumulative dose. Neuropsychiatric adverse events include agitation, tremors, hallucinations, psychosis, and seizures. [440] The low oral bioavailability profile of ciprofloxacin can be due to high secretory efflux and poor aqueous solubility. This inspired an investigation of the viability of prodrug methods as a means of enhancing the systemic delivery of the drug. Prodrugs have become a well-accepted path to address drug delivery challenges associated with parent antibiotics. [441, 442]

To date a variety of polymer architectures have been evaluated for use as drug scaffolds including hyperbranched structures (e.g., dendrimers and hyperbranched polymers). [443] For example, the research from B. Christensen[444] reported antibiotic-conjugated to PAMAM-dendrimer (**Figure 5.1**). In this study involves the covalent attachment of ciprofloxacin *via* a linker to a small PAMAM-dendrimer and tested against clinically relevant Gram-positive and Gram-negative bacteria. The dendrimer conjugated with ciprofloxacin had a significantly higher antibacterial activity than each of the components alone, which demonstrates a "synergy" of action between ciprofloxacin and the dendrimer. (**Figure 5.1**, dendrimer I) shows the structure of PAMAM dendrimer conjugates with four molecules of ciprofloxacin.

Figure 5.1 Dendrimer- ciprofloxacin conjugates

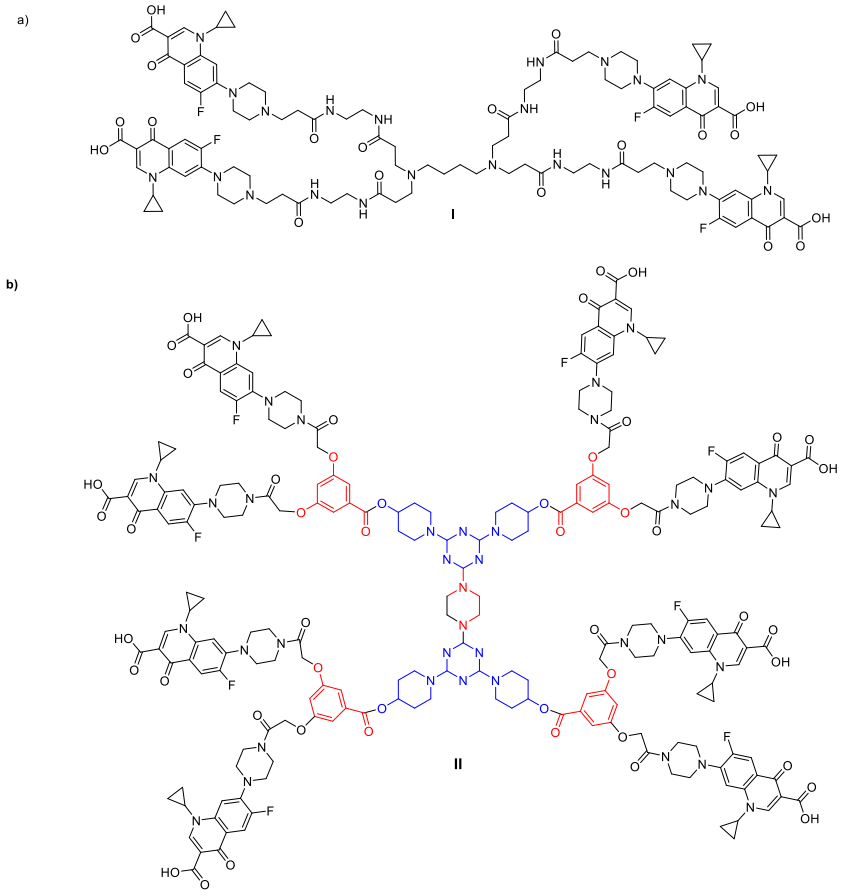

The covalent conjugation between fluoroquinolones and dendrimer has been also studied by Gopalakrishnan and co-workers, (**Figure 5.1,** dendrimer II). They establish the synthesis of piprazine core 1,3,5-triazine dendrimer with eight molecules of ciprofloxacin drug as a surface moiety. [445] They studied and evaluate the drug release from the dendrimer under different pH conditions, pH 1,2,3,4,5 and 6. It was found that 78% of the drug was released at a very lower pH (pH = 1), and in 14 hrs. It is concluded that this dendrimer-drug conjugate system is not efficient in the systematic administration of the drug.

Dendrimer-prodrug represents a creative approach for the treatment of UTIs. Accordingly, drug linkage chemistry is an important parameter for achieving antibiotic efficacy and can also influence the pK and biodistribution properties of the resulting conjugates. Thus, in the present study, we report the design of labile (Acyloxy)alkyl esters carbamate linkers to enable intracellular release of the antibiotic by enzymes such as esterase or acid catalyzed hydrolysis.

Another research to study the intracellular release of antibiotics from synthetic conjugates has been attempted by installing a variety of cleavable linker moieties between the drug carrier and antibiotic cargo. However, the majority of earlier examinations uncovered limitations. For example, ester linkers were employed to release of the antibiotic by intracellular esterase or acid catalyzed hydrolysis, but the hydrolytic lability of these linkers resulted in permature cleavage of the conjugates. [446]

A wide range of ciprofloxacin conjugates has also been studied by several groups, including conjugates with linkers which can be cleaved by enzymatic degradation of the siderophore. [69, 447] The Cip-linker **129 (Figure 5.2**), conjugated to siderophore was studied by Nolan and co-workers. However, experiments in enzyme-triggered ciprofloxacin showed that the hydrolytic lability of these linkers resulted in premature cleavage of the conjugates, hence the release of the antibiotic in the culture medium. [448]

Figure 5.2 Molecular structure of ciprofloxacin (Cip) and its conjugate linker analogue **129**

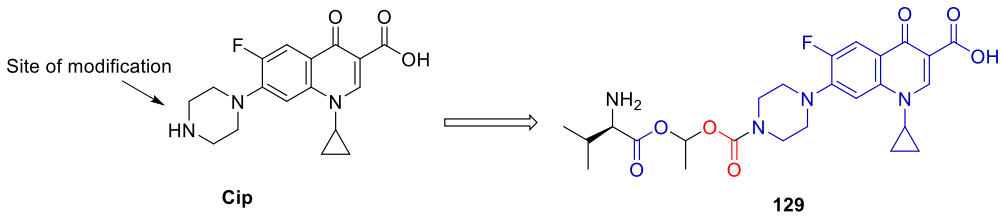

These results are encouraging, and we conclude that the stability of (acyloxy)alkyl- Cip may be improved by the incorporation on the dendrimer backbone. In this way, we are targeting ciprofloxacin efflux pump and drug target modification through a dendrimer-cleavable prodrug approach.

5.2 Ciprofloxacin-cleavable linker conjugate

In our studies, several different analogues of the monobasic amino acid were designed as depicted in (**Figure 5.3**), attached to ciprofloxacin *via* a carbamate linker to explore the steric effects and pH stability of both linkers. It is also possible that the conjugates **130**, **132**, and **133,** might have a better stability. [366, 449-451] In this chapter we explored only the synthesis of **132**, due to time constraints during my studying program.

Figure 5.3 The proposed ciprofloxacin linker conjugates

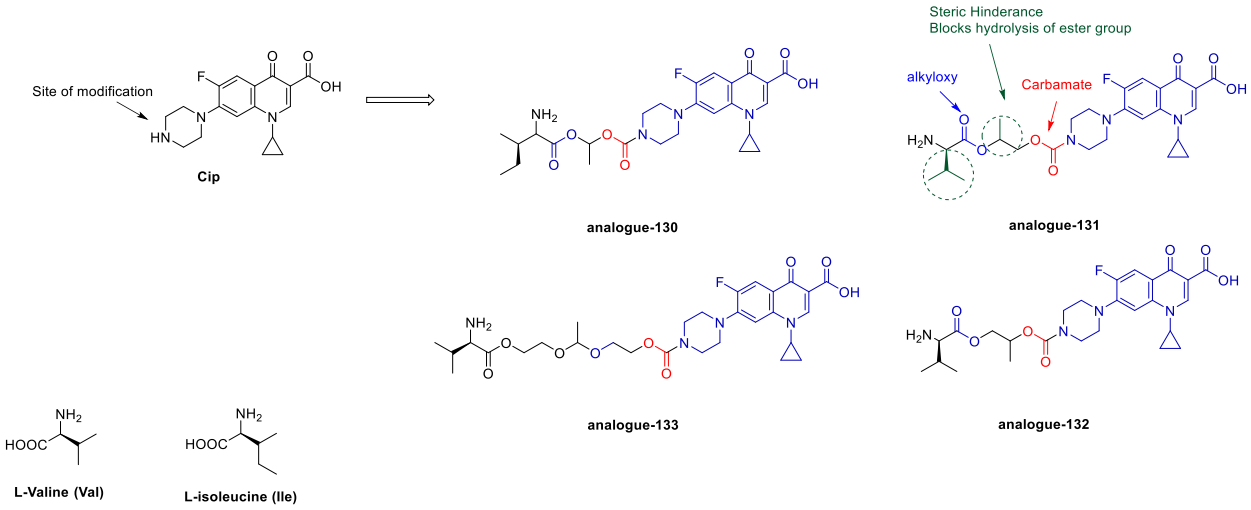

In this design, the size of the amino acid side chain is the method by which the rate of prodrug hydrolysis can be controlled. By placing a large sterically hindering group next to a carbonyl group, an attack on this carbon would be sterically blocked. It was crucial to investigate how the size of the side chain affects its capacity to sterically hinder hydrolysis. Among the cleavable linkers, L-Valine, Valine-Citruline (Val-Cit) or phenylalanine-lysine (Phe-lys) dipeptide linker spacers have been utilized in many drug delivery systems. [452] Thus, there were two possible approaches when designing Cip-Carbamate linker. [366]

Considering the steric hindrance of the linker and the symmetrically branched side chain of L-Valine (Val), this will boost the linker stability. In this study we recommend utilizing L-isoleucine (Ile), (**Figure 5.3**).

5.3 Results and discussion

We choose ciprofloxacin as the target drug molecule, a broad-spectrum antibiotic and its molecular structure bears several functional groups. [453] SAR[454] showed that the secondary amine in the piperazine ring of ciprofloxacin can be modified without a major loss of antimicrobial activity; this position was therefore chosen for conjugation with the linker. [455-457]

5.3.1 Synthesis of ciprofloxacin conjugate **132**

The development of the synthetic route for Cip-conjugate **132** was considered challenging. The synthetic overview is depicted in the (**Scheme 5.1**).

The synthesis of Cip-linker conjugates **132** is depicted in (**Scheme 5.1**). The synthesis started with the reaction of 2–chloro-1-propanol which is attached to Cip secondary amine group using 4-nitrophenyl chloroformate as the coupling agent. In this method 2–chloro-1-propanol **135** was reacted with 4-nitrophenyl chloroformate **134** [450, 458] in the presence of pyridine[418, 459] to obtain chloroethyl-4-nitrophenyl carbonate **136** which was purified and characterized by ^{1}H NMR spectroscopy. Because ciprofloxacin exhibits poor solubility in most organic solvents, the carboxylic acid moiety was protected in situ by the addition of trimethylsilyl chloride (TMSCl) prior to each coupling reaction. The reaction of TMS-protected ciprofloxacin with chloroethylcarbonate **136** afforded compound **137** as a yellow solid in 40% yield. Subsequent esterification by the reaction of Boc L-Valine **138** with compound **137** using DIPEA at 65^{o}C in DMF, afforded compound **139**. [460] Boc protecting group were removed by treatment with 20% of TFA in DCM to produce the Cip-linker free amine **132** in 71% yield.

Scheme 5.1 Synthesis of drug-linker conjugate **132**

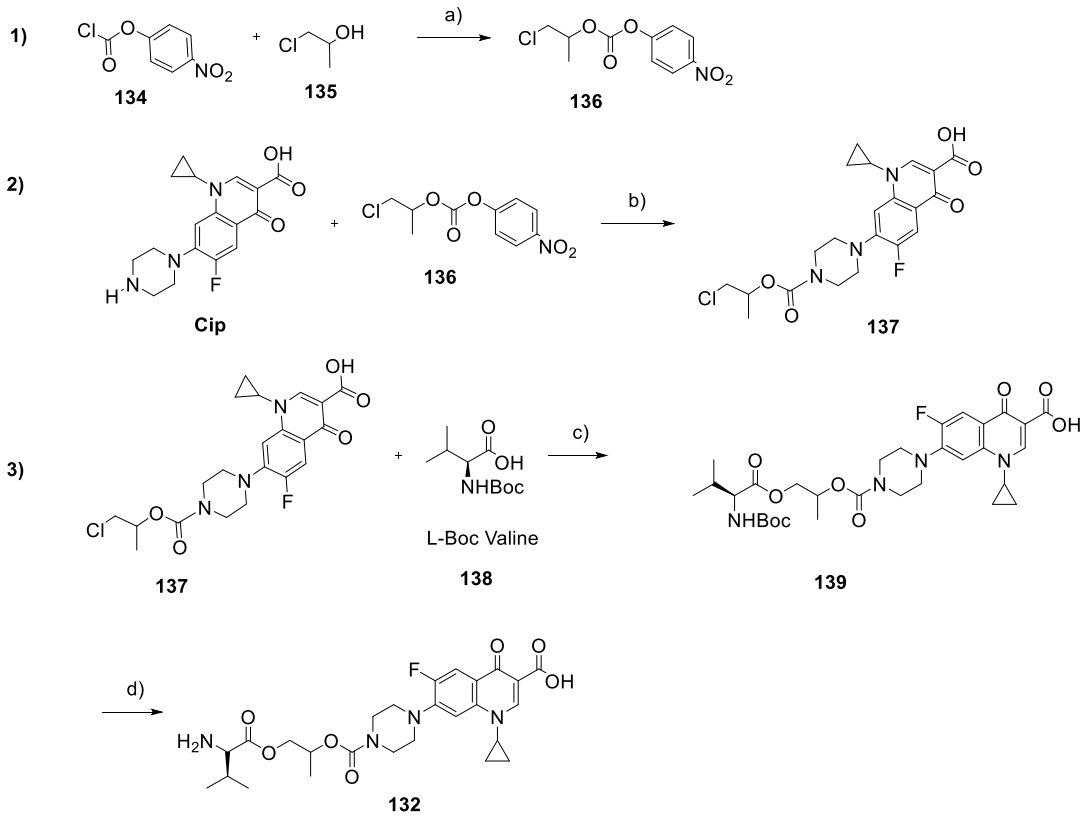

a) THF, pyridine, 0 ^{o}C- rt, 15 h, 60%; b) TMSCl, DCM, DIPEA, rt, o.n, 40%; c) TMSCl, DMF, DIPEA, 65 ^{o}C, o.n, 50%; d) 20% TFA/DCM, 0 ^{o}C- rt, 2.5 h, 71%.

Figure 5.4 shows the ^{1}H NMR analysis of compound **139.** Three protons were observed at a chemical shift of 8.77 to 7.36 ppm, these three protons originate from H_2, H_7, and H_{10}. Isopropyl was further confirmed by the appearance of peaks at 0.92-0.94 ppm. A singlet peak of *tert*-butyl group appeared at 1.44 ppm.

Figure 5.4 ^{1}H NMR analysis of compound **139**

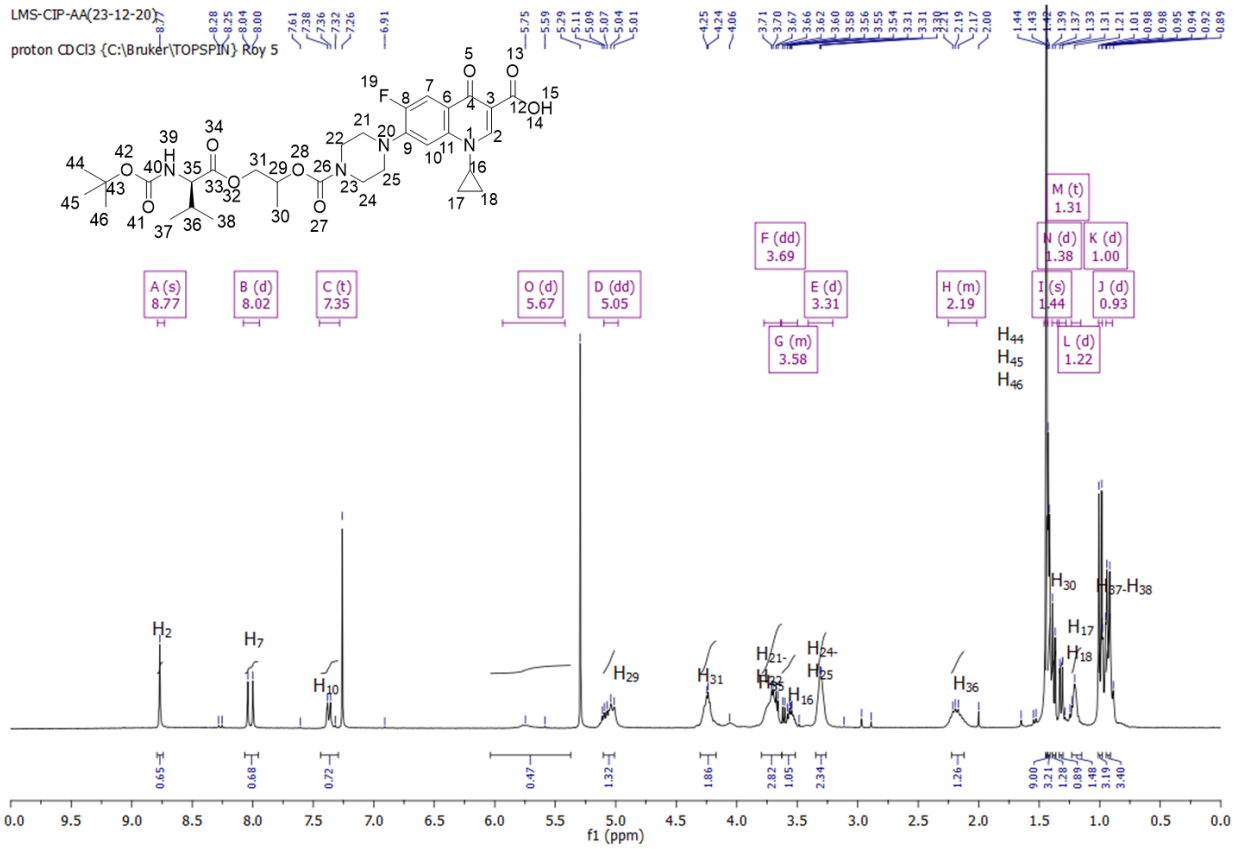

The linking between **137** and L-Boc Valine **138** was also confirmed by using electron ionization mass spectrometry (ESI-MS). In (**Figure 5.5**), two peaks of Cip-linker (compound **139**) were detected at a molecular weight of $[M+H]^+$ 634.1 and $[M+Na]^+$ 656.1 which is consistent with the theoretical molecular weight of compound **139**, $[C_{31}H_{41}FN_4O_9+H]^+$ 633.29, or $[C_{31}H_{41}FN_4O_9+Na]^+$ 655.29.

Figure 5.5 ESI-MS analysis of compound **139**

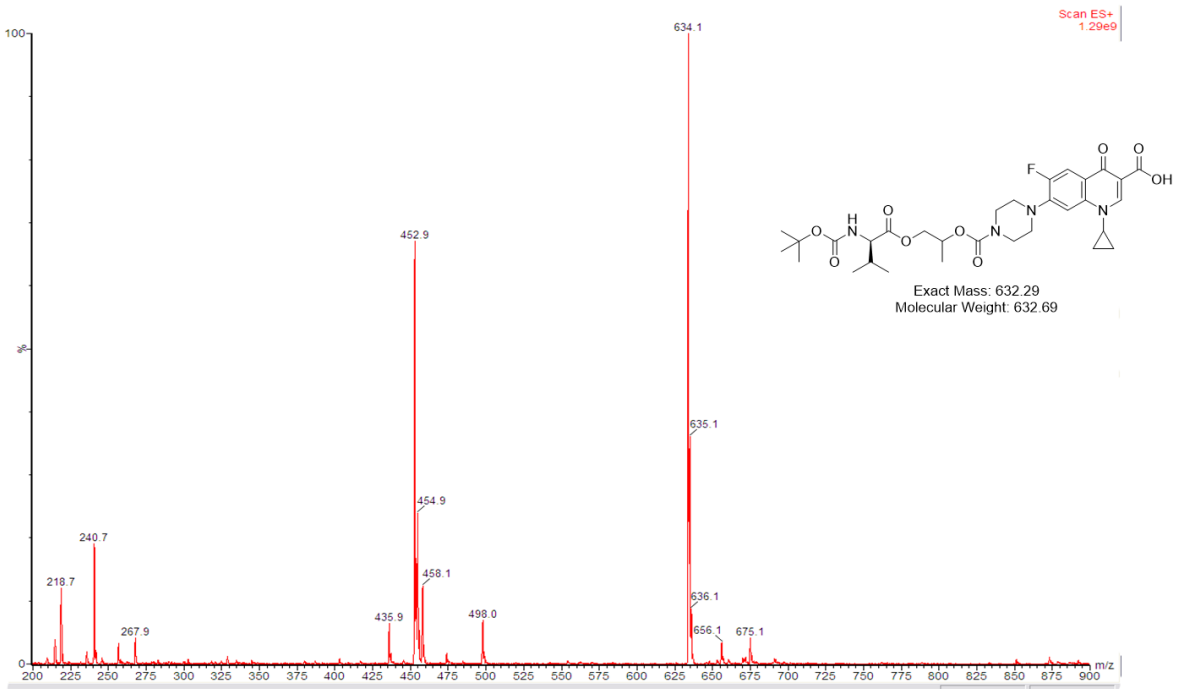

The structure of the final Cip-conjugate is confirmed by ^{1}H NMR and ^{19}F NMR. In (**Figure 5.6**) shows the ^{1}H NMR analysis for the final conjugate **132**, deprotection of *t*-Boc is confirmed by ^{1}H NMR by following the disappearance of 9H reseonance at δ = 1.44 ppm. A peak at molecular weight $[M+2H]^{+}$ 534.1 was observed in (**Figure 5.8**), which is consistent with the theoretical molecular weight of the desired product **132**, $[C_{26}H_{33}FN_4O_7+2H]^{+}$ 534.23.

Figure 5.6 ^{1}H NMR analysis of compound **132**

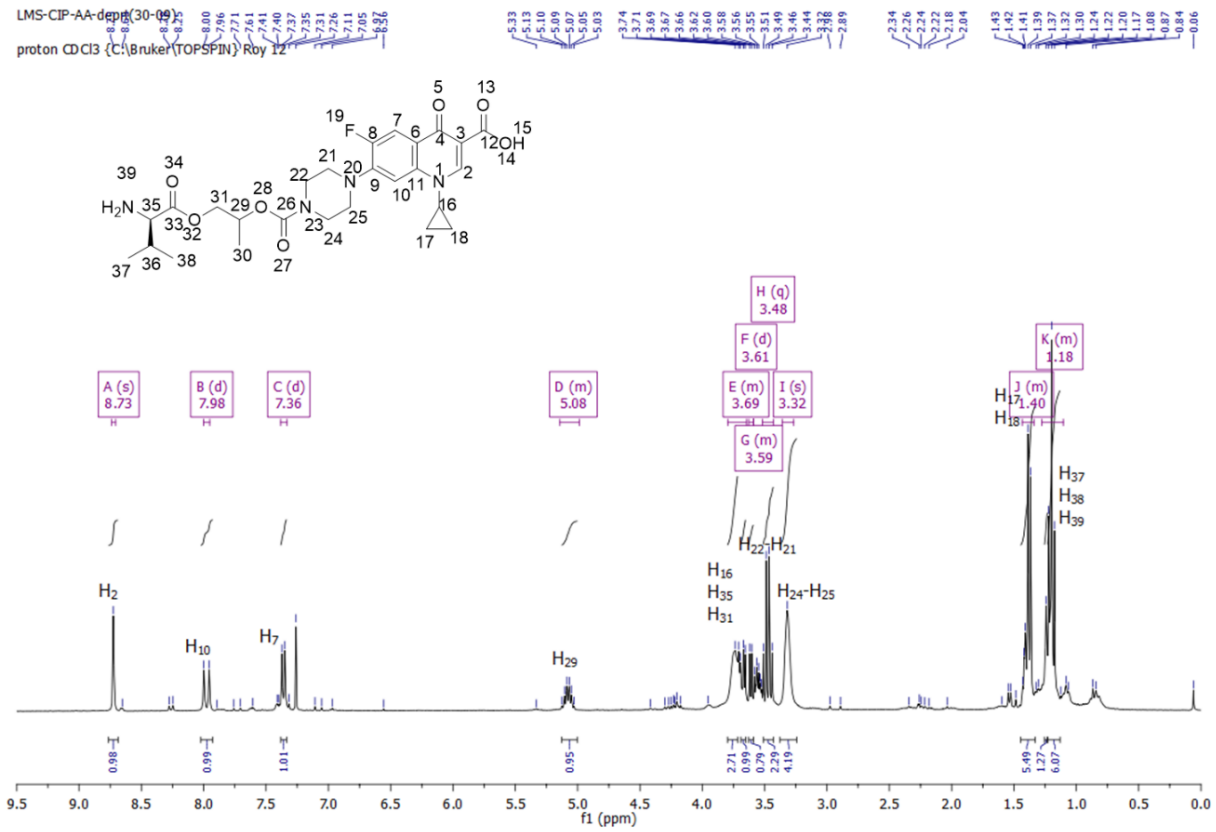

Figure 5.7 ^{19}F NMR of compound **132**

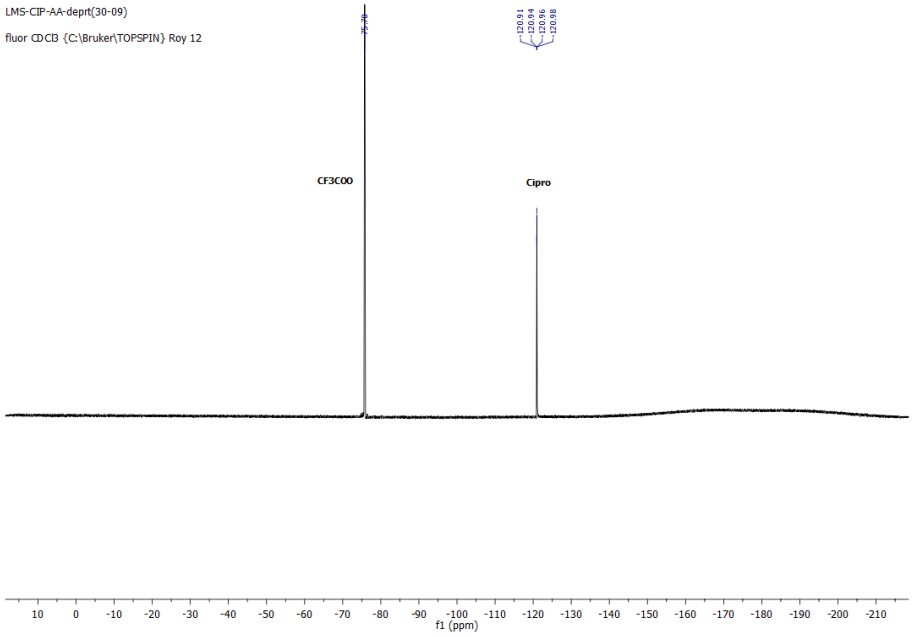

Figure 5.8 ESI-MS analysis of compound **132**

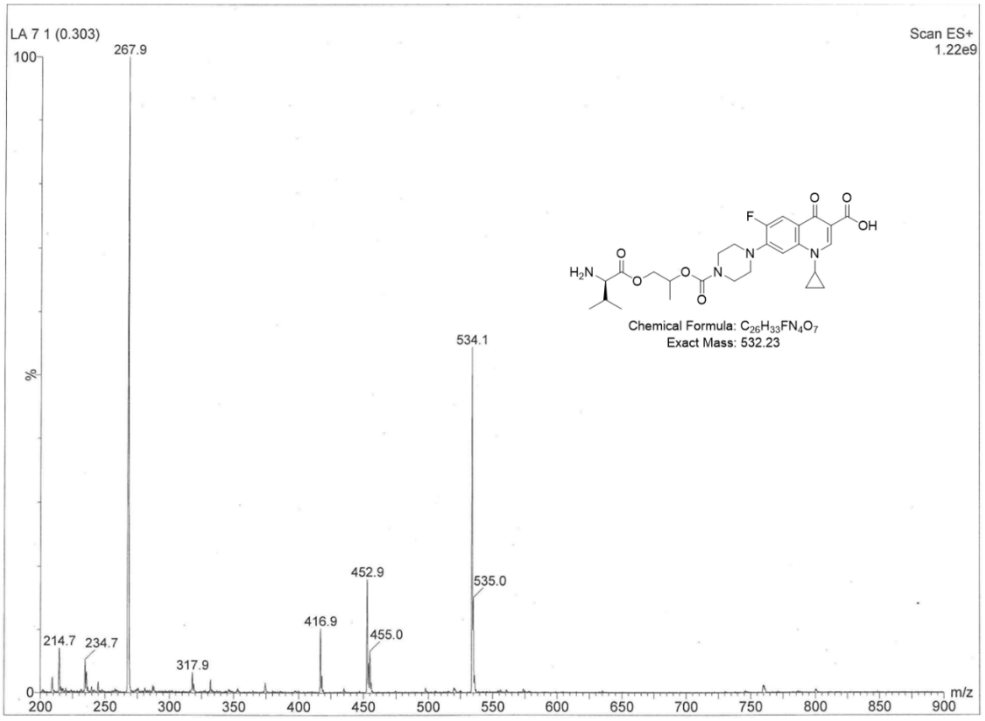

Next, we directed our attention to the synthesis of Cip-dendrimer prodrug by amide coupling with hydrophilic mannose/ or fucose dendrimer (**Scheme 5.2**). The Cip-spacer contains carbamate and (acyloxy) alkyl. Organic carbamates are structural elements of many approved therapeutic agents. Structurally, the carbamate functionality is related to amide-ester hybrid features and, in general, displays very good chemical and proteolytic stabilities. Carbamates are widely utilized as peptide bond surrogates in medicinal chemistry. This is mainly due to their chemical stability and capability to permeate cell membranes. Another unique feature of carbamates is their ability to modulate inter- and intramolecular interactions with target enzymes or receptors. [68, 461] In addition, the carbamate functionality participates in hydrogen bonding through the carbonyl group and backbone -NH. Therefore, substitution on the *O*- and *N*-termini of carbamate offers opportunities for modulation of biological properties and improvement in stability and pharmacokinetic properties.

Scheme 5.2 Schematic illustration showing the mannose/ or fucose targeted prodrug being binding to the cell following internalized and drug release

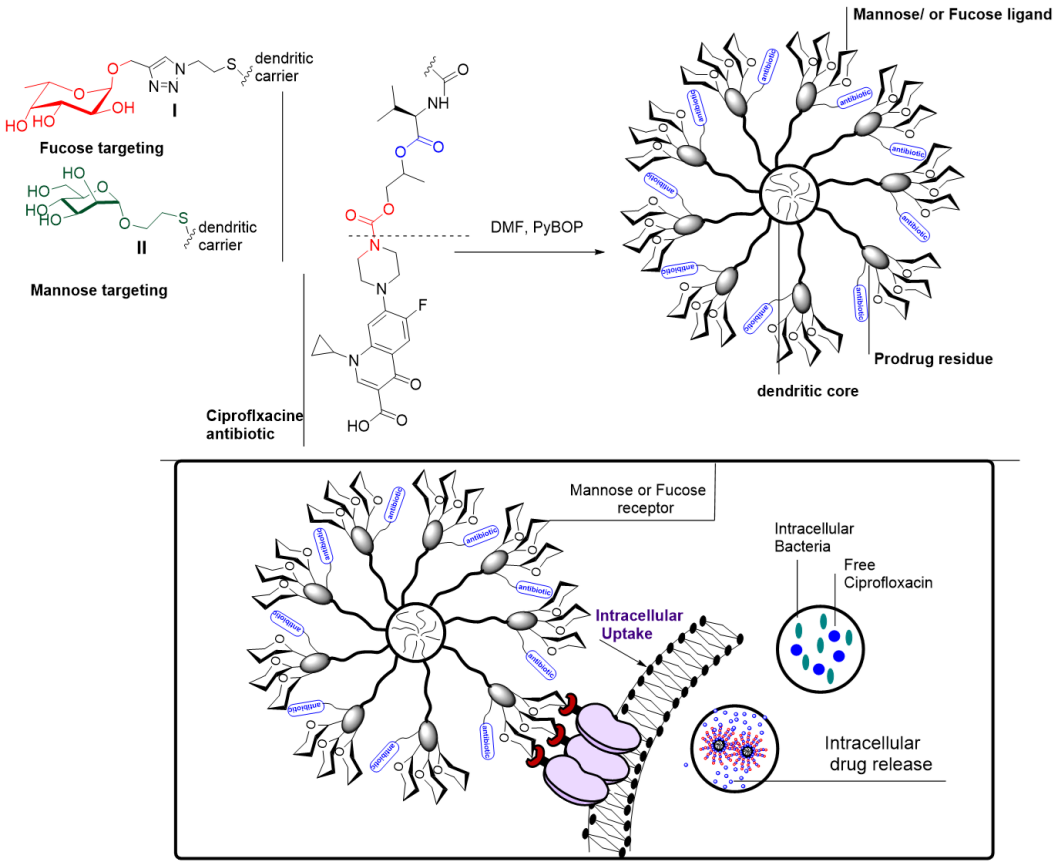

The ability to prepare Cip-dendrimer prodrug was next evaluated by conducting the amide coupling conditions using PyBOP as a standard amide coupling reagent. [429, 462] The dendrimer **85** was dissolved in DMF, to this mixture was added Cip-linker **132**, PyBOP, and DIPEA. The mixture was stirred at room temp. for 16 hr. The reaction mixture was then dialyzed using nanopure water at r.t using a dialysis membrane (1000 KDa cutoff) and then freeze-dried to remove water. The ^{1}HNMR of the product shows a low degree of drug conjugation (**Figure 5.9**).

Figure 5.9 Drug-dendrimer conjugates (In progress)

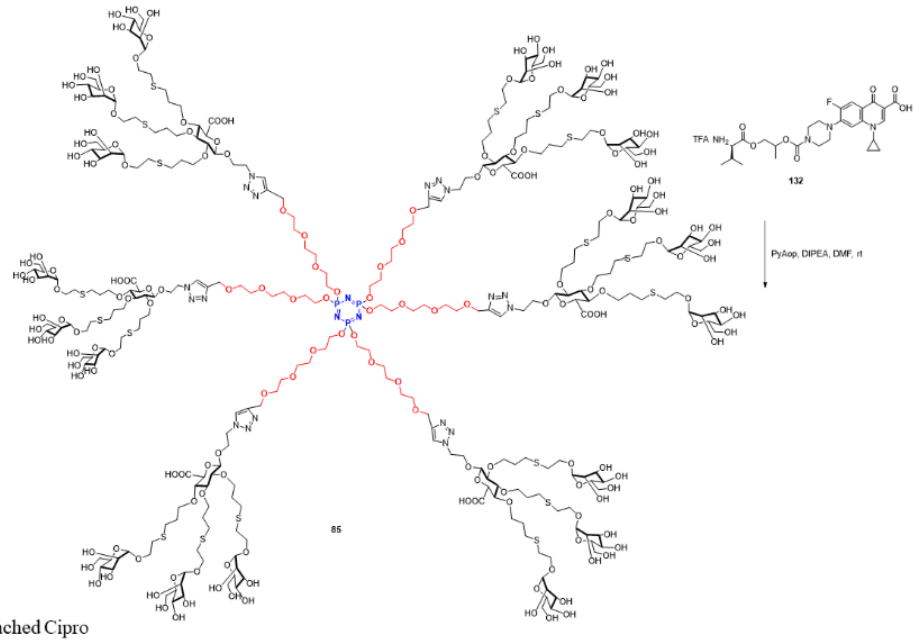

^{1}H NMR of attached Cipro

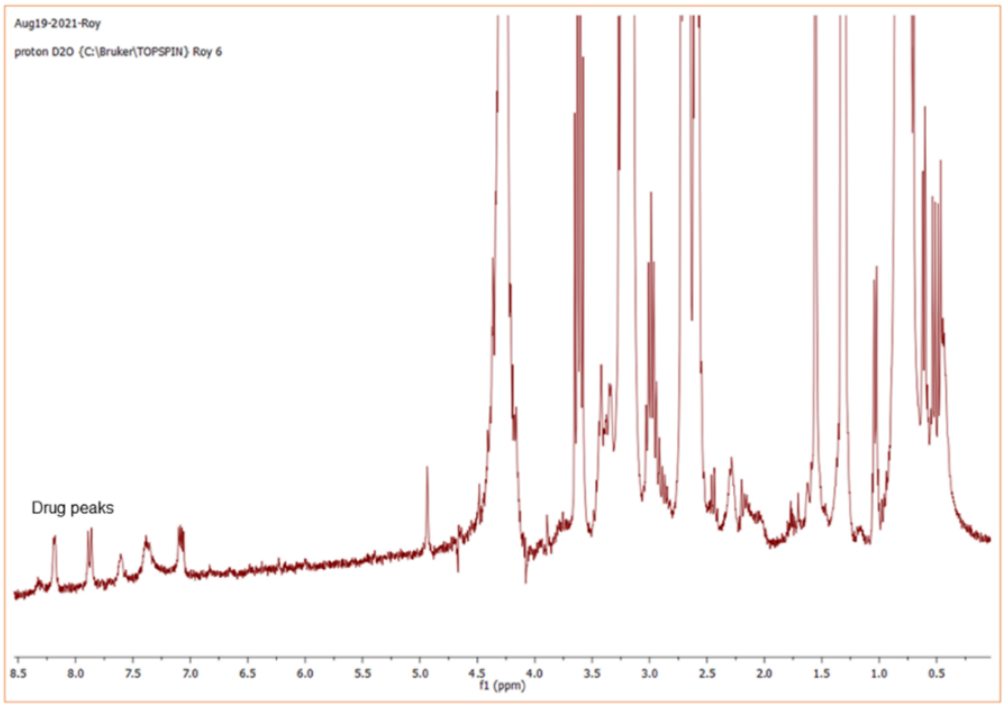

These results were obtained in the last months of my Ph.D. program, with time constraints that prevented us from looking into the causes of these outcomes or using numerous drug conjugation techniques.

5.3.2 Strategy of dendrimer-drug conjugation

The important feature of our synthesis involves the early-stage introduction of the drug as explained in (**Scheme 5.3A**). The second approach (**Scheme 5.3B**), is to attach the drug to the dendrimer backbone.

Scheme 5.3 Schematic approach of Cip-dendrimer conjugates

A) Early stage conjugates the drug to the dendron, followed by synthesis of dendrimer by click reaction

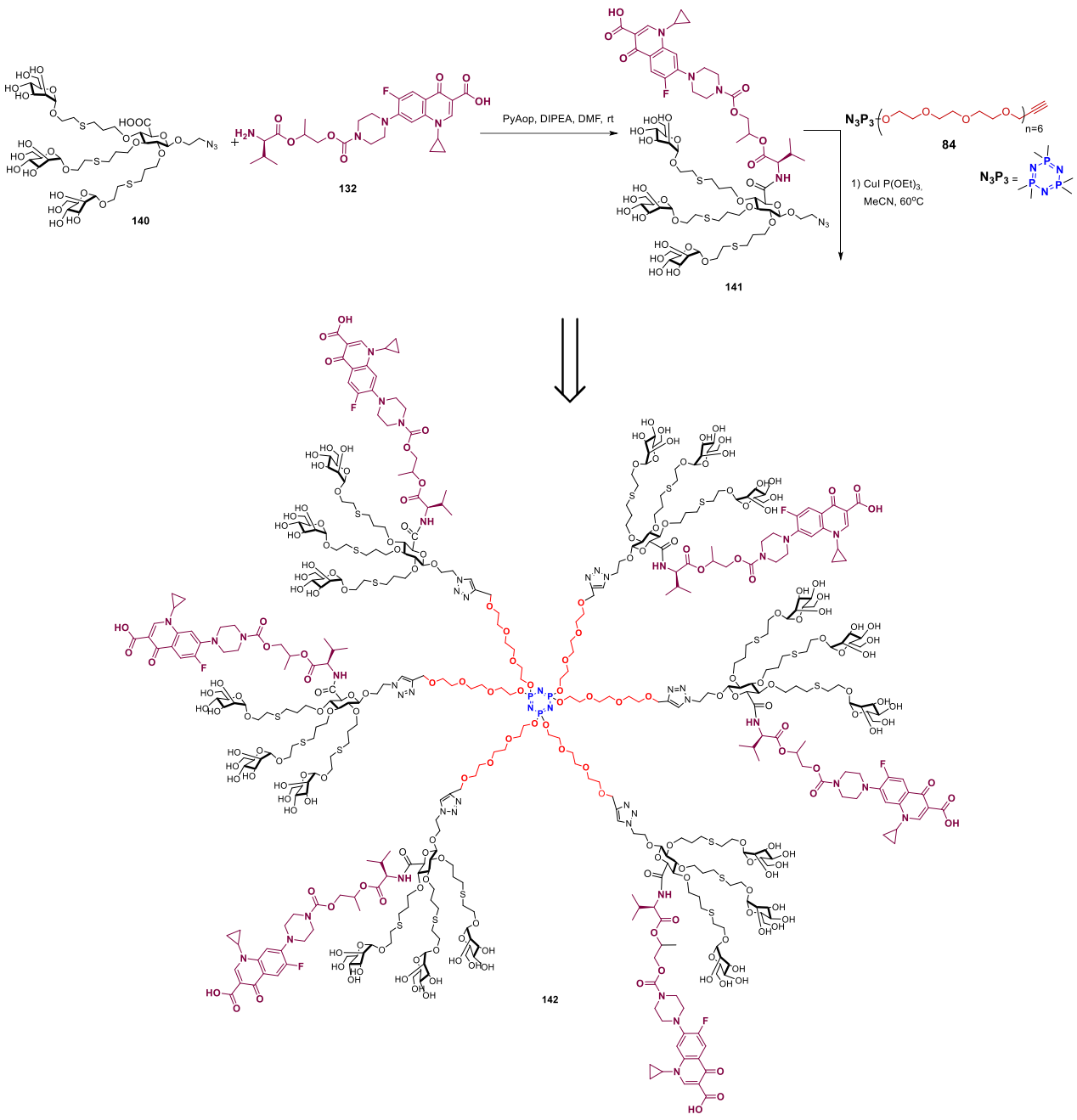

B) Late stage dendrimer-drug conjugates by amide coupling

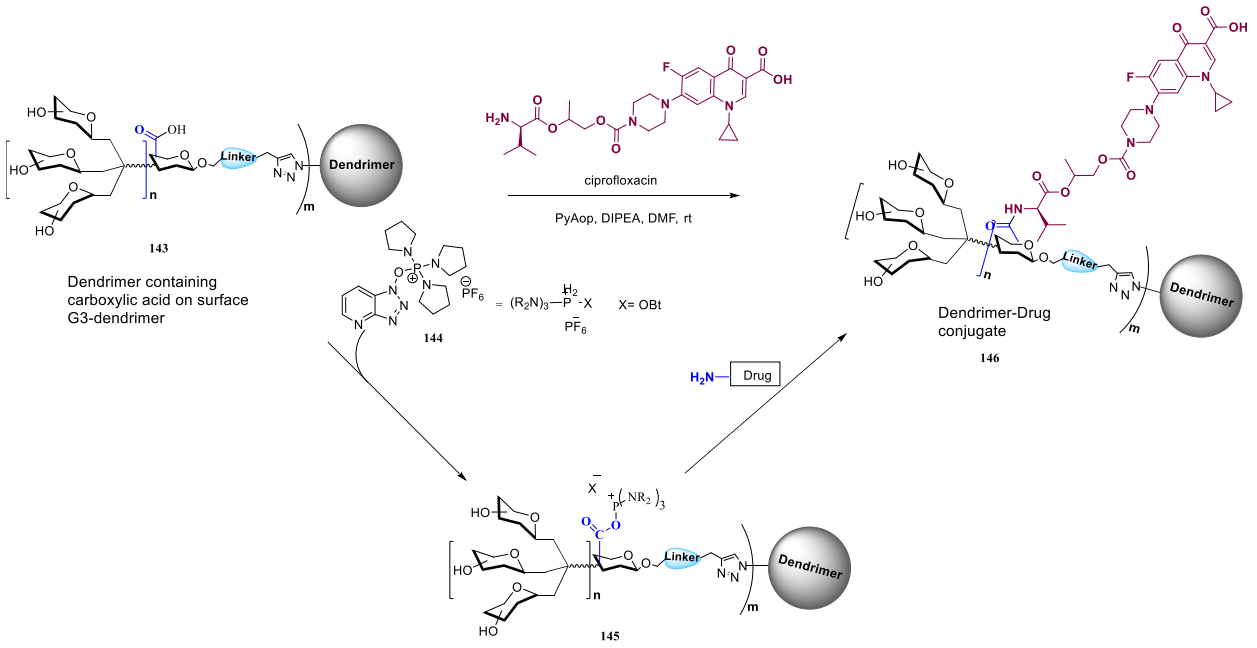

5.4 Mechanism of action of dendrimer ciprofloxacin conjugate

Successful penetration into the bacterial cell envelope is a prerequisite for the activity of antibiotics having intracellular targets. At physiological pH, fluoroquinolones are known to coexist in a zwitterionic and overall uncharged form and a neutral form, with only the latter form passively diffusing through cell membranes, such as the cytoplasmic membrane of Gram-negative and Gram-positives. [463] For Gram-negatives, however, the outer membrane and its lipopolysaccharides (LPS) layer constitute a second barrier. Penetration by fluoroquinolones of this barrier is suggested to be mediated by three mechanisms: (i) by a hydrophilic pathway through porins, (ii) by a hydrophobic pathway through the lipid bilayer, and (iii) by a "self-promoted" pathway involving displacement of divalent cations bridging adjacent LPS molecules. [464] Ciprofloxacin, uptake is mediated primarily by porins and by the self-promotion pathway. [465, 466] With ciprofloxacin having a mass of 331 Da it is easy for this hydrophilic molecule can cross the water-filled porins as they generally have an exclusion size of 600 Da. [467] However, the larger size of our dendrimer conjugate (ex.108 kDa), suggests that these dendrimers are instead transported by either the "self-promotion" pathway or by the hijacking of specific channels and high affinity lectins translocating larger dendrimer. [467] It will be of interest to examine further the mode of action of the dendrimer-ciprofloxacin conjugate.

CHAPTER 6
SYNTHESIS OF PEGYLATED CORES FOR THE DENDRIMER GROWTH

6.1 Introduction

As previously explained in **Chapter 1**, dendrimers are hyperbranched polymers with complex three-dimensional architectures for which the mass, size, shape, and surface chemistry can be highly controlled. Active functional groups present on the exterior of dendrimers enable the conjugation of biomolecular or contrast agents to the surface while drugs can be loaded in the interior. Overall, polymeric nanoparticles (NPs) are ideal candidates for drug delivery because they are biodegradable, water-soluble, biocompatible, biomimetic, and stable during storage. Their surfaces can be easily modified for additional targeting allowing them to deliver drugs to targeted tissues. [468] However, disadvantages of polymeric NPs include an increased risk of particle aggregation and toxicity. Only a small number of polymeric nanomedicines are currently FDA-approved and used in the clinic. [469]

6.2 Circulation stability and clearance

While in circulation, factors such as excretion, blood flow, coronas, and phagocytic cells can reduce NP stability and delivery. The specific effects of each of these environmental factors are independent of the physiochemical properties of the NPs platform, which has led to general design principles aimed to manipulate these characteristics to achieve favorable outcomes. In size, for example, NPs with a diameter less than 10 nm have generally been shown to be rapidly eliminated by the kidneys, whereas NPs larger than 200 nm risk activating the complement system, if not otherwise engineered. [470] Furthermore, to avoid rapid excretion based on surface properties, many NP formulations incorporate PEG as a stealth coating. PEGylation improves the circulation time by altering the NP size and solubility while shielding the NP surface from enzymes and antibodies that may induce degradation, secretion, and clearance, but this physical barrier does not completely prevent recognition by macrophages or other cells of the immune system.

Poly(organophosphazenes) have a number of attractive features for such biomedical uses, not the least of which is the broad synthetic versatility and the wide range of chemical and physical properties that can be built into specific macromolecules. [471] Hexachlorocyclotriphosphazene ($N_3P_3Cl_6$) is an old compound, first synthesized in 1832 by Liebig, [472] and correctly analyzed by Gladstone and Holmes in 1864. [473] The first X-ray diffraction structure of $N_3P_3Cl_6$ was determined in 1960, [474] showing that N_3P_3 cycle is very nearly planar. $N_3P_3Cl_6$ is a very interesting precursor in various fields. [475] Its thermal ring opening leads to

polyphosphazenes, whereas lots of publications describe its functionalization by nucleophilic substitutions of the chlorides. [476, 477] The most fascinating property of $N_3P_3Cl_6$ is certainly the possibility to regio- and stereochemically control the nucleophilic substitutions, to have one (or several) functions different from others. [475]

The ability of PEG to influence the pharmacokinetic properties of drugs and drug carriers is currently utilized in a wide variety of established and emerging applications in pharmaceutics. The change in the pharmacokinetics of administered drugs by being shielded by or bound to PEG results in prolonged blood circulation times. This consequently increases the chance that the drug will reach its site of action before being detected as a foreign substance and removed from the body. Therefore, the majority of conjugated drugs as well as liposomal and micellar formulations on the market or in advanced clinical trials, are PEG-containing products. [478, 479] PEGylated drugs, liposomes, and nanocarriers are characterized by reduced renal filtration, and diminished enzymatic degradation. For this reason, PEGylated drugs show a prolonged half-life in the body and thus, an enhanced bioavailability. As a result, it is possible to administer medications less frequently and in smaller doses, which enhances the patient quality of life and lowers clinical expenses. [480] Furthermore, PEG shows high solubility in organic solvents, and therefore, end-group modifications are relatively easy. PEG also has low inherent toxicity and is soluble in water, which renders the polymer ideally suited for biological applications. When attached to hydrophobic drugs or carriers, the hydrophilicity of PEG increases its solubility in aqueous media. It provides drugs with greater physical and thermal stability as well as prevents or reduces aggregation of the drugs in *vivo*. [481, 482]

6.3 Synthetic strategy

The retrosynthesis of the applied dendritic cores is described in (**Scheme 6.1**). In this present study, we report a novel cyclotriphosphazene core grafted with an equimolar amount of TEG, with the aim to study their chemistry and properties as new potential drug carriers. In order to synthesize our PEGylated dendrimers, we prepared a bifunctional PEG_3 linker bearing an alkyne on one side with a heterofunctional group on the other side.

Scheme 6.1 General strategy of PEGylated core synthesis

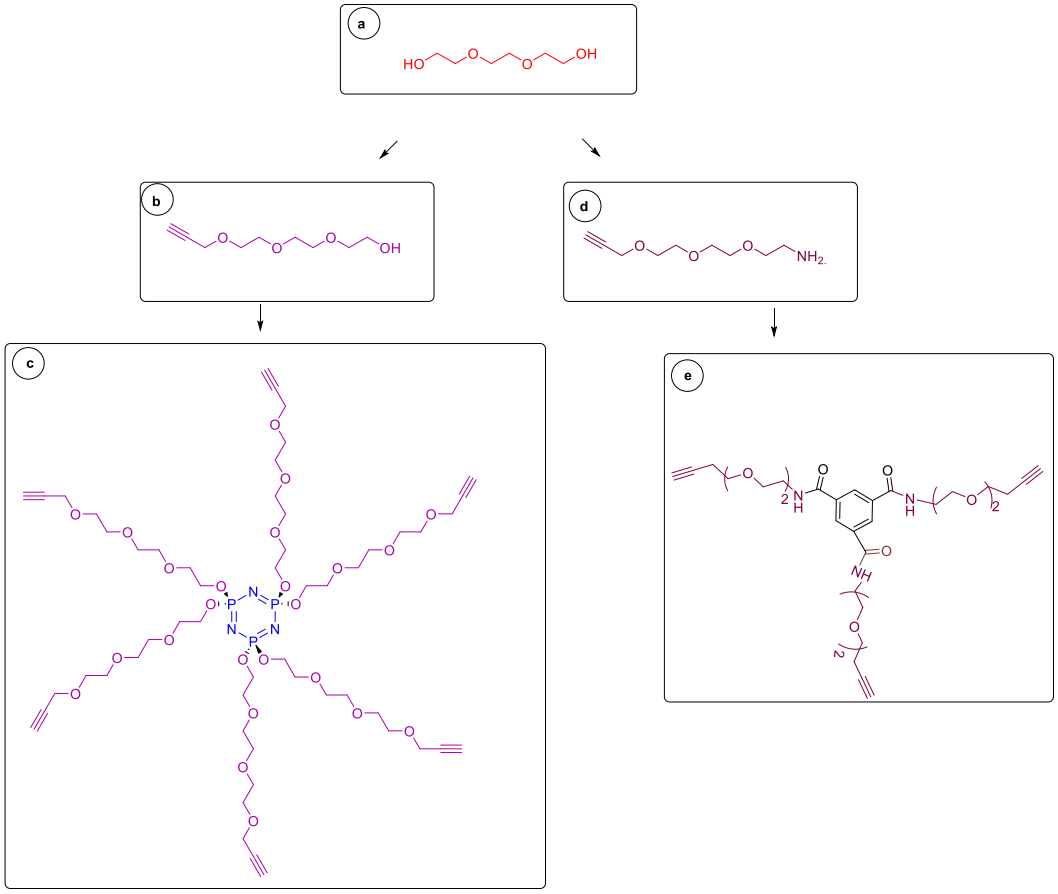

6.4 Cyclotriphosphazene core

Hexachlorocyclotriphosphazene (HCCP), is a six-membered ring system, with alternating phosphorus and nitrogen repeating atoms. Since its synthesis for the first time by J. Liebig and F. Wo¨hler, [483] and due to its relatively easy and versatile functionalization via selective substitutions on the chlorides, cyclotriphosphazene has received extensive attention. Over the last few years, cyclotriphosphazene has been developed in several pharmacological domains. The use of dendrimers in general and the dendrimers based HCCP core in particular represents a new strategy in nanomedicine. Majoral and Caminade are the pioneers in the synthesis of simple and straightforward macromolecular chemistry and the development of phosphorus dendrimers with HCCP core for instance, anticancer, [484] anti-Alzheimers, and anti-inflammatory. [485]

One of the characteristic features of cyclophosphazene chemistry is the chlorine atom replacement by a wide variety of alkoxy, aryloxy, or amino residues to yield species such as $[NP(OR)_2]_{3\text{ or }4}$, $[NP(NHR)_2]_{3\text{ or }4}$, or $[NP(NR_2)_2]_{3\text{ or }4}$, (**Scheme 6.2**). [486] In all these reactions, partly organo-substituted derivatives, as well as

fully substituted species, can usually be isolated. Moreover, two or more different organic substituents can be attached to the same ring. [487, 488]

Scheme 6.2 Nucleophilic substitution on phosphazene core

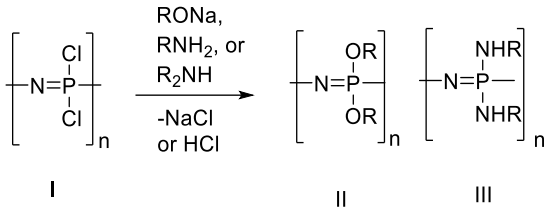

A number of dendrimers with cyclophosphazene as the core was synthesized and showed several interesting biological activities. [489, 490] Among various appending functionalities terminal alkyne-functionalized phosphazene central core has drawn increased interest in the scientific field, since it allows a facile placing of a variety of functional molecules *via* convenient click reaction without backbone degradation. [491] Click chemistry utilizing Cu(I)-catalyzed Huisgen 1,3-dipolar cycloaddition between azide and terminal alkyne is a highly reliable synthetic strategy because of its high selectivity, ease to perform, and broad functional group and reaction condition tolerance. [492, 493]

With continuous interest in the development of novel clickable dendrimers and exploration of their promising biomedical application, we designed propargylated PEGylated central core based phosphazene ring. Therefore, we have synthesized ω- hydroxyl propargylated PEG_3 linkers which feature a facile substitution on a phosphazene ring. The synthesis is easily and economically operational starting from HCCP, TEG, and propargyl bromide, since these starting materials are widely used in industry and can be supplied in large quantities and at low prices. [494] This route aims to limit steric hindrance by using tri ethylene glycol (PEG_3) and also facilitate the construction of dendrimer layers.

6.5 Results and discussion

6.5.1 Synthesis and characterization of PEG_3 linkers

Most commercially available PEG are monofunctional, containing only a single reactive hydroxyl group. Therefore, there is a need to synthesize heterobifunctional PEG_3 with highly reactive end groups, i.e., with one terminal alkyne functionality, which would render them suitable for biocompatible azide-alkyne dipolar cycloaddition reactions. In order to synthesize our PEGylated dendrimers, we prepared a bifunctional PEG_3 linker bearing an alkyne on one side and a hydroxyl or a primary amine on the other side. [354]

The bifunctional PEG_3 spacers with an alkyne and hydroxyl group **152** were synthesized from tri (ethylene glycol) (**151**, PEG_3) as shown in (**Scheme 6.3**). In order to synthesize mono propargyl TEG-OH, an equimolar amount of sodium hydride and propargyl bromide was used, in our case, mono propargylated Tri (ethylene glycol-OH) **152** were synthesized in 69% yield. A minor amount of di propargyl PEG_3 **153** was also formed.

Scheme 6.3 Synthesis of PEG_3 with terminal alkyne group

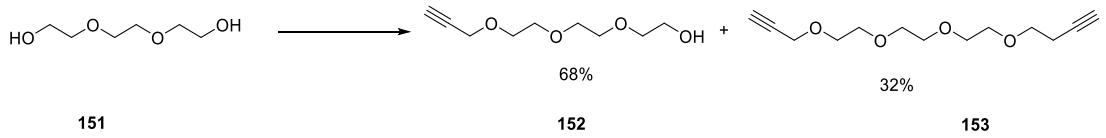

a) NaH, THF,  , 0 °C- rt, then 70 °C, 24 h, 68%

The ^1H NMR spectra of PEG_3 linker **152** exhibited a very characteristic triplet at δ 2.4 ppm assigned to the propargyl group, the remaining hydroxyl group on **152** was ready to react as a nucleophile to construct the core phosphazene.

6.5.2 Synthesis of PEG_3-triphosphazene dendrimer core

In general, halogen replacement reactions using $(NPCl_2)_3$ become more challenging with using TEG as a nucleophile. In this thesis, the cyclotriphosphazene core with a direct substituted PEG_3 linker represents the first example of this class of phosphazene core. [495] The synthetic route is shown in (**Scheme 6.4**), all the synthetic reactions were monitored by ^{31}P NMR spectroscopy.

Traditionally, the synthesis of an *O*-linked phosphazene requires the prior formation of an alkali metal salt and the use of the precipitation of the metal chloride to drive the process to completion. However, during the synthesis, the sodium salt PEG_3 **152** was insoluble, therefore, solution **154** was added to the insoluble salt **152**. During the addition, the salt became soluble, probably due to a facile reaction with the cyclic trimer. Full halogen replacement was completed within 24 h at 70 °C.

This linker contains two functional groups, a terminal alkyne and a hydroxyl group, it is possible to employ its hydroxyl group as a nucleophile under the basic conditions without affecting the terminal alkyne group. As shown in (**Scheme 6.4**) monopropargyl TEG as deprotected by NaH in THF, and the resulting alkoxide reacted with cyclotriphosphazene to give the final dendritic core **84**. [490]

Scheme 6.4 Synthesis of PEG_3-phosphazene core **84**

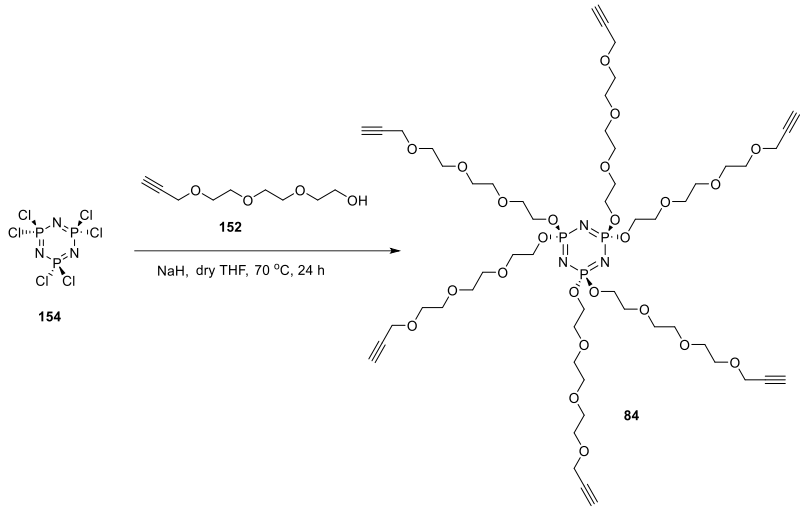

In (**Figure 6.1**) shows the ^1H NMR for core **84**. The ^1H NMR exhibits a distinct triplet peak at 2.45 ppm that is integrated for proton H_1. Another significant peak at 4.20 ppm that is equivalent to two protons H_2. Two distinct peaks at 4.00- 3.61 ppm, multiple patterns for $(-OCH_2-CH_2-O)_2$ (H_3-H_8). The final product showed a clean and sharp singlet peak of ^{31}P NMR at $\delta = 17$ ppm, (**Figure 6.2**).

Figure 6.1 ^1H NMR analysis of PEG_3-phosphazene conjugate **84**

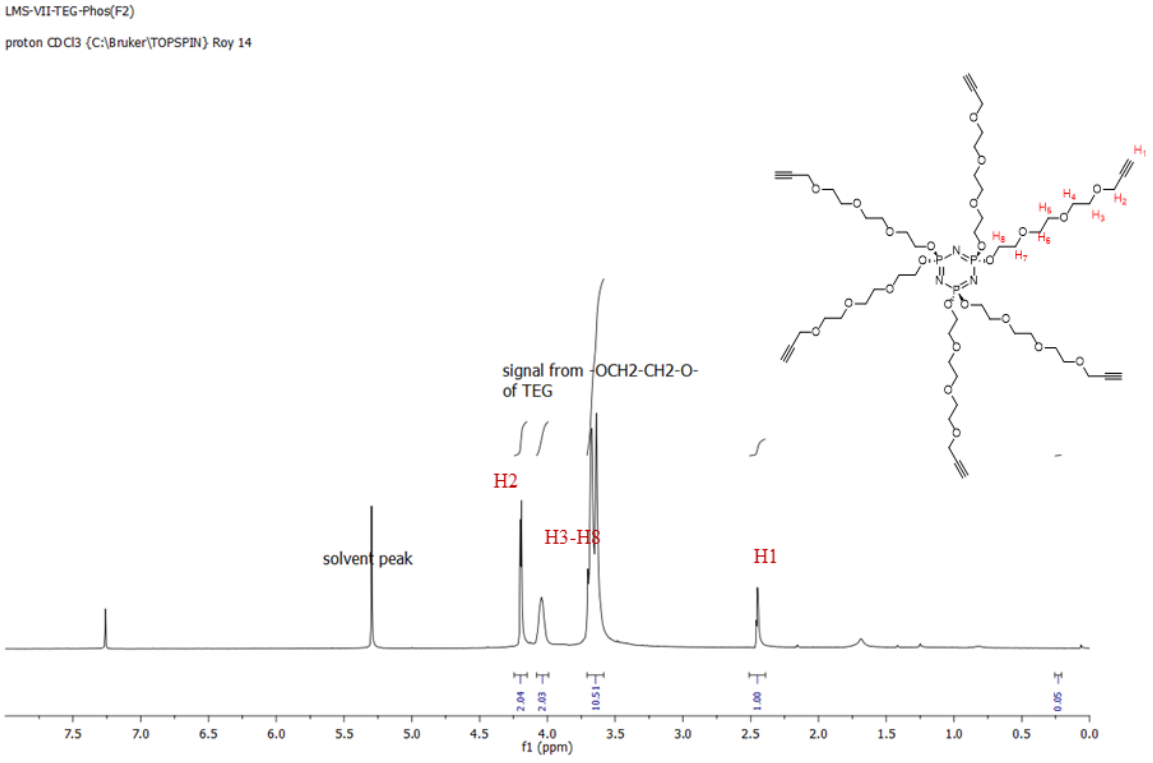

Figure 6.2 ^{31}P NMR analysis of PEG_3-phosphazene conjugate **84**

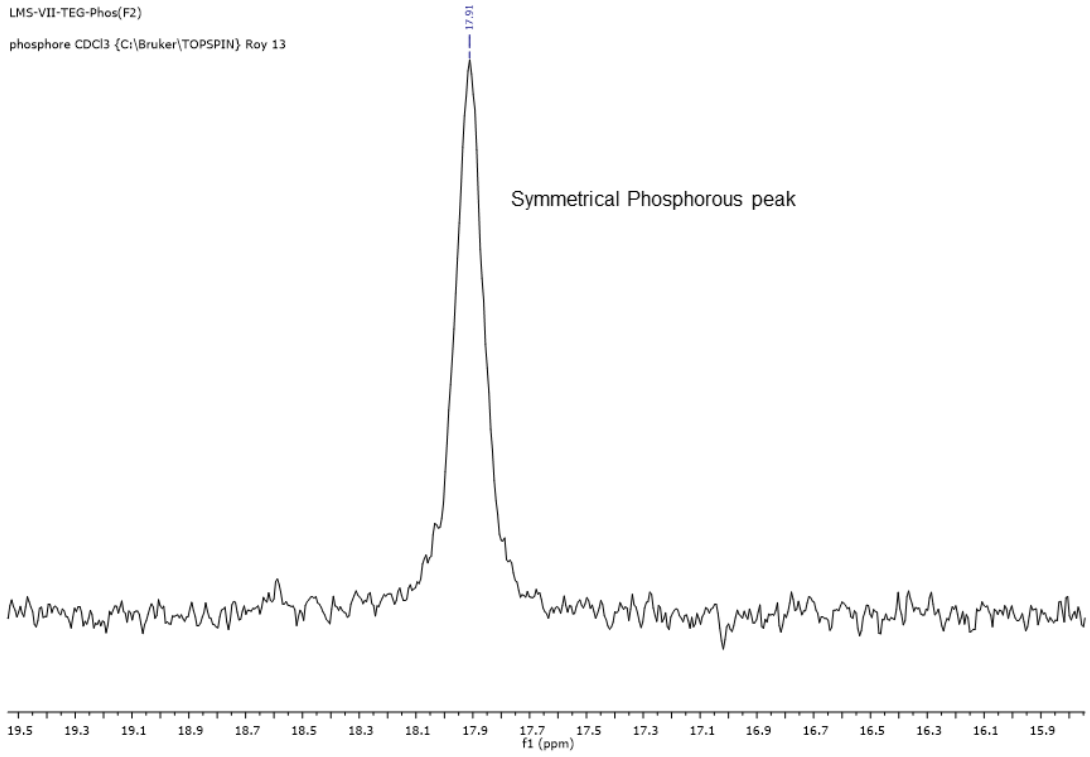

The product also was confirmed by using electron ionization mass spectrometry (ESI-MS), a peak of TEG_3-alkyne core **84** was detected at a molecular weight $[M+H]^+$1259.6 which matches the theoretical molecular weight of core **84** $C_{42}H_{66}N_3O_{18}P_3$ $[M+H]^+$ 1258.51.

Figure 6.3 ESI-MS of PEG_3-phosphazene conjugate **84**

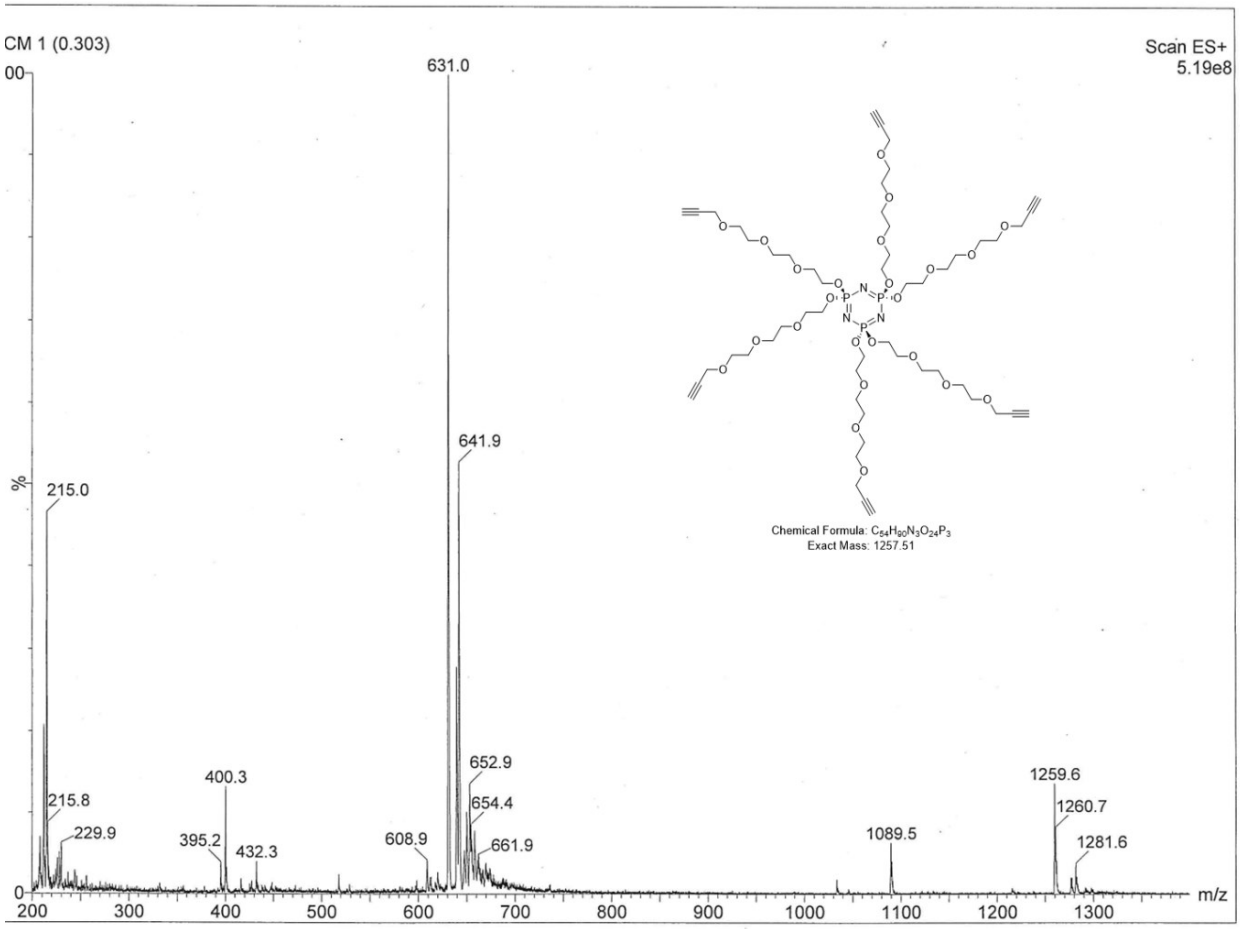

6.5.3 Diverse approaches to heterobifunctionalized PEG_3 linker

Here, we have investigated versatile synthesis routes for the preparation of heterobifunctionalized PEG_3 linkers, (illustrated in **Scheme 6.5**). Moreover, alkyne-TEG-NH_2 **161** can be obtained *via* two distinct routes starting from the same starting material. [496] A schematic overview for the synthesis of heterobifunctionalized PEG_3 linker is depicted in, (**Scheme 6.5**).

Scheme 6.5 Retrosynthesis and diverse approaches for synthesizing of PEG_3 heterobifunctional linkers

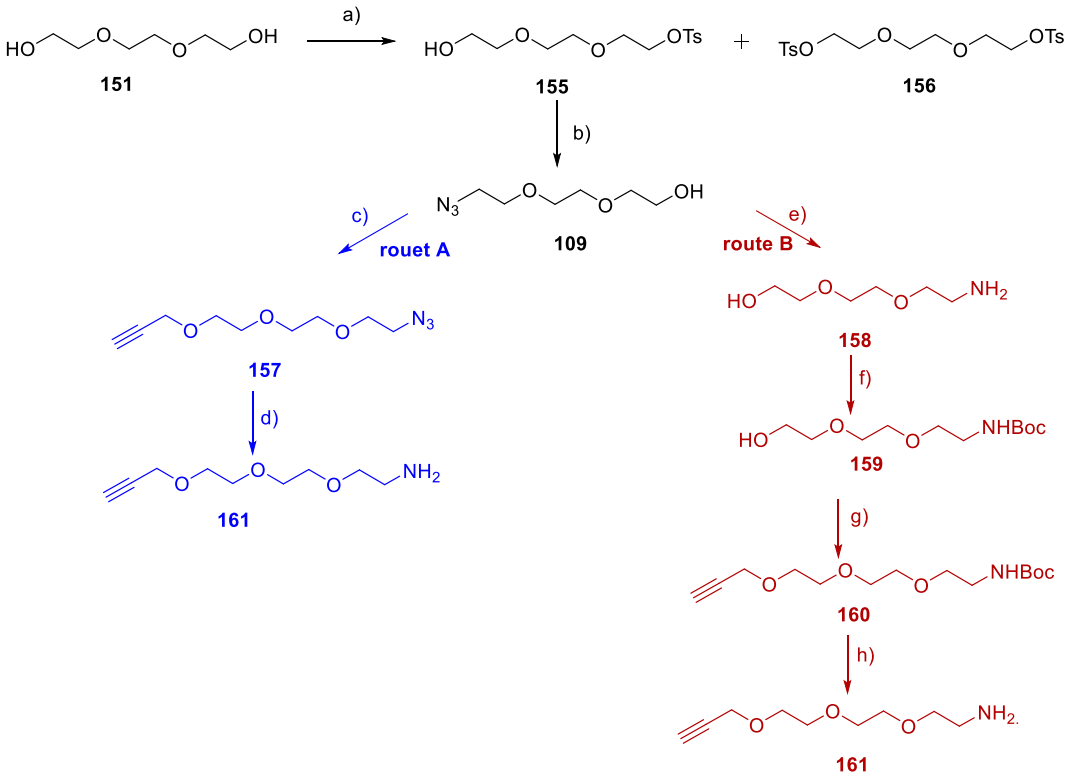

a) *p*-TsCl, NaOH, THF, 0 °C, 2.5 h; b) NaN_3, DMF, 70 °C, 16 h; c)  , NaH, THF, rt; d) PPh_3, THF/H_2O, 50 °C; e) PPh_3, Et_2O-5% aq. HCl, rt, 68%; f) $(Boc)_2O$, DCM, 0 °C- rt, 52%; g)  , NaH, DMF, 0 °C- rt; h) 20 % TFA, DCM, 0 °C- rt, 2 h.

The synthesis started with the reaction of tri (ethylene glycol) (**151**, PEG_3) with *p*-toluenesulfonyl chloride in presence of NaOH to afford mono PEG_3-tosylate **155** in 70%. In order to reduce the amount of di-tosylated compound, we attempted to use a large excess of TEG. The following step is the substitution of the tosylate with sodium azide in DMF at 70 °C. [497] Next, PEG_3- azide linker **109** was converted to mono-alkyne-PEG_3 **157** by the reaction with 1.1 equivalent of propargyl bromide in the presence of sodium hydride. Subsequent treatment of **157** with triphenylphosphine in THF-H_2O afforded alkyne-PEG_3-amine **161** in a low yield, (**Scheme 6.5**, *pathway A*). Alternatively, we applied a different route for the synthesis of linker **161**. As shown in (**Scheme 6.5**, *pathway B*), by reduction of the azide group of **109** to an amine *via* Staudinger reduction in a biphasic reaction medium (Et_2O-5% aq. HCl) [498] was found to produce **158** in a more facile manner and the overall yield was also considerably higher. The amine group was then protected as butyloxycarbonyl, followed by the reaction with propargyl bromide and sodium hydride to obtain **160**. Subsequent deprotection of Boc group in 20% TFA/DCM afforded PEG_3 linker with hetero functionality **161**, the data was in match with the reported one. [354]

6.5.4 Benzene-1,3,5-tricarbodimide (BTA-PEG_3) dendritic core

The synthesis of Benzene-1,3,5-tricarbodimide (BTA-PEG_3) dendritic core **93** as shown in (**Scheme 6.6**). Linker **161** was coupled to commercially available benzene-1,3,5-tricarboxylic acid **162**, using *N,N'*-Diisopropylcarbodiimide (DIC), 1-Hydroxybenzotriazole monohydrate (HOBt), tri ethylamine, in DMF as a solvent. The reaction mixture allowed to stir at room temperature for 16 h. Following the reaction work-up and purification, the desired alkyne scaffold **93** was obtained in a good yield. This core was characterized by ^{1}H NMR and ^{13}C NMR.

Scheme 6.6 Synthesis of Benzene-1,3,5-tricarbodimide (BTA-TEG_3) **93**

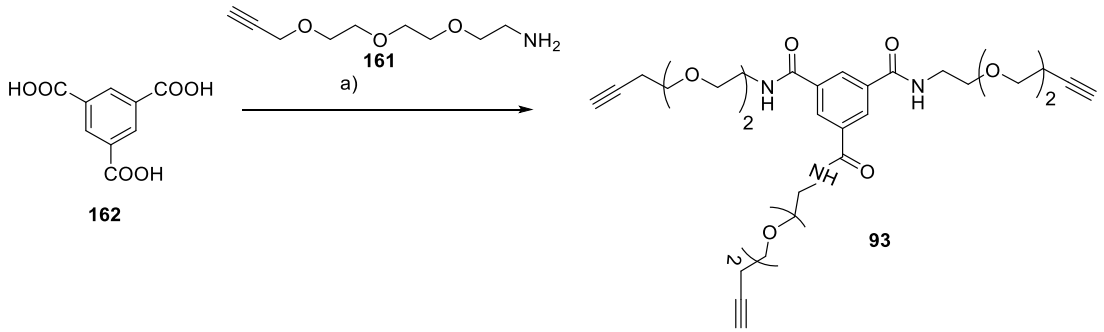

a) DIC, HOBt, Et_3N, DMF, 16 h, 0 °C- rt, 16 h.

The proton NMR for core **93** (**Figure 6.4**) showed a singlet peak at 8.39 ppm which integrates three aromatic protons. Other multiple significant peaks at 4.10- 3.53 ppm from TEG $[O\text{-}CH2\text{-}CH2\text{-}O]_2$. A distinct peak at 2.83 ppm which integrated for -CH bond.

Figure 6.4 ^{1}H NMR analysis of core **93**

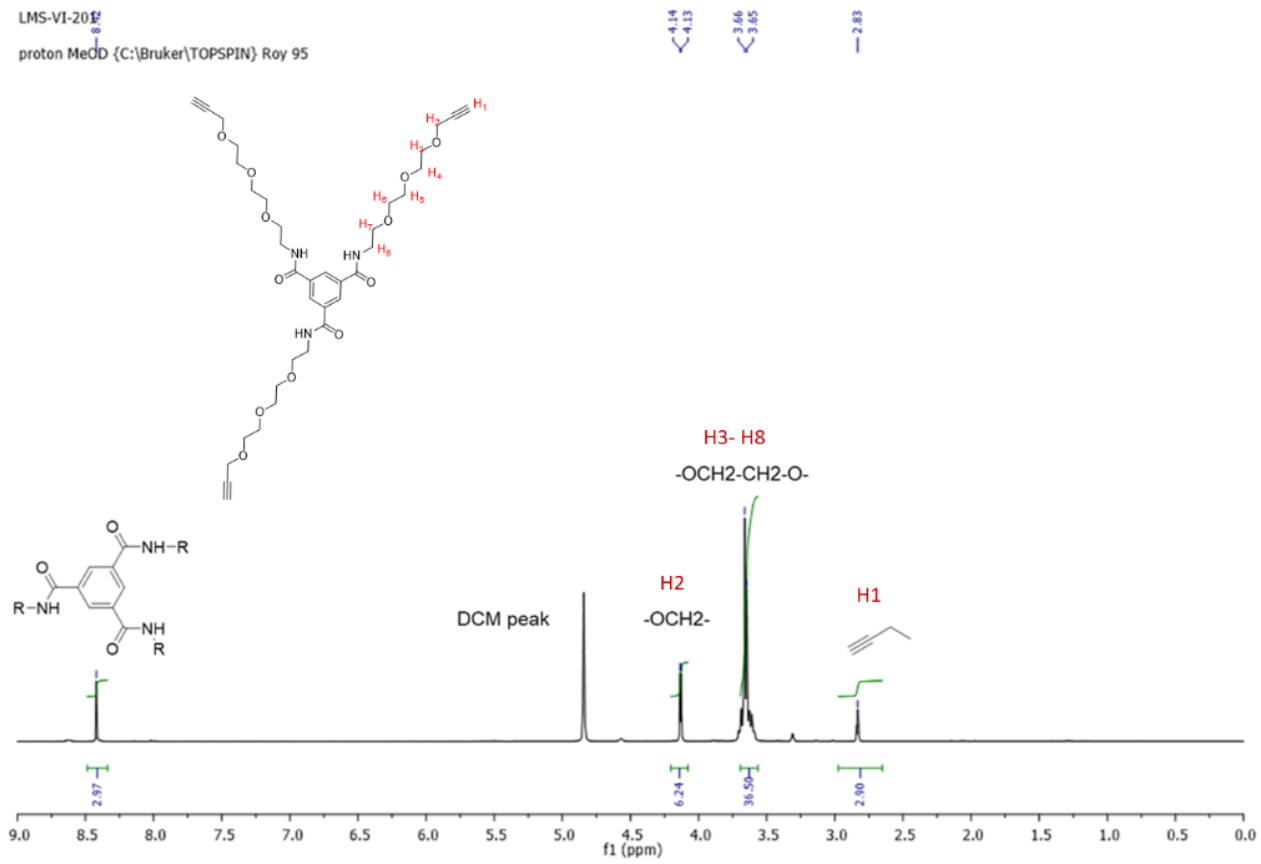

^{13}C NMR (**Figure 6.5**) showed a significant peak at 167.27 corresponds to amide carbonyl, confirming the amide bond synthesis. Peaks at 135.21- 128.70 correspond to aromatic carbon atoms. Another peaks at 79.21 and 74.71 which corresponds to alkyne carbon atom.

Figure 6.5 ^{13}C NMR analysis of core **93**

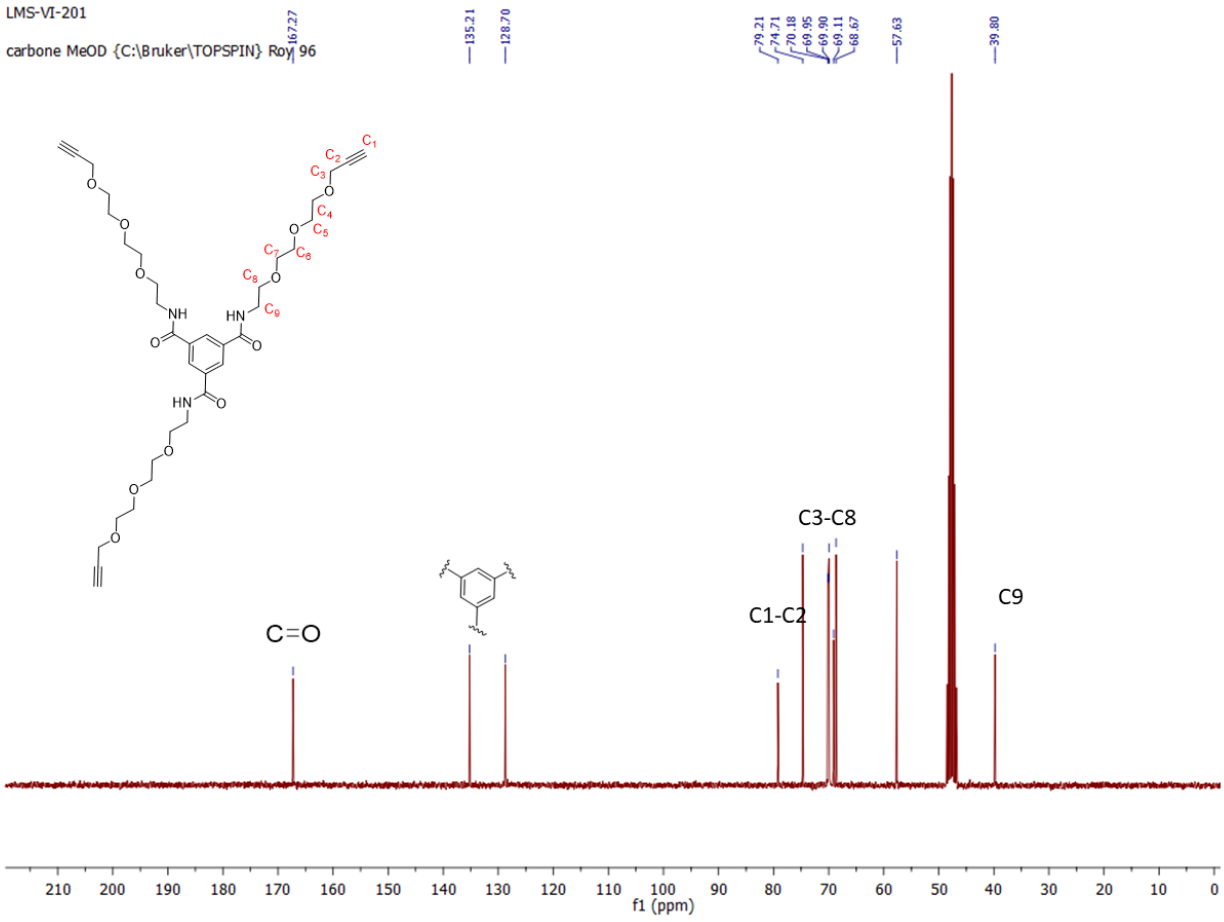

CONCLUSIONS AND FUTURE PERSPECTIVE

Gram-negative bacteria have developed mechanisms to protect themselves against antibiotics. Two of the major mechanisms that limit the activity of many antibiotics include efflux pumps and reduced uptake across the outer membrane (OM) barrier. One major challenge is to design new molecules to rapidly penetrate Gram-negative bacteria in order to achieve intracellular drug accumulation. The presented doctoral research had the objective to design a new glycodendrimer-prodrug approach in targeting bacterial adhesion and its application in the treatment of urinary tract infections and drug resistance. We apply the idea of dendrimers that use multivalent effects to exhibit enhanced susceptibility to prevent bacterial adhesion to host cells.

We are particularly interested in the dendrimer-based drug platforms that can deliver therapeutic compounds and combat bacterial resistance from both *P. aeruginosa* and *E. coli*, by carefully altering the surface properties of dendrimers. First, we demonstrated that shielding the secondary amine (-NH) of Cip will reduce the antibacterial resistance, therefore, can boost their ability to penetrate cell membranes. We designed a dendrimer-prodrug conjugate system that can modulate drug interaction with the body physiological environment and investigate the effectiveness of the suggested drug delivery system.

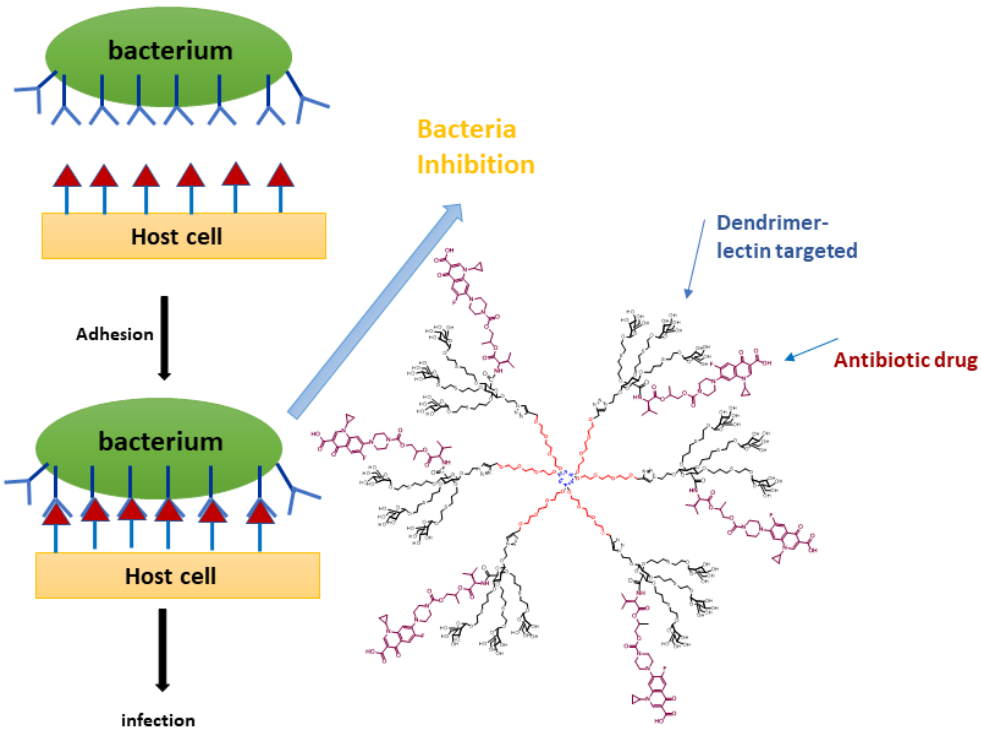

Successful application of a novel synthetic approach towards sequence-controlled multi-functionalized glycodendrimer was achieved by coupling sequence-defined monomers *via* thiol-ene click (TEC) and CuAAC coupling as schematically shown below (**Scheme 6.7**).

Scheme 6.7 Schematic overview of the synthetic approach towards construction of glycodendrimers *via* a combination of TEC and CuAAC reactions

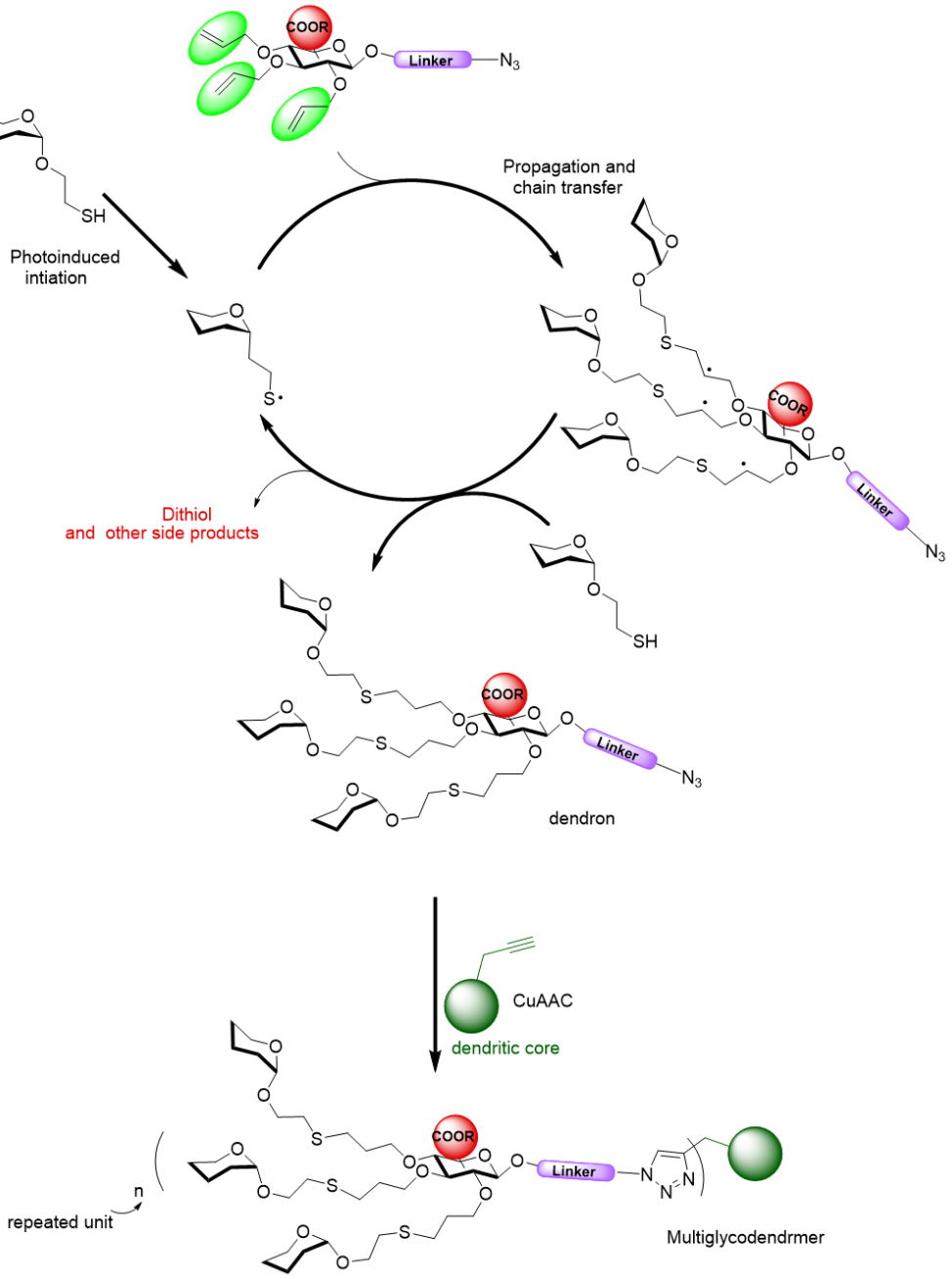

In the first part of the project, a detailed synthesis of monomers which represents different dendrimer generation (G), were discussed. In the first part, 1-azidoethanol-2,3,4-tri-allyl-β-D-glucuronic ester was synthesized from D-glucosepentaacetate. In this part, the first step is the synthesis of azidoethanol-β-D-glucopyranoside, which was separated as a single β-isomer in a high yield. Silylation of a primary OH group at C-6 position facilitates the allylation at positions *O*-2, *O*-3, and *O*-4. Finally, deprotection of *O*-TBDMS followed by one-step oxidation/esterification at C-6 position, accomplished *tert*-butyl-*β*-D-glucuronic ester in 74% yield. This new scaffold contains azide group (features click coupling), *tert*-butyl carboxylate group (for subsequent drug coupling), and terminal alkene, the latter is the active moiety in radical photoinduced thiol-ene reaction (TEC). The next part, we focused on the synthesis of lectin-targeted sugar. In this regard, two different monomers thiol were synthesized from commercially starting material, including L-fucose, and D-mannose, respectively. First, a productive approach has been developed for the synthesis of α-L-fucose thiol that has a rigid triazole linker. In this approach, several steps were applied including glycosylation, click, and hydroxyl group transformation to the xanthate functional group. For the following step of thiol synthesis, the reaction was performed using *n*-butylamine. Since the reactive thiol end-groups tend to oxidize and produce disulfides, therefore, several reaction parameters were evaluated. The first parameter is the number of *n*-butylamine equivalents added to the reaction mixture. The optimal amount was determined to be 1.3 equiv, reaching the highest yield. A second parameter studied was the duration required to liberate free thiol group. It was determined two hours as the optimal, and the product outcome was high yield (75%). The second example is α-D-mannose thiol synthesis. In this study, we be able to optimize the reaction parameters to reach the optimal yields.

The second part of the project focused on the synthesis of generation three (G3), in this step two different sequence glycomonomers produced from β-D-glucuronic ester, and α-L-fucose thiol or α-D-mannose thiol, were coupled by TEC using 2,2-Dimethoxy-2-phenylacetophenone as a radical initiator, therofore forming two different trithioglyco dendritic wedges (dendrons). Our main focus was devoted to the determination of the optimal reaction conditions, which involved various reaction parameters in order to achieve the maximum degree of coupling. To achieve the best reaction outcome, the monomers were combined in different ratios which is crucial for high conversion in the step-growth pathway. During the optimization, different reaction parameters were also varied to achieve high yield products. After choosing DMF as an adequate solvent ensuring good solubility of monomers, as well as an additional reactant during the entire course of the reaction, the first parameter that was optimized is the photoinitiator. It found that 2,2-Dimethoxy-2-phenylacetophenone (DMPA), the most suitable initiator for photoinduced TEC, with absorption maxima close to the emitted wavelength 365 nm. During the optimization, it was observed that the equimolar amount of 0.6 equiv DMPA (0.2 per each double bond) provides the best result of TEC reaction. The second parameter evaluated was the duration of UV irradiation. Studying determined 2-3 hours

as the optimal yield. With the optimized conditions two different molecules were obtained, trithiomannoside β-D-glucuronic ester, and trithiofucoside β-D-glucuronic ester carrying three α-D-mannoside or α-L-fucoside moieties in their side chain, respectively. The next step is the final dendrimer construction using the click reactions with dendrimer core. Unfortunately, the new synthesized molecules and the dendrimer core did not interact, and no desirable products were obtained. Under photolytic conditions, it is discovered that the azide group is unstable and vulnerable to reduction. Since the aforementioned synthesis was unable to produce the necessary dendrimers, a novel synthetic approach was taken. The addition of the protective group thus served to stop the azide group from being reduced. By conducting several experiments, it was found that NH-Fmoc protection following by diazo transfer methodology was the alternative synthetic route. Subsequently, thiol-ene reaction proceeded on NH-Fmoc-triallyl β-D-glucuronic ester. After optimization of the reaction parameters, two different novel building blocks including NH-Fmoc trithiomannoside-β-D-glucuronic ester, 79% yield, and NH-Fmoc trithiofucoside-β-D-glucuronic ester, 66% yield, were achieved when irradiating the reactants for a molar ratio of 6 :1 (Mannose thiol: alkene), or a molar ratio of 18 :1 (Fucose thiol: alkene), respectively under the presence of 50 mg photoinitiator DMPA using a total of 700 µl of a mixture of DMF and water in a ratio of (9:1). The increased ratio of applied fucose thiol could be explained by the reactivity of the thiol end group, as during the TEC reaction condition, fucose thiol was discovered to have a propensity to oxidize quickly in a short period of time, resulting in low conversion. As a result, it was discovered during optimization that using 18 equiv gave the best product outcomes. The timing for TEC was determined to be for 2.5 hours, even though in the case of mannose thiol almost no further increase in conversion was observed after 2 h. In addition, the reaction without adding water was tested, reaching a good yield, thereby showing there is no essential to add water to the reaction mixture.

The final NH-Fmoc trithiomannoside and /or trithiofucoside building blocks were subjected to a two-steps procedure, first removing all protecting groups in a mixture of ammonia/ methanol and thereby liberating the reactive amine group, followed by diazo transfer using 1H-imidazole-1-sulfonyl azide sulfate in a catalytic $CuSO_4$. The novel molecules with free azide group were obtained in 83% and 74 % for trimannoside, and trifucoside dendrons, respectively. These novel synthetic dendrons were clicked *via* CuAAC to different dendritic cores. For this task, several diverse pathways were used to synthesize different dendritic cores including PEG_3-cyclotriphosphazene and benzene-1,3,5-tricarbodimide (BTA-PEG_3) core functionalized with terminal alkyne moieties. The first pathway was to create a flexible hexavalent core, which started with the synthesis of PEG_3 linker. The reaction involved the addition of alkyne on one end of the PEG_3. Next, this linker is added to hexachlorocyclotriphosphazene (HCCP) to complete the synthesis of PEG_3-cyclotriphosphazene hexavalentcore. The second pathway explored synthesis of trivalent dendritic core. This pathway started with the synthesis of a heterobifunctional PEG_3-linker. This linker carries one

alkyne group on one end, and an amine group to the other end. Next step was the addition of this linker to Benzene tricarboxylic acid (BTA) under amide coupling condition to obtain benzene-1,3,5-tricarbodimide (BTA-PEG_3) dendritic core.

After establishing the click coupling conditions, a series of four new glycodendrimers were synthesized, with weight average molecular mass, Mw, between 11.246 kDa and 11.727 kDa, depending on the molecular weight of the incorporated dendritic wedges (dendrons), (**Scheme 6.8**). The exact masses of one presented dendrimer were slightly below the theoretical one, which could be reasoned to a degradation that happened during the MALDI process. With a hexavalent and/ or trivalent dendrimer, each dendron is incorporated 6 times and/ or 3 times in the final multiglycodednrimer, therefore obtaining glycodendrimers with final averages Man and/ or Fuc valencies between 18-9.

Scheme 6.8 A schematic overview of the synthetic approach towards glycodendrimers construction. A) the first set, assembled out of several glycomonomers using TEC, derived from β-D-glucuronic ester or β-D-glucosamine carrying alkene moieties and other α-D-mannoside or α-L-fucoside bearing active thiol; B) the second set, assembled out of the dendrons and a functionalized cores using CuAAC

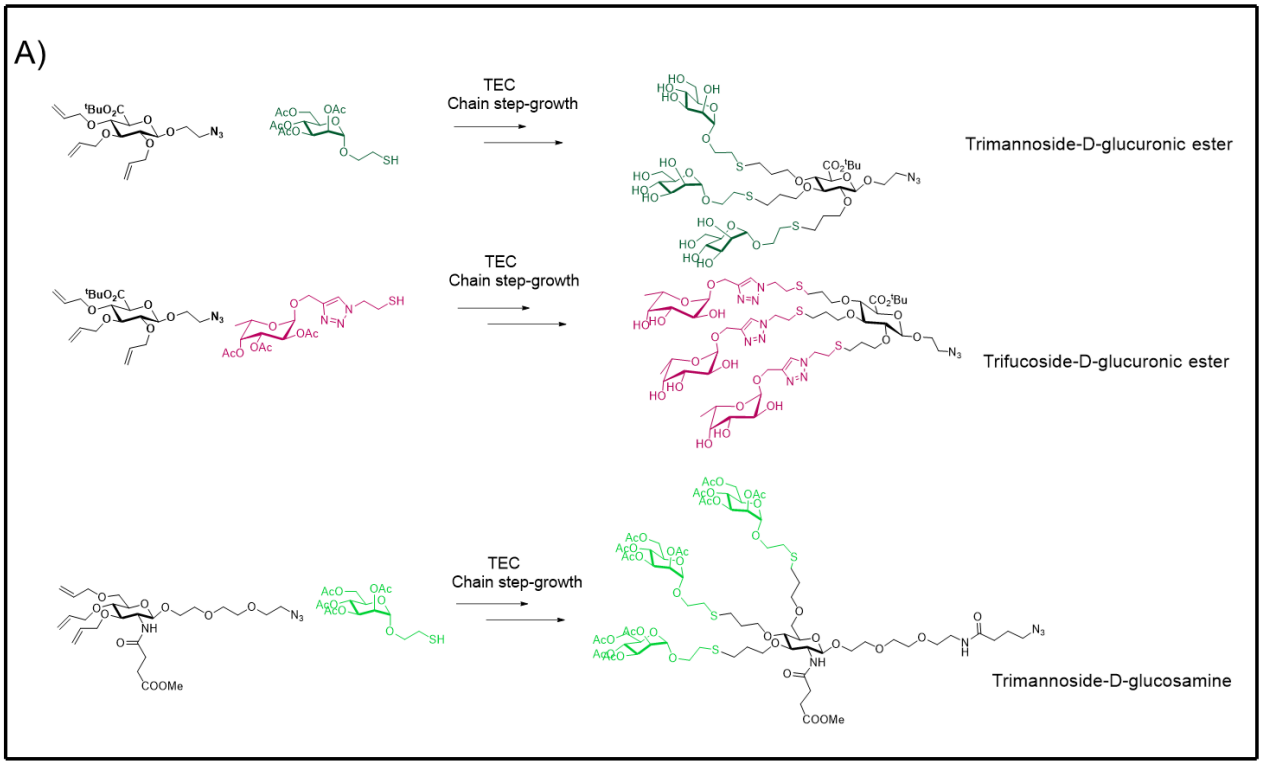

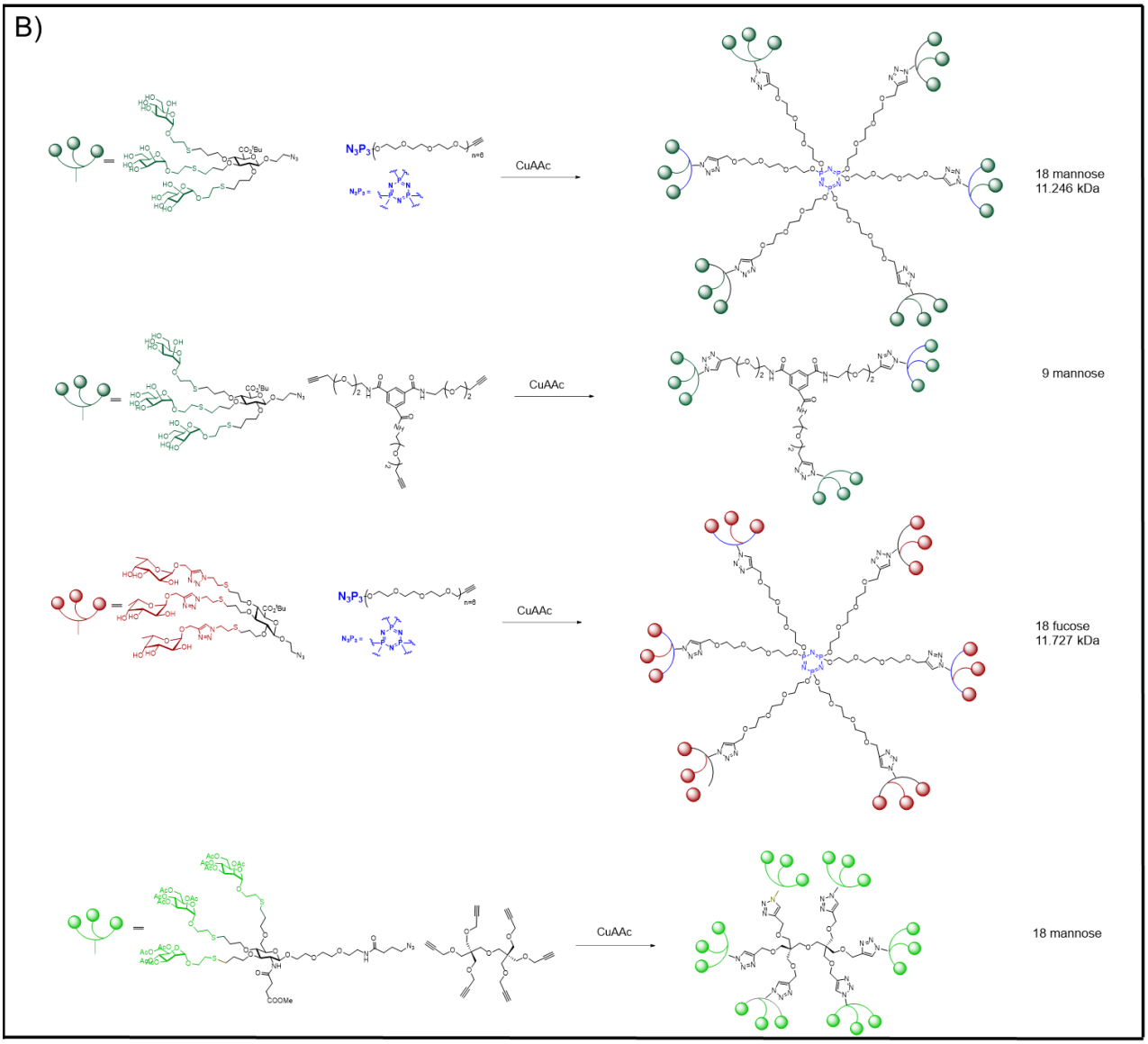

To study whether the introduction of rigid spacing affects the interactions towards the lectin, and subsequent drug delivery, therefore, the second set of the glycodendrimer-PEG_3 rigid spacer was synthesized (**Scheme 6.8**). In this context, a multivalent novel building block based on multifunctional β-D-glucosamine, was introduced. This novel building block was successfully synthesized starting from a fully protected tetra-*O*-acetyl-2-deoxy-2-phthalimido-D-glucopyranose key intermediate. These routes involved multi-step procedures which required the preparation and characterization of several key building blocks, equipped with appropriate orthogonal functionalities. In the first step of this approach, PEG_3 linker terminated with the azide group (PEG_3-N_3), was installed at the anomeric position, using $BF_3.Et_2O$ as the promoter. Next, the product was subjected to two steps. First, deprotection of *O*-acetyl groups using NaOMe/MeOH which was conducted under pH control, followed by the reaction with allyl bromide in the presence of a base, to

introduce allyl moieties at *O*-3, *O*-4, and *O*-6. By conducting several experiments we found that 2.5 h in the presence of base LiHMDS afforded the best reaction outcome. Deprotection of phthalimido group afforded D-glucosamine bearing free amine (NH_2) at position C-2, which was used to introduce an external linker bearing terminal carboxylic group. As linker 4-methoxy-oxobutanoic acid was chosen to conjugate with the amine group from D-glucosamine using *N,N*'-diisopropylcarbodiimide (DIC), and hydroxybenzotriazole (HOBt). This new key building block β-D-glucosamine-(PEG_3-N_3) was subjected to Staudinger reduction to afford free amine (PEG_3-NH_2) which subsequently protected with $(Boc)_2O$ group. The next step was to link α-D-mannose thiol to triallyl-β-D-glucosamine scaffold by using TEC coupling approach. A novel trithiomannoside dendritic molecule obtained in 85% yield, that contains two different orthogonal protecting groups, -NHBoc and -*O*Ac, which were selectivity removed by applying two continuous procedures, first removal of OAc in NaOMe/CH_3OH, then removal of Boc by TFA/DCM, resulting in trithiomannoside β-D-glucosamine building block carrying hydroxyl and free amine groups, this product was pure enough and subjected to the next step without any further purification. The resulting product coupled to 4-azidobutanoic acid linker by using bulk phosphonium salt type coupling reagents, benzotriazol-1-yl-oxy-tris-(pyrrolidino)-phosphonium hexafluorophosphate (PyBOP). For the step of the dendrimer synthesis, the dendritic wedge coupled to dipentaerythritol core (carrying hexa alkyne functional group) using CuAAC, resulting in a first set of a novel glycodendrimer carrying a total of 18 Man valency. The final process involves two steps of deprotection, first removal of acetyl groups by NaOMe/CH_3OH, then the removal of methyl ester groups using lithium hydroxide in a mixture of methanol and water, which is a continuing process. The resultant free carboxylic group subsequently will be coupled to the antibiotic.

The third part of this project was focused to introduce a cleavable linker to the secondary amine of Cip. (Acyloxy)methyl ester linker was chosen. Its free amine (-NH_2) functional group coupled onto the carboxylic group of the dendrimer using the standard amide coupling reagent (PyBOP). We disclosed the preliminary results involving the coupling of the Cip-linker to the dendrimer backbone using the standard coupling reagent PyBOP. The final synthetic pathway towards the dendrimer-drug conjugates is shown in (**Scheme 6.9**).

Scheme 6.9 Dendrimer-drug conjugate

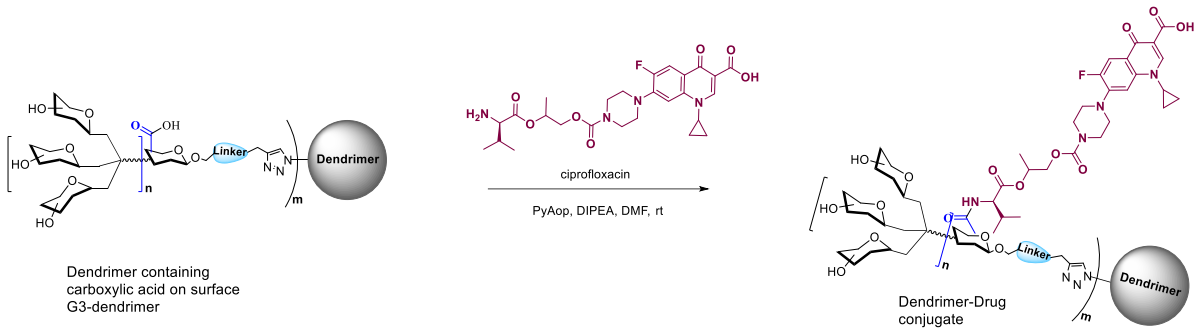

Some parts of this research cannot be completely undertaken due to time constraints. Evidently, there is a need to expand and build on the studies presented in this thesis especially as it relates to ciprofloxacin. We have demonstrated an approach to enhance the delivery of this class of drug in resistant Gram-negative bacteria, using glycodendrimer-based drug conjugate, and we envisage that the concept therein will be useful in developing a strategy to address the problem of antimicrobial resistance with different antibiotics. Based on the presented synthetic approach, new insights about the design and properties of glycodendrimer will be further extended in future studies. Due to the ease of introducing different biological ligands in the dendrons sequence during CuAAC in addition to the great tolerance of TEC procedure, the approach has great potential for a broad range of applications. Besides the application of the synthetic procedures, further research will be done on the impact of molecular weight and inter ligand spacing on multivalent binding processes during lectin interaction.

PERSPECTIVE

The concept of dendrimers and dendritic wedges (dendrons) containing internal functionality is an attractive area of research. Within this concept the design of dendritic core and wedges is still ongoing research.

Some plausible pathways towards expanding this project may include, but are not limited to:

6.6 Synthesis of dendrimer-Cip conjugate

Cip is a clinically used antibiotic against a wide range of Gram-negative bacteria. However, bacteria often express multiple resistance pathways that work in tandem to prevent the actions of antibiotics. In **chapter 1**, we demonstrate that Cip suffers from an efflux pump, wherein an outer membrane permeability may enhance intracellular uptake and reduce antibiotic resistance. To increase the drug metabolic stability, it is possible that the drug can be ligated to the dendrimer using stable amide linker, with the hope that the

targeted dendrimer-drug conjugate will anchor Cip across the porin of Gram-negative bacteria into the plasma where it will enzymatically be released.

Scheme 6.10 The dendrimer drug conjugates; (A) Fuc-based dendrimer coupling with Cip, (B) Man-based dendrimer- coupling with Cip, (C) D-glucosamine dendrimer Cip coupling

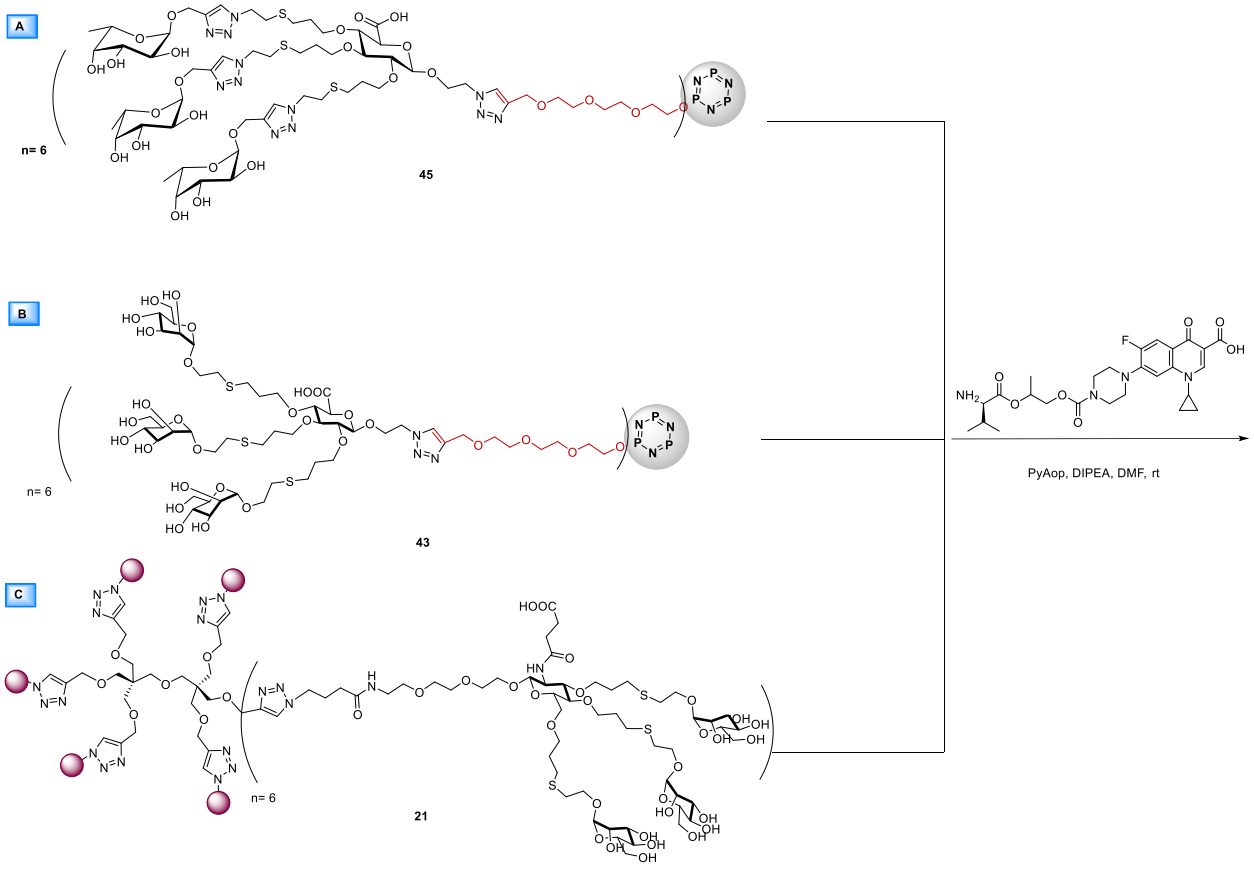

6.7 Sulfamethoxazole-dendrimer drug conjugate

Sulfamethoxazole (SMZ) and trimethoprim combination are used to treat infections including urinary tract infections. SMZ, a sulfonamide with known anti-bacterial properties, is not freely soluble in water and causes problems in its clinical application. Recently, urea derivatives obtained from SMZ have been proposed as potential antimicrobial agents. Importantly, we choose SMZ as a second antibiotic for the present study as a drug-dendrimer conjugates with the hope to reduce the number of the drug combination and possible pharmacokinetics interactions that may associate therein, (**Scheme 6.10)**.

Scheme 6.11 Sulfamethoxazole-dendrimer drug conjugate

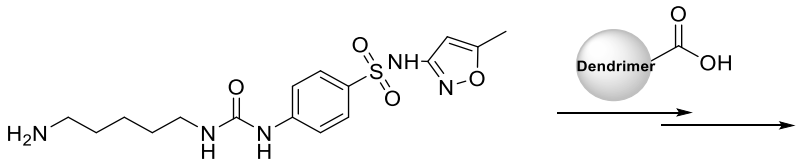

6.8 Biology

- Conjugation of antibiotic on glycodendrimer may have different mechanism for interaction with bacteria that requires further investigation in the future.

- To elucidate the fundamental mechanism of drug potency when localized on the dendrimer, the binding affinity of the Cip and Cip-dendrimer conjugate using a ligand displacement assay to assess what concentration of ligand is required to aborogat antibacterial activity.

- Dynamic light scattering (DLS) will be used to monitor the evolution of the hydrodynamic volume for the drug loading.

APPENDIX A

SUPPORTING INFORMATION

1. Solvents and reagents

Unless otherwise noted, all reactions were performed under an inert nitrogen atmosphere**.** All work-up and purification procedures were carried out with reagent-grade solvents under an ambient atmosphere. Reagents were purchased from commercial suppliers and were used without further purification. THF, DMF, CH_2Cl_2, were purified by passing through a solvent purification system and dried over activated Molecular Sieves, 4 Å pellets, prior to use. Amberlite IR120 H^+ form was washed with MeOH before using it for neutralization. Thin layer chromatography (TLC) was performed on Merck TLC plates (0.25 mm) pre-coated with silica gel 60 F254 and visualized by UV quenching and staining with ninhydrin, $KMnO_4$ and 10% H_2SO_4 in MeOH or by heating with orcinol.

2. Characterizations

NMR spectra were recorded on Bruker DPX-300 instruments and were calibrated using residual deuterated solvent as an internal reference ($CDCl_3$: 7.26 ppm ^1H NMR, 77.2 ppm ^{13}C NMR; MeOH-d4: 3.31 ppm ^1H NMR, 29.8 ppm ^{13}C NMR; acetone-*d6*: 2.05 ppm ^1H NMR, 29.8 ppm ^{13}C NMR; DMSO-*d6*: 2.50 ppm ^1H NMR, 39.5 ppm ^{13}C NMR. Chemical shifts (δ) are given in ppm relative to residual solvent peaks. Data for ^1H NMR are reported as follows: s (singlet), d (doublet), t (triplet), q (quartet), m (multiplet), br (broad), dd (doublet of doublet), dt (doublet of triplet). Spectrometer FT-IR instrument is reported in reciprocal centimeters (cm^{-1}). Elctron ionization Mass experiments were performed in LCMS. High-resolution mass spectroscopy (HRMS) analysis was performed using an ESI-QTOF spectrometer (UQAM) and Applied Biosystems MALDI TOF/TOF instrument (Research Institute of the McGill University Health Center).

Experimental, detailed synthetic procedures, and compounds characterization, are given within the supplementary materials.

Experimental part chapter 2

2-Azidoethyl 2,3,4,6-tetra-*O*-acetyl-β-D-glucopyranoside (33)

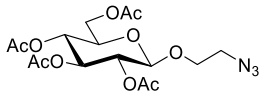

Step 1: 2-Chlorooethyl 2,3,4,6-tetra-*O*-acetyl-β-D-glucopyranoside

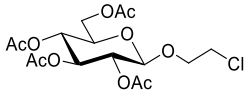

Experimental: A mixture of 1,2,3,4,6-penta-*O*-acetyl-β-D-gulcopyranose (652 mg, 1.67 mmol) and chloroethanol (220 µL, 3.23 mmol) in anhydrous CH_2Cl_2 (10 mL), containing 4 Å molecular sieves (powder, 900 mg) was stirred for 30 min. under nitrogen atmosphere, the mixture was then cooled to -40 °C, to this mixture $BF_3.Et_2O$ (250µL, 3.34 mmol) was added slowly. The reaction was allowed to stir for 10 h at which the temperature reached 10 °C. The mixture extracted with DCM, and the combined organic phases were washed with saturated aq. $NaHCO_3$, water, and brine. The organic phase was dried over anhydrous Na_2SO_4, the solvent was then evaporated under reduced pressure. The crude product was purified by flash column chromatography (Hexane/EtOAc 6:4 %) giving pure compound (480 mg, 70%), (R_f = 0.226). ^{1}H and ^{13}C NMR were consistent with reported data.^{1}H NMR (300 MHz, $CDCl_3$): δ 5.22 (q, *J* =9.55 Hz, 1H, H-3), 5.09 (t, *J*= 7.43 Hz, 1H, H-4), 4.93 (dd, *J*= 7.44 and 15.48Hz, 1H, H-2), 4.60 (d, *J* = 7.91Hz, 1H, H-1), 4.26(dd, $J_{6a,5}$ = 4.24, $J_{6a,6b}$= 12.3 Hz, 1H, H-6_a), 4.15 (dd, $J_{6b,5}$ = 3.25, $J_{6a,6b}$= 12.3 Hz, 1H, H-6_b), 4.13- 4.06 (m, 1H, OCH), 3.80- 3.73(m, 1H, OCH), 3.71 (q, $J_{5,6a}$ = 24.7 Hz, $J_{5,6b}$= 4.7 Hz, $J_{5,4}$= 9.9,1H, H-5), 3.62 (m, 2H, CH_2Cl), 2.09 (s, 3H, OAc), 2.06 (s, 3H, OAc), 2.03 (s, 3H, OAc), 2.01 (s, 3H, OAc) ^{13}C NMR (300 MHz, $CDCl_3$) δ 170.7, 170.4, 169.5, 169.5, 101.2, 72.7, 72.0, 71.1, 70.0, 68.4, 61.9, 42.6, 20.8, 20.8, 20.7, 20.7. [306]

Step 2:

Experimental: To a solution of the product from the previous step (480 mg, 1.17 mmol) in DMF, added tetra-*n*-Butyl ammonium iodide (*n*-Bu_4NI) (43 mg, 0.117 mmol), and sodium azide (380 mg, 5.85 mmol), the reaction mixture was heated at 80 °C for 16 h. The mixture was partitioned between ethyl acetate and water, then the organic phase dried over anhyd. Na_2SO_4, concentrated to give the product as a white precipitate. The data was obtained in accordance with the reported literature. [306] ^{1}H NMR (300 MHz,

$CDCl_3$): δ 5.21 (q, *J* =9.55 Hz, 1H, H-3), 5.09 (t, *J*= 7.43 Hz, 1H, H-4), 5.02 (dd, *J*= 7.44 and 15.48Hz, 1H, H-2), 4.59 (d, *J* = 7.91Hz, 1H, H-1), 4.25 (dd, $J_{6a,5}$ = 4.24, $J_{6a,6b}$= 12.3 Hz, 1H, H-6_a), 4.16 (dd, $J_{6b,5}$ = 3.25, $J_{6a,6b}$= 12.3 Hz, 1H, H-6_b), 4.03- 4.01 (m, 1H, OCH), 3.78- 3.60 (m, 2H, OCH and H5), 3.54- 3.38 (m, 1H, CH_2N_3), 3.33- 3.21(m, 1H, CH_2N_3), 2.08 (s, 3H, OAc), 2.04 (s, 3H, OAc), 2.02 (s, 3H, OAc), 2.00 (s, 3H, OAc); ^{13}C NMR (300 MHz, $CDCl_3$) δ 170.7, 170.3, 169.5, 169.4, 100.8, 72.9, 72.0, 71.0, 70.0, 68.6, 68.4, 61.9, 50.6, 20.8, 20.8, 20.7, 20.7.

2-Azidoethyl-β-D-glucopyranoside (34) [499]

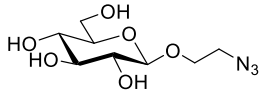

Experimental: β-D-glucoopyranoside derivative **33** (480 mg, 1.15 mmol) was dissolved in MeOH (10 mL) under a nitrogen atmosphere. Then sodium methoxide (74 mg, 1.4 mmol) in methanol was added with the syringe, and the reaction mixture was stirred at rt for 4 h after which TLC indicated full conversion. The reaction was neutralized by the addition of Amberlite IR120 H^+ form until the pH reached ~6 (checked using pH paper). The Amberlite was then filtered off, and the solvent was removed in *vacuo* to afford a pure product **34** as yellow oil residue (286 mg) which was used in the next step without any further purification. The data was obtained in accordance with the reported literature.

2-Azidoethyl-(6-*O*-tert-butyl-dimethylsilyl) β-D-glucopyranoside (35)

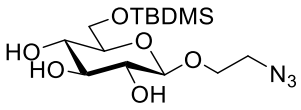

Experimental: A solution of the compound **34** (6g, 24.1 mmol) in dry DMF (20 mL) was cooled at 0 ºC, to this solution was added imidazole (2g, 29.4 mmol) and TBDMSCl (4g, 26.7 mmol). The reaction mixture was allowed stirring at 0 ºC for 7 h. The solvents were evaporated under reduced pressure with co-solvent toluene, such azeotropic drying with toluene was repeated several times to remove traces of DMF. The crude product was purified by column chromatography using (CH_2Cl_2/ MeOH, 99:5%) as eluent to afford compound **35** (5 g, 13.77 mmol, 57%) as colourless oil; R_f (0.176). ^{1}H NMR (300 MHz, CD_3OD): δ 4.91-4.53 (brs, 3H), 4.26 (d, 1H, *J* = 7.7 Hz, H_1), 3.99- 3.87 (m, 2H, CH_2), 3.79- 3.66 (m, 2H, CH_2, $H_{6a,b}$), 3.47-3.37 (m, 2H, CH_2), 3.31- 3.20 (m, 2H, H_2,H_3,H_4), 3.20- 3.13 (m, 1H, H_5), (s, 9H, 3xCH_3), 0.06 (d, 6H, *J* =

1.3 Hz, 2xCH$_3$). ^{13}C NMR (300 MHz, CD$_3$OD) δ 103.0, 76.7, 76.6, 73.6, 69.9, 68.1, 62.7, 50.6, 25.2, 17.9. ESI-HRMS: *m/z* calcd for $C_{14}H_{29}N_3O_6$ Si [M+Na] $^+$ 386.1718, found 386.1709.

Figure A1. ^{1}H NMR analysis of **35** (300 MHz, CD$_3$OD)

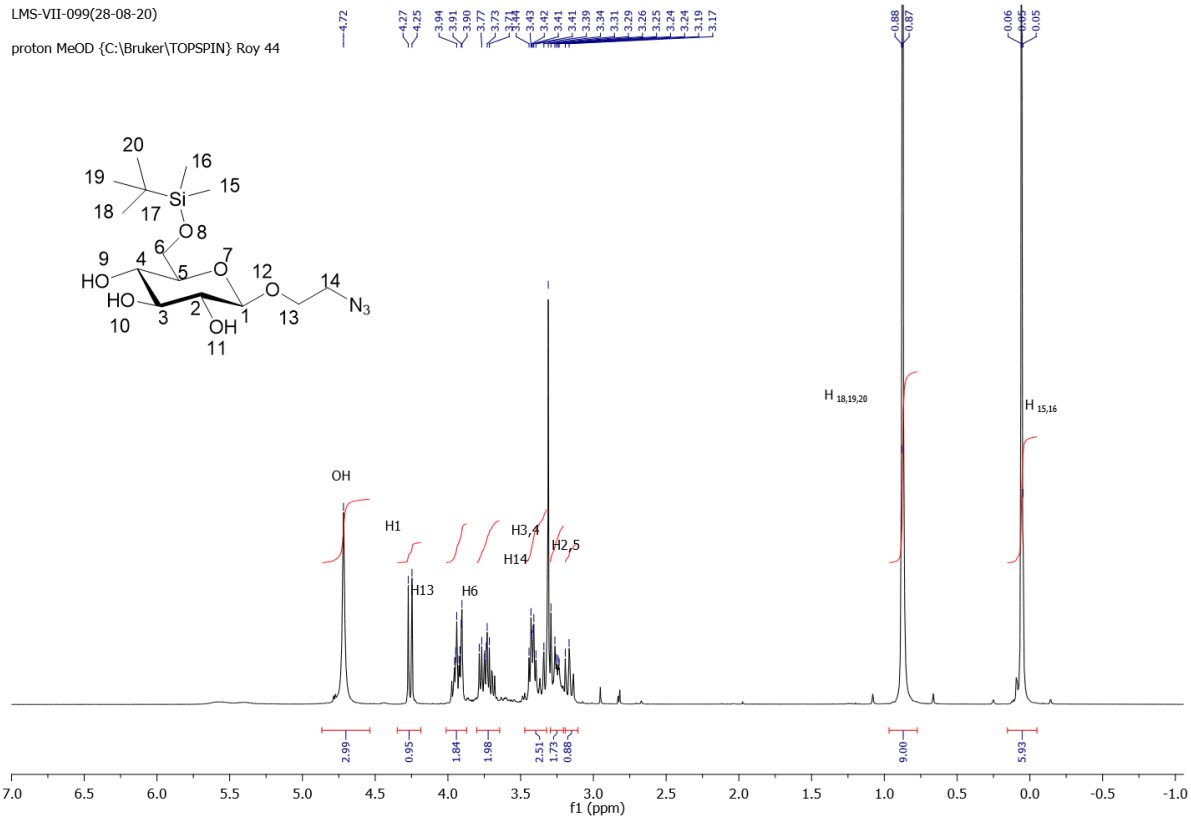

Figure A2. ^{13}C NMR analysis of **35** (300 MHz, CD_3OD)

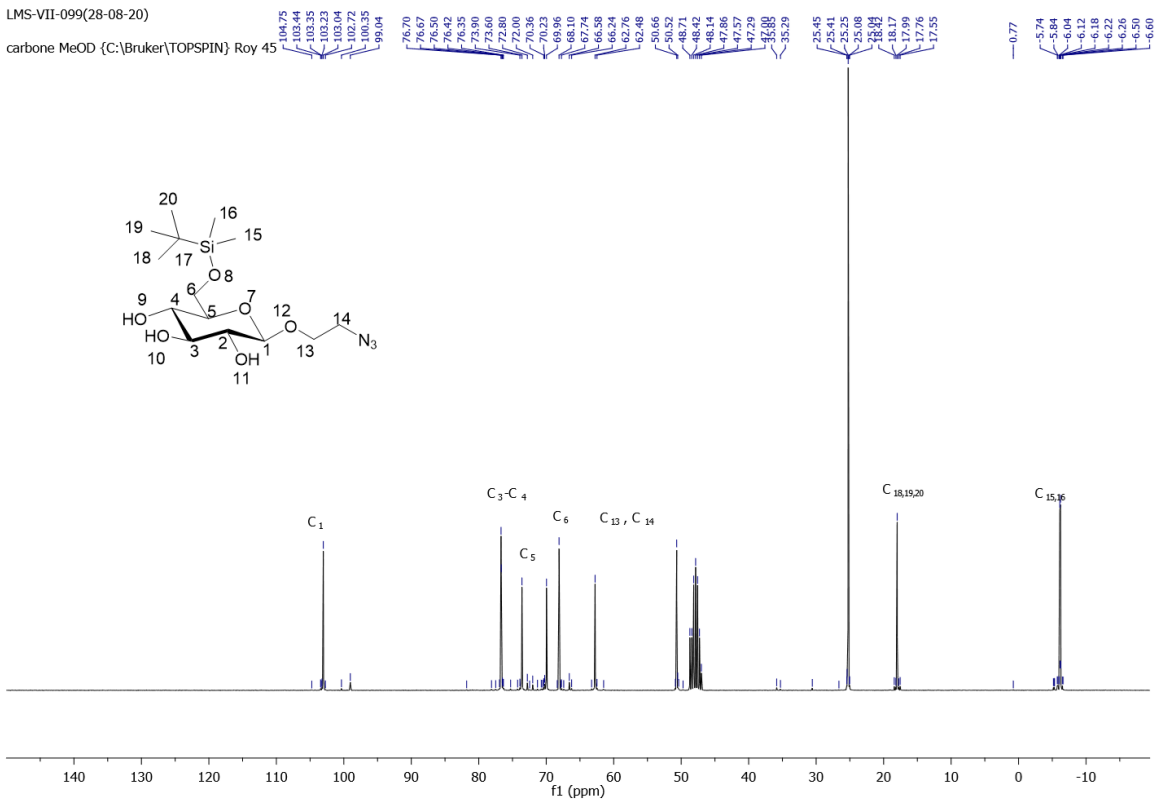

Figure A3. COSY analysis of **35** (300 MHz, CD_3OD)

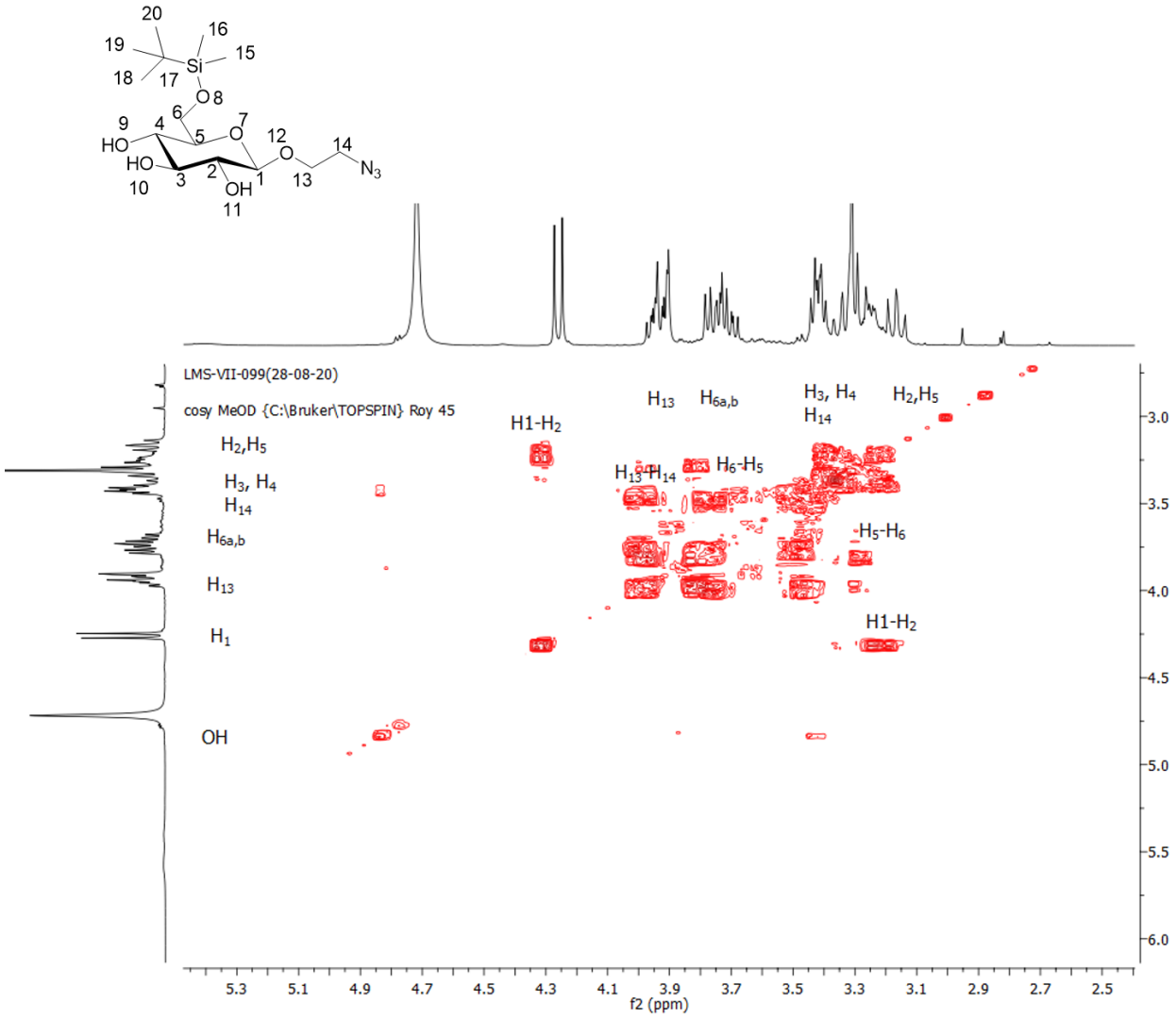

Figure A4. HSQC analysis of **35** (300 MHz, CD_3OD)

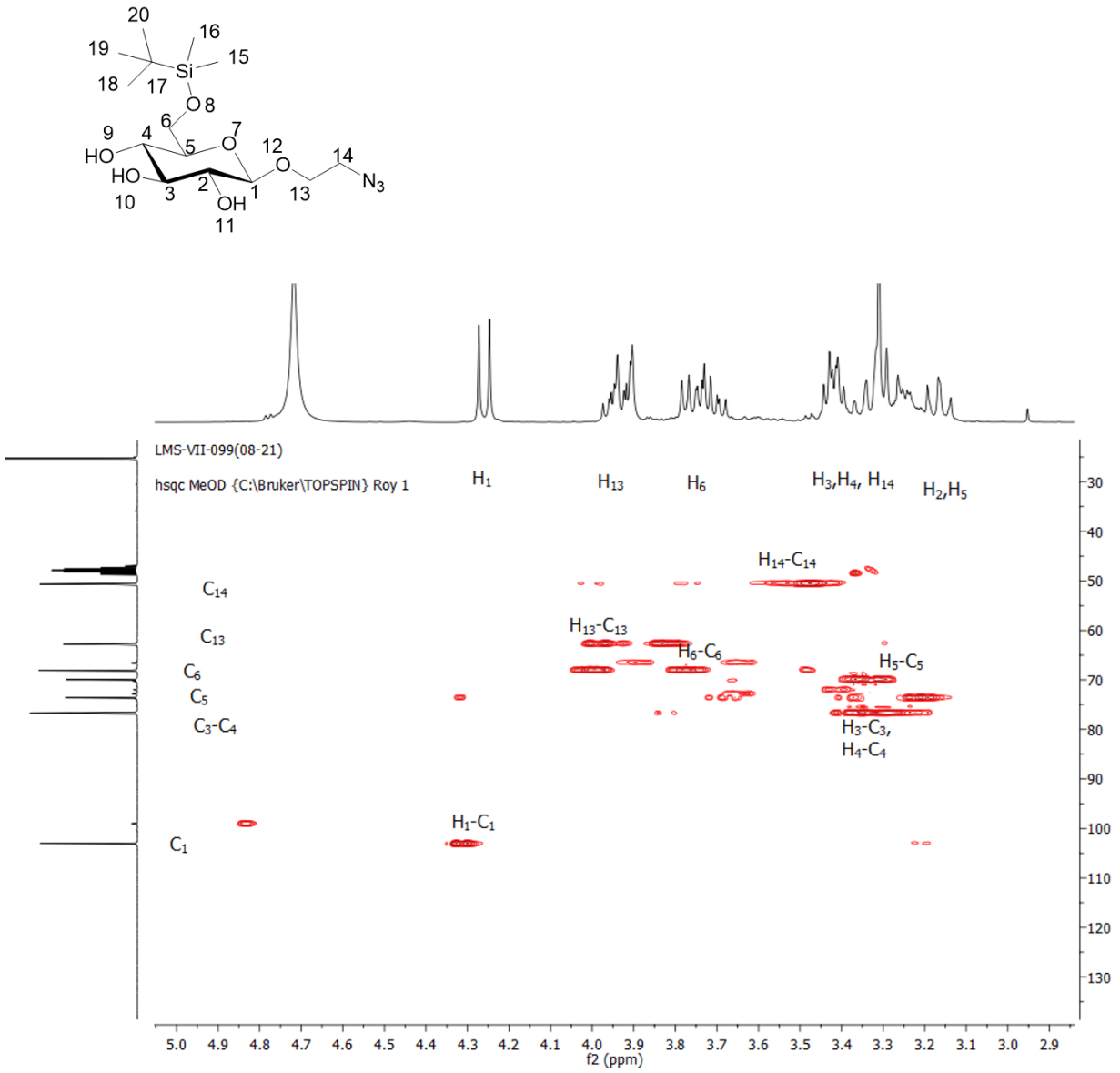

Compound 36

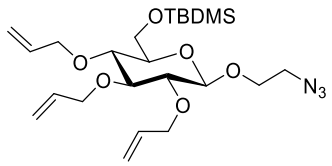

Experimental: To a solution of **35** (4 g, 11.02 mmol) in DMF (40 mL) at 0 ºC, was added sodium hydride (60%, 1.9 g, 49.59 mmol), after stirring at 0 ºC for 15 min. allyl bromide (6 mL, 66.12 mmol) was added. The reaction mixture was stirred at rt for extra 2.30 h. After, the reaction mixture was quenched by the addition of saturated aqueous NH_4Cl, then diluted with ethyl acetate and the organic layer was washed with water, brine, and dried over anhyd. Na_2SO_4. The organic layer is concentrated under reduced pressure. The crude residue was purified by column chromatography (Hexane/ EtOAc, 95:5%) to give pure product **36** as pale-yellow oil, yield (3 g, 57%). ^{1}H NMR (300 MHz, $CDCl_3$) δ 6.12- 5.74 (m, 3-H), 5.28- 5.00 (m, 6H), 4.40- 4.17 (m, 6H), 4.4- 4.14 (m, 6H, H_1), 3.99 (ddd,1H, *J* = 10.5, 5.6, 4.0 Hz, OCH_2), 3.87 – 3.73 (m, 2H, $H_{6a,b}$), 3.67 (ddd, 1H, *J* = 10.8, 6.8, 4.2 Hz, OCH_2), 3.49 – 3.39 (m, 2H, NCH_2), 3.41- 3.28 (m, 2H, CH_2), 3.22 – 3.12 (m, 2H, H_3, H_4), 3.20- 3.16 (m, 2H, H_2, H_5) 0.89 (s, 9H, 3x CH_3), 0.05 (s, 6H, 2x CH_3). ^{13}C NMR (300 MHz, $CDCl_3$) δ 116.7, 103.2, 84.1, 81.6, 74.4, 73.6, 73.6, 67.9, 62.1, 50.9, 25.8, 18.3, -5.1, -5.4.

Figure A5. ^{1}H NMR analysis of **36** (300 MHz, $CDCl_3$)

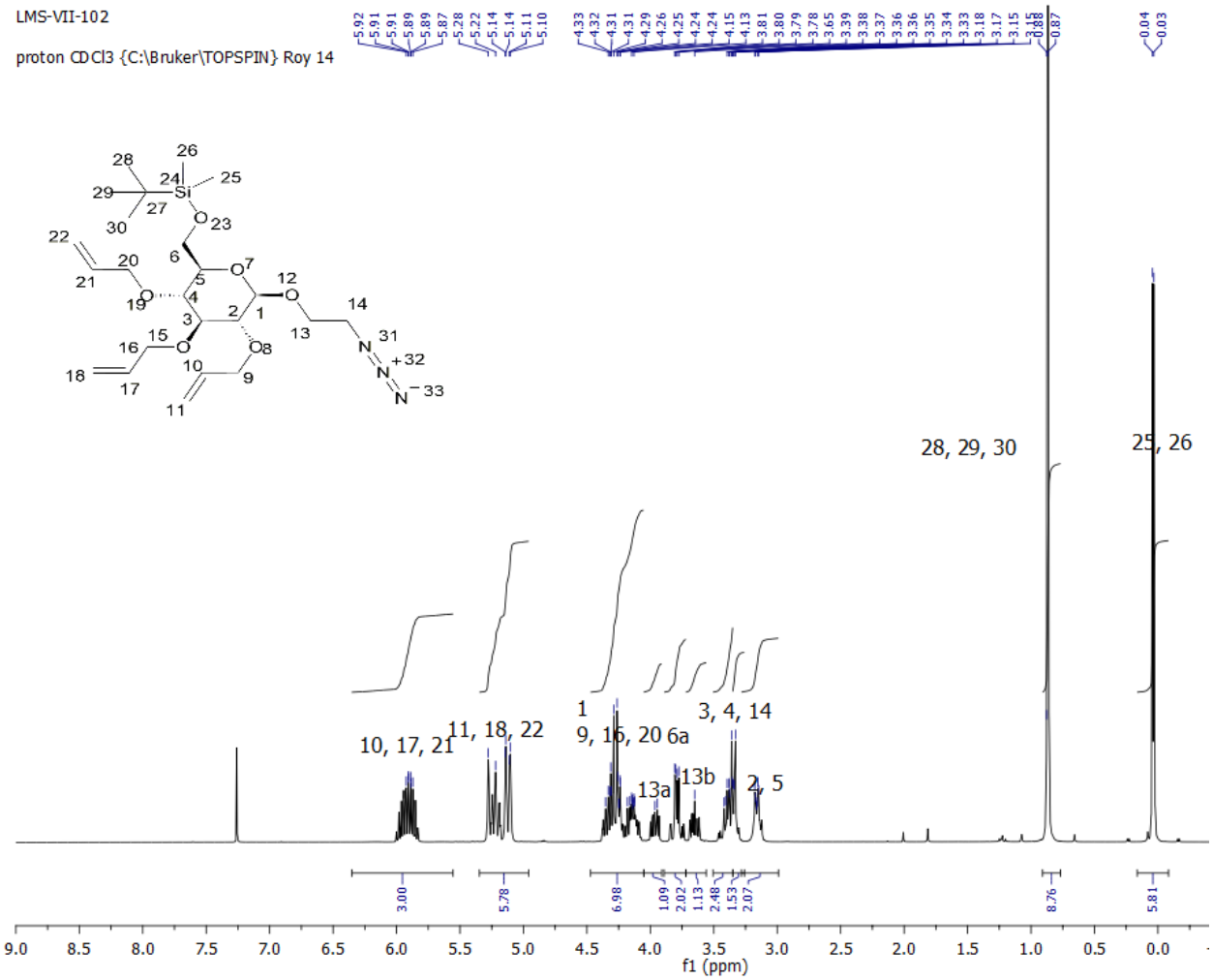

Figure A6. ^{13}C NMR analysis of **36** (300 MHz, $CDCl_3$)

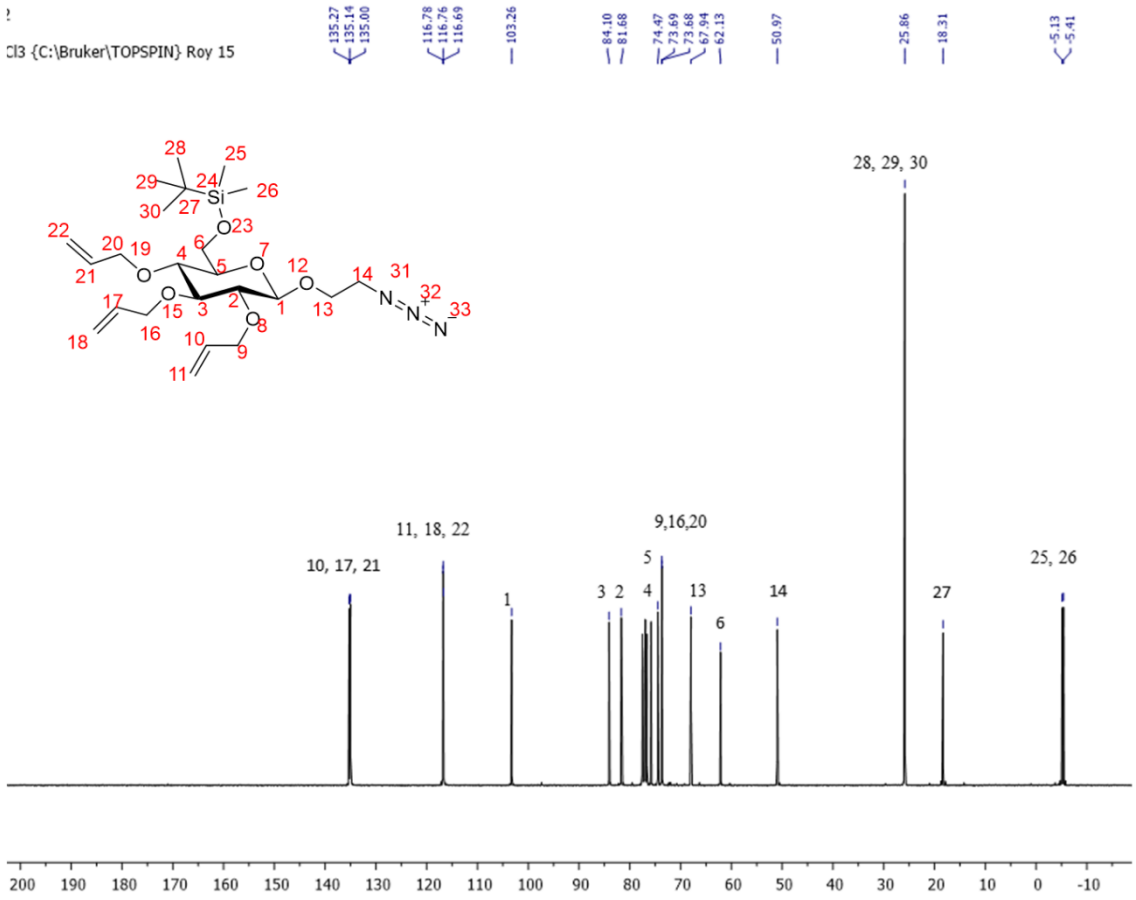

Figure A7. COSY analysis of **36** (300 MHz, $CDCl_3$)

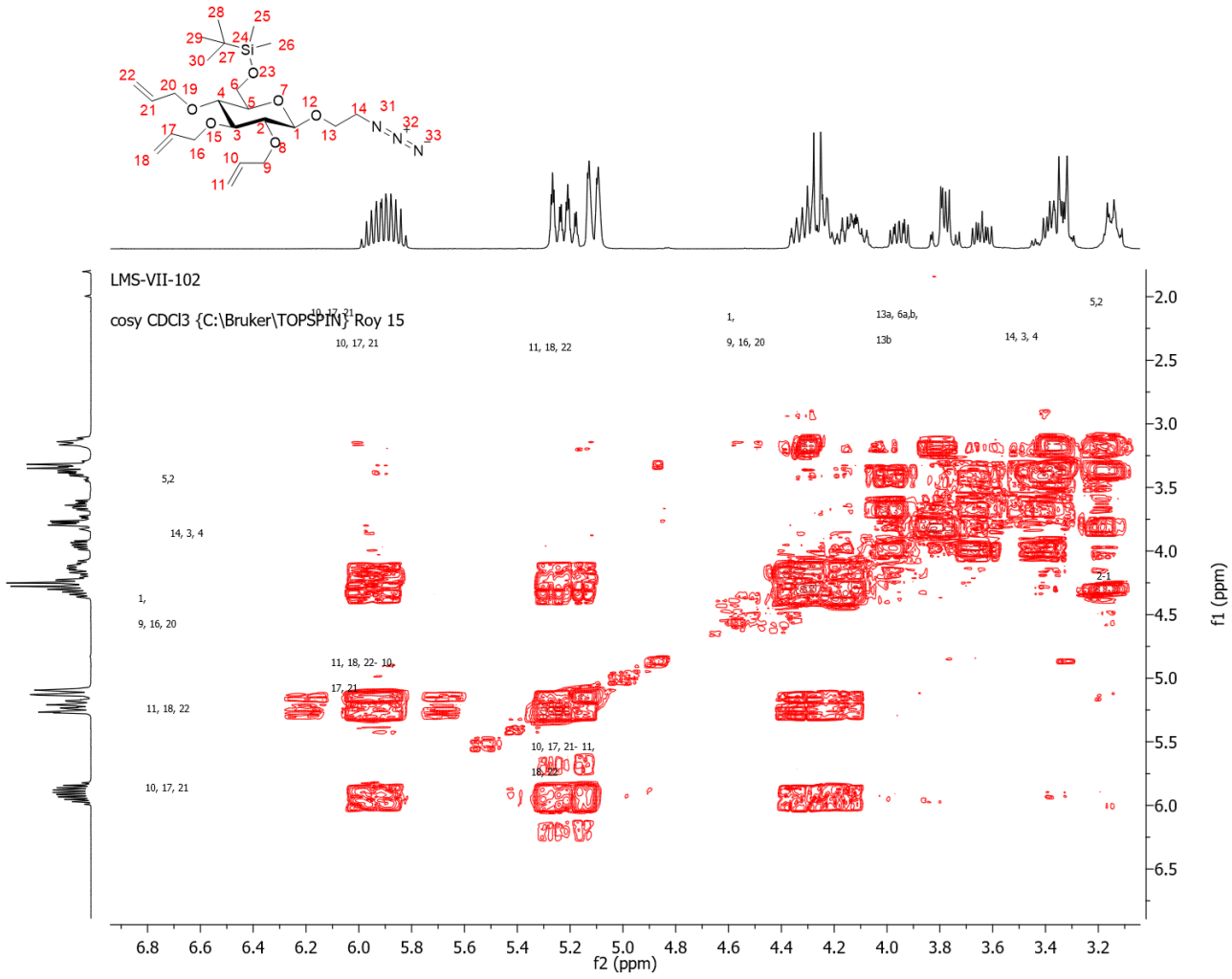

Figure A8. HSQC analysis of **36** (300 MHz, $CDCl_3$)

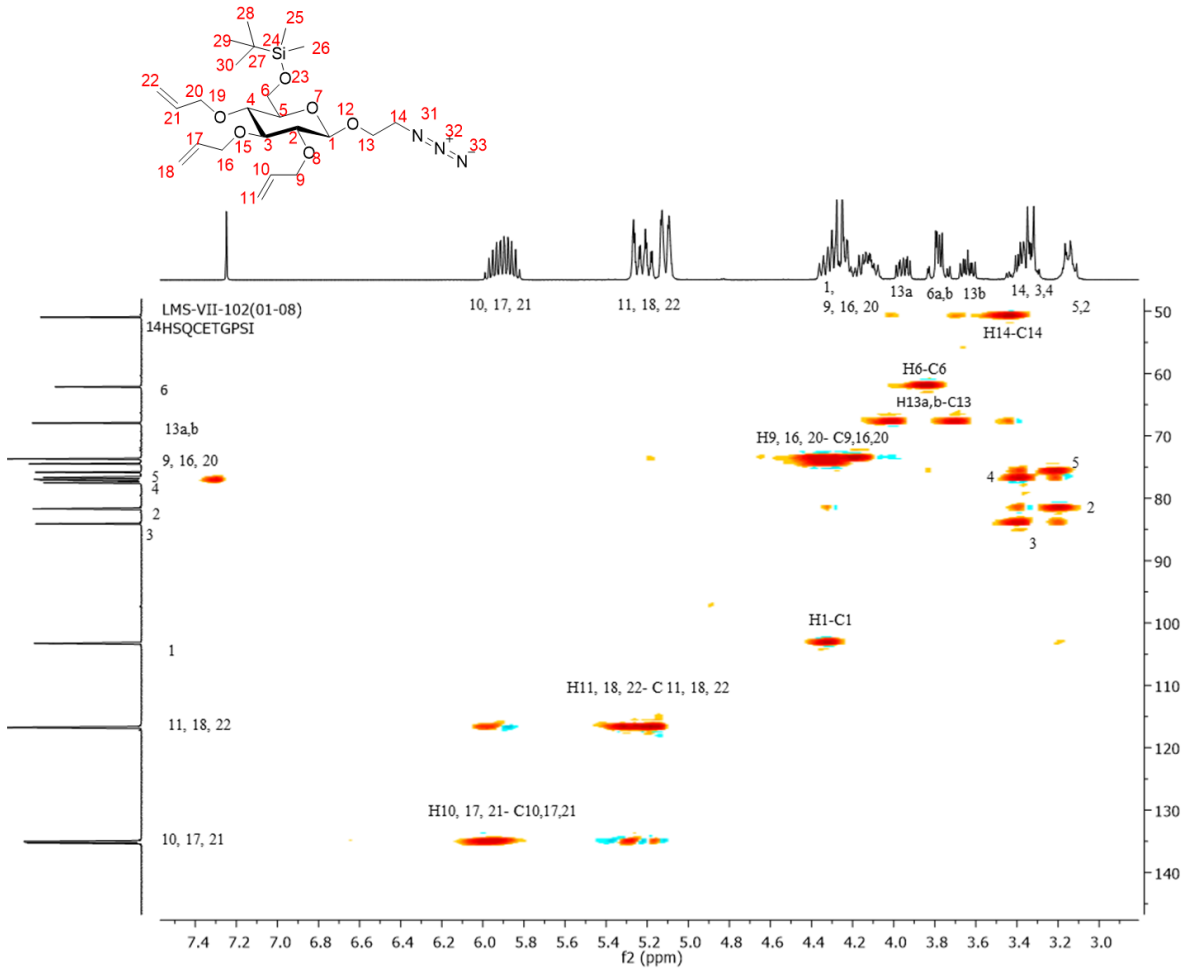

Figure A9. DEPT analysis of **36** (300 MHz, $CDCl_3$)

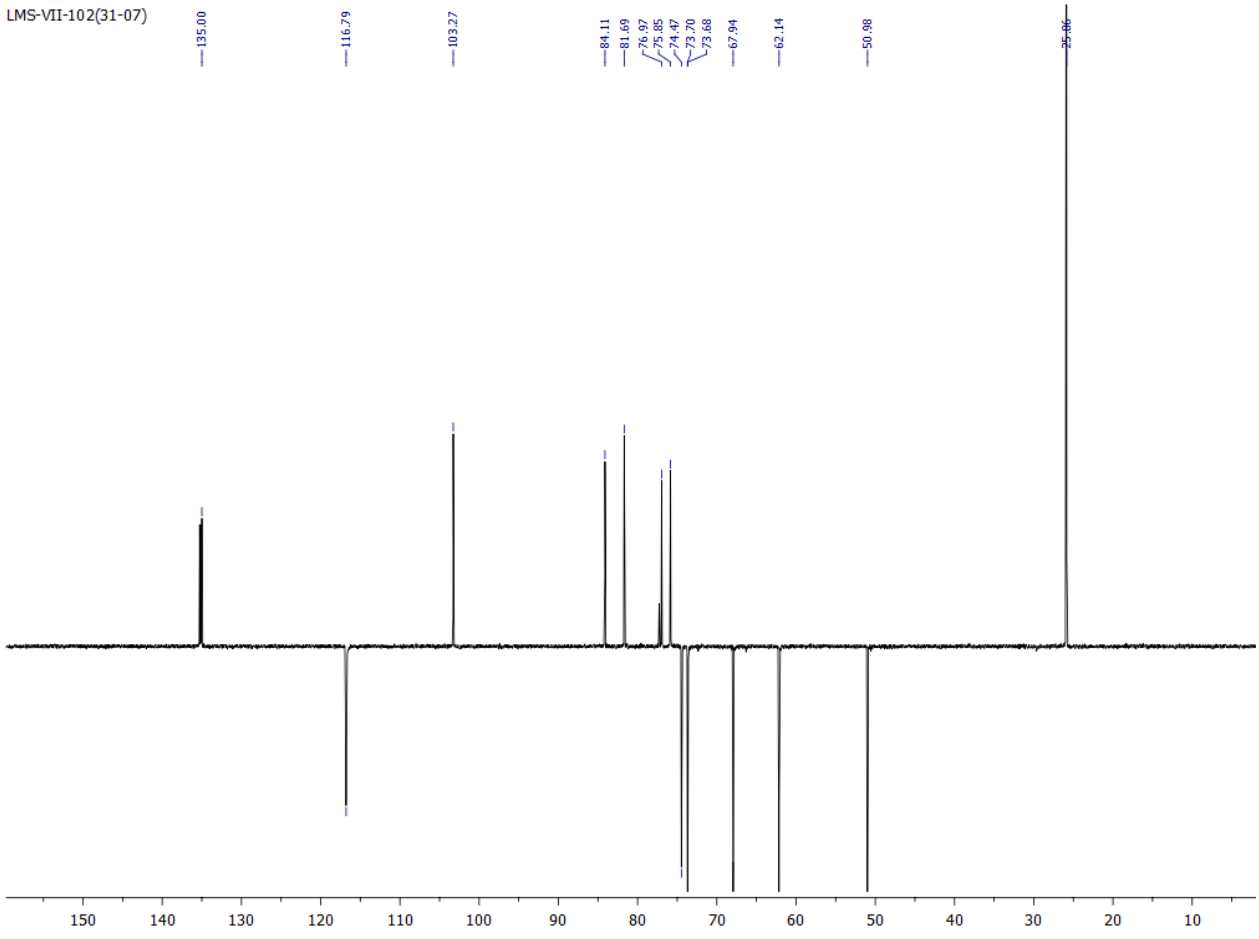

Compound (37)

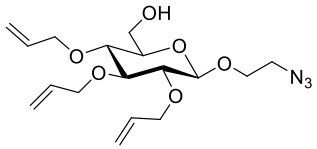

Experimental: TBAF (1M buffered with 20 mol % in THF, 13 mL, 3.266 mmol) was added at 0 ºC to a stirring solution of **36** (2g, 1.306 mmol) in dry THF (15 mL) under a nitrogen atmosphere. The resulting solution was stirred at rt for 10 h. When all the starting material was consumed as evident by TLC, the mixture was concentrated under reduced pressure. The crude residue was purified *via* flash column chromatography (EtOAc /Hexane, 40:60 %) to provide the desired product **37** as colorless oily residue (1.3 g, 87% yield). R_f= 0.304. ^{1}H NMR (300 MHz, $CDCl_3$) δ 6.11 – 5.69 (m, 3H), 5.40 – 5.00 (m, 6H, H_1), 4.05 – 3.92 (m, 1H, H_{13a}), 3.82 (ddd, 1H, *J* = 8.3, 6.9, 2.6 Hz, H_{6a}), 3.73 (dd, 1H, *J* = 4.5, 1.5 Hz, H_{6b}), 3.69 (dd,1H, *J* = 5.8, 4.8 Hz, H_{13b}), 3.46 – 3.39 (m, 2H, H_3,H_4), 3.35 (dd, 2H, *J* = 12.6, 4.8 Hz,H_{14}), 3.30 – 3.22 (m, 1H, H_2), 3.18 (dd, 1H, *J* = 16.8, 7.9 Hz, H_5), 2.09 (brs, 1H, OH).^{13}C NMR (300 MHz, $CDCl_3$) δ 117.3, 117.04, 116.7, 103.5, 81.5, 75.0, 74.4, 73.8, 73.7, 68.4, 61.9, 50.9.

Figure A10. ^{1}H NMR analysis of **37** (300 MHz, $CDCl_3$)

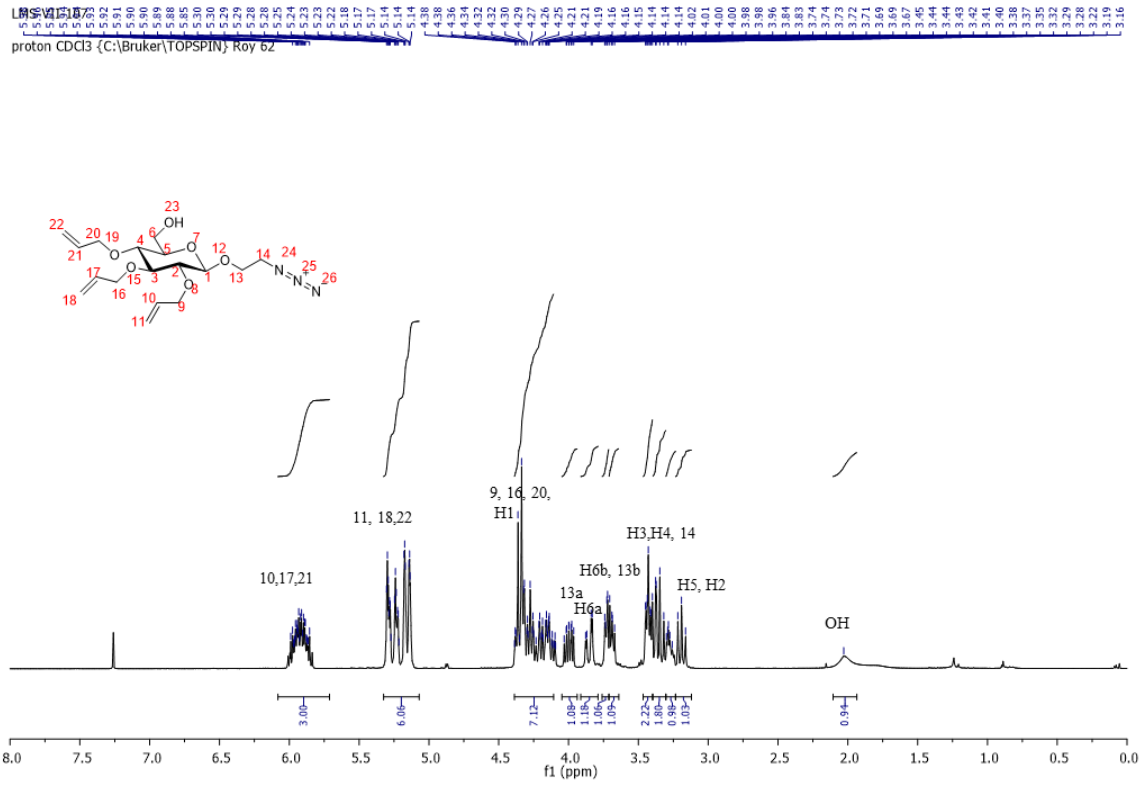

Figure A11. ^{13}C NMR analysis of **37** (300 MHz, $CDCl_3$)

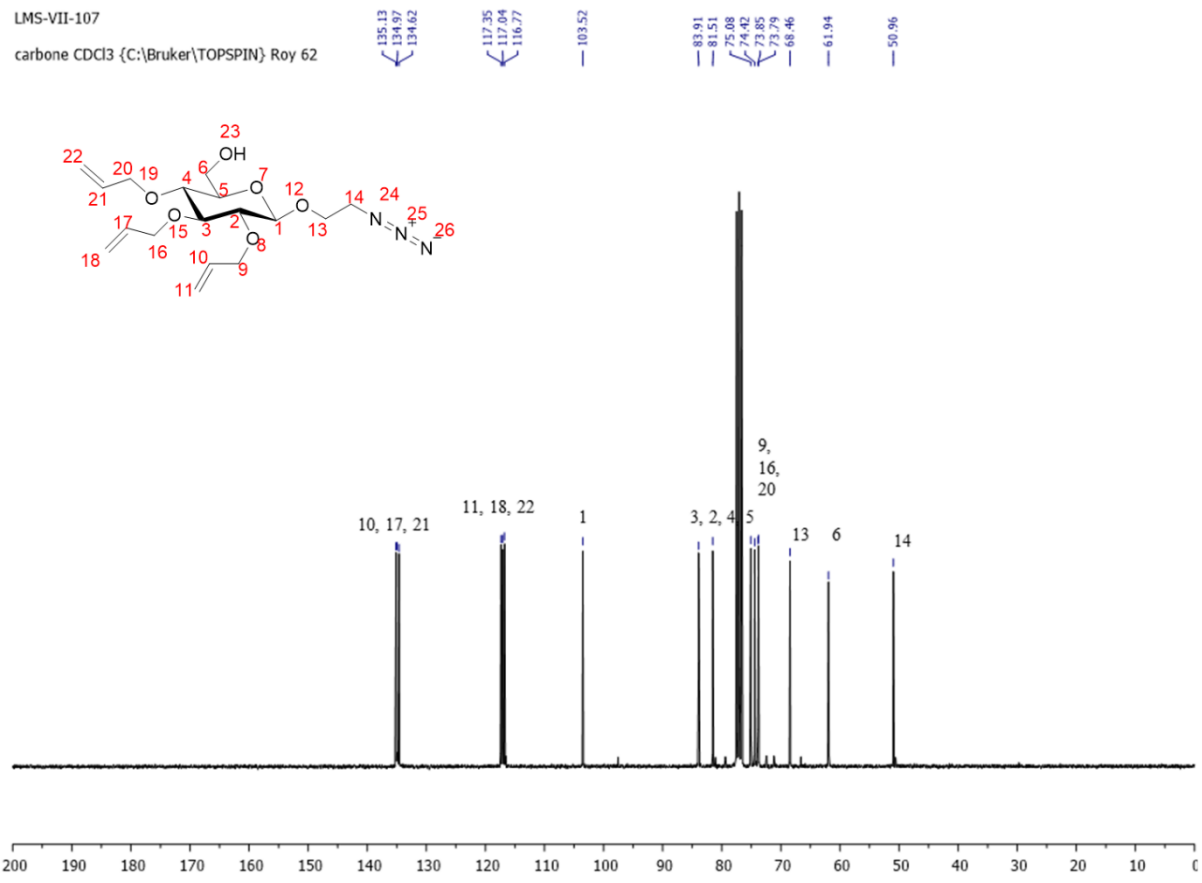

Figure A12. COSY analysis of **37** (300 MHz, $CDCl_3$)

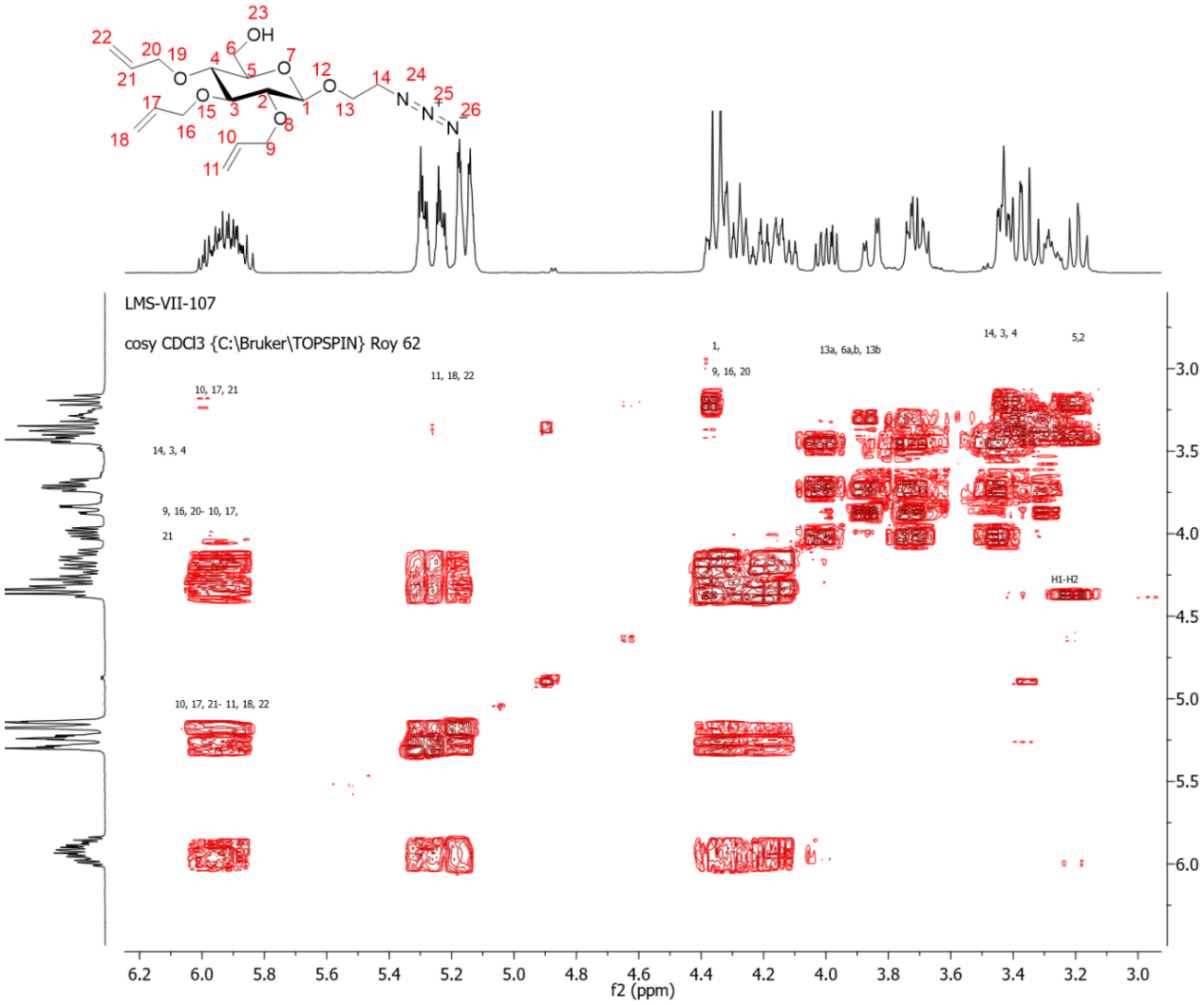

Figure A13. HSQC analysis of **37** (300 MHz, $CDCl_3$)

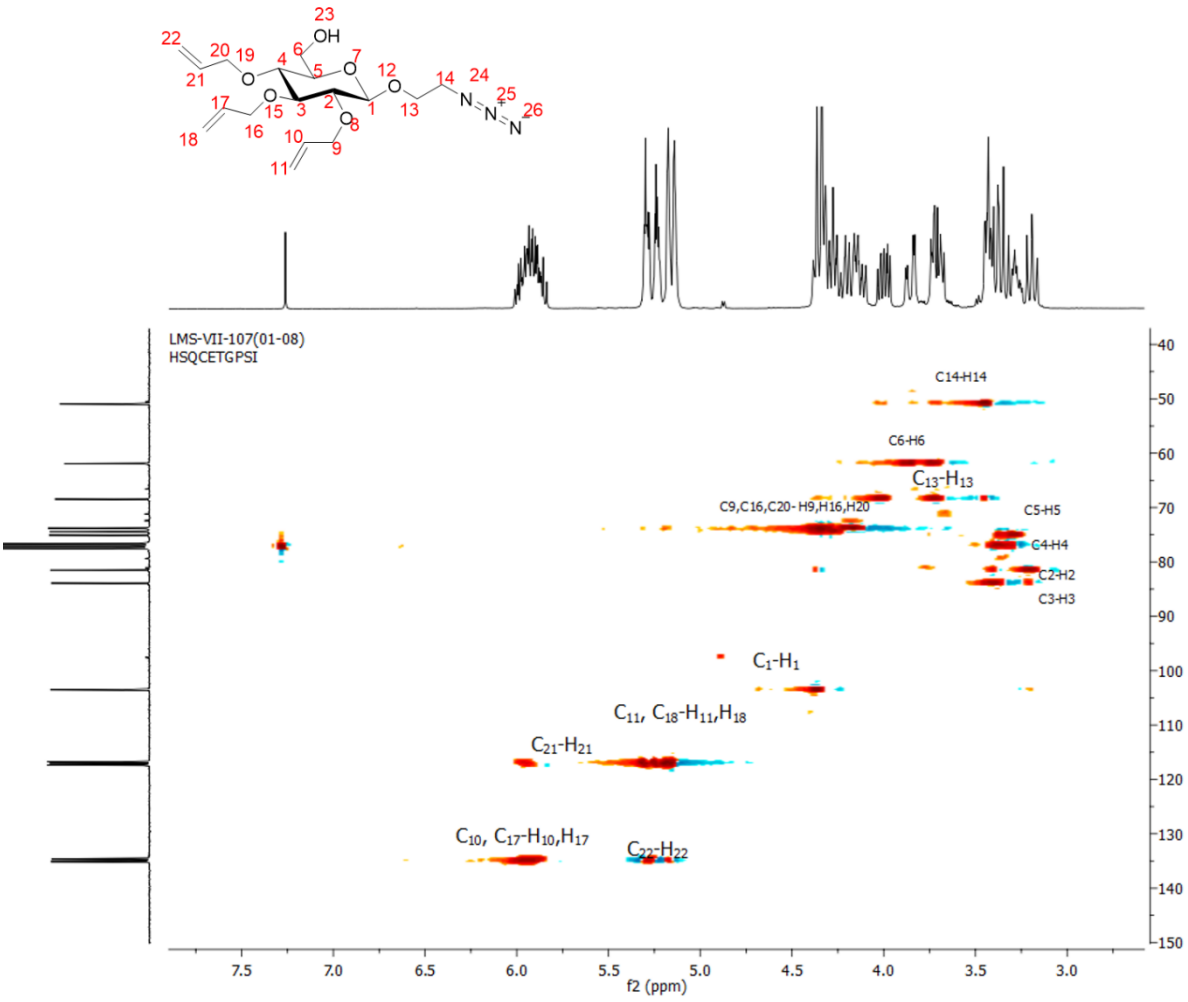

Figure A14. HMBC analysis of **37** (300 MHz, $CDCl_3$)

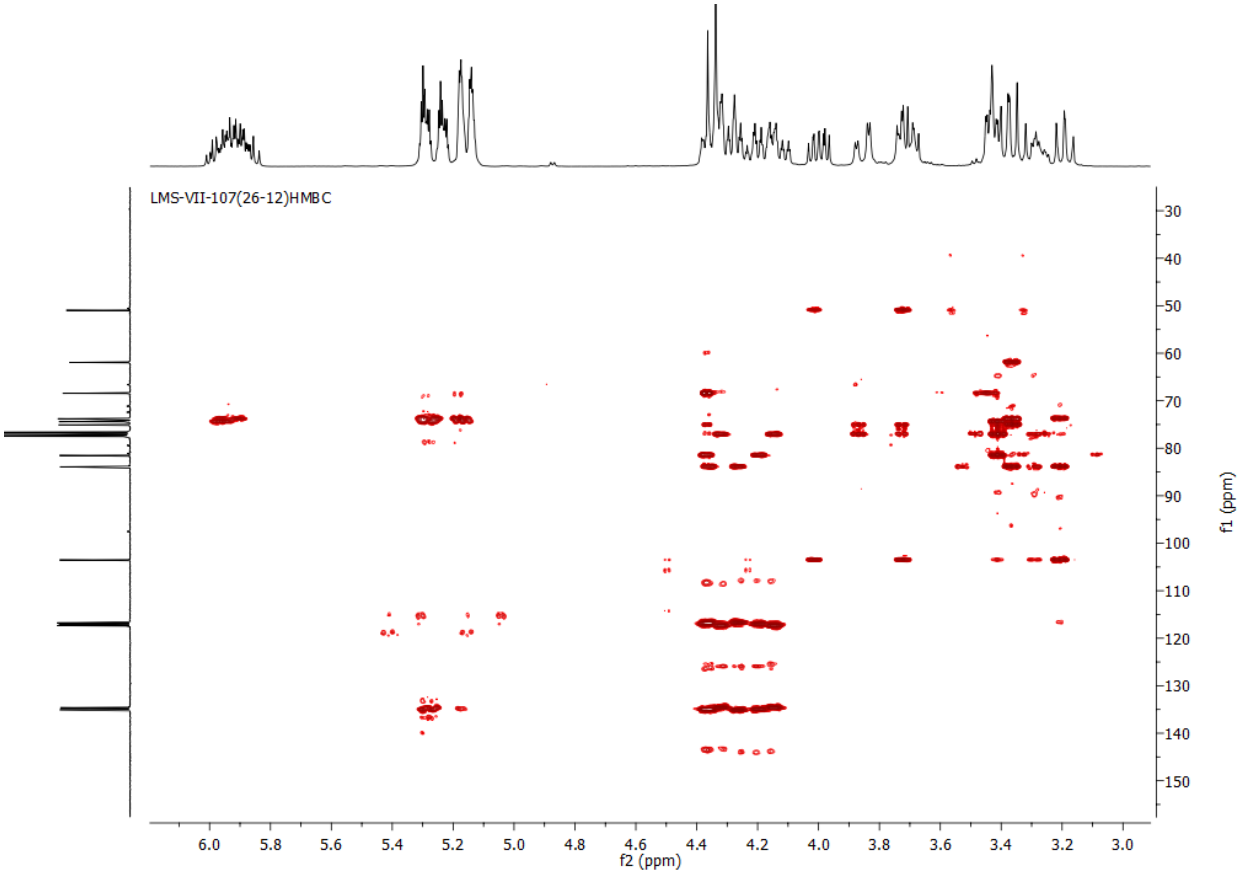

Figure A15. DEPT analysis of **37** (300 MHz, $CDCl_3$)

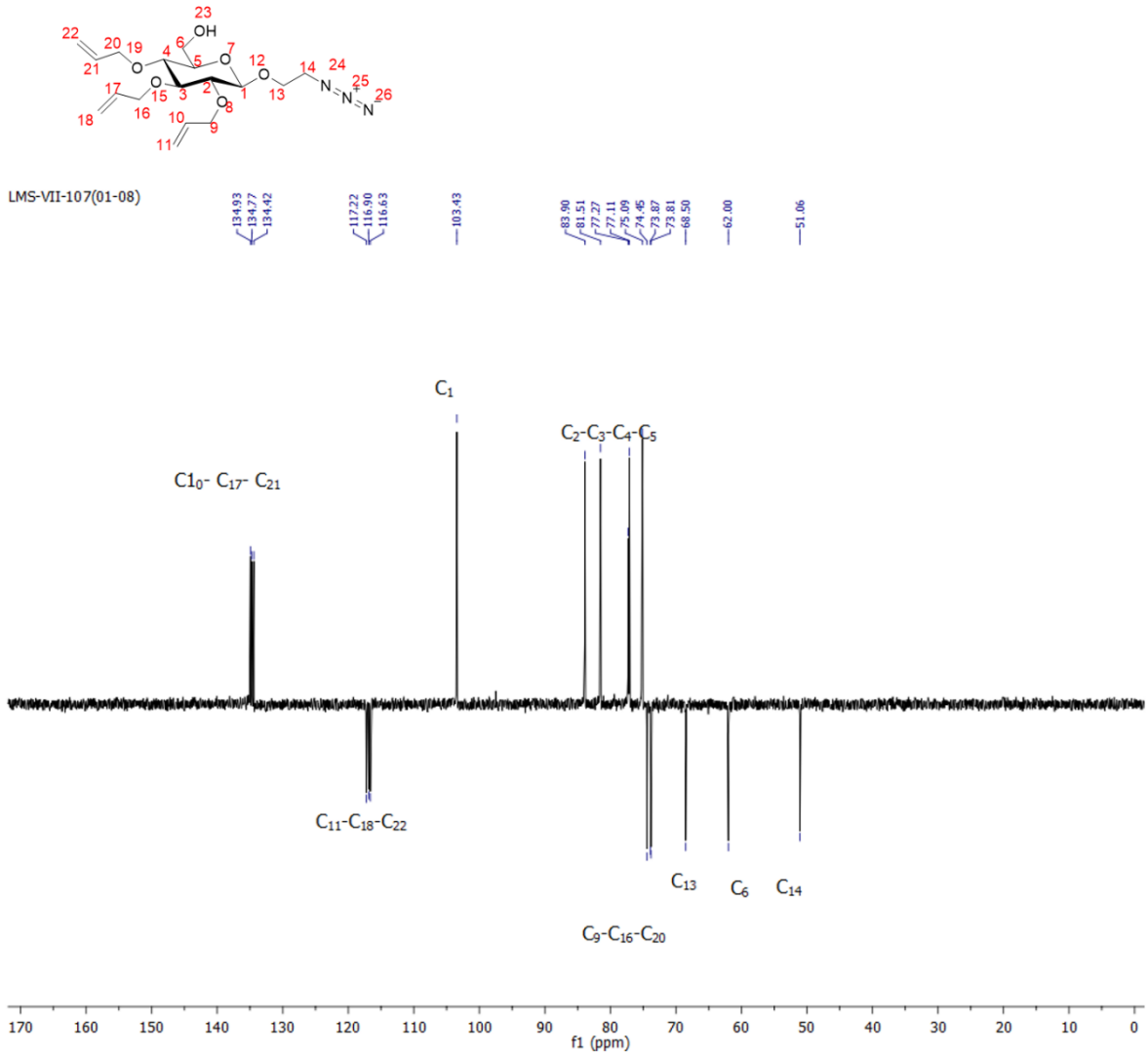

Compound 38

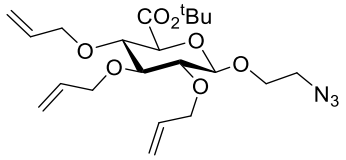

Experimental: To a solution of compound **37** (339 mg, 0.920 mmol) in dichloromethane (5.5 mL) were added acetic anhydride (0.9 mL, 9.2 mmol), *tert*-butyl alcohol (1.8 mL, 18.4 mmol) and pyridinium dichromate (0.69 g, 1.84 mmol), and the mixture was stirred for 6 h at ambient temperature. The mixture was then passed through a layer of silica gel (3x 5 cm) using ethyl acetate as eluent to remove the main part of chromium salts. The collected organic filtrate was washed with H_2O, brine, dried over anyd. Na_2SO_4. The collected organic phase was concentrated under reduced pressure, and the residue was purified by column chromatography (Hexane/ Ethyl acetate 9:1) to give the product **38** as white crystals (300 mg, 74 %), R_f = 0.230.^{1}H NMR (300 MHz, $CDCl_3$) δ 6.03 – 5.78 (m, 3H, 3xCH_2=<u>CH</u>-), 5.33 – 5.11 (m, 6H, 3x<u>CH_2</u>=CH-), 4.44 – 4.25 (m, 5H, H1, 2xCH_2=CH-<u>CH_2</u>-), 4.23 – 4.15 (m, 1H, H_5), 4.10 – 3.98 (m, 1H, (O-CH_2)$H_{13''}$), 3.78 – 3.62 (m, 3H, (O-CH_2)$H_{13'}$, CH_2=CH-<u>CH_2</u>-), 3.55 (dd, *J* = 9.7, 8.7 Hz, 1H, H_4), 3.54 – 3.33 (m, 3H, H_3, N-<u>CH_2</u>), 3.25 (dd, *J* = 9.1, 7.6 Hz, 1H, H_2), 1.50 (s, 9H).^{13}C-NMR ($CDCl_3$, 300 MHz), δ 167.6, 135.0, 134.8, 134.5, 117.1, 116.9, 116.8, 103.6, 83.3, 82.2, 81.1, 78.9, 75.3, 74.4, 73.8, 73.7, 68.3, 50.9, 27.9. ESI-HRMS: *m/z* calcd for $C_{21}H_{33}N_3O_7$ $[M+NH_4]^+$ 457.2687, found 457.2670.

Figure A16. ^{1}HNMR analysis of **38** (600 MHz, $CDCl_3$)

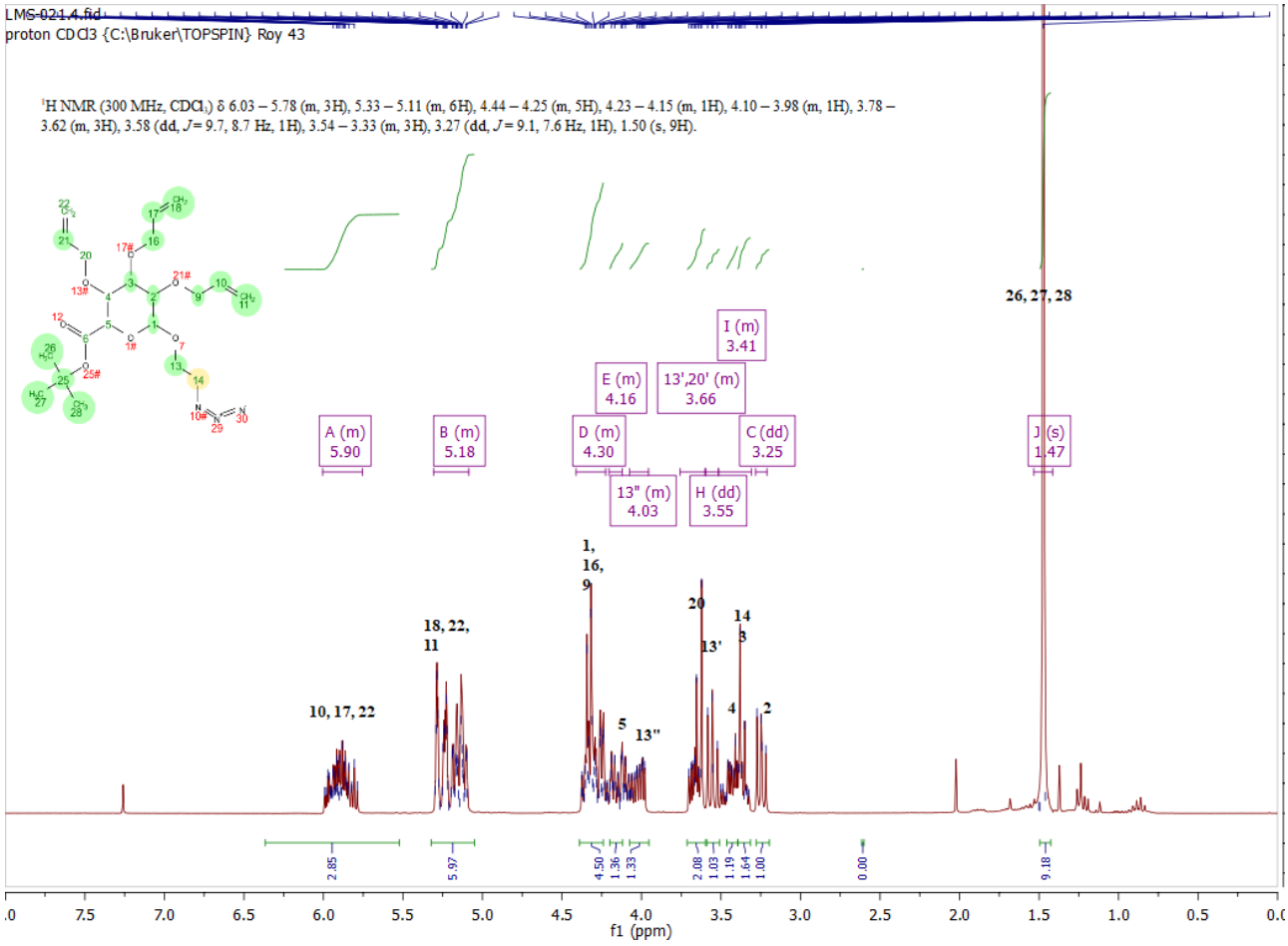

Figure A17. ^{13}C NMR analysis of **38** (600 MHz, $CDCl_3$)

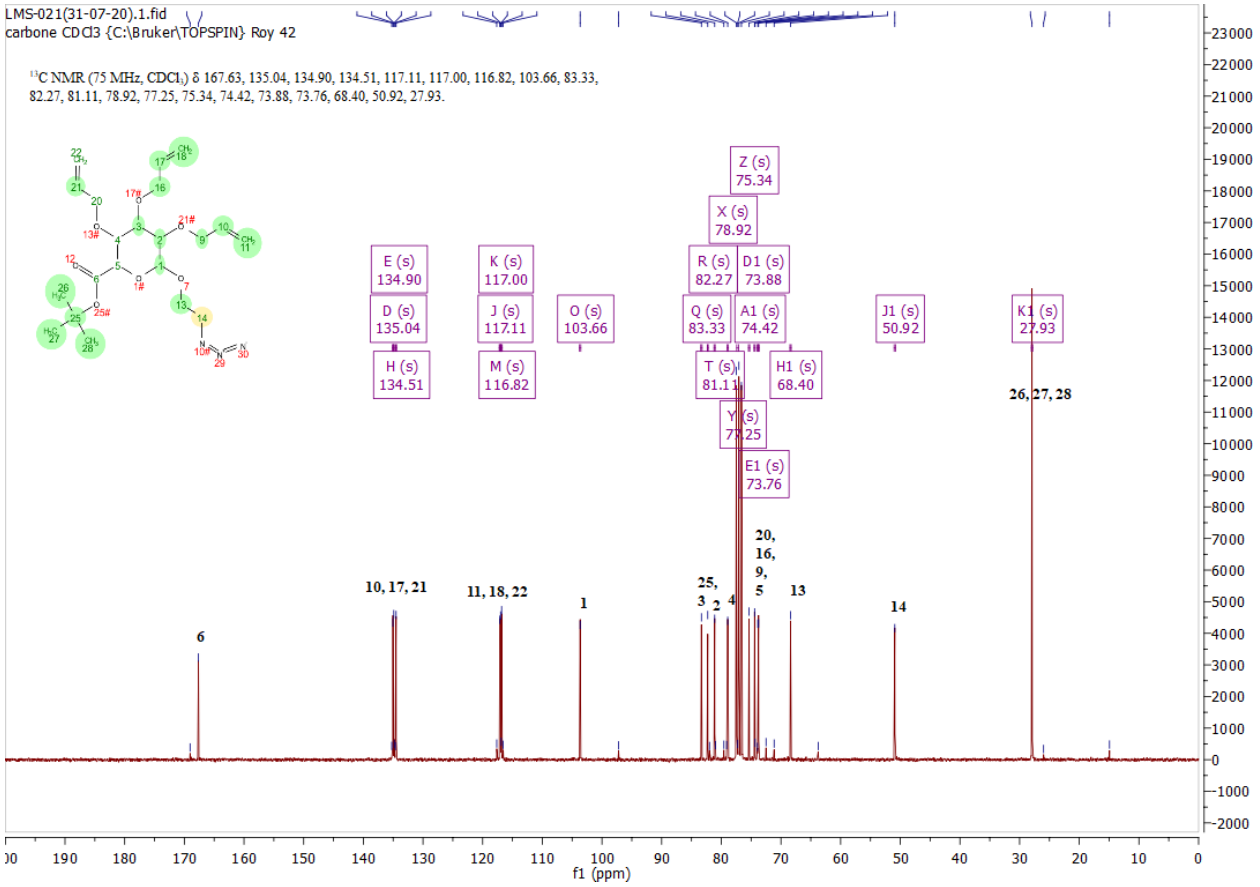

Figure A18. HMBC analysis of **38** (600 MHz, $CDCl_3$)

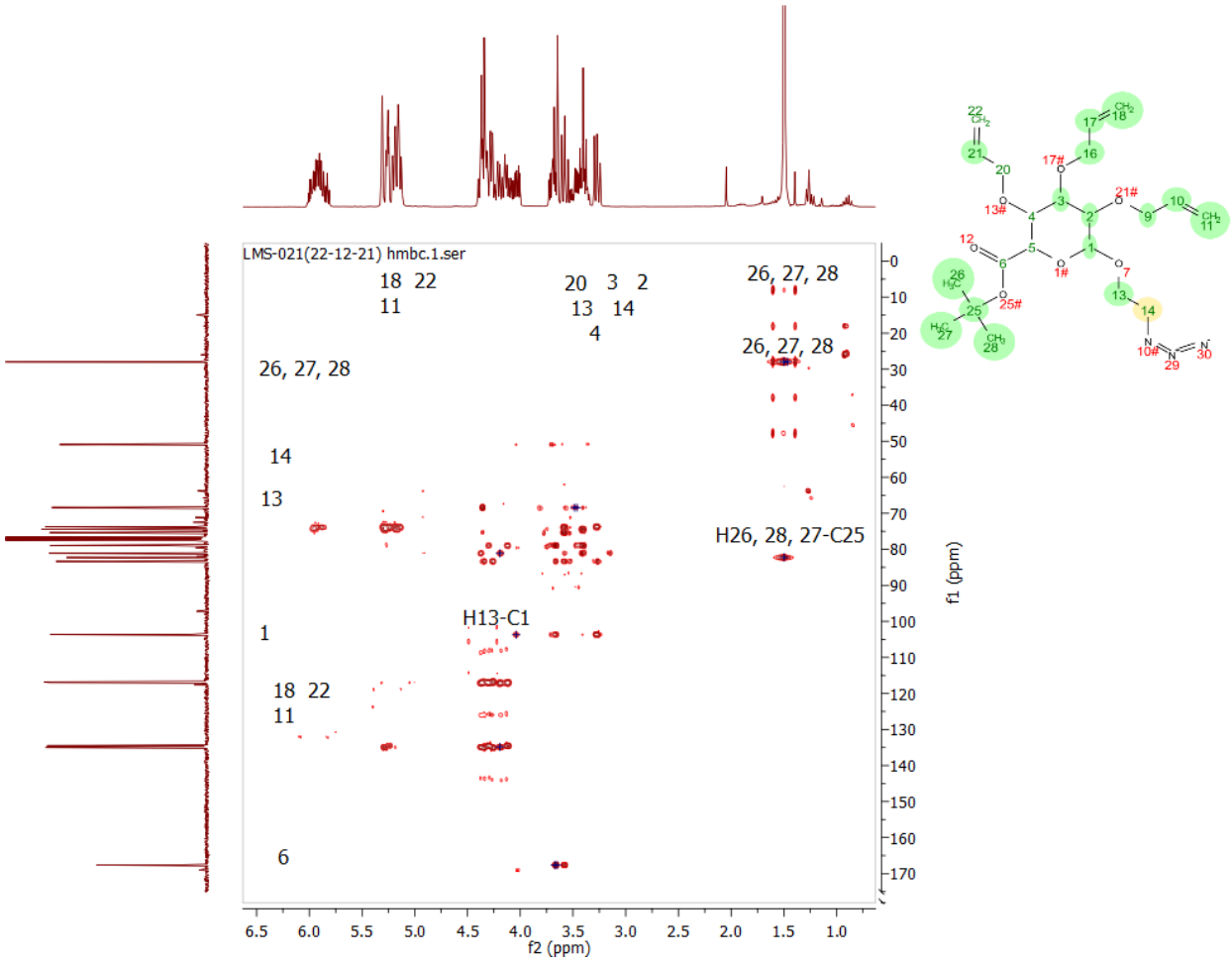

Figure A19. COSY analysis of **38** (600 MHz, $CDCl_3$)

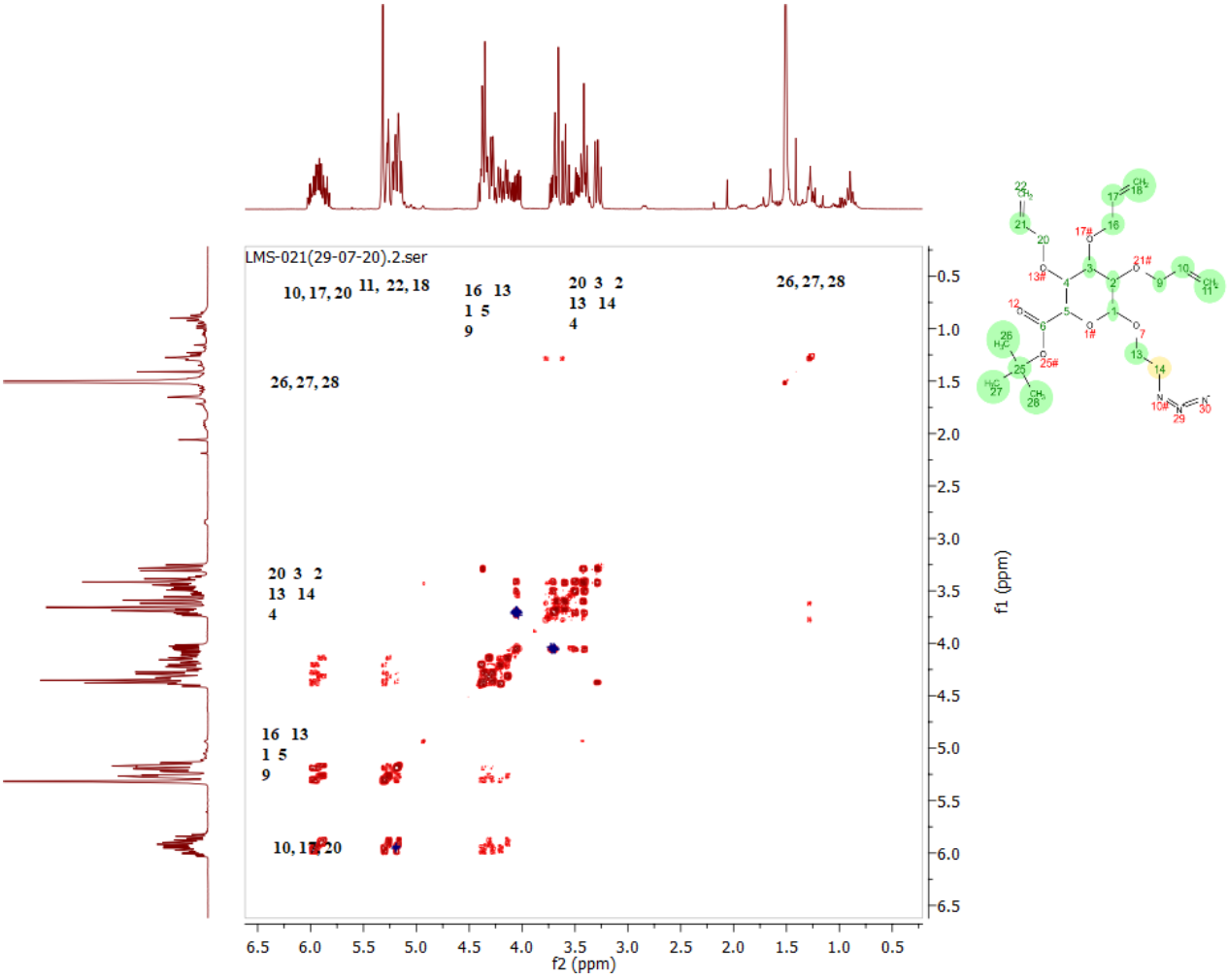

Figure A20. HSQC analysis of **38** (300 MHz, $CDCl_3$)

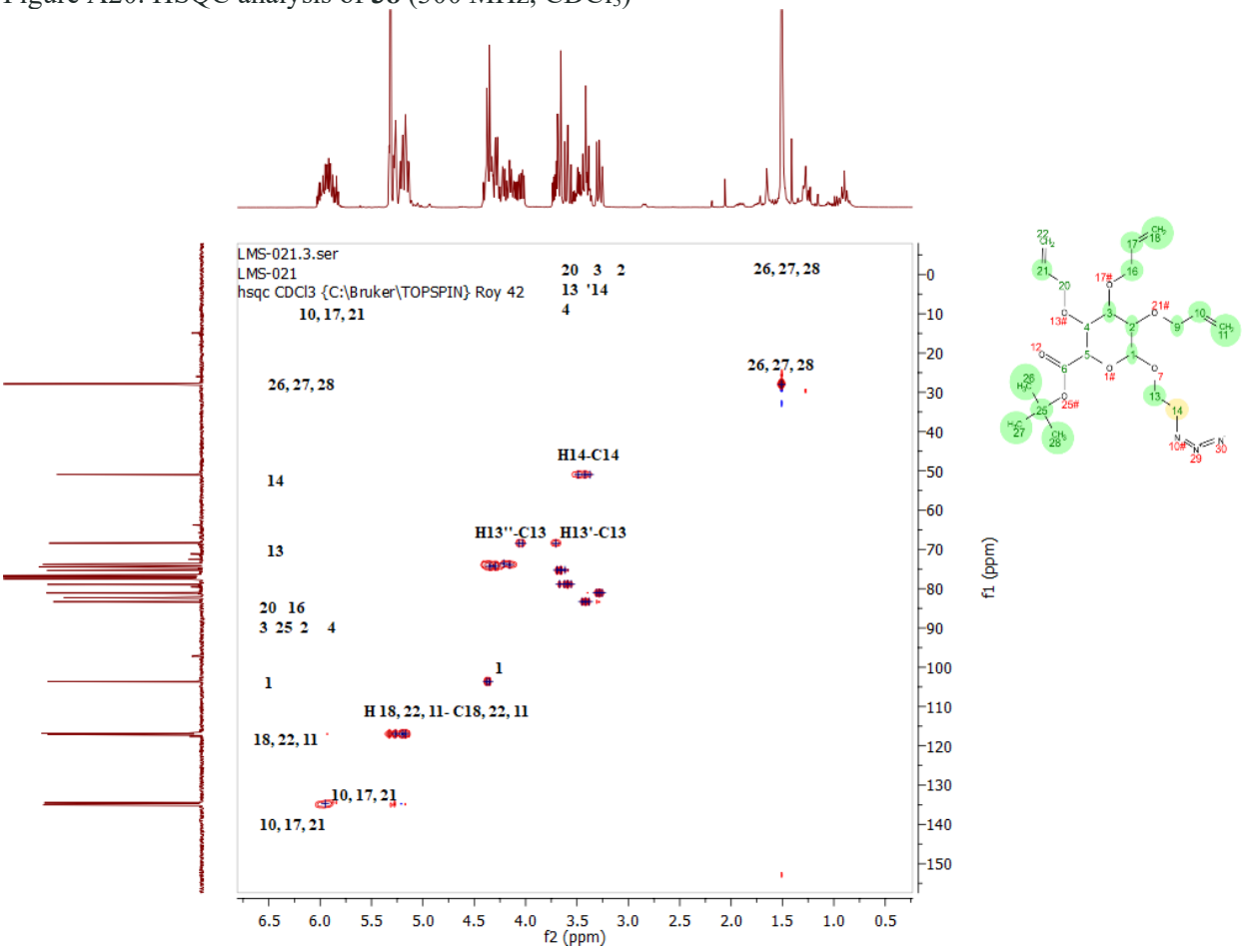

Figure A21. DEPT analysis of **38** (600 MHz, $CDCl_3$)

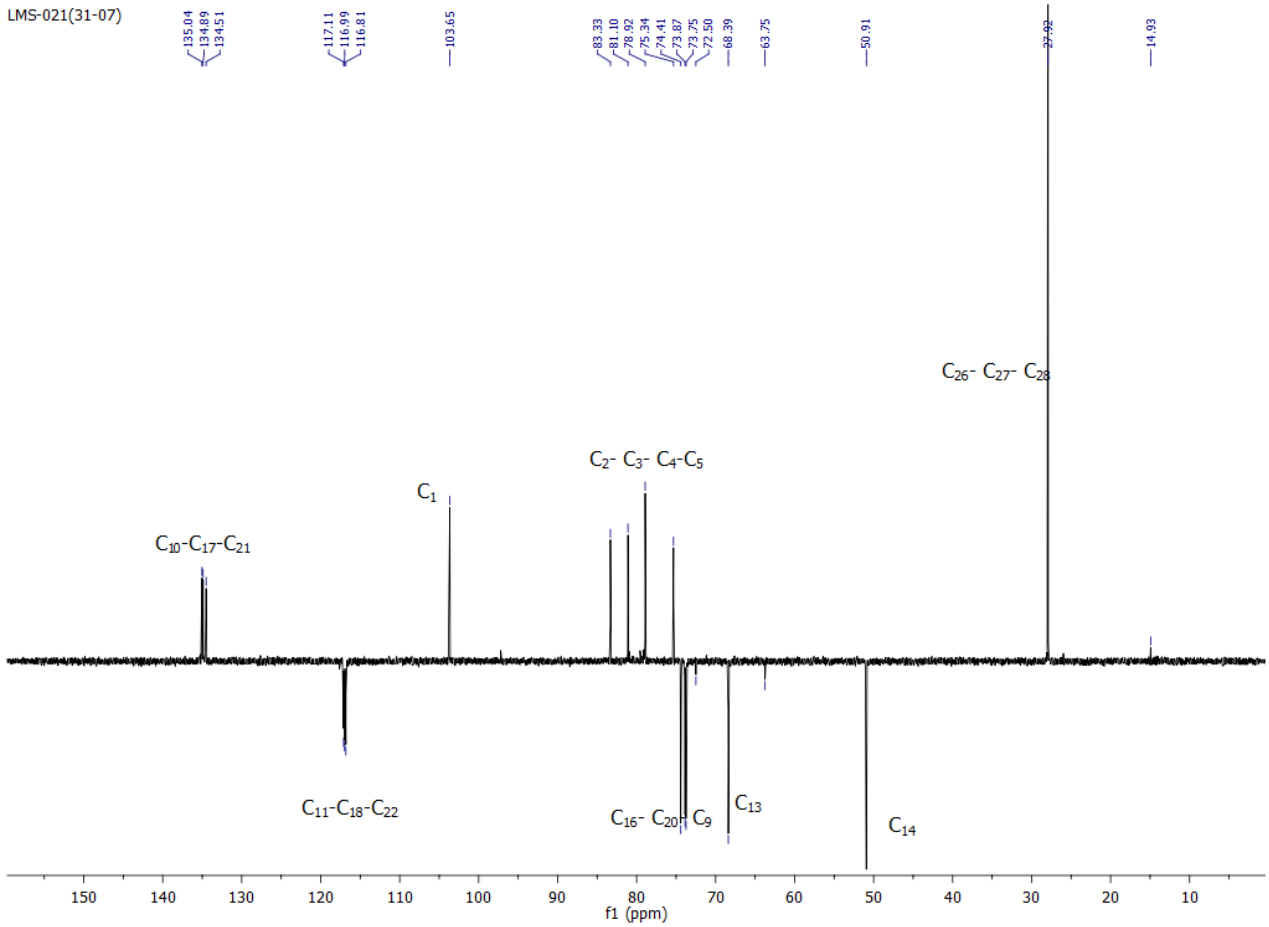

Experimental part chapter 3

1,2,3,4-Tetra-*O*-acetyl- α/β - L-fucopyranose 57

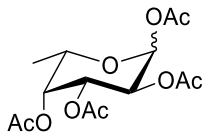

Experimental: L-fucose **56** (5.00 g, 15.06 mmol) was dissolved in pyridine (200 mL), the mixture was cooled at 0 ºC, in which acetic anhydride (40 mL) was added in a small portion, and the reaction mixture was stirred and gradually warmed to room temperature. The reaction remained stirring at room temp. overnight. After completion of the reaction, the solvent was evaporated under reduced pressure, then diluted with dichloromethane and washed with sat. $NaHCO_3$, brine and dried over anhydrous sodium sulfate, the filtrate concentrated under reduced pressure, the crude product was obtained as α/β mixture in 75% yield. All data of this compound is in accordance with literature data. [338]

2-propargy 2,3,4-tri-O-acetyl-α-L-fucopyranoside 58

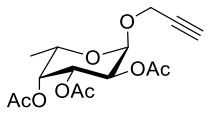

Experimental: L-fucosetetracetate **57** (200 mg, 0.602 mmol) dissolved in DCM (2 mL), after which propargyl alcohol (70 µL, 1.204 mmol) was added. The mixture was then stirred at 0 ºC and $BF_3.OEt_2$ (0.9 mL, 3.00 mmol) was added slowly over 15 min. the reaction mixture was stirred for 12 h, and then diluted with DCM and washed with aq. saturated $NaHCO_3$ and brine. The organic phase was dried over anhydrous Na_2SO_4, and the solvent was removed under reduced pressure. The crude product was separated by flash column chromatography (Hexane/EtOAc 8:2) to afford pure product **58** (140 mg, 73%). ^{1}H NMR (300 MHz, $CDCl_3$): δ (ppm) 5.31 (dd, 1H, J = 10.8, 3.3 Hz, H_3), 5.26 (dd, 1H, J = 3.4, 1.1 Hz, H_4), 5.21 (d, 1H, J = 3.7 Hz, H_1), 5.11 (dd, 1H, J = 10.8, 3.8 Hz, H_2), 4.21 (d,2H, J = 4.0 Hz, $H_{9,9'}$), 2.49 (t,1H, J= 2.5 H, H_7), 2.12 (s, 3H, $COCH_3$), 2.04 (s, 3H, $COCH_3$), 1.94 (s, 3H, $COCH_3$), 1.10 (d, 3H, J = 6.6 Hz, CH_3).^{13}C NMR (300 MHz, $CDCl_3$) δ (ppm) 170.5, 170.3, 169.9, 95.0, 78.5, 74.8, 71.0, 67.8, 67.8, 65.0, 55.2, 20.7, 20.6, 20.6, 15.7. ESI-MS (m/z) calcd for $C_{15}H_{20}O_8$ $[M+Na]^+$ 351.6, found 351.5.

Figure A22. ^{1}H NMR analysis of compound **58** (300 MHz, $CDCl_3$)

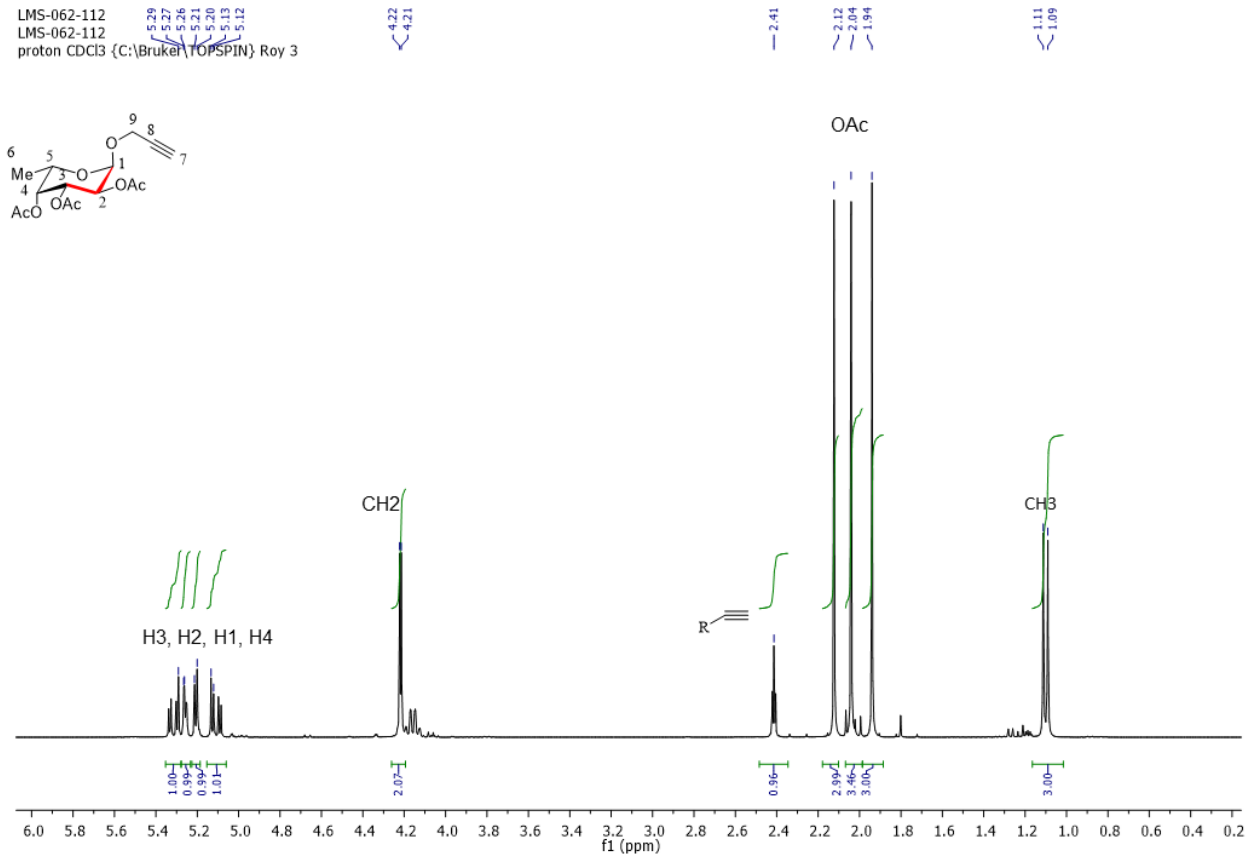

Figure A23. ^{13}C NMR analysis of compound **58** (300MHz, $CDCl_3$)

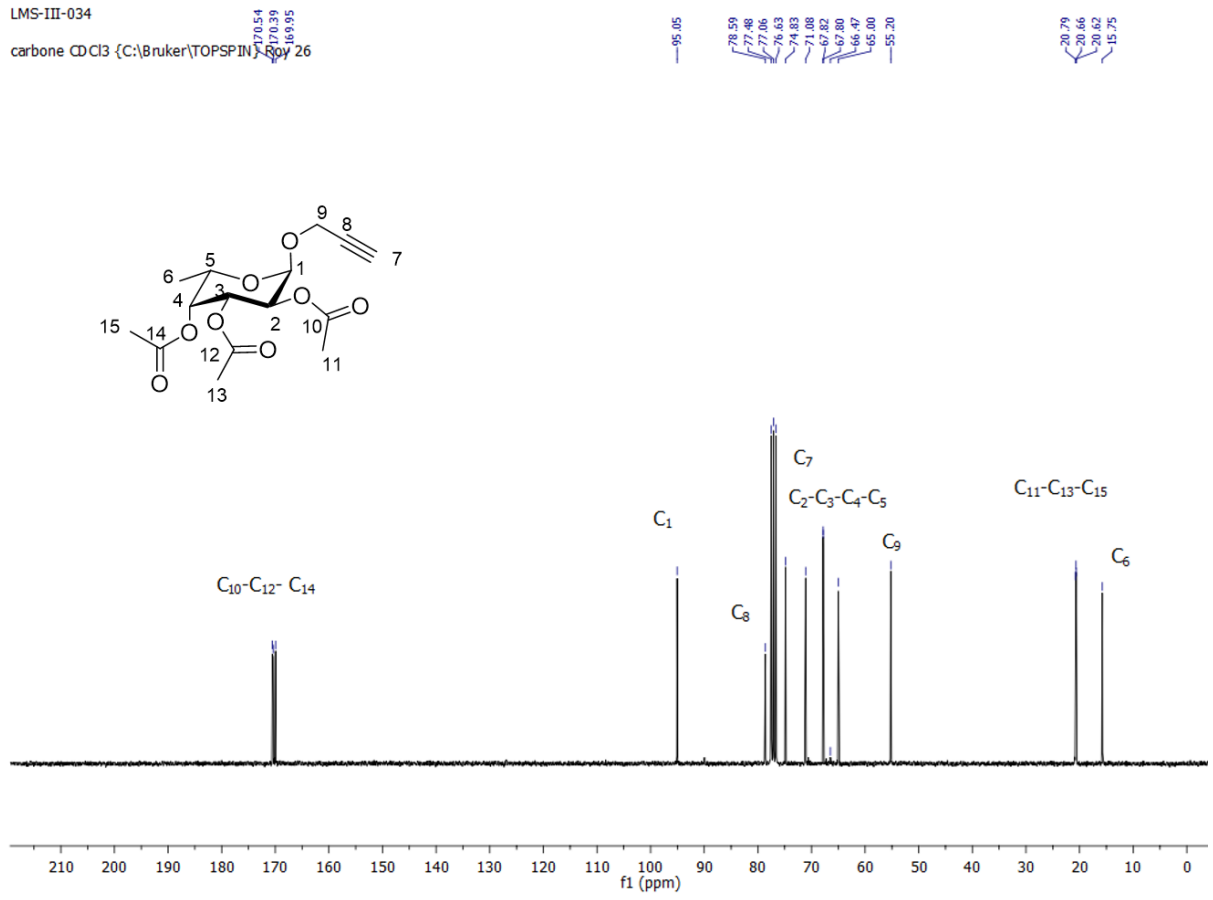

2-Azido ethanol, was synthesized following ref. [500]

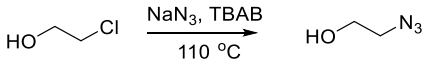

Compound 60

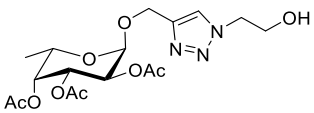

Experimental: α-L-fucopyranoside **58** (260 mg, 0.794 mmol) and 2-azidoethanol (120 µL, 0.589 mmol) were combined in a vial equipped with a magnetic stir bar and dissolved in THF/ H_2O (4:1), To this solution was added while stirring at rt, a freshly prepared aqueous solution of sodium ascorbate (52 mg, 0.262 mmol), and copper (II) sulfate pentahydrate (20 mg, 0.131 mmol). The reaction mixture was allowed to stir at room temperature for 12 h. After completion of the reaction, ethyl acetate was added and quenched with EDTA

to remove excess of copper, then the organic phase was washed with water, brine, dried over anhyd. Na_2SO_4, and concentrated. The crude product was separated by flash chromatography (DCM/MeOH 98:2%) giving pure product **60** (280 mg, 85%).^{1}H NMR (300 MHz, $CDCl_3$) δ (ppm) 7.65 (s, 1H, Triazole), 5.32 (dd,1H, *J*= 3.3, 10.8 Hz, H_3), 5.27 (dd,1H, *J*= 1.7, H4) , 5.16 (d, 1H, *J* = 3.7 Hz, H_1), 4.92 (dd,1H, *J* = 10.8, 3.8 Hz, H_2), 4.80(d, 1H, *J*= 12.6 Hz, O$\underline{CH_2}$), 4.68 (d,1H, *J* = 12.5 Hz, O$\underline{CH_2}$), 4.52 (d,2H, *J* = 12.6 Hz, N$\underline{CH_2}$), 4.20(q, 1H, *J*= 6.4 Hz, H_5), 4.01 (dd, 1H, *J*= 5.2, 10.4 Hz, $\underline{CH_2}$OH), 2.04 (s, 3H, CH_3-Acetyl), 1.89 (s, 3H, CH_3-Acetyl), 1.85 (s, 3H, CH_3-Acetyl), 1.02 (dd, 3H, *J* = 6.4, 3.8 Hz, CH_3). ^{13}C NMR (300 MHz, $CDCl_3$) δ 170.7, 170.6, 170.1, 143.3, 124.3, 95.0, 71.0, 68.2, 67.8, 64.6, 61.1, 60.8, 60.7, 53.3, 52.7, 20.6, 20.5, 20.5, 15.7. ESI-HRMS: *m/z* calcd for $C_{17}H_{25}N_3O_9$ $[M+H]^+$ 416.1664, found 416.1651.

Figure A24. ^{1}H NMR analysis of compound **60** (300MHz, $CDCl_3$)

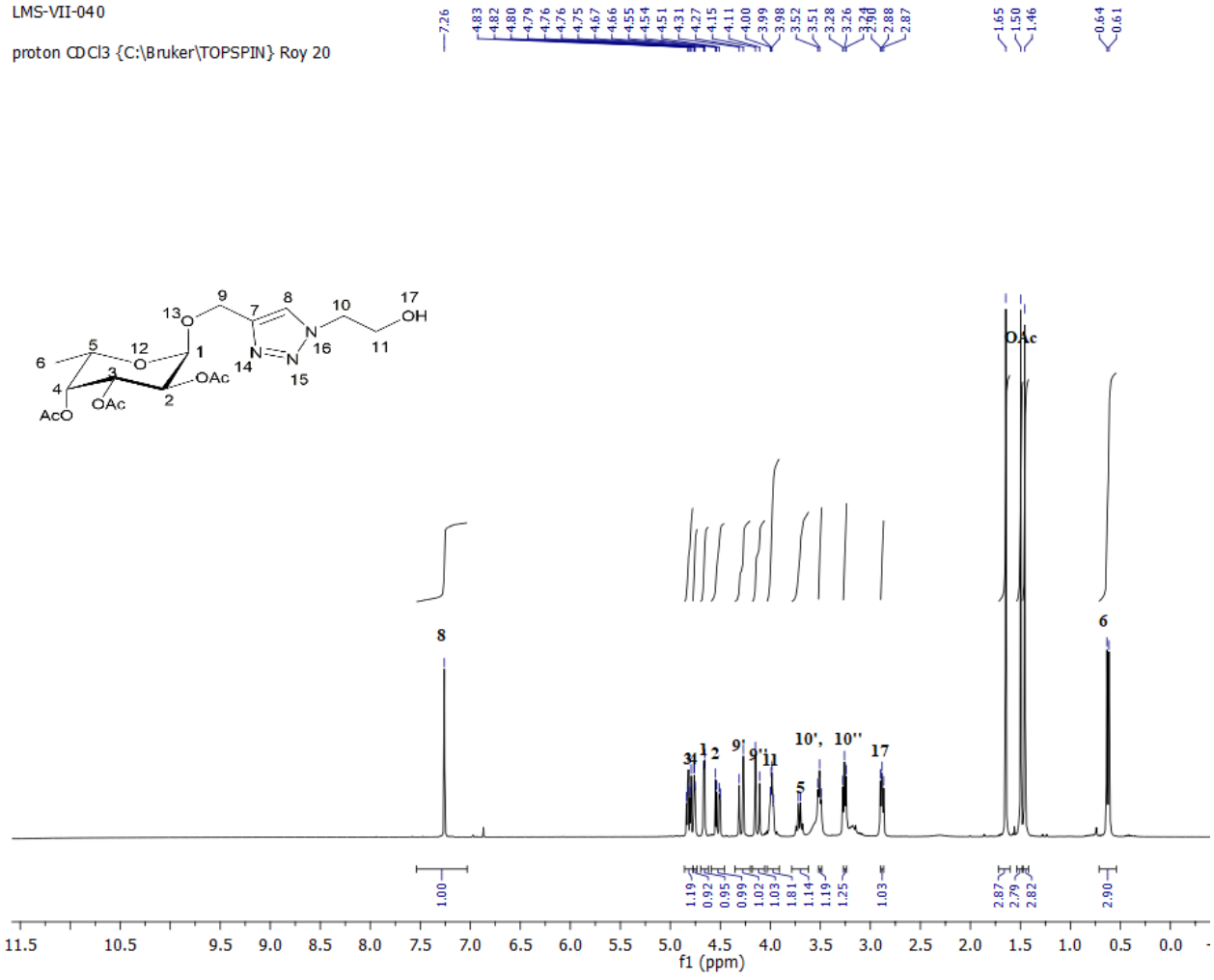

Figure A25. ^{13}C NMR analysis of compound **60** (300 MHz, $CDCl_3$)

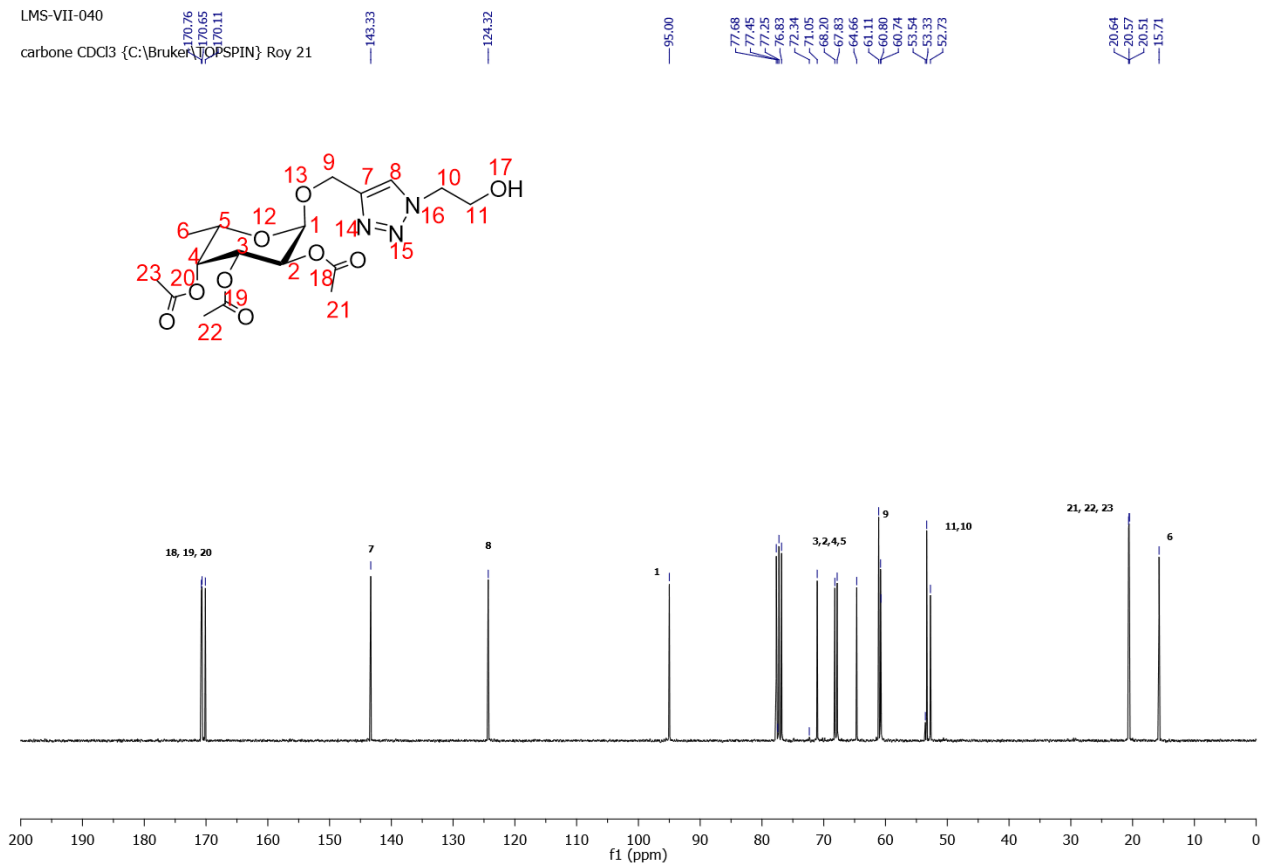

Figure A26. HSQC analysis of compound **60** (300 MHz, $CDCl_3$)

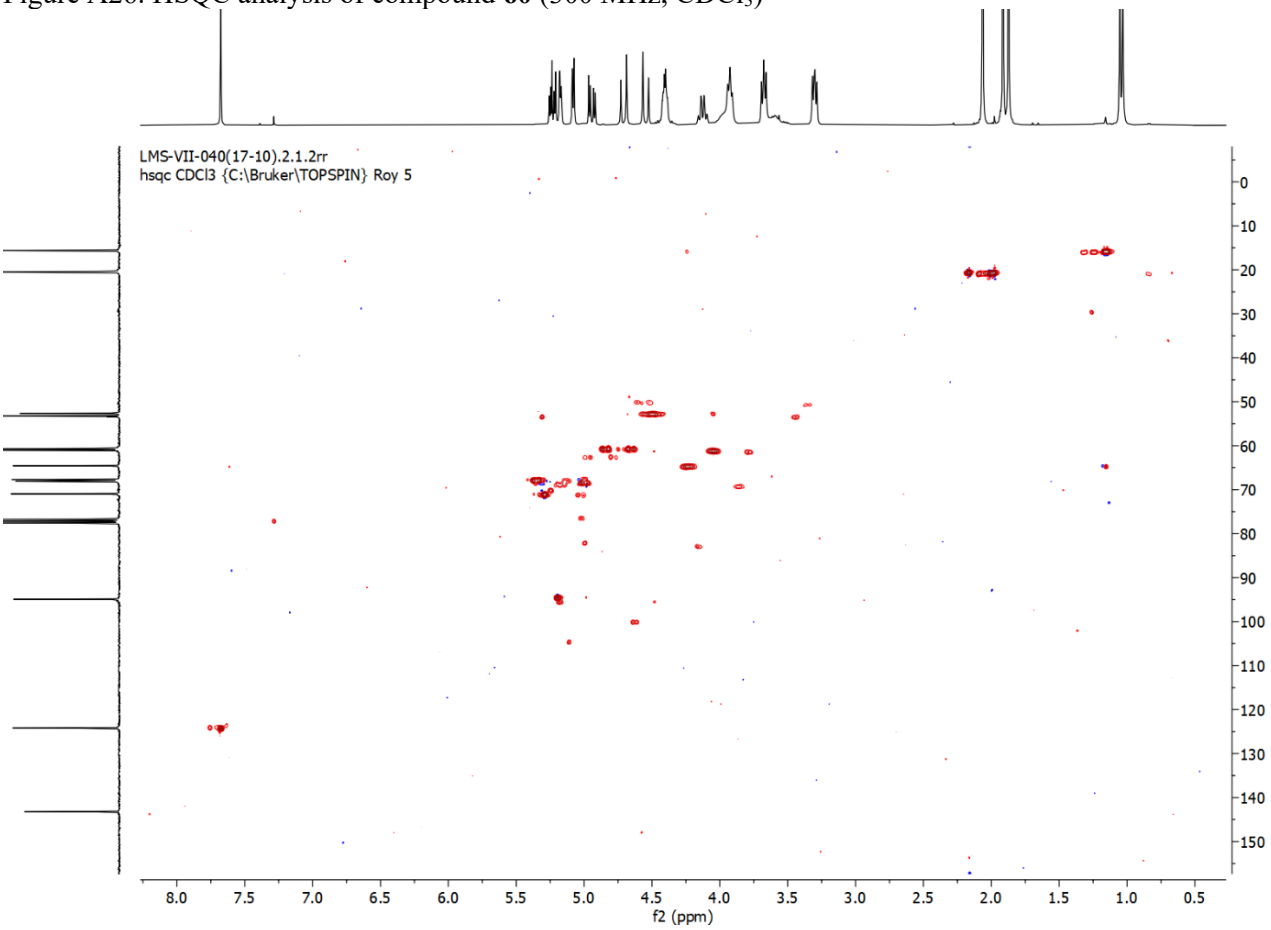

Figure A27. DEPT analysis of compound **60** (300 MHz, $CDCl_3$)

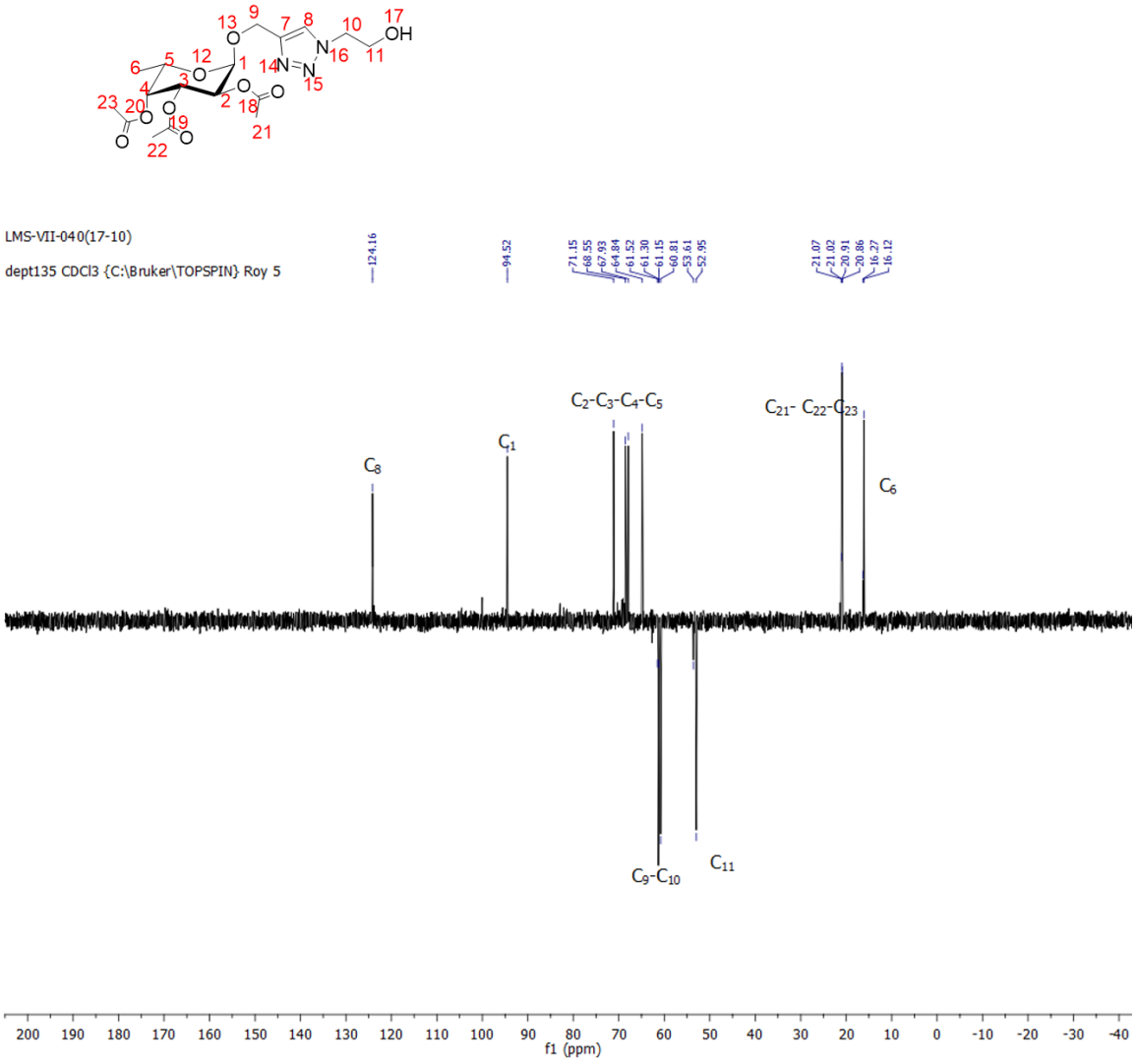

The thiol segment was accessed *via* three steps:

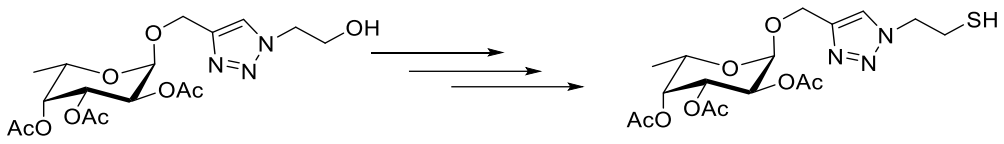

Step 1: **Compound 61**

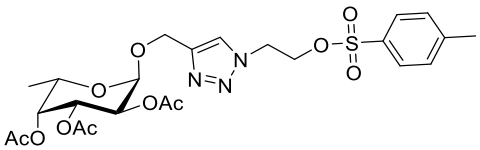

Experimental: To a solution of **60** (2 g, 4.819 mmol) in CH_2Cl_2 (50 mL), was added triethylamine (1.5 mL, 10.78 mmol), the mixture cooled at 0°C, a solution of *p*-TSCl (1.5 g, 7.8 mmol) in 10 mL CH_2Cl_2 was added slowly, then the reaction allowed to stir at room temperature for 10 h. The organic phase was washed with saturated NaCl and dried over anhyd. Na_2SO_4, filtered, and concentrated *in vacuo*. The crude product was purified on column chromatography (DCM/MeOH 99:1%) to give the primary tosylate ether **61** (2.5 g, 95%) as a colorless viscous oil. ^{1}H NMR (300 MHz, $CDCl_3$) δ 7.77- 7.65 (m, 2H, Ar), 7.62 (s, 1H, triazole), 7.33 (d, 2H, *J* = 8.0 Hz, Ar), 5.35 (dd, 1H, *J* = 10.3, 3.4 Hz, H-3), 5.29 (dd,1H, *J* = 3.3, 1.2 Hz, H-4), 5.17 (t, 1H, *J* = 2.8 Hz, H-1), 5.13 (t, 1H, *J* = 5.2 Hz, H-2), 4.81 (d, 1H, *J* = 12.4 Hz, -*O*CH_2) , 4.64 (dd, 2H, *J* = 5.7, 4.5 Hz, -*O*CH_2-tosylate), 4.61(1H, -*O*CH_2), 4.44- 4.33 (m, 2H, -*N*CH_2), 4.20 (q, 1H, *J* = 6.2 Hz, H-5), 2.44 (s, 3H, CH_3-Acetyl), 2.16 (s, 3H, CH_3-Acetyl), 2.05 (s, 3H, CH_3-Acetyl), 1.97 (s, 3H), 1.14 (dd, *J* = 12.6, 6.8 Hz, 3H). ^{13}C NMR (300 MHz, $CDCl_3$) δ 170.6, 170.4, 170.0, 145.6, 144.2, 131.9, 130.1, 123.8, 95.7, 71.1, 67.9, 67.9, 67.6, 64.7, 61.1, 49.1, 21.6, 20.8, 20.7, 20.6, 15.8. ESI-HRMS: *m/z* calcd for $C_{24}H_{31}N_3O_{11}S$ $[M+H]^+$ 570.1752, found 570.1739.

Figure A28. ^{1}H NMR analysis of compound **61** (300 MHz, $CDCl_3$)

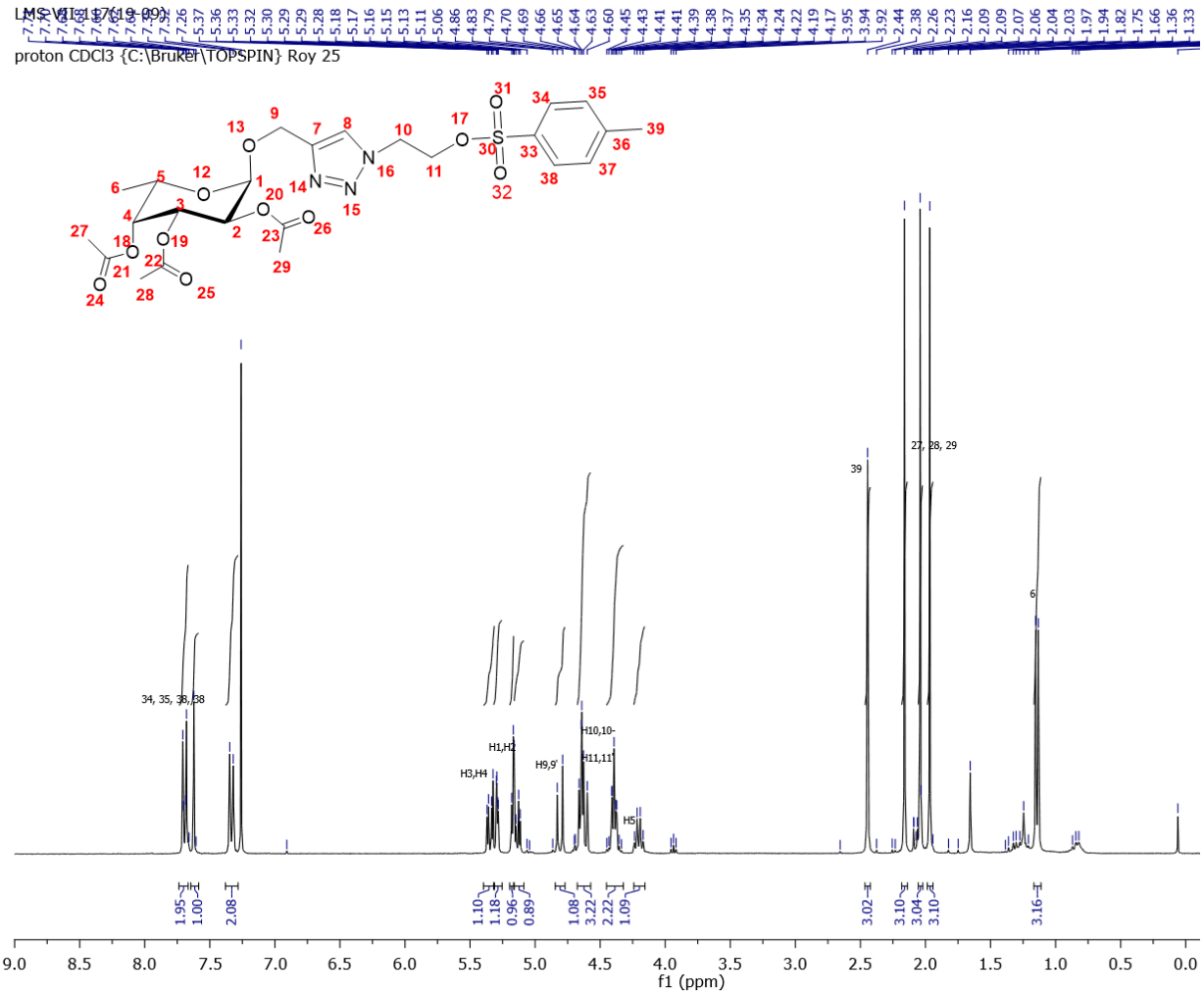

Figure A29. ^{13}C NMR analysis of compound **61** (300MHz, $CDCl_3$)

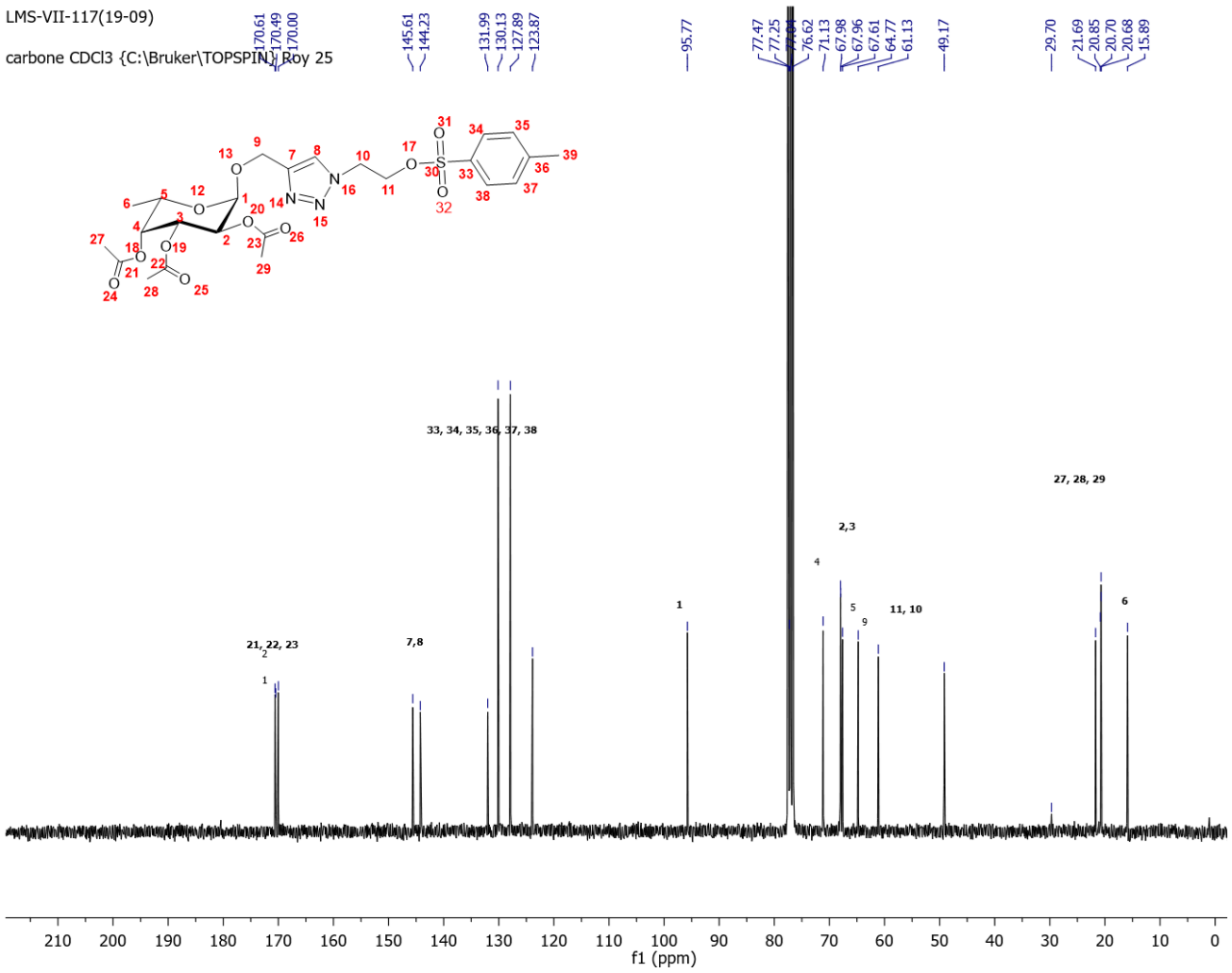

Figure A30. COSY analysis of compound **61** (300 MHz, $CDCl_3$)

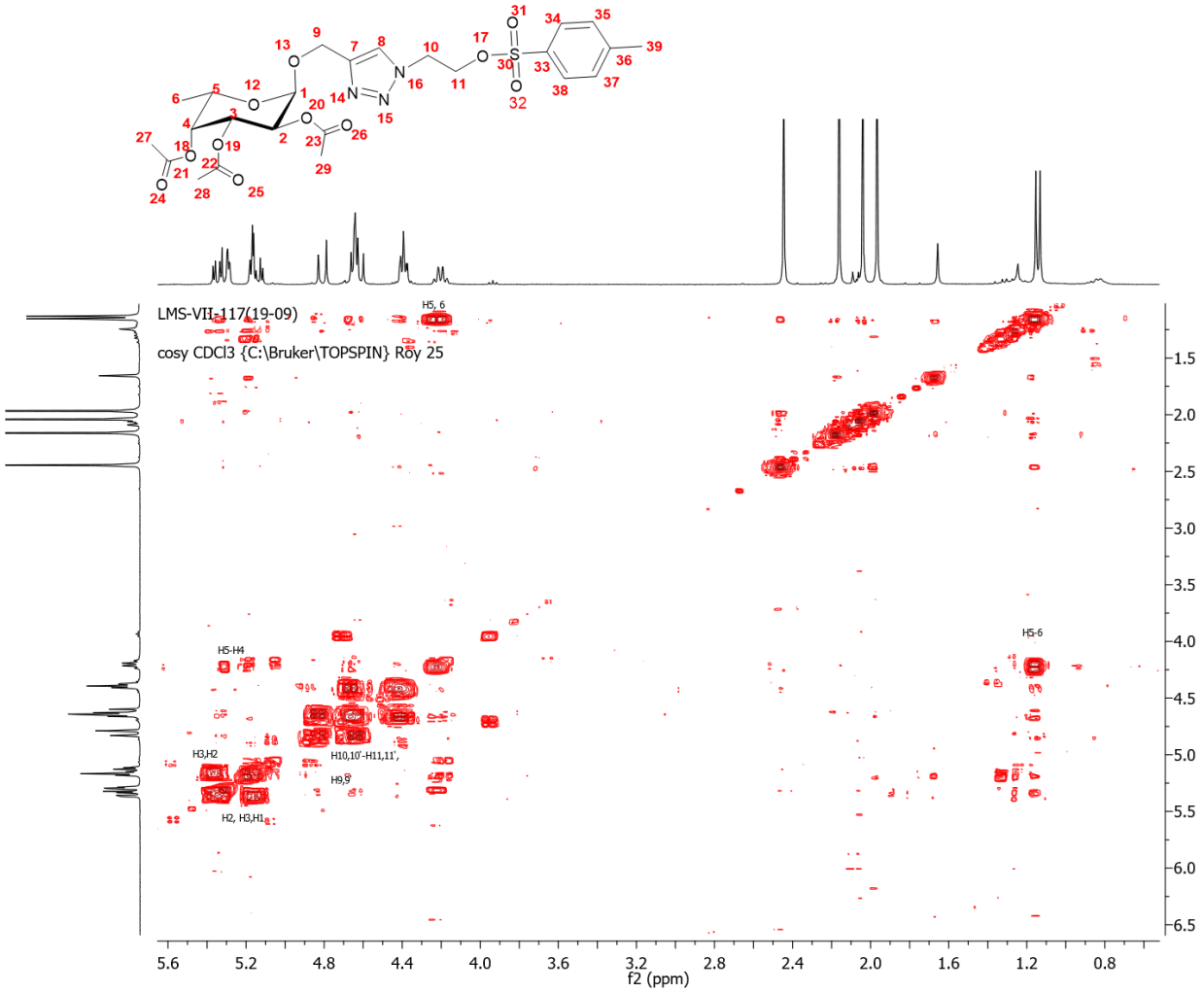

Figure A31. HSQC analysis of compound **61** (300 MHz, $CDCl_3$)

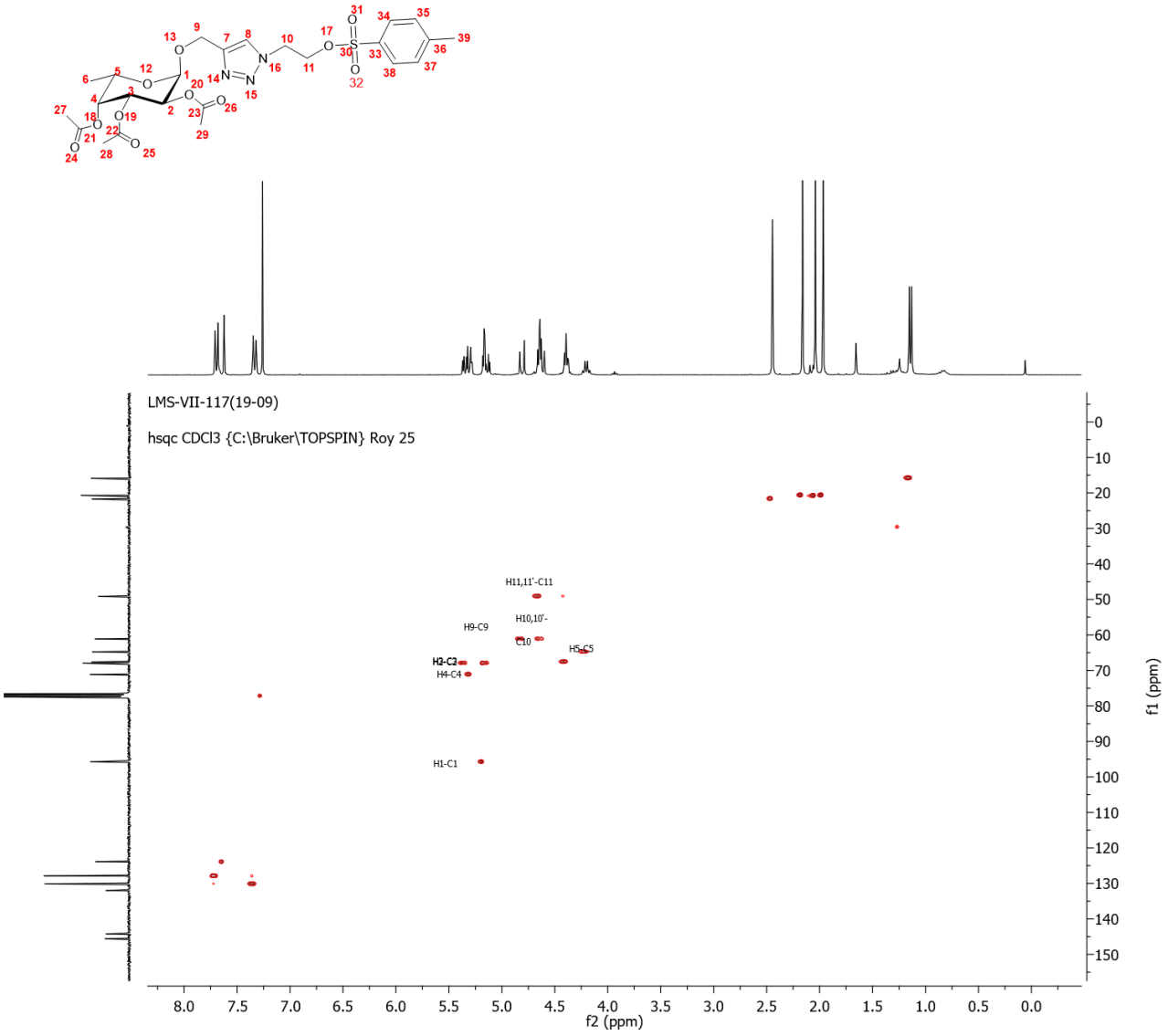

Figure A32. DEPT analysis of compound **61** (300 MHz, $CDCl_3$)

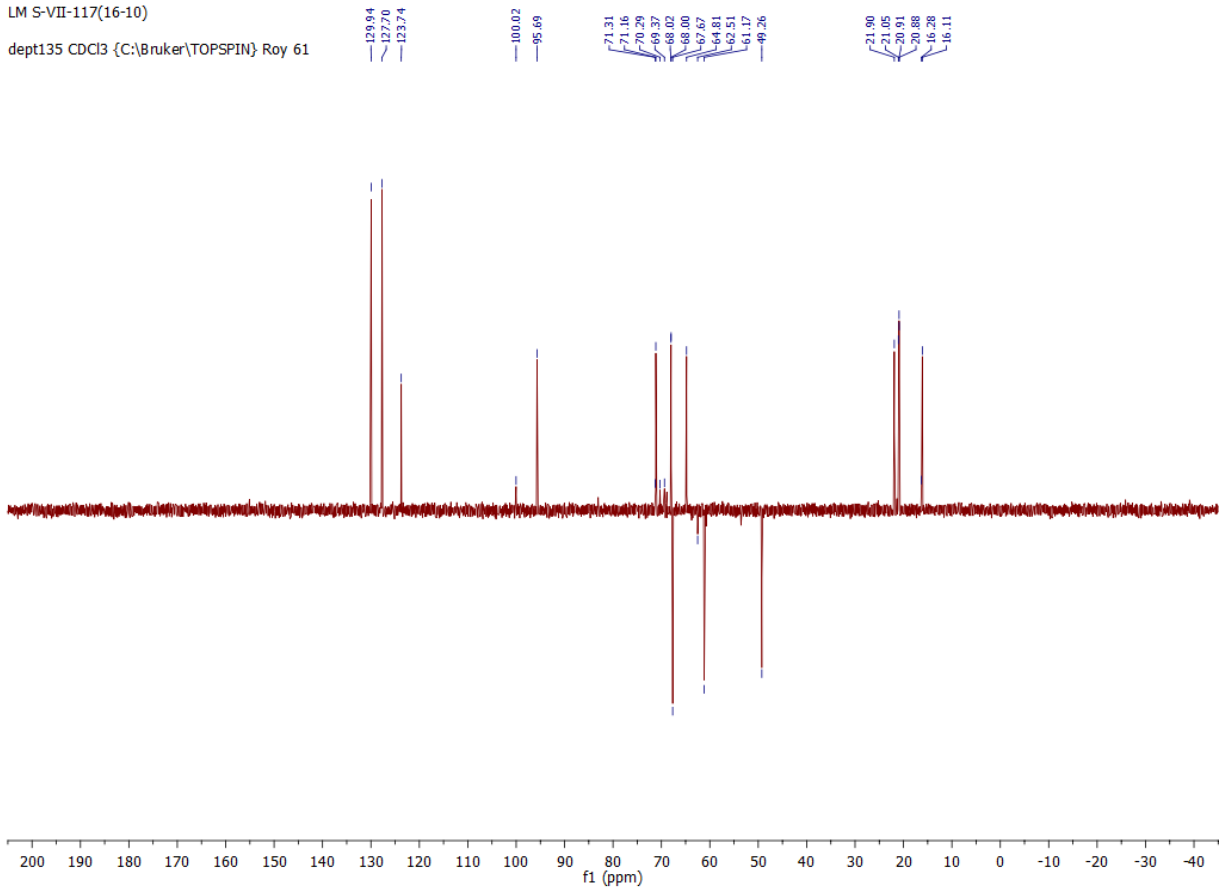

Figure A33. DEPTq analysis of compound **61** (300 MHz, $CDCl_3$)

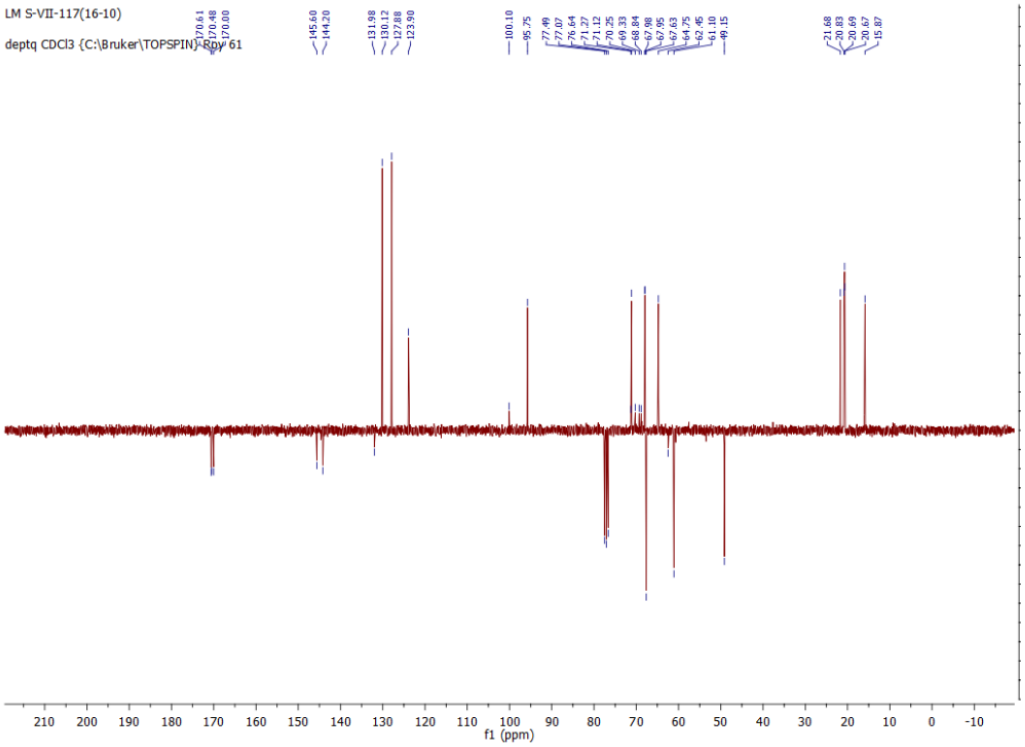

Figure A34. HRMS analysis of compound **61**

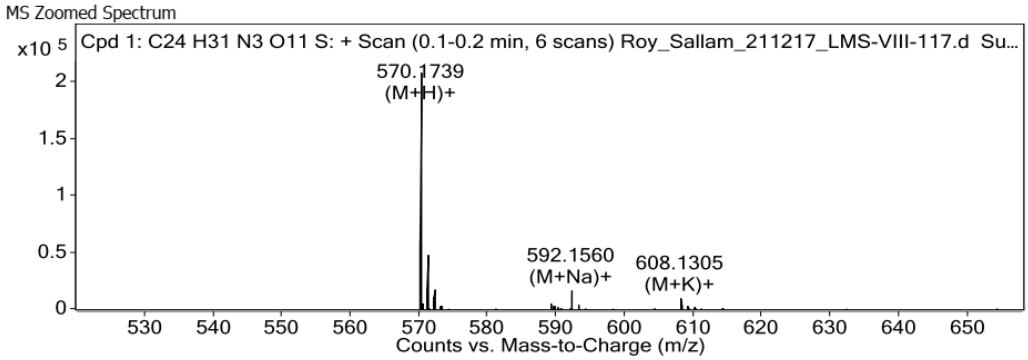

MS Spectrum Peak List

m/z	*Calc m/z*	Diff(ppm)	z	Abund	Formula	Ion
570.1739	570.1752	-2.26		212297	C24 H32 N3 O11 S	(M+H)+
570.4798				5985		
571.1773	571.1783	-1.71		51756	C24 H32 N3 O11 S	(M+H)+
572.1756	572.1766	-1.76		17578	C24 H32 N3 O11 S	(M+H)+
573.1772	573.1782	-1.59		3411	C24 H32 N3 O11 S	(M+H)+
592.156	592.1572	-1.88	1	17568	C24 H31 N3 Na O11 S	(M+Na)+
593.1591	593.1602	-1.78	1	4615	C24 H31 N3 Na O11 S	(M+Na)+
608.1305	608.1311	-0.91	1	10397	C24 H31 K N3 O11 S	(M+K)+
609.1346	609.1341	0.81	1	2913	C24 H31 K N3 O11 S	(M+K)+
610.1356	610.1312	7.33	1	1831	C24 H31 K N3 O11 S	(M+K)+

--- End Of Report ---

Step 2: Compound 62

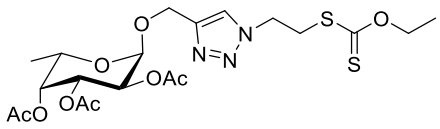

Experimental: To a solution of compound **61** (150 mg, 0.263 mmol) in dry acetone (3 mL) was added potassium ethyl xanthate (63 mg, 0.395 mmol). The mixture was stirred at rt for 12 h. The solution was filtered from inorganic material over celite® and the filtrate and acetone were evaporated. The mixture was redissolved in DCM and washed with H_2O. The combined organic layers were collected, dried over anhyd. Na_2SO_4 and concentrated under reduced pressure. The residue was purified by flash column chromatography (DCM/MeOH 99:1%) to afford **62** (120 mg, 85%) as a colorless viscous oil.^{1}H NMR (300 MHz, $CDCl_3$) δ 7.60 (s, 1H), 5.31 (dd, 1H, *J* = 8.8, 4.8 Hz, H_3), 5.26 (d, 1H, *J* = 3.2 Hz, H_4), 5.15 (d, 1H, *J* = 3.5 Hz, H1), 5.10 (dd, 1H, *J* = 10.7, 3.6 Hz, H_2), 4.80 (d, 2H, *J* = 12.4 Hz, -*O*CH_2), 4.68 (m, 2H, *J* = 43.4, 8.2 Hz, -*O*CH_2- Xanthate), 4.64 (m, 2H, *J* = 5.7 Hz, -*N*CH_2), 4.63- 4.58 (m, 2H, -SCH_2), 4.18 (q, 1H, *J* = 6.4 Hz, H_5), 3.60 (t, 2H, *J* = 6.7 Hz, -*S*CH_2-Xanthate), 2.12 (s, 3H, CH_3-Acetyl), 2.02 (s, 3H, CH_3-Acetyl), 1.94 (s, 3H, CH_3-Acetyl), 1.41 (td, 3H, *J* = 7.1, 0.9 Hz, CH_3), 1.11 (d, 3H, *J* = 6.5 Hz, CH_3).^{13}C NMR (300 MHz, $CDCl_3$) δ 213.1, 170.5, 170.3, 169.9, 144.0, 123.2, 95.6, 71.1, 70.8, 68.0, 67.9, 64.7, 61.2, 48.6, 35.3, 20.8, 20.6, 20.6, 15.8, 13.7. ESI-HRMS: *m/z* calcd for $C_{20}H_{29}N_3O_9S_2$ $[M+H]^+$ 520.1418, found 520.1407.

Figure A35. ^{1}H NMR analysis of compound **62** (300 MHz, $CDCl_3$)

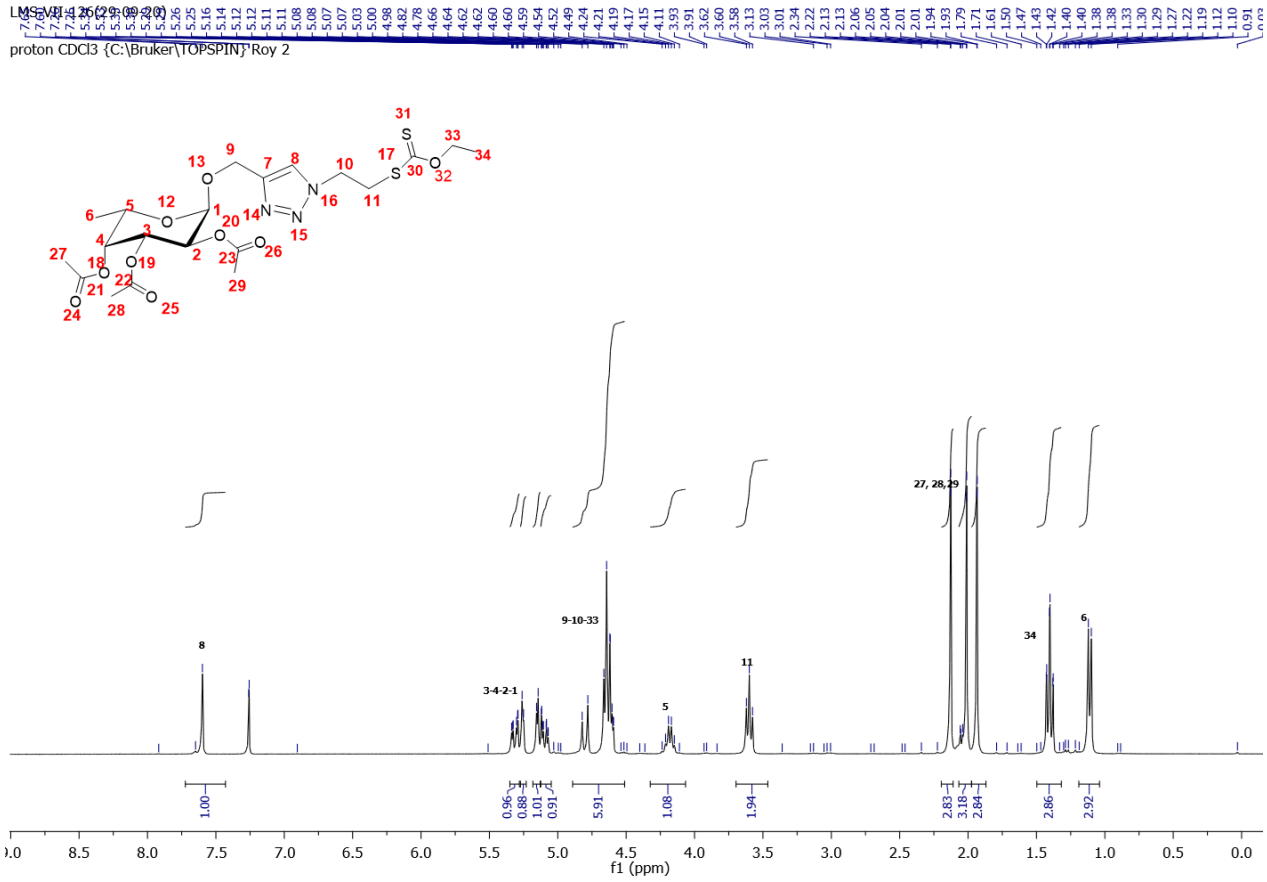

Figure A36. ^{13}C NMR analysis of compound **62** (300 MHz, $CDCl_3$)

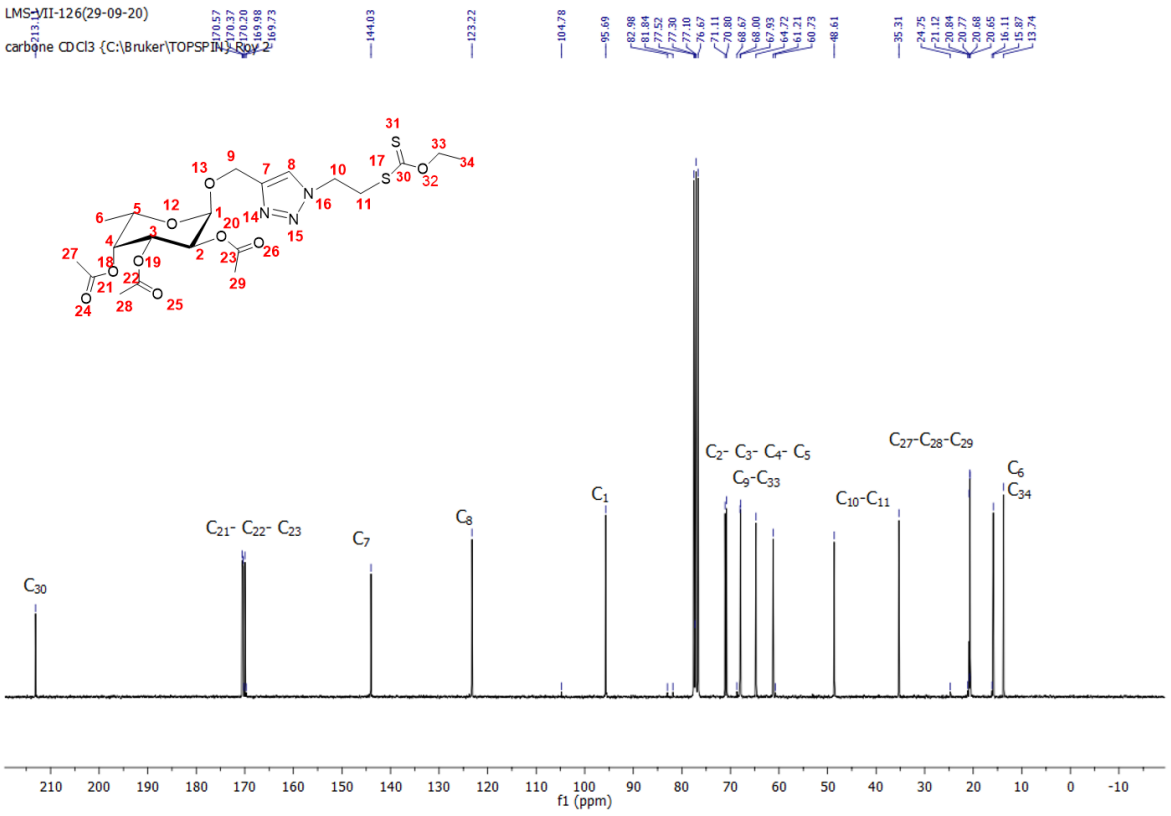

Figure A37. COSY analysis of compound **62** (300 MHz, $CDCl_3$)

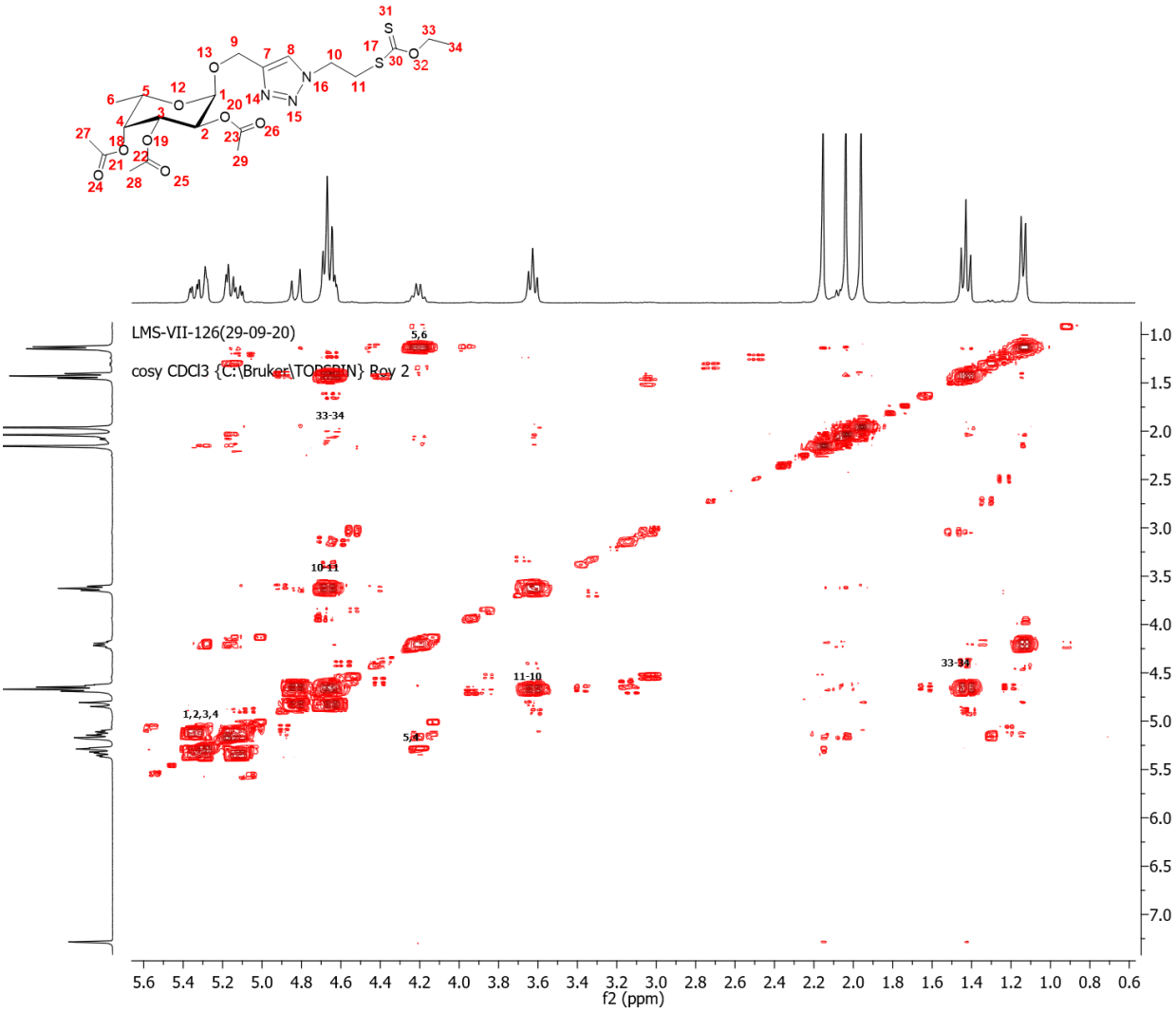

Figure A38. HSQC analysis of compound **62** (300 MHz, $CDCl_3$)

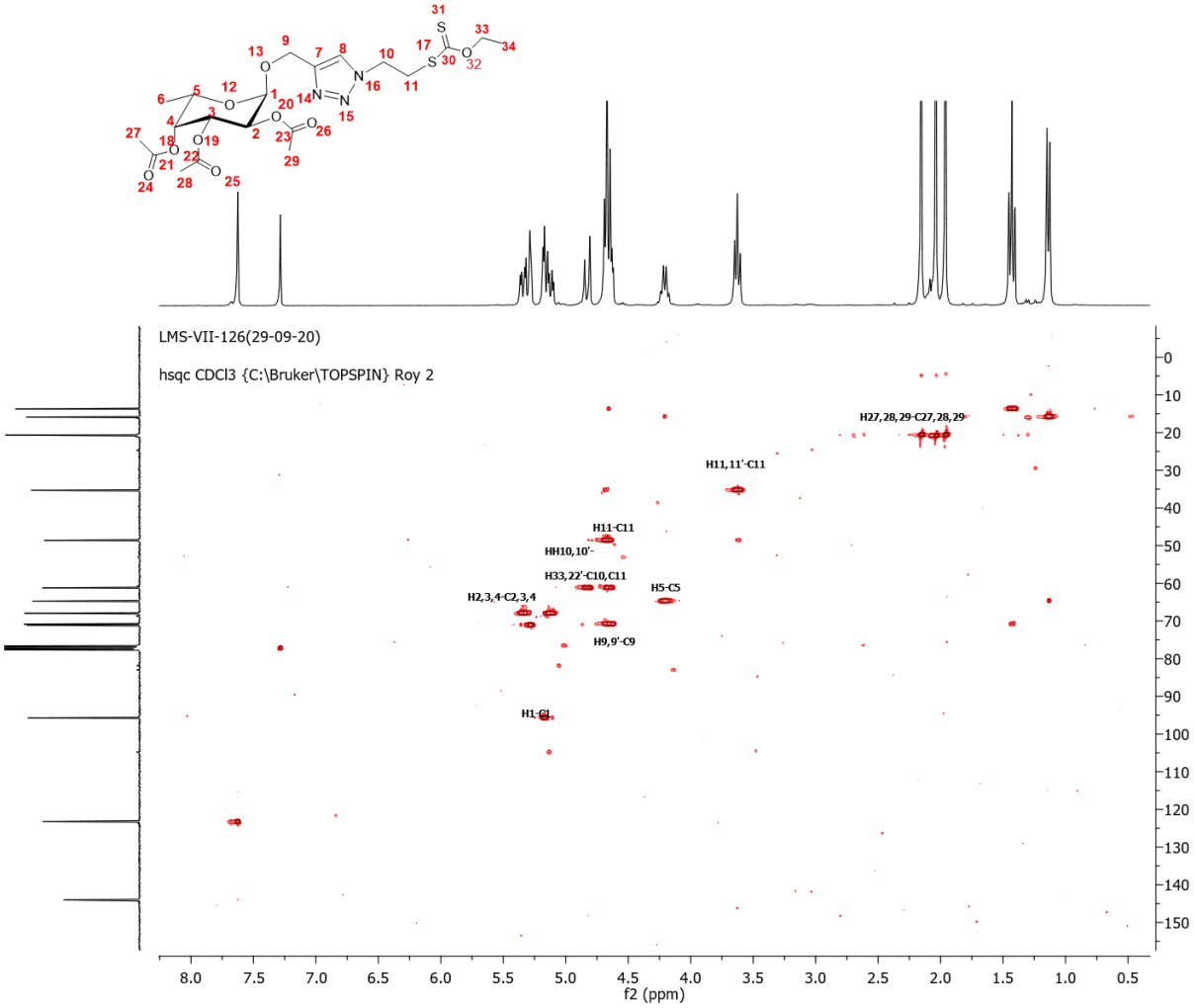

Figure A39. DEPT analysis of compound **62** (300 MHz, $CDCl_3$)

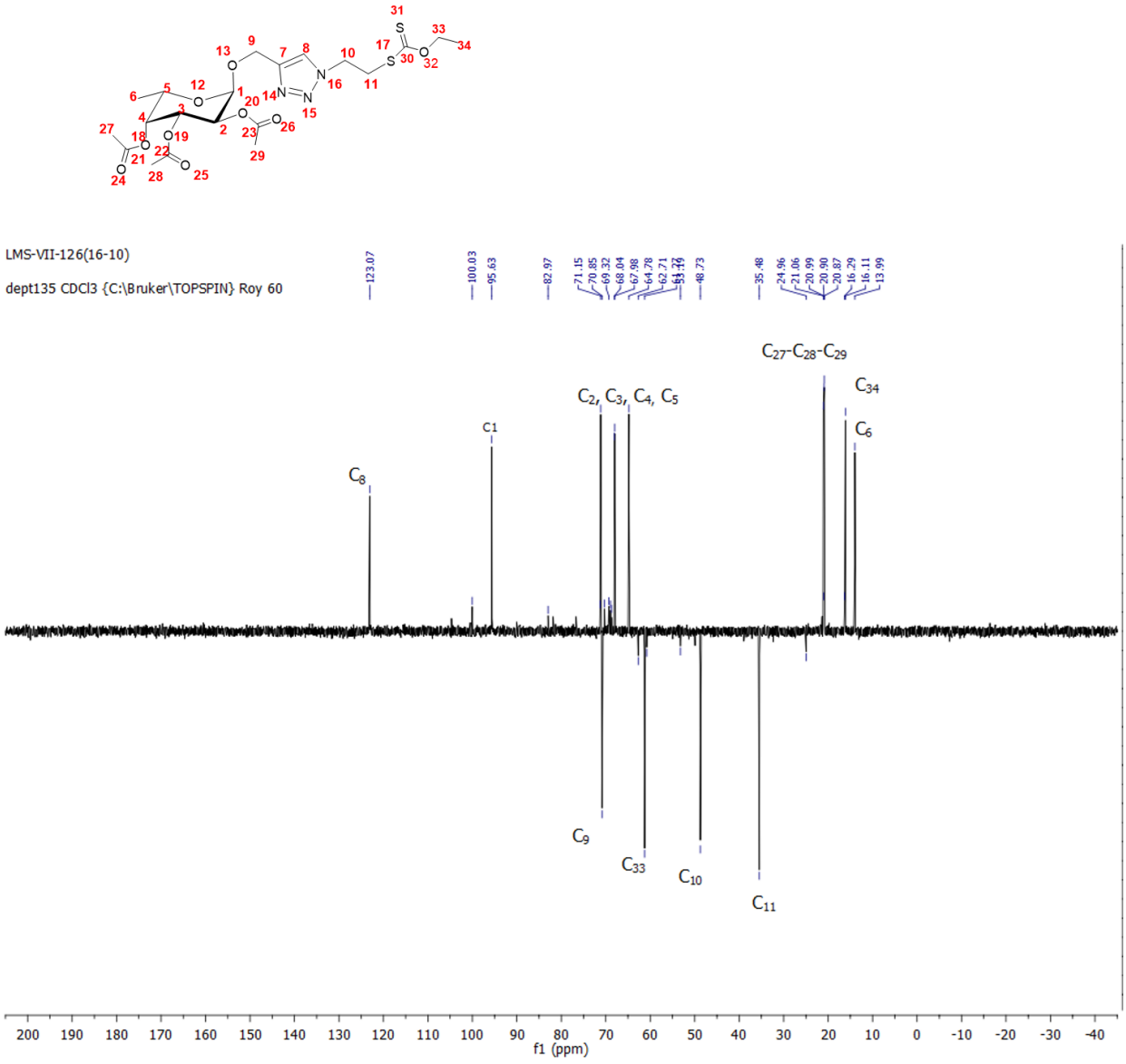

Figure A40. HRMS analysis of compound **62**

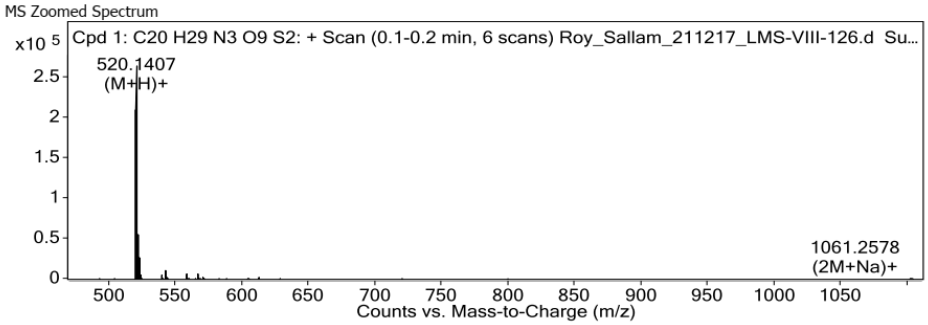

MS Spectrum Peak List

m/z	*Calc m/z*	Diff(ppm)	z	Abund	Formula	Ion
520.1407	520.1418	-2.16		267523	C20 H30 N3 O9 S2	(M+H)+
520.432				9250		
521.1436	521.1447	-2.12		57158	C20 H30 N3 O9 S2	(M+H)+
522.1399	522.1409	-1.92		28460	C20 H30 N3 O9 S2	(M+H)+
523.1417	523.1427	-1.95		5345	C20 H30 N3 O9 S2	(M+H)+
542.1223	542.1237	-2.72	1	11879	C20 H29 N3 Na O9 S2	(M+Na)+
543.126	543.1266	-1.1	1	2931	C20 H29 N3 Na O9 S2	(M+Na)+
558.0963	558.0977	-2.45	1	6802	C20 H29 K N3 O9 S2	(M+K)+
559.1007	559.1006	0.23	1	1703	C20 H29 K N3 O9 S2	(M+K)+
1061.2578	1061.2583	-0.41	1	510	C40 H58 N6 Na O18 S4	(2M+Na)+

--- End Of Report ---

Step 3: α-L-fucose thiol 63

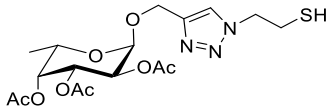

Experimental: THF Solvent was degassed prior to use by bubbling nitrogen through the solutions for 30 min. The exclusion of oxygen is important to keep thiols in reduced form.

To a flame-dried round bottom flask was added a solution of **62** (250 mg, 0.480 mmol, 1.0 eqv.) in dry THF (6 mL) under nitrogen atmosphere, *n*-butylamine was added (60 µL, 0.626 mmol, 1.3 eqv.), the reaction allowed to stir for 2 h at room temperature. The progress of the reaction was followed using TLC, after completion of the reaction the solvent was removed, the residue was redissolved in CH_2Cl_2, and washed with sat. aq. NH_4Cl. The organic layers were dried over anhydrous Na_2SO_4 and evaporated to dryness. The product was then purified by silica gel flash chromatography (DCM/MeOH 99:1%) to give pure compound **63** as a viscous oil (150 mg, 75%). The thiol product was flushed with nitrogen and closed, kept at - 20 ºC. ^{1}H NMR (300 MHz, $CDCl_3$) δ 7.58 (s, 1H), 5.20 (dd, 1H, *J* = 10.8, 3.3 Hz, H_3), 5.14 (dd, 1H, *J* = 3.3, 0.9 Hz, H_4), 5.03 (dd, 1H, *J* = 9.4, 2.7 Hz, H1), 4.95 (dd, 1H, *J* = 10.8, 3.7 Hz, H_2), 4.73- 4.51 (m, 2H, OCH_2), 4.43 (t, 2H, *J* = 6.6 Hz, NCH_2), 4.08 (q, 1H, *J* = 6.3 Hz, H_5), 2.91 (dt, 2H, *J* = 8.7, 6.6 Hz, SCH_2), 2.02 (s, 3H, CH_3-Acetyl), 1.88 (s, 3H, CH_3-Acetyl), 1.83 (s, 3H, CH_3-Acetyl), 1.44 (t, 1H, *J* = 8.7 Hz, -SH), 1.00 (d, 3H, *J* = 6.5 Hz, CH_3). ^{13}C NMR (300 MHz, $CDCl_3$) δ 170.4, 170.2, 169.8, 143.6, 123.5, 95.3, 70.9, 67.9,

67.8, 64.5, 60.9, 52.9, 24.6, 20.7, 20.6, 20.5, 15.7. ESI-MS (*m/z*) calcd for $C_{17}H_{25}N_3O_8S$ $[M+ Na]^+$ 454.46, found 455.0.

Figure A41. ^1H NMR analysis of compound **63** (300 MHz, $CDCl_3$)

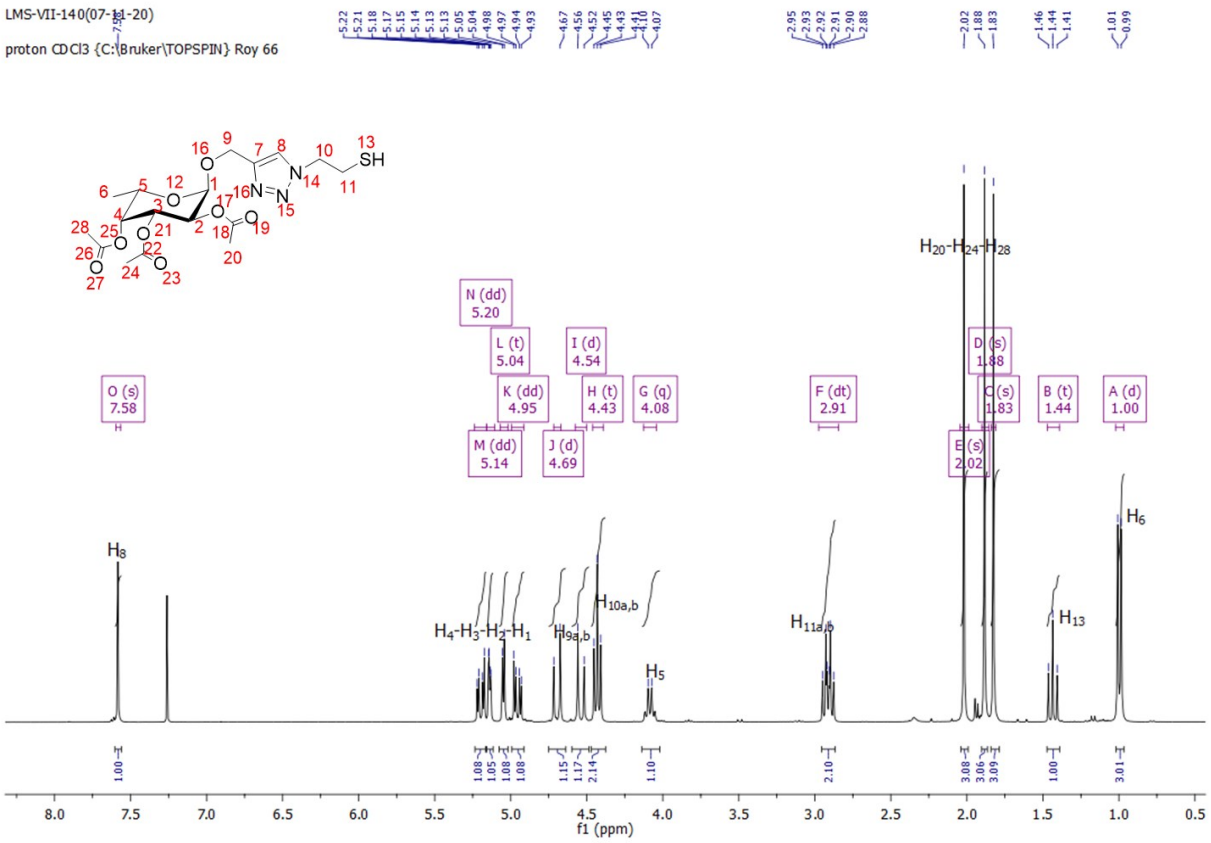

Figure A42. ^{13}C NMR analysis of compound **63** (300 MHz, $CDCl_3$)

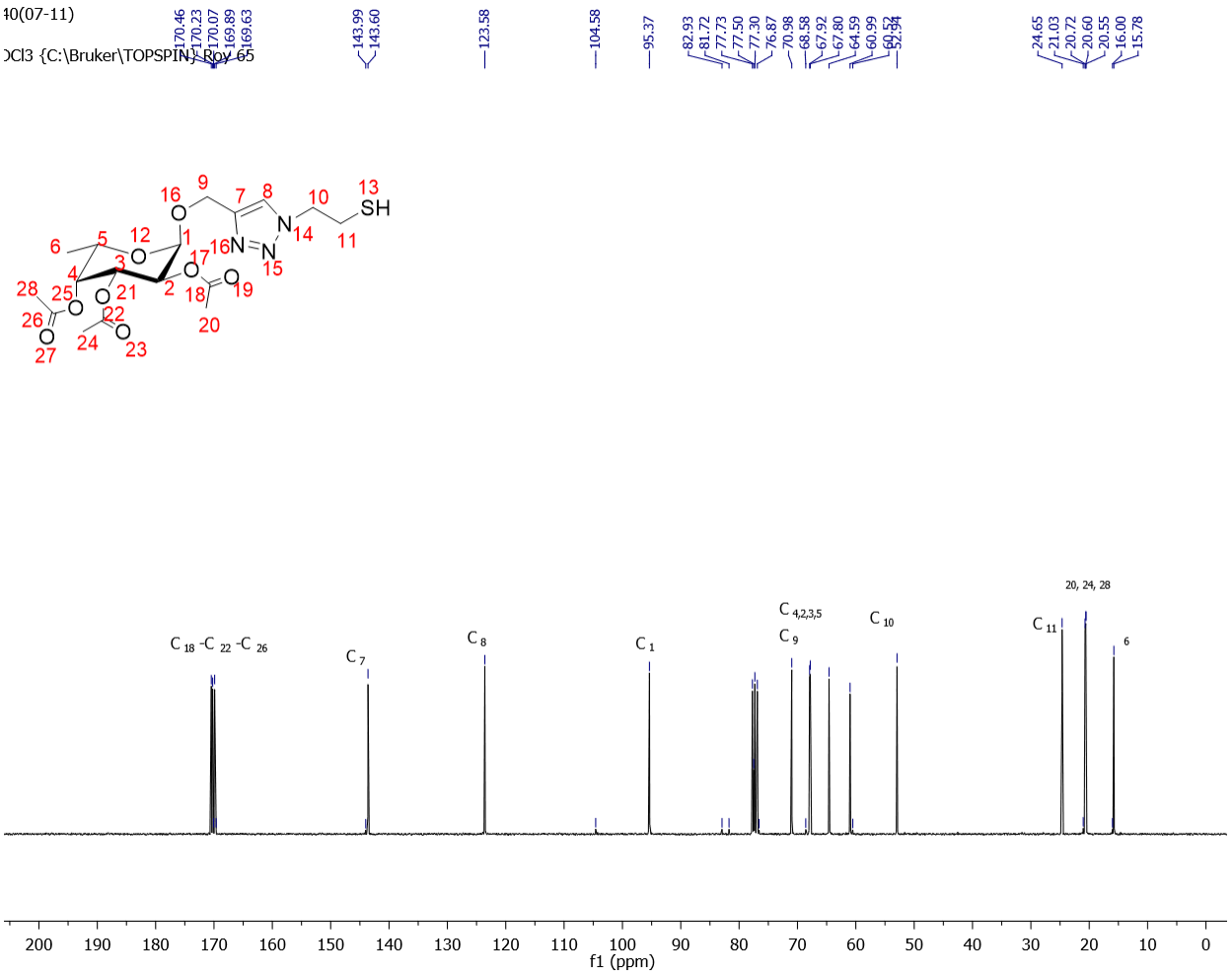

Figure A43. COSY analysis of compound **63** (300 MHz, $CDCl_3$)

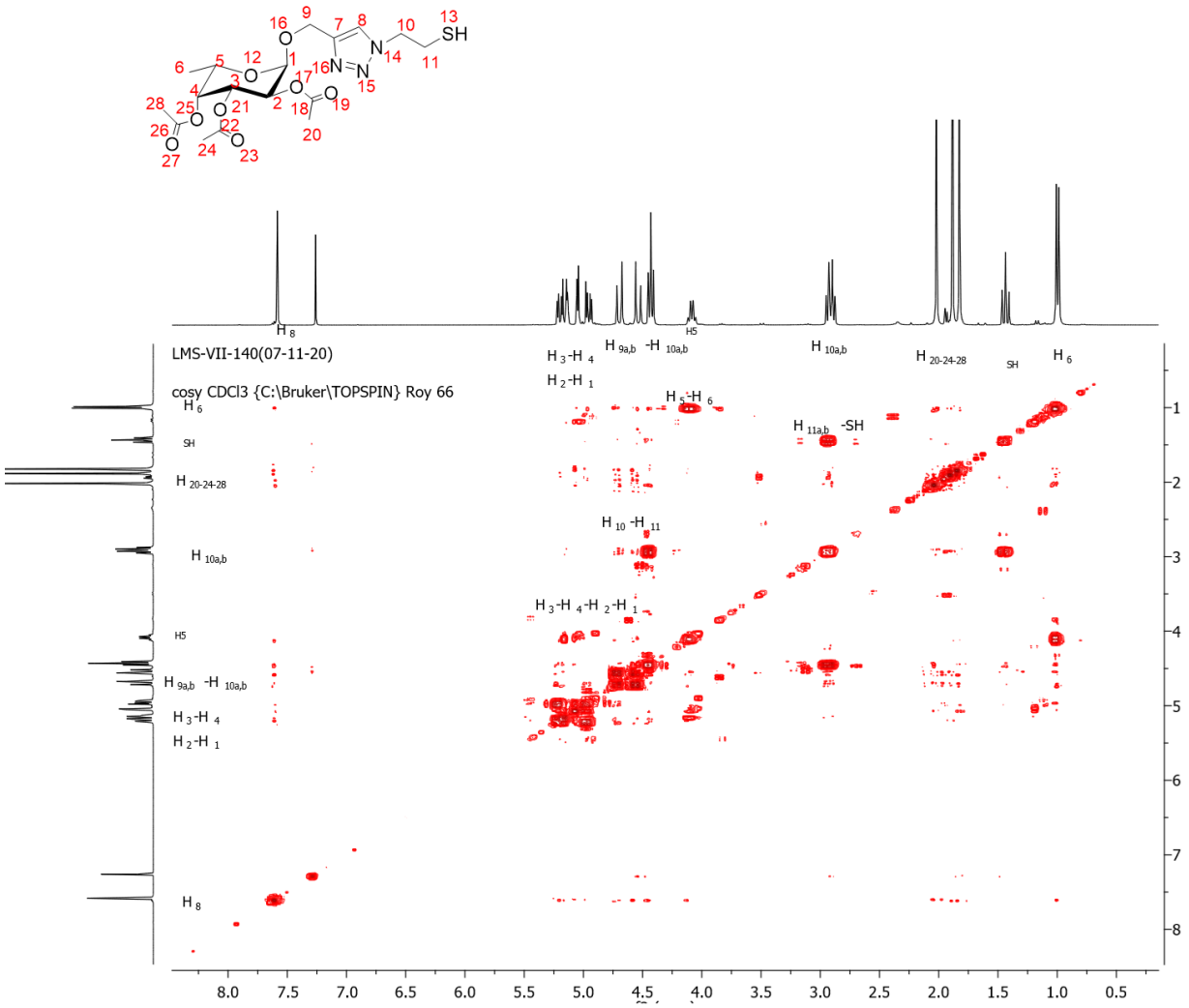

Figure A44. HSQC analysis of compound **63** (300 MHz, $CDCl_3$)

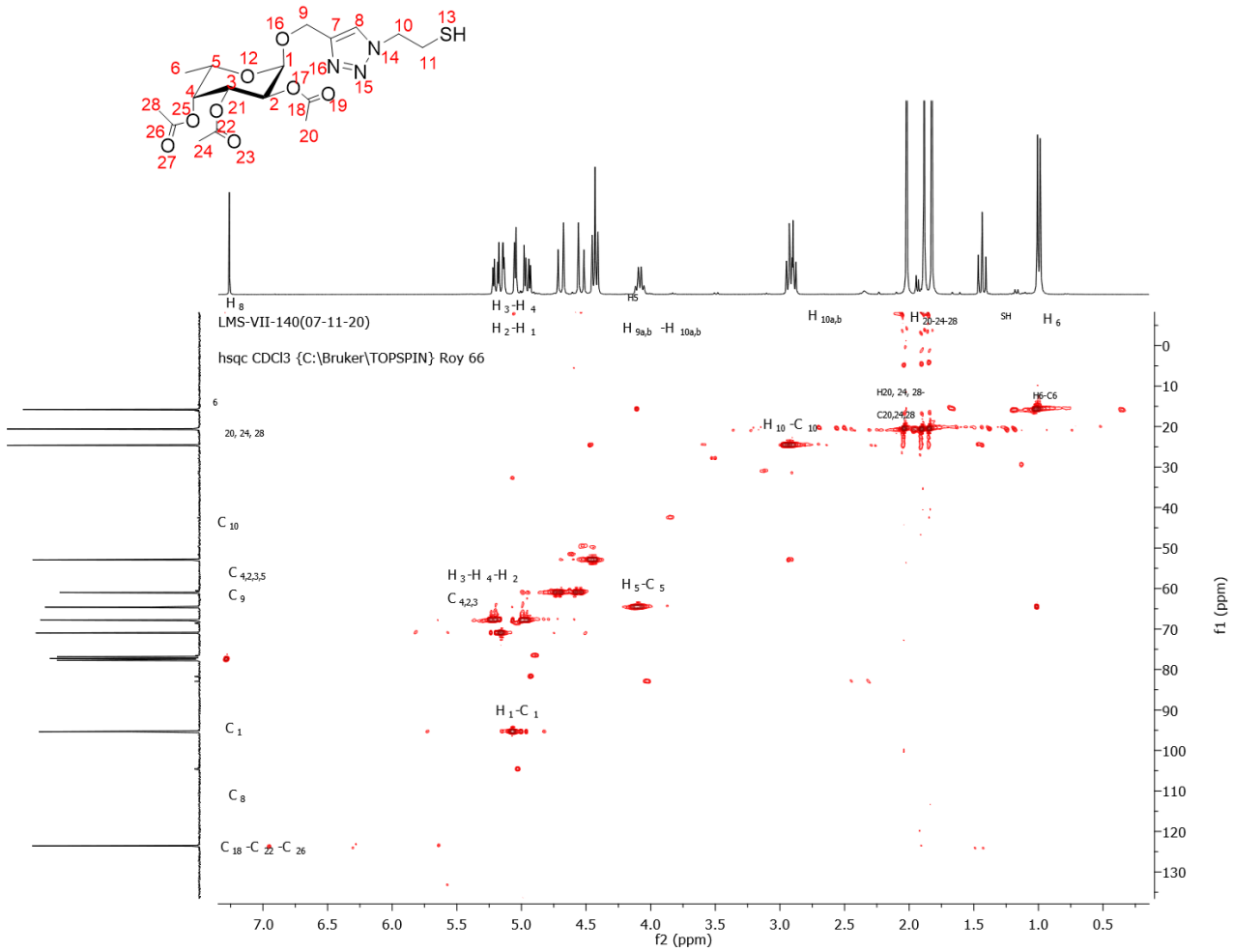

Synthesis of 1,5-triazole isomer 64, using catalyst $Cp^*RuCl(PPh_3)_2$

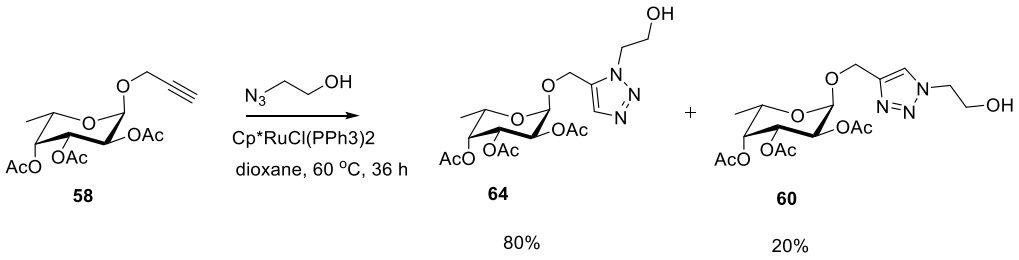

58 **64** 80% + **60** 20%

Experimental: To a solutionof α-L-fucoside **58** (100 mg, 0.304 mmol) and 2-azidoethanol (52 mg, 0.609 mmol) in 0.5 mL of dioxane was added to $Cp^*RuCl(PPh_3)_2$ (12 mg, 5 mol%) dissolved in 2.5 mL of dioxane. The vial was purged with nitrogen, sealed, and heated in an oil bath at 60 °C for 36 h, at which point TLC indicated complete consumption of the alkyne starting materials. The mixture was purified on chromatography (DCM/MeOH 9 :1%) to afford a product **64** as pale-yellow oil (200 mg, yield 75 %).

Figure A45. ^{1}H NMR analysis of Fuc-1,5 triazole **64**

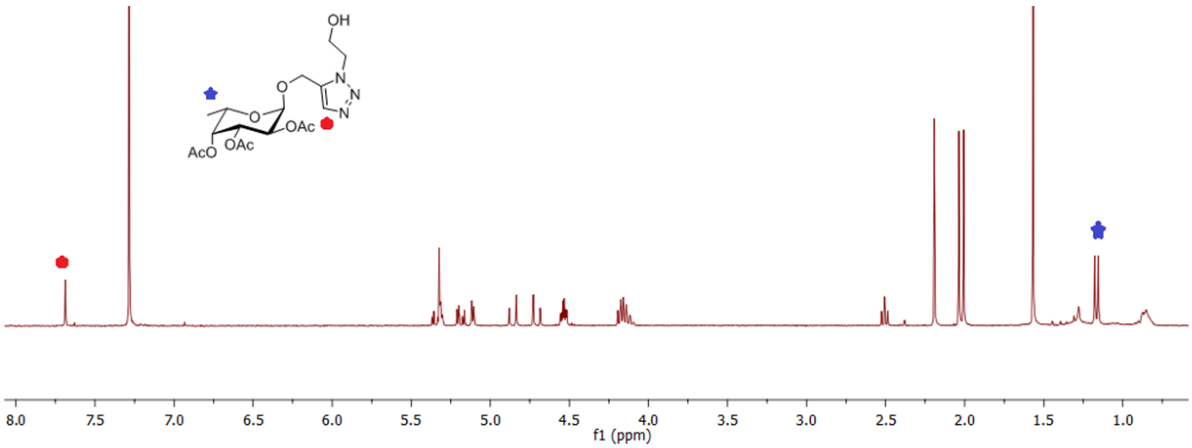

Synthesis of α-L-fucose thiol 65

Following the previous sequence, the synthesis of α-L-fucoside thiol analogue **65**, was prepared in 70 %.

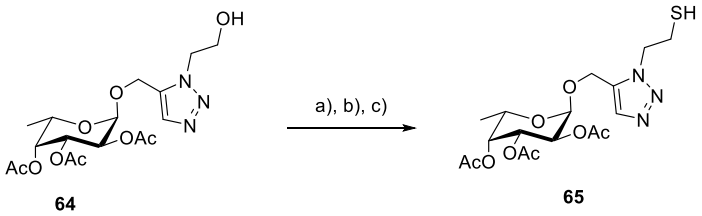

a) *p*-TSCl, NEt_3, DCM, rt, 7r, 95%; b)  , acetone, rt, 12 h, 90%; c) *n*-$BuNH_2$, THF, rt, 2h, 70%.

Compound 71

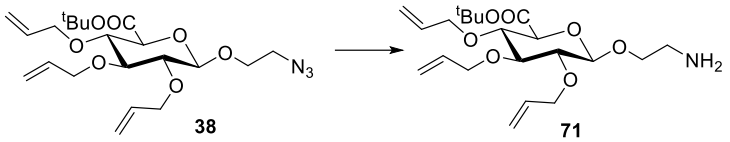

Experimental: To a solution of β-D- glucuronic ester **38** (2 g, 5.46 mmol) in freshly degassed THF (100 mL) was added PPh_3 (12.5 g, 47.7 mmol), and water (8 mL). The reaction mixture was stirred at room temperature for 12h. The mixture was evaporated under a high vacuum and purified on column chromatography packed with dry silica (CH_2Cl_2/ MeOH 70: 3%) to afford the desired amine **71** as white oily residue (500 mg, 80%). ^{1}H NMR ($CDCl_3$, 300 MHz), 56.22-5.51(m, 3H, 3x CH_2=CH-), 5.39- 4.91 (m, 6H, 3x CH_2=CH-), 4.34- 4.13 (m, 5H, 2xCH_2=CH-CH_2-, H_1), 4.09 – 4.05 (m, 1H, H5), 4.03 (d, 1 H, J = 5.6 Hz, OCH_2), 3.88 – 3.76 (m, 1H, H_4), 3.74 – 3.51 (m, 2H, CH_2=CH-CH_2-), 3.51 (dd,1H, J = 14.4, 5.6 Hz, OCH_2), 3.33 (t, 1H, J = 8.9 Hz, H_3), 3.18 (dd, 1H, J = 9.1, 7.7 Hz, H_2), 2.88-2.79 (m, 2H, -NCH_2), 1.60 (brs, 2H, NH_2), 1.43 (s, 9H, *t-Butyl*).^{13}C NMR (300 MHz, $CDCl_3$) δ 167.6, 135.0, 134.8, 134.5, 116.9, 116.9, 116.7, 103.7, 83.3, 82.1, 81.2, 79.0, 75.2, 74.3, 73.8, 73.7, 72.6, 41.9, 27.8. ESI-HRMS (*m/z*) calcd for $C_{21}H_{35}NO_7$ $[M+H]^+$ 414.2486, found 414.2474.

Figure A46. ^{1}H NMR analysis of compound **71** (300 MHz, $CDCl_3$)

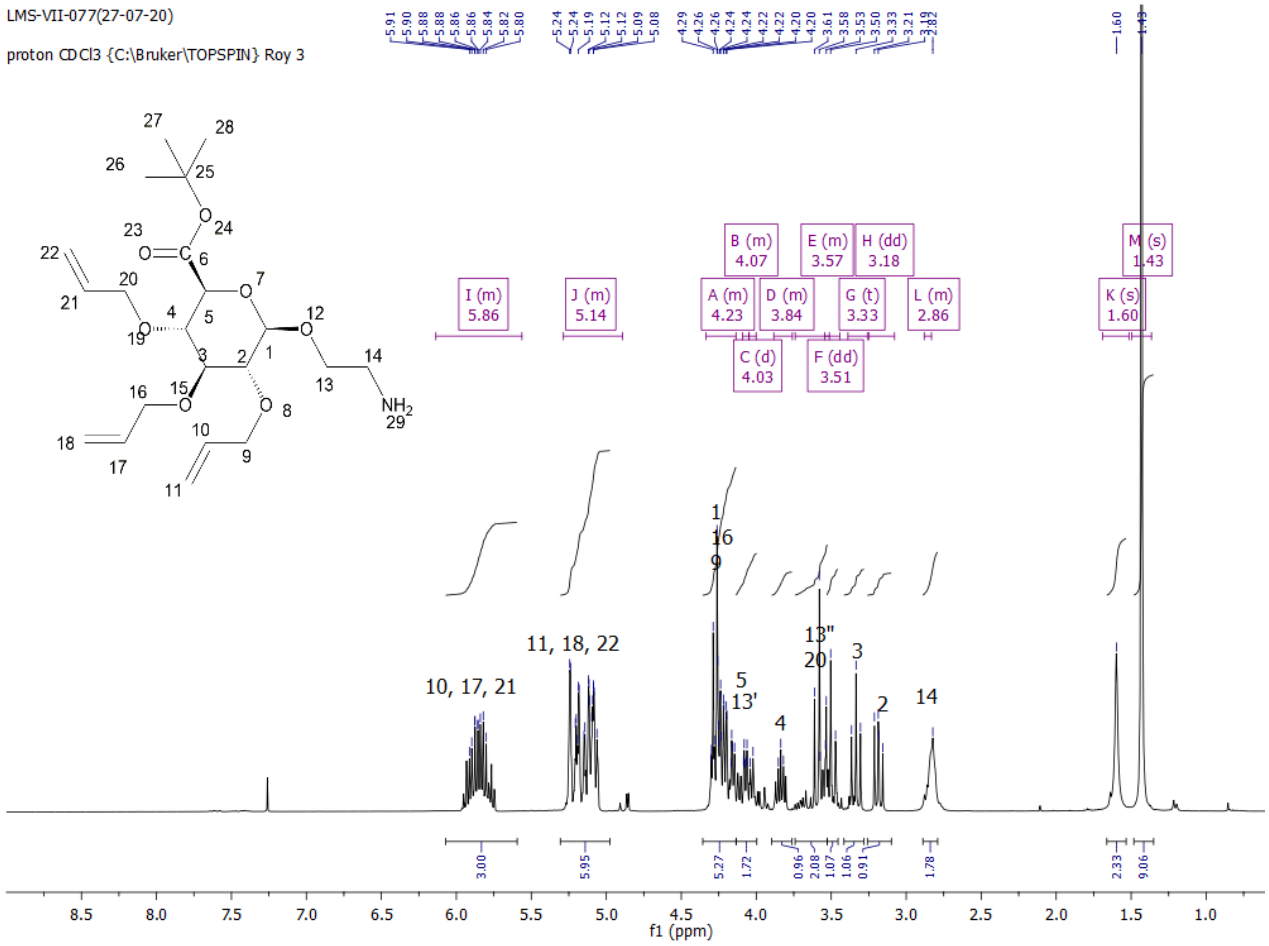

Figure A47. ^{13}C NMR analysis of compound **71** (300 MHz, $CDCl_3$)

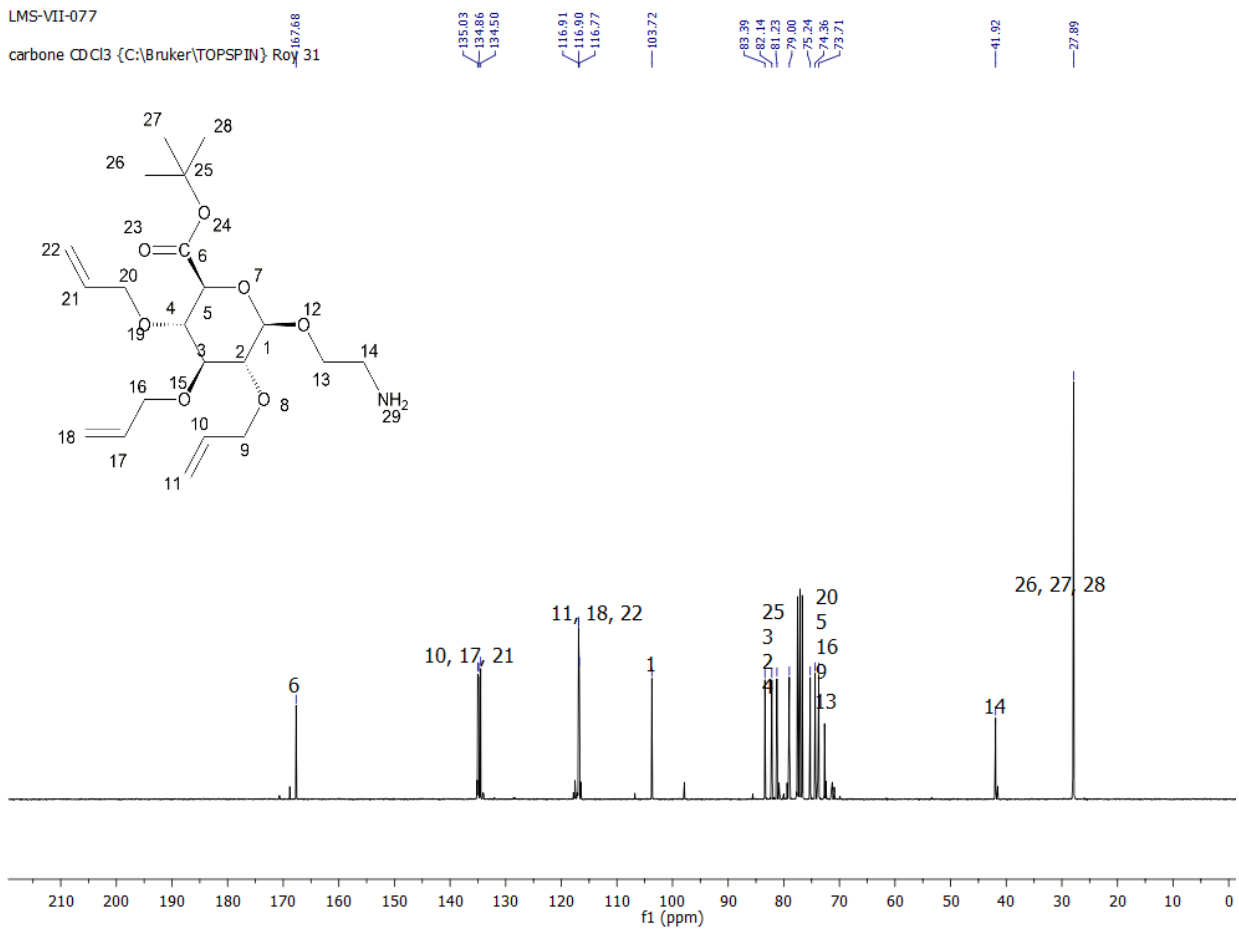

Figure A48. COSY analysis of compound **71** (300 MHz, $CDCl_3$)

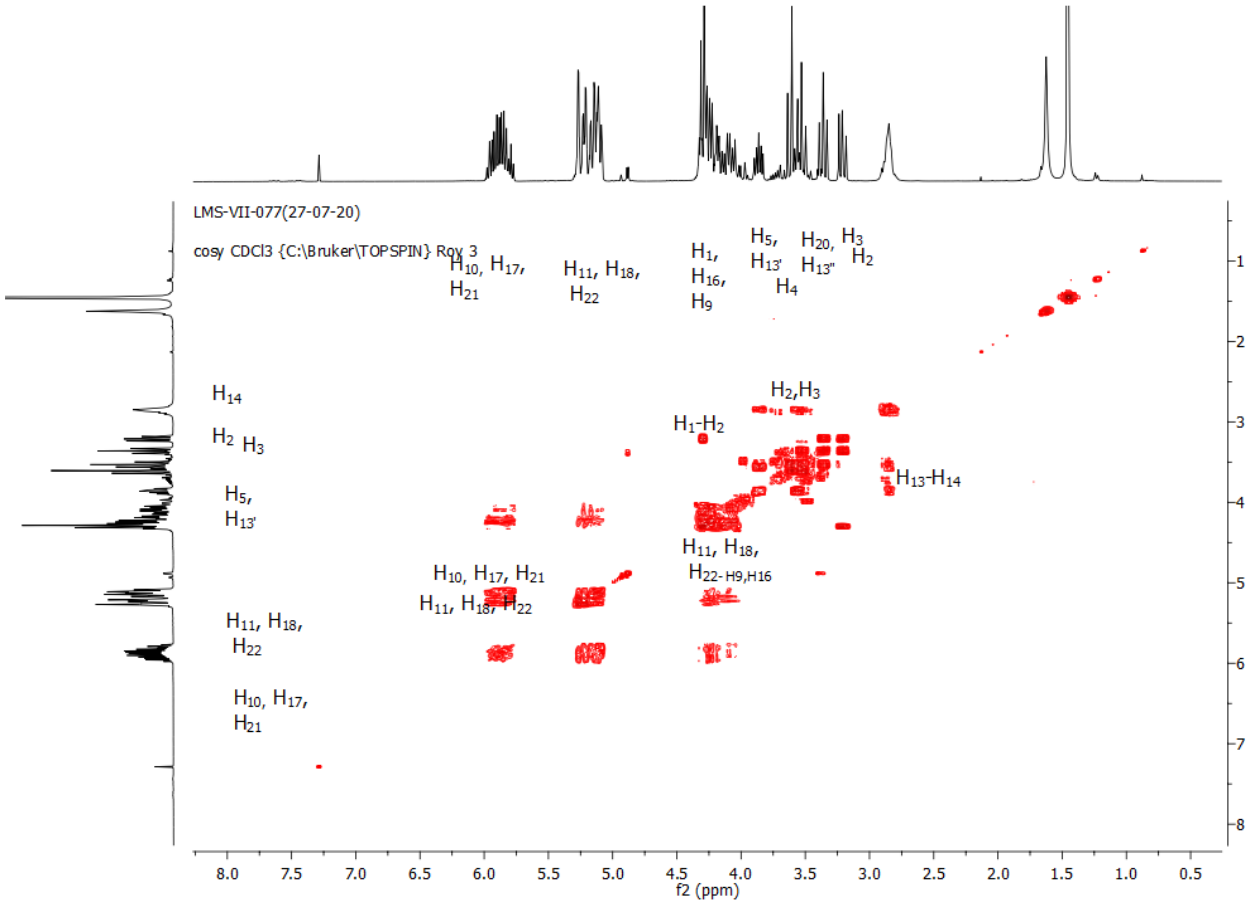

Figure A49. HSQC analysis of compound **71** (300 MHz, $CDCl_3$)

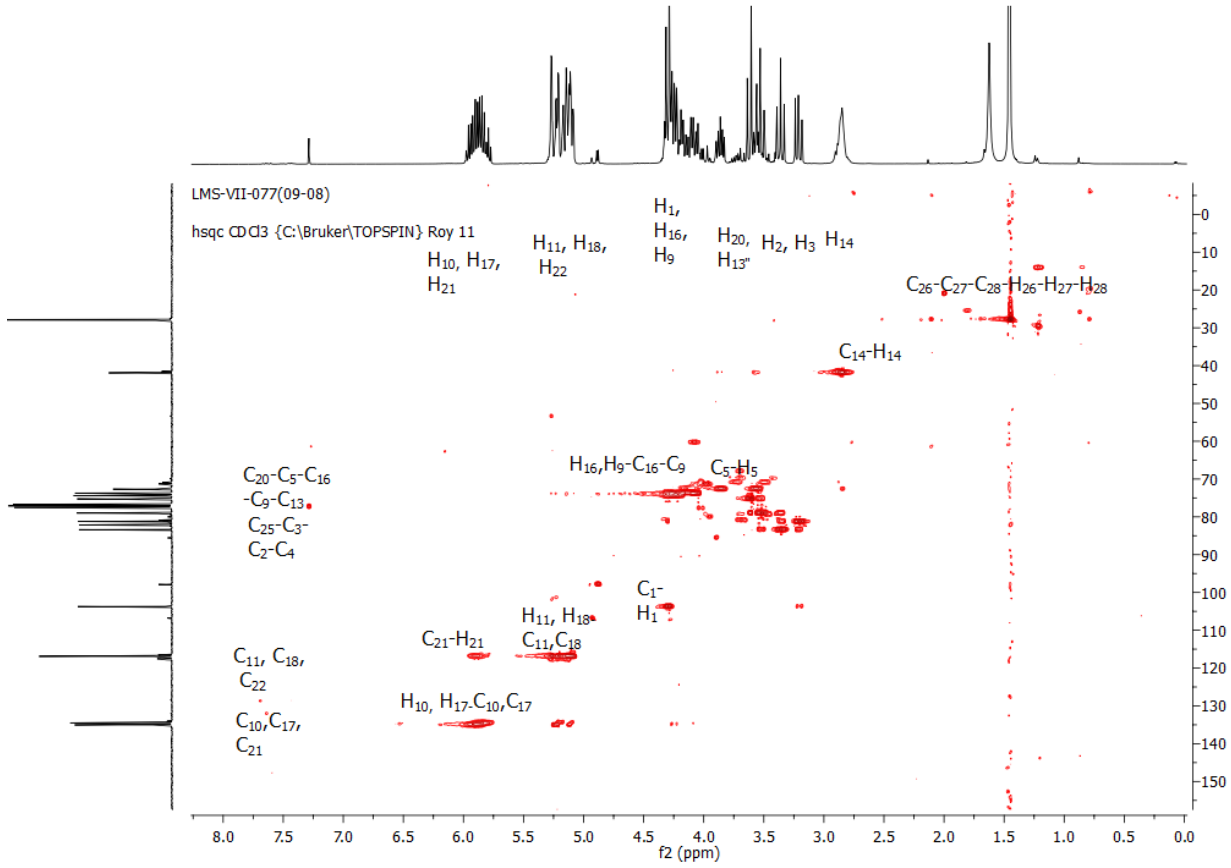

Figure A50. HMBC analysis of compound **71** (300 MHz, $CDCl_3$)

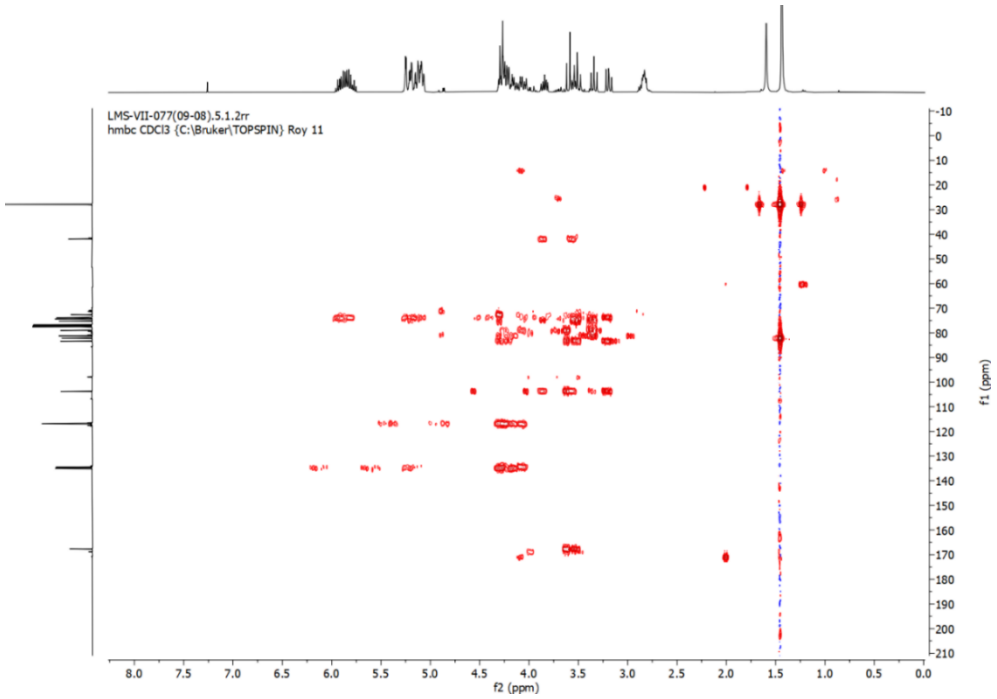

Figure A51. DEPT analysis of compound **71** (300 MHz, $CDCl_3$)

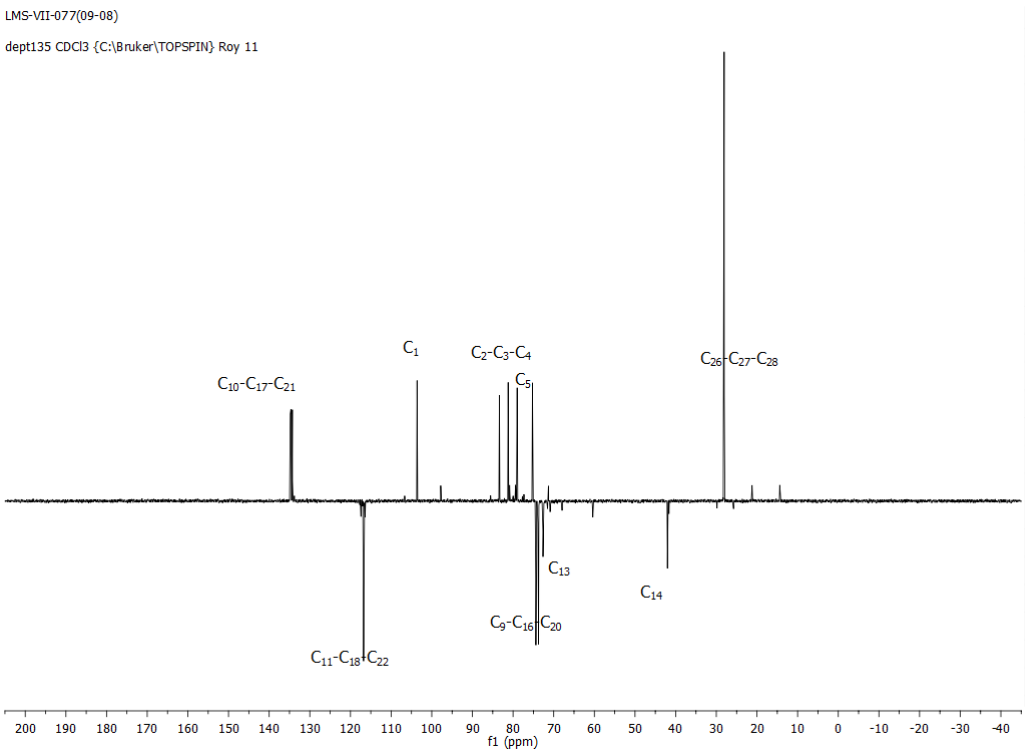

Figure A52. HRMS analysis of compound **71**

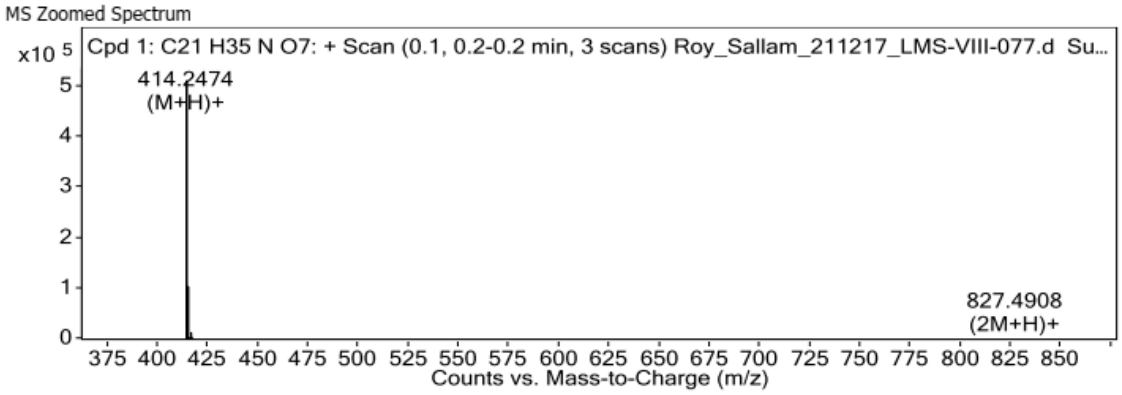

MS Spectrum Peak List

m/z	*Calc m/z*	Diff(ppm)	z	Abund	Formula	Ion
413.2622	413.2646	-5.75		130	C21 H37 N2 O6	(M+NH4)+[-H2O]
414.2474	414.2486	-2.87		518989	C21 H36 N O7	(M+H)+
414.5003				30719		
415.2508	415.2519	-2.88		110464	C21 H36 N O7	(M+H)+
415.5055				2599		
416.253	416.2544	-3.55		15728	C21 H36 N O7	(M+H)+
417.2527	417.2571	-10.56		1991	C21 H36 N O7	(M+H)+
436.2268	436.2306	-8.7	1	1132	C21 H35 N Na O7	(M+Na)+
452.2009	452.2045	-8.07	1	478	C21 H35 K N O7	(M+K)+
827.4908	827.49	1.04	1	182	C42 H71 N2 O14	(2M+H)+

--- End Of Report ---

Compound 75

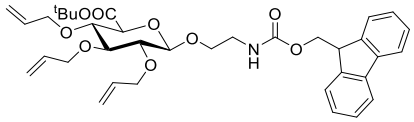

Experimental: To a solution of **71** (1.00 g, 2.42 mmol) in dry dichloromethane (20 mL) was added Fmoc-OSu (1.3 g, 3.86 mmol) and triethylamine (1.2 mL, 8.63 mmol). The reaction mixture was allowed to stir at room temperature overnight before being concentrated and purified by column chromatography (EtOAc/Hexane, 2: 8 %) to give the desired product **75** as a white viscous oil (1.2 g, 78 %). ^{1}H NMR ($CDCl_3$, 300 MHz), 7.76 (d, 2H, *J* = 7.4 Hz, Fm-Ar), 7.60 (d, 2H, *J* = 7.3 Hz, Fm-Ar), 7.40 (t, *J* = 7.3 Hz, 2H, Fm-Ar), 7.31 (td, *J* = 7.4, 1.1 Hz, 2H, Fm-Ar), 6.13 – 5.67 (m, 3H, 3x CH_2=CH-), 5.36 – 5.14 (m, 6H, 3x CH_2=CH), 4.39 (d, 2H, *J* = 6.9 Hz, Fm-CH_2), 4.34 – 4.25 (m, 5H, 2x CH_2=CH-CH_2), 4.22 (d, 1H, *J* = 4.8 Hz, Fm-CH), 4.17 – 4.07 (m, 1H, H_5), 3.90 (dd, 1H, *J* = 9.9, 5.0 Hz, OCH_2), 3.79 – 3.68 (m, 1H, OCH_2), 3.66 (d, 1H, *J* = 9.7 Hz, H_4), 3.59 (d, 1H, *J* = 8.7 Hz, H_3), 3.40 (t, 2H, *J* = 8.8 Hz, -NCH_2), 3.25 (t,1H, H_2), 1.48 (s, 9H, *t-butyl*). ^{13}C NMR (300 MHz, $CDCl_3$) δ 167.6, 156.4, 144.0, 143.9, 141.3, 135.0, 134.8, 134.5, 127.6, 127.0, 125.1, 119.9, 117.1, 117.0, 116.9, 103.7, 83.4, 82.4, 81.1, 78.9, 74.4, 73.8, 73.7, 69.6, 66.7, 47.2, 41.1, 27.9. HRMS (ESI, Q-TOF) *m/z* calcd for $C_{36}H_{45}NO_9$ $[M+Na]^+$ 658.2986, found 658.2981.

Figure A53. ^{1}H NMR analysis of compound **75** (300 MHz, $CDCl_3$)

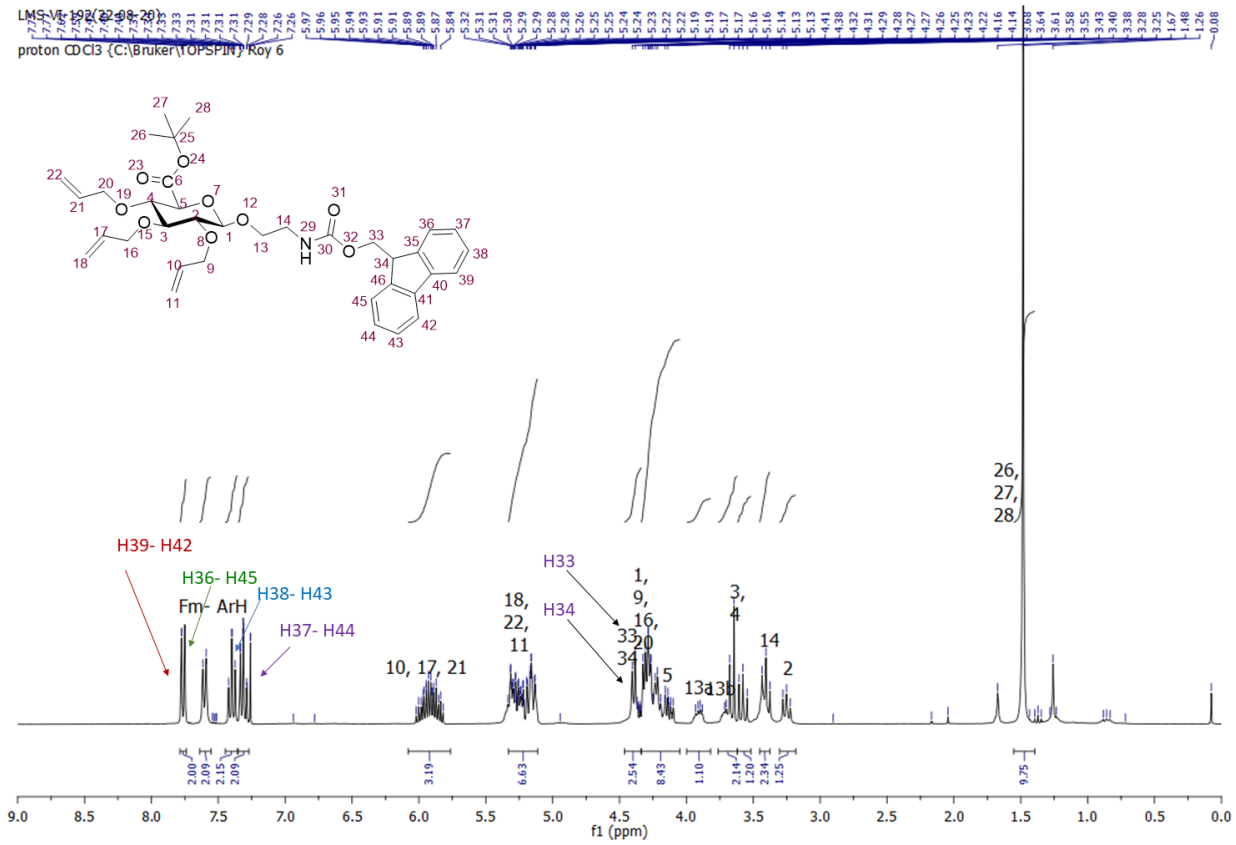

Figure A54. ^{13}C NMR analysis of compound **75** (300 MHz, $CDCl_3$)

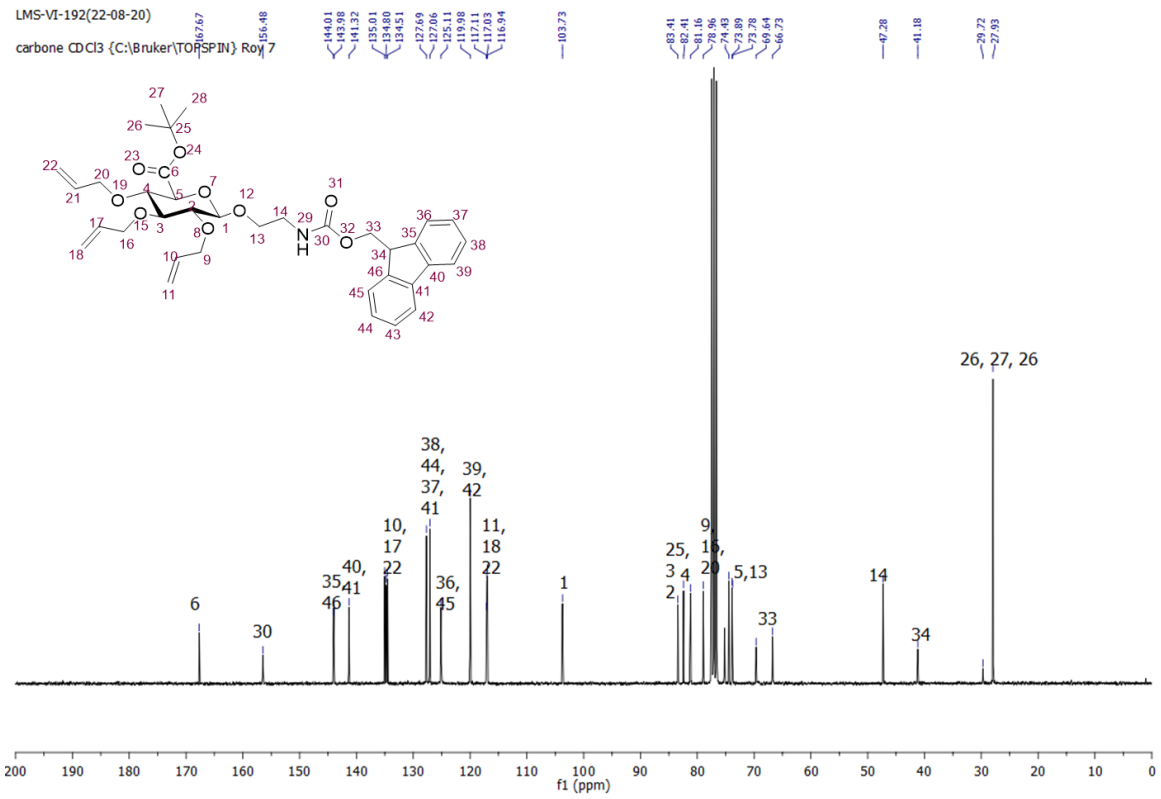

Figure A55. COSY analysis of compound **75** (300 MHz, $CDCl_3$)

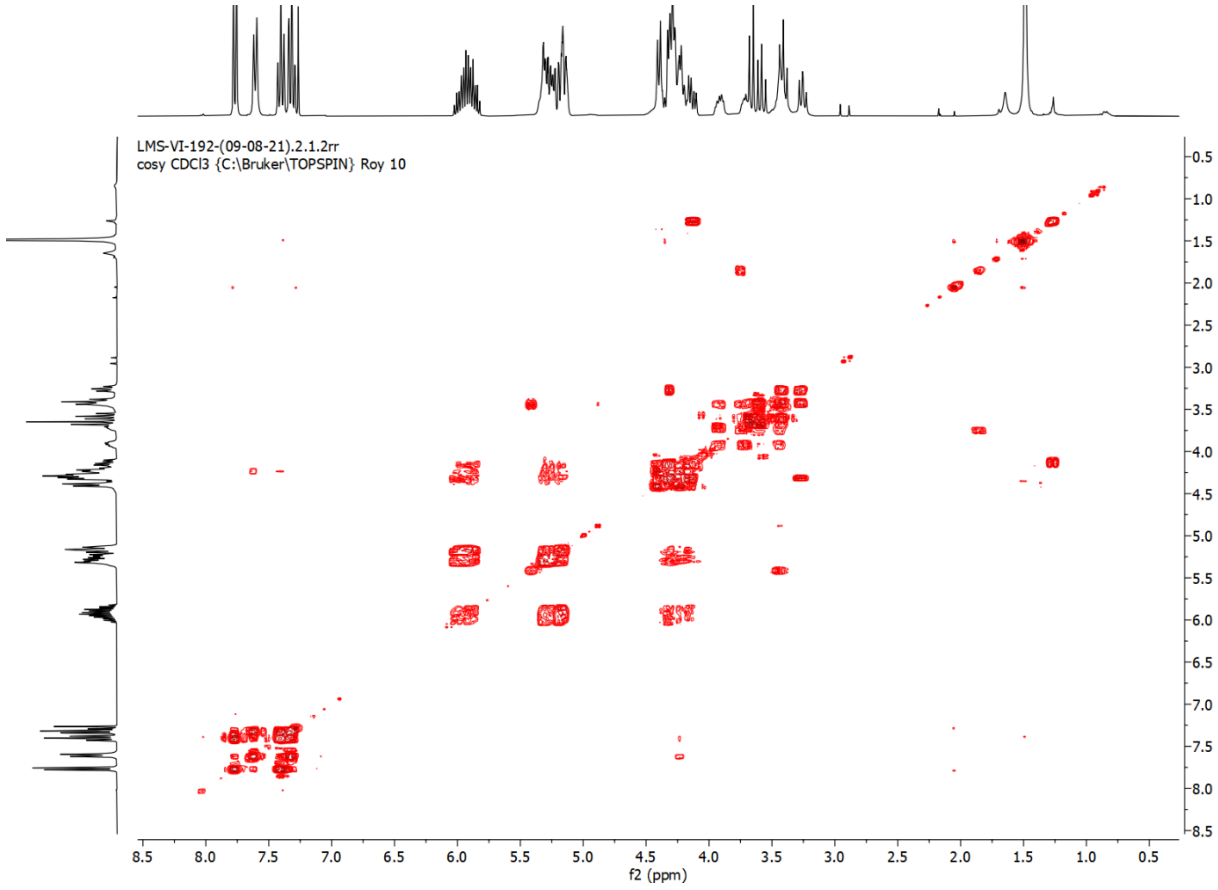

Figure A56. HSQC analysis of compound **75** (300 MHz, $CDCl_3$)

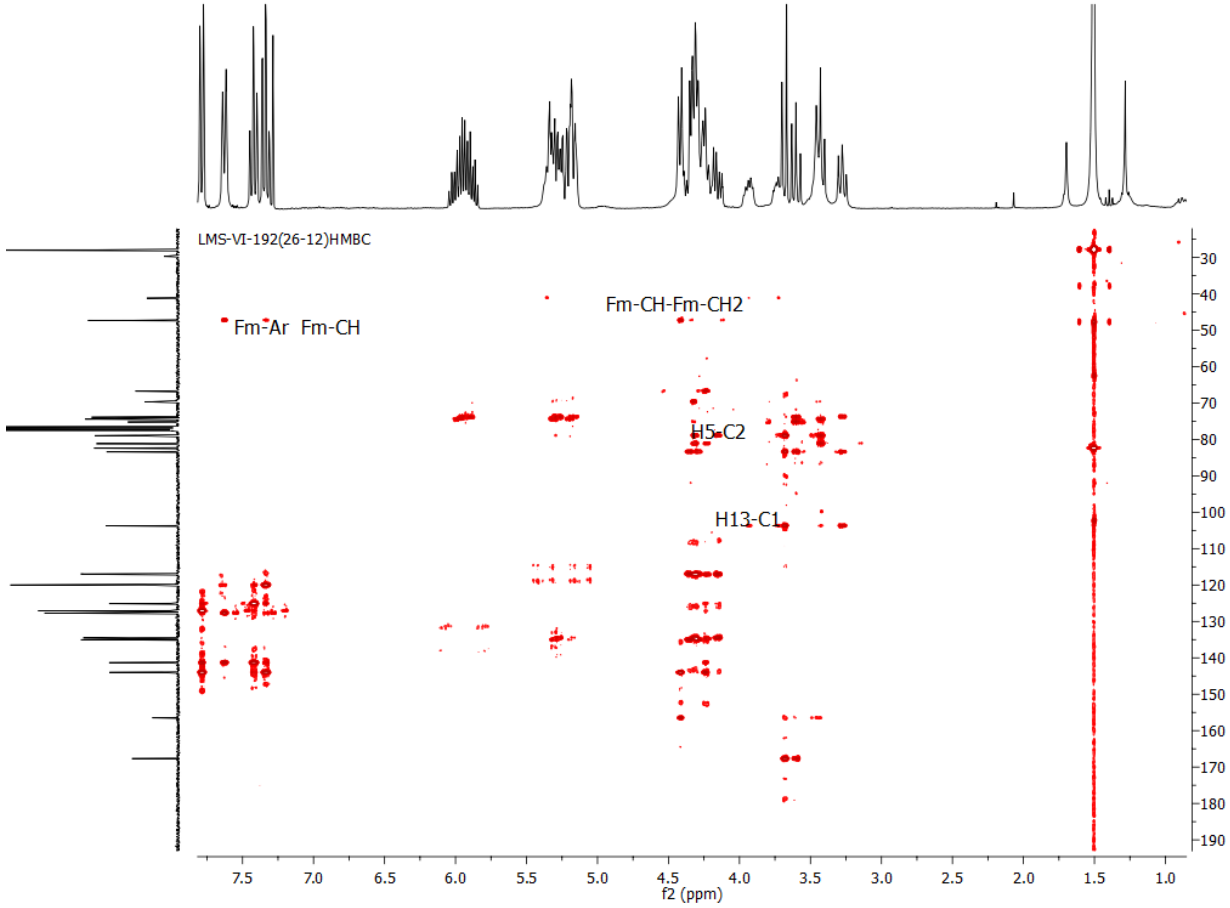

Figure A57. HRMS (ESI, Q-TOF) of compound **75** (300 MHz, $CDCl_3$)

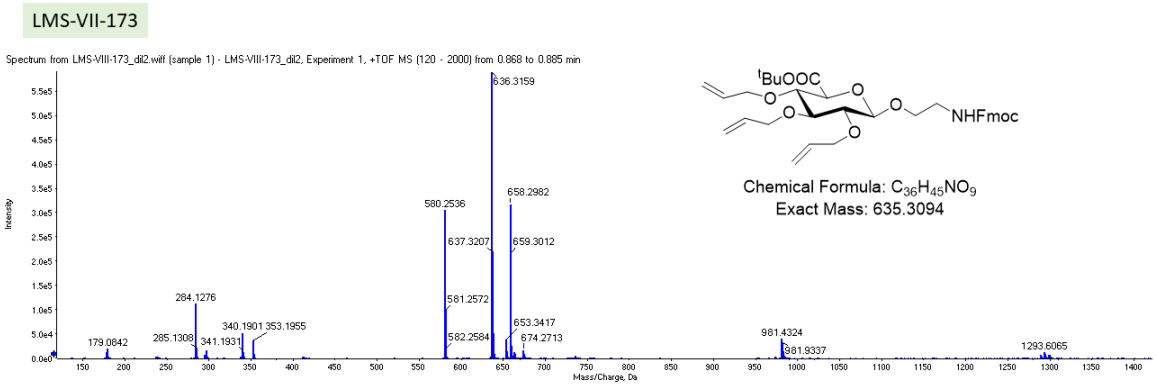

Sample	Formula	Adduct	Neutral mass Da	Calculated *m/z*	Observed *m/z*	PPM	Intensity
LMS-VII-173	C36H45NO9	+H	635.30943	636.31671	636.31634	-0.6	2889311
LMS-VII-173 +Na	C36H45NO9	+Na	635.30943	658.29865	658.29818	-0.7	1545423
LMS-VII-173 - tBu	C32H37NO9	+H	579.24683	580.25411	580.25371	-0.7	1492512
LMS-VII-173 +NH4	C36H45NO9	+NH4	635.30943	653.34326	653.34216	-1.7	187390

Trithiomannoside β-D-glucuronic ester dendron synthesis and characterization

General Photoreaction configuration

All photochemical reactions were conducted using UV-A Hand Lamp-365 nm, the temperature was 25°C. A small stir bar is required for efficient stirring when using Vial.

General Procedure (A), photochemical thiol-ene reaction

Experimental: To a vial equipped with a stir bar was charged with a solution of compound **75** (100 mg, 0.157 mmol), and α-D-mannose thiol (0.44 g, 0.942 mmol) in DMF (0.7 mL). The mixture was sparged by bubbling with nitrogen for 5 minutes. Followed by addition 2,2-Dimethoxy-2-phenylacetophenone **163** (44 mg, 0.172 mmol, 0.2 eq. per each double bond), the reaction mixture was irradiated for 2.5 hours under 356 nm. Following irradiation, the reaction was diluted with ethyl acetate, washed with water, brine, dried over anhyd. Na_2SO_4, and concentrated. The desired product was isolated by flash column chromatography (Hexane/ Ethylacetate 3: 7 %) to afford the product **76** as a white oily crystals (230 mg, 79%).

Photointiator: 2,2-Dimethoxy-2-Phenylacetophenone (DMPA) **163**

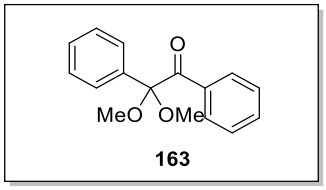

163

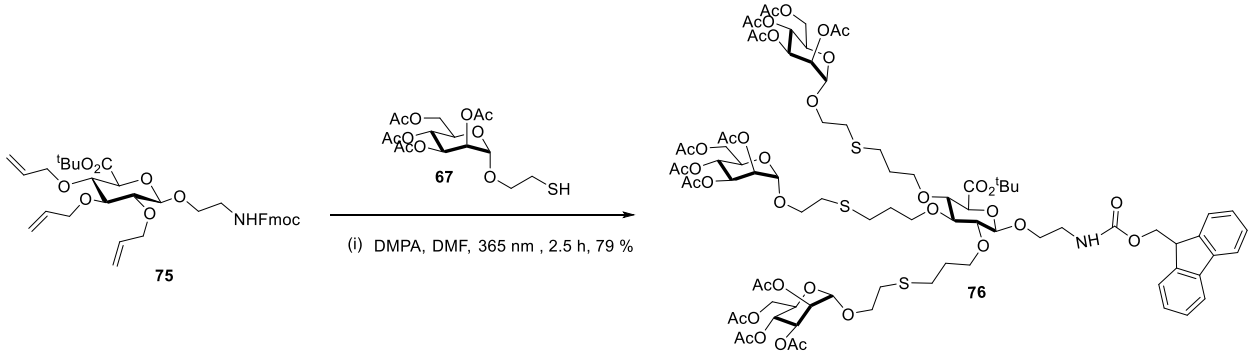

Mannoside dendron 76 characterization

^{1}H NMR (300 MHz, $CDCl_3$) δ 7.74 (d, 2H, *J* = 7.4 Hz, Ar), 7.59 (d, 2H, *J* = 7.3 Hz, Ar), 7.33 (ddd, 4H, *J* = 13.9, 11.1, 6.9 Hz, Ar), 5.39- 5.10 (m 3.93 – 3.72 (m, 4H), 9H, H2-H4 man), 4.93- 4.76 (m, 3H, H1 man), 4.54- 4.14 (m, 7H), 3.74- 3.52 (m, 7H), 3.52- 3.29 (m, 3H), 3.24 (t, 1H, *J* = 8.8 Hz), 3.10 (t, 1H, *J* = 8.2 Hz), 2.8- 2.64 (m, 12H), 2.14 (s, 9H), 2.08 (s, 9H), 2.02 (s, 9H), 1.96 (s, 9H), 1.91–1.69 (m, 6H), 1.48 (s, 9H). ^{13}C NMR (300 MHz, $CDCl_3$) δ 170.6, 170.0, 169.8, 169.8, 169.8, 169.7, 167.6, 156.4, 144.0, 143.9, 141.2, 127.6, 127.0, 125.1, 119.9, 103.7, 97.6, 83.9, 82.3, 81.7, 77.2, 77.0, 76.6, 75.2, 71.7, 71.2, 70.9, 69.5, 69.0, 68.7, 67.9, 67.9, 66.6, 66.0, 62.4, 60.3, 47.2, 41.2, 31.1, 30.5, 30.5, 30.3, 29.3, 29.2, 27.9, 20.8, 20.7, 20.7, 20.6, 14.2. HRMS (ESI, Q-TOF): *m/z* calcd for $C_{84}H_{117}NO_{39}S_3$ [M+Na$^+$] 1882.62571, found 1882.6239.

Figure A58. ^{1}H NMR analysis of **76 (**300 MHz**,** $CDCl_3$**)**

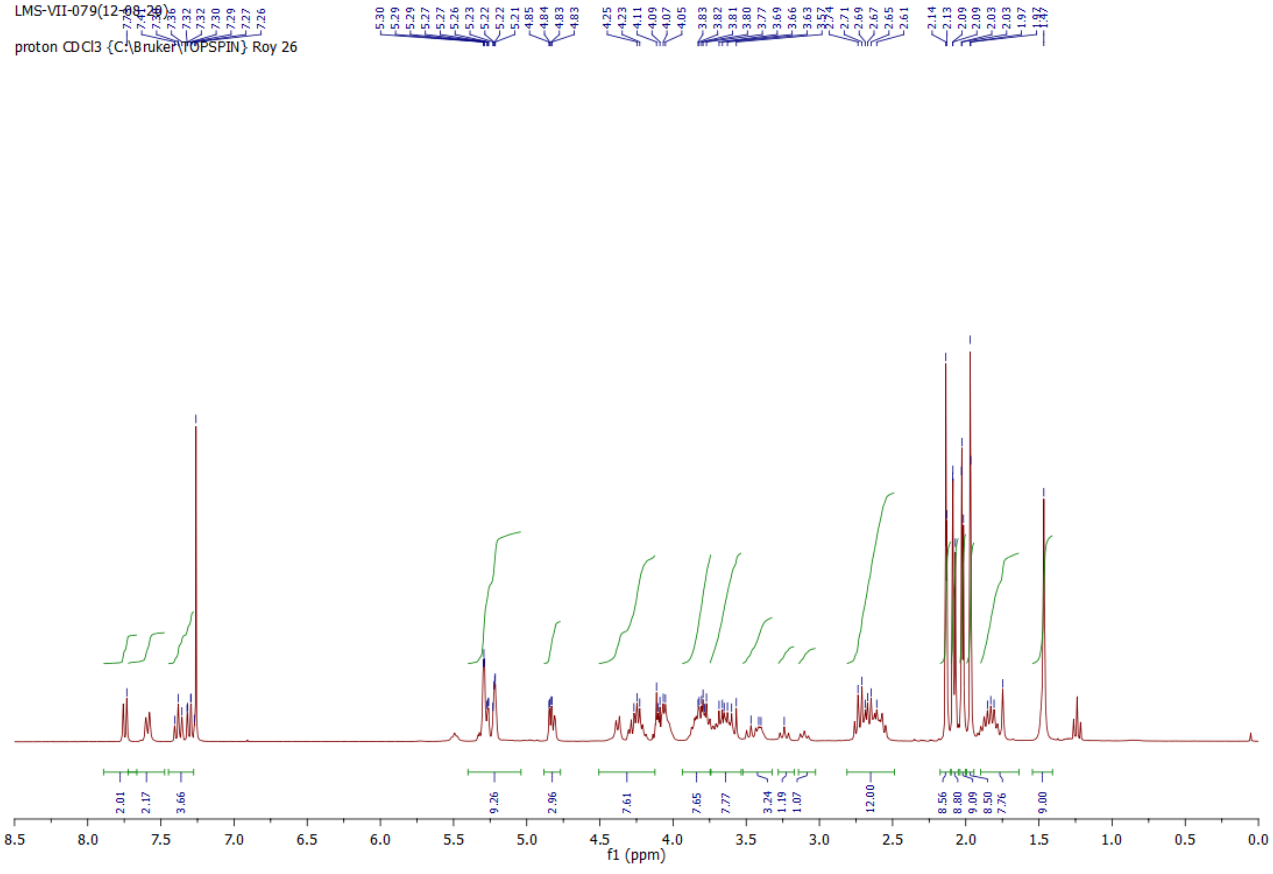

Figure A59. ^{13}C NMR analysis of **76 (**300 MHz**,** $CDCl_3$**)**

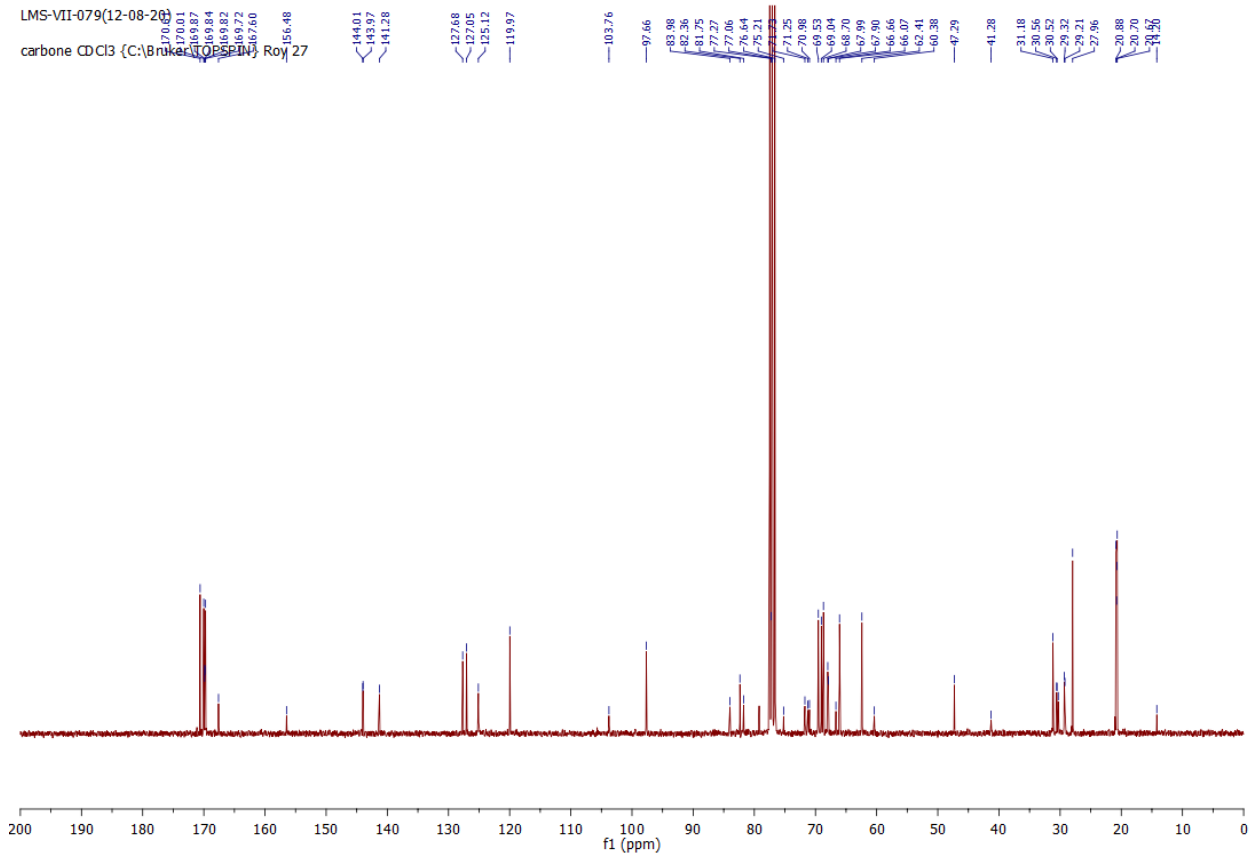

Figure A60. COSY analysis of **76** (300 MHz, $CDCl_3$)

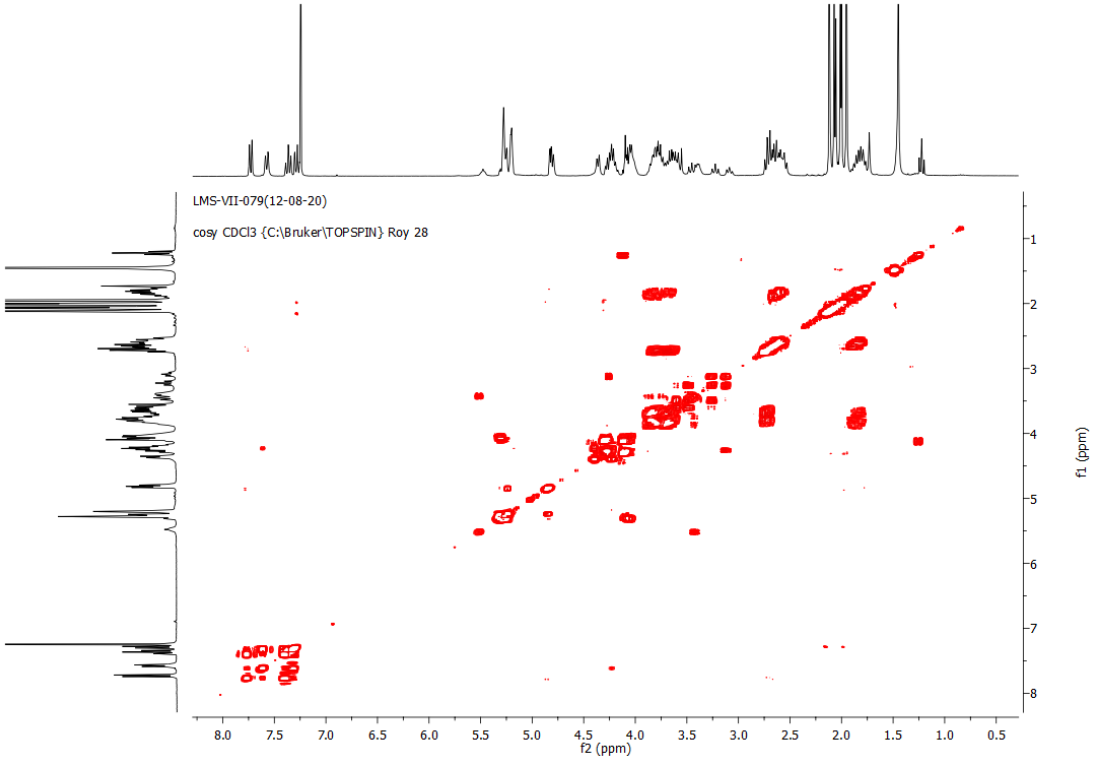

Figure A61. HRMS TOF **(**QTOF) analysis of compound **76**

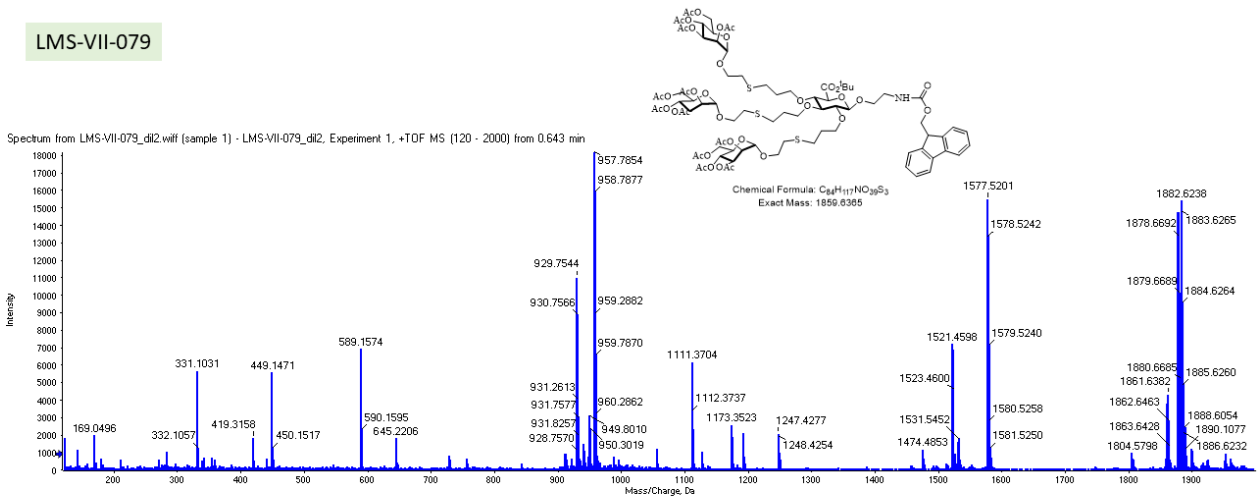

Sample	Formula	Adduct	Neutral mass Da	Calculated *m/z*	Observed *m/z*	PPM	Intensity
LMS-VII-079 MH+	C84H117NO39S3	+H	1859.63649	1860.64377	1860.6403	-1.9	15881
LMS-VII-079 +NH4	C84H117NO39S3	+NH4	1859.63649	1877.67032	1877.66782	-1.3	56217
LMS-VII-079 + Na	C84H117NO39S3	+Na	1859.63649	1882.62571	1882.6239	-1	60608
LMS-VII-079 [M+2H]+2	C84H117NO39S3	+2H	1859.63649	930.82552	930.82337	-2.3	18649
LMS-VII-079- Fmoc	C67H100O36S3	+H	1576.51565	1577.52292	1577.5213	-1	63401
LMS-VII-079 - Fmoc - tBu	C63H92O36S3	+H	1520.45305	1521.46032	1521.45862	-1.1	30327

General Procedure for deprotection in ammonia/methanol (gram scale)

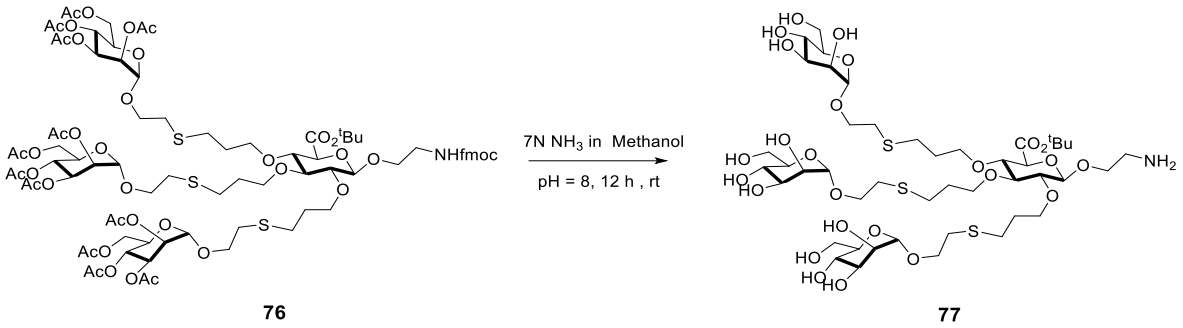

76 77

Experimental: A solution of compound **69** (600 mg, 0.332 mmol) was dissolved in 7N solution of ammonia/methanol (200 mL) at 0 ºC and the reaction mixture was adjusted to pH= 8. The reaction mixture stirred at room temperature for 12 h. After evaporation of the solvent under reduced pressure, the resulting residue redissolved in methanol and filtered through a bed of celite. The filtrate evaporated under reduced pressure, the resulting residue was extensively rinsed with chloroform several times to remove the side products, then left under vacuum to dryness to afford the product as a white amorphous mass. The yield was determined by ^{1}H NMR analysis of the crude product (0.33 g, 90%).^{1}H NMR (300 MHz, D_2O) δ 5.03- 4.83 (m, 10H), 4.13-3.84 (m, 14H), 3.86 – 3.71 (m, 12H), 3.65 (dt, 12H, *J* = 15.5, 11.7 Hz), 3.52-3.40 (m, 3H), 3.00 (d, 3H, *J* = 5.4 Hz), 2.95-2.74 (m, 6H), 2.77 – 2.53 (m, 6H), 2.00-1.75 (m, 6H), 1.53 (s, 9H); ESI-HRMS (*m/z*) calcd for $C_{45}H_{83}NO_{25}S_3$ $[M+H]^+$ 1134.4489, found: 1134.4504.

Figure A62. ^{1}H NMR analysis of **77** (300 MHz, D_2O)

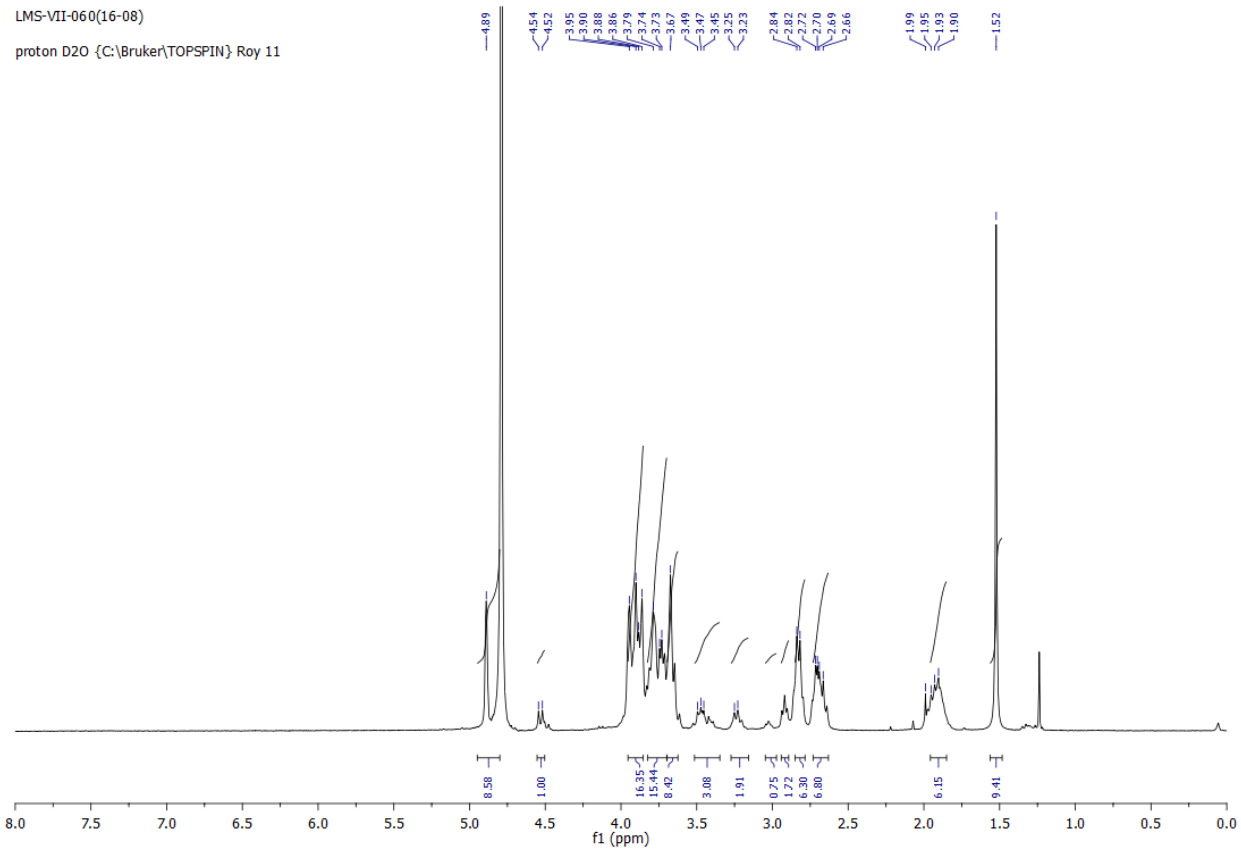

Figure A63. ^{13}C NMR analysis of **77** (300 MHz, D_2O)

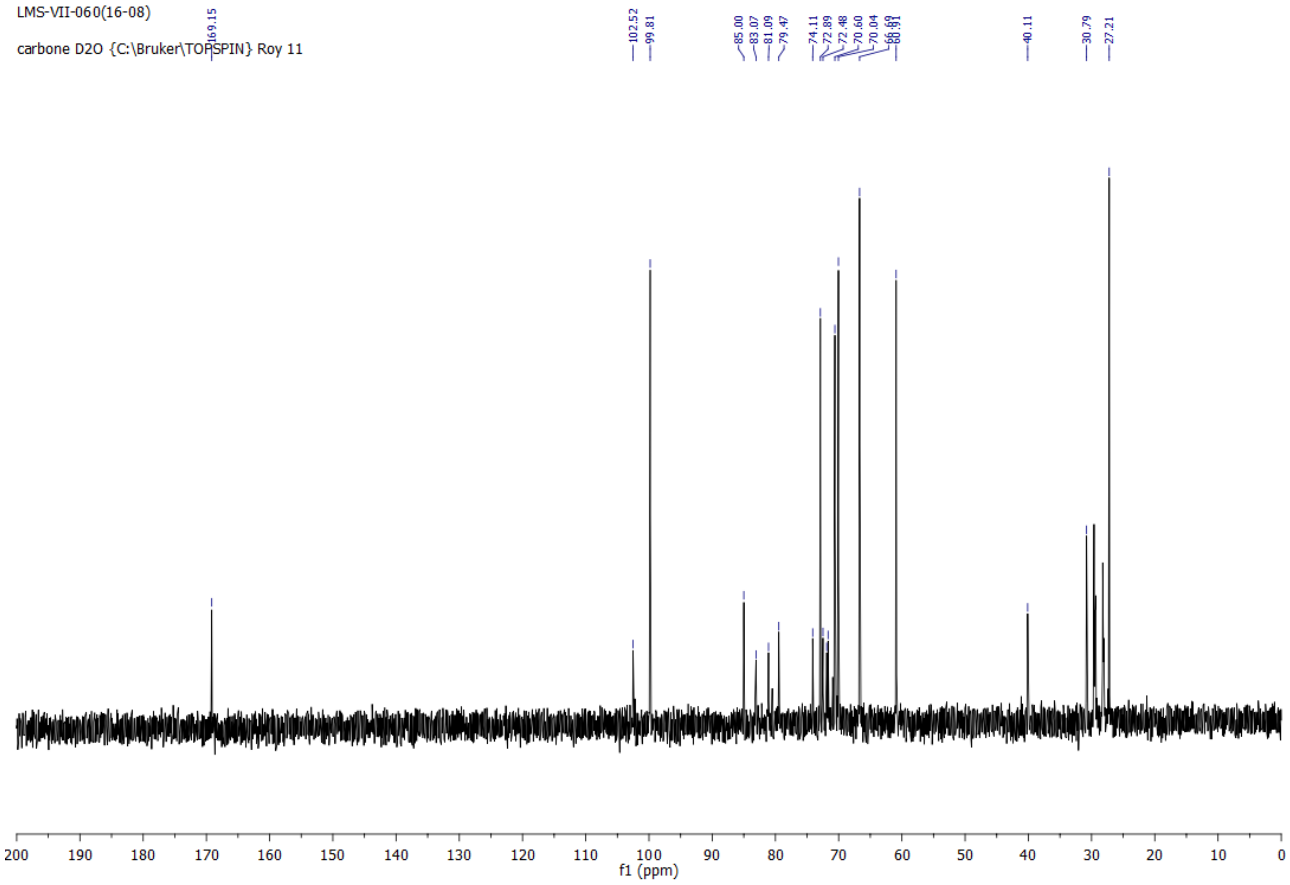

Figure A64. COSY analysis of **77** (300 MHz, D_2O)

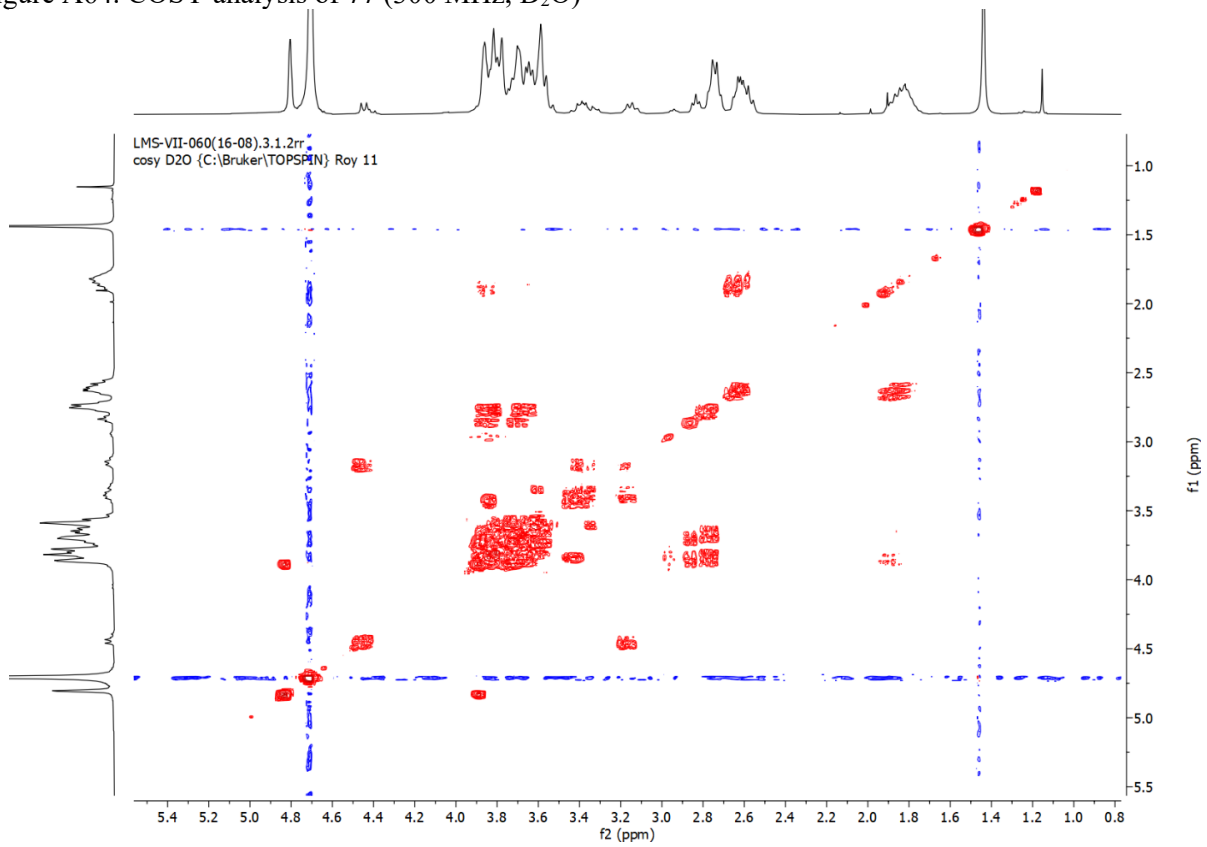

Figure A65. HSQC analysis of **77** (300 MHz, D_2O)

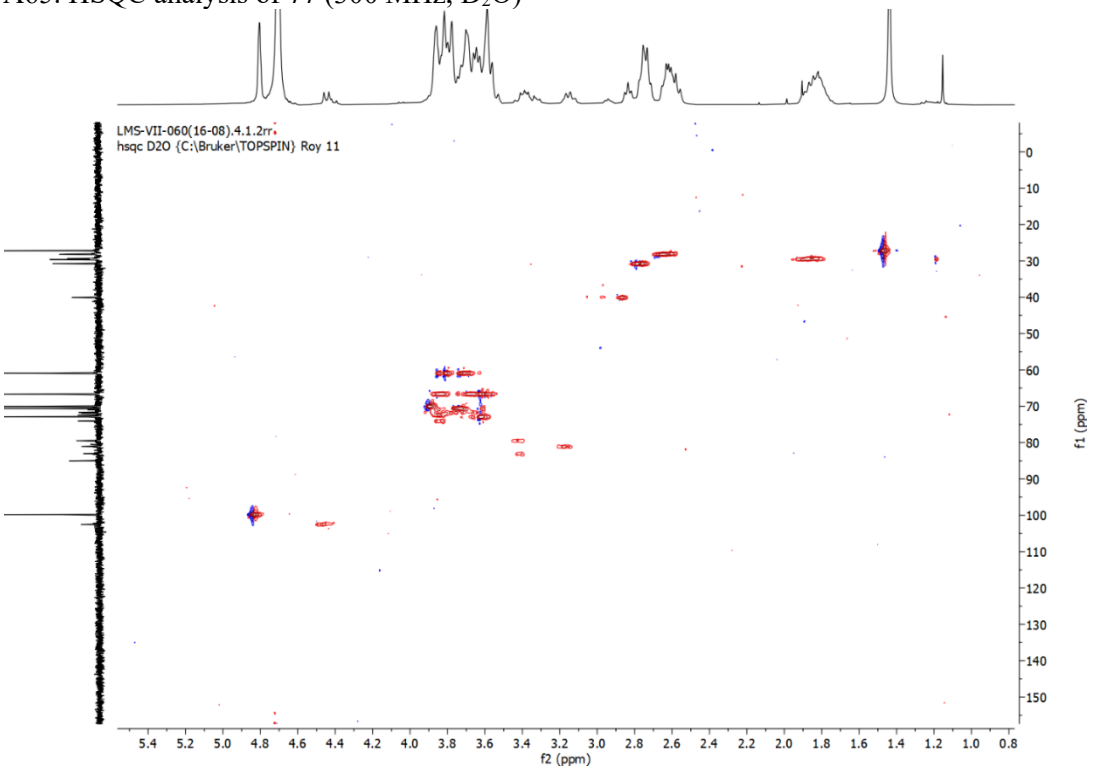

Figure A66. HRMS analysis of **77**

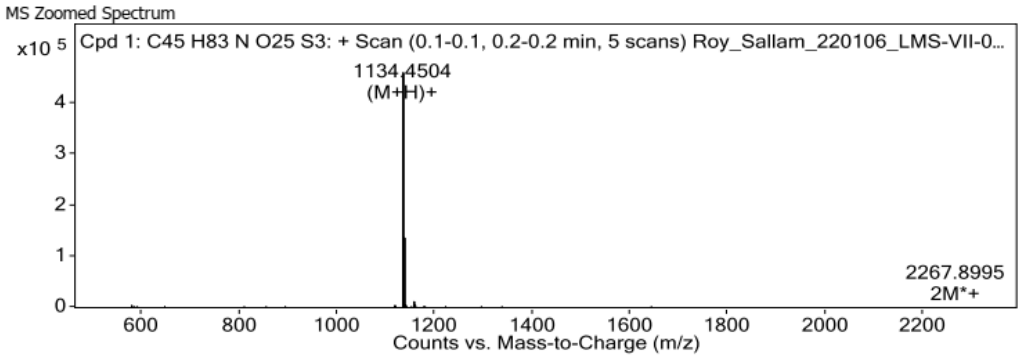

MS Spectrum Peak List

m/z	*Calc m/z*	Diff(ppm)	z	Abund	Formula	Ion
567.7295	567.7281	2.46	2	174	C45 H85 N O25 S3	(M+2H)+2
1116.4391	1116.4383	0.68	1	4893	C45 H82 N O24 S3	(M+H)+[-H2O]
1133.4408	1133.4411	-0.28		162	C45 H83 N O25 S3	M*+
1134.4504	1134.4489	1.36		460509	C45 H84 N O25 S3	(M+H)+
1135.4536	1135.4521	1.3		241666	C45 H84 N O25 S3	(M+H)+
1136.4524	1136.4506	1.61		136341	C45 H84 N O25 S3	(M+H)+
1156.433	1156.4309	1.86	1	14203	C45 H83 N Na O25 S3	(M+Na)+
1172.4119	1172.4048	6.08	1	574	C45 H83 K N O25 S3	(M+K)+
2267.8995	2267.8859	5.97	1	311	C90 H166 N2 O50 S6	2M*+
2289.8862	2289.8725	5.99	1	64	C90 H166 N2 Na O50 S6	(2M+Na)+

--- End Of Report ---

Diazo transfer procedure using imidazole-1-sulfonyl azide

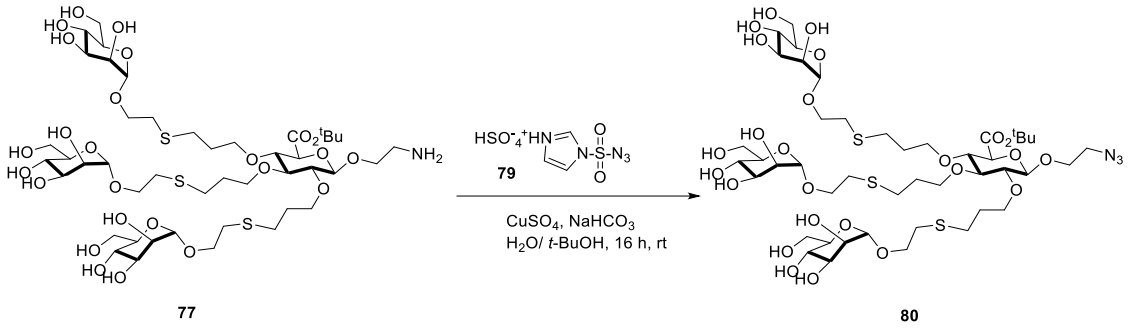

Stick reagent **79** has been synthesized according to the literature. [380]

Experimental: To a mixture of (200 mg, 0.176 mmol, 1 equiv), $NaHCO_3$ (60 mg, 0.71 mmol, 4 equiv), water (2 mL), and 1 M aq $CuSO_4$ (0.04 equiv) were added imidazolsulfonyl azide sulfate (70 mg, 0.26 mmol, 1.5 eqv.), followed by *t*-BuOH (14 mL), such that the final ratio of H_2O/*t*-BuOH was 1/6.7. The solution was stirred vigorously at room temperature for 16 h. The crude reaction was filtered through a pad of celite, washed multiple times with methanol, and the filtrate was concentrated under reduced pressure and loaded onto dry silica gel. The product was purified using (Acetonitile /H_2O 80 :20 %), the fractions collected and the solvent removed under reduced pressure. Subsequently the product was freeze-dried to remove water. The desired product **80** was isolated as a pale-yellow oil (180 mg, 83%). ^{1}H NMR (600 MHz, D_2O) 4.96- 4.86 (m, 1H), 4.54 (dd, 2H, J = 27.7, 7.5 Hz), 4.05 (dd, 2H, J = 53.9, 43.0 Hz), 3.90 (dd, 14H, J = 44.1, 31.5 Hz), 3.85- 3.71 (m, 14H), 3.71- 3.62 (m, 7H), 3.61- 3.40 (m, 5H), 3.36 (s, 1H), 3.22 (dd, 2H, J = 41.3, 33.1 Hz), 2.98- 2.79 (m, 6H), 2.66 (dd, 6H, J = 26.8, 20.2 Hz), 2.11- 1.75 (m, 6H), 1.54 (s, 9H).^{13}C NMR (300 MHz, D_2O) δ 99.9, 82.8, 72.8, 70.8, 70.2, 66.8, 66.4, 60.8, 30.9, 30.1, 29.3, 28.6, 27.7, 21.7, 20.3; ESI-HRMS (*m/z*) calcd for $C_{45}H_{81}N_3O_{25}S_3$ $[M+Na]^+$ 1182.4213, found 1182.4216.

Figure A67. ^{1}H NMR analysis of **80** (300 MHz, D_2O)

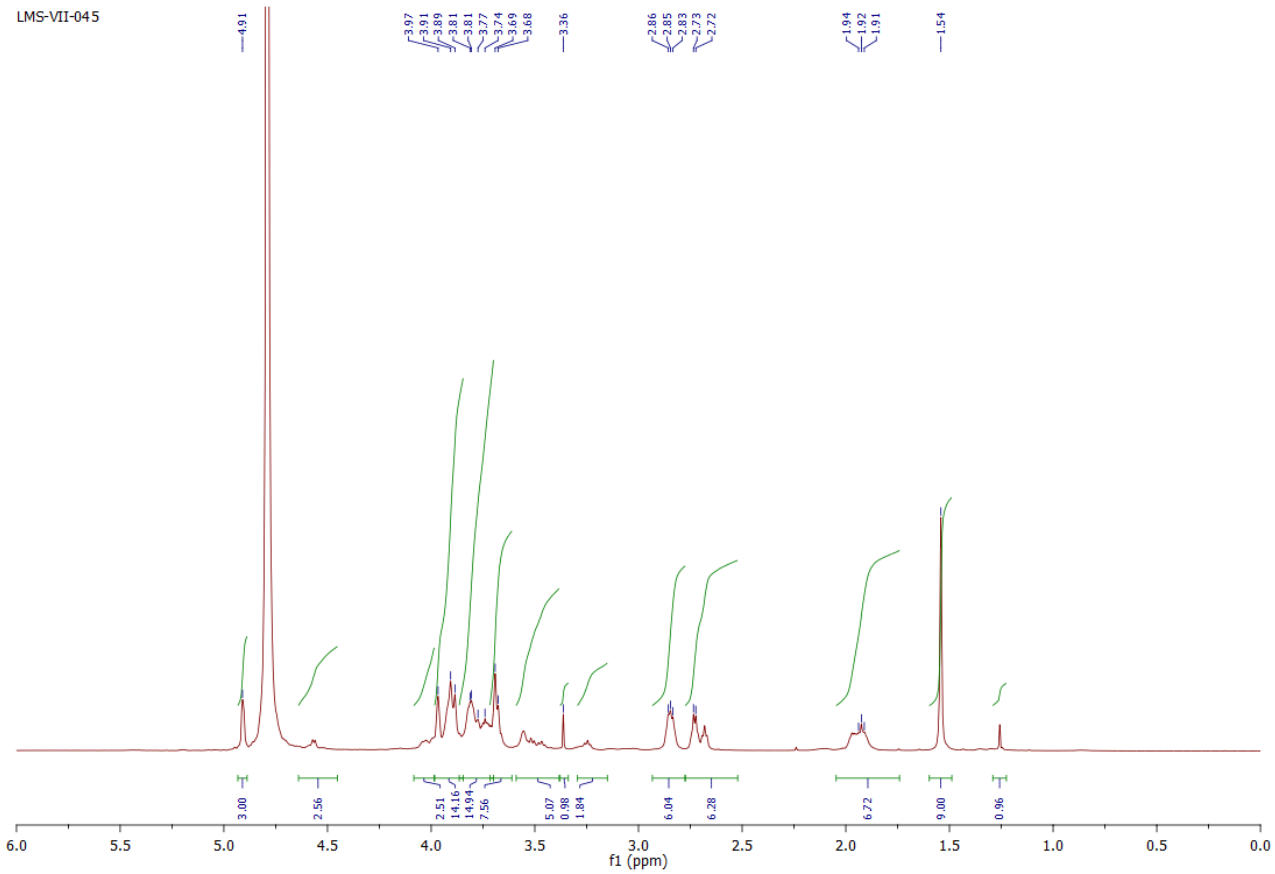

Figure A68. ^{13}C NMR analysis of **80** (300 MHz, D_2O)

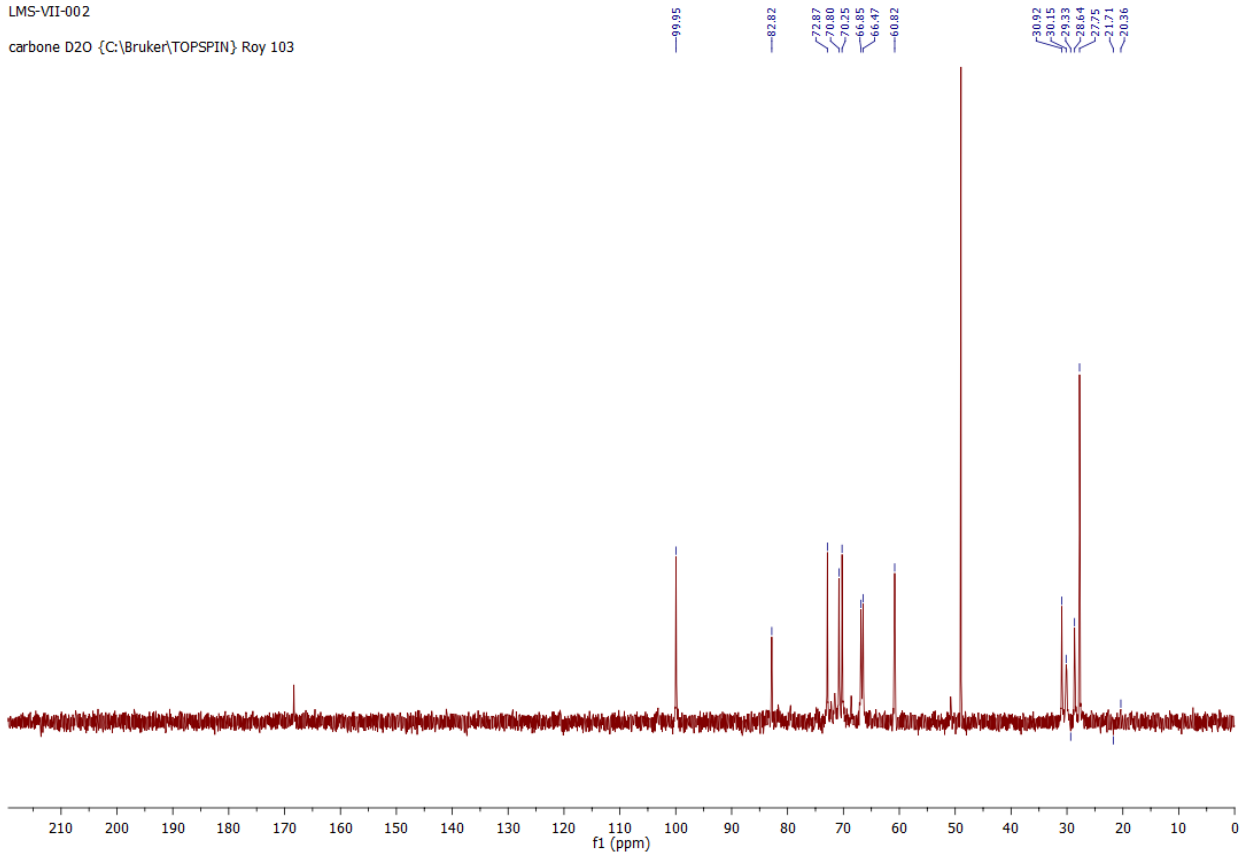

Figure A69. IR analysis of **80**

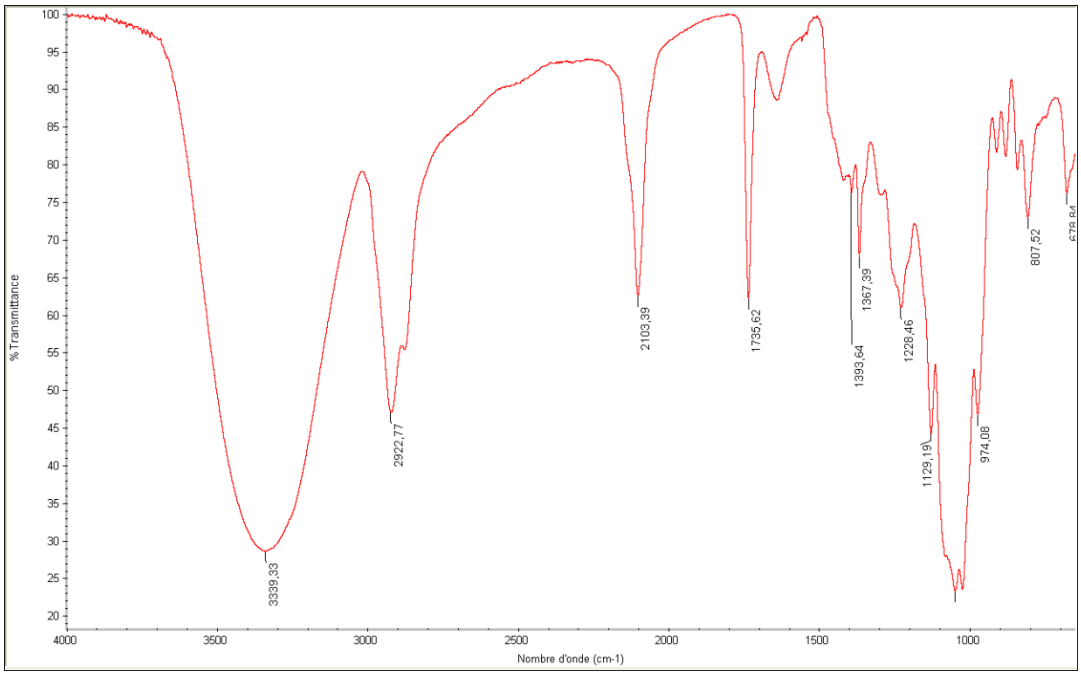

Figure A70**.** HRMS analysis of **80**

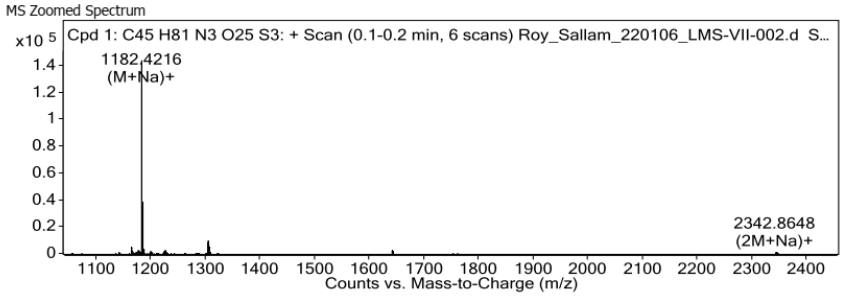

MS Spectrum Peak List

m/z	*Calc m/z*	Diff(ppm)	z	Abund	Formula	Ion
1142.4265	1142.4288	-2.01	1	1407	C45 H80 N3 O24 S3	(M+H)+[-H2O]
1159.4404	1159.4316	7.57	1	289	C45 H81 N3 O25 S3	M*+
1164.4114	1164.4108	0.52	1	5442	C45 H79 N3 Na O24 S3	(M+Na)+[-H2O]
1177.4551	1177.466	-9.2	1	3547	C45 H85 N4 O25 S3	(M+NH4)+
1182.4216	1182.4213	0.21		144732	C45 H81 N3 Na O25 S3	(M+Na)+
1183.4246	1183.4245	0.13		70452	C45 H81 N3 Na O25 S3	(M+Na)+
1184.4238	1184.423	0.71		39443	C45 H81 N3 Na O25 S3	(M+Na)+
2323.8486	2323.8429	2.45	1	61	C90 H160 N6 Na O49 S6	(2M+Na)+[-H2O]
2341.8557	2341.8535	0.94	1	1376	C90 H162 N6 Na O50 S6	(2M+Na)+
2357.839	2357.8274	4.9	1	67	C90 H162 K N6 O50 S6	(2M+K)+

--- End Of Report ---

Trithiofucoside β-D-glucuronic ester dendron synthesis and characterization

General Procedure for photochemical reaction

Experimental: To a vial equipped with a stir bar was charged with a solution of β-D-glucuronic ester derivative **75** (100 mg, 0.157 mmol), and α-L-fucose thiol **63** (0.9 g, 2.088 mmol) in DMF (0.7 mL). The mixture was sparged by bubbling with nitrogen for 5 minutes. Followed by addition 2,2-Dimethoxy-2-phenylacetophenone (44 mg, 0.22 mmol, 0.2 eq. per each double bond) the reaction mixture was irradiated for 3 hours under 356 nm. The reaction was diluted with ethyl acetate, washed with water, brine, dried over anhyd. Na_2SO_4, and concentrated. The crude reaction mixture was purified by flash column chromatography using (DCM/ MeOH 3:97%), to afford the desired product **81** as a white solid crystals (200 mg, 66 %).

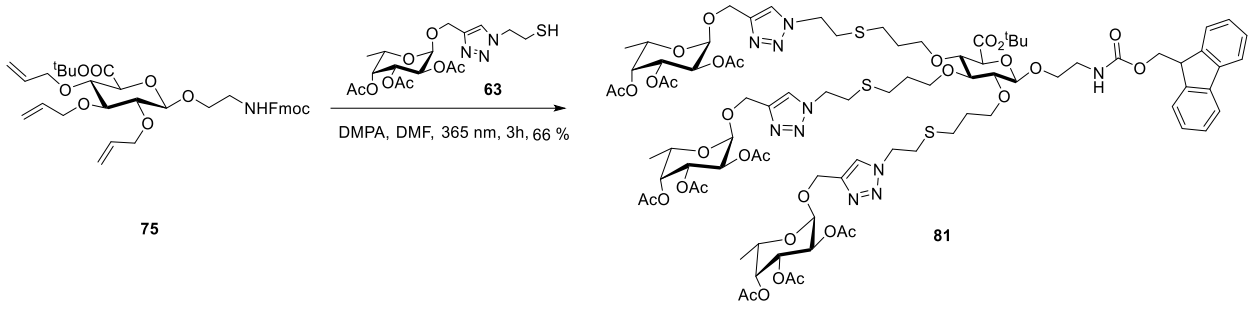

Characteriazation of Fuc-dendron **81**

^{1}H NMR (300 MHz, $CDCl_3$) δ 7.75 (d, 2H, *J* = 7.4 Hz, Ar), 7.63 (dd, 3H, *J* = 9.4, 5.9 Hz, triazole), 7.61-7.52 (m, 2H, Ar), 7.34 (dt, 4H, *J* = 25.9, 6.5 Hz, Ar), 5.33 (ddd, 3H, *J* = 10.5, 3.2, 1.8 Hz, H1, Fucoside), 5.27 (d, 3H, *J* = 3.3 Hz), 5.19 – 5.05 (m, 8H), 4.81 (dt, 3H, *J* = 12.9, 6.5 Hz), 4.70 – 4.60 (m, 6H), 4.53 (d, 6H, *J* = 7.4 Hz), 4.53 (dd, 1H, *J* = 14.0, 6.6 Hz), 4.39 (d, 1H, *J* = 6.9 Hz, H1, Gluc.), 4.19 (dd, 3H, *J* = 6.1, 3.1 Hz), 3.86 – 3.68 (m, 7H), 3.67– 3.48 (m, 3H), 3.50 – 3.35 (m, 2H), 3.28 – 3.11 (m, 3H), 3.09 – 2.88 (m, 6H), 2.65 – 2.41 (m, 6H), 2.15 (s, 9H, OAc), 2.02 (s, 9H, OAc), 1.95 (s, 9H, OAc), 7.75 (d, *J* = 7.4 Hz, 1H), 1.82 (dt, 6H, *J* = 18.7, 6.7 Hz), 1.47 (s, 9H, *tert*-butyl), 1.12 (dt, *J* = 6.1, 2.7 Hz, 9H, 3xCH_3). ^{13}C NMR (300 MHz, $CDCl_3$) δ 170.6, 170.3, 170.0, 167.5, 156.4, 143.9, 141.2, 127.7, 127.0, 125.1, 123.4, 123.1, 120.0, 95.7, 95.6, 95.6, 83.9, 82.4, 81.7, 79.2, 71.1, 68.0, 67.9, 64.7, 61.2, 61.1, 61.1, 50.0, 48.7, 47.2, 37.7, 31.9, 30.3, 28.9, 28.8, 27.9, 20.8, 20.7, 20.6, 15.8. ESI-HRMS (*m/z*) calcd for $C_{87}H_{120}N_{10}O_{33}S_3$ $[M+H]^+$ 1929.7207, found 1930.7310.

Figure A71. ^{1}H NMR analysis of **81 (**300 MHz, $CDCl_3$**)**

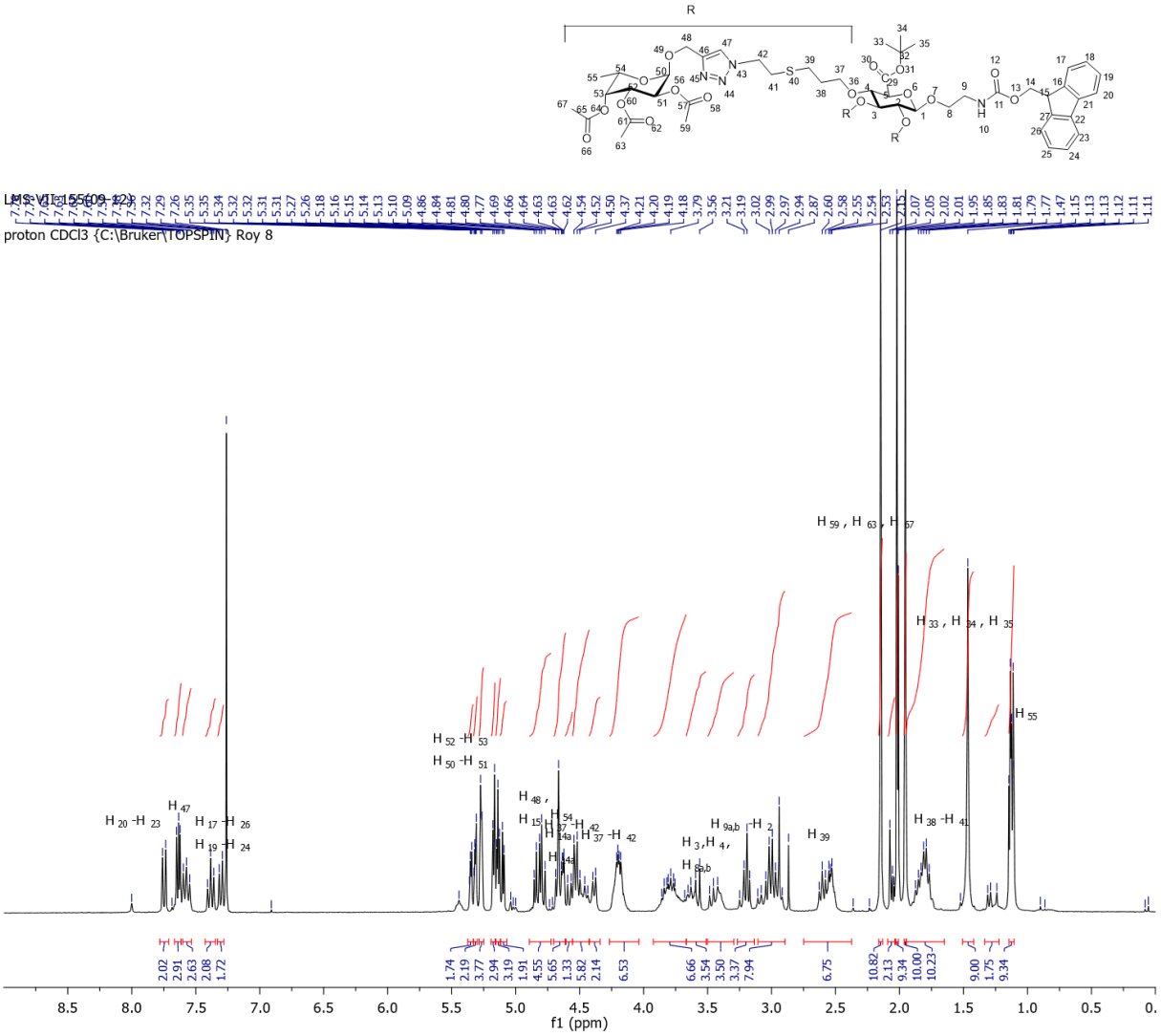

Figure A72. ^{13}C NMR analysis of **81** (300 MHz, $CDCl_3$)

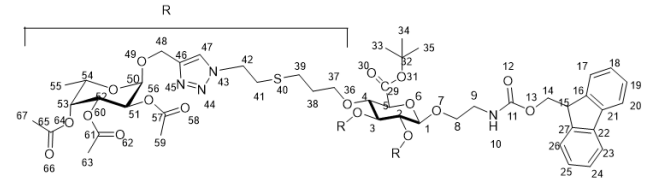

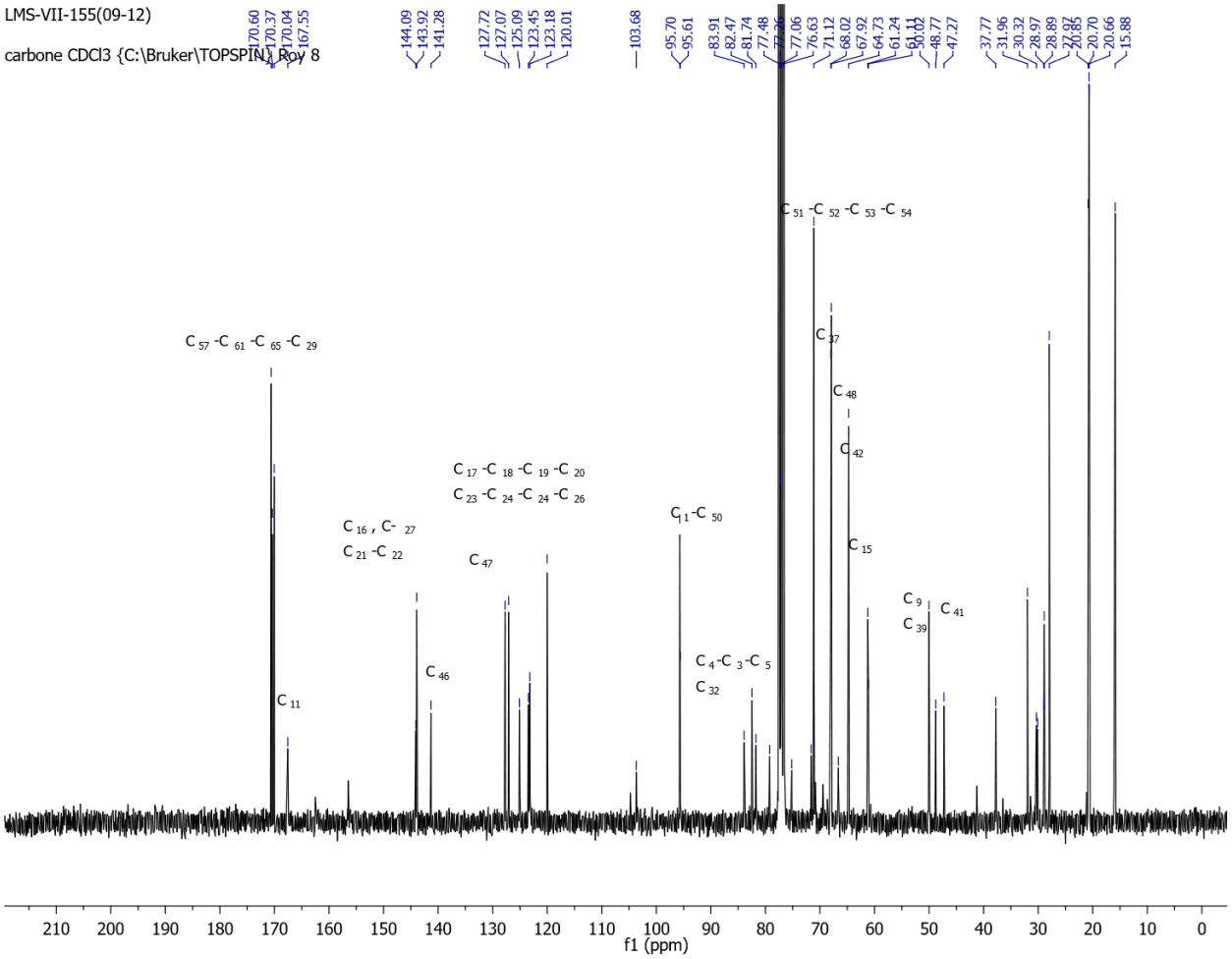

Figure A73. COSY analysis of **81** (300 MHz, $CDCl_3$)

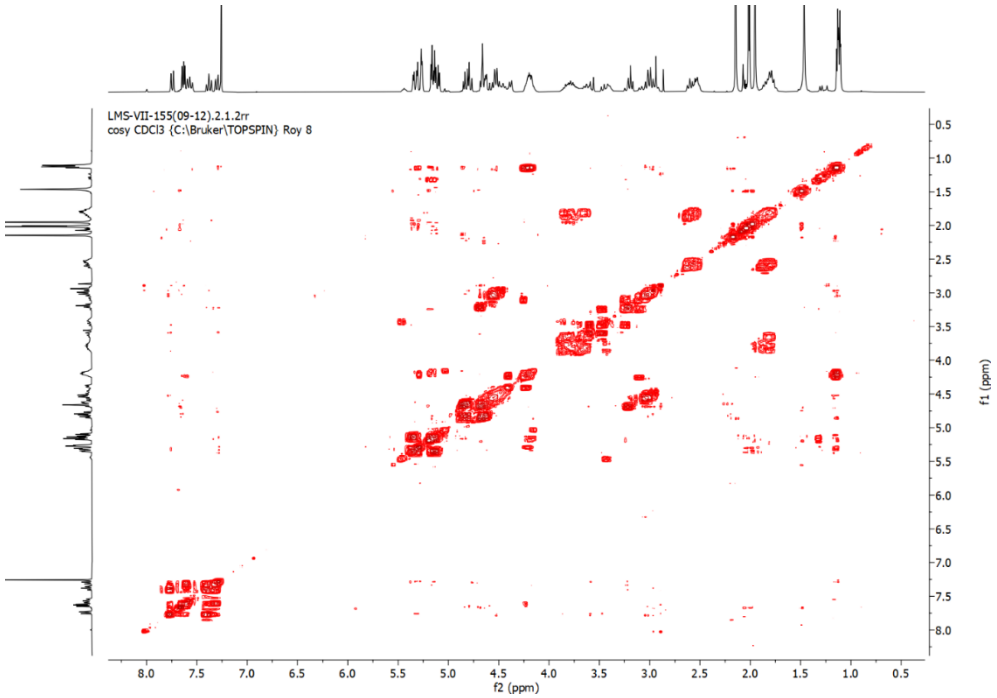

Figure A74. HMBC analysis of **81** (300 MHz, $CDCl_3$)

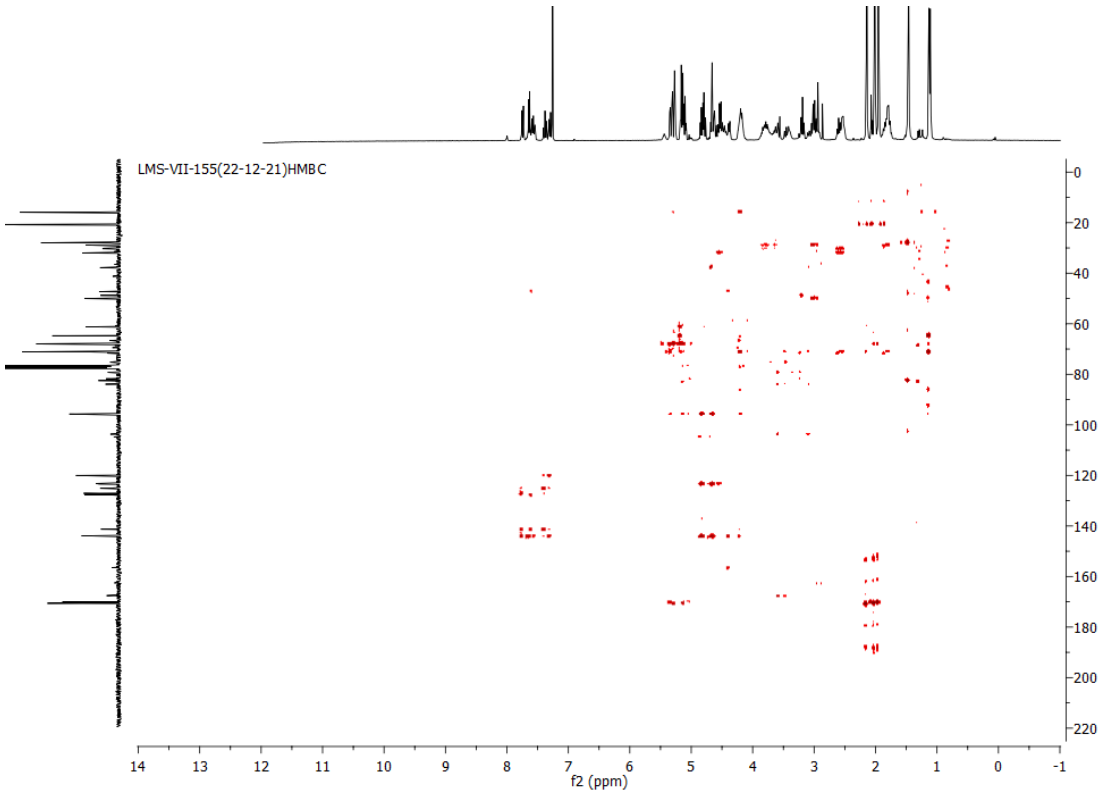

Figure A75. HSQC analysis of **81** (300 MHz, $CDCl_3$)

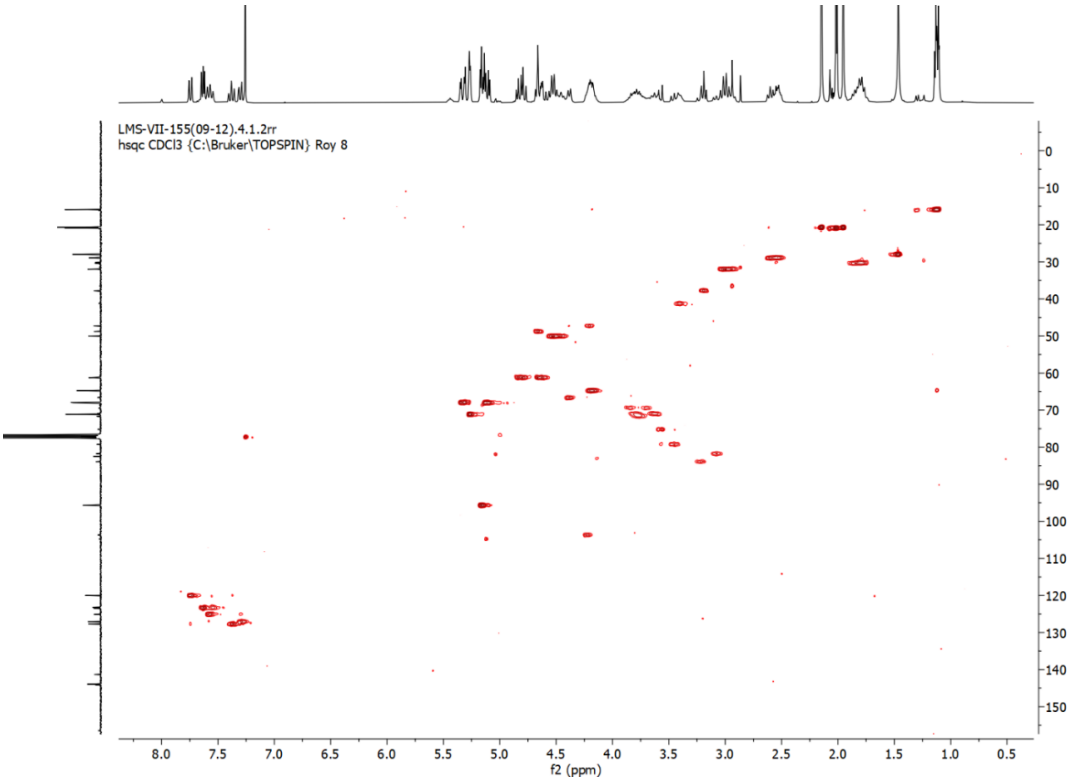

Figure A76. ESI-MS analysis of compound **81**

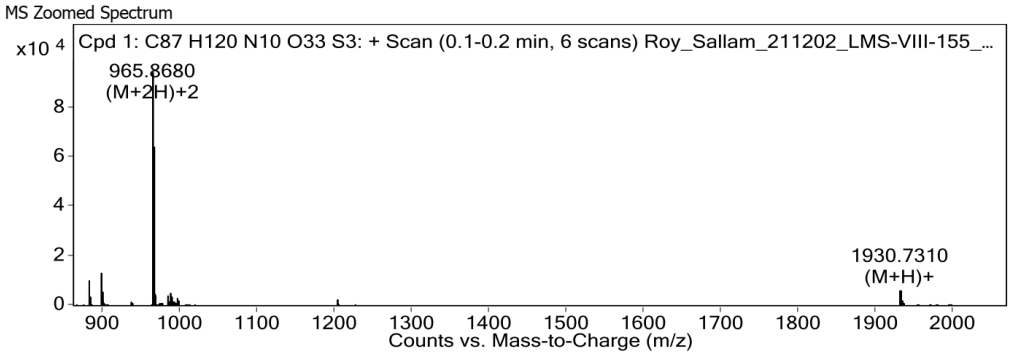

MS Spectrum Peak List

m/z	*Calc m/z*	Diff(ppm)	z	Abund	Formula	Ion
965.3658	965.3663	-0.56		92081	C87 H122 N10 O33 S3	(M+2H)+2
965.868	965.8679	0.16		94290	C87 H122 N10 O33 S3	(M+2H)+2
966.3683	966.3684	-0.04		64065	C87 H122 N10 O33 S3	(M+2H)+2
966.8688	966.8689	-0.15		31880	C87 H122 N10 O33 S3	(M+2H)+2
967.369	967.3694	-0.47		13650	C87 H122 N10 O33 S3	(M+2H)+2
1003.8317	1003.8238	7.91	2	63	C87 H120 K2 N10 O33 S3	(M+2K)+2
1929.7284	1929.7207	4	1	6179	C87 H120 N10 O33 S3	M*+
1947.7637	1947.755	4.43	1	70	C87 H124 N11 O33 S3	(M+NH4)+
1951.713	1951.7074	2.91	1	575	C87 H120 N10 Na O33 S3	(M+Na)+
1967.6818	1967.6813	0.26	1	373	C87 H120 K N10 O33 S3	(M+K)+

Compound 82

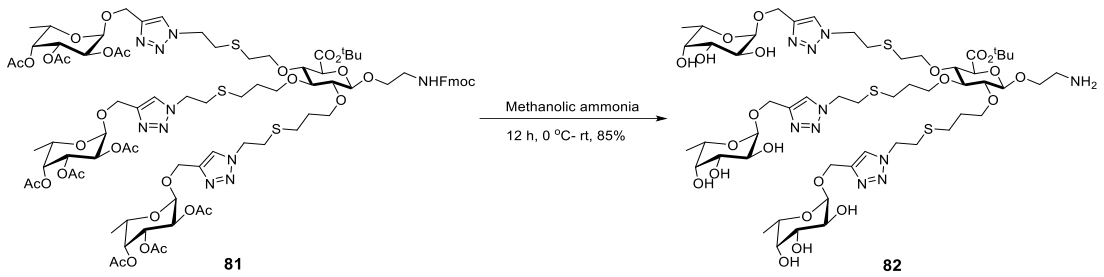

Experimental: deprotection of *O*-Ac and -NHFmoc groups of compound **81** (600 mg) was carried out in a mixture of ammonia/methanol, as described previously, to afford **82** (350 mg, 85%) as an amorphous mass. ^{1}H NMR (300 MHz, D_2O) δ 8.07 (s, 3H, triazole), 4.99 (d, 3x 1H, *J* = 2.5 Hz, H-1 Fuc.), 4.76 (s, 3x 2H, OCH_2), 4.73- 4.56 (m, 3x2H, N-CH_2), 4.51- 4.48 (m, 1H, H-1, D-Glu.) 3.89 (dd, 3x2H, *J* = 19.1, 12.7 Hz, $\underline{CH_2}$-CH_2-S-), 3.83- 3.69 (m, 3x4H, $H_{2,3,4,5}$ Fuc.), 3.24 (dd, 3x2H, *J* = 38.5, 32.2 Hz, O-$\underline{CH_2}$-CH_2), 3.00 (d, 3x2H, *J* = 38.9 Hz, S-$\underline{CH_2}$-CH_2), 2.51- 2.47 (m, 3x2H, O-CH_2-CH_2-$\underline{CH_2}$-S-), 2.00- 1.56 (m, 3x2H, O-CH_2-$\underline{CH_2}$-CH_2-S). 1.49 (s, 9H, *t*-butyl), 1.10 (d, 3x3H, *J* = 5.0 Hz, CH_3). ^{13}C NMR (300MHz, MeOD) δ 168.3, 144.4, 144.2, 124.3, 124.2, 103.4, 98.7, 87.4, 83.6, 82.1, 81.8, 79.5, 74.9, 72.2, 71.5, 70.8, 70.2, 68.5, 66.4, 60.3, 60.2, 49.7, 48.5, 48.2, 47.9, 47.6, 47.4, 47.1, 46.8, 41.0, 37.3, 31.3, 30.1, 30.0, 29.9, 28.1, 28.0, 26.9, 15.4, 15.3. ESI-MS (*m/z*) calcd for $C_{54}H_{92}N_{10}O_{22}S_3$ $[M+2H]^+$ 1330.5, found 1330.9.

Figure A77. ^{1}H NMR analysis of **82** (300 MHz, D_2O)

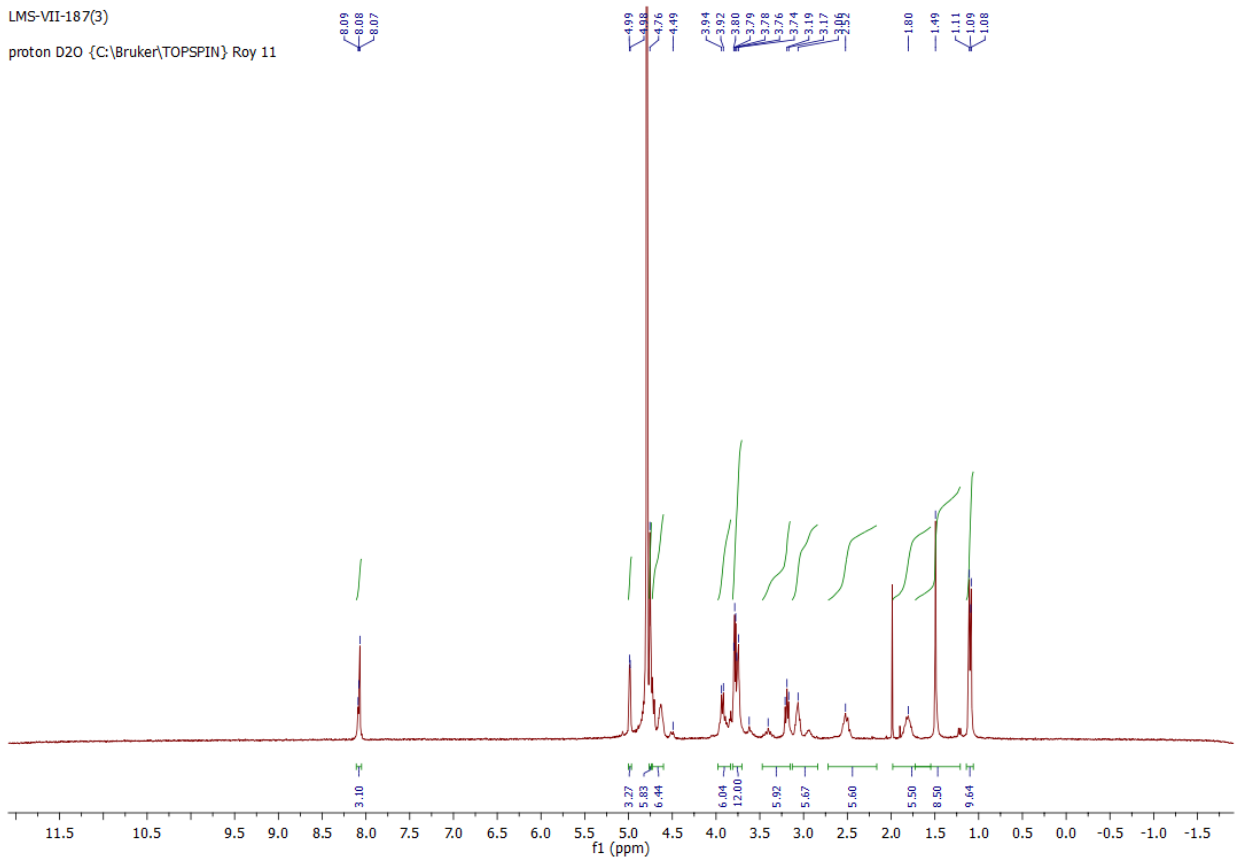

Figure A78. ^{13}C NMR analysis of **82 (**300 MHz, D_2O)

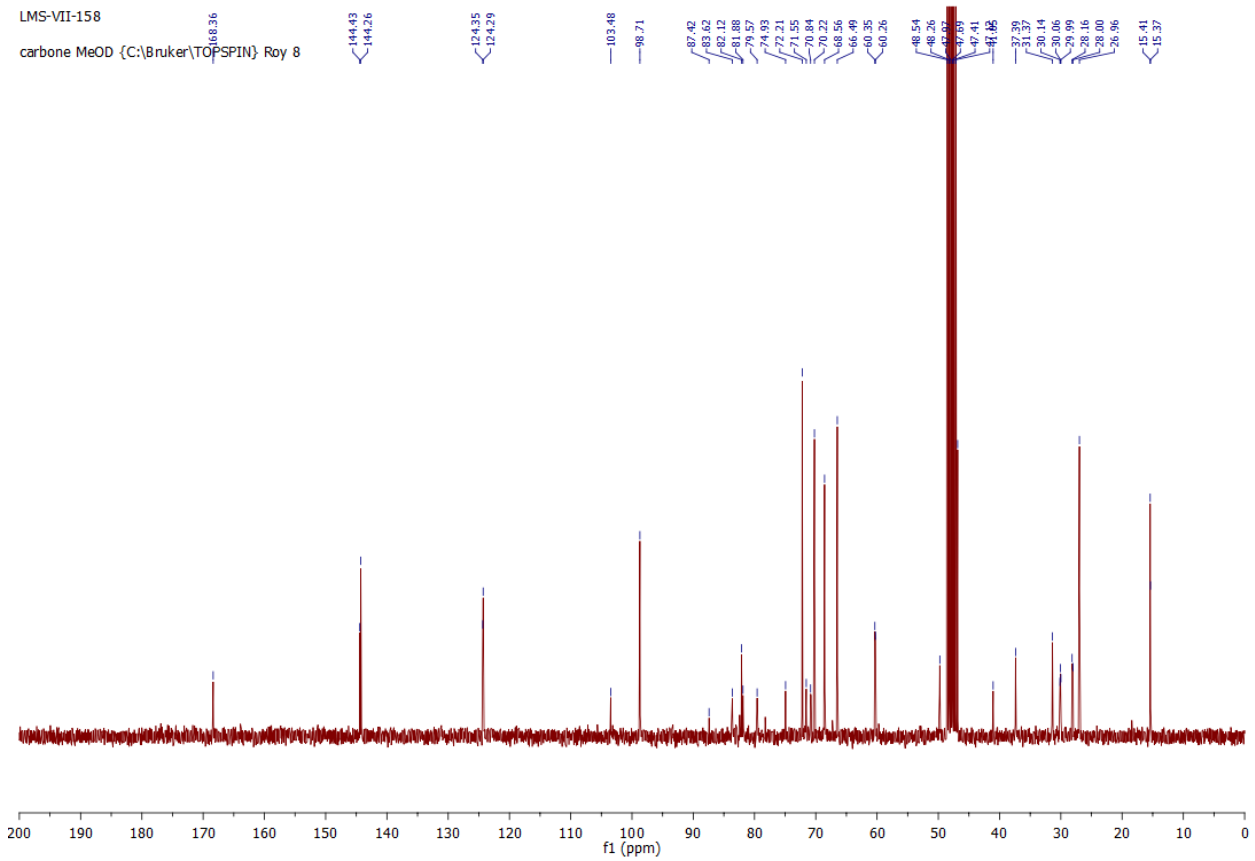

Figure A79. COSY analysis of **82** (300 MHz, D_2O)

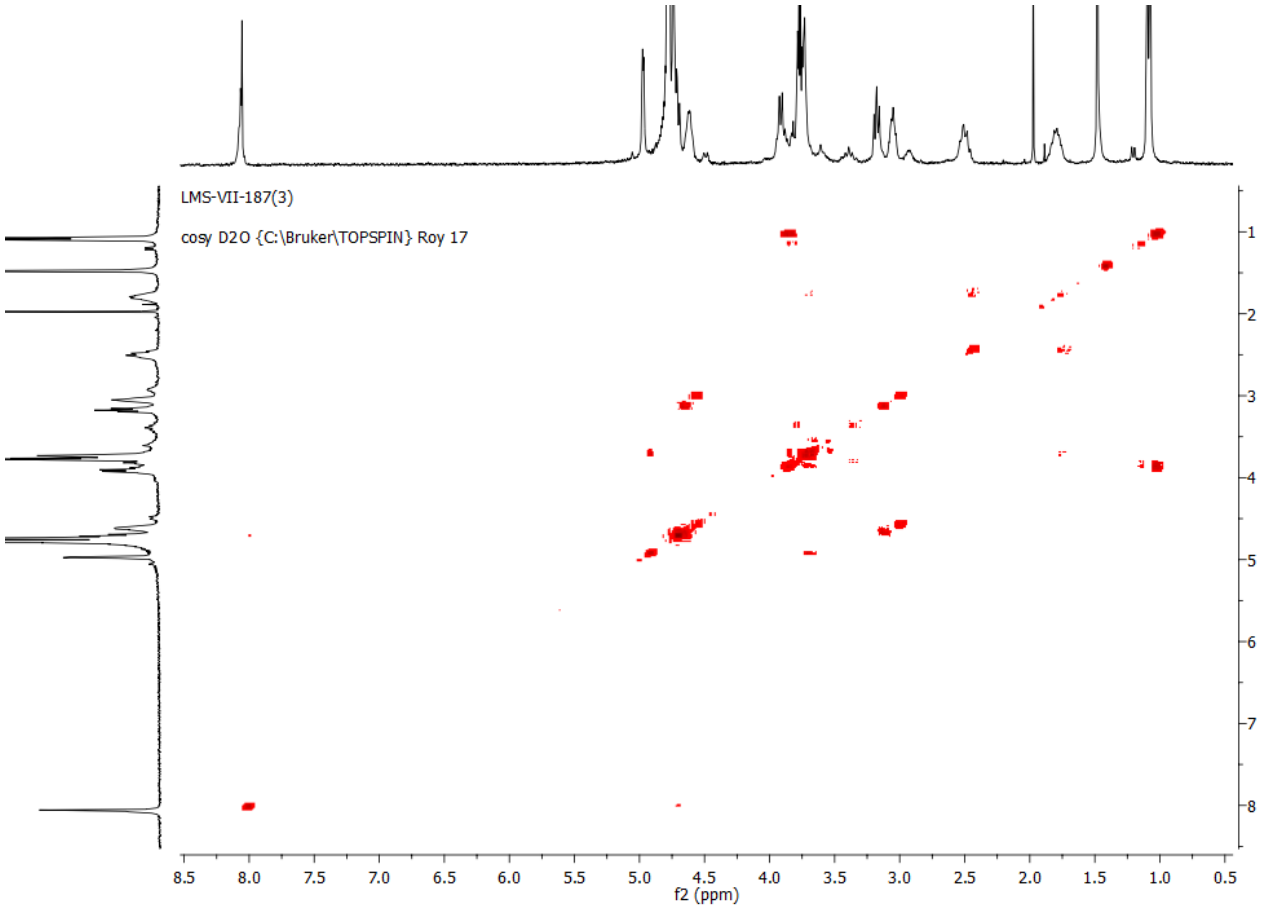

Figure A80. HSQC analysis of **82** (300 MHz, D_2O)

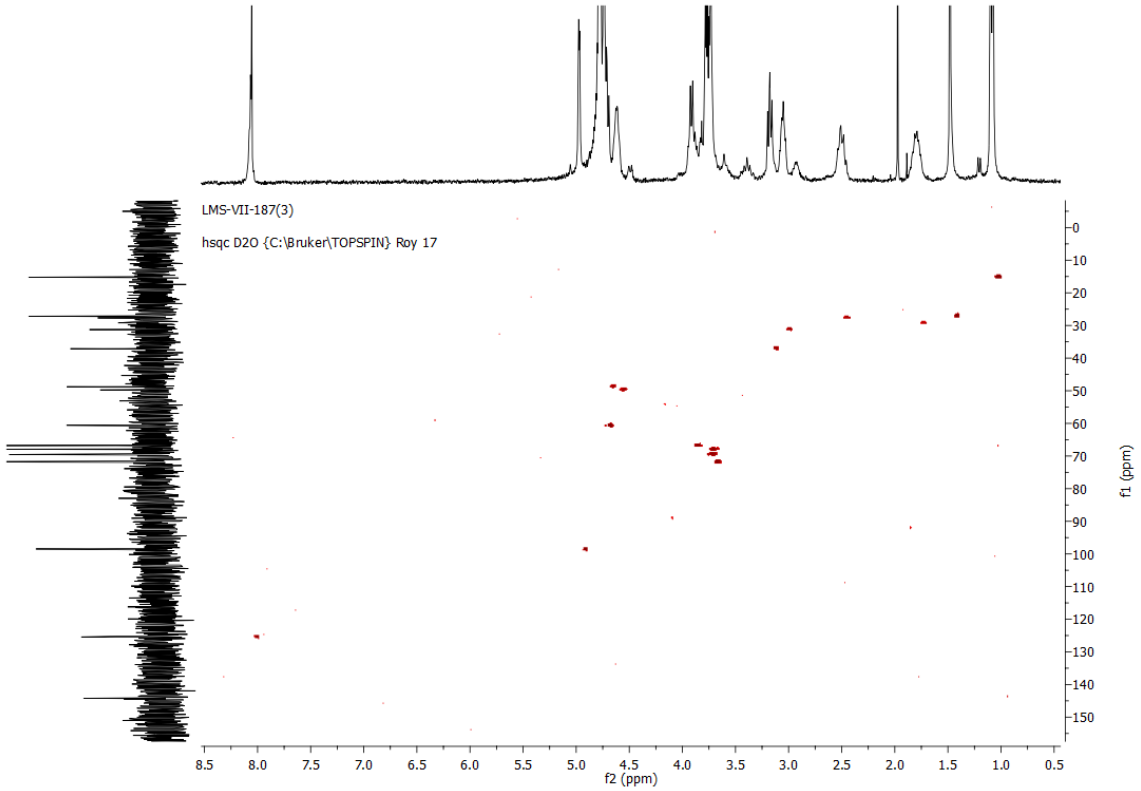

Compound 83

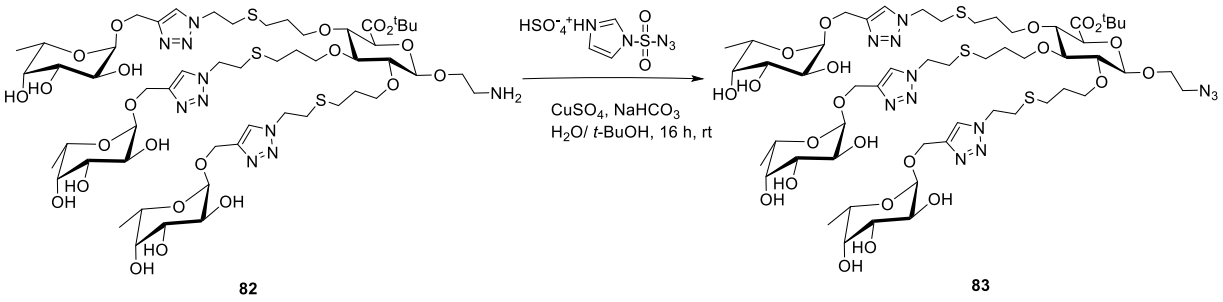

Diazo transfer was done following the procedure previously described, to provide the product **83** (150 mg, 74%). ^{1}H NMR (300 MHz, D_2O) δ 8.08 (s, 3H, triazole), 4.96 (d, 3x 1H, J = 22.3 Hz, H-1 Fuc.), 4.76-4-70 (m, 3x 2H, OCH_2), 4.73 – 4.58 (m, 3x3H, -OH), 4.57(d, J = 14.8 Hz, 1H, H-1, Glu.) , 4.04- 3.83 (m, 3x2H, N-CH2-CH2-S-), 3.85 – 3.69 (m, 3x3H, H35, H36, H37 Fuc.), 3.64-.22 (m, 3x2H, O-CH_2-CH_2), 3.26 – 3.15 (m, 4H, H2, H3, H4, H5, Glu) , 3.21-2.97 (m, 3x2H, S-CH_2-CH_2), 2.54 – 2.47 (m, 3x2H, O-CH_2-CH_2-CH_2-S-), 2.00 – 1.57(m, 3x2H, O-CH_2-CH_2-CH_2-S). 1.50 (s, 9H, *t-butyl*, 1.11(d, 3x3H, J= 5.0 Hz, CH_3). ESI-MS (*m/z*) calcd for $C_{54}H_{90}N_{12}O_{22}S_3$ $[M+Na]^+$ 1377.55, found 1378.7.

Figure A81. ^{1}H NMR analysis of **83** (300 MHz, D_2O)

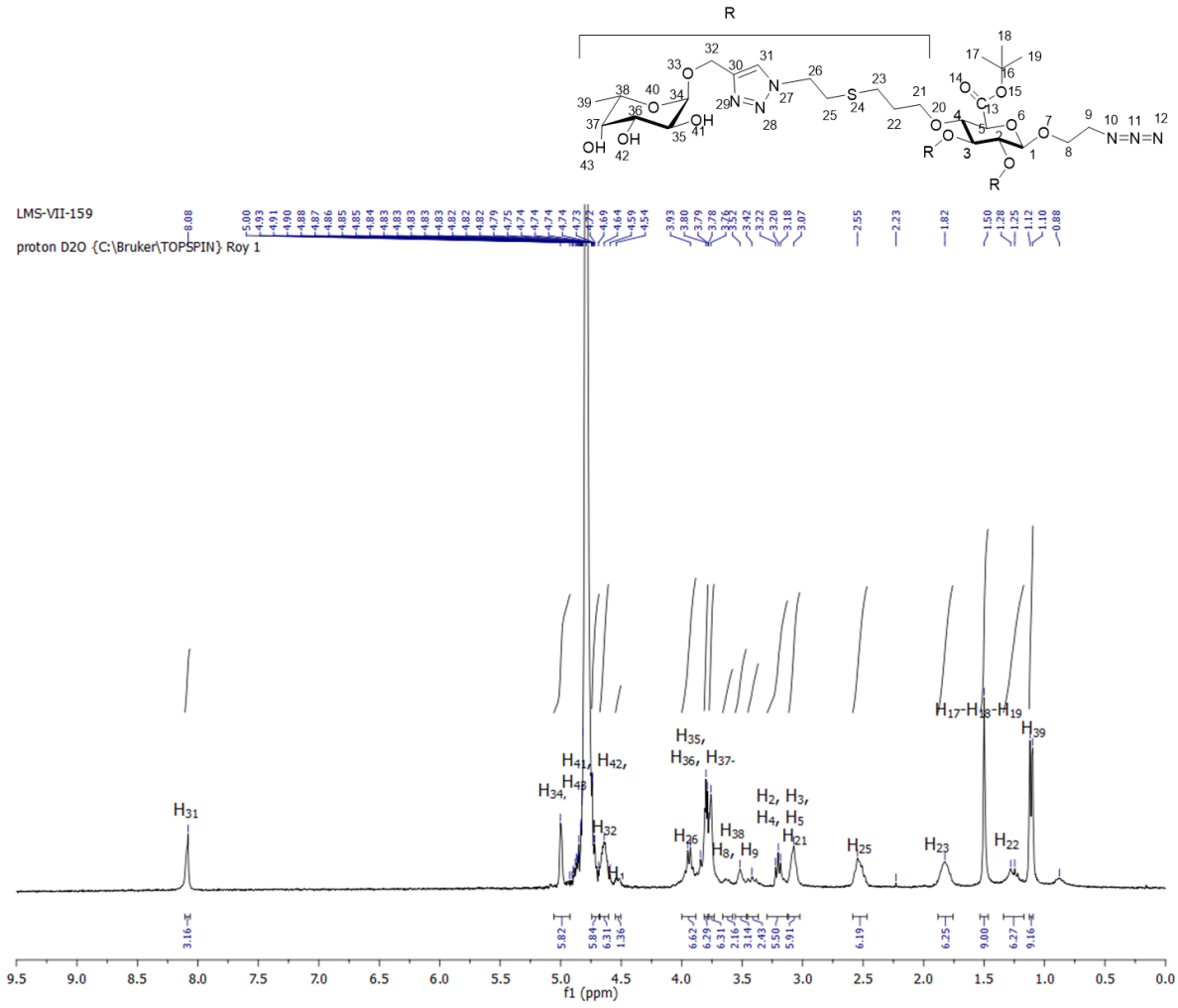

Copper Catalyzed Addition of azide- alkyne (CuAAC) (General Procedure A)

A flame dried flask equipped with a magnetic stirring bar was charged with a solution of dendron (6 eqv.), in dry methanol, after which a solution of alkyne (1 equiv.) in dry acetonitrile and *N,N*-diiso propyl ethyl amine (15 eqv.) were added. To this mixture a solution of CuI $P(OEt)_3$ (0.7 eqv.) in dry acetonitrile was added via syringe under a nitrogen atmosphere. The resulting mixture was heated at 80 ºC for 24 h. The solvents were evaporated under reduced pressure. The crude product was cooled to 0 ºC, pyridine and Ac_2O were added, the mixture was stirred for 12 h at rt. The solvent was evaporated with co-solvent toluene under reduced pressure, after complete drying, the crude was extracted with ethyl acetate, and the organic extract was washed successively with saturated aqueous $NaHCO_3$, Saturated aqueous Na_3EDTA solution, water

and then dried over Na_2SO_4. After evaporation of volatiles under reduced pressure, the crude mixture was purified by silica gel column chromatography (DCM/MeOH 97: 3%) to give the desired products.

Phosphite ligand and copper (I) complex CuI [$P(OEt)_3$]

Freshly recrystallized $CuI.P(OEt)_3$ must be used for optimal yields. $CuI.P(OEt)_3$ used was synthesized according to the procedure reported therein. Most often, these complexes were prepared by the method introduced by A. Arbuzov (A. Arbuzov, Ber., 38, 117 (1905), and A. Arbuzov (A. Arbuzov, J.Russ.Phys. Chem. Soc., 38, 161, 193, 687 (1906), and more recently used by Y. Nishizawa. [501] In this procedure, the phosphite was mixed with the appropriate mole ratio of copper (I) halide in benzene, followed by evaporation to dryness and recrystallization.

Synthesis and characterization of dendrimer 85

The reaction performed according to the general procedure A:

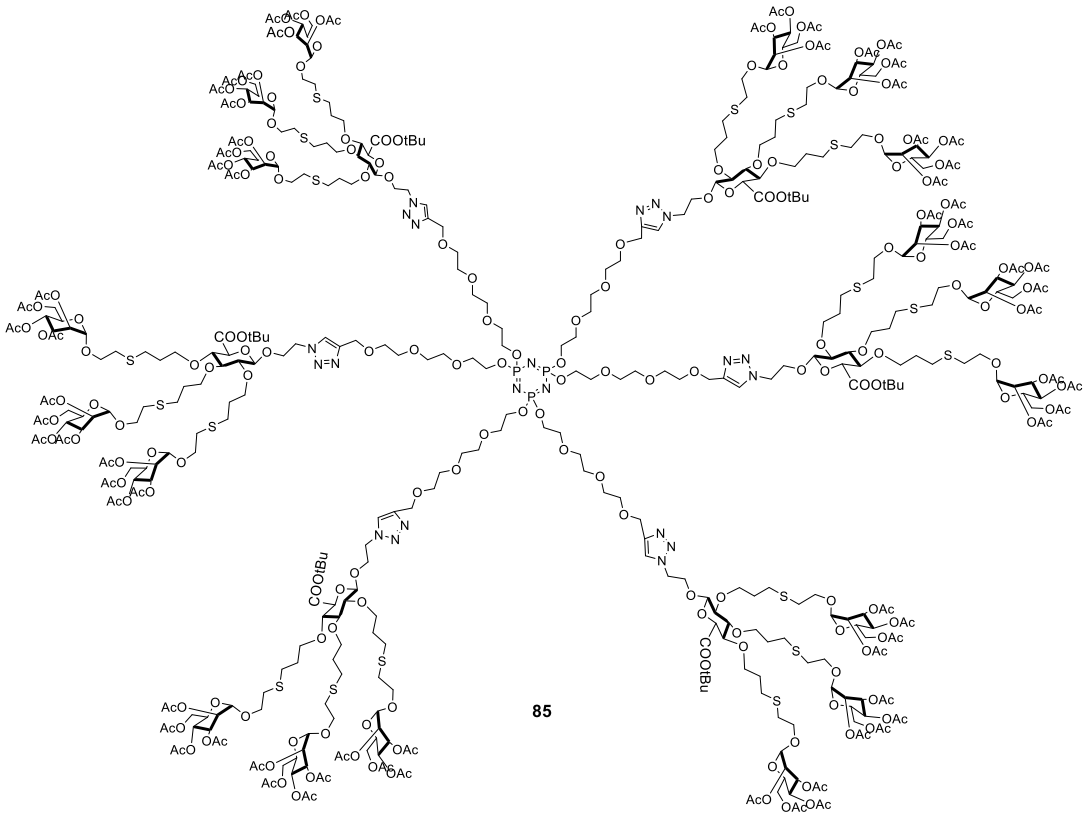

^{1}H NMR (300 MHz, $CDCl_3$) δ 7.67 (s, 3x1H, triazole), 5.28 (d, 6x6H, J = 7.9 Hz), 5.21 (s, 6x3H), 4.84 (s, 6x3H), 4.63 (s, 6x2H), 4.56 (s, 6x2H), 4.37- 4.20 (m, 6x5H), 4.10 (d, 6x2H J = 8.1 Hz), 4.08- 3.94 (m, 6x6 H), 3.89- 3.67 (m, 6x6H), 3.62 (dd, 6x14H, J = 17.2, 8.7 Hz), 3.41 (dd, 6x2H, J = 23.7, 14.3 Hz), 3.21 (t, 6x1H J = 8.8 Hz), 3.13- 2.94 (m, 6x1H), 2.69 (dt,6x6H, J = 15.3, 6.0 Hz), 2.59 (dt, 6x6H, J = 19.7, 7.0 Hz), 2.14 (s, 6x9H), 2.09 (s, 6x9H), 2.03 (s, 6x9H), 1.97 (s, 6x9H), 1.91- 1.66 (m, 6x8H), 1.47 (s, 6x9H). ^{13}C 170.6, 170.0, 169.8, 169.7, 167.5, 130.9, 128.8, 123.6, 103.7, 97.6, 83.8, 82.3, 81.6, 79.2, 71.2, 70.9, 70.5, 69.6, 69.5, 69.0, 68.6, 67.9, 67.8, 66.0, 62.4, 50.1, 31.1, 29.1, 28.0, 20.8, 20.7, 20.7, 20.6, 14.1, 1.0. MALDI-TOF MS: *m/z* calcd for $C_{468}H_{720}N_{21}O_{246}P_3S_{18}$ $[M+Na]^+$ 11269.81, found 11267.33.

[Since the product is very large, the peaks were integrated for 1/6 of the full compound, **Figure A83**]

Figure A82.^{1}H NMR analysis of **85** (300 MHz, $CDCl_3$)

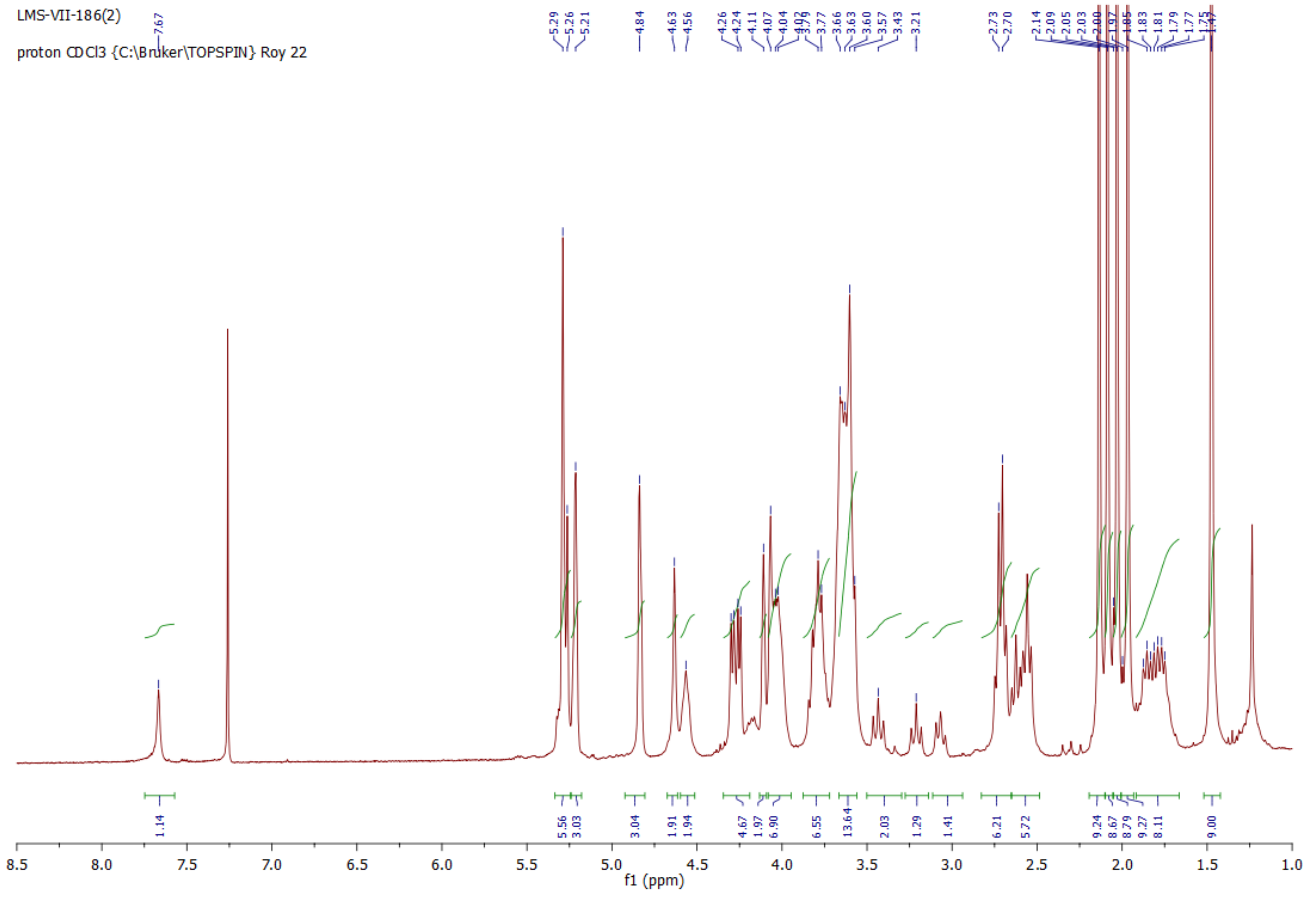

[Full integration of dendrimer **85**, **Figure A84**]

Figure A83.[1]H NMR analysis of **85** (300 MHz, $CDCl_3$)

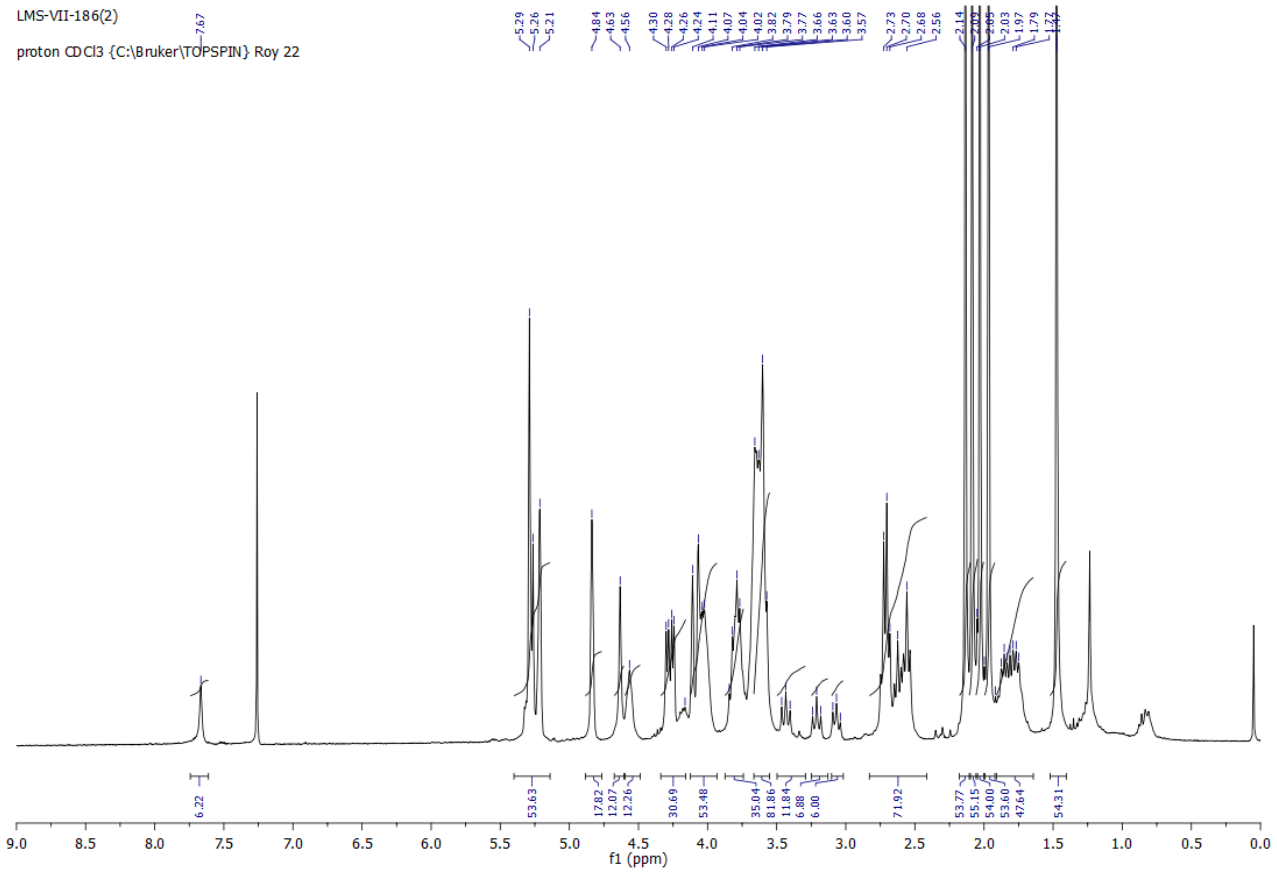

Figure A84. ^{13}C NMR analysis of **85** (300 MHz, $CDCl_3$)

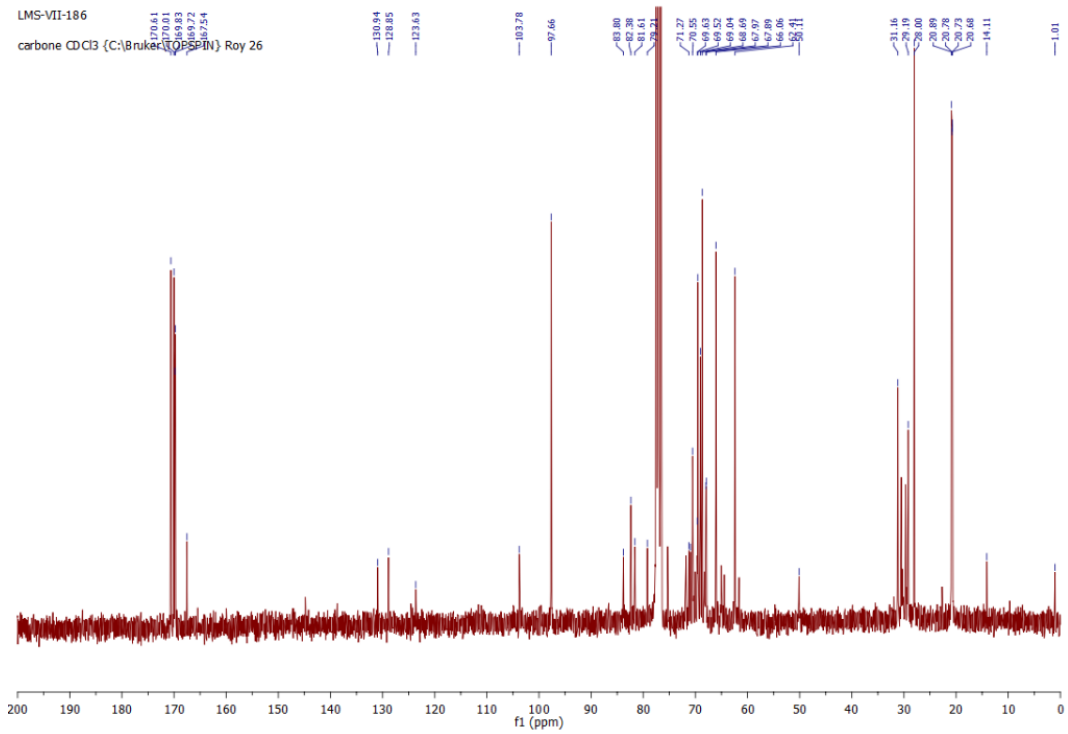

Figure A85. ^{31}P NMR analysis of **85** (300 MHz, $CDCl_3$)

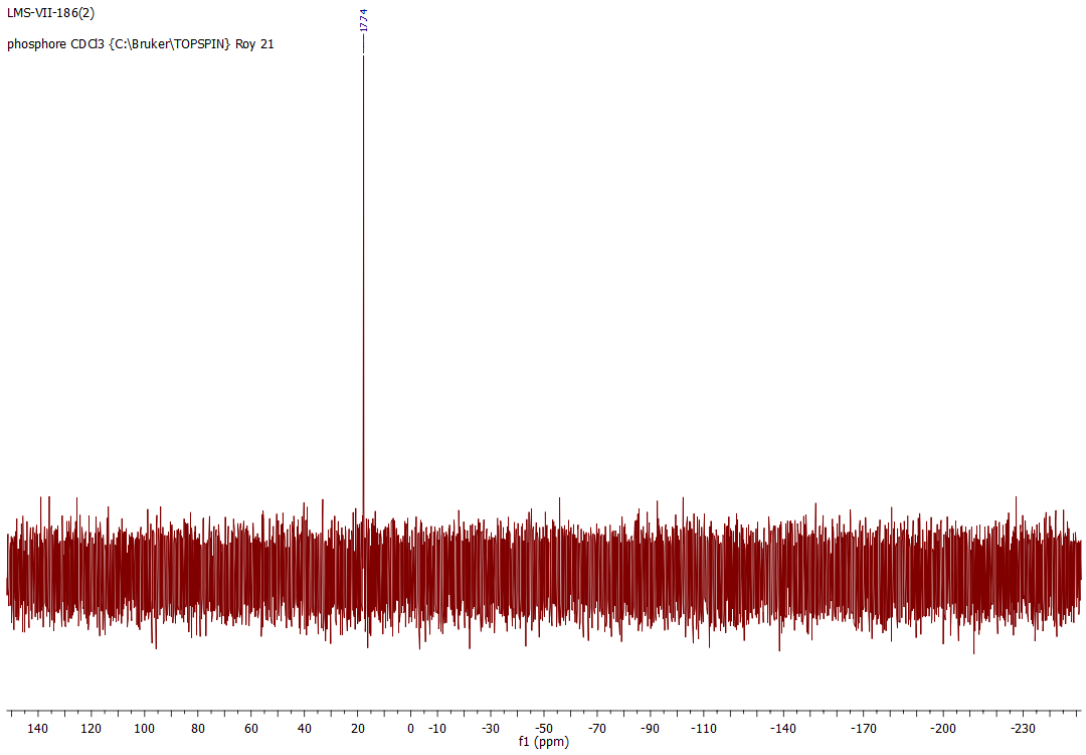

Figure A86. MALDI-TOF ANALYSIS of fully clicked dendrimer **85**

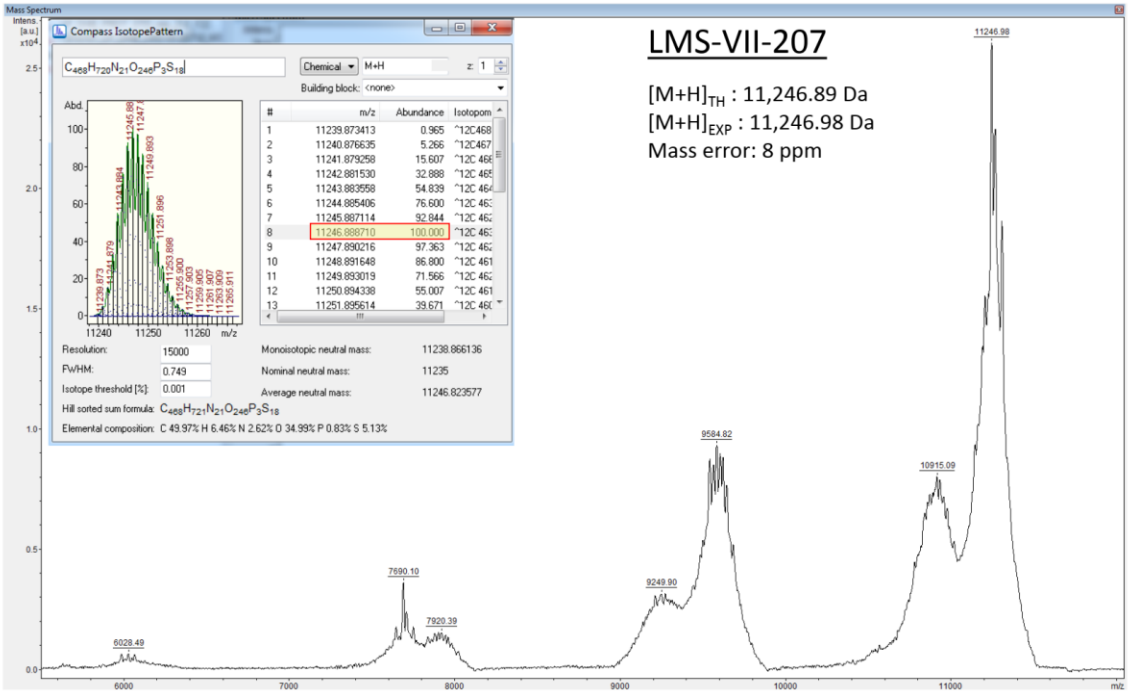

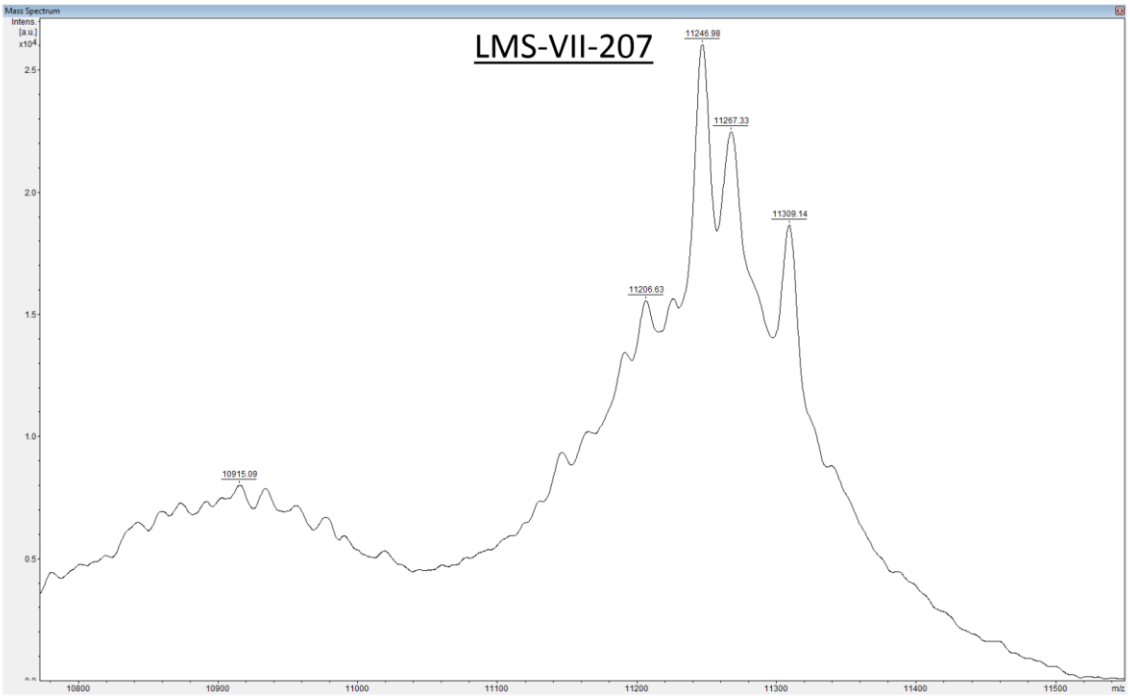

Synthesis and characterization of dendrimer 88

The reaction performed according to the general procedure A

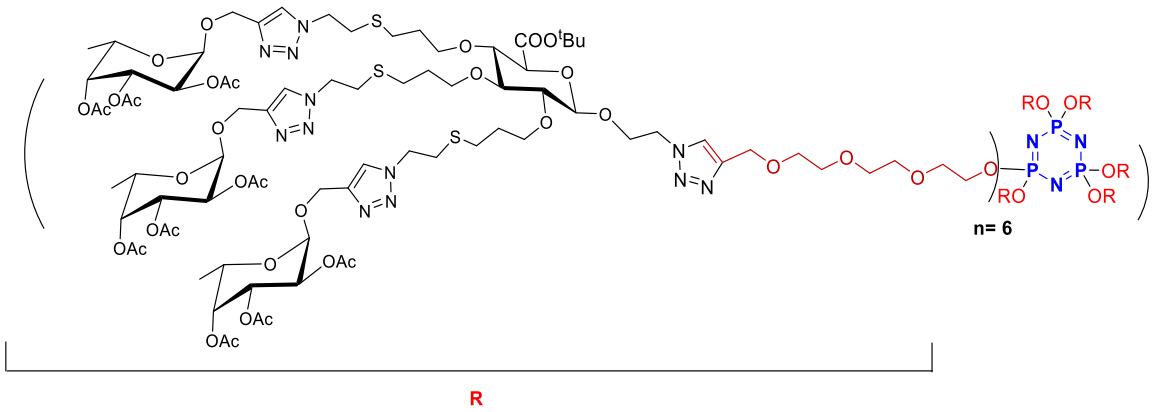

^{1}H NMR (300 MHz, $CDCl_3$) δ 7.88- 7.52 (m, 24H, triazole), 5.28 (dd, 36 H, *J* = 22.7, 12.6 Hz, H1, H3, Fuc.), 5.11 (dt, 36H, *J* = 24.7, 10.3 Hz, H2, H4, Fuc.), 4.81 (d,18H, *J* = 12.3 Hz, H5), 4.62 (dd, 36H, *J* = 13.3, 6.9 Hz, O-CH_2- Fuc), 4.59 – 4.44 (m, 36H, S-CH_2-CH_2), 4.31 – 4.09 (m, 36H, O-CH_2), 4.12 – 3.88 (m, 36H, O-CH_2-CH_2), 3.65 (s, 84H, TEG), 3.62 (s, 72H), 3.43 (d, 12H, *J* = 8.3 Hz, CH_2, Gu), 3.15 (dd, 12H, *J* = 24.7, 16.5 Hz, CH_2, Gu), 2.99 (d, 36H, *J* = 6.5 Hz, -SCH_2), 2.77- 2.25 (m, 55H), 2.14 (s, 54H, OAc), 2.01 (s, 54H, OAc), 1.95 (s, 54H, OAc), 1.88 -1.53 (m, 47H), 1.47 (s, 54H, *tert.Butyl*), 1.11 (d, 54H, *J* = 6.4 Hz, CH_3), 0.79 (dd, 60H, *J* = 28.6, 21.3 Hz). ^{13}C NMR (300 MHz, $CDCl_3$) δ 170.6, 170.3, 170.0, 167.5, 143.9, 130.9, 123.2, 103.5, 95.6, 82.4, 79.7, 74.7, 71.1, 70.6, 70.3, 70.0, 69.1, 68.0, 67.9, 64.7, 61.2, 58.3, 50.0, 31.9, 30.2, 30.1, 29.6, 29.3, 28.8, 27.9, 22.6, 20.8, 20.6, 20.6, 16.0, 15.8, 14.1. MALDI-TOF MS (*m/z*) calcd for $C_{486}H_{738}N_{75}O_{210}P_3S_{18}$ 11661.57, found 11727.

Figure A87. ^{1}H NMR analysis of **88** (300 MHz, $CDCl_3$)

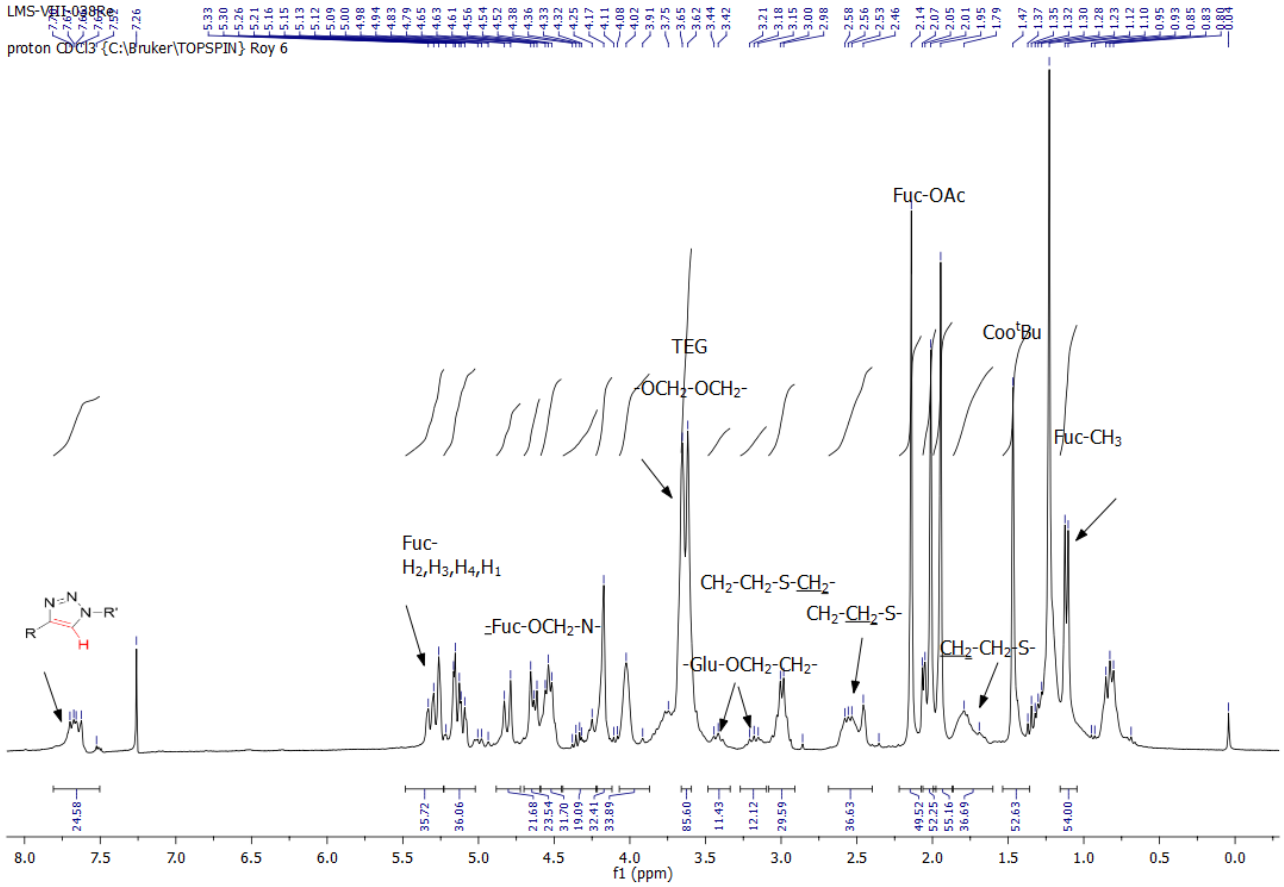

Figure A88. ^{13}C NMR analysis of **88** (300 MHz, $CDCl_3$)

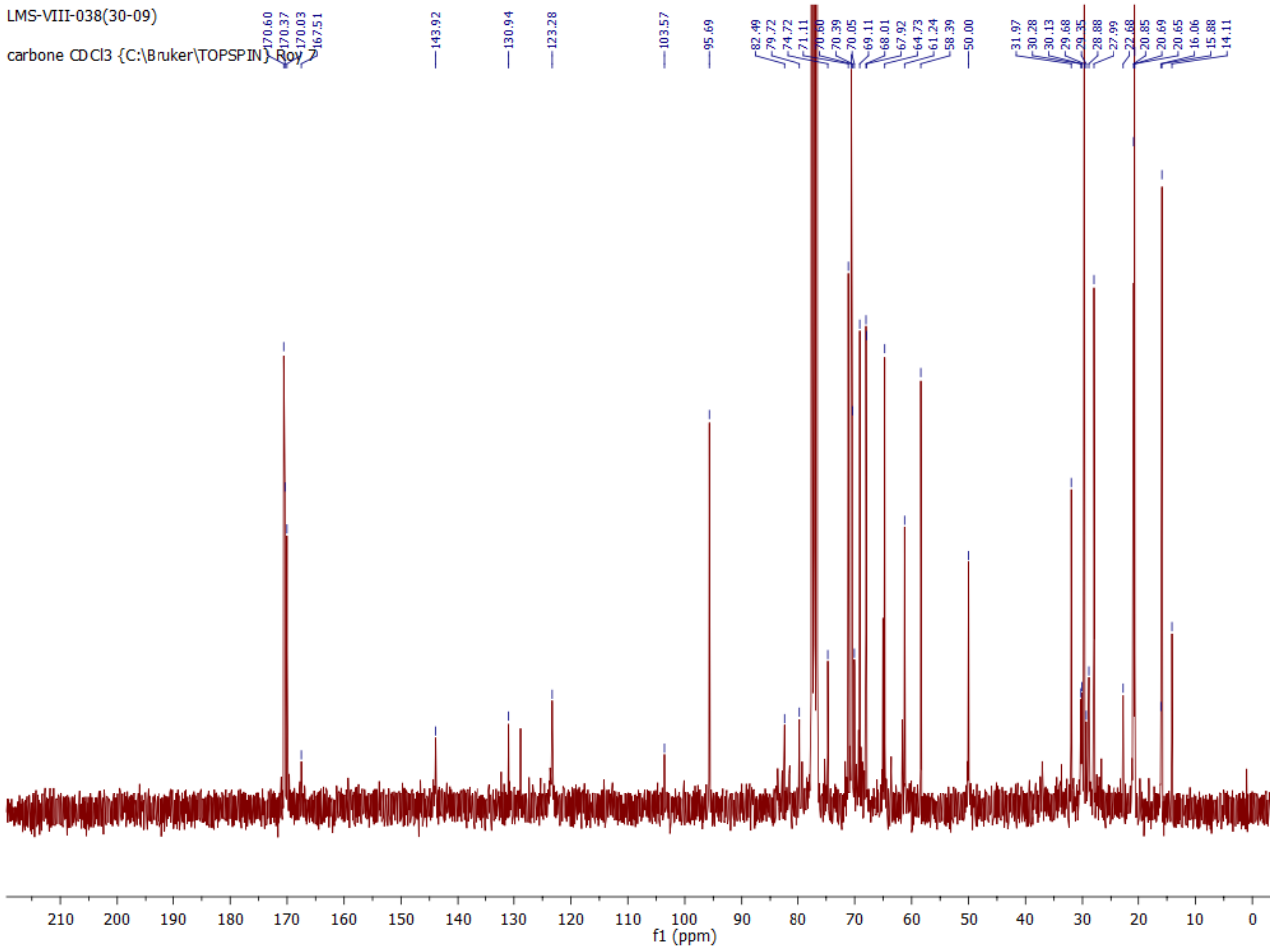

Figure A89. ^{31}P NMR analysis of **88** ($CDCl_3$)

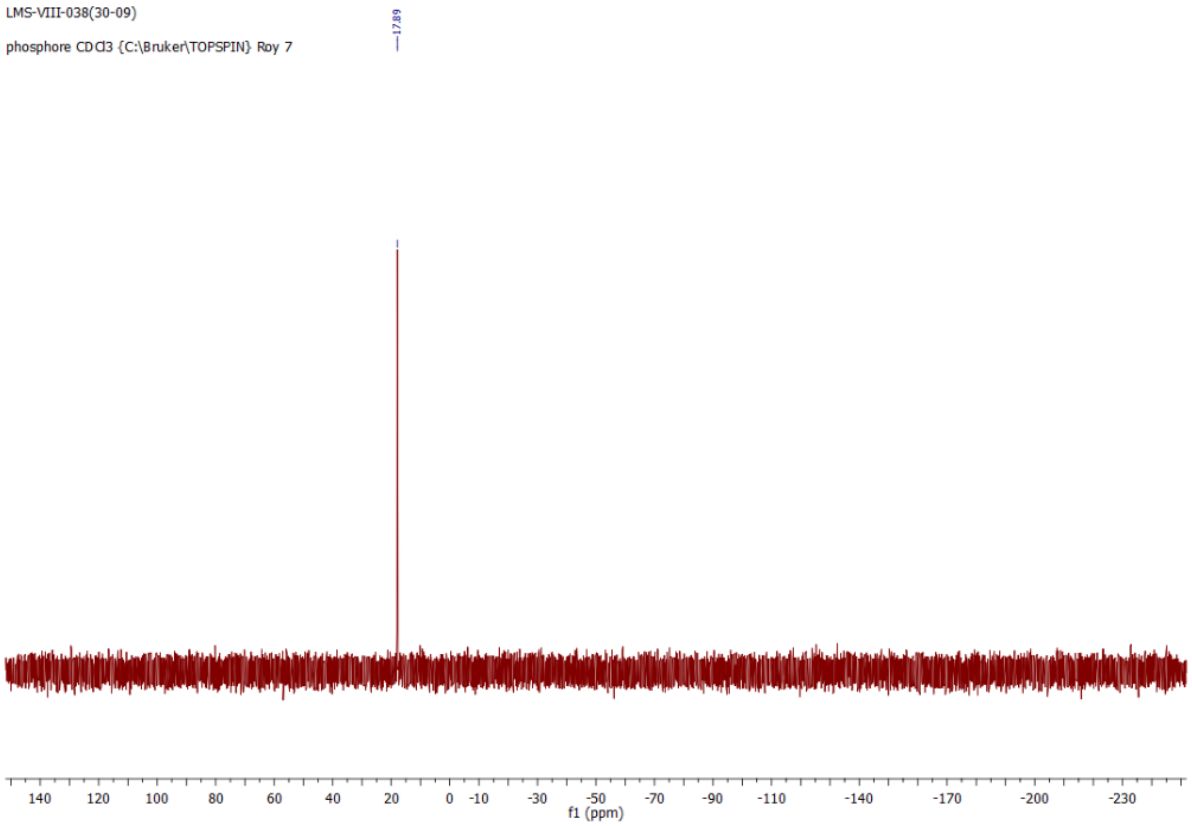

Synthesis and characterization of dendrimer 92

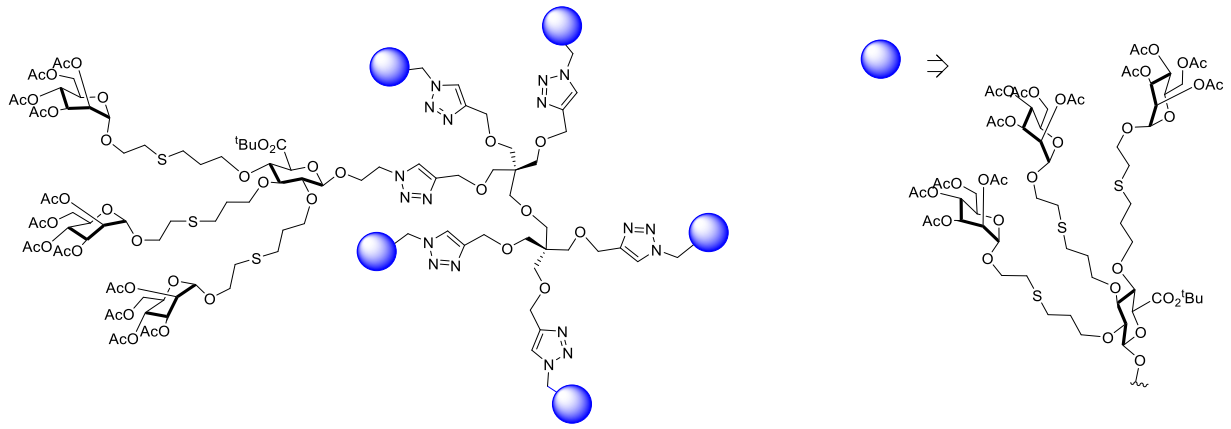

The reaction performed according to the general procedure A to afford product **92** as a colorless oil, ^{1}H NMR (300 MHz, $CDCl_3$) δ 7.65 (s, 1H), 5.34- 5.20 (m, 6H, H_2-H_3), 5.18 (d, 3H, J = 0.8 Hz, H_4), 4.81 (dd, 3H, J = 3.6, 1.5 Hz, H_1), 4.49 (d, 4H, J = 26.5 Hz), 4.24 (dd, 4H, J = 12.4, 5.1 Hz), 4.24 (dd, 7H, J = 12.4, 5.1 Hz), 3.77 (dd, 6H, J = 10.0, 5.6 Hz), 3.68- 3.49 (m, 6H), 3.41 (d, 3H, J = 9.3 Hz), 3.18 (m, 1H), 3.05 (d, 1H, J = 7.9 Hz), 2.86 – 2.25 (m, 12H), 2.10 (s, 9H), 2.06 (s, 9H), 2.00 (s, 9H), 1.94 (s, 9H), 1.88- 1.61 (m, 6H), 1.44 (s, 9H). ^{13}C NMR (300 MHz, $CDCl_3$) δ 170.5, 169.9, 169.8, 169.7, 167.5, 145.0, 123.4, 103.7, 97.6, 83.7, 82.3, 81.6, 79.2, 75.2, 71.8, 71.2, 70.9, 69.4, 69.0, 68.6, 68.2, 67.9, 67.9, 67.8, 66.0, 62.3, 49.8, 31.1, 30.5, 30.3, 29.2, 29.1, 27.9. No HRMS data were obtained for this dendrimer.

Figure A90. ^{1}H NMR analysis of **92** (300 MHz, $CDCl_3$)

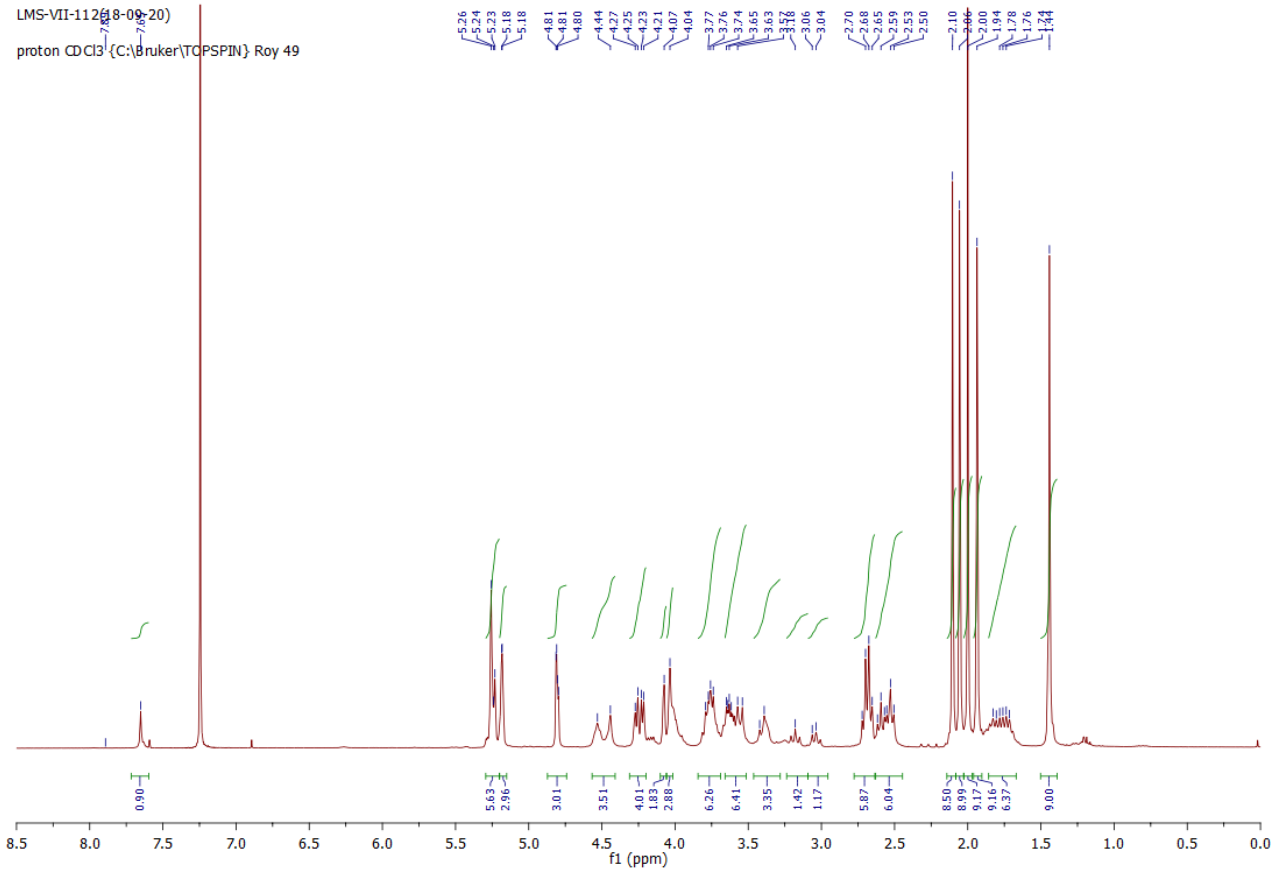

Figure A91.^{13}C NMR analysis of **92** (300 MHz, $CDCl_3$)

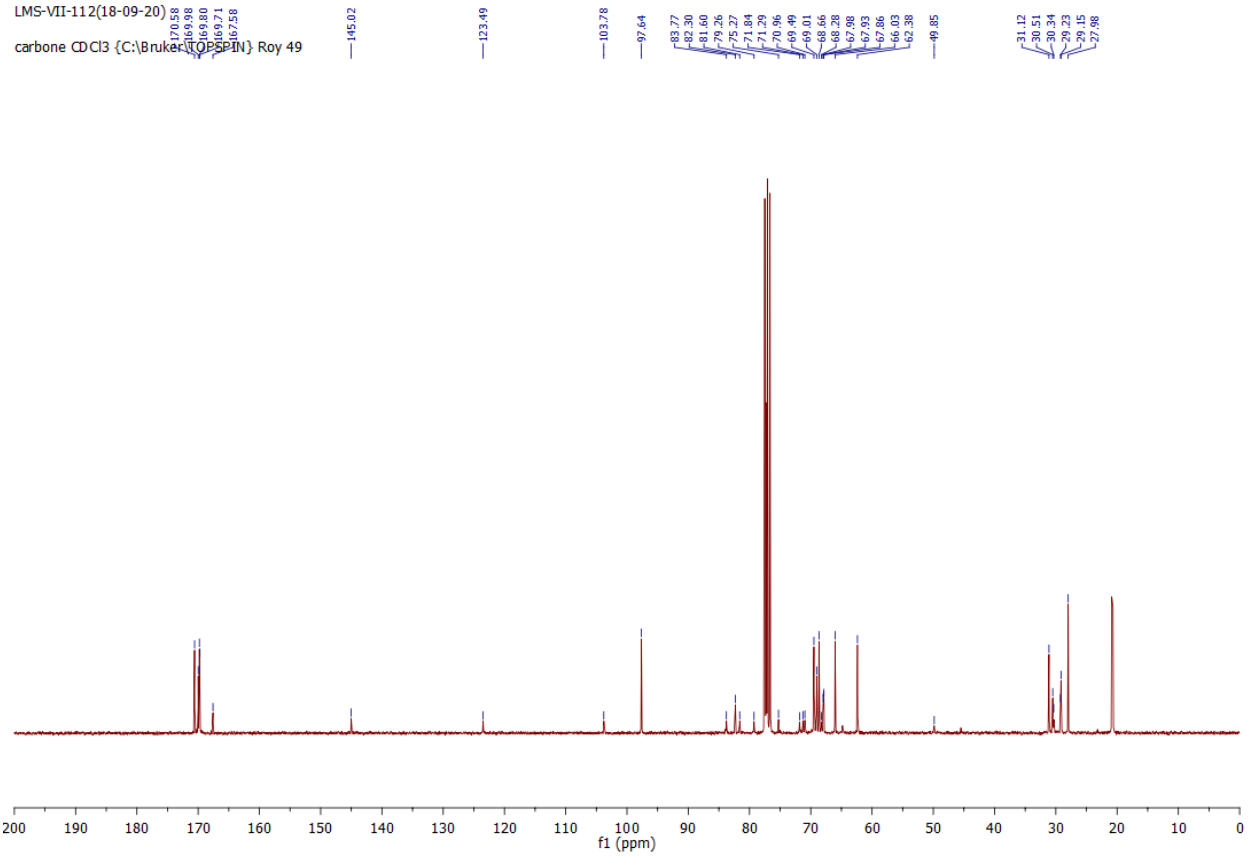

Synthesis and characterization of dendrimer 94

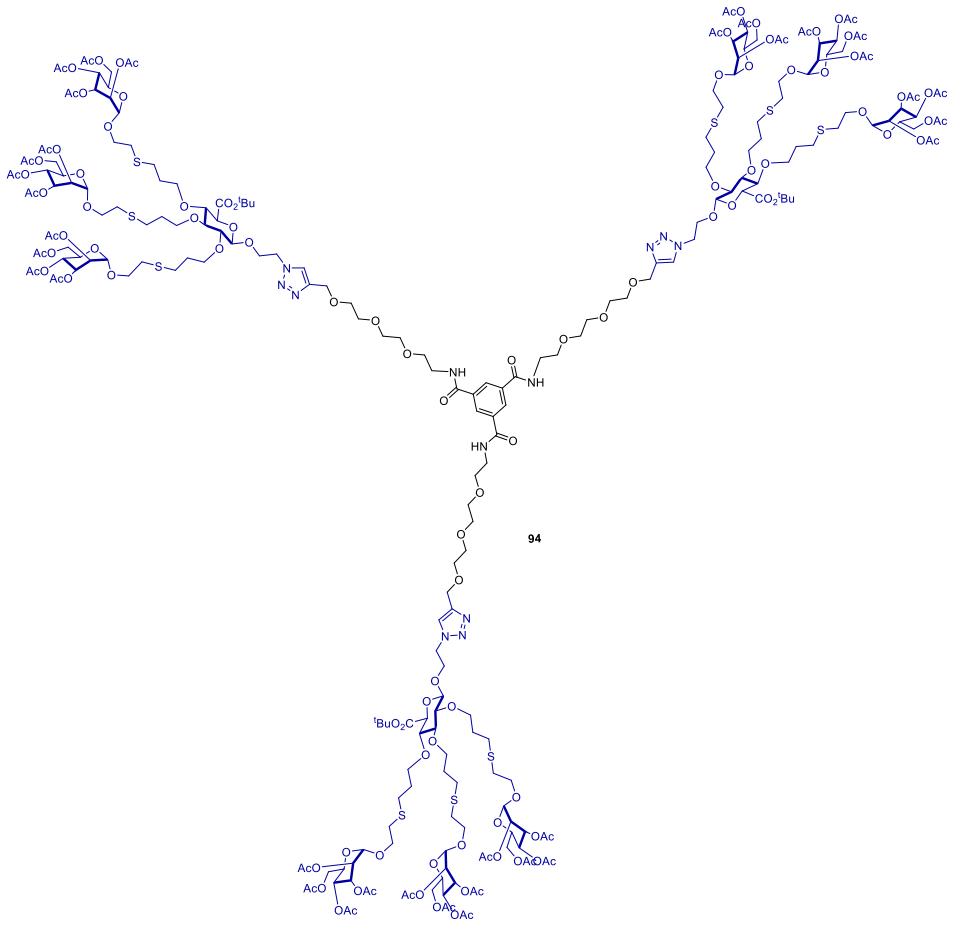

The reaction performed according to the general procedure A to afford product **94** as a colorless oil. ^{1}H NMR (300 MHz, $CDCl_3$) δ 8.38 (s, 3H), 7.65 (s, 3H), 7.35 (s, 3H), 5.36- 5.24 (m, 16H), 5.22 (d, 8H, J = 5.2 Hz), 5.00 – 4.70 (m, 9H), 4.61 (s, 5H), 4.55 (s, 6H), 4.37 – 4.21 (m, 12H), 4.20 – 4.13 (m, 3H), 4.10 (d,5H, J = 7.8 Hz), 4.06 (d, J = 6.9 Hz, 3H), 4.06 (d, 6H, J = 6.8 Hz), 4.05 – 3.93 (m, 8H), 3.62 (dd, 52H, J = 17.4, 7.9 Hz), 3.51 – 3.30 (m, 5H), 3.21 (t, 4H, J = 8.9 Hz), 3.14 – 2.95 (m, 4H), 2.91 – 2.36 (m, 33H), 2.14 (s, 27H), 2.09 (s, 27H), 2.05 (s, 27H), 2.03 (s, 27H), 1.97 – 1.61 (m, 18H), 1.47 (s, 27H), 1.33 – 1.06 (m, 6H), 0.85 (d, 3H, J = 7.6 Hz). No HRMS data were obtained for this dendrimer.

Figure A92. ^{1}H NMR analysis of **94** (300 MHz, $CDCl_3$)

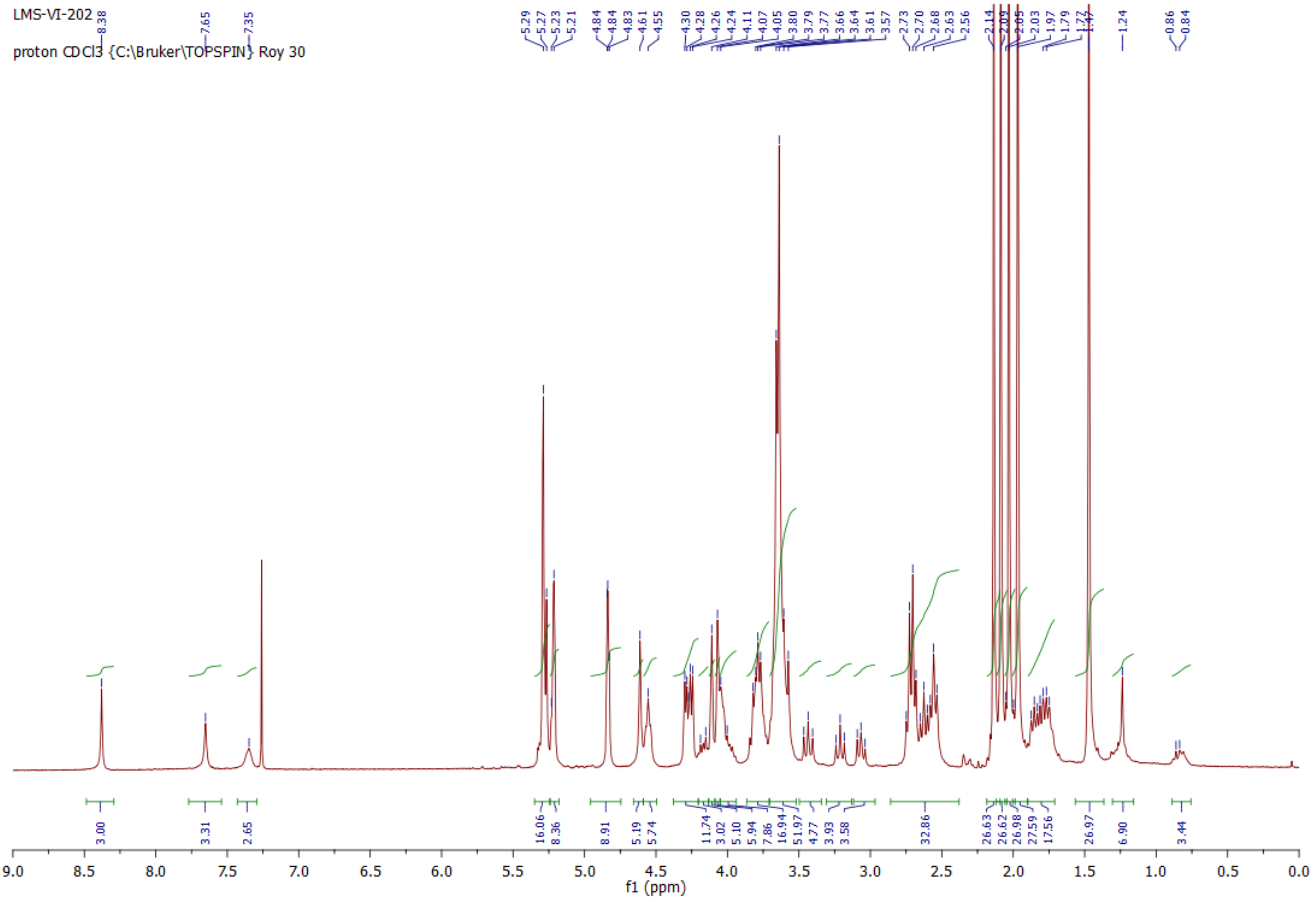

The general procedure of dendrimer deprotection

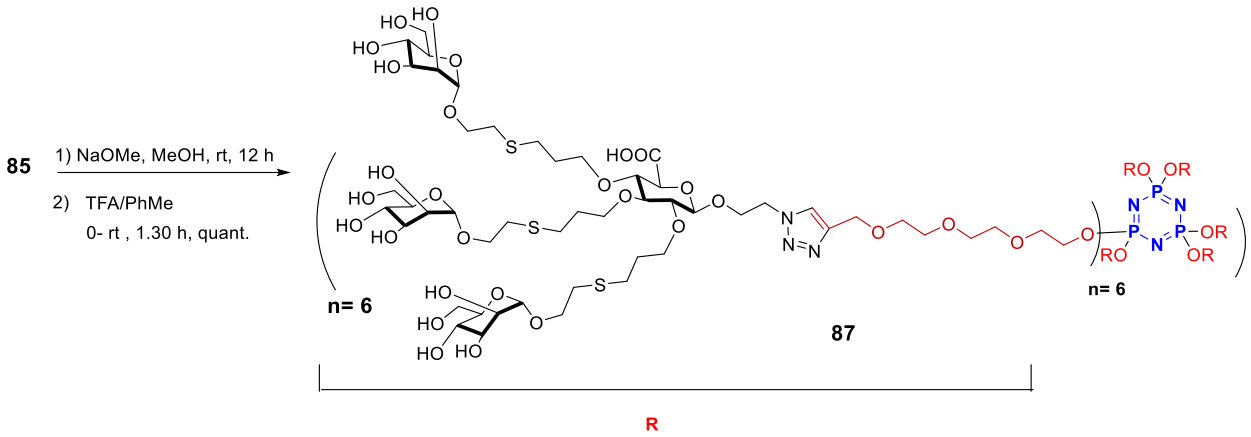

General procedure B

To a solution of dendrimer **85** (150 mg, 1.2 mmol) in MeOH (15 mL), was added 1.0 M of NaOMe in MeOH (700 µL), and the solution was allowed to stir for 12 h at room temperature. Then Amberlyst 15 was added under gentle stirring until the pH reached ~7. The Amberlyst was then filtered off, and the solvent was evaporated till dryness to afford the fully deprotected dendrimer bearing hydroxyl groups (60 mg). The product from the first step was dissolved in a premixed solvent of TFA/toluene (1 mL, v/v= 10/1) at 0 ºC and was stirred at room temperature for 90 min. The mixture was further diluted and concentrated under reduced pressure to remove solvents. The crude product was purified by dialysis (membrane 3000 cut-off). The obtained product was sent to lyophilization to afford product **87** in 90% yield. ^{1}H NMR (600 MHz, D_2O) 8.14 (s, 6H), 4.90 (s, 18H), 4.70 (s, 36H), 4.48- 4.38 (m, 6H), 4.34 (d, 4H), 4.25- 4.02 (m, 24H), 3.94 (d, 24H), 3.93- 3.86 (m, 60H), 3.79 (dd, *J* = 23.8, 9.5 Hz, 72H), 3.75- 3.61 (m, 156H), 3.45- 3.25 (m, 24H), 3.19- 3.03 (m, 12H), 2.92- 2.74 (m, 36H), 2.66 (dt, *J* = 41.4, 21.0 Hz, 36H), 2.52 (dt, *J* = 82.2, 38.5 Hz, 12H), 2.00- 1.72 (m, 36H), 1.59 (d, *J* = 75.7 Hz, 12H).^{13}C NMR (600 MHz, D_2O) δ 175.1, 144.0, 125.3, 102.2, 99.8, 99.7, 83.1, 81.1, 80.4, 76.3, 72.9, 72.3, 71.5, 71.2, 70.6, 70.5, 70.1, 70.0, 69.8, 69.6, 69.5, 69.1, 67.7, 66.7, 66.7, 65.7, 63.2, 62.5, 60.9, 50.3, 30.8, 30.6, 29.7, 29.5, 28.3, 28.1. MALDI-TOF (*m/z)* calcd for $C_{300}H_{528}N_{21}O_{174}P_3S_{18}$ 7883.50, found 7892.

Figure A93.[1]H NMR analysis of **87** (600 MHz, D_2O)

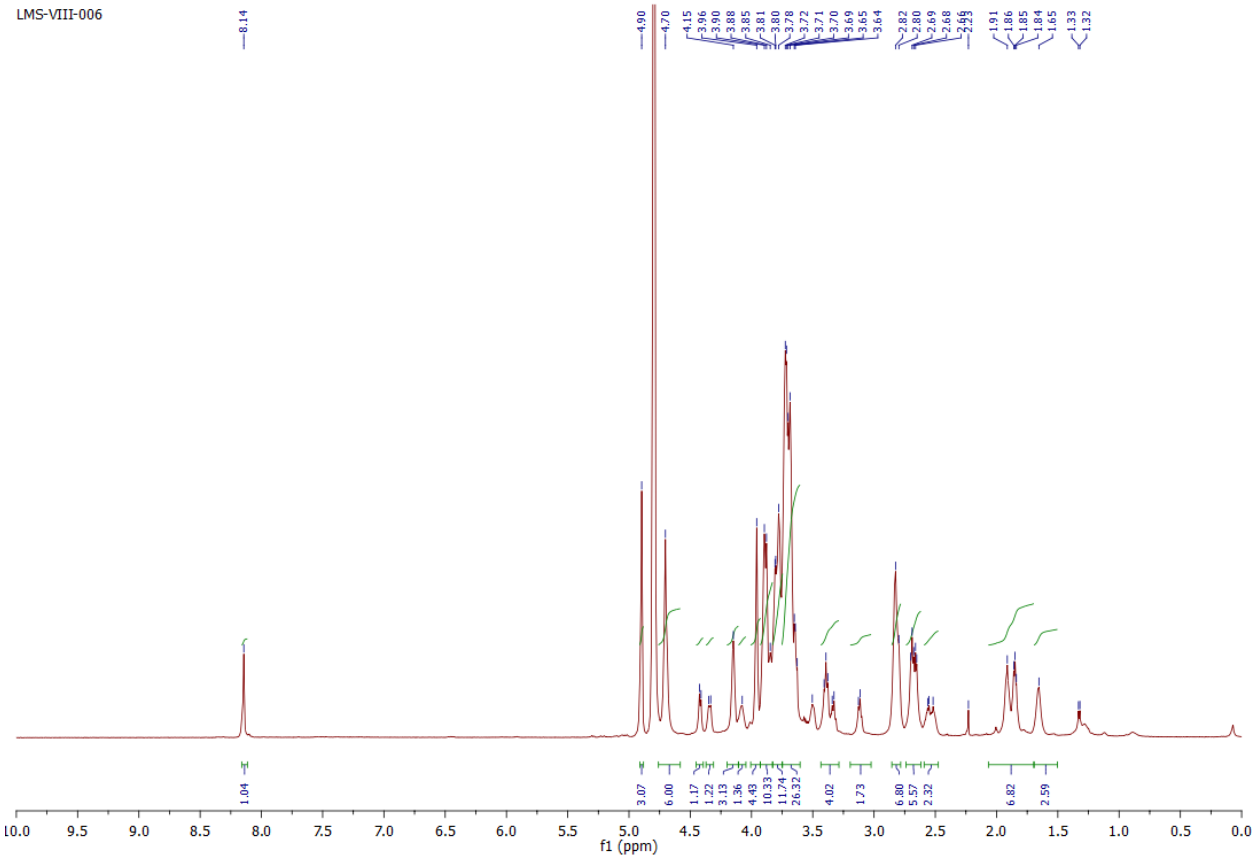

Figure A94.^{13}C NMR analysis of **87** (600 MHz, D_2O)

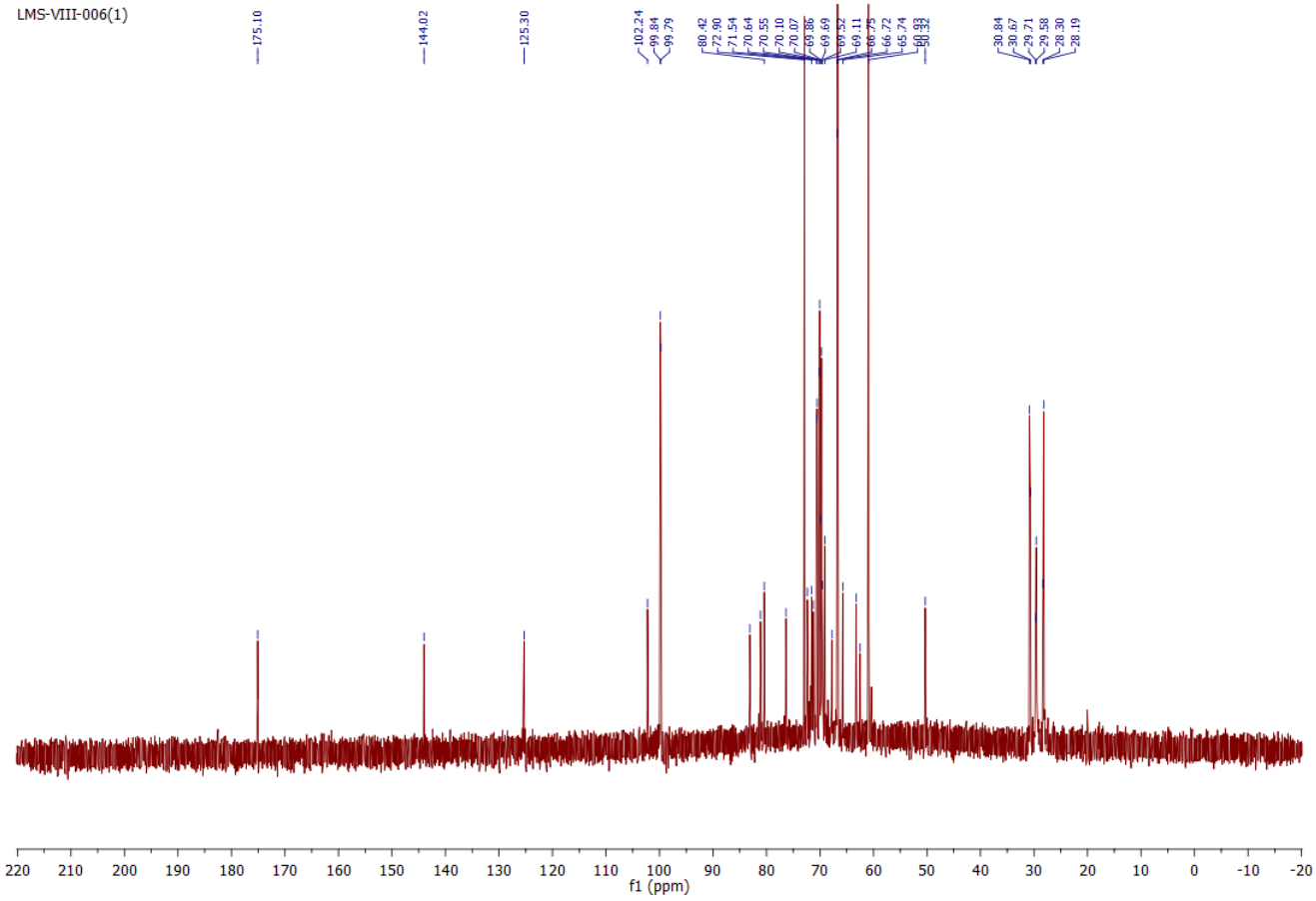

Figure A95. ^{31}P NMR analysis of **87** (600 MHz, D_2O)

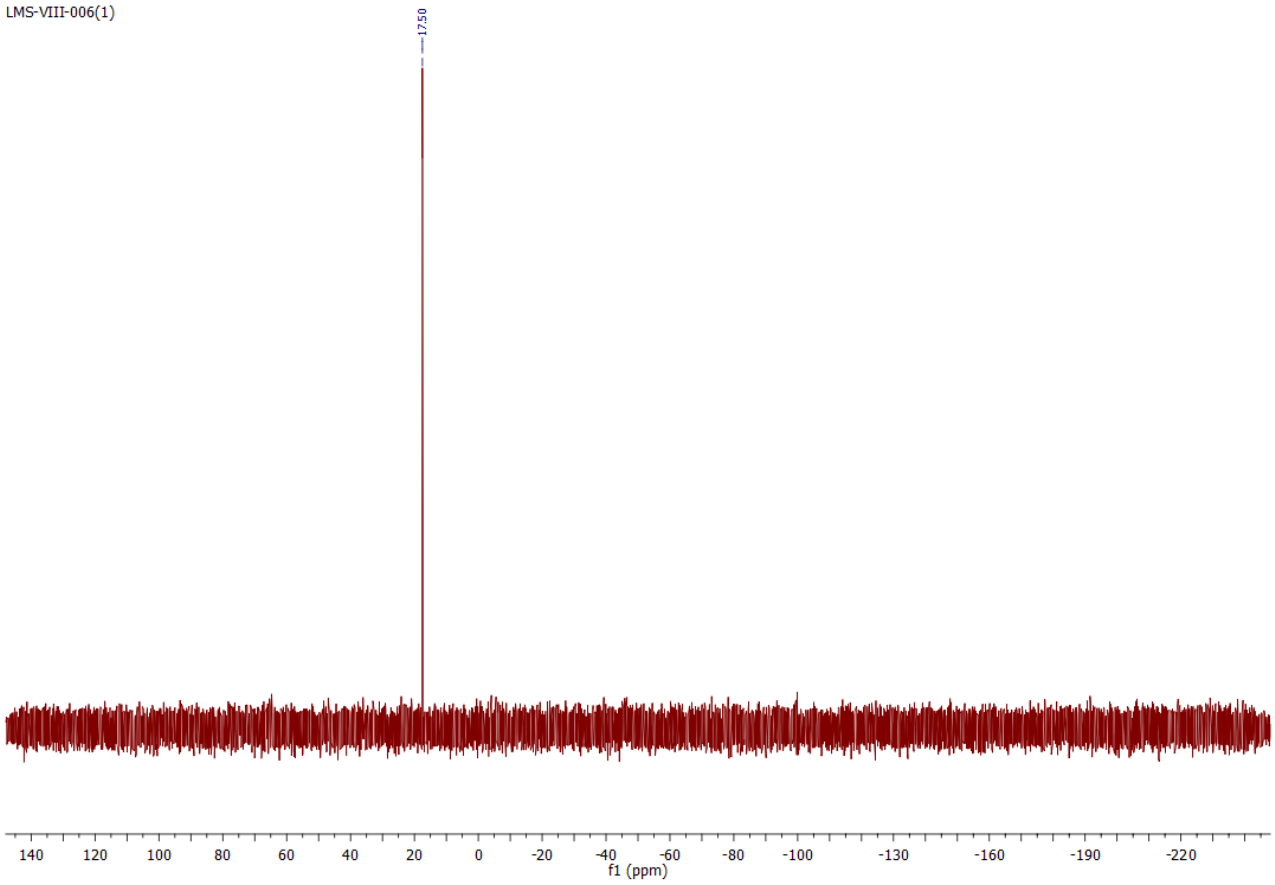

LMS-VIII-006

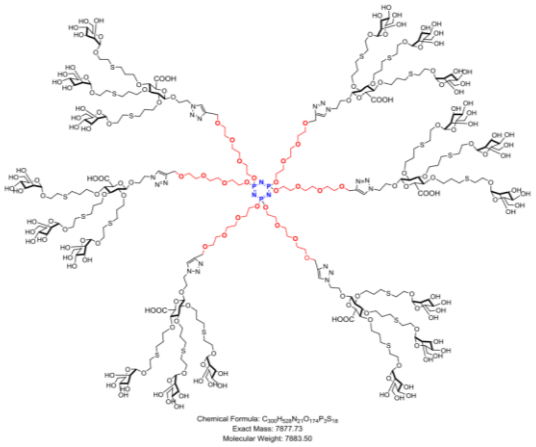

Figure A96. MALDI-TOF ANALYSIS **87**

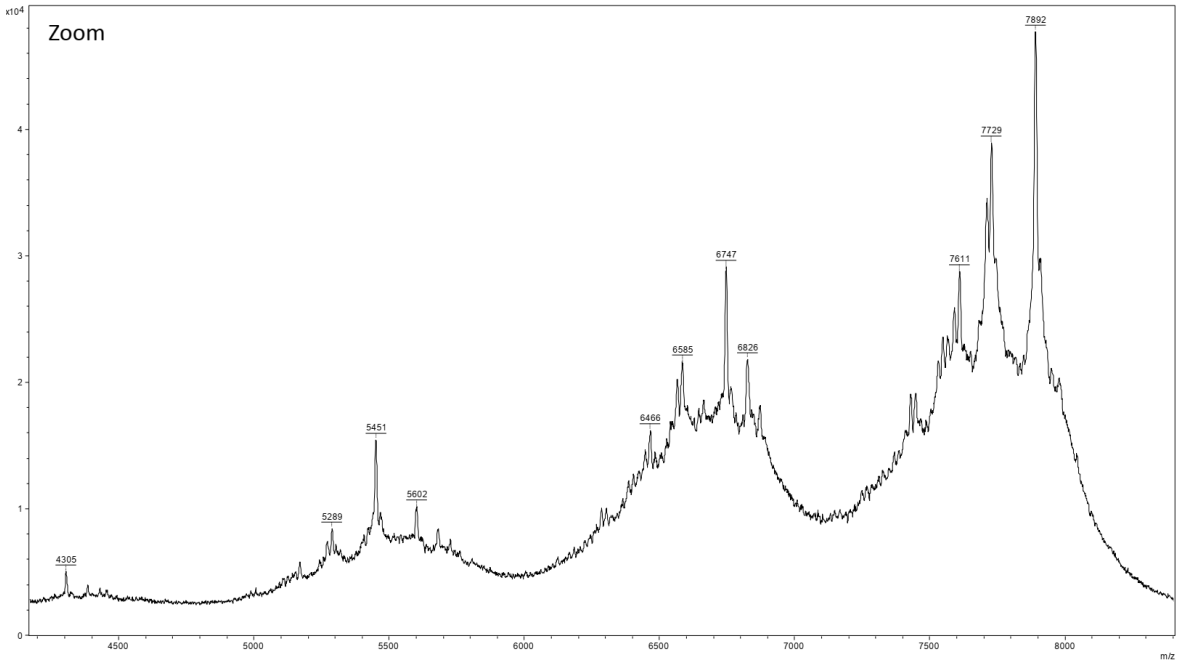

Synthesis and characterization of dendrimer 90

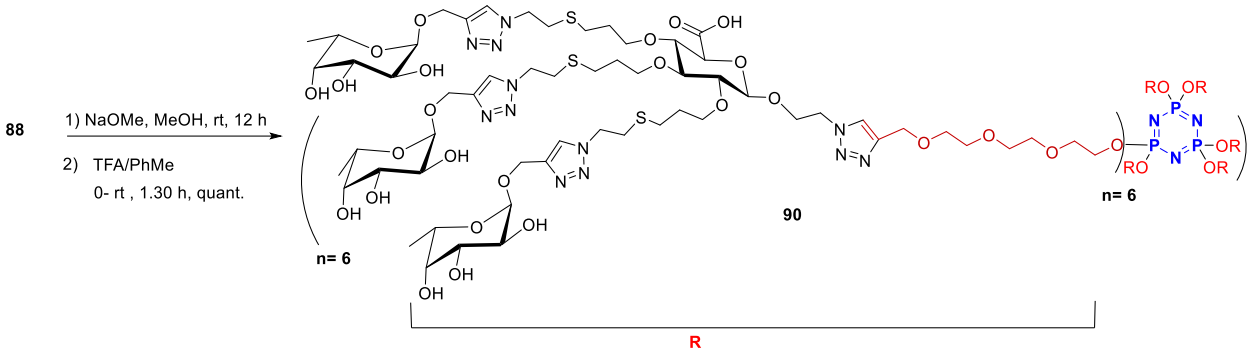

The reaction performed according to the general procedure B to afford product **90**. ^{1}H NMR (300 MHz, D_2O) δ 8.01- 8.13 (m, 24H, triazole), 4.95 (d, 22H, J = 3.0 Hz), 4.74 – 4.64 (m, 36H), 4.66 – 4.46 (m, 36H), 4.21 (d, 12H, J = 2.4 Hz), 4-08- 4.16 (m, 27 H), 3.89 (d, 27H, J = 5.1 Hz), 3.79 – 3.73 (m, 73H), 3.72- 3.59 (m, 128H), 3.22- 3.10 (m, 17H), 3.05- 2.95 (m, 28H), 2.93-2.88 (m, 11H), 2.45 (dd, 30H, J = 77.1, 55.9 Hz), 1.66 (d, 24H, J = 48.7 Hz), 1.42 – 1.10 (m, 37H), 1.06 (d, 54H, J = 6.6 Hz).

Figure A97. ^{1}H NMR analysis of **90** (300 MHz, D_2O)

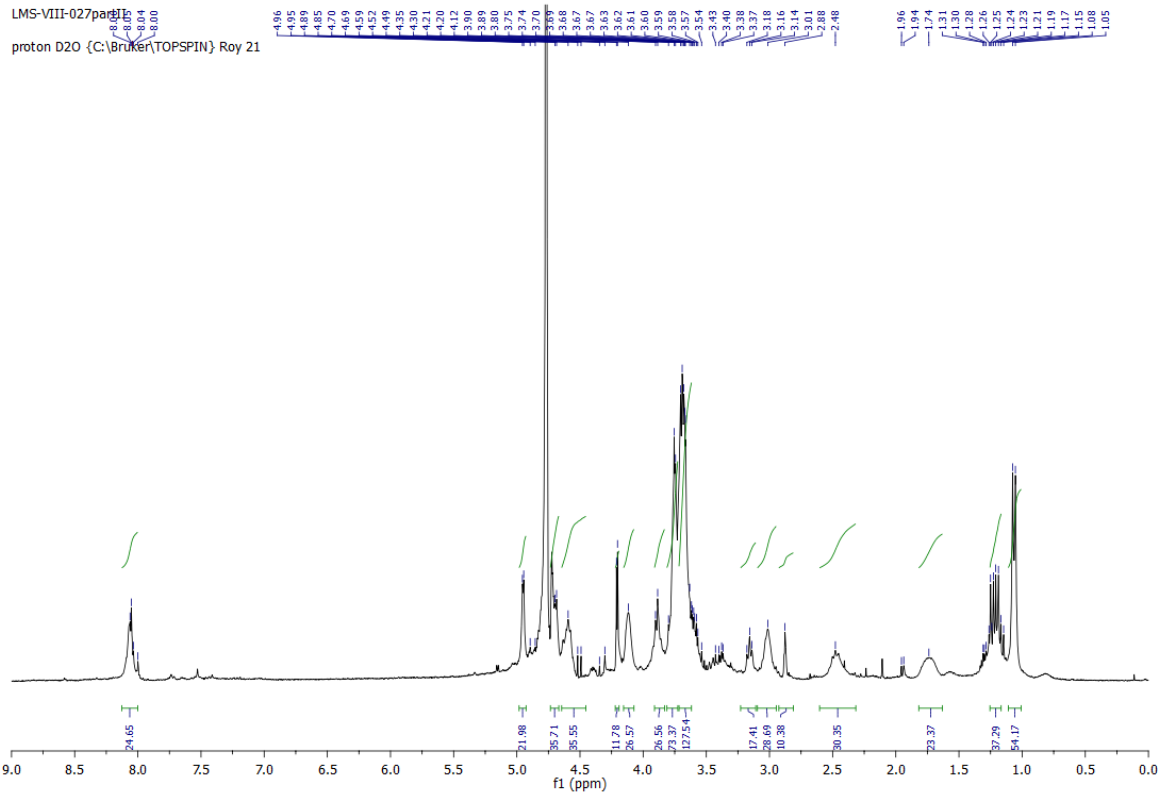

Figure A98.^{31}P NMR analysis of **90** (300 MHz, D_2O)

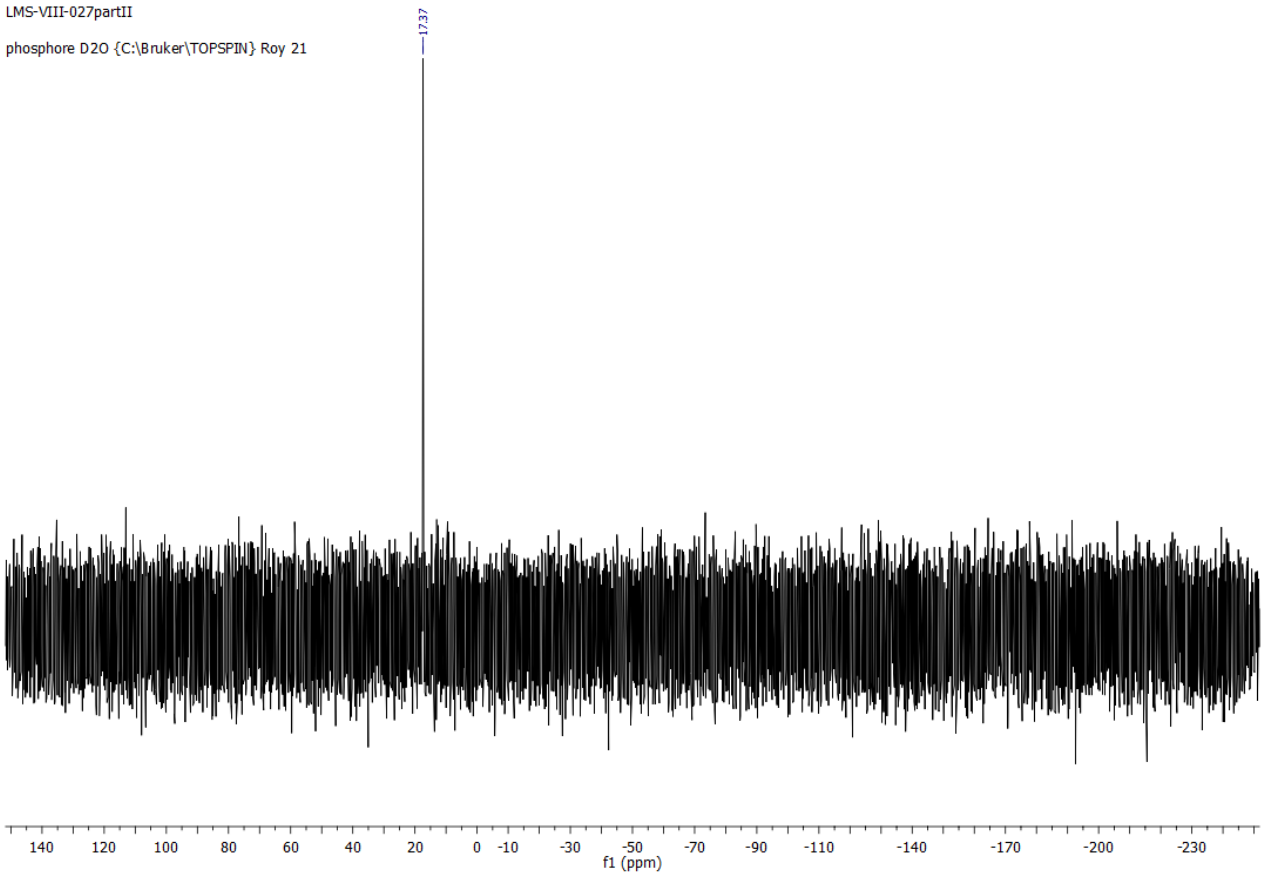

Experimental part chapter 4

1,3,4,6-Tetra-*O*-acetyl-2-phthalimido-2-deoxy-β-D-glucopyranoside (108)

Experimental: 1 M NaOMe (232 mL), was slowly added at 0 °C to D-glucosamine hydrochloride **107** (50 g, 0.232 mol). The reaction mixture was stirred for 2 h at r.t, then treated with finely ground phthalic anhydride (19 g, 0.128 mol) and stirred for another 45 min. The mixture was charged with the second portion of phthalic anhydride (19 g, 0.128 mol), Et_3N (35.5 mL, 0.255 mol), and MeOH (230 mL) and stirred for another 24. The intermediate phthalamate (and salts) were precipitated as a white solid by cooling the mixture to -20 °C for 4 h. These were filtered and thoroughly washed with cold MeOH, then dried overnight under reduced pressure. The solid was redispersed in pyridine (500 mL) with stirring and cooled to -5 °C, followed by treatment with Ac_2O (330 mL). The mixture was stirred at r.t for 48 h. This was redispersed in toluene and concentrated several times for the azeotropic removal of pyridine. The remaining slurry was redissolved in ethyl acetate and washed with saturated $NaHCO_3$, and brine. The combined aqous layer was extracted twice with ethyl acetate. The combined organic layer was dried over anhydrous sod. Sulphate, concentrated under reduced pressure. The crude product was dissolved in a minimal amount of hot EtOAc (100 mL), then diluted with hexanes (400 mL) and left to cool at –5 °C. The recrystallized product was collected by filtration, washed with cold hexanes, and dried to yield the desired tetraacetate (85.3 g, 77%). As the major β-isomer; mp 94-95 °C. All data of this compound is exactly matching with those previously reported. [407]

Compound 110

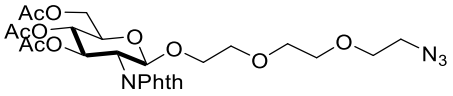

Experimental: To a solution of D-Gulcosamine tetraacetate **108** (3 g, 9.06 mmol) in dry DCM (40 mL), was added PEG_3-azide (3g, 17.14 mmol). The reaction mixture was cooled at 0 °C followed by slow addition of $BF_3.OEt_2$ (10 mL, 57.09 mmol). Reaction allowed stirring at rt overnight. The organic phases were washed with saturated aq. $NaHCO_3$, and water. The organic layer was dried over anhyd. Na_2SO_4 and the solvent evaporated under reduced pressure. The crude product was purified by flash column chromatography (hexanes/ethyl acetate, 60: 40%) to afford the product as oily residue (2 g, 55%). ^1H NMR (300 MHz, $CDCl_3$) δ 7.85 (dd, 2H, J = 5.4, 3.0 Hz, Ar), 7.74 (dd,2H, J = 5.4, 3.1 Hz, Ar), 5.81 (dd, 1H, J =

10.6, 9.2 Hz, H-3), 5.43 (d,1H, J = 8.5 Hz, H-1), 5.17 (t, 1H, J = 9.6 Hz, H-4), 4.38- 4.32 (m, 1H, H-2), 4.30 (dd, 1H, J = 8.0, 2.6 Hz, H_{6a}), 4.23- 4.08 (m, 1H, H_{6b}), 3.94- 3.82 (m, 1H, H5), 3.76 – 3.59 (m, 3H), 3.56 – 3.44 (m, 4H), 3.42 – 3.25 (m, 6H), 2.11 (s, 3H), 2.03 (s, 3H), 1.86 (s, 3H). ^{13}C NMR (300 MHz, $CDCl_3$) δ 170.7, 170.1, 169.5, 134.2, 131.5, 123.5, 98.2, 71.8, 70.7, 70.5, 70.4, 70.0, 69.94, 69.1, 69.0, 62.0, 54.6, 50.6, 29.7, 20.8, 20.6, 20.4. ESI-HRMS (*m/z*) calcd. for $C_{26}H_{32}N_4O_{12}$ 610.2355 $[M+NH_4]^+$, found 610.2352.

Figure A99. ^{1}H NMR analysis of compound **110** (300 MHz, $CDCl_3$)

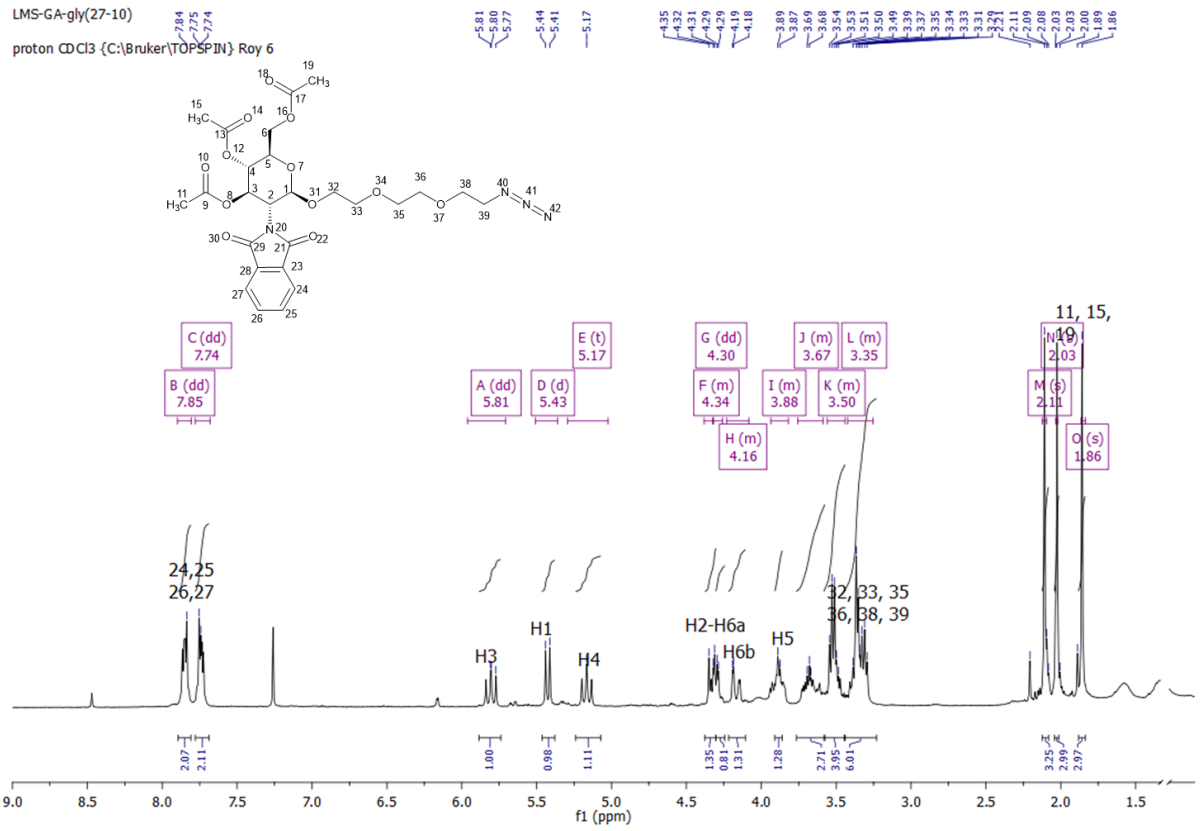

Figure A100. ^{13}C NMR analysis of compound **110** (300 MHz, $CDCl_3$)

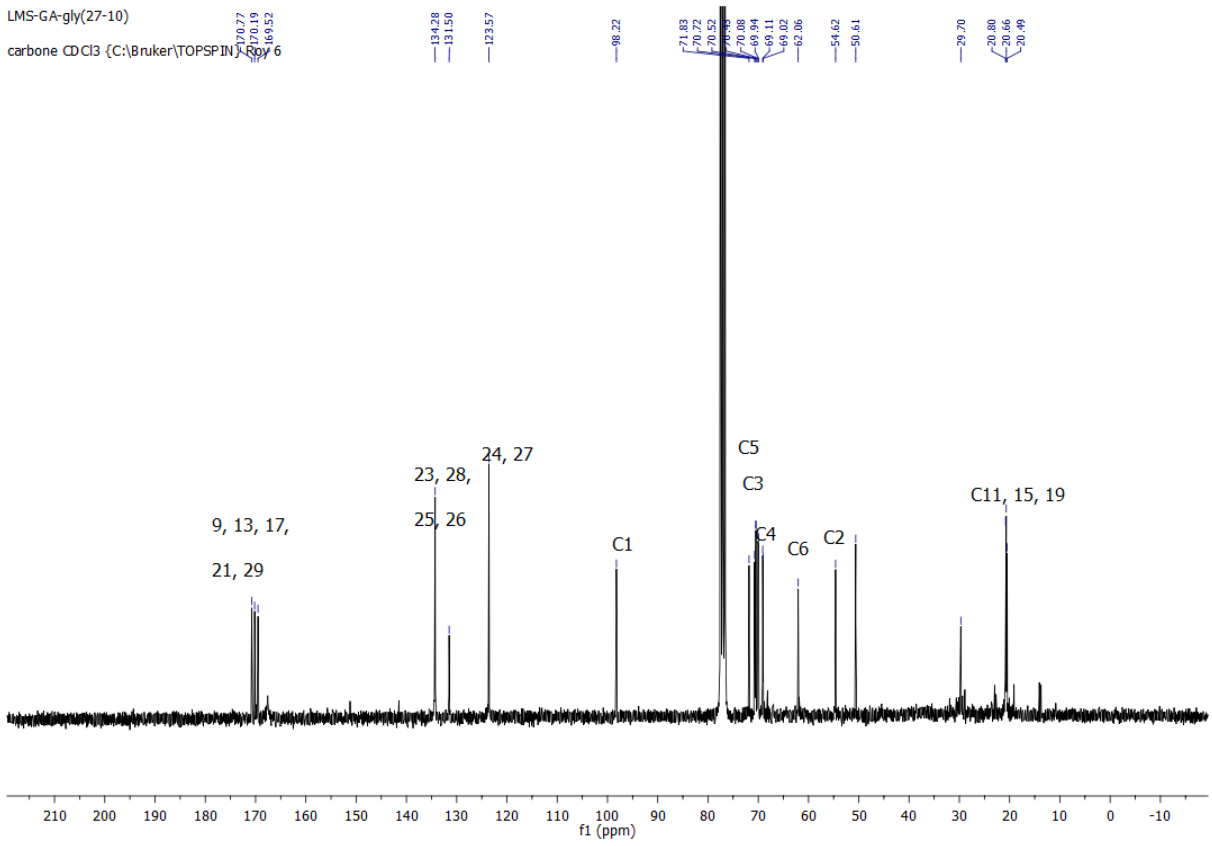

Figure A101. COSY analysis of compound **110** (300 MHz, $CDCl_3$)

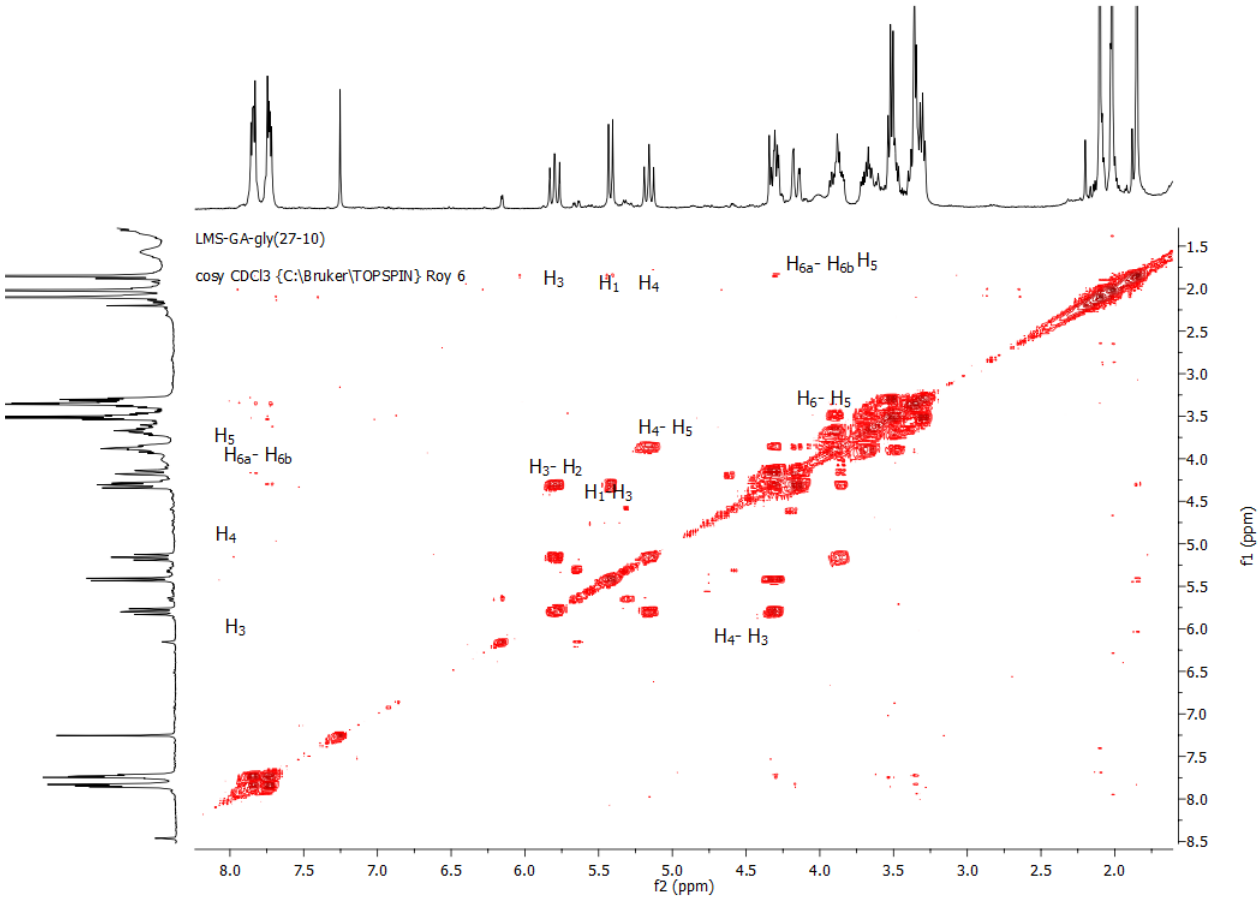

Figure A102. DEPT analysis of compound **110** (300 MHz, $CDCl_3$)

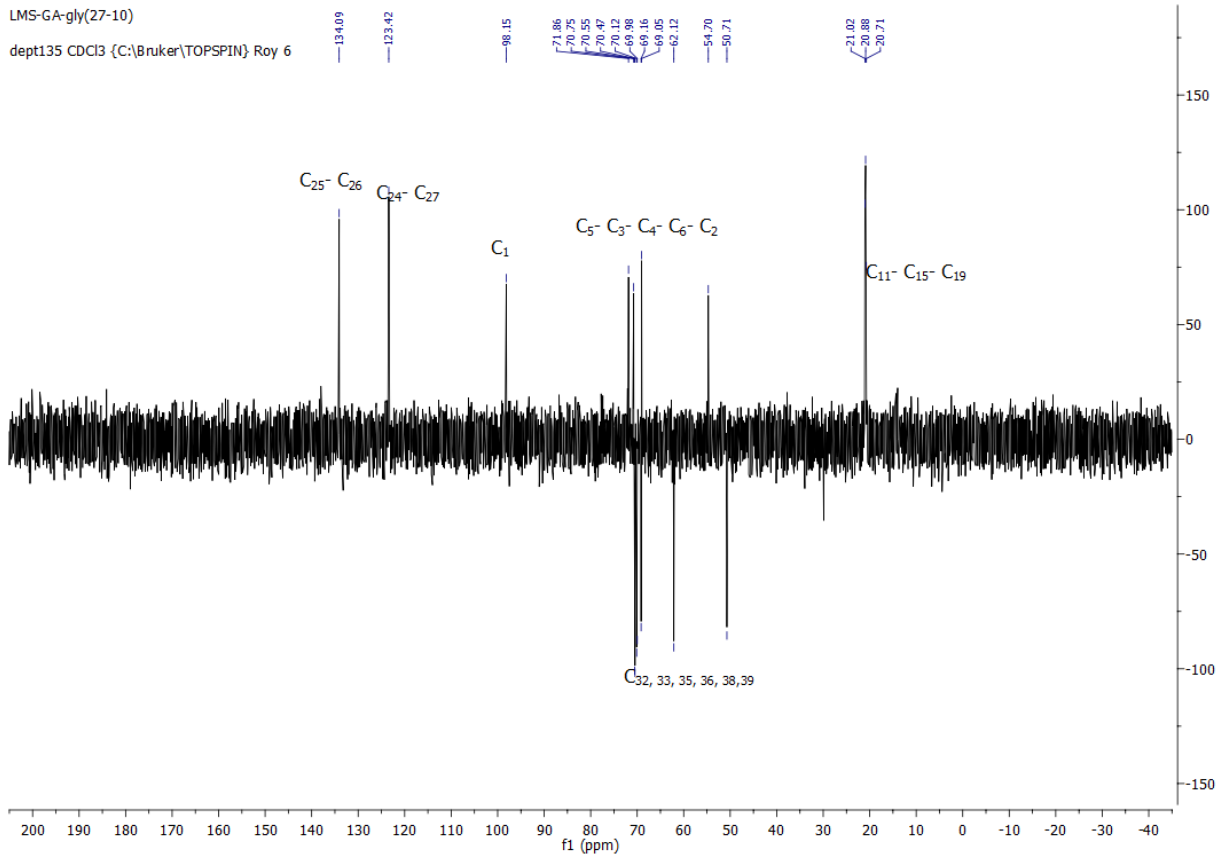

Compound 111

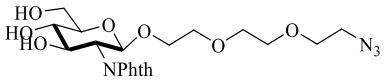

Experimental: Compound **110** (1.2g, 2.69 mmol) was dissolved in MeOH (50 mL), then MeONa/MeOH (1M, 1g, 18.6 mmol) was added till pH 7. The reaction mixture was stirred at rt for 5 hr. Then the reaction was neutralized with acidic resin (Amberlyst IR-120H), and was filtered through bad of celite, and the filtrate was then evaporated under reduced pressure to obtain product **111** as oily residue (0.9 g, 95%). ^{1}H NMR (600 MHz, CD_3OD) δ 7.91-7.86 (m, 2H, Ar), 7.86 -7.80 (m, 2H, Ar), 5.23 (d, 1H, J = 8.5 Hz, H_1), 4.28 (dd,1H, J = 10.7, 8.3 Hz, H_3), 3.99 (dd, 1H, J = 10.7, 8.5 Hz, H_2), 3.93 (dd, 1H, J = 12.0, 2.1 Hz, H_{6a}), 3.79 – 3.71 (m, 1H, H_{6b}), 3.40 (dd, 1H, J = 11.7, 6.3 Hz, H_4), 3.40 (dd, 1H, J = 11.7, 6.3 Hz, H5).^{13}C NMR (600 MHz, CD_3OD) δ 168.5, 168.2, 134.1, 131.7, 122.7, 98.2, 76.8, 71.2, 71.1, 70.0, 69.8, 69.7, 69.6, 68.4, 61.3, 57.1, 50.2. ESI-HRMS (*m/z*) calcd for C_{20} H_{26} N_4 O_9 $[M+Na]^+$ 489.1592, found 489.1577.

Figure A103. ^{1}H NMR analysis of compound **111** (600 MHz, CD_3OD)

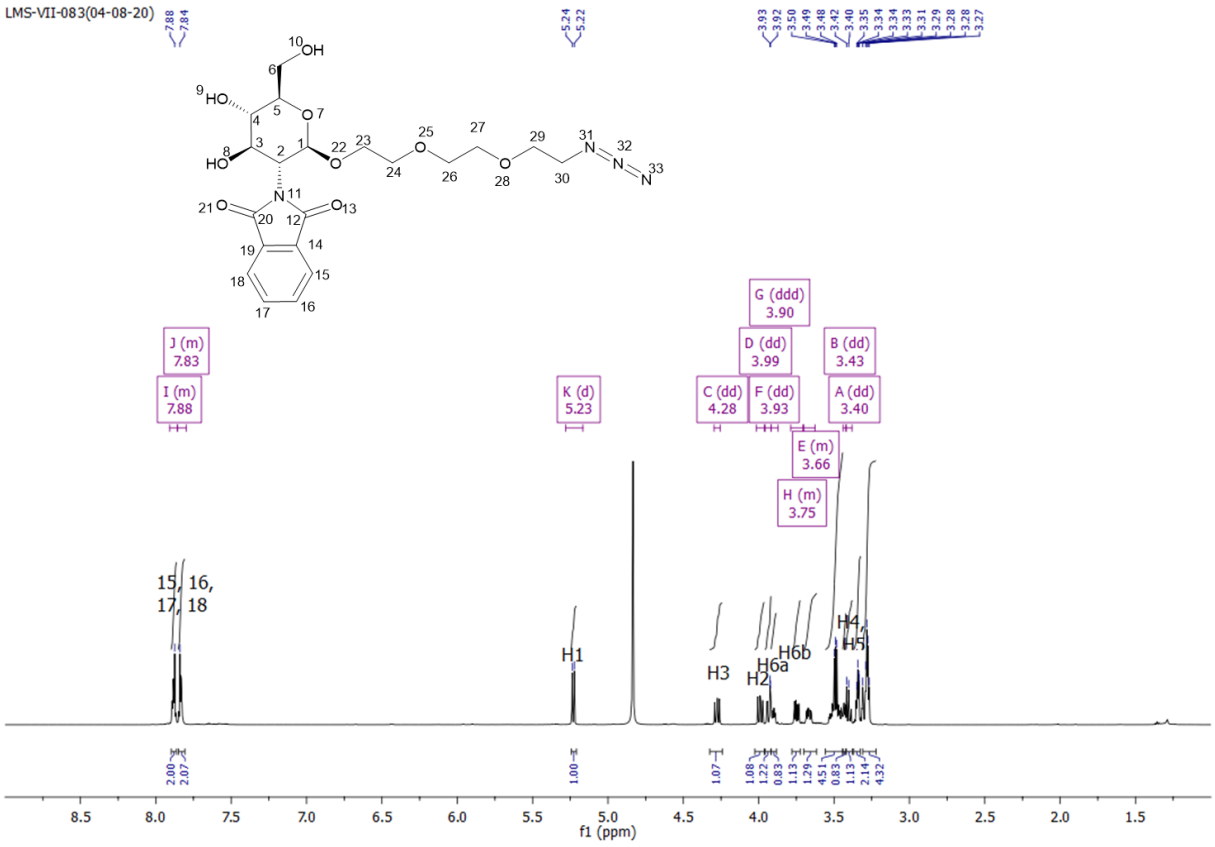

Figure A104. ^{13}C NMR analysis of compound **111** (600 MHz, CD_3OD)

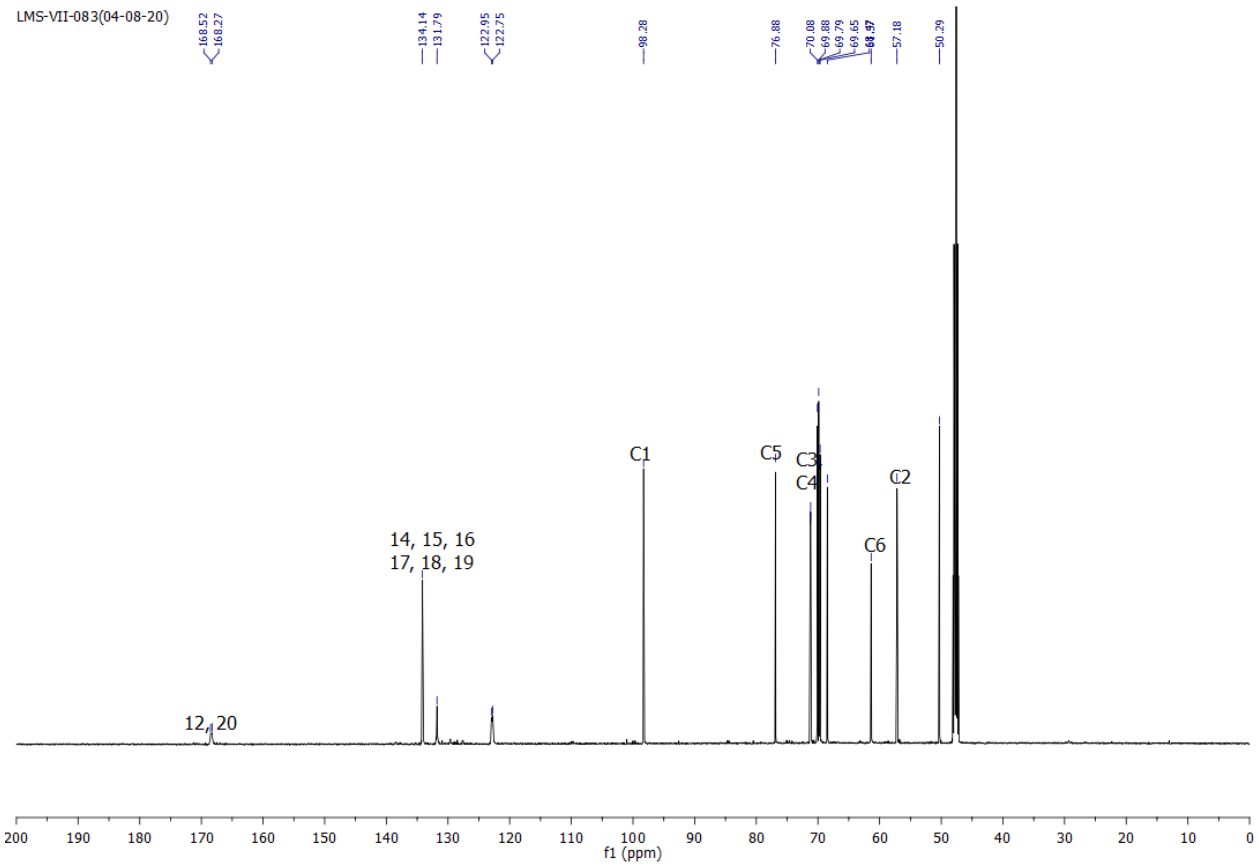

Figure A105. COSY analysis of compound **111** (600 MHz, CD_3OD)

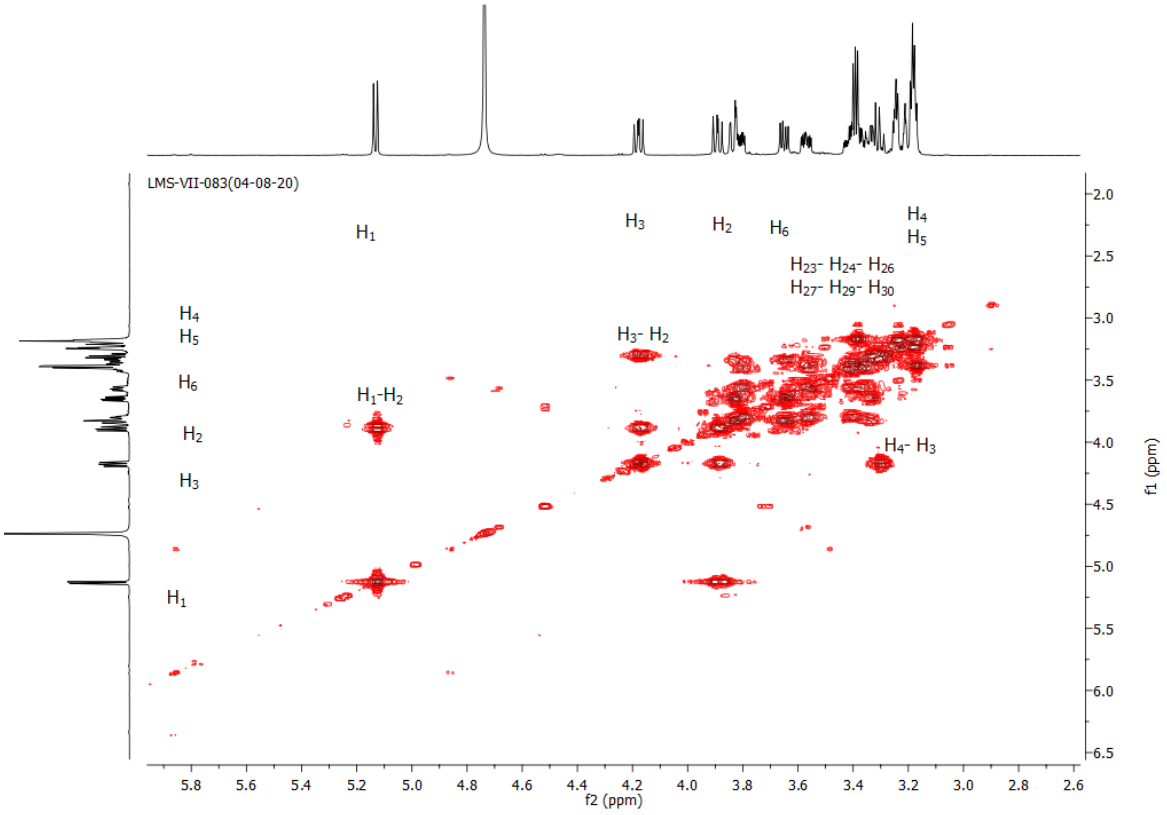

Compound 113

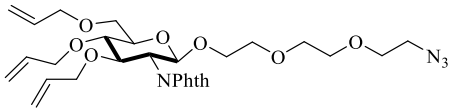

Experimental: To a solution of **111** (5.5 g, 11.8 mmol) in DMF (90 mL) was added a freshly prepared solution of LiHMDS (1.0 M in Toluene, 60 mL) at -75 ºC. The mixture was stirred for 30 min before allyl bromide (23 mL, 76.7 mmol) was added, and the mixture was allowed to stir at room temperature for 2 h. before being quenched by sat. aq. NH_4Cl. The mixture was diluted with EtOAc, washed with brine twice, dried over anhyd. Na_2SO_4, the filtrate evaporated in *vacuo* and purified by silica gel flash chromatography (Hexane/ EtOAc 6 :4) to give allylated product as oily residue (4.2 g, 60%). ^{1}H NMR (300 MHz, $CDCl_3$) δ 7.94-7.75 (m, 2H, Ar), 7.74 (dd, 2H, J = 5.5, 3.1 Hz, Ar), 6.09- 5.74 (m, 2H-allyl), 5.62-5.47 (m, 1H- allyl), 5.40- 5.07 (m, 6H-allyl, H_1), 5.01 (dd, 1H, J = 17.2, 3.1, 1.5 Hz, H_3), 4.80 (dd, 1H, J = 10.3, 1.6 Hz, H_4), 4.42-4.00 (m, 7H-allyl, H_2), 3.95-3.82 (m, 1H, H_5), 3.72 (dd, 2H, J = 5.7, 2.6 Hz, $H_{6,6}$), 3.69-3.58(m, 2H, CH_2), 3.58 – 3.42 (m, 6H, 3xCH_2), 3.41-3.35 (m, 2H, CH_2), 3.34-3.27 (m, 2H, CH_2).^{13}C NMR (300 MHz,

$CDCl_3$) δ 134.7, 134.6, 134.4, 134.0, 131.8, 117.0, 116.9, 98.3, 79.0, 78.8, 75.0, 73.6, 72.5, 70.5, 70.4, 70.0, 69.9, 68.7, 55.9, 50.6. ESI-HRMS (*m/z*) calcd for $C_{29}H_{38}N_4O_9$ $[M+ NH_4]^+$ 604.2977, found 604.2971.

Figure A106. ^1H NMR analysis of compound **113** (300 MHz, $CDCl_3$)

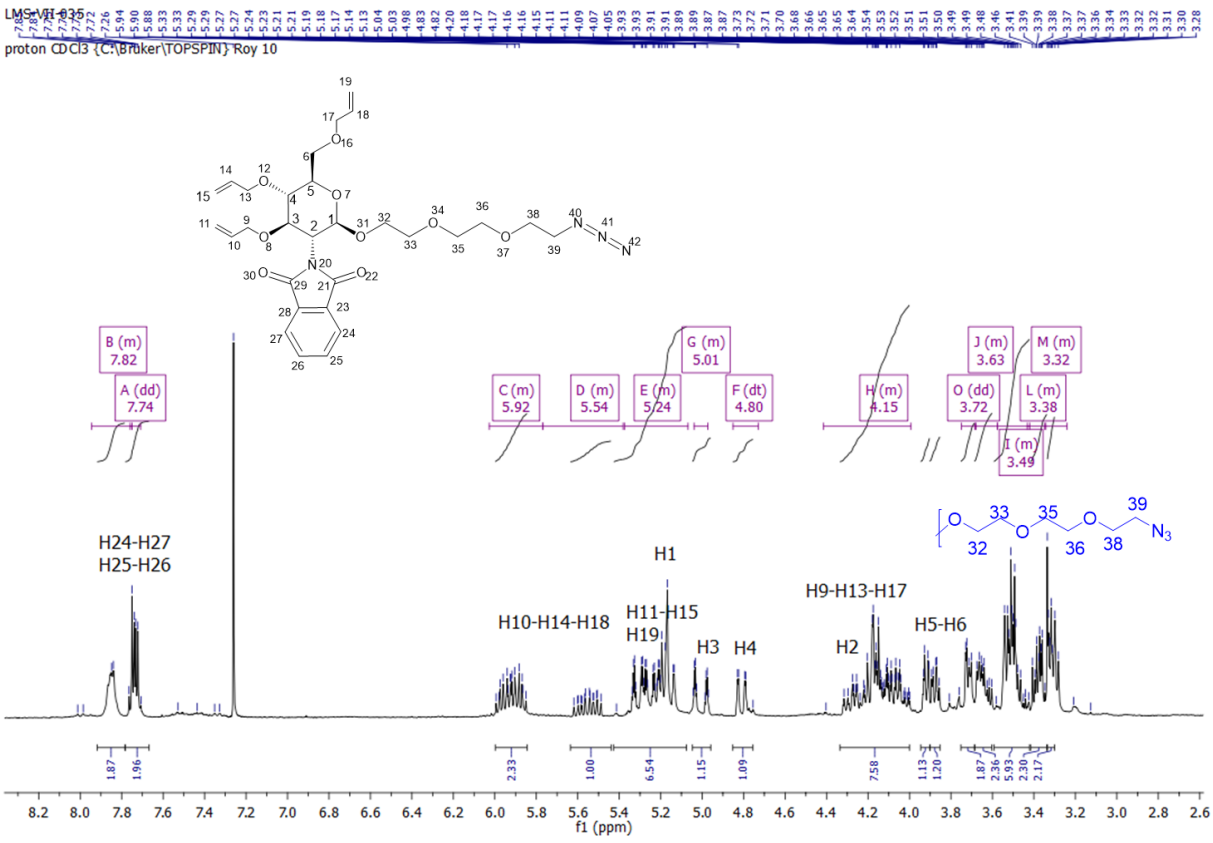

Figure A107. ^{13}C NMR analysis of compound **113** (300 MHz, $CDCl_3$)

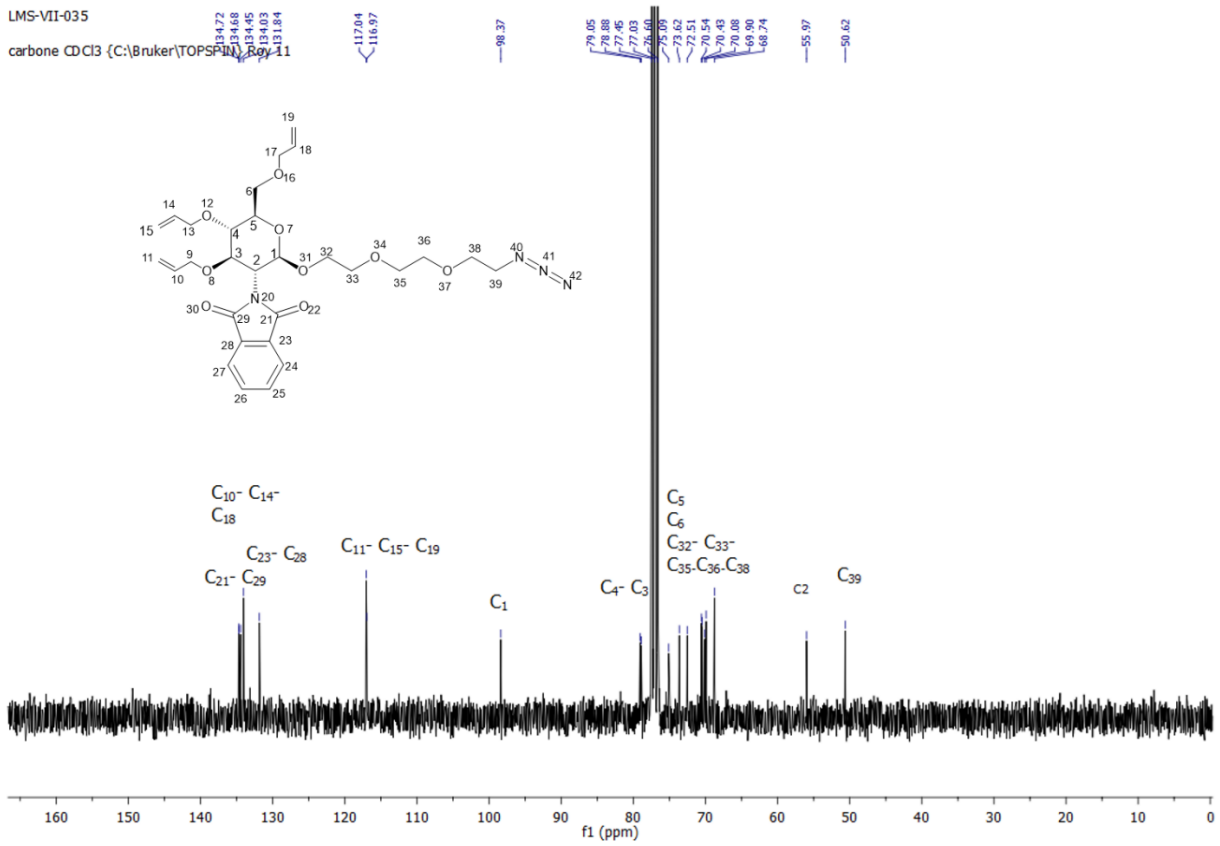

Figure A108. COSY analysis of compound **113** (300 MHz, $CDCl_3$)

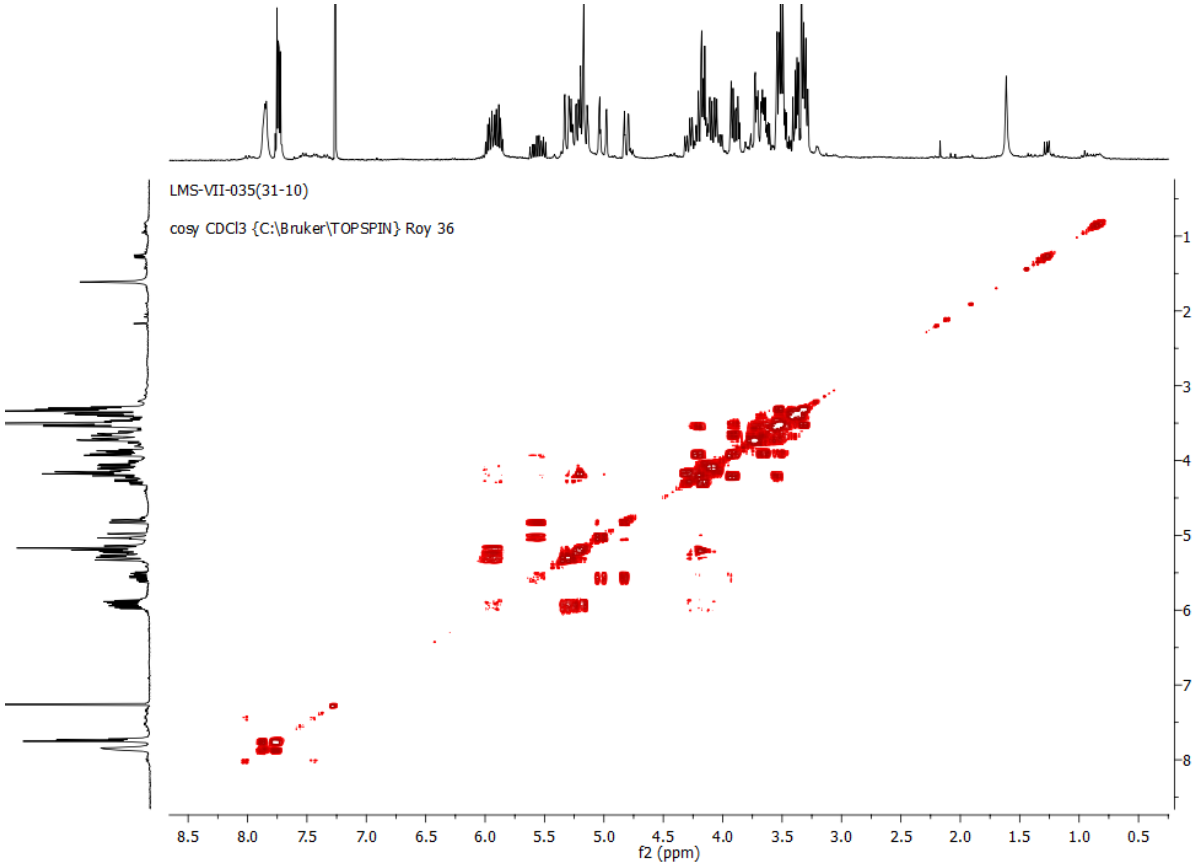

Figure A109. HSQC analysis of compound **113**(300 MHz, $CDCl_3$)

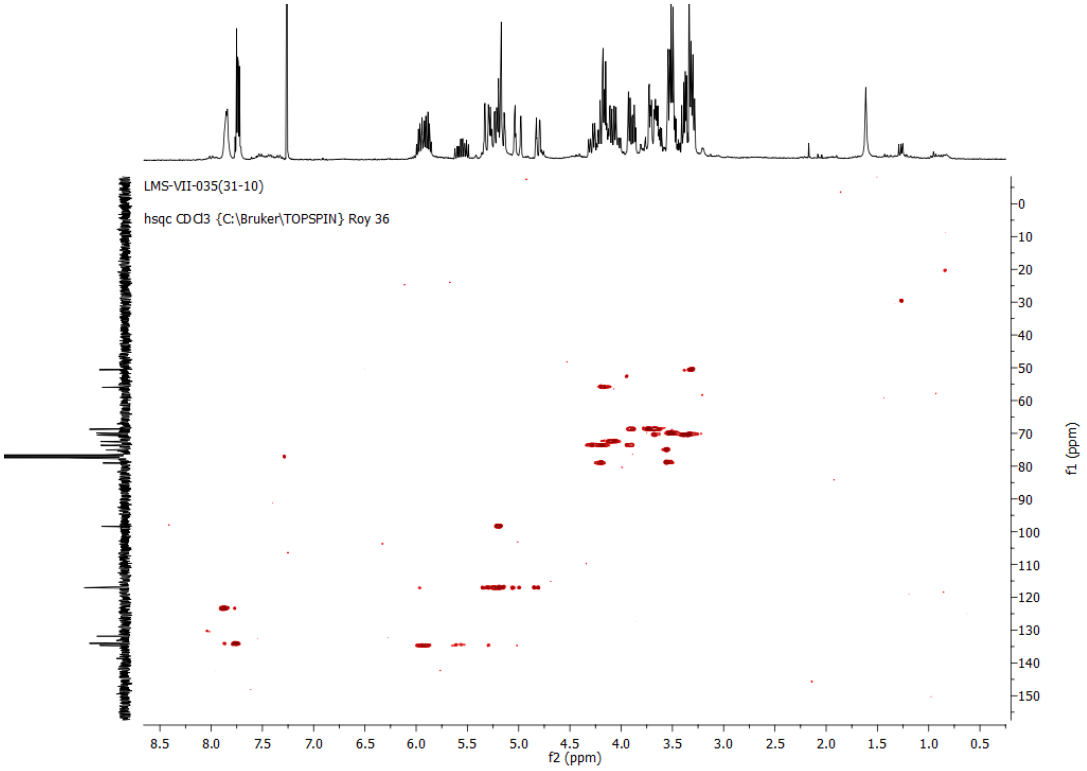

Compound 114

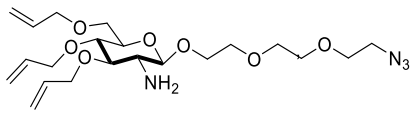

Experimental: Ethylenediamine (0.80 mL, 8.64 mmol) was added dropwise at 0 ºC to a stirred solution of compound **113** (400 mg, 0.234 mmol) in *n*-butanol (10 mL). The reaction mixture was stirred for 2 h at 85 °C. The solvent was removed under reduced pressure and repeatedly evaporated with co-solvent toluene. The resulting residue was purified by flash chromatography packed with dry silica gel (DCM/Methanol 97: 3%), to obtain the product as oily residue, (260 mg , 83%).^{1}H NMR (300 MHz, $CDCl_3$) δ 6.11-5.68 (m, 3H), 5.42-5.05 (m, 6H), 4.59-3.93 (m, 8H), 3.77-3.71 (m, 1H), 3.72-3.63 (m, 10H, PEG_3), 3.64-3.58 (m, 1H), 3.47- 3.34 (m, 4H), 3.33-3.25 (m, 1H), 2.80 (dd, *J* = 9.7, 8.0 Hz, 1H), 1.89 (s, 2H).^{13}C NMR (300 MHz, $CDCl_3$) δ 134.8, 134.6, 123.0, 117.1, 117.0, 112.2, 103.9, 84.7, 78.2, 75.2, 74.1, 73.5, 72.4, 70.7, 70.5, 70.3, 70.0, 68.8, 56.8, 50.7. ESI-HRMS (*m/z*) calcd for $C_{21}H_{36}N_4O_7$ $[M+H]^+$ 457.2657; found 457.2651.

Figure A110. ESI-MS *m/z* analysis of compound **114**

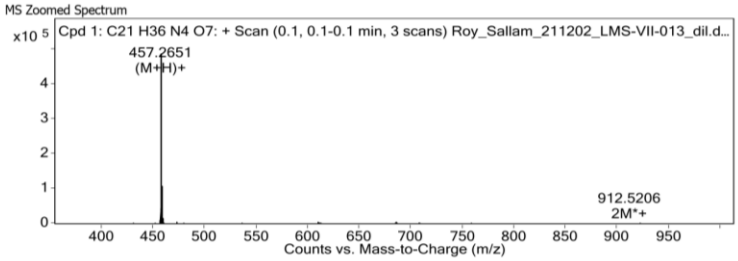

MS Spectrum Peak List

m/z	*Calc m/z*	Diff(ppm)	z	Abund	Formula	Ion
456.2564	456.2579	-3.12		520	C21 H36 N4 O7	M*+
457.2651	457.2657	-1.26		504081	C21 H37 N4 O7	(M+H)+
457.532				27156		
458.2676	458.2687	-2.4		111639	C21 H37 N4 O7	(M+H)+
458.5347				2669		
459.2707	459.2712	-1.02		17109	C21 H37 N4 O7	(M+H)+
460.2737	460.2737	0.06		2264	C21 H37 N4 O7	(M+H)+
479.2468	479.2476	-1.7	1	2799	C21 H36 N4 Na O7	(M+Na)+
495.2265	495.2216	9.93	1	900	C21 H36 K N4 O7	(M+K)+
912.5206	912.5163	4.79	1	52	C42 H72 N8 O14	2M*+

Figure A111. ^{1}H NMR analysis of compound **114** (300 MHz, $CDCl_3$)

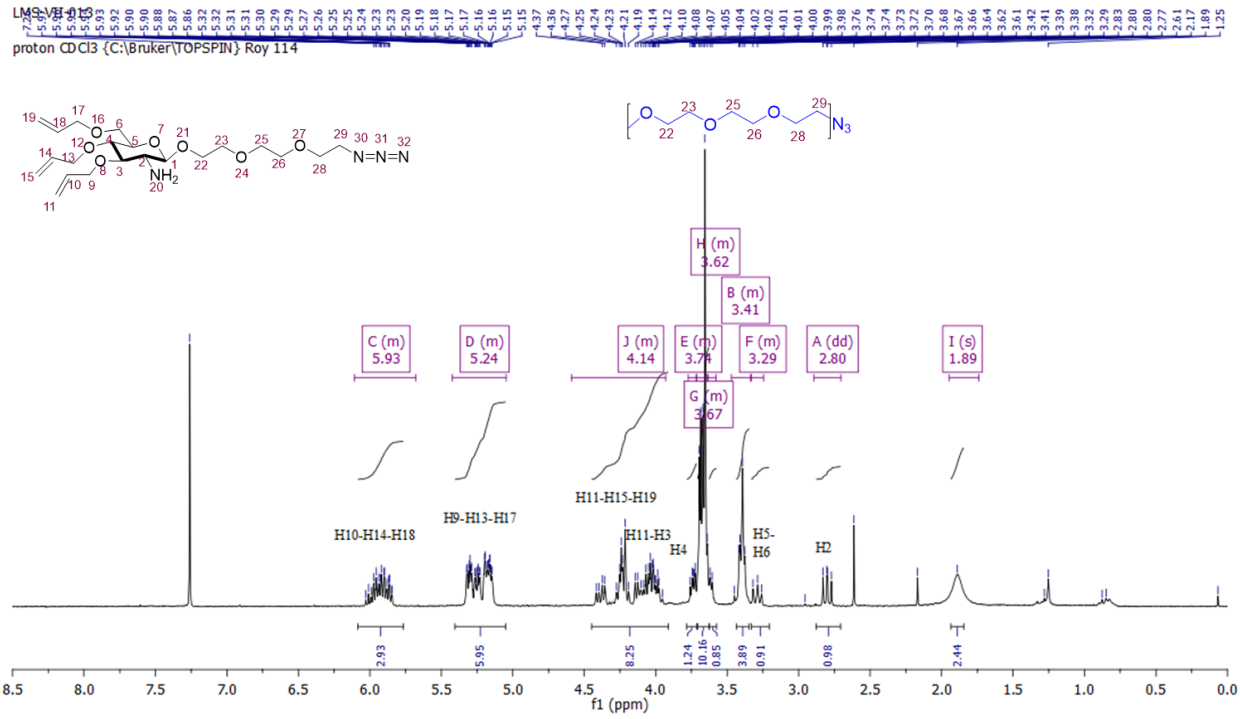

Figure A112. ^{13}C NMR analysis of compound **114** (300 MHz, $CDCl_3$)

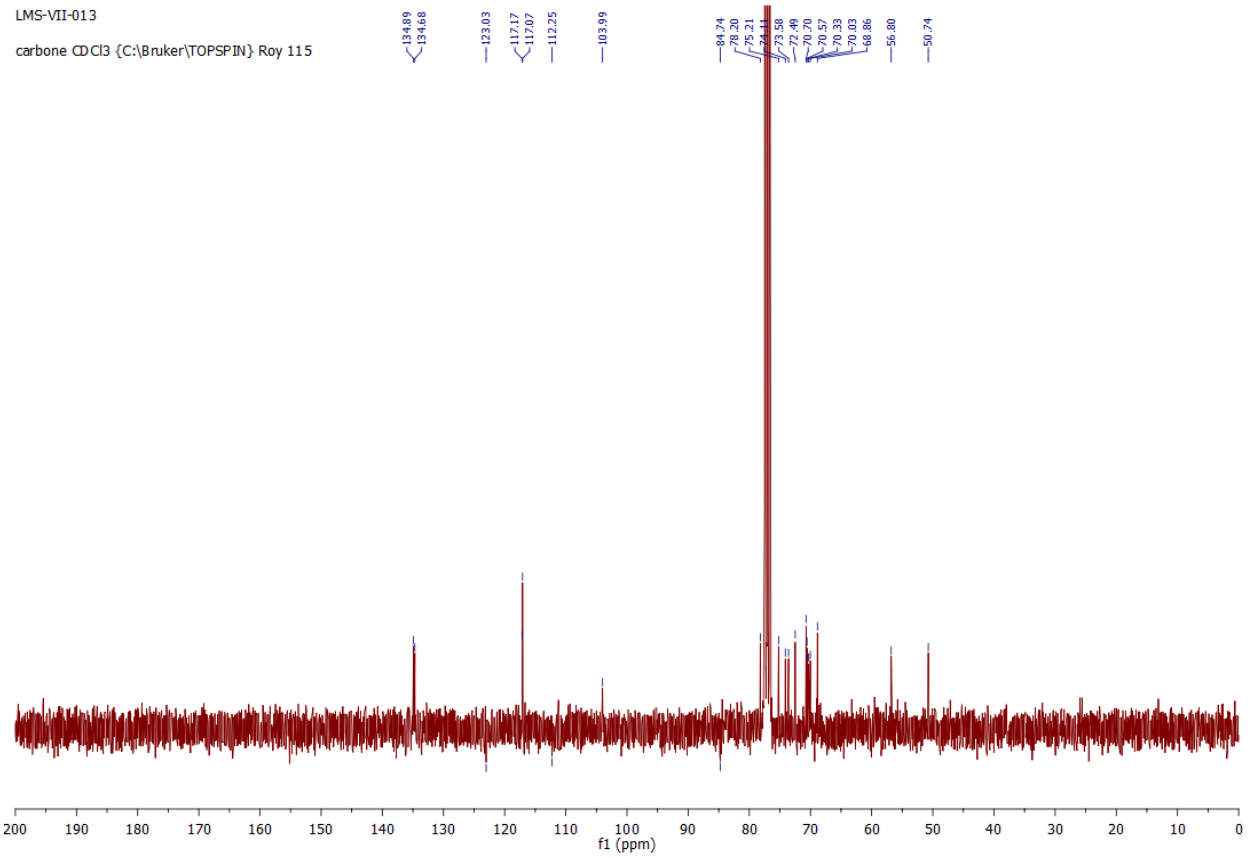

Compound 117

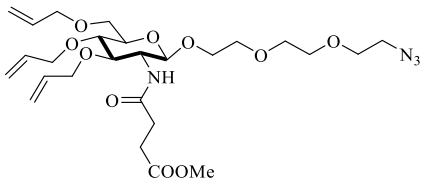

Experimental: Compound **114** (0.4 g, 0.877 mmol) and methoxy butanoic acid **115** (0.12 g, 0.877 mmol) were dissolved in DMF (6 mL). To this solution was added 1-Hydroxybenzotriazole hydrate (HOBt) (0.12g, 0.877 mmol) and Et_3N (0.4 mL, 2.89 mmol). After stirring the resultant solution for 5 minutes, it was cooled to 0 ºC, and *N,N*-diisopropylcarbodimide (DIC) (0.3 mL, 1.32 mmol) was added at once. The reaction mixture was allowed to warm to room temperature and continue stirring for 18 h. The resulting mixture was partitioned between EtOAc and water and extracted three times with EtOAc. The organic layers were combined and sequentially washed with sat. aq. $NaHCO_3$, sat. aq. NH_4Cl, and brine. The organic layer was dried over Na_2SO_4 and concentrated under reduced pressure. The resulting crude solid was purified by flash

coloumn chromatography (EtOAc/ hexane 7:3%) yielding **117** as a white oily residue (0.35 g, 72%). ^{1}H NMR (300 MHz, $CDCl_3$) δ 6.27 (d, 1H, J = 8.1 Hz, NH), 6.02- 5.64 (m, 3H, 3xCH allyl), 5.34- 4.84 (m, 6H, 3xCH_2 allyl), 4.70 (d, 1H, J = 8.2 Hz, H1), 4.29- 3.93 (m, 6H, CH_2, allyl), 3.83 (ddd, 1H, J = 11.9, 7.8, 4.4 Hz, H_3), 3.79- 3.66 (m, 2H, H_2, H_5), 3.61 (s, 3H, CH_3), 3.65- 3.52 (m, 8H), 3.43 (t,1H, J = 7.1 Hz, H_4), 3.40- 3.24 (m, 2H, 2xH6, CH_2), 2.59 (t,2H, J = 6.8 Hz, CH_2), 2.44 (t, 2H, J = 6.8 Hz, $NHCH_2$). ^{13}C NMR (300 MHz, $CDCl_3$) δ 173.2, 171.5, 135.1, 134.7, 134.7, 116.8, 116.7, 116.5, 100.4, 81.0, 74.8, 73.3, 72.3, 70.6, 70.6, 70.4, 69.8, 68.9, 68.3, 56.5, 51.7, 50.5, 41.8, 30.9, 29.1, 23.4.

Figure A113. ^{1}H NMR analysis of compound **117** (300 MHz, $CDCl_3$)

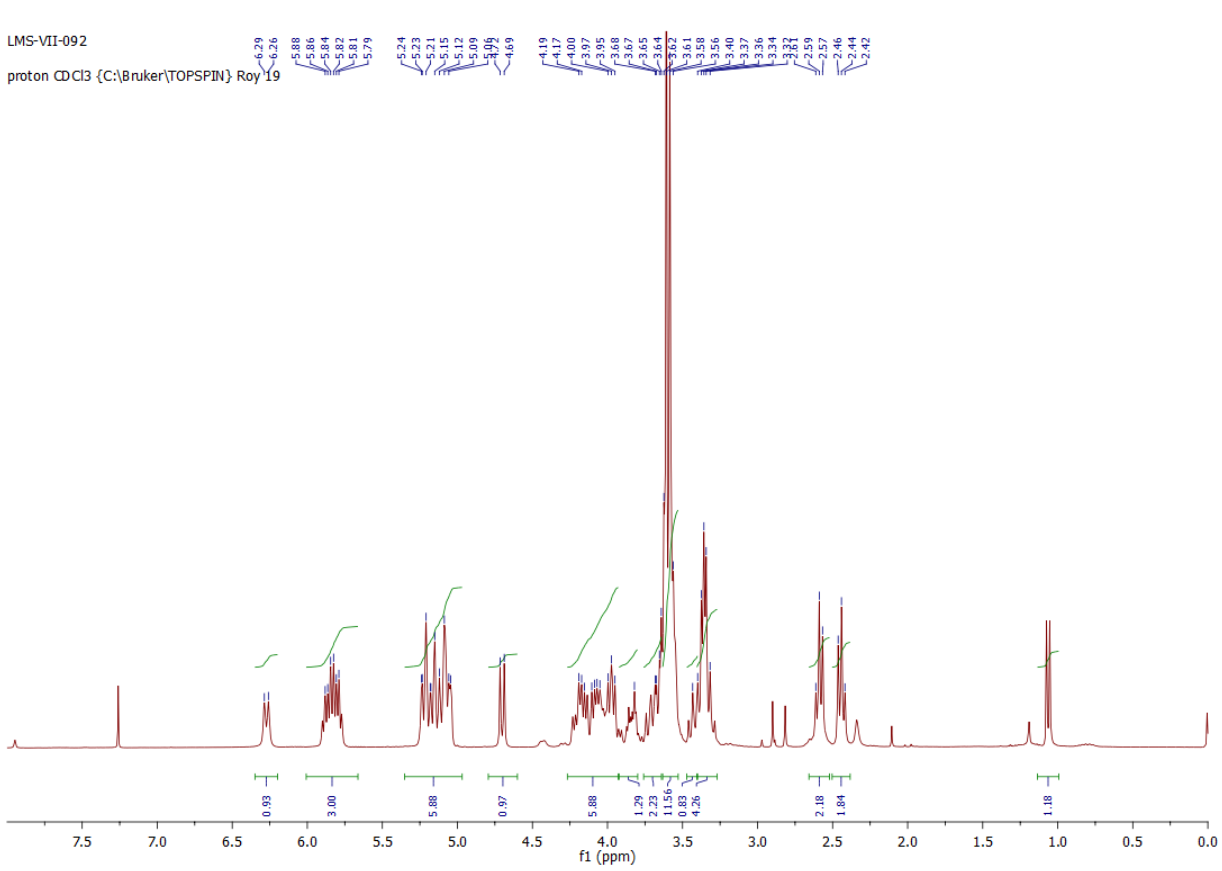

Figure A114. ^{13}C NMR analysis of compound **117** (300 MHz, $CDCl_3$)

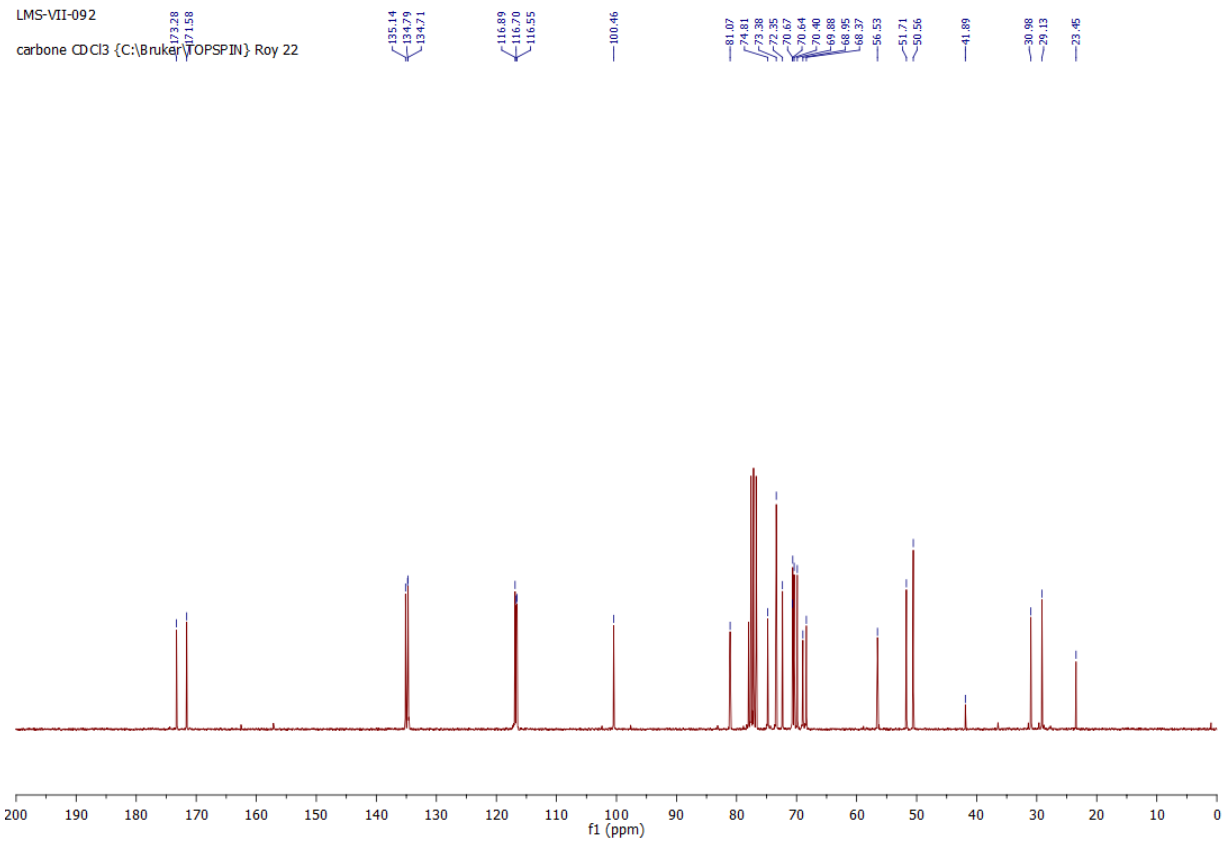

Compound 118

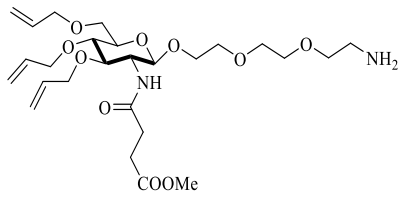

Experimental: To a solution of compound **117** (100 mg, 0.175 mmol) in THF (3 mL), was added triphenyl phosphine (80 mg, 0.305 mmol), and 0.2 mL of water. The reaction mixture is allowed to stir overnight at rt. The solvent was evaporated under reduced pressure. The crude mixture was Purified by column chromatography packed with dry silica (DCM/ MeOH 70: 30%), to afford product **118** as oily crystals (50 mg, 52%).^{1}H NMR (300 MHz, $CDCl_3$) δ 6.27 (d, 1H, J = 8.1 Hz, NH), 6.14- 5.65 (m, 3H, 3xCH allyl), 5.25- 4.98 (m, 6H, 3xCH_2 allyl), 4.71(d, 1H, J = 8.2 Hz, H_1), 4.32- 3.71 (m, 6H, CH_2, allyl), 3.82 – 3.25 (m, 15H), 3.15 (s, 1H), 2.80 (dd, 4H, J = 25.7, 14.8 Hz), 2.50 (d, 2H, J = 11.5 Hz), 1.80 (dt, 12H, J = 75.4, 30.4 Hz).

Compound 119

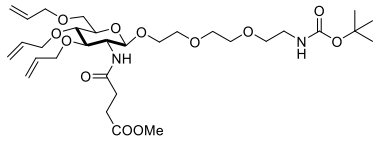

Experimental: The product from previous step **118** (100 mg, 0.18 mmol), was dissolved in dry dichloromethane (10 mL), to this solution was added Et_3N (0.1 mL, 0.59 mmol) and Boc_2O (50 mg, 0.24 mmol), the resulting mixture was allowed to stir at room temperature for 16 h then concentrated under vacuum and the residue was purified on column chromatography (DCM/ MeOH 97: 3 %) to afford the desired product as a colorless oil (100 mg, 84%).^{1}H NMR (300 MHz, $CDCl_3$) δ 6.34 (d, J = 7.1 Hz, 1H), 5.98 – 5.67 (m, 3H), 5.34 – 4.97 (m, 6H), 4.76 (d, J = 8.2 Hz, 1H), 4.29 – 3.80 (m, 6H), 3.86 (dt, J = 11.0, 3.8 Hz, 1H), 3.70 – 3.57 (m, 2H), 3.70 – 3.45 (m, 15H), 3.45 – 3.08 (m, 3H), 2.70 – 2.49 (m, 2H), 2.49 – 2.37 (m, 2H), 1.39 (s, 9H). ^{13}C NMR (300 MHz, $CDCl_3$) δ 173.3, 171.6, 156.0, 135.1, 134.7, 134.7, 116.9, 116.7, 116.5, 100.2, 80.8, 79.1, 74.8, 73.4, 72.3, 70.6, 70.4, 70.2, 68.9, 68.3, 56.6, 51.7, 40.2, 30.9, 29.1, 28.4. HRMS (ESI, Q-TOF): *m/z* calcd for $C_{31}H_{52}N_2O_{12}$ [M+Na$^+$]: 667.3412, found, 667.3397.

Figure A115**.** ^{1}H NMR analysis of compound **119** (300 MHz, $CDCl_3$)

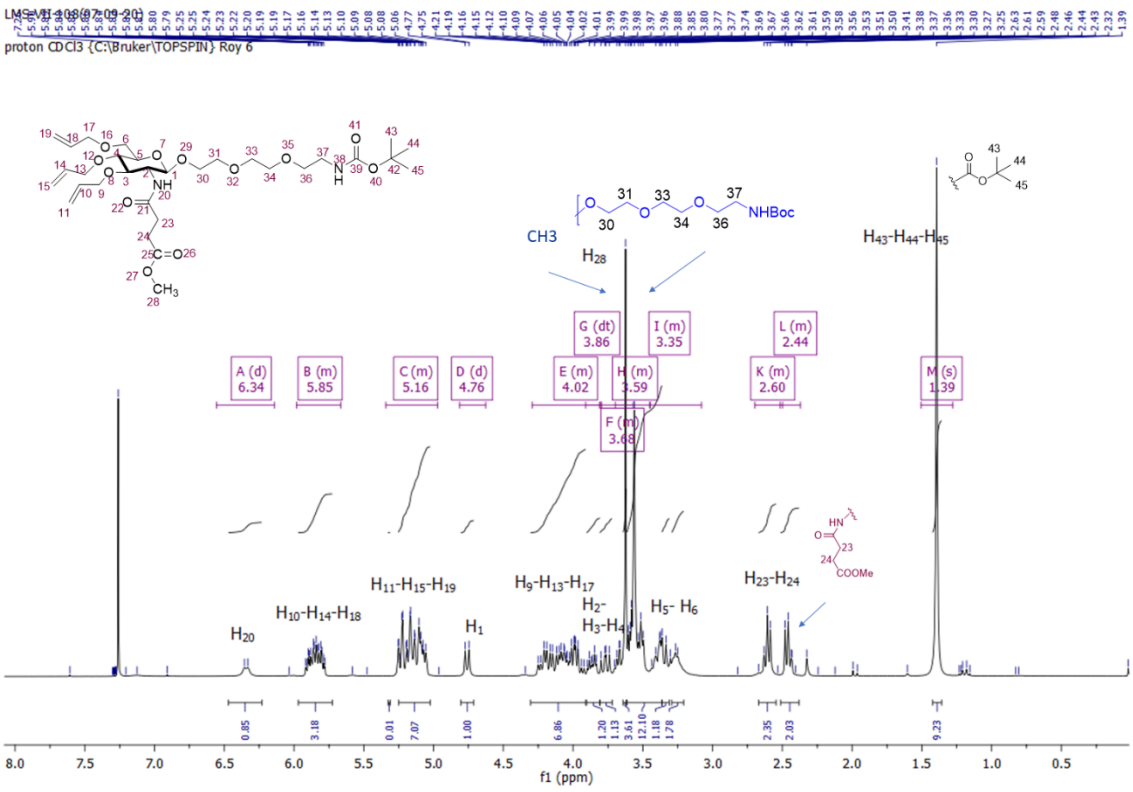

Figure A116. ^{13}C NMR analysis of compound **119** (300 MHz, $CDCl_3$)

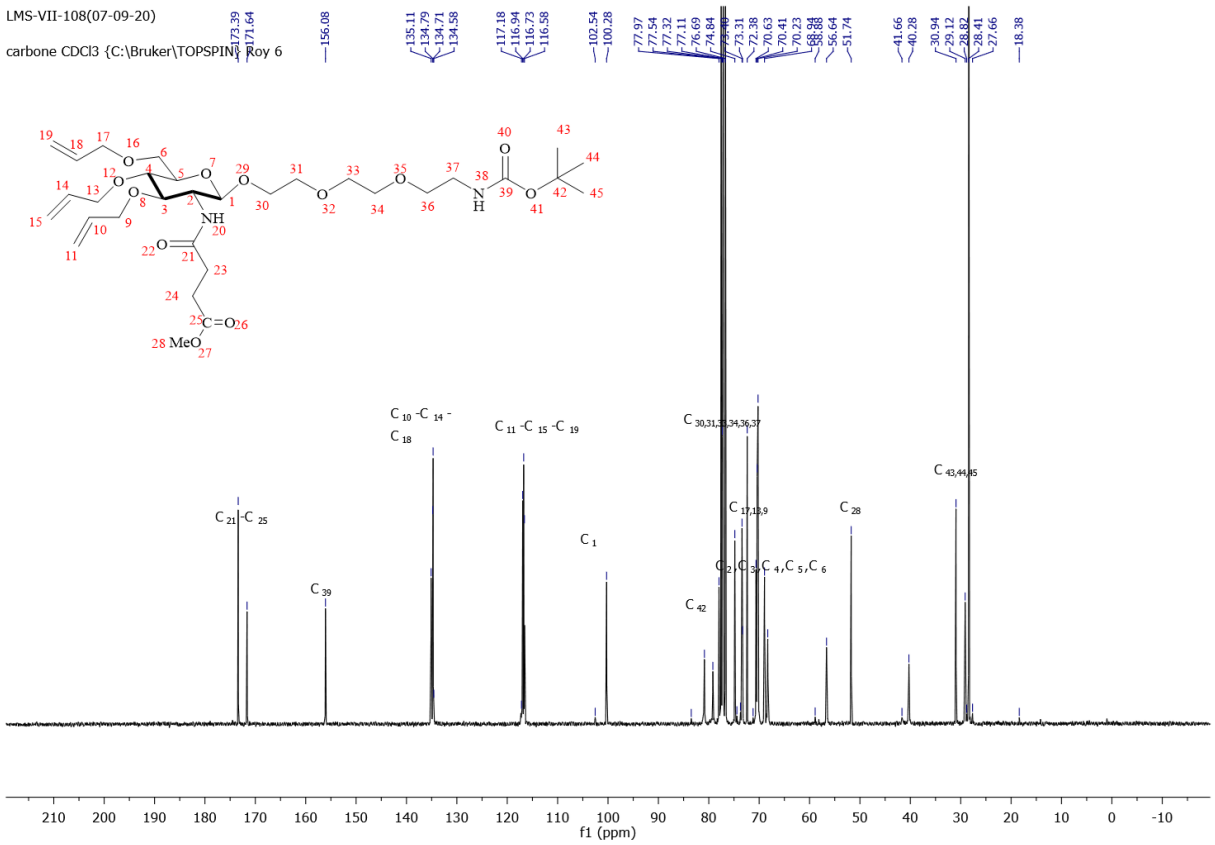

Figure A117. COSY analysis of compound **119** (300 MHz, $CDCl_3$)

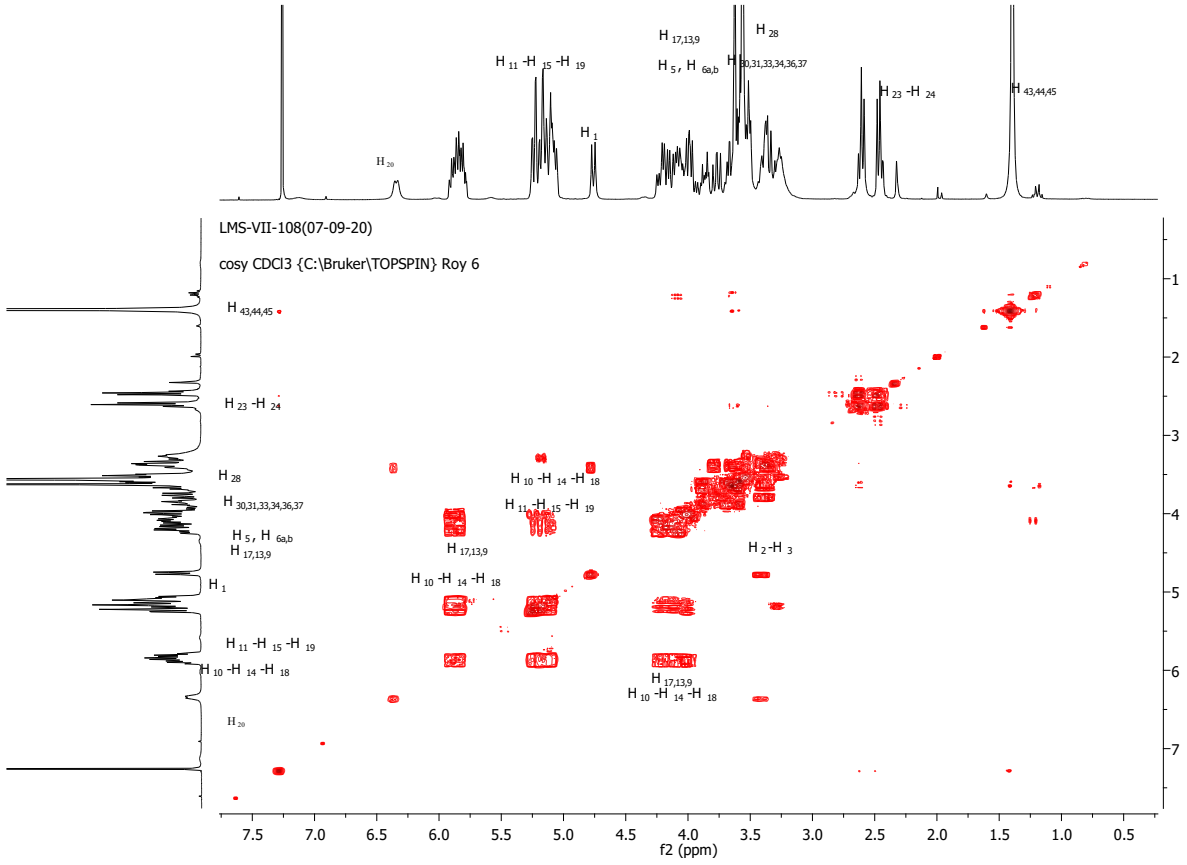

Figure A118. HSQC analysis of compound **119** (300 MHz, $CDCl_3$)

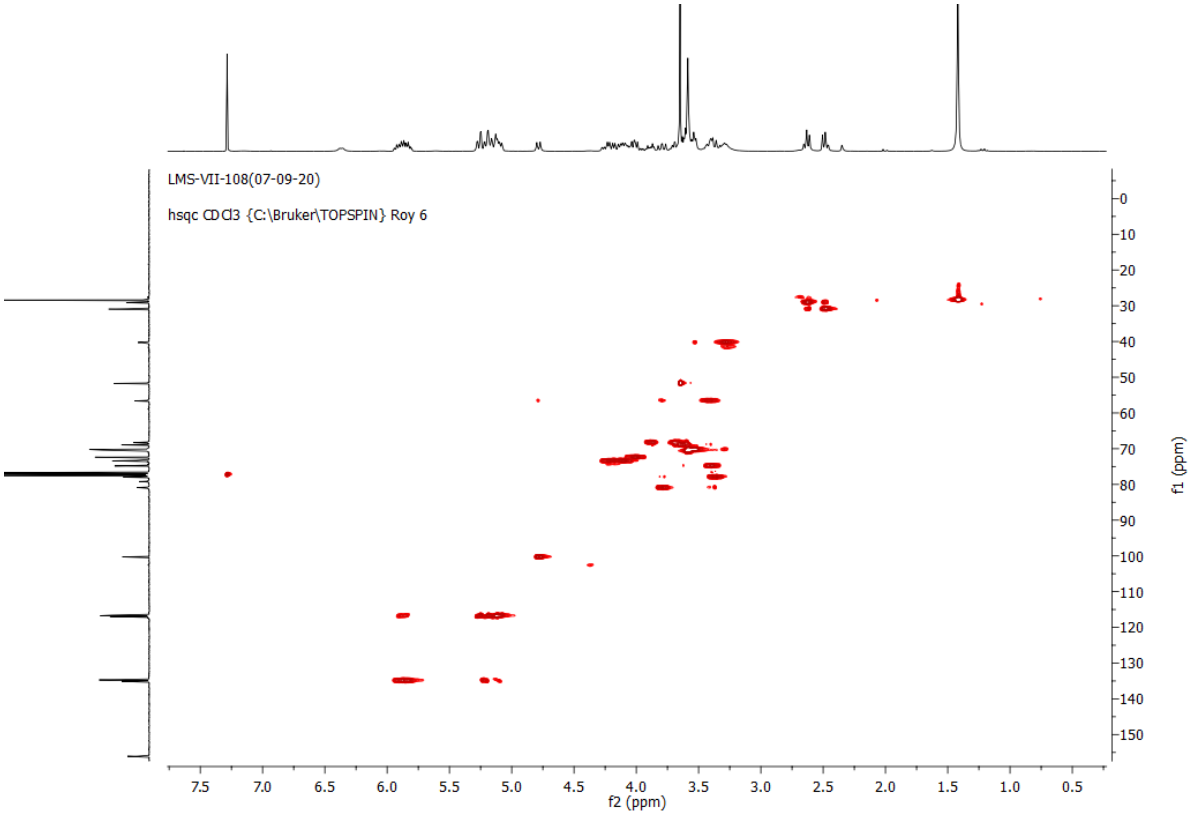

Figure A119. DEPT analysis of compound **119** (300 MHz, $CDCl_3$)

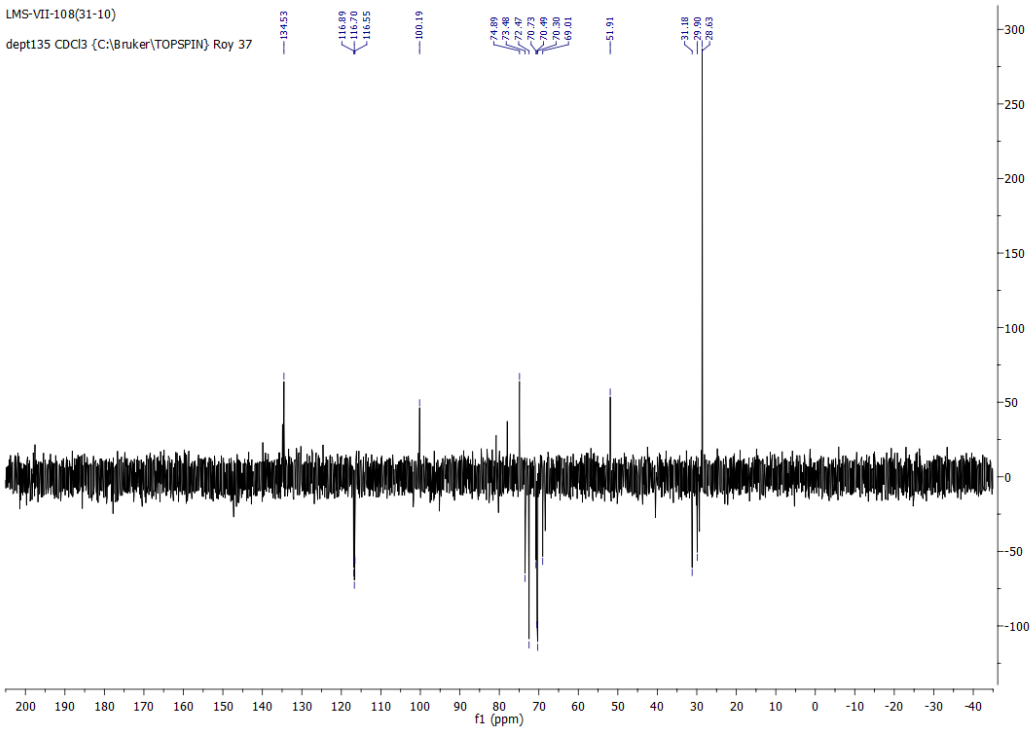

Figure A120. HRMS TOF **(**QTOF**)** analysis of compound **119**

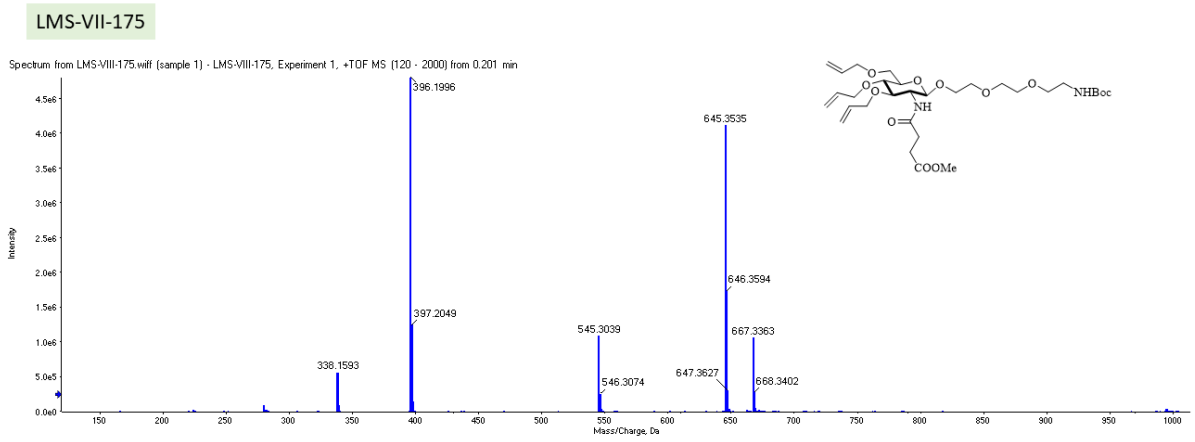

Sample	Formula	Adduct	Neutral mass Da	Calculated *m/z*	Observed *m/z*	PPM	Intensity
LMS-VII-175	C31H52N2O12	+H	644.35203	645.3593	645.35699	-3.6	7014274
LMS-VII-175 +Na	C31H52N2O12	+Na	644.35203	667.34125	667.33979	-2.2	1994292
LMS-VII-175 - Boc	C26H44N2O10	+H	544.2996	545.30687	545.30614	-1.4	2279107
LMS-VII-175 - Boc - C6H15O3	C20H29NO7	+H	395.1944	396.20168	396.20072	-2.4	7155479

Compound 120

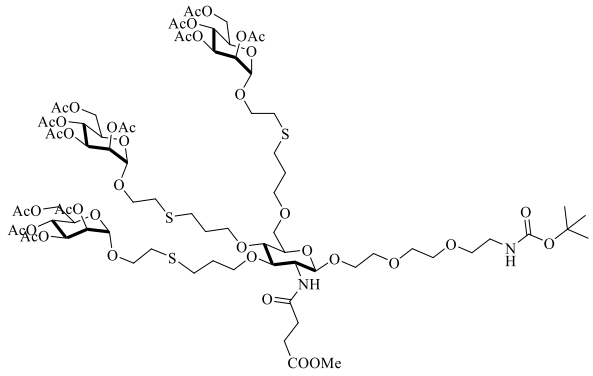

Experimental: To a vial equipped with a stir bar was charged with a solution of compound **119** (150 mg, 0.232 mmol), and α-D-mannose thiol **67** (600 mg, 1.413 mmol) in DMF (0.7 mL). The mixture was sparged by bubbling with nitrogen for 5 minutes. Followed by the addition of 2,2-Dimethoxy-2-phenylacetophenone (DMPA) (60 mg, 0.33 mmol, 0.2 eq. per each double bond). The reaction mixture was irradiated for 2.5 hours (λmax= 356 nm) at room temperature. After complete conversion of the starting material, the reaction was diluted with ethyl acetate, washed with water, brine, dried over anhyd. Na_2SO_4, and concentrated. The desired product was isolated as a white oily residue following purification by column chromatography (DCM/MeOH 97: 3%), to afford the desired product **120** (350 mg, 81%). ^{1}H NMR (300 MHz, $CDCl_3$) δ 6.44 (s, 1H, NH), 5.35 – 5.19 (m, 9H, 3x H2,3,4, man), 4.84 (d, 3H, J = 1.4 Hz, H1, man.), 4.71 (d, 1H, J = 8.2 Hz, H1 glu), 4.30 (d, 1H, J = 5.2 Hz, H3, Glu), 4.26 (d, 2H, J = 5.1 Hz, H 2,5, D-Glucosamine), 4.16 – 4.01 (m, 6H, 3xH6, man), 3.9- 3.73 (m, 6H, 3x CH2), 3.71- 3.67 (m, 2H, H6, Glu), 3.66 (s, 3H, CH_3), 3.55-3.42 (m, 6H, 2xO-CH_2), 3.39- 3.14 (m, 6H, 2x O-CH_2), 2.71 (ddd, 8H, J = 14.1, 8.5, 5.3 Hz, 3xS-CH_2, CH_2), 2.64- 2.43 (m, 8H, 3xS-CH_2, CH_2), 2.14 (s, 3H, OAc), 2.09 (s, 3H, OAc), 2.04 (s, 3H, OAc), 1.98 (s, 3H, OAc), 1.88- 1.78 (m, 2H, 3xCH_2), 1.43 (s, 9H, t-Butyl). ^{13}C NMR (300 MHz, $CDCl_3$) δ 173.4, 170.6, 170.6, 170.0, 169.8, 169.7, 156.0, 97.6, 81.6, 79.2, 78.3, 77.4, 76.6, 74.9, 70.7, 70.4, 70.2, 69.7, 69.5, 69.1, 69.0, 68.6, 68.0, 66.0, 62.4, 56.4, 51.7, 50.8, 40.3, 31.1, 31.0, 30.9, 30.4, 29.8, 29.7, 29.2, 29.0, 28.4. HRMS (ESI, Q-TOF): (*m/z*) calcd for $C_{79}H_{124}N_2O_{42}S_3$ $[M+Na]^+$: 1891.6683, found 1891.66861.

Figure A121. ^{1}H NMR analysis of compound **120** (300 MHz, $CDCl_3$)

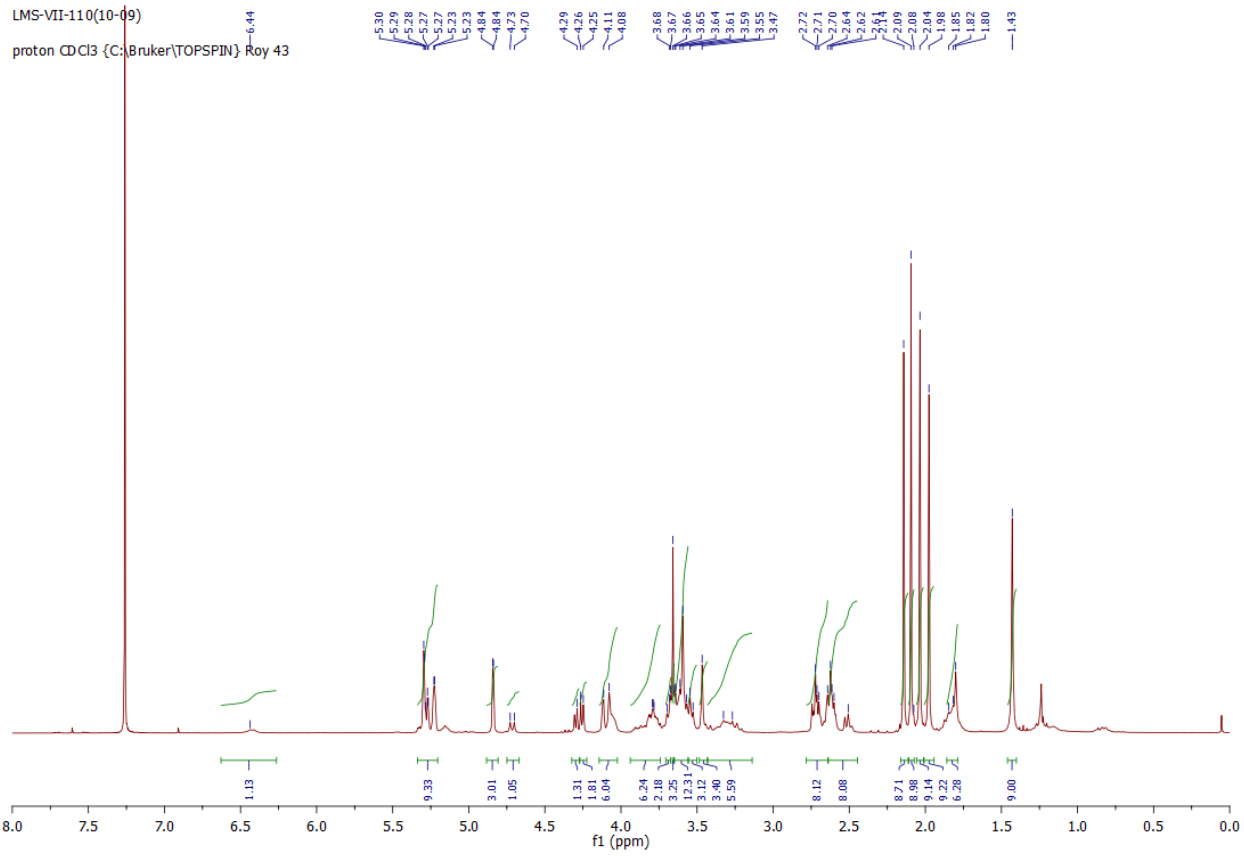

Figure A122. ^{13}C NMR analysis of compound **120** (300 MHz, $CDCl_3$)

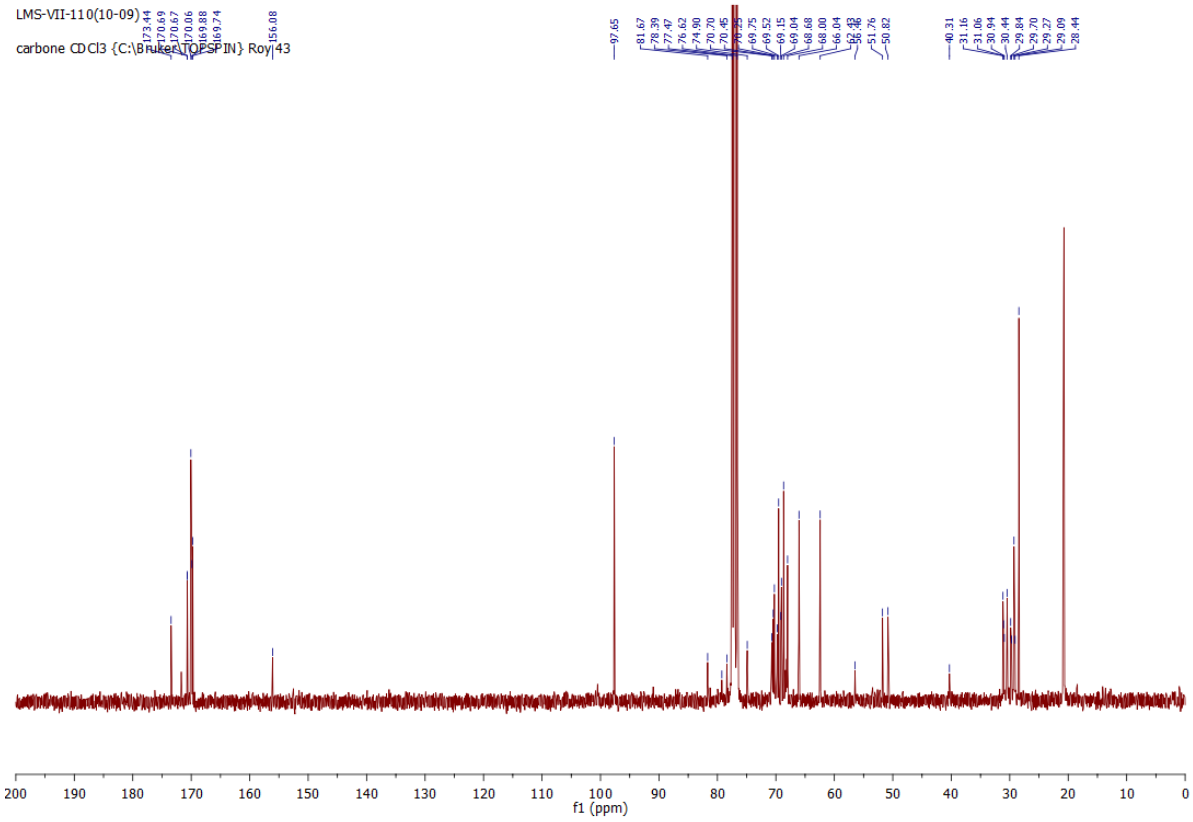

Figure A123. HSQC analysis of compound **120** (300 MHz, $CDCl_3$)

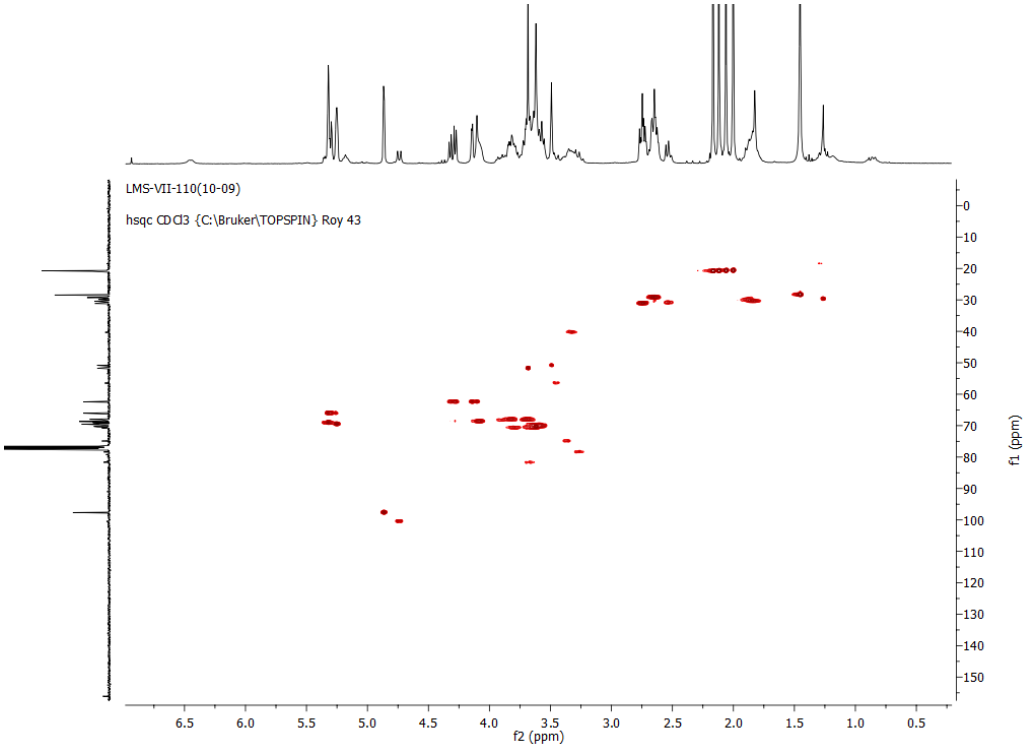

Figure A124. COSYanalysis of compound **120** (300 MHz, $CDCl_3$)

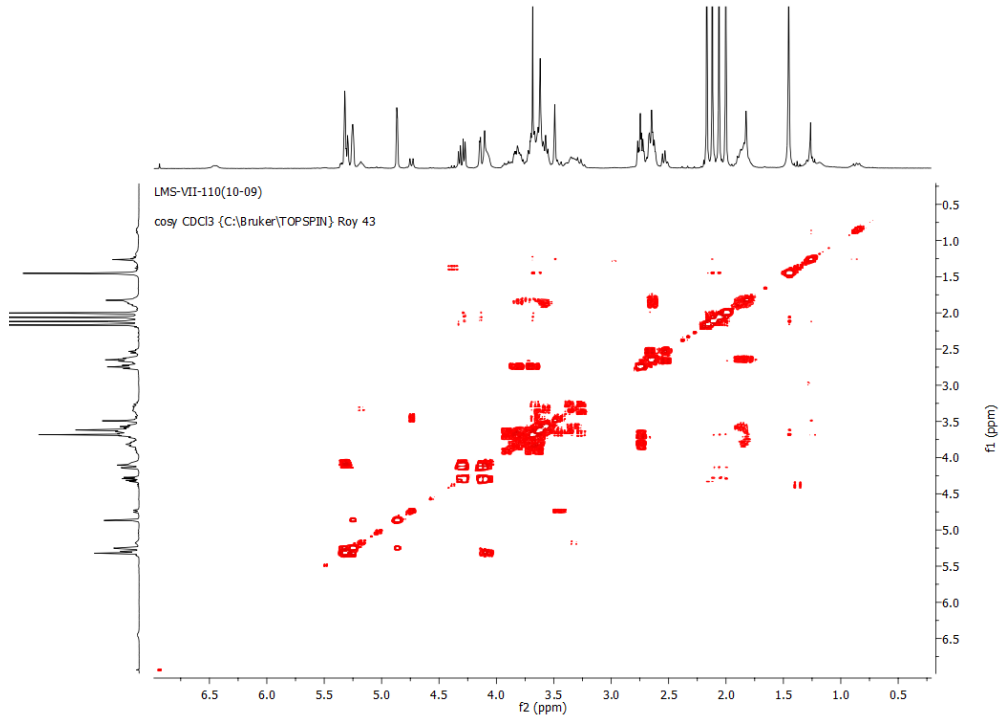

Figure A125. HRMS TOF (**QTOF**) of compound **120**

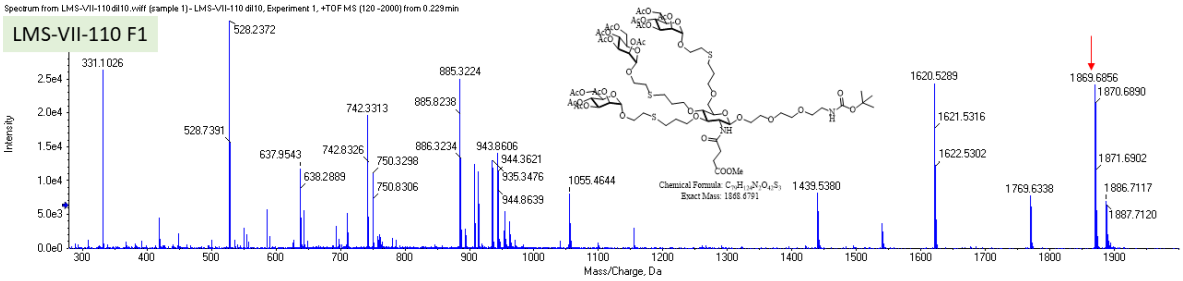

Sample	Formula	Adduct	Neutral mass Da	Calculated *m/z*	Observed *m/z*	PPM	Intensity
LMS-VII-110	C79H124N2O42S3	+H	1868.67908	1869.6864	1869.68543	-0.5	89592
and	C79H124N2O42S3	+Na	1868.67908	1891.6683	1891.66861	0.2	15333
LMS-VII-198	C79H124N2O42S3	+NH4	1868.67908	1886.7129	1886.7118	-0.6	32035

Compound 122

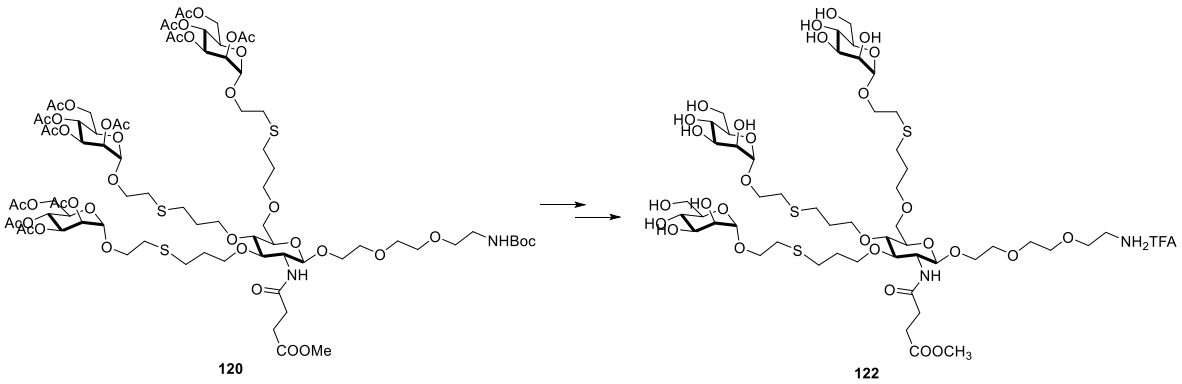

Experimental: To a solution of compound **120** (100 mg, 0.053 mmol) in MeOH (25 mL), added a solution of 1.0 M of NaOMe in MeOH (0.1mL), NaOMe solution was added dropwise till pH= 8. The solution allowed to stir for 12 hr at room temperature. Then Amberlyst IR-120H; was added under gentle stirring until the pH reached ~7, then the resin was filtered off, and the solvent was evaporated till dryness to afford the fully deprotected acetyl groups as oily residue (80 mg). This residue was dissolved in a pre-mixed solution of 20 % TFA/DCM at 0 ºC, the reaction was stirred for 2 h at rt. TFA was removed by azeotropic evaporation using toluene, under reduced pressure with a temperature lower than 40 ºC, and concentrated under reduced pressure, to afford the desired product **115** (58 mg, 87%). ^{1}H NMR (300 MHz, D_2O) δ 7.95 (d, 1H, *J* = 8.3 Hz, NH), 7.60 (d, 1H, *J* = 8.3 Hz, NH), 4.95- 4.84 (m, 9H), 4.60- 4.44 (m, 3H), 3.99 (d, 2H, *J* = 8.1 Hz), 3.95 (dt, 10H, *J* = 6.1, 3.1 Hz), 3.89 (dd, 20H, *J* = 11.3, 4.5 Hz), 3.79 (dt, 19H, *J* = 10.2, 4.4 Hz), 3.76- 3.70 (m, 20H), 3.70- 3.59 (m, 40H), 3.59- 3.31 (m, 13H), 3.19- 2.94 (m, 14H), 2.81 (dt, 16H, *J*

= 14.3, 7.3 Hz), 2.69 (tt, 16H, J = 17.7, 8.9 Hz), 2.58- 2.50 (m, 6H), 2.49- 2.41 (m, 6H), 1.89 (dt, 16H, J = 14.2, 7.3 Hz), 1.37-1.20 (m, 2H).^{13}C NMR (300 MHz, D_2O) δ 180.4, 175.9, 132.6, 129.2, 101.0, 99.7, 82.0, 77.8, 73.6, 72.8, 71.6, 70.5, 70.5, 70.0, 69.7, 69.6, 69.5, 69.4, 69.0, 66.6, 66.6, 54.7, 52.4, 39.4, 33.2, 30.7, 30.7, 28.2, 28.1. MALDI-TOF MS: *m/z* calcd for $C_{50}H_{93}N_2O_{28}S_3[M+Na]^+$ 1268.51, found 1268.5105.

Figure A126. ^{1}H NMR analysis of compound **122** (300 MHz, D_2O)

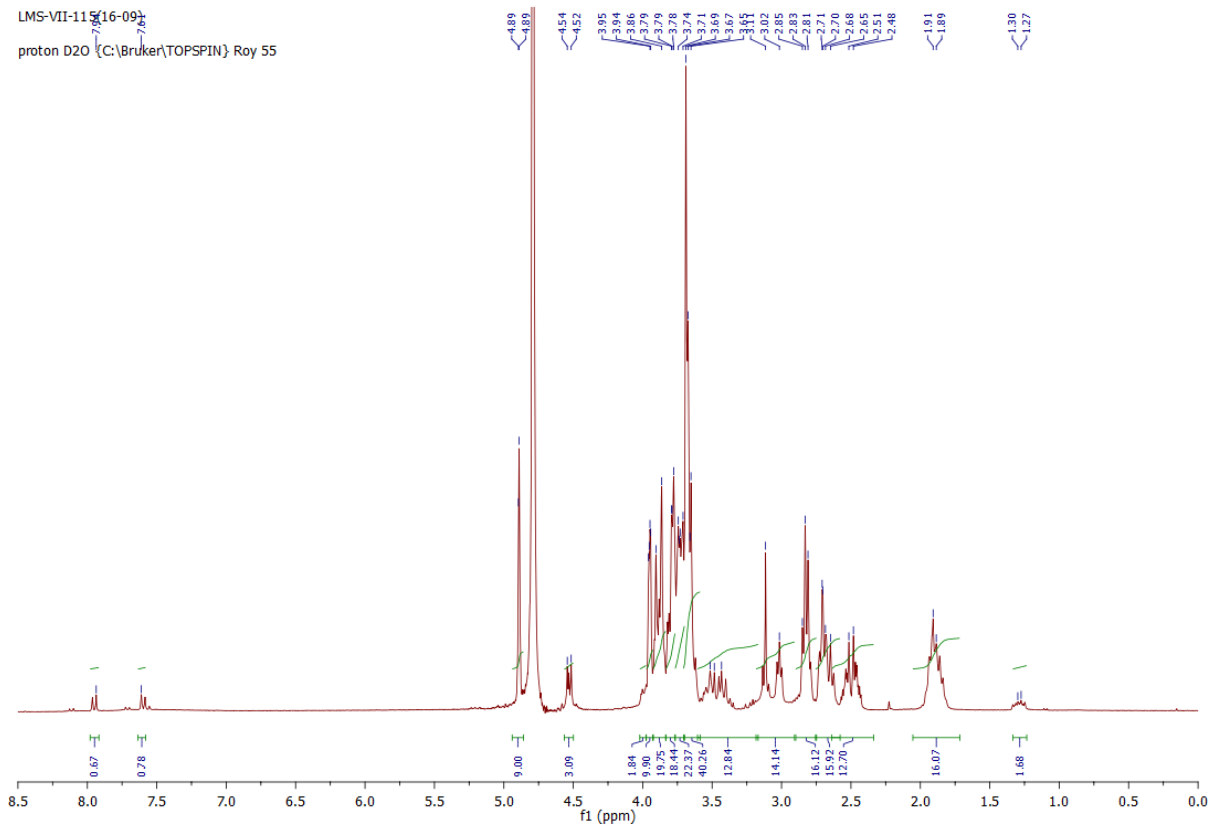

Figure A127. ^{13}C NMR analysis of compound **122** (300 MHz, D_2O)

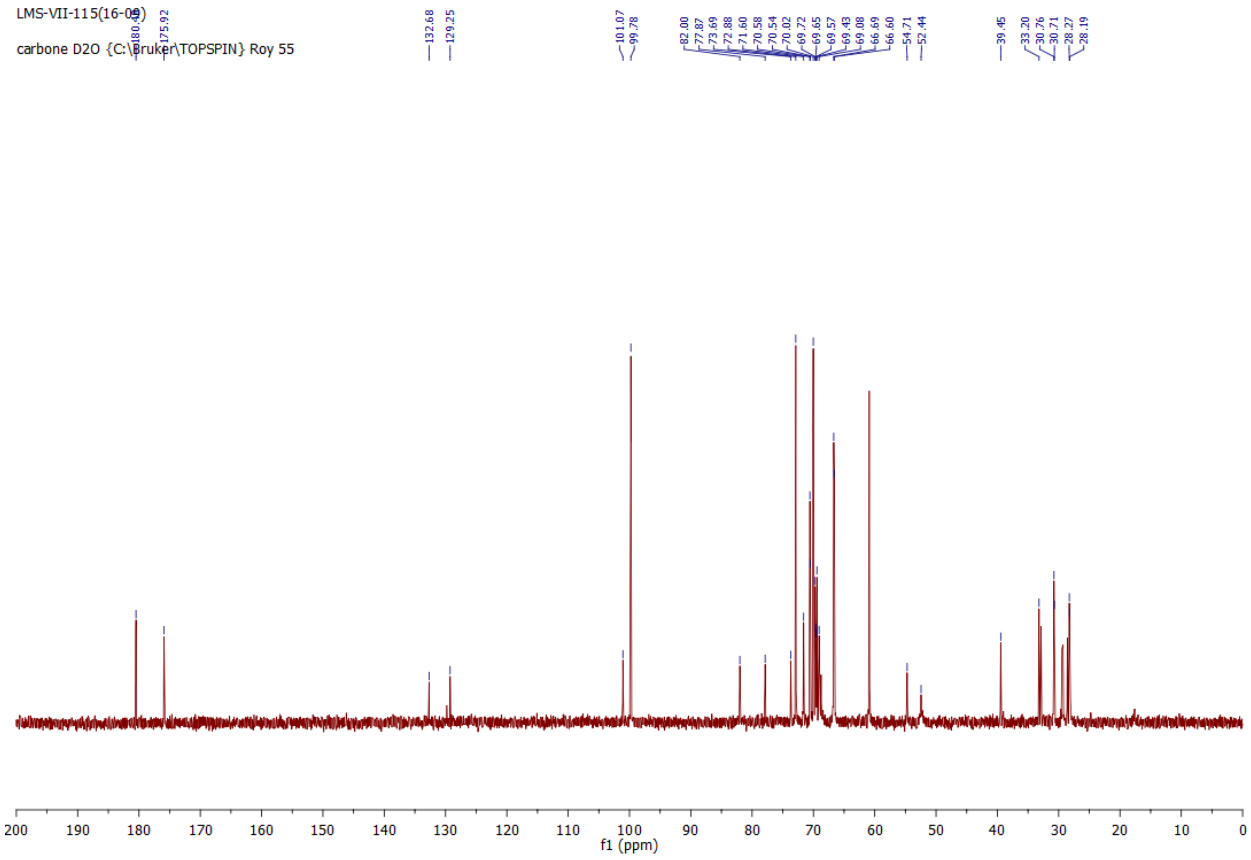

Figure A128. ^{13}C NMR analysis of compound **122** (300 MHz, CD_3OD)

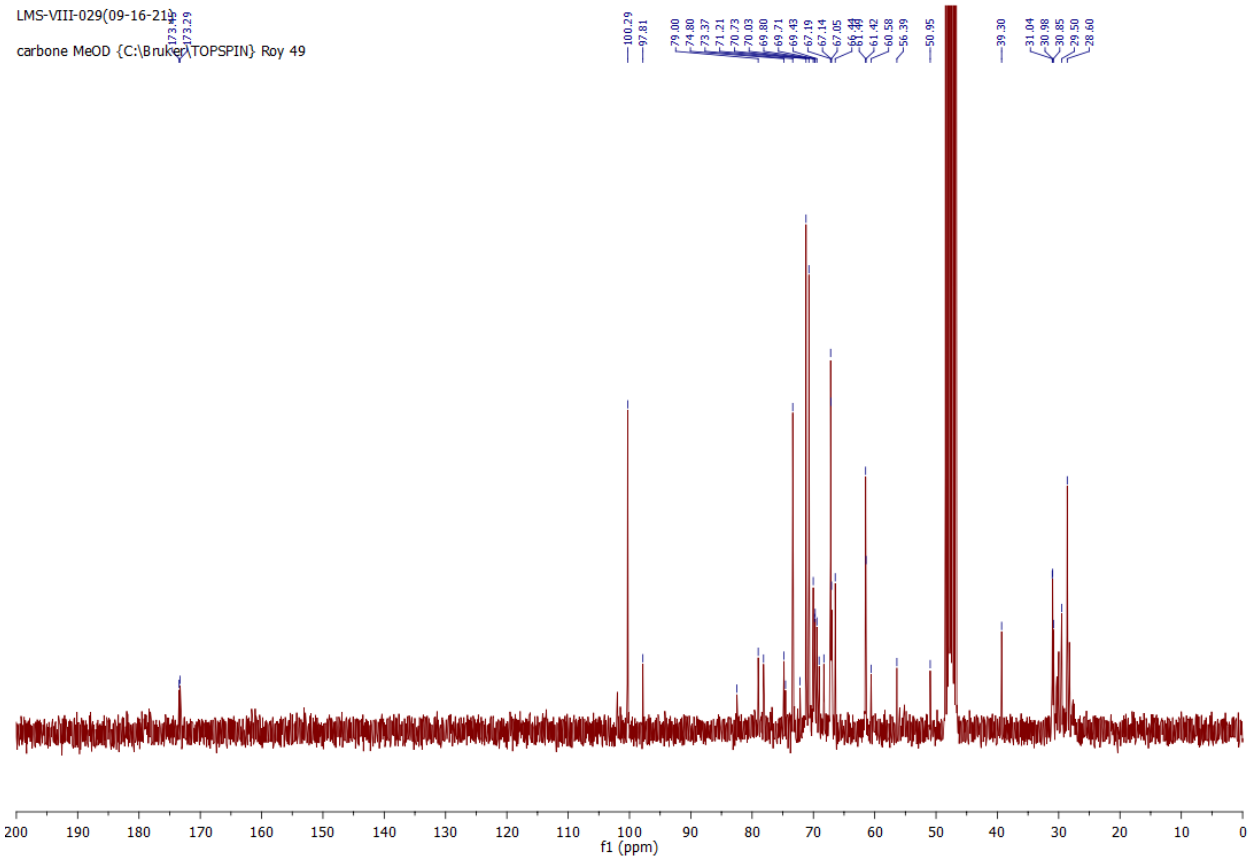

Figure A129. DEPT analysis of compound **122** (300 MHz, CD_3OD)

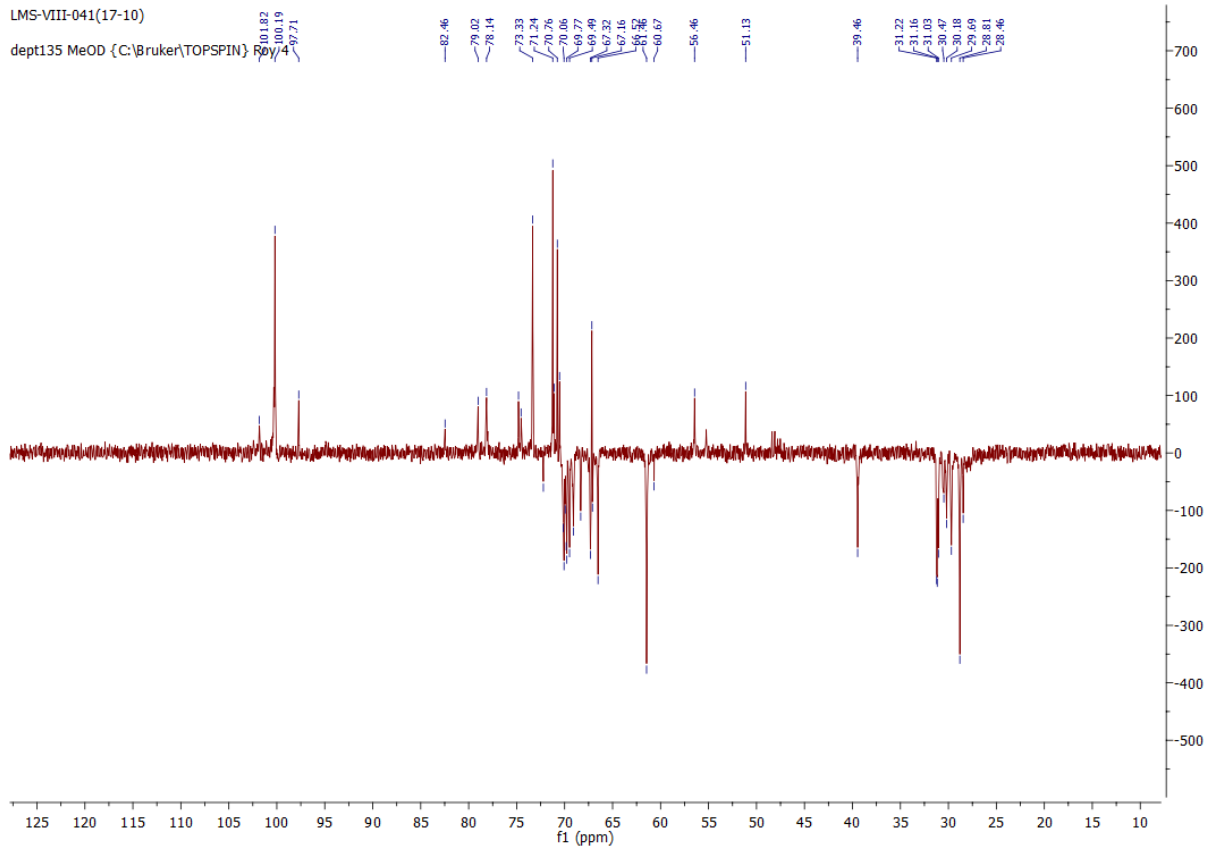

Compound 124

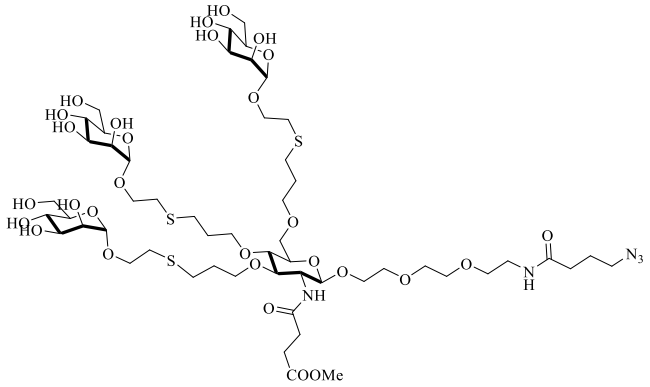

Experimental: The compound **122** (80 mg, 0.063 mmol), and 4-azobutanoic acid (25 mg, 0.208 mmol) were dissolved in anhydrous DMF (2 mL) and DIPEA (0.2 mL, 1.162 mmol) and PyBop (100 mg, 0.129 mmol) were added. The reaction mixture was stirred at toom temperature for 16 h and then concentrated to dryness under reduced pressure. The crude product was purified by flash column chromatography on dry silica, (Acetonitrite/H_2O 80: 20%) to provide the product **124.** (NMR not shown).

Note: in the case of PyBOP coupling reagent, a significant peak overlap of UV-active by products was observed, which overlap with the product. As a result, the product from this step was directly acetylated providing compound **125** with all of its acetylated hydroxyl groups:

Compound 125

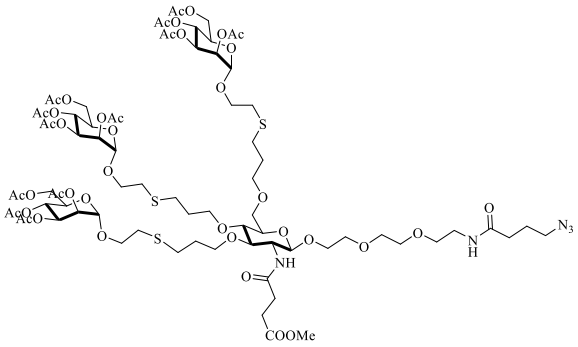

Experimental: The product from the previous step **124** (700 mg) was dissolved in a mixture of pyridine (30 mL), and acetic anhydride (15 mL) at 0 ºC degree. The reaction was allowed to stir for 12 h at room temperature. The solvent evaporated under reduced pressure and the residue was then redissolved in DCM, washed with sat $NaHCO_3$, brine, and dried over anhydrous sodium sulfate. The crude product was purified on coloumn chromatography (DCM/MeOH 97 :3%) to afford **125** (300 mg, 60%).

^{1}H NMR (300 MHz, $CDCl_3$) δ 7.68 (d, 1H, J = 23.5 Hz, NH), 6.51 (d, 1H, J = 34.6 Hz, NH), 5.41 – 4.99 (m, 9H), 4.95 (d, 1H, J = 8.3 Hz, H1), 4.73 (s, 3H), 4.27 – 4.03 (m, 4H), 3.93 (t, 9H, J = 21.1 Hz), 3.54 (t, 4H, J = 9.4 Hz, 1H), 3.54 (t, 12H, J = 9.4 Hz), 3.31 – 3.11 (m, 4H), 2.78 – 2.29 (m, 20H), 2.29 – 2.10 (m, 3H), 2.02 (s, 9H, OAc), 1.97 (s, 9H, OAc), 1.92 (s, 9H, OAc), 1.86 (s, 9H, OAc), 1.76 – 1.62 (m, 6H), 1.44 (t, 2H, J = 41.7 Hz, CH_2), 1.16 (dt, 2H, J = 14.2, 8.9 Hz, CH_2).^{13}C NMR (300 MHz, $CDCl_3$) δ 178.1, 177.0, 173.3, 172.1, 171.9, 171.5, 171.4, 170.4, 170.4, 169.8, 169.8, 169.6, 169.6, 169.5, 157.3, 156.9, 121.6, 117.7, 113.9, 97.4, 79.0, 78.0, 77.7, 77.5, 74.8, 70.6, 70.2, 70.1, 69.9, 69.5, 69.3, 69.2, 68.9, 68.6, 68.5, 68.3, 67.8, 67.7, 65.9, 65.8, 62.3, 60.1, 56.1, 53.5, 51.6, 50.7, 50.3, 50.2, 39.6, 32.8, 31.0, 30.8, 30.7, 30.2, 29.6, 29.4, 29.1, 23.8, 20.7, 20.6, 20.5, 20.5, 14.0.

Figure A130. ^{1}H NMR analysis of compound **125** (300 MHz, $CDCl_3$)

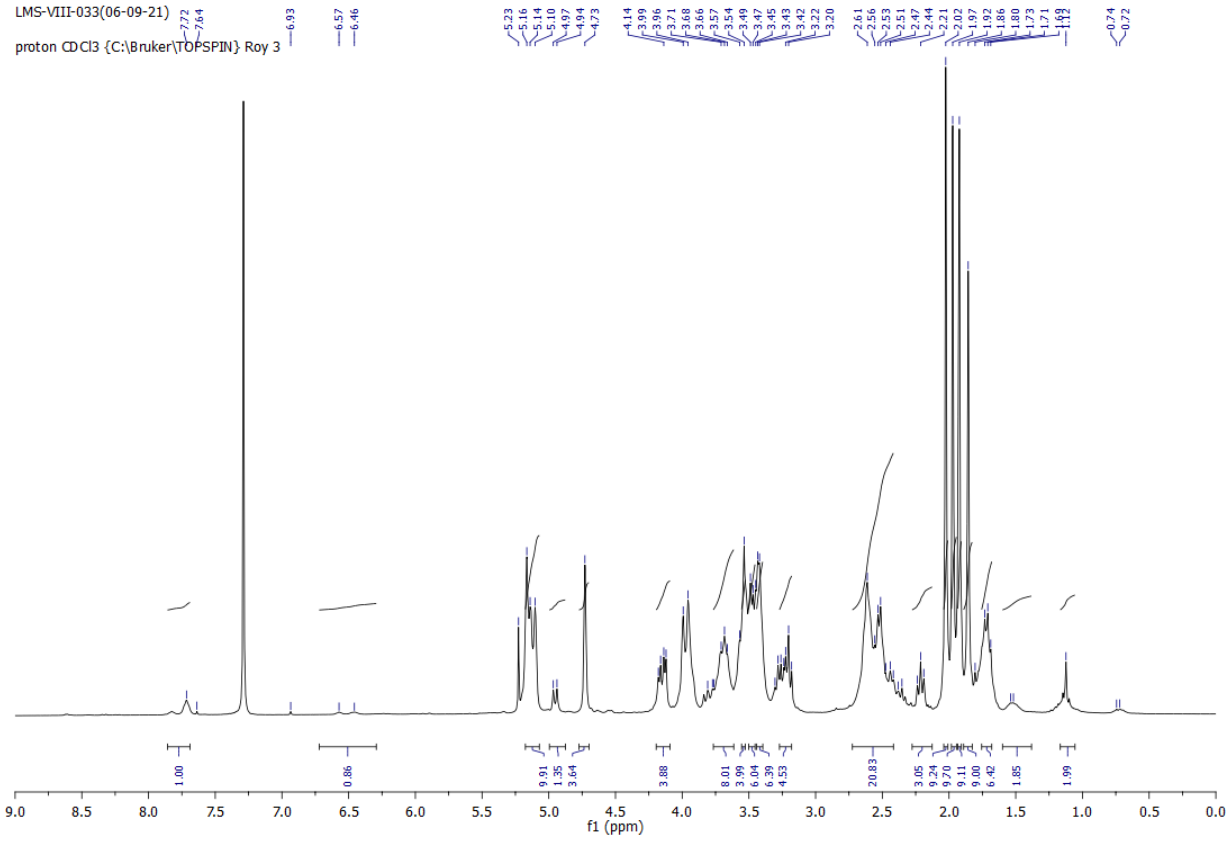

Figure A131. ^{13}C NMR analysis of compound **125** (300 MHz, $CDCl_3$)

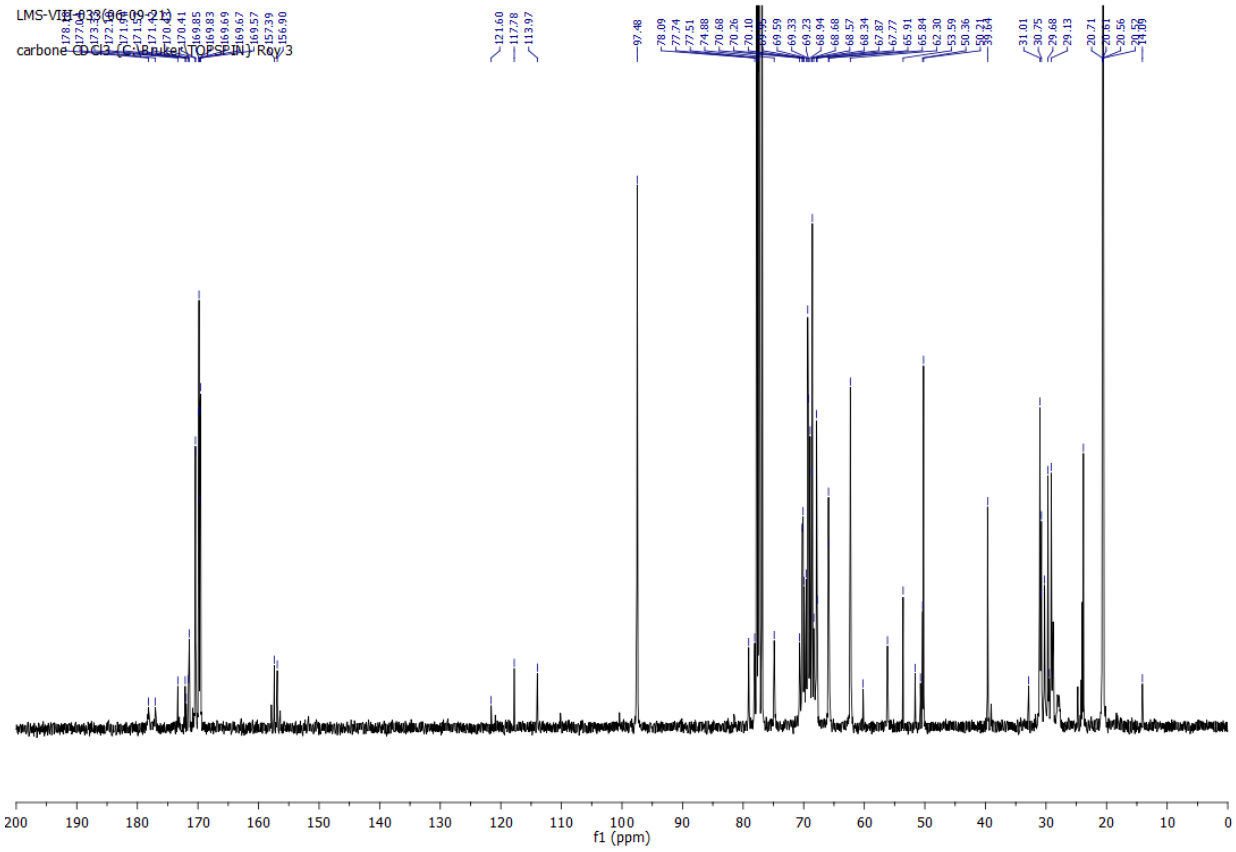

Figure A132**.** DEPT analysis of compound **125** (300 MHz, $CDCl_3$)

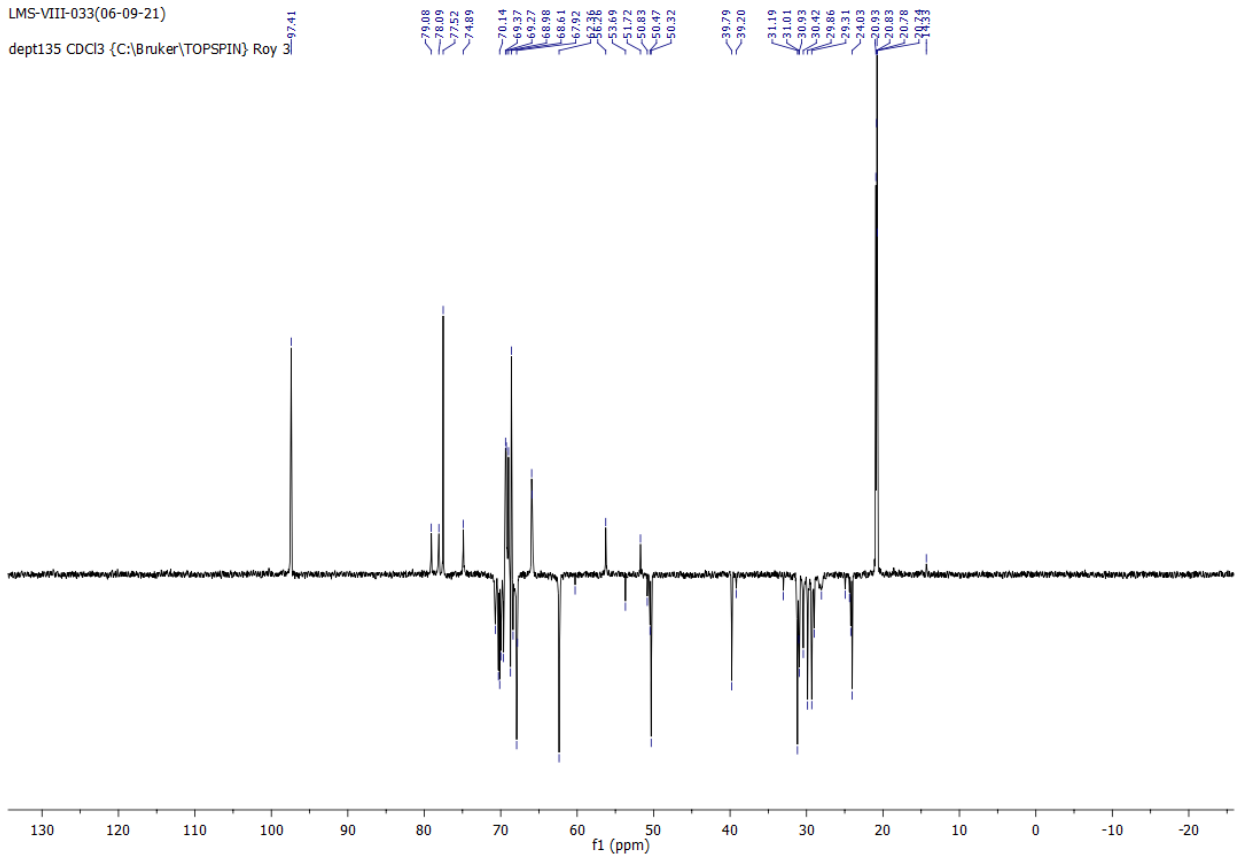

Figure A133. HSQC analysis of compound **125** (300 MHz, $CDCl_3$)

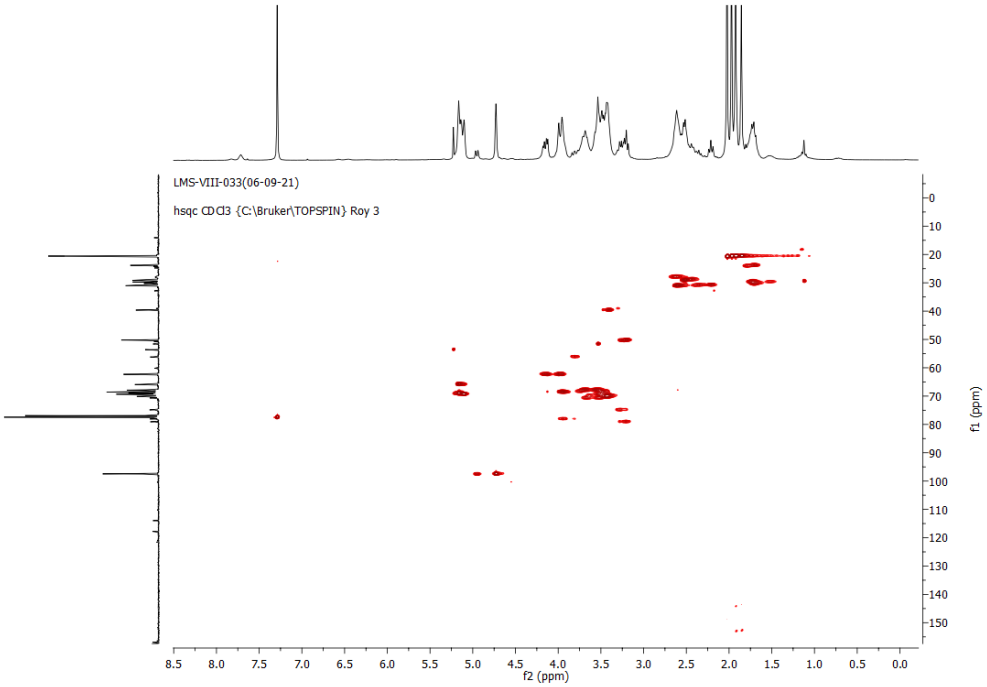

Figure A134. COSY analysis of compound **125** (300 MHz, $CDCl_3$)

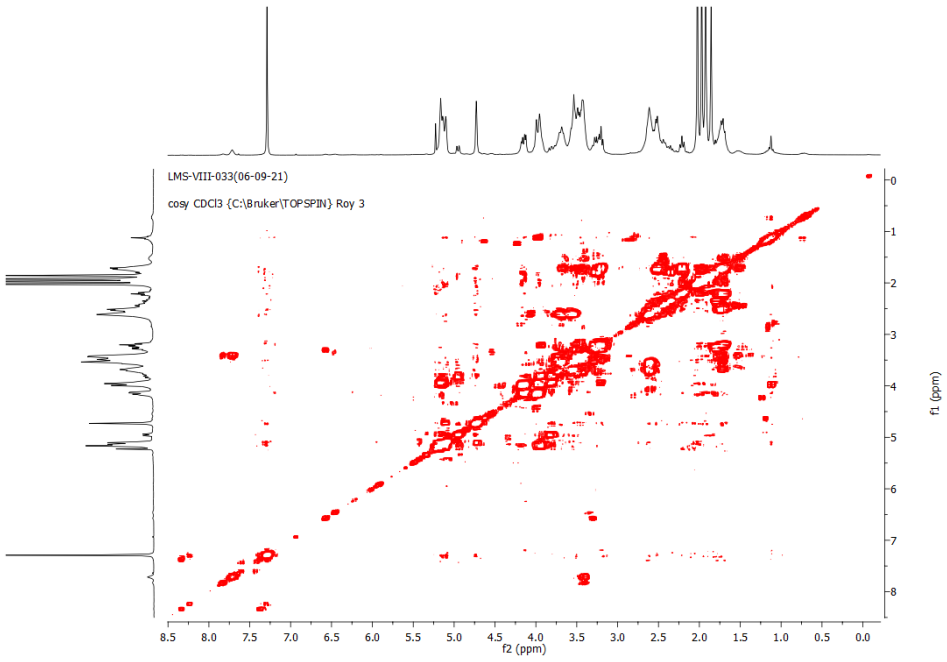

Figure A135**.** IR analysis of compound **125**

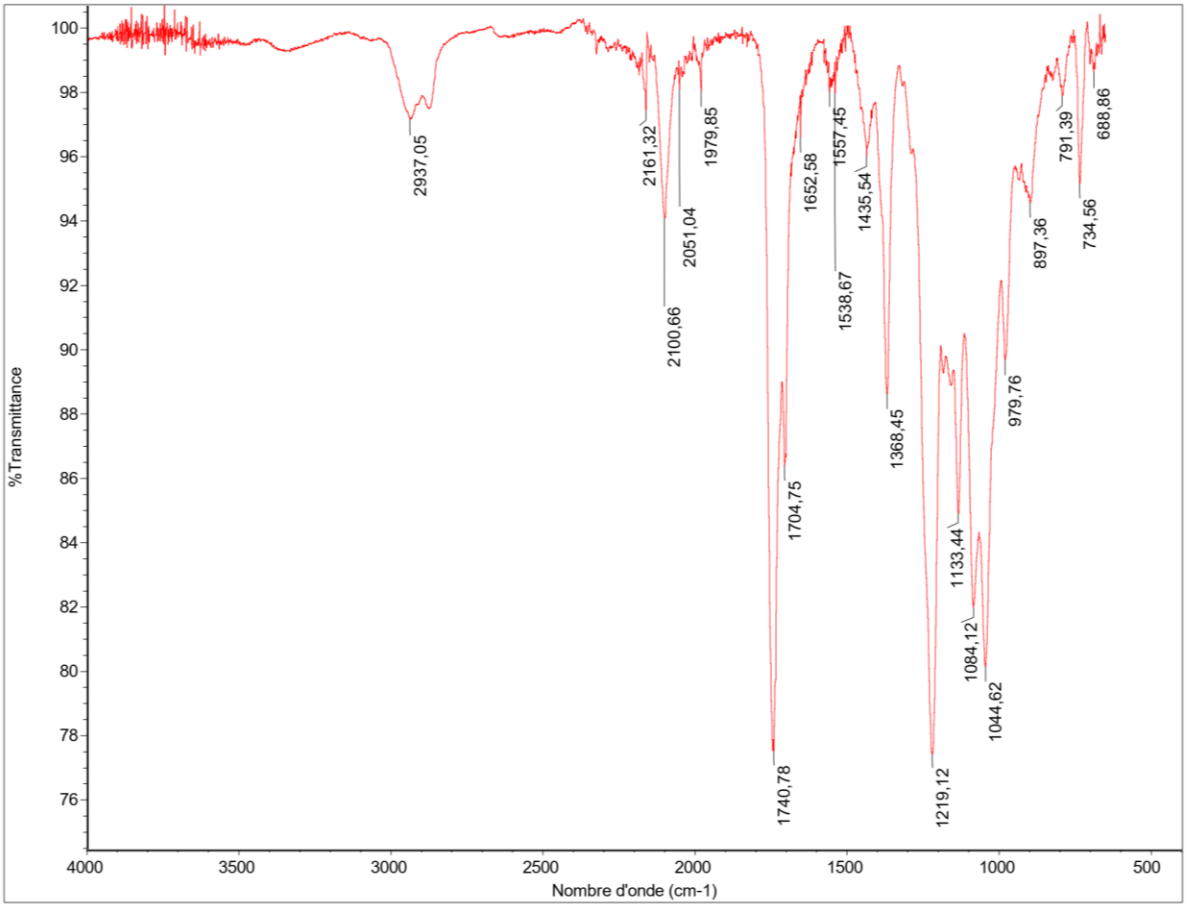

Compound 126

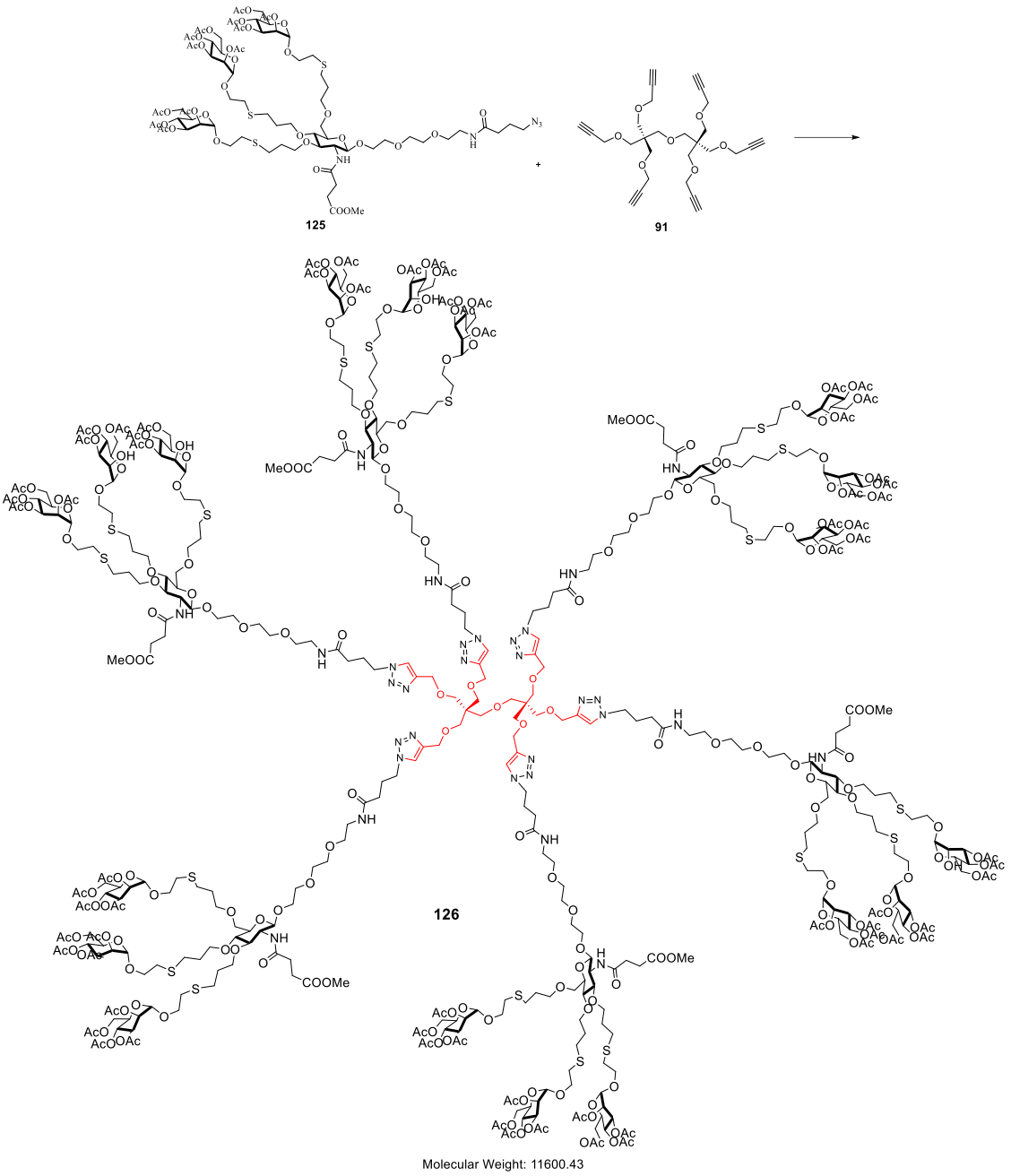

Experimental: To a solution of D-Glc thiomannoside **125** (400 mg, 0.213 mmol), and hexapropargylated dipentaerythritol **91** (15 mg, 0.023 mmol) in anhydrous toluene, were subsequently added DIPEA (1mL, 5.75 mmol), and CuI.P(OEt)$_3$ (30 mg). The reaction was stirred for 24 h at 80 ºC in an oil bath under a nitrogen atmosphere. The reaction mixture was cooled to ambient temperature, diluted with ethyl acetate, washed with repeatedly with EDTA, finally washed with water, and dried over anhydrous Na_2SO_4. After

the solvent was removed, the crude product was purified by column chromatography to obtain **126** (100 mg. ^{1}H NMR ($CDCl_3$, 300 MHz) δ 8.47-7.33 (m, 1H, triazole ring), 5.47-5.12 (m, 54H), 5.06 (d, 6H, J = 8.3 Hz), 4.83 (s, 18H), 4.38- 4.16 (m, 23H), 4.15- 3.94 (m, 88H), 3.91-3.68 (m, 65H), 3.70- 3.42 (m, 109H), 3.46- 3.10 (m, 25H), 2.862.55 (m, 83H), 2.57- 2.44 (m, 16H), 2.39- 2.17 (m, 18H), 2.13 (s, 54H), 2.08 (s, 54H), 2.02 (s, 54H), 1.96 (s, 54H), 1.94- 1.67 (m, 46H), 1.70- 1.40 (m, 8H), 1.39- 1.24 (m, 18H), 0.78 (dd, 18 H) . ^{13}C NMR (300 MHz, $CDCl_3$) δ 170.6, 170.0, 169.8, 169.7, 157.5, 97.6, 79.2, 78.1, 77.5, 77.3, 77.1, 74.9, 70.3, 70.1, 70.0, 69.7, 69.4, 69.3, 69.0, 68.8, 68.6, 68.3, 67.9, 39.7, 31.1, 29.7, 29.6, 29.2, 20.8, 20.7, 20.6, 20.6. HRMS data could not be obtained for this compond.

Figure A136**.** ^{1}H NMR analysis of obtained product **126** (300 MHz, $CDCl_3$)

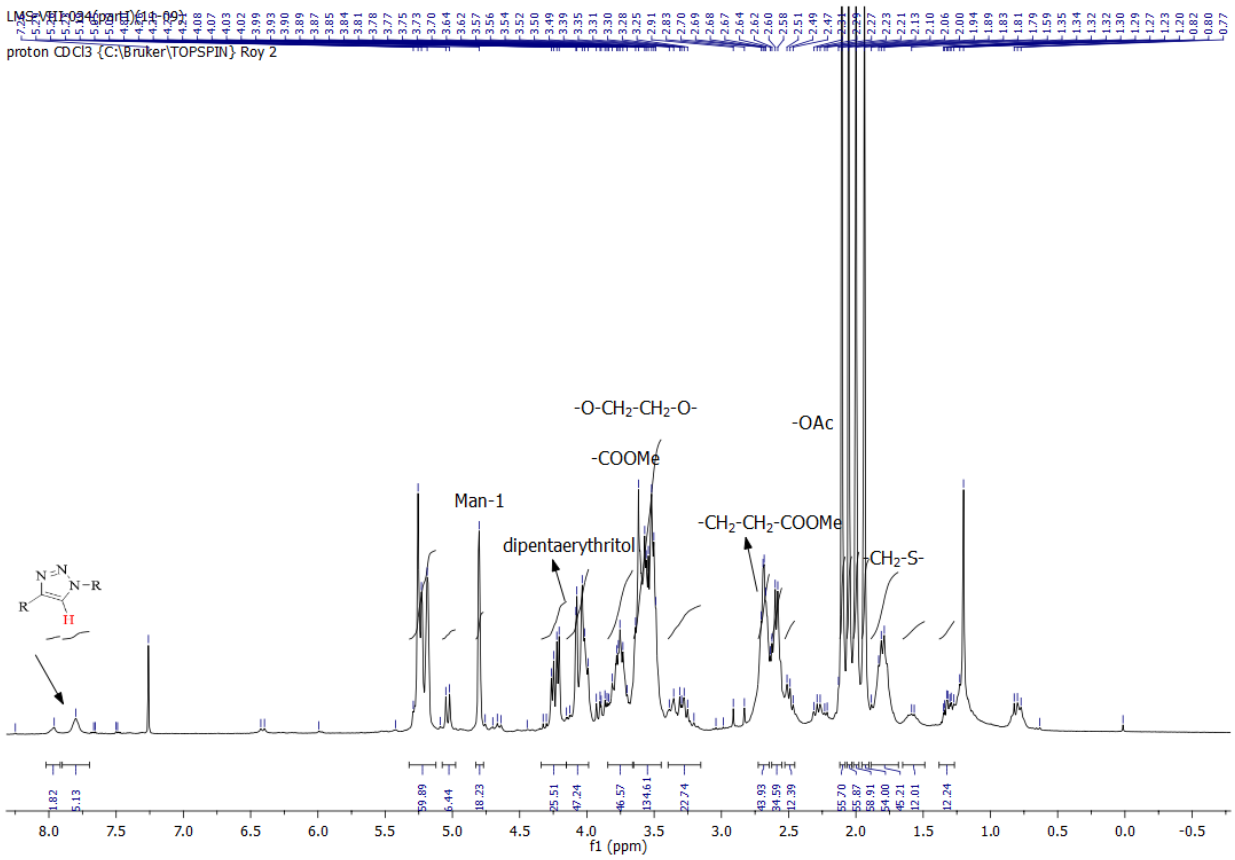

Figure A137.[13]C NMR analysis product **126** (300 MHz, $CDCl_3$)

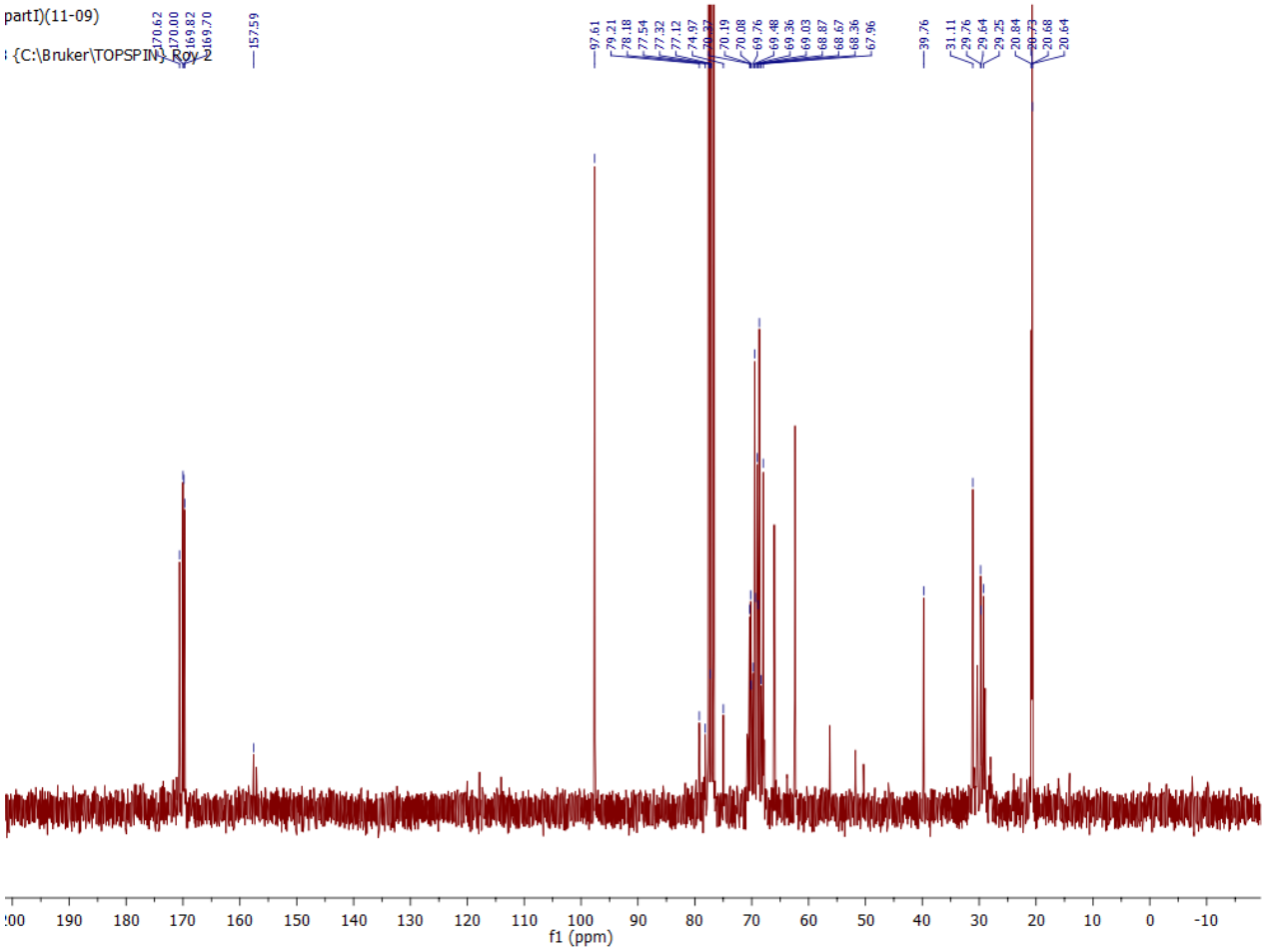

Figure A138. COSY analysis of obtained product **126 (**300 MHz, $CDCl_3$)

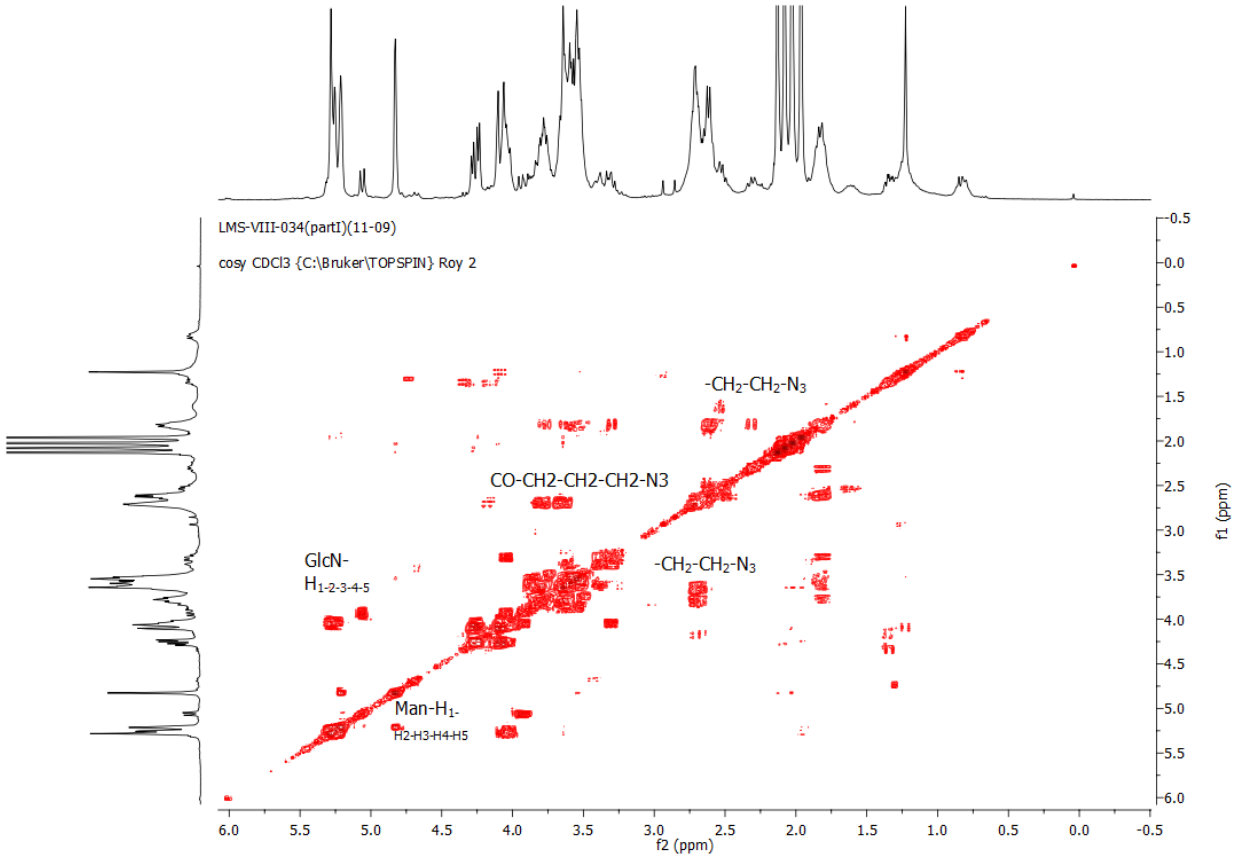

Figure A139. DEPT analysis of obtained product **126 (**300 MHz, $CDCl_3$)

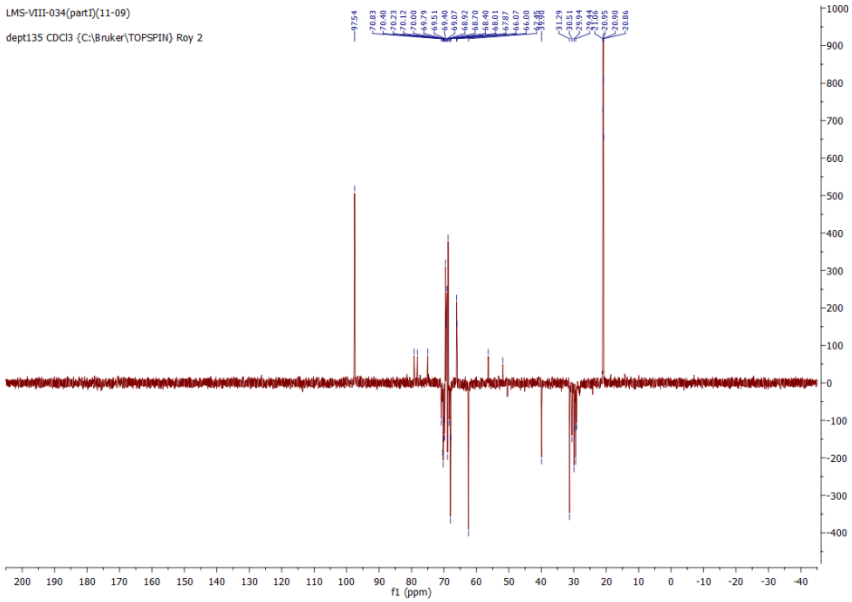

Experimental part chapter 5

2-chloro propyl (4- nitro phenyl) carbonate (136)

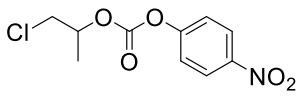

Experimental: A stirring mixture of 4-nitrophenyl chloroformate **134** (4g, 19.9 mmol) and pyridine (8 mL) in dry THF (40 mL) was cooled to 0 ºC for 15 min, and a solution of 2-chloro-1-propanol **135** (4g, 42.55 mmol) in dry THF (40 mL) of was added slowly. The mixture was allowed to stir at room temperature for 15 h. The mixture was then concentrated under reduced pressure to dryness. The resulting residue was purified by flash column chromatography (Hexane/ Ethyl acetate 9:1) to give product **136** (3g, 60%) as white solid crystals. ^{1}H NMR (300 MHz, $CDCl_3$) δ 8.44- 8.14 (m, 2H, Ar), 7.56- 7.31 (m, 2H, Ar), 5.40- 4.67 (m, 1H), 1.48 (d, 3H, J = 6.4 Hz, CH_3).

Figure A140.[1]H NMR analysis of compound **136** (300 MHZ, $CDCl_3$)

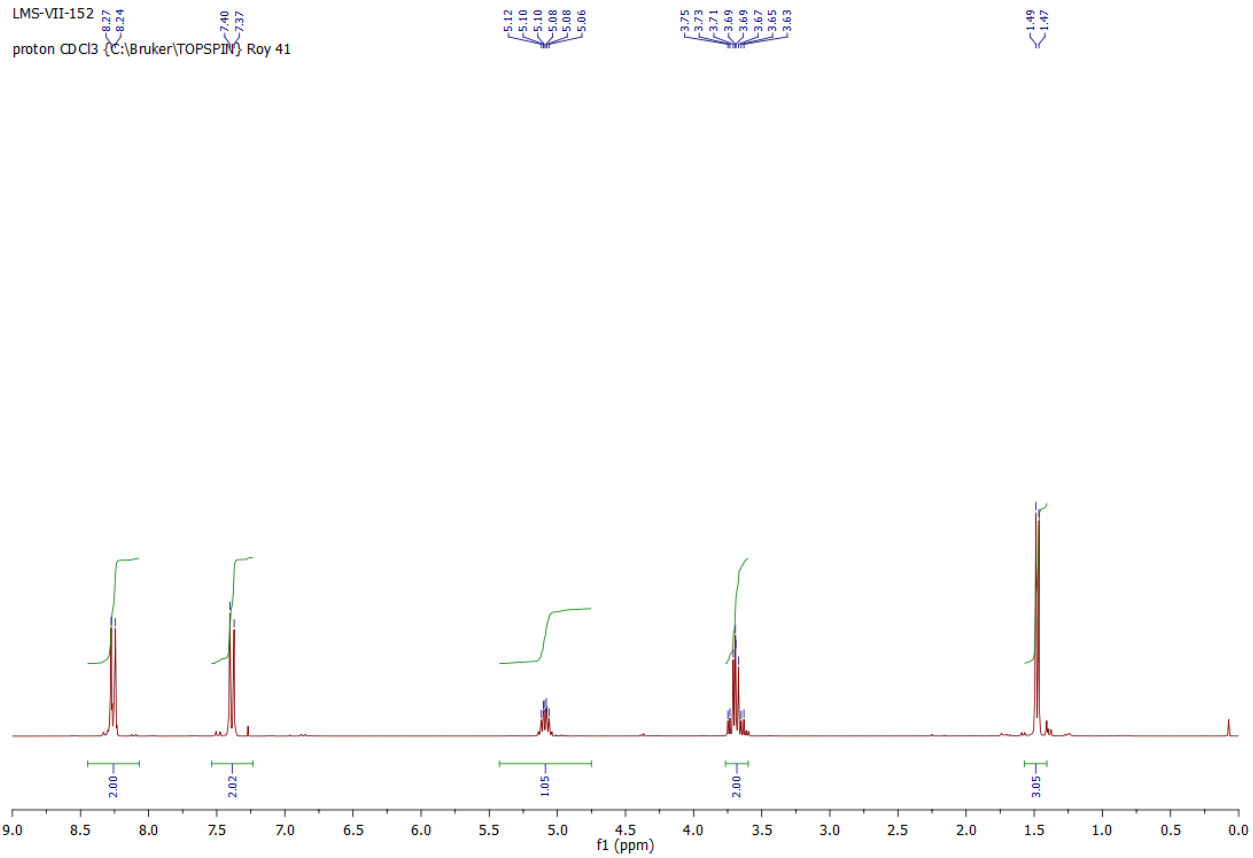

Compound (137)

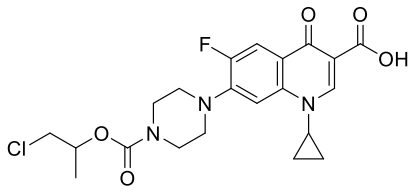

Experimental: Ciprofloxacin **129** (0.9 g, 3.0 mmol, 1 eqv.) and TMS-Cl (800 µL, 6.18 mmol, 2.06 eqv.) were combined in dry CH_2Cl_2 (50 mL). The mixture was stirred for 10 min at rt and DIPEA (5.1 mL, 29 mmol, 9 eqv.) was added to afford a clear light-yellow solution. 2-chloro propyl (4- nitro phenyl) carbonate **136** (0.9 g, .9 mmol, 1.3 eqv.) in DCM (5 mL) was then added slowly, during which time the solution turned dark orange and some smoke formed. The reaction was stirred overnight at rt and diluted with MeOH (10 mL), and the mixture was stirred vigorously for another 30 min. The solution was concentrated, and the

resulting residue was dissolved in CH_2Cl_2. The solution was washed with 0.1 M HCl (3 x 30 mL) and H_2O, then dried over Na_2SO_4, and concentrated to give product **137** (500 mg, 40 %). The product purified on column chromatography (DCM: MeOH 99:1%). ^{1}H NMR (300 MHz, $CDCl_3$) δ 8.76 (s, 1H), 8.03 (d, 2H, *J* = 12.9 Hz), 7.37 (d, 2H, *J* = 7.1 Hz), 5.17- 4.71 (m, 1H), 3.81-3.68 (m, 4H), 3.67 (d, 2H, *J* = 4.3 Hz), 3.62 (d, 2H, *J* = 5.3 Hz), 3.53 (ddd, 2H, *J* = 36.1, 21.1, 17.1 Hz), 3.32 (s, 4H), 1.44- 1.39 (m, 2H), 1.38 (d, 3H, *J* = 6.4 Hz), 1.28- 1.03 (m, 2H).

Figure A141.^{1}H NMR analysis of compound **137** (300 MHZ, $CDCl_3$)

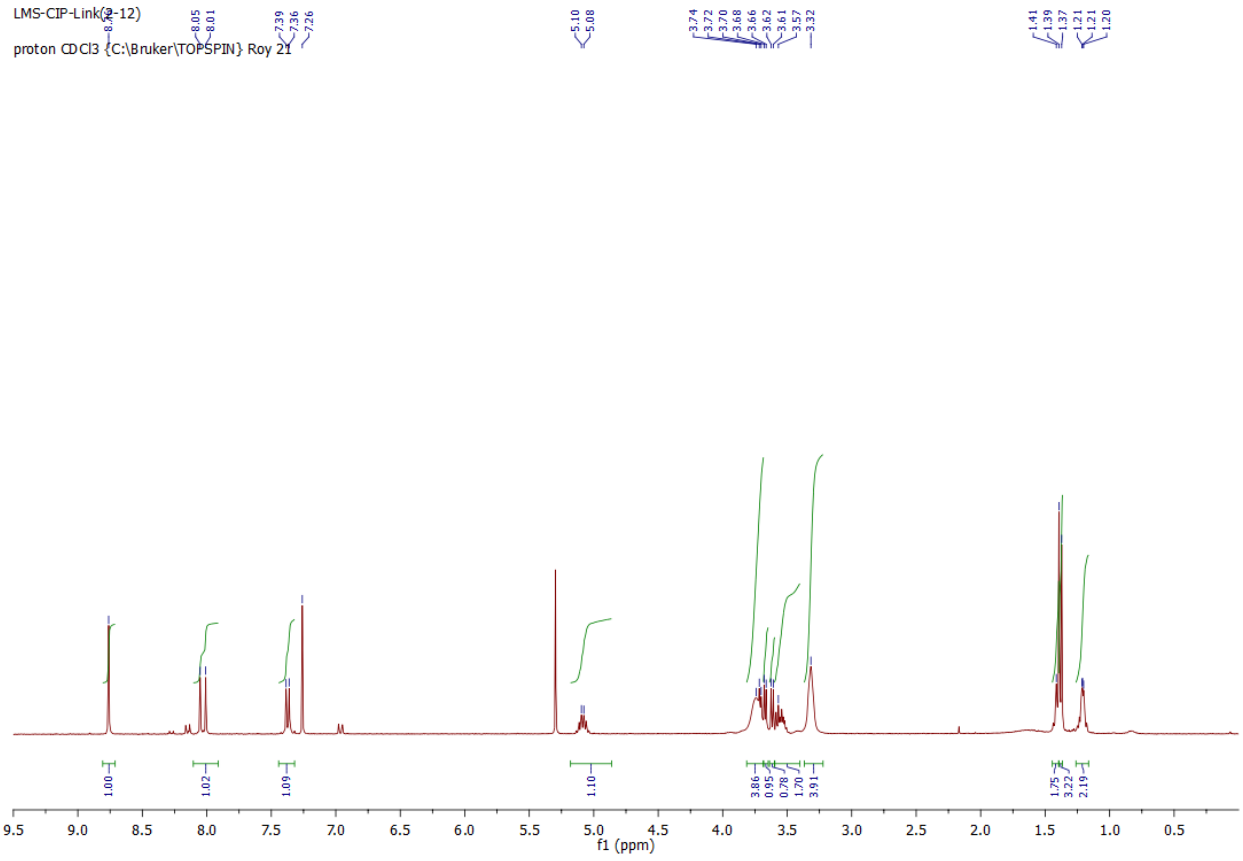

Figure A142. ^{19}F NMR analysis of compound **137** (300 MHz, $CDCl_3$)

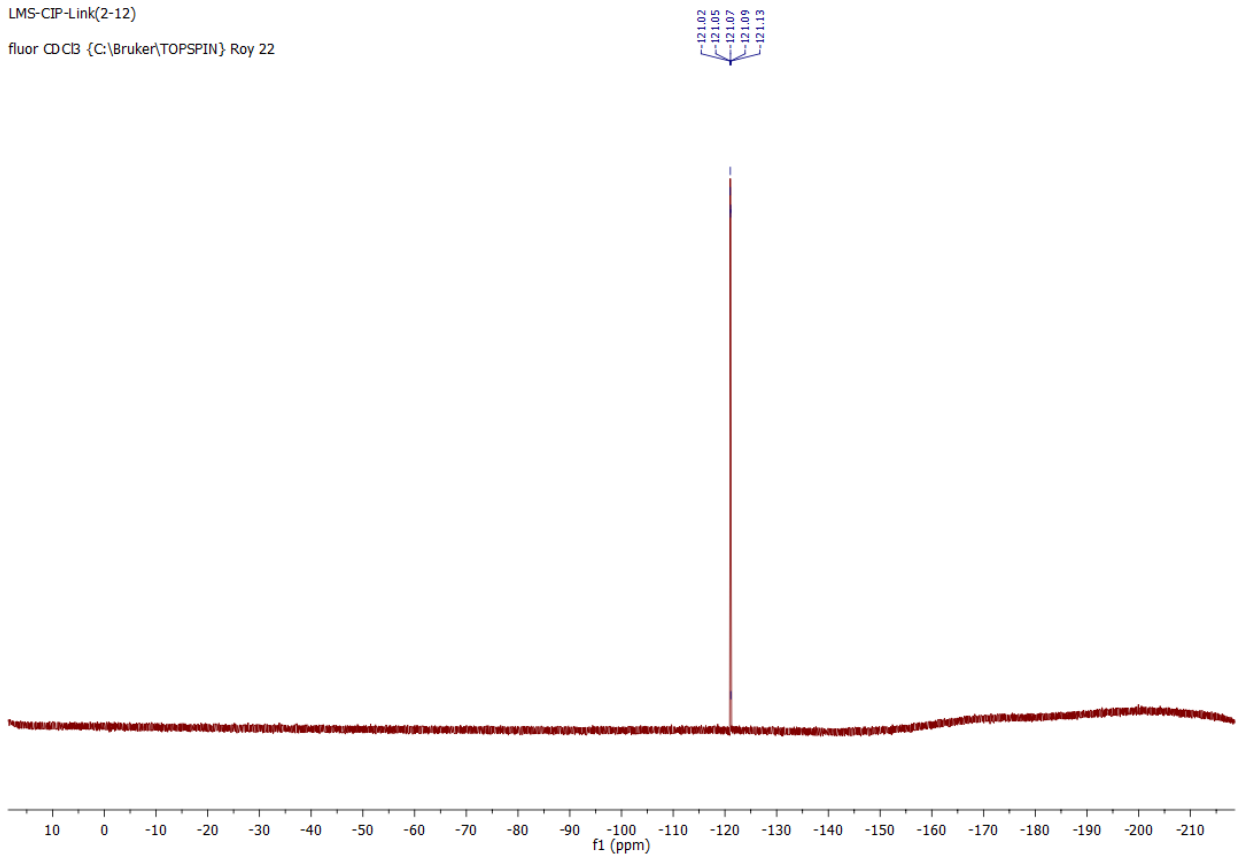

Boc L-Valine (138). [502, 503]

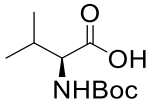

Experimental: A solution of L-valine (2.34g, 20 mmol) in a mixture of THF (30 mL), water (15 mL), and 1M NaOH (20 mL) was stirred and cooled in an ice bath. Afterward, di-*tert*-butyldicarbonate $(Boc_2)O$ (4.8 g, 22 mmol) was added and the reaction mixture was further stirred for 12 h at room temperature. Then it was acidified with 1M HCl and extracted with ethyl acetate. The organic layer was dried over anhydrous sodium and evaporated under reduced pressure to give a gummy mass, yield 90%. All the data are in accordance with the reported one.^1H NMR (300 MHz, $CDCl_3$) δ; 0.92-0.89 (m, 6H, $CH(CH_3)_2$), 1.44 (s, 9H, Boc, $(CH_3)_3$), 2.07–2.10 (m, 1H, β-CH), 4.19-4.23 (m, 1H, α-CH), 8.10 (br s, 1H, NH); ^{13}C NMR (300 MHz, $CDCl_3$), δ 17.4, 18.9, 28.2, 31.0, 58.3, 80.0, 155.8, 176.6.

Figure A143.[1]H NMR analysis of Boc L-Valine **138.**

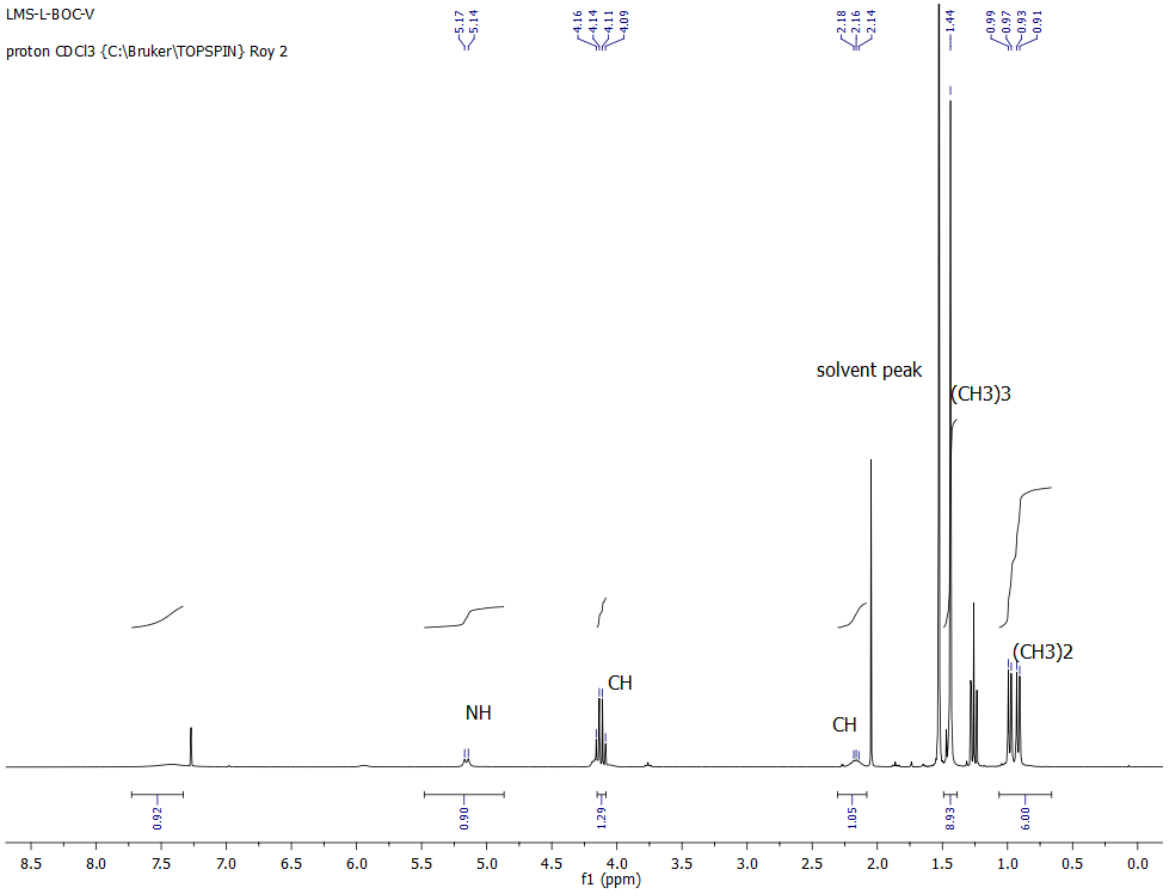

Compound 139

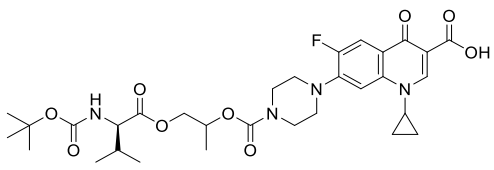

Experimental: TMSCl (300 µL, 2.355 mmol), DIPEA (700 µL, 397 mmol) and **137** (300 mg, 0.653 mmol) were combined in dry DMF (9 mL) and stirred for 5 min. at rt to give a light-yellow solution. N-Boc L-Valine **138** (400 mg, 1.78mmol, 2.5 eqv.) and DIPEA (700 µL, 3.6 mmol, 2 equiv) were combined in 6 mL dry DMF to give a colorless solution. The solutions were combined and the reaction was stirred overnight at 65°C. MeOH (9 mL) was added to the reaction and the resulting mixture was stirred for another 15 min, the mixture was concentrated and the resulting solid was dissolved in EtOAc. The organic phase was washed with brine and dried over anhyd. Na_2SO_4. The crude product was purified by flash chromatography on silica

gel (DCM: MeOH 97: 3%) to afford the desired product as brown solid (200 mg, 50%). ^{1}H NMR (300 MHz, $CDCl_3$) δ 8.77 (s, 1H, H2), 8.02 (d, *J* = 12.9 Hz, 1H, H7), 7.35 (t, *J* = 9.6 Hz, 1H, H10), 5.67 (brs, 1H, NH),, 5.05 (dd, *J* = 17.1, 7.3 Hz, 2H, H29), 3.69 (dd, *J* = 11.5, 4.3 Hz, 1H, H31), 3.63 – 3.50 (m, 3H, H21-H22, H16), 3.31 (d, *J* = 2.5 Hz, 1H, H24-H25), 2.25 – 2.02 (m, 1H, H36), 1.44 (s, 9H-*tert-butyl*), 1.38 (d, J = 6.4 Hz, 1H, H17), 1.31 (t, *J* = 6.5 Hz, 1H, H17'), 1.22 (d, *J* = 6.0 Hz, 2H, H18), 1.00 (d, *J* = 6.9 Hz, 3H, H37), 0.93 (d, J = 6.9 Hz, 3H, H38). ESI-MS (*m/z*) calcd for $C_{31}H_{41}FN_4O_9$ $[M+H]^+$ 633.29; found 634.10

Figure A144.^{1}H NMR analysis of compound **139** ($CDCl_3$)

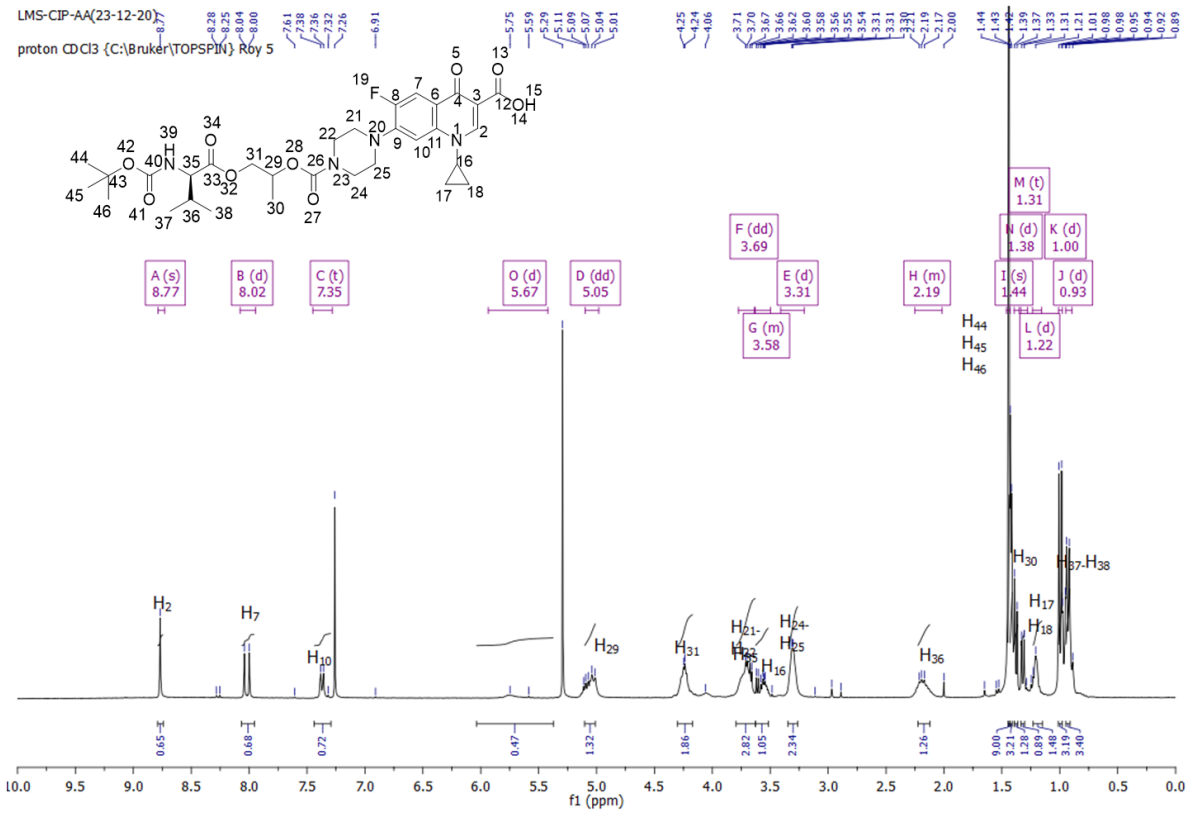

Figure A145. ^{19}F NMR analysis of compound **139** (300 MHZ, $CDCl_3$)

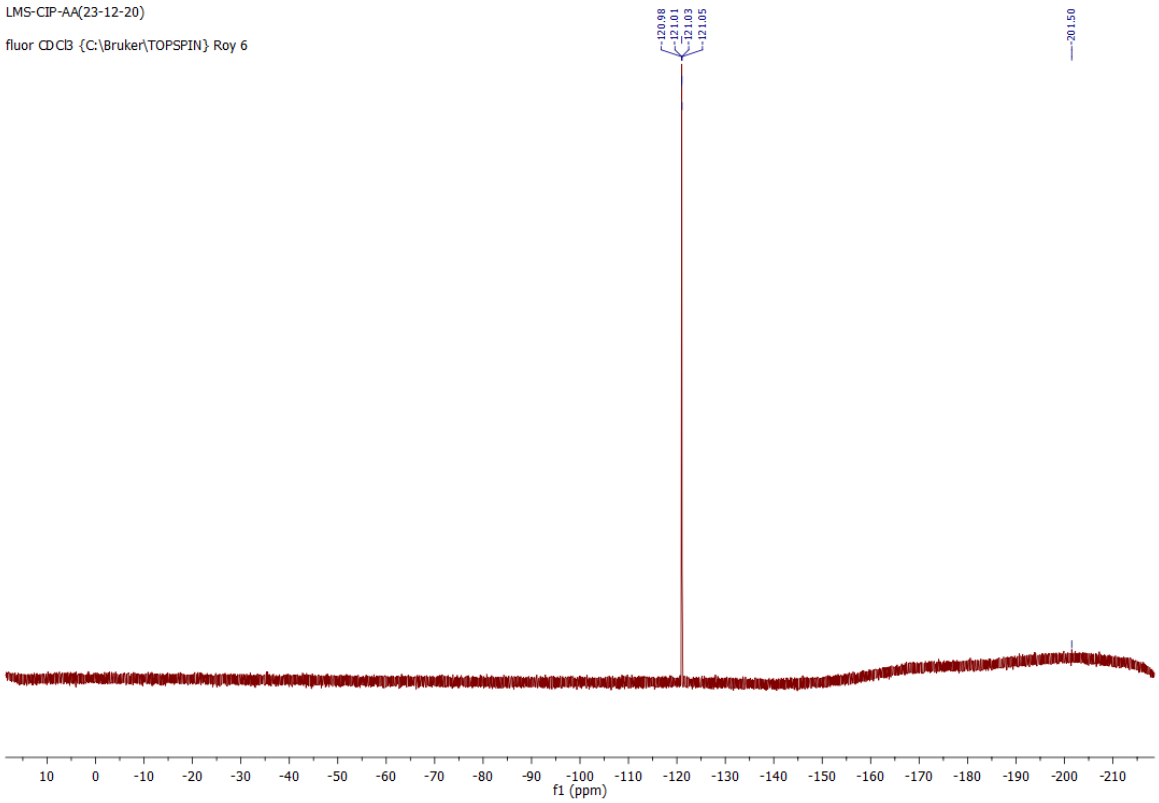

Figure A146. Mass spectrum of compound **139**

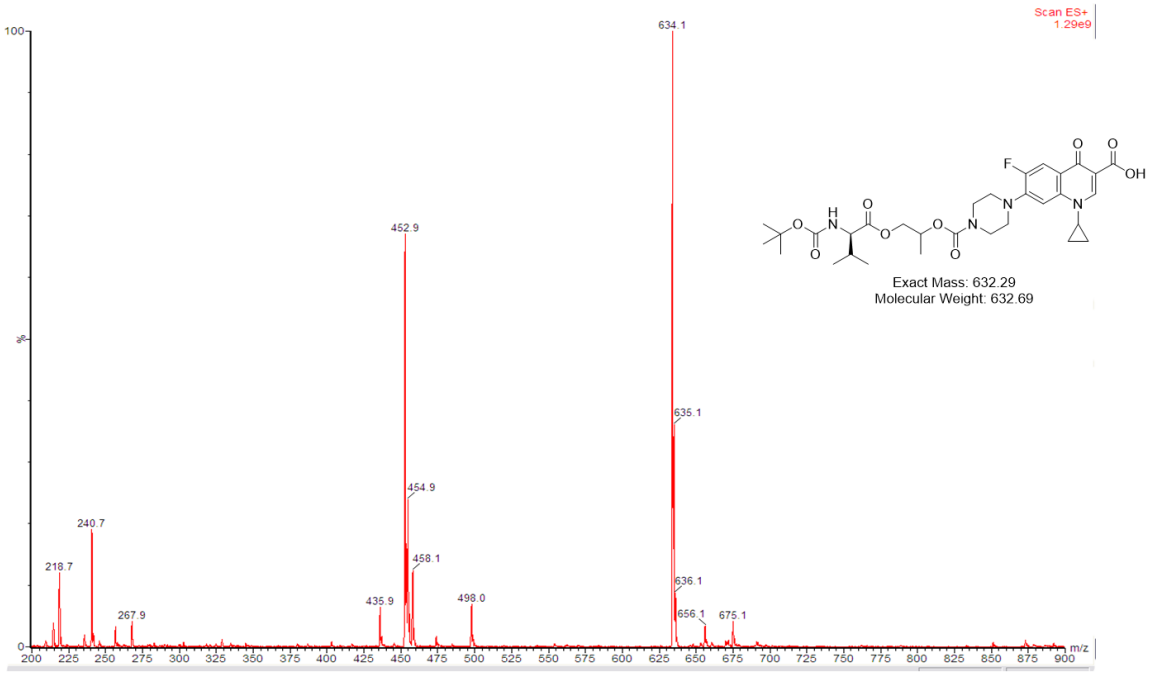

Compound 132

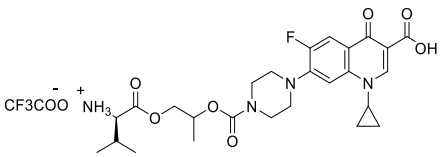

Experimental: A portion of **139** (150 mg, 0.237 mmol) was dissolved in 20% TFA/DCM (3 mL), which was stirred for 2.5 h at rt. The reaction was then concentrated under reduced pressure with co-solvent toluene, resulting in the precipitation of an orange solid **132** (90 mg, 71 % yield). The mixture was dried, and pure enough to be injected and used for the next step without further purification. ^{1}H NMR (300 MHz, $CDCl_3$) δ 8.73 (s, 1H, H2), 7.98 (d, *J* = 12.9 Hz, 1H, H10), 7.36 (d, *J* = 7.1 Hz, 1H, H7), 5.14 – 4.99 (m, 1H, H29), 3.80 – 3.65 (m, 2H, H31), 3.61 (d, *J* = 5.3 Hz, 1H, H16-H16), 3.59 – 3.59 (m, 1H, H35), 3.48 (q, *J* = 7.0 Hz, 2H, H21-H22), 3.32 (s, 4H, H24-H25-NH2), 1.43 – 1.34 (m, 6H, H17-H18), 1.28 – 1.10 (m, 7H, H36-H37-H38). ^{13}C NMR (300 MHz, $CDCl_3$) δ 177.0, 177.0, 167.0, 155.3, 154.4, 151.9, 147.5, 145.6, 139.0, 128.9, 125.1, 122.2, 120.1, 120.0, 112.6, 112.3, 108.0, 105.1, 105.1, 70.9, 65.8, 54.6, 49.6, 47.4, 43.5, 35.3, 30.3, 29.7, 21.4, 17.9, 15.2, 8.2. ESI-MS (*m/z*) calcd for $C_{26}H_{33}FN_4O_7$ $[M+2H]^+$ 534.23; found 535.00.

Figure A147.[1]H NMR analysis of compound **132** (300 MHz, $CDCl_3$)

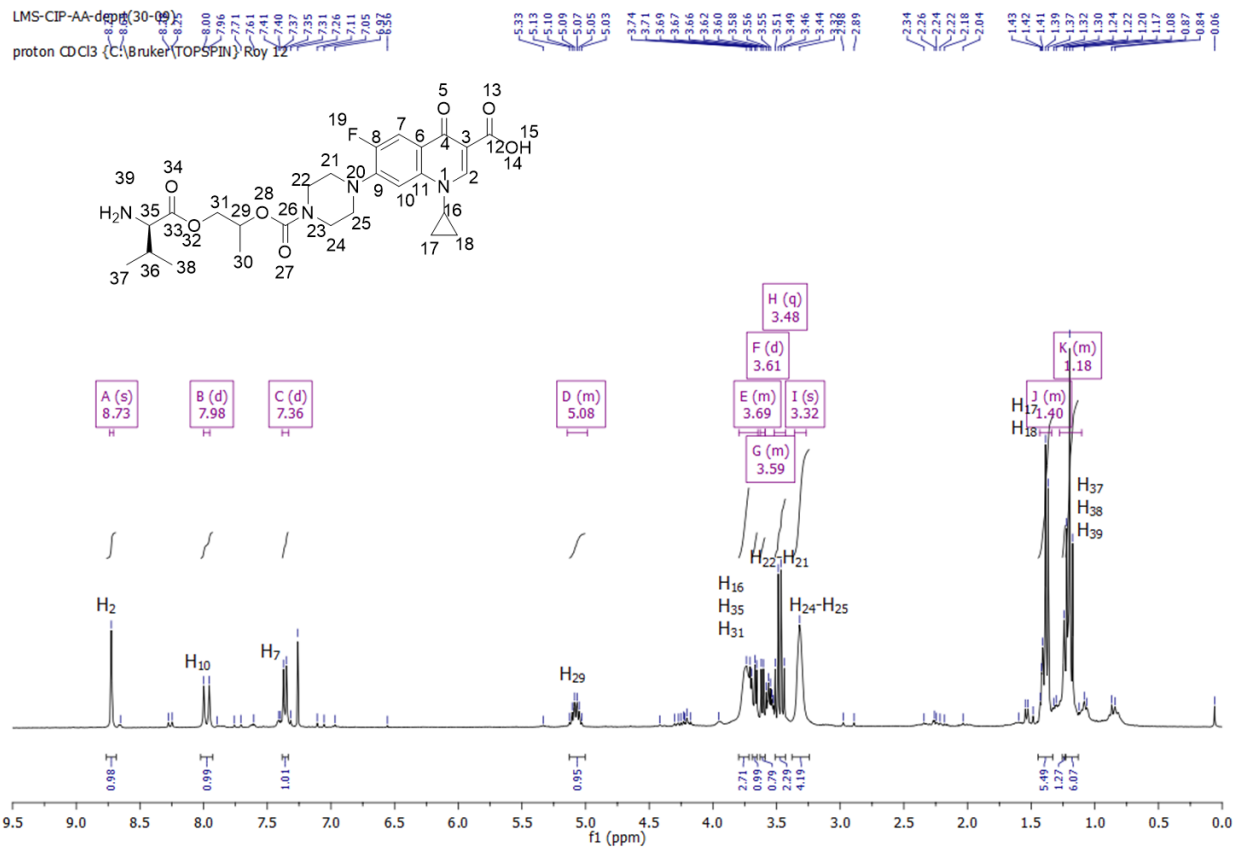

Figure A148. ^{13}C NMR analysis of compound **132** (300 MHz, $CDCl_3$)

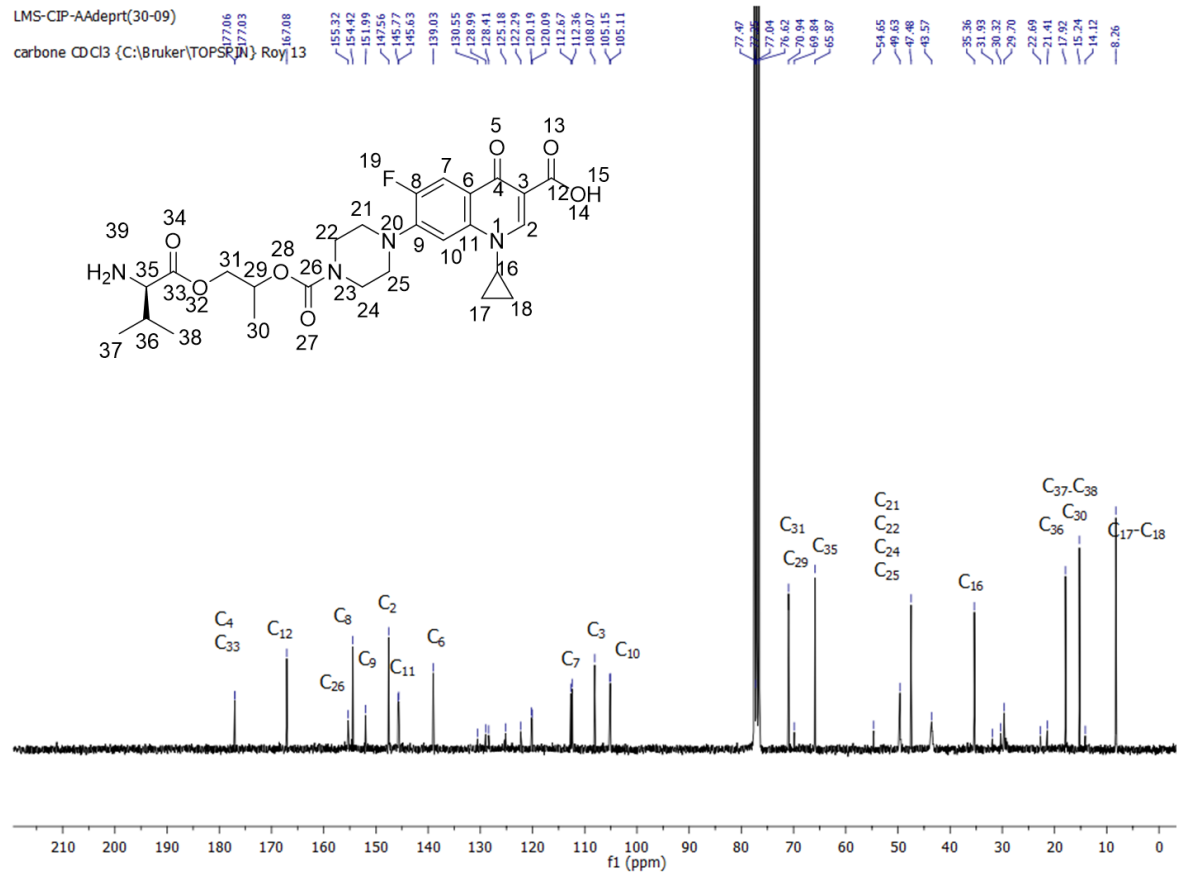

Figure A149. ^{19}F NMR analysis of compound **132** (300 MHz, $CDCl_3$)

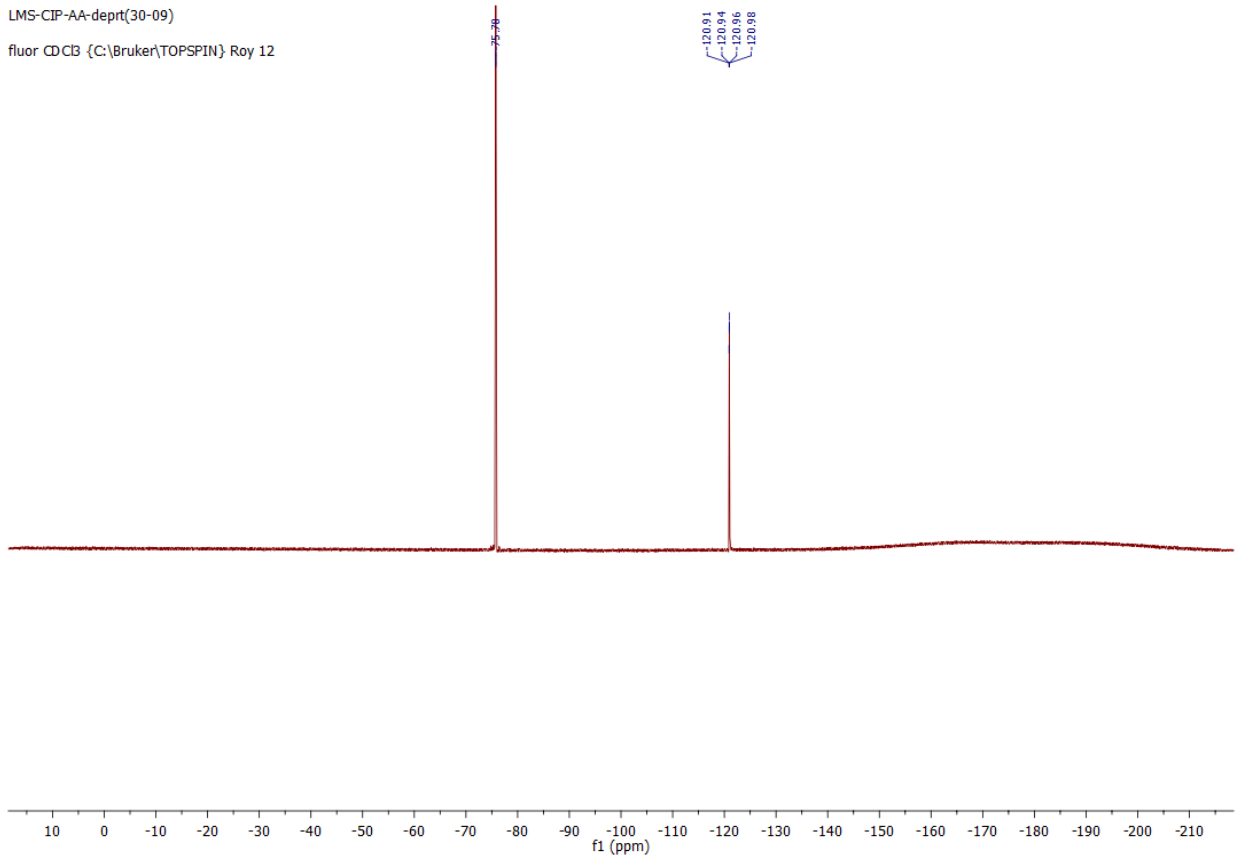

Figure A150. Mass spectrum of compound **132**

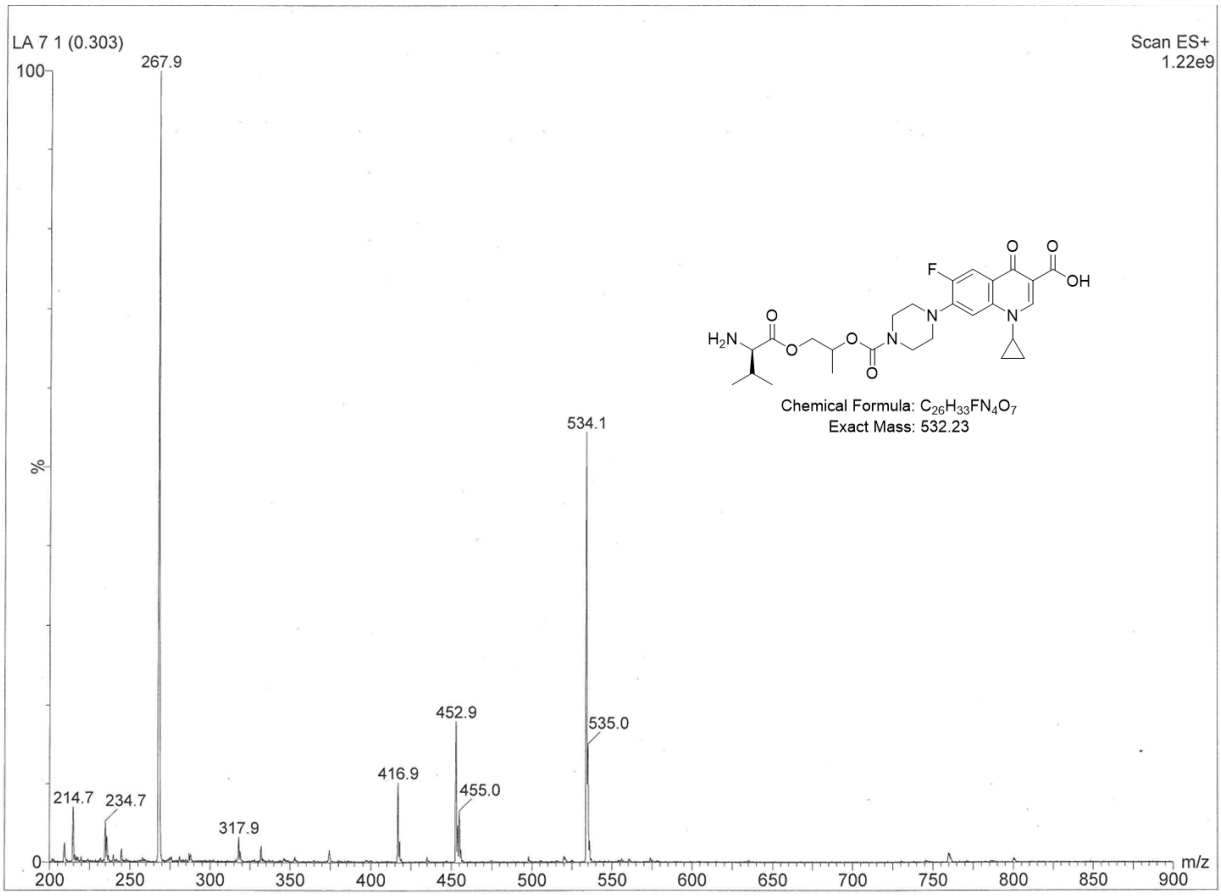

Experimental part chapter 6

Synthesis of cyclotriphosphazene PEG_3 core (84)

Step 1: synthesis of Mono alkyne terminated tri ethylene glycol (**152**)

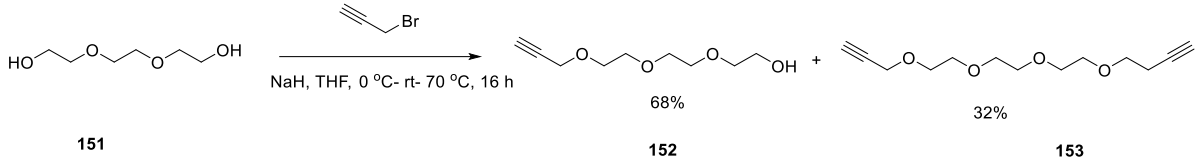

Experimental: in a two-neck round-bottom flask NaH (60%, 1.3 g, 32.66 mmol, 0.7 eqv.) was added to THF (23 mL) at 0 ºC, with extensive stirring, and a solution of Tri ethylene glycol **151** (7 g, 46.66mmol, 1.0 eq) in THF (30 mL) was added over 30 min. The reaction was stirred for 1 h at room temperature, and a solution of propargyl bromide (5 mL, 46.66mmol, 1.0 eq) in THF (23 mL) was then added over 1 h. The solution was stirred for 1 h at room temperature and then an additional 15 h at 60 °C. The reaction mixture was extracted with DCM, quenched with 3% HCl (100 mL), and washed with brine. The organic layer was dried over Na_2SO_4 and concentrated in *vacuo* to obtain the crude residue as a colorless oil. The residue was purified by silica gel column chromatography (gradient eluent: 0-1-2-3-4-5% MeOH in DCM) to obtain the pure product as colorless oil (6 g, 68%).

Step II- core synthesis

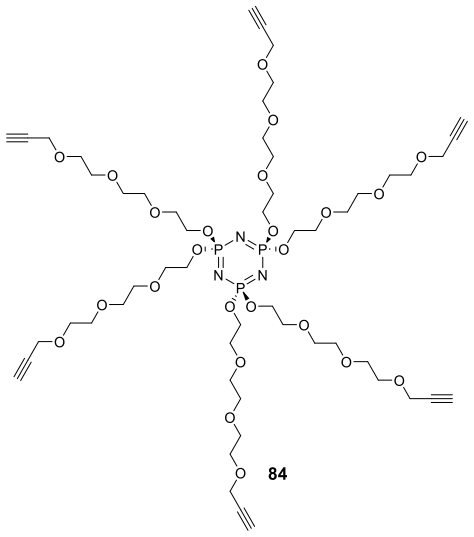

Chemical Formula: $C_{54}H_{90}N_3O_{24}P_3$
Exact Mass: 1257.51

Experimental: TEG monopropargyl **152** (5g, 26.39 mmol) was dissolved in dry THF (400 mL) and added to a suspension of NaH (60%, 1.00 g, 21.27 mmol) in THF (50 mL). The resultant solution was stirred at room temperature for 1 h, at which point the sodium salt precipitated from the solution. Hexachlorocyclotriphosphazene (HCCP) (0.5 g, 1.32 mmol) dissolved in THF (5 mL) was added dropwise to the salt solution over a period of 1 h, during which the sodium salt dissolved. The resultant solution was then heated at 70 °C for 24 h, followed by the removal of the solvent under reduced pressure. The oily residue was redissolved in dichloromethane, washed with nanopure water, and subsequently dried over magnesium sulfate, filtered, and concentrated under *vacuum*. The crude product was purified by column chromatography (DCM/ MeOH 99:1%) to afford the product as a colorless oil residue (1 g, 75%). ^{1}H NMR (300 MHz, $CDCl_3$) δ 4.20 (d, 2H, J = 2.3 Hz, CH_2, H_2C—≡), 4.00- 4.09 (m, 2H, CH_2), 3.70 – 3.61 (m, 10H), 2.45 (t, 1H, J = 2.3 Hz, ≡–H). ESI/MS *m/z* calcd for $C_{54}H_{90}N_3O_{24}P_3$ $[M+H]^+$ 1258.51; found 1259.6.

Figure A151. ^{1}H NMR analysis of core **84** (300 MHz, $CDCl_3$)

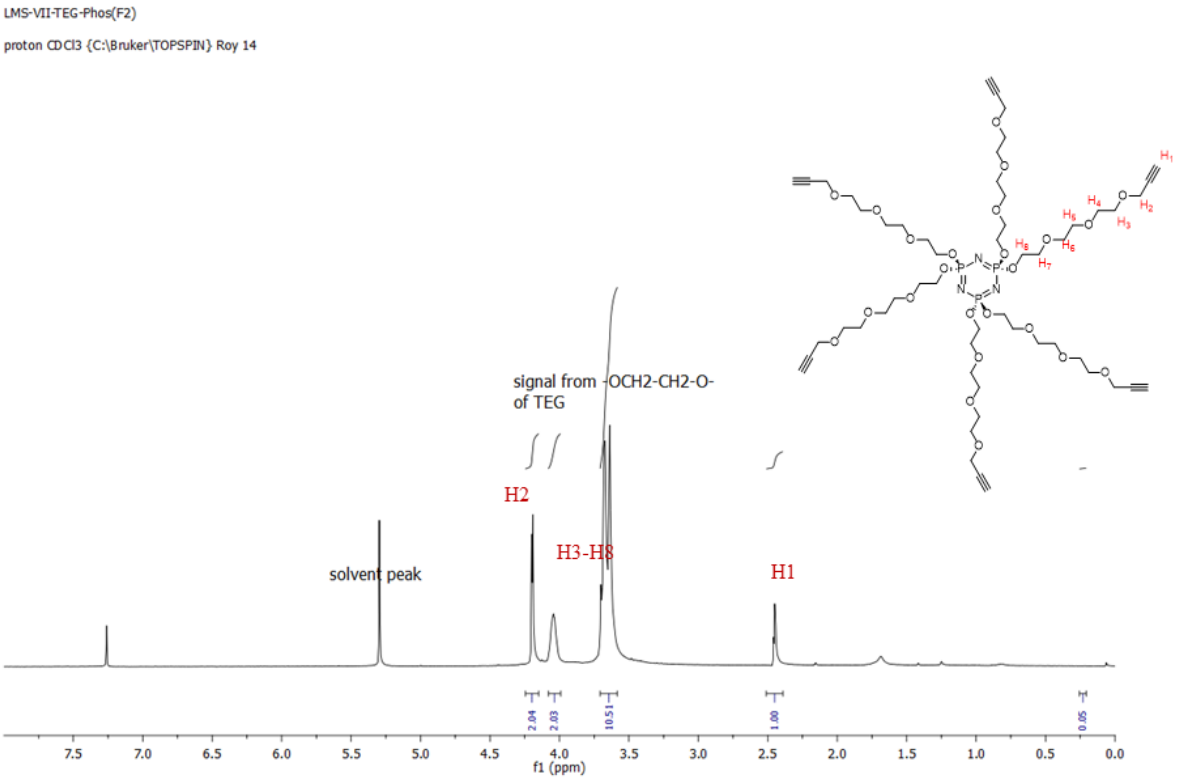

Figure A152.^{31}P NMR analysis of core **84** (300 MHz, $CDCl_3$)

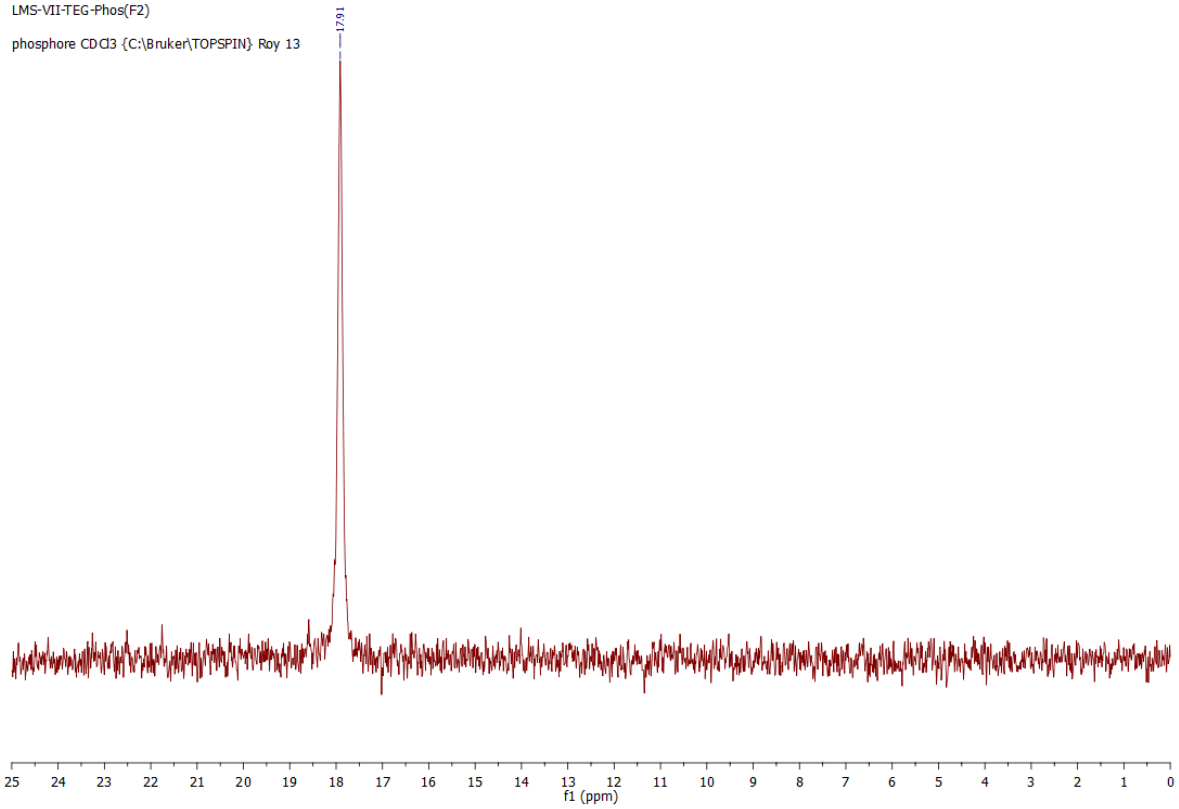

Heterobifunctionalized tri (ethylene glycol) Linkers Synthesis

Synthesis of HO-TEG-N_3 (109)

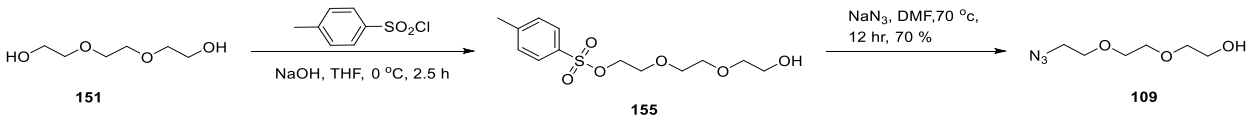

Experimental: To a solution of the TEG **151** (30g, 199.7 mmol, 2.5 equiv) in THF-H_2O (2:1) at 0 °C was added a solution of NaOH 0.5 M (50 mL). The resultant mixture was stirred at 0 °C for 15 min. a solution of *p*-Tosyl chloride (15 g, 78.9 mmol, 1 equiv) in THF (50 mL) was added, the reaction mixture was allowed to stir at 0 °C for 2.5 h. The mixture was poured into ice water, and slightly acidified with 3% HCl (pH = 6). The crude product was extracted with dichloromethane, dried over Na_2SO_4, filtered, and concentrated under reduced pressure. Purification of the crude product by flash column chromatography (DCM-MeOH 95:5%) afforded TEG mono tosylate as a pale-yellow oil (30g, 50%). The resulting monotosylated PEG product was reacted with NaN_3 (5.0 eq) in DMF at 70 °C for 15 h. the reaction was allowed to cool to rt, then filtered over celite, DMF was removed in vacuo, diluted with ethyl acetate, washing with water, dried

over anhyd. Na_2SO_4 and concentrated to give the pure product as a pale-yellow oil in quantitative yield, which injected to the next step without further purification. The NMR matched with the reported one. [504] ^1H NMR (300 MHz, $CDCl_3$) δ 3.66- 3.50 (m, 8H), 3.47 (dd, 2H, J = 5.2, 3.9 Hz, CH_2), 3.26 (dt, 2H, J = 20.7, 11.6 Hz, CH_2). 3.13 (br, 1H, OH). ^{13}C NMR (300 MHz, $CDCl_3$) δ 72.5, 70.4, 70.2, 69.8, 61.4, 50.4.

Figure A153.^1H NMR analysis of linker **109** (300 MHz, $CDCl_3$)

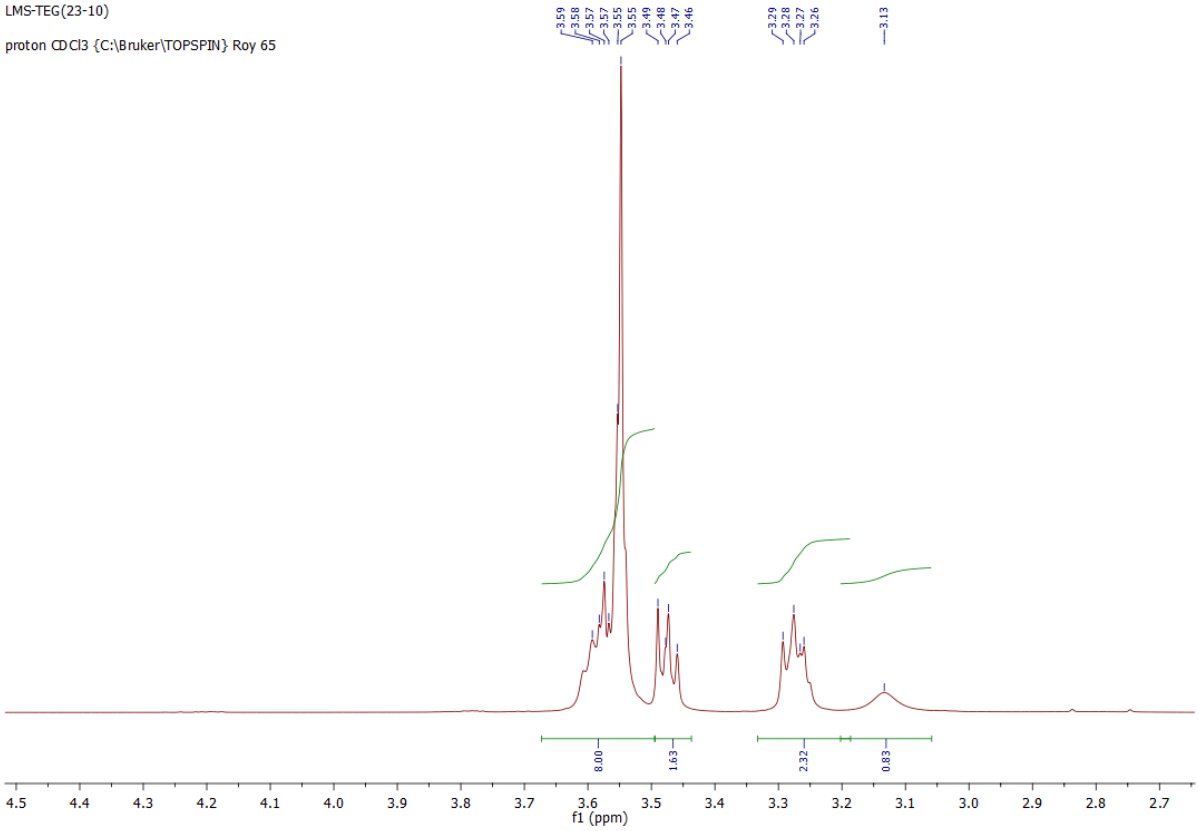

Figure A154.^{13}C NMR analysis of linker **109** (300 MHz, $CDCl_3$)

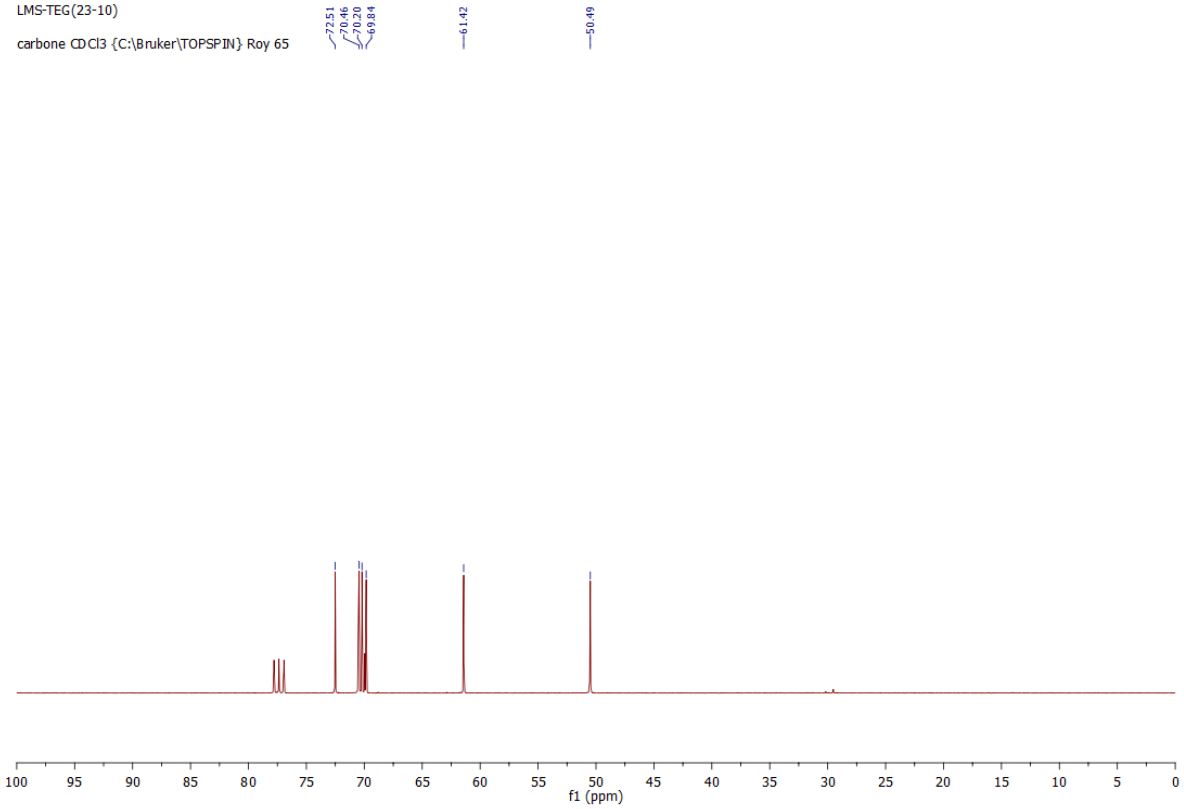

Synthesis of Alkyne-TEG-NH2 161; route A

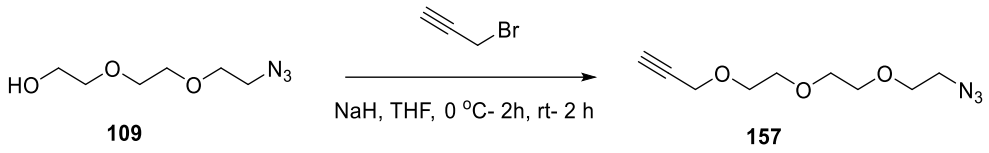

Experimental: To a solution of linker **109** (4,00 g, 22.85 mmol) in 20 mL of THF was added NaH (60%, in mineral oil, 1.00 g, 41.66 mmol, 1.8 equiv) at 0 °C. After stirring for 15 min. propargyl bromide (80% in toluene, 3.5 mL, 39.59 mmol, 1.7 equiv) was added slowly, and the mixture was stirred at 0 °C for 2 h and then at 23°C for an additional 2 h. The reaction mixture was extracted with DCM, quenched with 3% HCl (50 mL), and washed with brine. The organic layer was dried over Na_2SO_4 and concentrated in *vacuo*. The crude residue was purified by silica gel column chromatography (gradient eluent: 0-1-2-3 % MeOH in DCM). The pure product **157** was obtained as a colorless oil in low yield (1.9 g, 39%).

Step 2 :

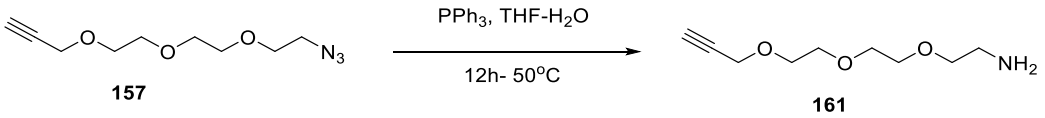

Experimental: To a solution of linker **157** (1.9 g, 8.92 mmol, 1.0 eqv.) in THF (20 mL) and triphenyl phosphine (3.2 g, 12.33mmol, 0.9 eqv.) was added water (5 mL). The mixture allowed to stir at 50 ^{0}C for 12. After the solution was evaporated under reduced pressure. The crude product was acidified with 1N HCl to pH= 3, followed by washing with ethyl acetate to remove the side product and unreacted materials. The aqueous layer was collected and a solution of sat. $NaHCO_3$ was added to it until the pH of the solution was basic, then the aqueous layer extracted several times with $CHCl_3$, drying over Na_2SO_4 and then in *vacuo*, to afford **161** (500 mg, 30 %) which injected to the next step without any further purification. ^{1}H NMR (300 MHz, $CDCl_3$): δ 3.72-3.51 (m, 8H), 3.37-3.27 (m, 4H), 3.40 (dd, 2H, *J* = 5.2, 3.9 Hz, CH_2), 3.26 (dt, 2H, *J* = 20.7, 11.6 Hz, CH_2),2.44 (t, 1H, *J*= 2.5 Hz), 1.7 (brs, 2H, NH_2). The data were in match with the reported one. [496]

Synthesis of Alkyne-TEG-NH_2 161; route B

Step 1 : Synthesis of HO-TEG-NH_2 (158)

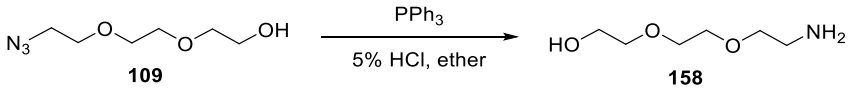

Experimental: To **109** (2.4 g,13.7 mmol, 1.0 equiv), 5% HCl (26 mL) was added with vigorous stirring at room temperature. A solution of triphenyl phosphine (3.2 g, 12.33mmol, 0.9 equiv) in Et_2O (40 mL) was added to this mixture over 3 hours. The mixture was allowed to react at room temperature for further 24 hours. The reaction mixture was washed with ethyl acetate to remove the unreacted starting materials and triphenylphosphine oxide that was formed during the reaction. The aqueous layer was collected, cooled to 0 ^{o}C, and concentrated potassium hydroxide was added to it until the pH of the solution was basic (~12). The product was extracted as a pale-yellow oil by washing the aqueous layer with DCM, drying over Na_2SO_4 and then in *vacuo*, to afford HO-TEG-NH_2 **158** (1.4 g, 68%) which injected to the next step without any further purification. ^{1}H NMR (300 MHz, $CDCl_3$) δ 3.72- 3.52 (m, 8H), 3.40 (dd, 2H, *J* = 5.2, 3.9 Hz, CH_2), 3.26 (dt, 2H, *J* = 20.7, 11.6 Hz, CH_2).

Step 2:

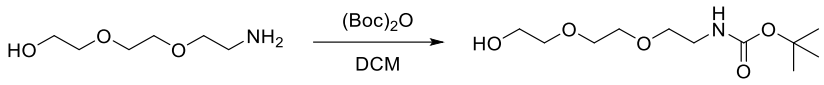

158 159

Experimental: Boc_2O anhydride (2.6 g, 12.18 mmol) was added to a solution of HO-TEG-NH_2 **158** (1.2 g, 8.12 mmol) in dichloromethane (10 mL) at 0 ºC, and the reaction continue stirring at room temperature overnight. Concentrated and precipitated with a large amount of ether. The suspension was filtered, and the residue was collected and dried to afford the product **159** as a white powder (1.05 g, 52%). ^{1}H NMR (300 MHz, $CDCl_3$): δ 3.72-3.51 (m, 8H), 3.37-3.27 (m, 4H), 1.44 (s, 9H). The data were in match with the reported one. [496]

Step 3 : Synthesis of Alkyne-TEG-NH(Boc) (160)

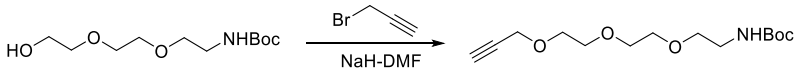

159 160

Experimental: A solution of the compound **159** (3.00 g, 12.04 mmol) in DMF (5 mL) was added to a suspension of sodium hydride (60% dispersion in mineral oil, 0.2 g, 5.06 mmol) in DMF (5 mL) at 0 ºC. The mixture was stirred ar rt for 30 min. after that, propargyl bromide (0.3 mL, 2.80 mmol) was added deropwise and reaction was left stirring at rt for 24 h. The reaction was quenched with water, extracted with ethyl acetate, and purified by column chrmotography, to afford yellowish powder **160** (2.00 g, 57 %). ^{1}H NMR (300 MHz, $CDCl_3$): δ 3.72-3.51 (m, 8H), 3.37-3.27 (m, 4H), 3.40 (dd, 2H, J = 5.2, 3.9 Hz, CH_2), 3.26 (dt, 2H, J = 20.7, 11.6 Hz, CH_2), 2.44 (t, 1H, J= 2.5 Hz), 1.44 (s, 9H). The data were in match with the reported one. [496]

Step 4: Alkyne-TEG-NH_2 (161)

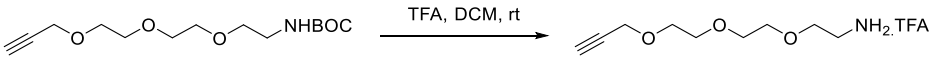

160 161

Experimental: Compound **160** (1 g, 3.48 mmol) was dissolved in 30 mL dry dichloromethane and cooled to 0 ºC. Trifluoroacetic acid (3 mL) was added dropwise, and the reaction was stirred at room temperature for 2 h. Evaporation to remove TFA and DCM. Following using of a large amount of ether, the precipitate

was collected and dried to afford linker **161** as a white powder (500 mg, 76 %). ^{1}H NMR (300 MHz, $CDCl_3$): δ 3.72-3.51 (m, 8H), 3.37-3.27 (m, 4H), 3.40 (dd, 2H, *J* = 5.2, 3.9 Hz, CH_2), 3.26 (dt, 2H, *J* = 20.7, 11.6 Hz, CH_2),2.44 (t, 1H, *J*= 2.5 Hz), 1.7 (brs, 2H, NH_2). The data were in match with the reported one. [496]

Dendritic core (93)

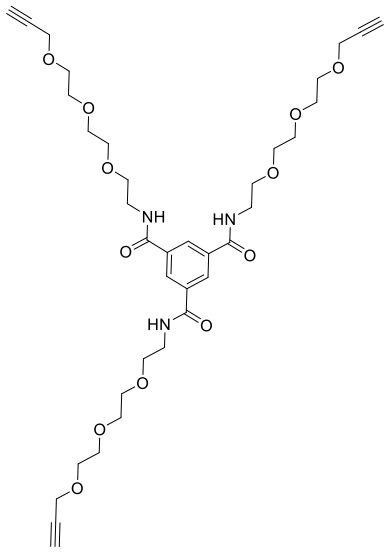

Experimental: Tri carboxylic benzoic acid 4 (500 mg, 2.4 mmol, 1 equiv) was dissolved in DMF (10 mL), and cooled at 0 ºC. DIC (1.3 mL, 8.41 mmol, 3.6 equiv), 1-Hydroxybenzotriazolehydrate (HOBt) (1.4 g, 10.4 mmol, 4.5 equiv) and Et_3N (2 mL, 82.5 mmol, 6 equiv) were added. After 10 min. alkyne-TEG-NH_2 **161** (2g, 10.8 mmol, 4.5 equiv.) was slowly added. The reaction mixture was allowed to warm to room temperature Stirred at rt for 36 h. The resulting mixture was diluted with DCM, washed with sat. $NaHCO_3$, followed by sat. NH_4Cl and brine, then it is dried over Na_2SO_4, filtered, and concentrated, the crude product is purified on silica gel using (DCM/MeOH, 96-3 %.) to afford core **93** (700 mg, 41%). ^{1}H NMR (300 MHz, CD_3OD) δ 8.39 (s, 3H, 3xNH), 4.10 (d, 6H, *J* = 2.4 Hz), 3.84- 3.53 (m, 36H), 2.83 (t, 3H, *J* = 2.4 Hz).^{13}C NMR (300 MHz, CD_3OD) δ 167.2, 135.2, 128.7, 79.2, 74.7, 70.1, 69.9, 69.9, 69.1, 68.6, 57.6, 39.8.

Figure A155. ^{1}H NMR analysis of core **93** (300 MHz, CD_3OD)

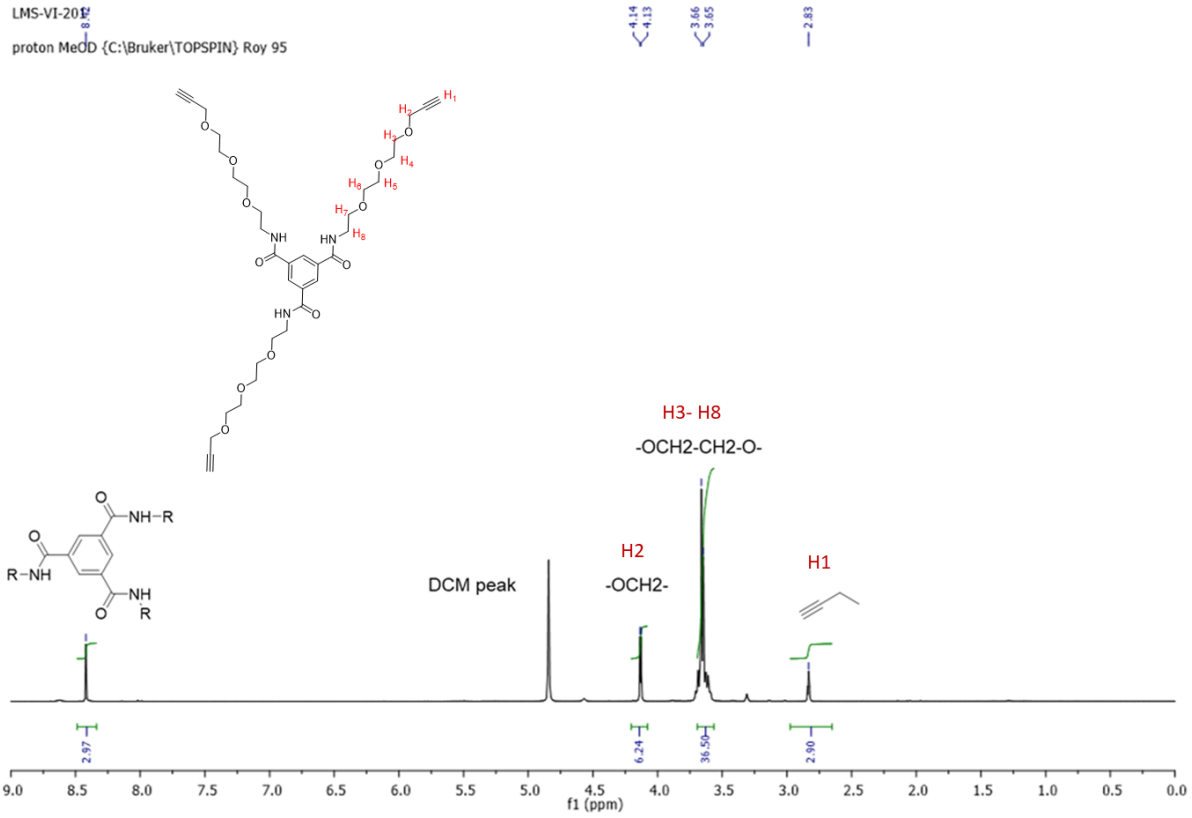

Figure A156. ^{1}H NMR analysis of core **93** (300 MHz, $CDCl_3$)

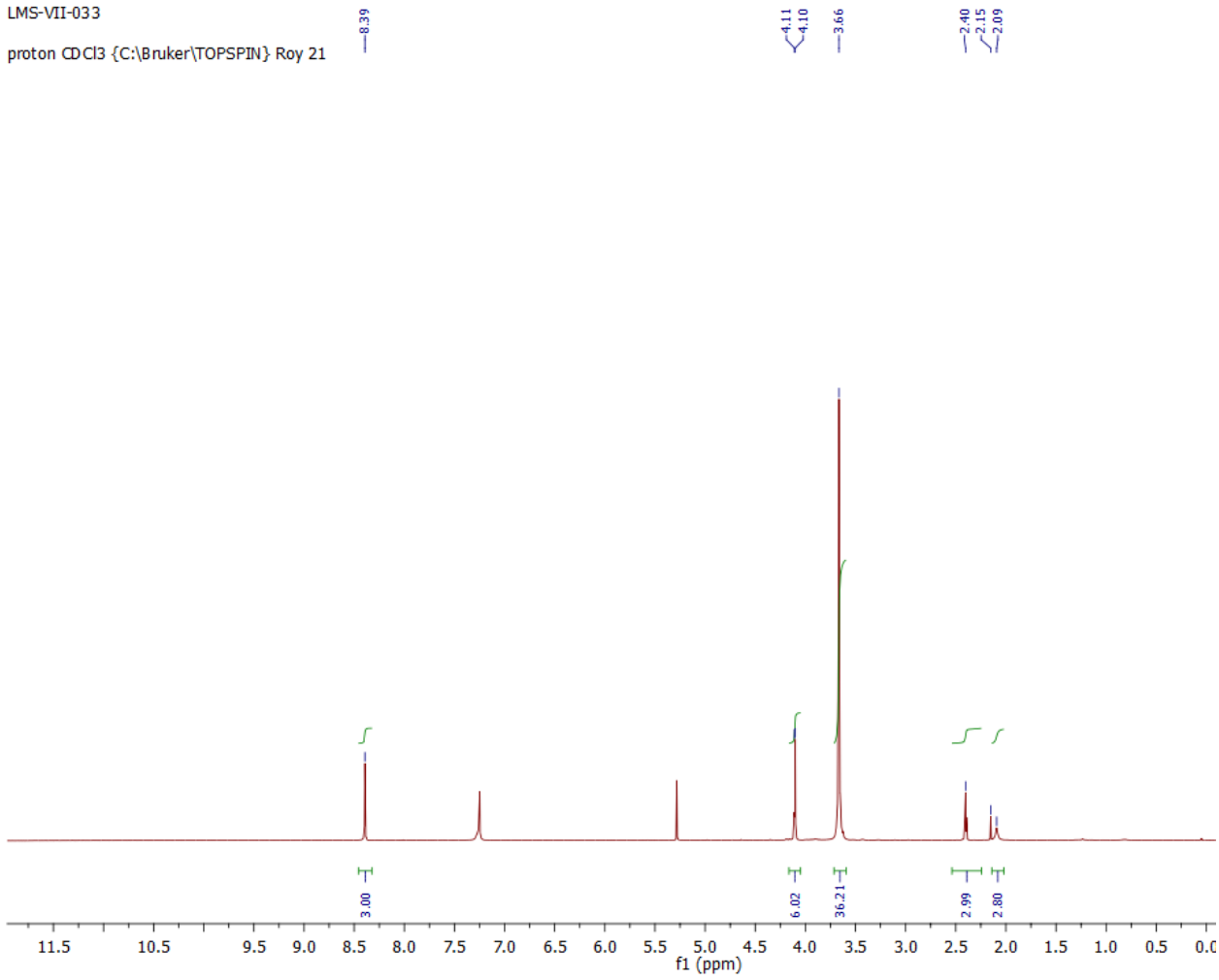

Figure A157. ^{13}C NMR analysis of core **93** (300 MHz, CD_3OD)

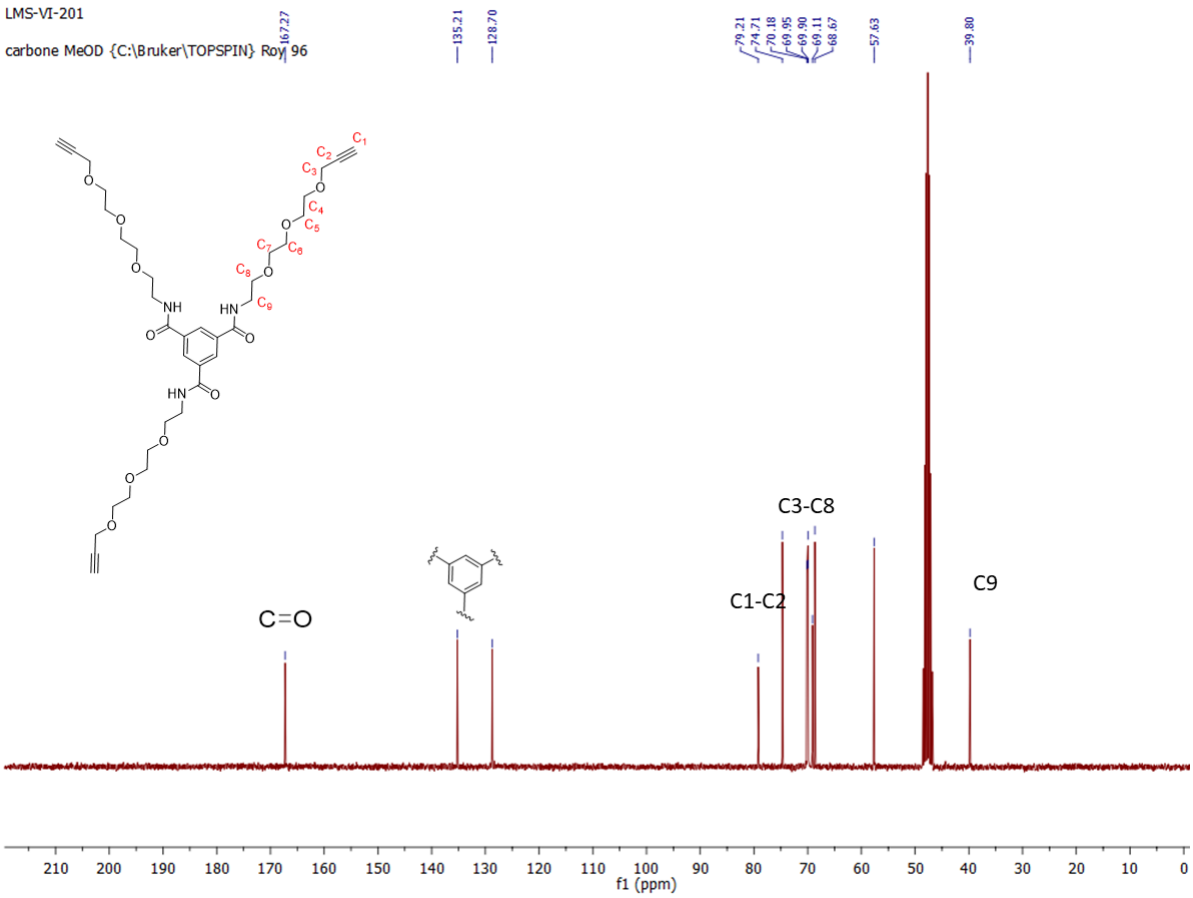

Methyl succinate linker 116

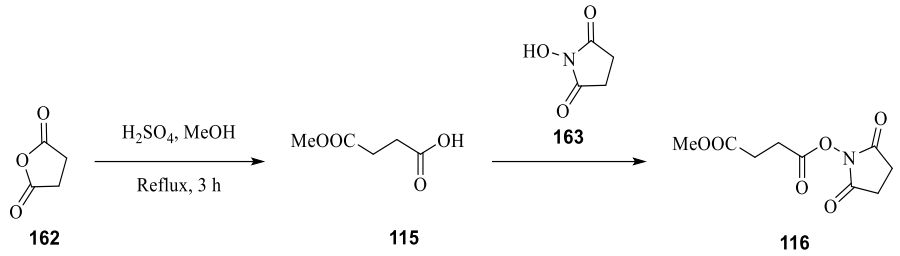

Experimental: To a mixture of acid **115** (1g, 7.575 mmol) and *N, N'*-Diisopropylcarbodiimide (1.7 g, 8.252 mmol) in DCM (100 mL), then add N-hydroxysuccinimide (4.3 g, 37.875 mmol) under vigorous stirring. The mixture was stirred at room temperature for 20 h. The organic layer was washed with 5% of citric acid; then with aq. Sat. $NaHCO_3$ was added, finally with brine. The crude product was purified on silica gel flash chromatography (Hexane: EtOAc 5 :5%) to afford the product **116** as solid white crystals (70 mg, 40% yield). ^{1}H NMR (300MHz, $CDCl_3$): δ 4.36- 3.89 (m, 1H), 3.73 (s, 3H), 2.96 (t, 2H, J = 7.1 Hz), 2.84 (s, 3H), 2.75 (t, 2H, J = 7.0 Hz), 1.26 (t, 2H, J = 7.1 Hz).

Figure A158. ^{1}H NMR analysis of compound **116** (300 MHz, $CDCl_3$)

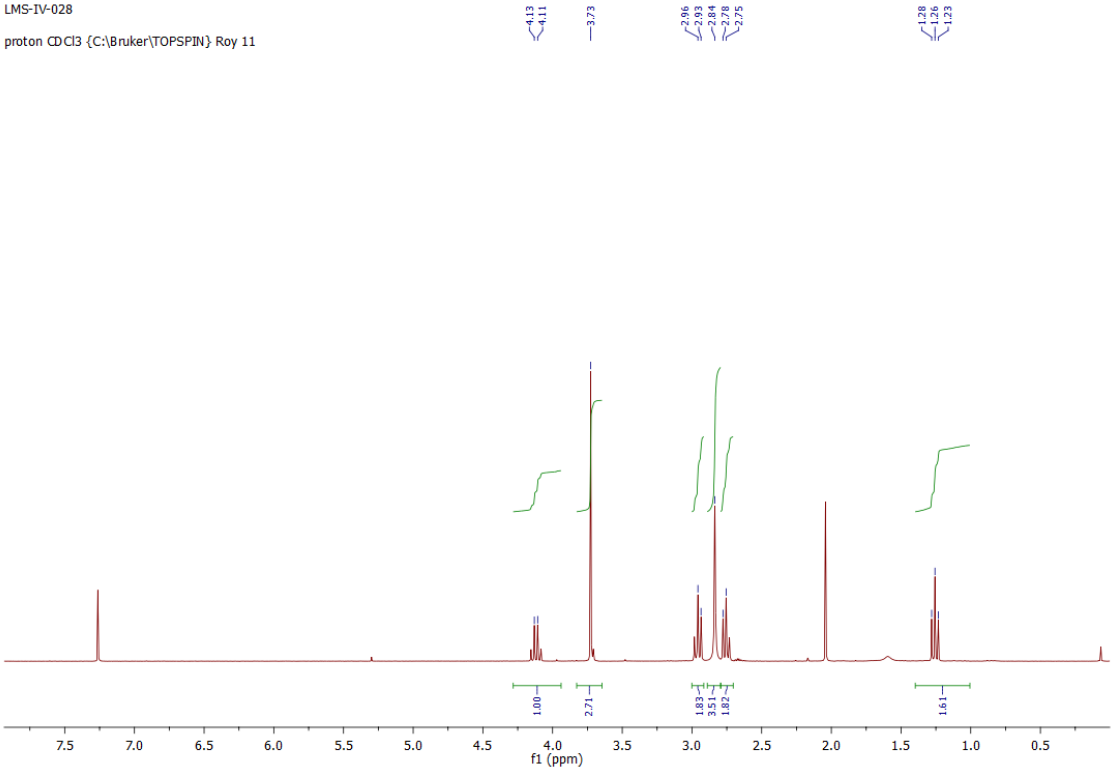

Synthesis of succinimidyl-4-azidobutyrate 166

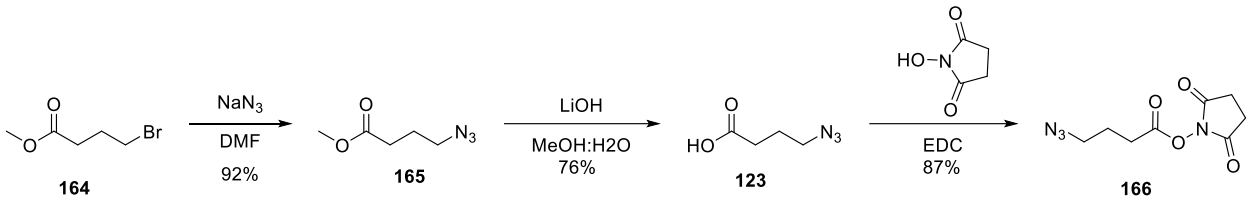

It has been synthesized through three steps as follow:

Step 1: Methyl 4-azidobutyrate (165)

Experimental: To a solution of methyl 4-bromobutyrate (2.7 g, 15 mmol) in DMF (4 mL), sodium azide (1.95 g, 30 mmol) was added. The mixture was heated at 80 °C overnight and was diluted with ethyl acetate (50 mL). The organic layer was washed with $NaHCO_3$, water, and brine, and dried over anhydrous Na_2SO_4. The solvent was removed under vacuum to yield a pale-yellow liquid (1.32 g, 62%). ^{1}H NMR ($CDCl_3$, 300MHz): δ 3.66 (s, 3 H), 3.32 (t, *J* = 7.8 Hz, 3 H), 2.38 (t, *J* = 7.5 Hz, 2 H), 1.86 (m, 2 H).

Step 2: 5-azidovaleric acid (123)

Experimental: To a solution of **165** (1.29 g, 9 mmol) in MeOH (15 mL) was added an aqoues solution of LiOH (20 mmol in 5 mL water). The suspension was stirred overnight. MeOH was removed under vacuum. The resulting residue was diluted by ethyl acetate (50 mL) and washed with 1.0 M HCl, water and brine. The organic layer was dried over anhydrous Na_2SO_4, and evaporated to dryness under *vacuum* yielding **123** as a pale-yellow oil (0.89 g, 76%). ^{1}H NMR ($CDCl_3$, 300 MHz): δ 3.38 (t, *J* = 6.6 Hz, 3 H), 2.48 (t, *J* = 7.2 Hz, 2 H), 1.90 (m, 2 H).

Step 3: Succinimidyl 5-Azidovalerate (166)

Experimental: To a mixture of acid **123** (180 mg, 1.40 mmol) and *N*-hydroxysuccinimide (173 mg, 1.50 mmol) in CH_2Cl_2 (20 mL), 1-(3-dimethylaminopropyl) -3- ethylcarbodiimide hydrochloride (EDC; 287 mg, 1.50 mmol) was added. The mixture was stirred at room temperature for 20 h. The organic layer was washed with 5% of citric acid; then with aq. Sat. $NaHCO_3$ was added, finally with brine The organic layer dried over anhyd. Na_2SO_4. The collected organic layers was evaporated under *vacuum* to afford **166** as a white solid (277 mg, 87%). ^{1}H NMR ($CDCl_3$): δ 3.45 (t, *J* = 6.6 Hz, 2 H), 2.87 (s, 4 H), 2.73 (t, *J* = 7.2Hz, 2 H), 2.00 (m, 4 H).

Figure A159. IR analysis of compound **166**

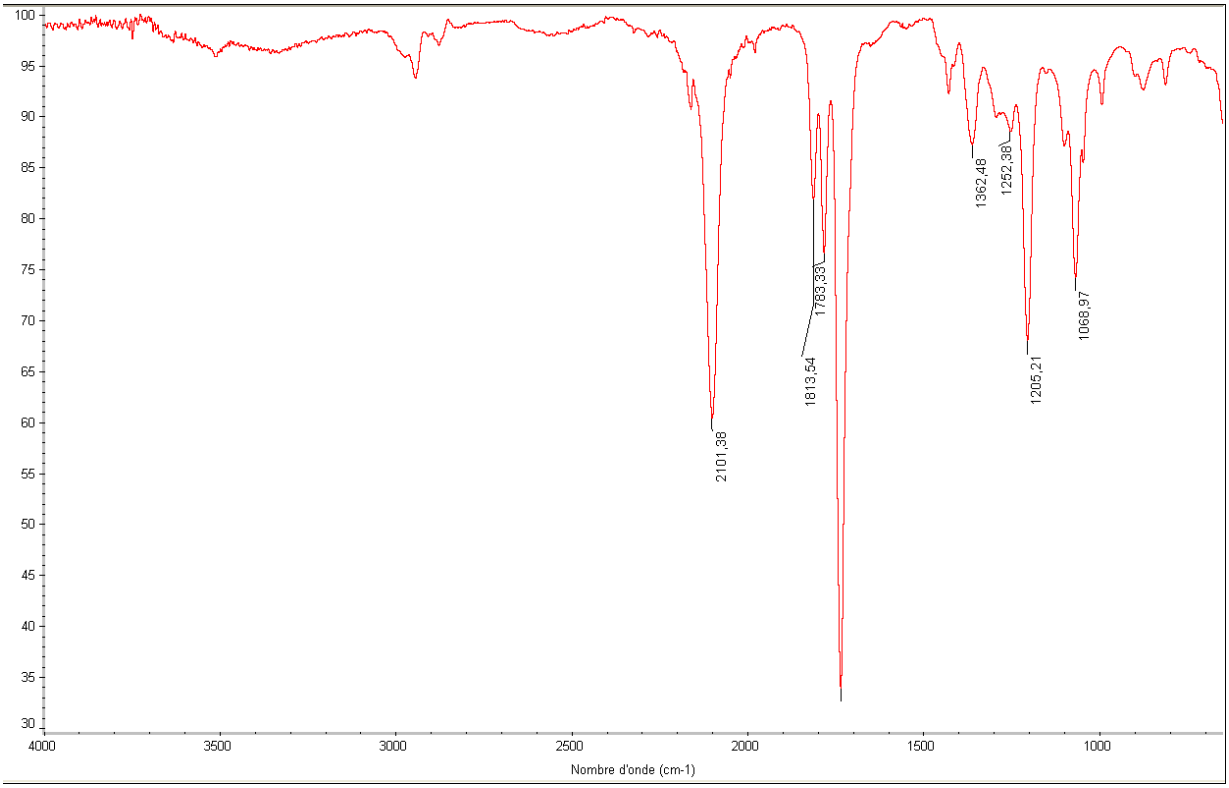

REFERENCES

1. Cano, A.; Ettcheto, M.; Espina, M.; López-Machado, A.; Cajal, Y.; Rabanal, F.; Sánchez-López, E.; Camins, A.; García, M. L.; Souto, E. B., State-of-the-art polymeric nanoparticles as promising therapeutic tools against human bacterial infections. *Journal of Nanobiotechnology* **2020,** *18* (1), 156.

2. Nicolle, L. E., Catheter-Related Urinary Tract Infection. *Drugs & Aging* **2005,** *22* (8), 627-639.

3. Stamm, W. E.; Norrby, S. R., Urinary Tract Infections: Disease Panorama and Challenges. *The Journal of Infectious Diseases* **2001,** *183* (Supplement_1), S1-S4.

4. Harding, G. K. M.; Ronald, A. R., The management of urinary infections; what have we learned in the past decade? *International Journal of Antimicrobial Agents* **1994,** *4* (2), 83-88.

5. Foxman, B., The epidemiology of urinary tract infection. *Nature Reviews Urology* **2010,** *7* (12), 653-660.

6. Foxman, B., Urinary Tract Infection Syndromes: Occurrence, Recurrence, Bacteriology, Risk Factors, and Disease Burden. *Infectious Disease Clinics of North America* **2014,** *28* (1), 1-13.

7. Hooton, T. M., Uncomplicated Urinary Tract Infection. *New England Journal of Medicine* **2012,** *366* (11), 1028-1037.

8. Lichtenberger, P.; Hooton, T. M., Complicated urinary tract infections. *Current Infectious Disease Reports* **2008,** *10* (6), 499-504.

9. Levison, M. E.; Kaye, D., Treatment of Complicated Urinary Tract Infections With an Emphasis on Drug-Resistant Gram-Negative Uropathogens. *Current Infectious Disease Reports* **2013,** *15* (2), 109-115.

10. Clatworthy, A. E.; Pierson, E.; Hung, D. T., Targeting virulence: a new paradigm for antimicrobial therapy. *Nat Chem Biol* **2007,** *3* (9), 541-8.

11. Gaspar, M. C.; Couet, W.; Olivier, J. C.; Pais, A. A.; Sousa, J. J., Pseudomonas aeruginosa infection in cystic fibrosis lung disease and new perspectives of treatment: a review. *Eur J Clin Microbiol Infect Dis* **2013,** *32* (10), 1231-52.

12. McGowan, J. E., Jr., Antimicrobial resistance in hospital organisms and its relation to antibiotic use. *Rev Infect Dis* **1983,** *5* (6), 1033-48.

13. Anderson, R.; Groundwater, P. W.; Todd, A.; Worsley, A., *Antibacterial agents: chemistry, mode of action, mechanisms of resistance and clinical applications*. John Wiley & Sons: 2012.

14. Rice, L. B., Federal Funding for the Study of Antimicrobial Resistance in Nosocomial Pathogens: No ESKAPE. *The Journal of Infectious Diseases* **2008,** *197* (8), 1079-1081.

15. Boucher, H. W.; Talbot, G. H.; Bradley, J. S.; Edwards, J. E.; Gilbert, D.; Rice, L. B.; Scheld, M.; Spellberg, B.; Bartlett, J., Bad bugs, no drugs: no ESKAPE! An update from the Infectious Diseases Society of America. *Clin Infect Dis* **2009,** *48* (1), 1-12.

16. Fernández, L.; Hancock Robert, E. W., Adaptive and Mutational Resistance: Role of Porins and Efflux Pumps in Drug Resistance. *Clin Microbiol Rev* **2012,** *25* (4), 661-681.

17. Fair, R. J.; Tor, Y., Antibiotics and bacterial resistance in the 21st century. *Perspect Medicin Chem* **2014,** *6*, 25-64.

18. Aslam, B.; Wang, W.; Arshad, M. I.; Khurshid, M.; Muzammil, S.; Rasool, M. H.; Nisar, M. A.; Alvi, R. F.; Aslam, M. A.; Qamar, M. U.; Salamat, M. K. F.; Baloch, Z., Antibiotic resistance: a rundown of a global crisis. *Infect Drug Resist* **2018,** *11*, 1645-1658.

19. Bhullar, K.; Waglechner, N.; Pawlowski, A.; Koteva, K.; Banks, E. D.; Johnston, M. D.; Barton, H. A.; Wright, G. D., Antibiotic resistance is prevalent in an isolated cave microbiome. *PLoS One* **2012,** *7* (4), e34953.

20. Sun, S.; Selmer, M.; Andersson, D. I., Resistance to β-lactam antibiotics conferred by point mutations in penicillin-binding proteins PBP3, PBP4 and PBP6 in Salmonella enterica. *PLoS One* **2014,** *9* (5), e97202.

21. Wright, G. D., Molecular mechanisms of antibiotic resistance. *Chemical Communications* **2011,** *47* (14), 4055-4061.

22. Sohmen, D.; Harms, J. M.; Schlünzen, F.; Wilson, D. N., Enhanced SnapShot: Antibiotic inhibition of protein synthesis II. *Cell* **2009,** *139* (1), 212-212.e1.

23. De Oliveira, D. M. P.; Forde, B. M.; Kidd, T. J.; Harris, P. N. A.; Schembri, M. A.; Beatson, S. A.; Paterson, D. L.; Walker, M. J., Antimicrobial Resistance in ESKAPE Pathogens. *Clin Microbiol Rev* **2020,** *33* (3).

24. Walsh, T. R.; Weeks, J.; Livermore, D. M.; Toleman, M. A., Dissemination of NDM-1 positive bacteria in the New Delhi environment and its implications for human health: an environmental point prevalence study. *Lancet Infect Dis* **2011,** *11* (5), 355-62.

25. Paterson, D. L., Resistance in gram-negative bacteria: Enterobacteriaceae. *Am J Infect Control* **2006,** *34* (5 Suppl 1), S20-8; discussion S64-73.

26. Cornaglia, G.; Akova, M.; Amicosante, G.; Cantón, R.; Cauda, R.; Docquier, J. D.; Edelstein, M.; Frère, J. M.; Fuzi, M.; Galleni, M.; Giamarellou, H.; Gniadkowski, M.; Koncan, R.; Libisch, B.; Luzzaro, F.; Miriagou, V.; Navarro, F.; Nordmann, P.; Pagani, L.; Peixe, L.; Poirel, L.; Souli, M.; Tacconelli, E.; Vatopoulos, A.; Rossolini, G. M., Metallo-beta-lactamases as emerging resistance determinants in Gram-negative pathogens: open issues. *Int J Antimicrob Agents* **2007,** *29* (4), 380-8.

27. Okusu, H.; Ma, D.; Nikaido, H., AcrAB efflux pump plays a major role in the antibiotic resistance phenotype of Escherichia coli multiple-antibiotic-resistance (Mar) mutants. *Journal of Bacteriology* **1996,** *178* (1), 306.

28. Aeschlimann, J. R., The role of multidrug efflux pumps in the antibiotic resistance of Pseudomonas aeruginosa and other gram-negative bacteria. Insights from the Society of Infectious Diseases Pharmacists. *Pharmacotherapy* **2003,** *23* (7), 916-24.

29. Lister Philip, D.; Wolter Daniel, J.; Hanson Nancy, D., Antibacterial-Resistant Pseudomonas aeruginosa: Clinical Impact and Complex Regulation of Chromosomally Encoded Resistance Mechanisms. *Clin Microbiol Rev* **2009,** *22* (4), 582-610.

30. Nikaido, H., Role of permeability barriers in resistance to beta-lactam antibiotics. *Pharmacol Ther* **1985,** *27* (2), 197-231.

31. Ghai, I.; Ghai, S., Exploring bacterial outer membrane barrier to combat bad bugs. *Infect Drug Resist* **2017,** *10*, 261-273.

32. Delcour, A. H., Outer membrane permeability and antibiotic resistance. *Biochim Biophys Acta* **2009,** *1794* (5), 808-16.

33. Pechère, J. C.; Köhler, T., Patterns and modes of beta-lactam resistance in Pseudomonas aeruginosa. *Clin Microbiol Infect* **1999,** *5 Suppl 1*, S15-S18.

34. Hooper, D. C., Mechanisms of action of antimicrobials: focus on fluoroquinolones. *Clin Infect Dis* **2001,** *32 Suppl 1*, S9-S15.

35. Strateva, T.; Yordanov, D., Pseudomonas aeruginosa - a phenomenon of bacterial resistance. *J Med Microbiol* **2009,** *58* (Pt 9), 1133-1148.

36. Domagala, J. M., Structure-activity and structure-side-effect relationships for the quinolone antibacterials. *Journal of Antimicrobial Chemotherapy* **1994,** *33* (4), 685-706.

37. Foxman, B., The epidemiology of urinary tract infection. *Nat Rev Urol* **2010,** *7* (12), 653-60.

38. Aldred, K. J.; Kerns, R. J.; Osheroff, N., Mechanism of quinolone action and resistance. *Biochemistry* **2014,** *53* (10), 1565-74.

39. Hernandez, A.; Sanchez, M.; Martinez, J., Quinolone Resistance: Much More than Predicted. *Frontiers in Microbiology* **2011,** *2* (22).

40. Fàbrega, A.; Madurga, S.; Giralt, E.; Vila, J., Mechanism of action of and resistance to quinolones. *Microb Biotechnol* **2009,** *2* (1), 40-61.

41. Redgrave, L. S.; Sutton, S. B.; Webber, M. A.; Piddock, L. J., Fluoroquinolone resistance: mechanisms, impact on bacteria, and role in evolutionary success. *Trends Microbiol* **2014,** *22* (8), 438-45.

42. Hooper, D. C.; Jacoby, G. A., Topoisomerase Inhibitors: Fluoroquinolone Mechanisms of Action and Resistance. *Cold Spring Harb Perspect Med* **2016,** *6* (9).

43. Correia, S.; Poeta, P.; Hébraud, M.; Capelo, J. L.; Igrejas, G., Mechanisms of quinolone action and resistance: where do we stand? *J Med Microbiol* **2017,** *66* (5), 551-559.

44. Tillotson, G. S., Quinolones: structure-activity relationships and future predictions. *J Med Microbiol* **1996,** *44* (5), 320-4.

45. Andersson, M. I.; MacGowan, A. P., Development of the quinolones. *J Antimicrob Chemother* **2003,** *51 Suppl 1*, 1-11.

46. Valdés, L.; Pérez, I.; de Ménorval, L. C.; Altshuler, E.; Fossum, J. O.; Rivera, A., A simple way for targeted delivery of an antibiotic: In vitro evaluation of a nanoclay-based composite. *PLoS One* **2017,** *12* (11), e0187879.

47. Nelson, R. G.; Rosowsky, A., Dicyclic and tricyclic diaminopyrimidine derivatives as potent inhibitors of Cryptosporidium parvum dihydrofolate reductase: structure-activity and structure-selectivity correlations. *Antimicrob Agents Chemother* **2001,** *45* (12), 3293-303.

48. Nikaido, H., Molecular basis of bacterial outer membrane permeability revisited. *Microbiol Mol Biol Rev* **2003,** *67* (4), 593-656.

49. Nikaido, H.; Thanassi, D. G., Penetration of lipophilic agents with multiple protonation sites into bacterial cells: tetracyclines and fluoroquinolones as examples. *Antimicrob Agents Chemother* **1993,** *37* (7), 1393-1399.

50. Hancock, R. E., The bacterial outer membrane as a drug barrier. *Trends Microbiol* **1997,** *5* (1), 37-42.

51. Kohanski, M. A.; Dwyer, D. J.; Collins, J. J., How antibiotics kill bacteria: from targets to networks. *Nat Rev Microbiol* **2010,** *8* (6), 423-35.

52. Hooper, D. C., Structure of grepafloxacin relative to activity and safety profile. *Clin Microbiol Infect* **1998,** *4 Suppl 1*, S15-s20.

53. Aldred, K. J.; Kerns, R. J.; Osheroff, N., Mechanism of Quinolone Action and Resistance. *Biochemistry* **2014,** *53* (10), 1565-1574.

54. Grkovic, S.; Brown, M. H.; Skurray, R. A., Regulation of bacterial drug export systems. *Microbiol Mol Biol Rev* **2002,** *66* (4), 671-701, table of contents.

55. Chapman, J. S.; Georgopapadakou, N. H., Routes of quinolone permeation in Escherichia coli. *Antimicrob Agents Chemother* **1988,** *32* (4), 438-42.

56. Ziha-Zarifi, I.; Llanes, C.; Köhler, T.; Pechere, J. C.; Plesiat, P., In vivo emergence of multidrug-resistant mutants of Pseudomonas aeruginosa overexpressing the active efflux system MexA-MexB-OprM. *Antimicrob Agents Chemother* **1999,** *43* (2), 287-91.

57. Mitscher, L. A., Bacterial topoisomerase inhibitors: quinolone and pyridone antibacterial agents. *Chem Rev* **2005,** *105* (2), 559-92.

58. Emmerson, A. M.; Jones, A. M., The quinolones: decades of development and use. *J Antimicrob Chemother* **2003,** *51 Suppl 1*, 13-20.

59. Baba, T.; Ara, T.; Hasegawa, M.; Takai, Y.; Okumura, Y.; Baba, M.; Datsenko, K. A.; Tomita, M.; Wanner, B. L.; Mori, H., Construction of Escherichia coli K-12 in-frame, single-gene knockout mutants: the Keio collection. *Mol Syst Biol* **2006,** *2*, 2006.0008-2006.0008.

60. Alam, M. K.; Alhhazmi, A.; DeCoteau, J. F.; Luo, Y.; Geyer, C. R., RecA Inhibitors Potentiate Antibiotic Activity and Block Evolution of Antibiotic Resistance. *Cell Chem Biol* **2016,** *23* (3), 381-91.

61. Robicsek, A.; Jacoby, G. A.; Hooper, D. C., The worldwide emergence of plasmid-mediated quinolone resistance. *Lancet Infect Dis* **2006,** *6* (10), 629-40.

62. Hooper, D. C.; Jacoby, G. A., Mechanisms of drug resistance: quinolone resistance. *Ann N Y Acad Sci* **2015,** *1354* (1), 12-31.

63. Wang, S.; Jia, X.-D.; Liu, M.-L.; Lu, Y.; Guo, H.-Y., Synthesis, antimycobacterial and antibacterial activity of ciprofloxacin derivatives containing a N-substituted benzyl moiety. *Bioorganic & medicinal chemistry letters* **2012,** *22* (18), 5971-5975.

64. Ross, A. G.; Benton, B. M.; Chin, D.; De Pascale, G.; Fuller, J.; Leeds, J. A.; Reck, F.; Richie, D. L.; Vo, J.; LaMarche, M. J., Synthesis of ciprofloxacin dimers for evaluation of bacterial permeability in atypical chemical space. *Bioorganic & Medicinal Chemistry Letters* **2015,** *25* (17), 3468-3475.

65. Panda, S. S.; Liaqat, S.; Girgis, A. S.; Samir, A.; Hall, C. D.; Katritzky, A. R., Novel antibacterial active quinolone–fluoroquinolone conjugates and 2D-QSAR studies. *Bioorganic & Medicinal Chemistry Letters* **2015,** *25* (18), 3816-3821.

66. Ross, A. G.; Benton, B. M.; Chin, D.; De Pascale, G.; Fuller, J.; Leeds, J. A.; Reck, F.; Richie, D. L.; Vo, J.; LaMarche, M. J., Synthesis of ciprofloxacin dimers for evaluation of bacterial permeability in atypical chemical space. *Bioorg Med Chem Lett* **2015,** *25* (17), 3468-75.

67. Neumann, W.; Nolan, E. M., Evaluation of a reducible disulfide linker for siderophore-mediated delivery of antibiotics. *JBIC Journal of Biological Inorganic Chemistry* **2018,** *23* (7), 1025-1036.

68. Alexander, J.; Cargill, R.; Michelson, S. R.; Schwam, H., (Acyloxy)alkyl carbamates as novel bioreversible prodrugs for amines: increased permeation through biological membranes. *Journal of Medicinal Chemistry* **1988,** *31* (2), 318-322.

69. Rivault, F.; Liébert, C.; Burger, A.; Hoegy, F.; Abdallah, M. A.; Schalk, I. J.; Mislin, G. L., Synthesis of pyochelin-norfloxacin conjugates. *Bioorg Med Chem Lett* **2007,** *17* (3), 640-4.

70. Gogate, U. S.; Repta, A. J.; Alexander, J., N-(Acyloxyalkoxycarbonyl) derivatives as potential prodrugs of amines. I. kinetics and mechanism of degradation in aqueous solutions. *International Journal of Pharmaceutics* **1987,** *40* (3), 235-248.

71. Ortmann, R.; Wiesner, J.; Reichenberg, A.; Henschker, D.; Beck, E.; Jomaa, H.; Schlitzer, M., Alkoxycarbonyloxyethyl Ester Prodrugs of FR900098 with Improved In Vivo Antimalarial Activity. *Archiv der Pharmazie* **2005,** *338* (7), 305-314.

72. Ayre, J.; Redmond, J. M.; Vitulli, G.; Tomlinson, L.; Weaver, R.; Comeo, E.; Bosquillon, C.; Stocks, M. J., Design, Synthesis, and Evaluation of Lung-Retentive Prodrugs for Extending the Lung Tissue Retention of Inhaled Drugs. *Journal of Medicinal Chemistry* **2022,** *65* (14), 9802-9818.

73. Gogate, U.; Repta, A., N-(Acyloxyalkoxycarbonyl) derivatives as potential prodrugs of amines. II. esterase-catalysed release of parent amines from model prodrugs. *International journal of pharmaceutics* **1987,** *40* (3), 249-255.

74. Peer, D.; Karp, J. M.; Hong, S.; Farokhzad, O. C.; Margalit, R.; Langer, R., Nanocarriers as an emerging platform for cancer therapy. *Nat Nanotechnol* **2007,** *2* (12), 751-60.

75. Matsumura, Y.; Maeda, H., A new concept for macromolecular therapeutics in cancer chemotherapy: mechanism of tumoritropic accumulation of proteins and the antitumor agent smancs. *Cancer Res* **1986,** *46* (12 Pt 1), 6387-92.

76. Astruc, D.; Boisselier, E.; Ornelas, C., Dendrimers Designed for Functions: From Physical, Photophysical, and Supramolecular Properties to Applications in Sensing, Catalysis, Molecular Electronics, Photonics, and Nanomedicine. *Chemical Reviews* **2010,** *110* (4), 1857-1959.

77. Chou, L. Y. T.; Ming, K.; Chan, W. C. W., Strategies for the intracellular delivery of nanoparticles. *Chemical Society Reviews* **2011,** *40* (1), 233-245.

78. Kumari, A.; Singla, R.; Guliani, A.; Yadav, S. K., Nanoencapsulation for drug delivery. *Excli j* **2014,** *13*, 265-86.

79. Shi, N.-Q.; Qi, X.-R., Preparation of Drug Liposomes by Reverse-Phase Evaporation. In *Liposome-Based Drug Delivery Systems*, Lu, W.-L.; Qi, X.-R., Eds. Springer Berlin Heidelberg: Berlin, Heidelberg, 2021; pp 37-46.

80. Wang, S.; Yu, S.; Lin, Y.; Zou, P.; Chai, G.; Yu, H. H.; Wickremasinghe, H.; Shetty, N.; Ling, J.; Li, J.; Zhou, Q., Co-Delivery of Ciprofloxacin and Colistin in Liposomal Formulations with Enhanced In Vitro Antimicrobial Activities against Multidrug Resistant Pseudomonas aeruginosa. *Pharmaceutical Research* **2018,** *35* (10), 187.

81. Wang, Y., Liposome as a delivery system for the treatment of biofilm-mediated infections. *Journal of Applied Microbiology* **2021,** *131* (6), 2626-2639.

82. Wang, S.; Yu, S.; Lin, Y.; Zou, P.; Chai, G.; Yu, H. H.; Wickremasinghe, H.; Shetty, N.; Ling, J.; Li, J.; Zhou, Q. T., Co-Delivery of Ciprofloxacin and Colistin in Liposomal Formulations with Enhanced In Vitro Antimicrobial Activities against Multidrug Resistant Pseudomonas aeruginosa. *Pharm Res* **2018,** *35* (10), 187.

83. Karathanasis, E.; Ayyagari, A. L.; Bhavane, R.; Bellamkonda, R. V.; Annapragada, A. V., Preparation of in vivo cleavable agglomerated liposomes suitable for modulated pulmonary drug delivery. *Journal of Controlled Release* **2005,** *103* (1), 159-175.

84. Chauhan, A. S., Dendrimers for Drug Delivery. *Molecules* **2018,** *23* (4).

85. Ma, M.; Cheng, Y.; Xu, Z.; Xu, P.; Qu, H.; Fang, Y.; Xu, T.; Wen, L., Evaluation of polyamidoamine (PAMAM) dendrimers as drug carriers of anti-bacterial drugs using sulfamethoxazole (SMZ) as a model drug. *Eur J Med Chem* **2007,** *42* (1), 93-8.

86. Kumar, P. V.; Asthana, A.; Dutta, T.; Jain, N. K., Intracellular macrophage uptake of rifampicin loaded mannosylated dendrimers. *J Drug Target* **2006,** *14* (8), 546-56.

87. Kumar, P. V.; Asthana, A.; Dutta, T.; Jain, N. K., Intracellular macrophage uptake of rifampicin loaded mannosylated dendrimers. *Journal of Drug Targeting* **2006,** *14* (8), 546-556.

88. Tomalia, D. A.; Reyna, L. A.; Svenson, S., Dendrimers as multi-purpose nanodevices for oncology drug delivery and diagnostic imaging. *Biochem Soc Trans* **2007,** *35* (Pt 1), 61-67.

89. Najlah, M.; D'Emanuele, A., Synthesis of dendrimers and drug-dendrimer conjugates for drug delivery. *Curr Opin Drug Discov Devel* **2007,** *10* (6), 756-67.

90. Agarwal, A.; Saraf, S.; Asthana, A.; Gupta, U.; Gajbhiye, V.; Jain, N. K., Ligand based dendritic systems for tumor targeting. *Int J Pharm* **2008,** *350* (1-2), 3-13.

91. Quintana, A.; Raczka, E.; Piehler, L.; Lee, I.; Myc, A.; Majoros, I.; Patri, A. K.; Thomas, T.; Mulé, J.; Baker, J. R., Jr., Design and function of a dendrimer-based therapeutic nanodevice targeted to tumor cells through the folate receptor. *Pharm Res* **2002,** *19* (9), 1310-6.

92. Kono, K.; Liu, M.; Fréchet, J. M. J., Design of Dendritic Macromolecules Containing Folate or Methotrexate Residues. *Bioconjugate Chemistry* **1999,** *10* (6), 1115-1121.

93. Rautio, J.; Kumpulainen, H.; Heimbach, T.; Oliyai, R.; Oh, D.; Järvinen, T.; Savolainen, J., Prodrugs: design and clinical applications. *Nature Reviews Drug Discovery* **2008,** *7* (3), 255-270.

94. Takagi, T.; Ramachandran, C.; Bermejo, M.; Yamashita, S.; Yu, L. X.; Amidon, G. L., A Provisional Biopharmaceutical Classification of the Top 200 Oral Drug Products in the United States, Great Britain, Spain, and Japan. *Molecular Pharmaceutics* **2006,** *3* (6), 631-643.

95. Jornada, D. H.; dos Santos Fernandes, G. F.; Chiba, D. E.; de Melo, T. R.; dos Santos, J. L.; Chung, M. C., The Prodrug Approach: A Successful Tool for Improving Drug Solubility. *Molecules* **2015,** *21* (1), 42.

96. Wong, P. T.; Tang, S.; Mukherjee, J.; Tang, K.; Gam, K.; Isham, D.; Murat, C.; Sun, R.; Baker, J. R.; Choi, S. K., Light-controlled active release of photocaged ciprofloxacin for lipopolysaccharide-targeted drug delivery using dendrimer conjugates. *Chemical Communications* **2016,** *52* (68), 10357-10360.

97. Schmidt, M.; Harmuth, S.; Barth, E. R.; Wurm, E.; Fobbe, R.; Sickmann, A.; Krumm, C.; Tiller, J. C., Conjugation of Ciprofloxacin with Poly(2-oxazoline)s and Polyethylene Glycol via End Groups. *Bioconjugate Chemistry* **2015,** *26* (9), 1950-1962.

98. Bosnjakovic, A.; Mishra, M. K.; Ren, W.; Kurtoglu, Y. E.; Shi, T.; Fan, D.; Kannan, R. M., Poly(amidoamine) dendrimer-erythromycin conjugates for drug delivery to macrophages involved in periprosthetic inflammation. *Nanomedicine* **2011,** *7* (3), 284-94.

99. Wrońska, N.; Felczak, A.; Zawadzka, K.; Poszepczyńska, M.; Różalska, S.; Bryszewska, M.; Appelhans, D.; Lisowska, K., Poly(Propylene Imine) Dendrimers and Amoxicillin as Dual-Action Antibacterial Agents. *Molecules* **2015,** *20* (10).

100. Michaud, G.; Visini, R.; Bergmann, M.; Salerno, G.; Bosco, R.; Gillon, E.; Richichi, B.; Nativi, C.; Imberty, A.; Stocker, A.; Darbre, T.; Reymond, J.-L., Overcoming antibiotic resistance in Pseudomonas aeruginosa biofilms using glycopeptide dendrimers. *Chemical Science* **2016,** *7* (1), 166-182.

101. Svenson, S.; Tomalia, D. A., Dendrimers in biomedical applications—reflections on the field. *Advanced Drug Delivery Reviews* **2005,** *57* (15), 2106-2129.

102. Kevin, B.; Robert, W.; Iain, G.; Kevin, D., Design of Ester Prodrugs to Enhance Oral Absorption of Poorly Permeable Compounds: Challenges to the Discovery Scientist. *Current Drug Metabolism* **2003,** *4* (6), 461-485.

103. Testa, B., Prodrugs: bridging pharmacodynamic/pharmacokinetic gaps. *Current Opinion in Chemical Biology* **2009,** *13* (3), 338-344.

104. Tomalia, D. A.; Baker, H.; Dewald, J.; Hall, M.; Kallos, G.; Martin, S.; Roeck, J.; Ryder, J.; Smith, P., A New Class of Polymers: Starburst-Dendritic Macromolecules. *Polymer Journal* **1985,** *17* (1), 117-132.

105. Hawker, C. J.; Frechet, J. M. J., Preparation of polymers with controlled molecular architecture. A new convergent approach to dendritic macromolecules. *Journal of the American Chemical Society* **1990,** *112* (21), 7638-7647.

106. Svenson, S.; Chauhan, A. S., Dendrimers for enhanced drug solubilization. *Nanomedicine (Lond)* **2008,** *3* (5), 679-702.

107. Sahoo, S. K.; Dilnawaz, F.; Krishnakumar, S., Nanotechnology in ocular drug delivery. *Drug Discovery Today* **2008,** *13* (3), 144-151.

108. Aillon, K. L.; Xie, Y.; El-Gendy, N.; Berkland, C. J.; Forrest, M. L., Effects of nanomaterial physicochemical properties on in vivo toxicity. *Advanced Drug Delivery Reviews* **2009,** *61* (6), 457-466.

109. He, C.-X.; Tabata, Y.; Gao, J.-Q., Non-viral gene delivery carrier and its three-dimensional transfection system. *International Journal of Pharmaceutics* **2010,** *386* (1), 232-242.

110. Esumi, K.; Houdatsu, H.; Yoshimura, T., Antioxidant Action by Gold−PAMAM Dendrimer Nanocomposites. *Langmuir* **2004,** *20* (7), 2536-2538.

111. Morgan, M. T.; Carnahan, M. A.; Finkelstein, S.; Prata, C. A. H.; Degoricija, L.; Lee, S. J.; Grinstaff, M. W., Dendritic supramolecular assemblies for drug delivery. *Chemical Communications* **2005,** (34), 4309-4311.

112. Tian, W.-d.; Ma, Y.-q., Insights into the endosomal escape mechanism via investigation of dendrimer–membrane interactions. *Soft Matter* **2012,** *8* (23), 6378-6384.

113. Kim, T. I.; Seo, H. J.; Choi, J. S.; Jang, H. S.; Baek, J. U.; Kim, K.; Park, J. S., PAMAM-PEG-PAMAM: novel triblock copolymer as a biocompatible and efficient gene delivery carrier. *Biomacromolecules* **2004,** *5* (6), 2487-92.

114. Dobrovolskaia, M. A.; Patri, A. K.; Simak, J.; Hall, J. B.; Semberova, J.; De Paoli Lacerda, S. H.; McNeil, S. E., Nanoparticle Size and Surface Charge Determine Effects of PAMAM Dendrimers on Human Platelets in Vitro. *Molecular Pharmaceutics* **2012,** *9* (3), 382-393.

115. Klajnert, B.; Bryszewska, M., Dendrimers: properties and applications. *Acta Biochim Pol* **2001,** *48* (1), 199-208.

116. Hatton, F. L.; Chambon, P.; McDonald, T. O.; Owen, A.; Rannard, S. P., Hyperbranched polydendrons: a new controlled macromolecular architecture with self-assembly in water and organic solvents. *Chemical Science* **2014,** *5* (5), 1844-1853.

117. Ihre, H.; Padilla De Jesús, O. L.; Fréchet, J. M. J., Fast and Convenient Divergent Synthesis of Aliphatic Ester Dendrimers by Anhydride Coupling. *Journal of the American Chemical Society* **2001,** *123* (25), 5908-5917.

118. Parrott, M. C.; Benhabbour, S. R.; Saab, C.; Lemon, J. A.; Parker, S.; Valliant, J. F.; Adronov, A., Synthesis, radiolabeling, and bio-imaging of high-generation polyester dendrimers. *J Am Chem Soc* **2009,** *131* (8), 2906-16.

119. Malkoch, M.; Malmström, E.; Hult, A., Rapid and Efficient Synthesis of Aliphatic Ester Dendrons and Dendrimers. *Macromolecules* **2002,** *35* (22), 8307-8314.

120. Rosselgong, J.; Armes, S. P.; Barton, W. R. S.; Price, D., Synthesis of Branched Methacrylic Copolymers: Comparison between RAFT and ATRP and Effect of Varying the Monomer Concentration. *Macromolecules* **2010,** *43* (5), 2145-2156.

121. Bugno, J.; Hsu, H.-J.; Hong, S., Tweaking dendrimers and dendritic nanoparticles for controlled nano-bio interactions: potential nanocarriers for improved cancer targeting. *J Drug Target* **2015,** *23* (7-8), 642-650.

122. Svenson, S.; Tomalia, D. A., Dendrimers in biomedical applications--reflections on the field. *Adv Drug Deliv Rev* **2005,** *57* (15), 2106-29.

123. Sowinska, M.; Urbanczyk-Lipkowska, Z., Advances in the chemistry of dendrimers. *New Journal of Chemistry* **2014,** *38* (6), 2168-2203.

124. Nanjwade, B. K.; Bechra, H. M.; Derkar, G. K.; Manvi, F. V.; Nanjwade, V. K., Dendrimers: emerging polymers for drug-delivery systems. *Eur J Pharm Sci* **2009,** *38* (3), 185-96.

125. Wooley, K. L.; Hawker, C. J.; Fréchet, J. M. J., A "Branched-Monomer Approach" for the Rapid Synthesis of Dendimers. *Angewandte Chemie International Edition in English* **1994,** *33* (1), 82-85.

126. Kawaguchi, T.; Walker, K. L.; Wilkins, C. L.; Moore, J. S., Double Exponential Dendrimer Growth. *Journal of the American Chemical Society* **1995,** *117* (8), 2159-2165.

127. Freeman, A. W.; Fréchet, J. M. J., A Rapid, Orthogonal Synthesis of Poly(benzyl ester) Dendrimers via an "Activated" Monomer Approach. *Organic Letters* **1999,** *1* (4), 685-688.

128. Lee, J. W.; Kim, J. H.; Kim, B.-K., Synthesis of azide-functionalized PAMAM dendrons at the focal point and their application for synthesis of PAMAM-like dendrimers. *Tetrahedron letters* **2006,** *47* (16), 2683-2686.

129. Rijkers, D. T. S.; van Esse, G. W.; Merkx, R.; Brouwer, A. J.; Jacobs, H. J. F.; Pieters, R. J.; Liskamp, R. M. J., Efficient microwave-assisted synthesis of multivalent dendrimeric peptides using cycloaddition reaction (click) chemistry. *Chemical Communications* **2005,** (36), 4581-4583.

130. Helms, B.; Mynar, J. L.; Hawker, C. J.; Fréchet, J. M. J., Dendronized Linear Polymers via "Click Chemistry". *Journal of the American Chemical Society* **2004,** *126* (46), 15020-15021.

131. Ihre, H.; Hult, A.; Fréchet, J. M. J.; Gitsov, I., Double-Stage Convergent Approach for the Synthesis of Functionalized Dendritic Aliphatic Polyesters Based on 2,2-Bis(hydroxymethyl)propionic Acid. *Macromolecules* **1998,** *31* (13), 4061-4068.

132. Agrahari, A. K.; Singh, A. S.; Mukherjee, R.; Tiwari, V. K., An expeditious click approach towards the synthesis of galactose coated novel glyco-dendrimers and dentromers utilizing a double stage convergent method. *RSC Advances* **2020,** *10* (52), 31553-31562.

133. Wooley, K. L.; Hawker, C. J.; Frechet, J. M. J., Hyperbranched macromolecules via a novel double-stage convergent growth approach. *Journal of the American Chemical Society* **1991,** *113* (11), 4252-4261.

134. Geng, Z.; Shin, J. J.; Xi, Y.; Hawker, C. J., Click chemistry strategies for the accelerated synthesis of functional macromolecules. *Journal of Polymer Science* **2021,** *59* (11), 963-1042.

135. Espeel, P.; Du Prez, F. E., "Click"-Inspired Chemistry in Macromolecular Science: Matching Recent Progress and User Expectations. *Macromolecules* **2015,** *48* (1), 2-14.

136. Pasini, D., The Click Reaction as an Efficient Tool for the Construction of Macrocyclic Structures. *Molecules* **2013,** *18* (8).

137. Huisgen, R.; Szeimies, G.; Möbius, L., 1.3-Dipolare Cycloadditionen, XXXII. Kinetik der Additionen organischer Azide an CC-Mehrfachbindungen. *Chemische Berichte* **1967,** *100* (8), 2494-2507.

138. Kolb, H. C.; Finn, M. G.; Sharpless, K. B., Click Chemistry: Diverse Chemical Function from a Few Good Reactions. *Angew Chem Int Ed Engl* **2001,** *40* (11), 2004-2021.

139. Zhang, L.; Chen, X.; Xue, P.; Sun, H. H. Y.; Williams, I. D.; Sharpless, K. B.; Fokin, V. V.; Jia, G., Ruthenium-Catalyzed Cycloaddition of Alkynes and Organic Azides. *Journal of the American Chemical Society* **2005,** *127* (46), 15998-15999.

140. Himo, F.; Lovell, T.; Hilgraf, R.; Rostovtsev, V. V.; Noodleman, L.; Sharpless, K. B.; Fokin, V. V., Copper(I)-catalyzed synthesis of azoles. DFT study predicts unprecedented reactivity and intermediates. *J Am Chem Soc* **2005,** *127* (1), 210-6.

141. Rodionov, V. O.; Fokin, V. V.; Finn, M. G., Mechanism of the ligand-free CuI-catalyzed azide-alkyne cycloaddition reaction. *Angew Chem Int Ed Engl* **2005,** *44* (15), 2210-5.

142. Bock, V. D.; Hiemstra, H.; van Maarseveen, J. H., CuI-Catalyzed Alkyne–Azide "Click" Cycloadditions from a Mechanistic and Synthetic Perspective. *European Journal of Organic Chemistry* **2006,** *2006* (1), 51-68.

143. Horne, W. S.; Stout, C. D.; Ghadiri, M. R., A Heterocyclic Peptide Nanotube. *Journal of the American Chemical Society* **2003,** *125* (31), 9372-9376.

144. Zhu, L.; Brassard, C. J.; Zhang, X.; Guha, P. M.; Clark, R. J., On the Mechanism of Copper(I)-Catalyzed Azide-Alkyne Cycloaddition. *Chem Rec* **2016,** *16* (3), 1501-17.

145. Neumann, S.; Biewend, M.; Rana, S.; Binder, W. H., The CuAAC: Principles, Homogeneous and Heterogeneous Catalysts, and Novel Developments and Applications. *Macromolecular Rapid Communications* **2020,** *41* (1), 1900359.

146. Pérez-Balderas, F.; Ortega-Muñoz, M.; Morales-Sanfrutos, J.; Hernández-Mateo, F.; Calvo-Flores, F. G.; Calvo-Asín, J. A.; Isac-García, J.; Santoyo-González, F., Multivalent neoglycoconjugates by regiospecific cycloaddition of alkynes and azides using organic-soluble copper catalysts. *Org Lett* **2003,** *5* (11), 1951-4.

147. Marmuse, L.; Nepogodiev, S. A.; Field, R. A., "Click chemistry" en route to pseudo-starch. *Organic & Biomolecular Chemistry* **2005,** *3* (12), 2225-2227.

148. Ladmiral, V.; Mantovani, G.; Clarkson, G. J.; Cauet, S.; Irwin, J. L.; Haddleton, D. M., Synthesis of neoglycopolymers by a combination of "click chemistry" and living radical polymerization. *J Am Chem Soc* **2006,** *128* (14), 4823-30.

149. Díez-González, S., Well-defined copper(i) complexes for Click azide–alkyne cycloaddition reactions: one Click beyond. *Catalysis Science & Technology* **2011,** *1* (2), 166-178.

150. Parrish, B.; Emrick, T., Soluble Camptothecin Derivatives Prepared by Click Cycloaddition Chemistry on Functional Aliphatic Polyesters. *Bioconjugate Chemistry* **2007,** *18* (1), 263-267.

151. Lal, S.; McNally, J.; White, A. J. P.; Díez-González, S., Novel Phosphinite and Phosphonite Copper(I) Complexes: Efficient Catalysts for Click Azide–Alkyne Cycloaddition Reactions. *Organometallics* **2011,** *30* (22), 6225-6232.

152. Kitov, P. I.; Sadowska, J. M.; Mulvey, G.; Armstrong, G. D.; Ling, H.; Pannu, N. S.; Read, R. J.; Bundle, D. R., Shiga-like toxins are neutralized by tailored multivalent carbohydrate ligands. *Nature* **2000,** *403* (6770), 669-672.

153. Pérez-Balderas, F.; Ortega-Muñoz, M.; Morales-Sanfrutos, J.; Hernández-Mateo, F.; Calvo-Flores, F. G.; Calvo-Asín, J. A.; Isac-García, J.; Santoyo-González, F., Multivalent Neoglycoconjugates by Regiospecific Cycloaddition of Alkynes and Azides Using Organic-Soluble Copper Catalysts. *Organic Letters* **2003,** *5* (11), 1951-1954.

154. Chen, Q.; Yang, F.; Du, Y., Synthesis of a C3-symmetric (1→6)-N-acetyl-β-d-glucosamine octadecasaccharide using click chemistry. *Carbohydrate Research* **2005,** *340* (16), 2476-2482.

155. Fernandez-Megia, E.; Correa, J.; Riguera, R., "Clickable" PEG−Dendritic Block Copolymers. *Biomacromolecules* **2006,** *7* (11), 3104-3111.

156. Fernandez-Megia, E.; Correa, J.; Rodríguez-Meizoso, I.; Riguera, R., A Click Approach to Unprotected Glycodendrimers. *Macromolecules* **2006,** *39* (6), 2113-2120.

157. Collman, J. P.; Devaraj, N. K.; Chidsey, C. E. D., "Clicking" Functionality onto Electrode Surfaces. *Langmuir* **2004,** *20* (4), 1051-1053.

158. Díaz, D. D.; Punna, S.; Holzer, P.; McPherson, A. K.; Sharpless, K. B.; Fokin, V. V.; Finn, M. G., Click chemistry in materials synthesis. 1. Adhesive polymers from copper-catalyzed azide-alkyne cycloaddition. *Journal of Polymer Science Part A: Polymer Chemistry* **2004,** *42* (17), 4392-4403.

159. Wu, P.; Feldman, A. K.; Nugent, A. K.; Hawker, C. J.; Scheel, A.; Voit, B.; Pyun, J.; Fréchet, J. M. J.; Sharpless, K. B.; Fokin, V. V., Efficiency and Fidelity in a Click-Chemistry Route to Triazole Dendrimers by the Copper(I)-Catalyzed Ligation of Azides and Alkynes. *Angewandte Chemie International Edition* **2004,** *43* (30), 3928-3932.

160. Yang, F.; Du, Y., A practical synthesis of a (1→6)-linked β-d-glucosamine nonasaccharide. *Carbohydrate Research* **2003,** *338* (6), 495-502.

161. Stenzel, M. H., Bioconjugation Using Thiols: Old Chemistry Rediscovered to Connect Polymers with Nature's Building Blocks. *ACS Macro Letters* **2013,** *2* (1), 14-18.

162. Northrop, B. H.; Coffey, R. N., Thiol–Ene Click Chemistry: Computational and Kinetic Analysis of the Influence of Alkene Functionality. *Journal of the American Chemical Society* **2012,** *134* (33), 13804-13817.

163. Goyard, D.; Baldoneschi, V.; Varrot, A.; Fiore, M.; Imberty, A.; Richichi, B.; Renaudet, O.; Nativi, C., Multivalent Glycomimetics with Affinity and Selectivity toward Fucose-Binding Receptors from Emerging Pathogens. *Bioconjugate Chemistry* **2018,** *29* (1), 83-88.

164. Ernst, B.; Magnani, J. L., From carbohydrate leads to glycomimetic drugs. *Nat Rev Drug Discov* **2009,** *8* (8), 661-77.

165. Caumes, C.; Gillon, E.; Legeret, B.; Taillefumier, C.; Imberty, A.; Faure, S., Multivalent thioglycopeptoids via photoclick chemistry: potent affinities towards LecA and BC2L-A lectins. *Chemical Communications* **2015,** *51* (61), 12301-12304.

166. Dondoni, A.; Marra, A., Recent applications of thiol–ene coupling as a click process for glycoconjugation. *Chemical Society Reviews* **2012,** *41* (2), 573-586.

167. Kelemen, V.; Csávás, M.; Hotzi, J.; Herczeg, M.; Poonam; Rathi, B.; Herczegh, P.; Jain, N.; Borbás, A., Photoinitiated Thiol-Ene Reactions of Various 2,3-Unsaturated O-, C- S- and N-Glycosides - Scope and Limitations Study. *Chem Asian J* **2020,** *15* (6), 876-891.

168. Krannig, K.-S.; Schlaad, H., pH-Responsive Bioactive Glycopolypeptides with Enhanced Helicity and Solubility in Aqueous Solution. *Journal of the American Chemical Society* **2012,** *134* (45), 18542-18545.

169. Wojcik, F.; O'Brien, A. G.; Götze, S.; Seeberger, P. H.; Hartmann, L., Synthesis of Carbohydrate-Functionalised Sequence-Defined Oligo(amidoamine)s by Photochemical Thiol□Ene Coupling in a Continuous Flow Reactor. *Chemistry – A European Journal* **2013,** *19* (9), 3090-3098.

170. Reynolds, M.; Marradi, M.; Imberty, A.; Penadés, S.; Pérez, S., Influence of ligand presentation density on the molecular recognition of mannose-functionalised glyconanoparticles by bacterial lectin BC2L-A. *Glycoconj J* **2013,** *30* (8), 747-57.

171. Reymond, J.-L.; Bergmann, M.; Darbre, T., Glycopeptide dendrimers as Pseudomonas aeruginosa biofilm inhibitors. *Chemical Society Reviews* **2013,** *42* (11), 4814-4822.

172. Berthet, N.; Thomas, B.; Bossu, I.; Dufour, E.; Gillon, E.; Garcia, J.; Spinelli, N.; Imberty, A.; Dumy, P.; Renaudet, O., High Affinity Glycodendrimers for the Lectin LecB from Pseudomonas aeruginosa. *Bioconjugate Chemistry* **2013,** *24* (9), 1598-1611.

173. Zusinaite, E.; Ianevski, A.; Niukkanen, D.; Poranen, M. M.; Bjørås, M.; Afset, J. E.; Tenson, T.; Velagapudi, V.; Merits, A.; Kainov, D. E., A Systems Approach to Study Immuno- and Neuro-Modulatory Properties of Antiviral Agents. *Viruses* **2018,** *10* (8).

174. Dwek, R. A., Glycobiology: Toward Understanding the Function of Sugars. *Chem Rev* **1996,** *96* (2), 683-720.

175. Rademacher, T. W.; Parekh, R. B.; Dwek, R. A., Glycobiology. *Annu Rev Biochem* **1988,** *57*, 785-838.

176. Linhardt, R. J.; Toida, T., Role of glycosaminoglycans in cellular communication. *Acc Chem Res* **2004,** *37* (7), 431-8.

177. Gabius, H. J.; Siebert, H. C.; André, S.; Jiménez-Barbero, J.; Rüdiger, H., Chemical biology of the sugar code. *Chembiochem* **2004,** *5* (6), 740-64.

178. Roseman, S., Reflections on glycobiology. *J Biol Chem* **2001,** *276* (45), 41527-42.

179. Imberty, A.; Varrot, A., Microbial recognition of human cell surface glycoconjugates. *Curr Opin Struct Biol* **2008,** *18* (5), 567-76.

180. Mager, M. D.; LaPointe, V.; Stevens, M. M., Exploring and exploiting chemistry at the cell surface. *Nat Chem* **2011,** *3* (8), 582-9.

181. Tu, T.; Drăguşanu, M.; Petre, B. A.; Rempel, D. L.; Przybylski, M.; Gross, M. L., Protein-peptide affinity determination using an h/d exchange dilution strategy: application to antigen-antibody interactions. *J Am Soc Mass Spectrom* **2010,** *21* (10), 1660-7.

182. de Mattos, L. C., Structural diversity and biological importance of ABO, H, Lewis and secretor histo-blood group carbohydrates. *Rev Bras Hematol Hemoter* **2016,** *38* (4), 331-340.

183. Croce, M. V.; Isla-Larrain, M.; Rabassa, M. E.; Demichelis, S.; Colussi, A. G.; Crespo, M.; Lacunza, E.; Segal-Eiras, A., Lewis x is highly expressed in normal tissues: A comparative immunohistochemical study and literature revision. *Pathology & Oncology Research* **2007,** *13* (2), 130.

184. Behren, S.; Yu, J.; Pett, C.; Shorlemer, M.; Heine, V.; Fischöder, T.; Elling, L.; Westerlind, U., Bacteria Lectin Recognition Towards Fucose Binding Motifs Highlights the Impact of Presenting Mucin Core Glycopeptides. **2021**.

185. Imberty, A.; wimmerová, M.; Mitchell, E. P.; Gilboa-Garber, N., Structures of the lectins from Pseudomonas aeruginosa: insight into the molecular basis for host glycan recognition. *Microbes Infect* **2004,** *6* (2), 221-8.

186. Gilboa-Garber, N., Pseudomonas aeruginosa lectins. *Methods Enzymol* **1982,** *83*, 378-85.

187. Mitchell, E.; Houles, C.; Sudakevitz, D.; Wimmerova, M.; Gautier, C.; Pérez, S.; Wu, A. M.; Gilboa-Garber, N.; Imberty, A., Structural basis for oligosaccharide-mediated adhesion of Pseudomonas aeruginosa in the lungs of cystic fibrosis patients. *Nat Struct Biol* **2002,** *9* (12), 918-21.

188. Hauber, H. P.; Schulz, M.; Pforte, A.; Mack, D.; Zabel, P.; Schumacher, U., Inhalation with fucose and galactose for treatment of Pseudomonas aeruginosa in cystic fibrosis patients. *Int J Med Sci* **2008,** *5* (6), 371-6.

189. Fasting, C.; Schalley, C. A.; Weber, M.; Seitz, O.; Hecht, S.; Koksch, B.; Dernedde, J.; Graf, C.; Knapp, E. W.; Haag, R., Multivalency as a chemical organization and action principle. *Angew Chem Int Ed Engl* **2012,** *51* (42), 10472-98.

190. Mahon, C. S.; Fulton, D. A., Mimicking nature with synthetic macromolecules capable of recognition. *Nat Chem* **2014,** *6* (8), 665-72.

191. Mahon, E.; Barboiu, M., Synthetic multivalency for biological applications. *Organic & Biomolecular Chemistry* **2015,** *13* (43), 10590-10599.

192. Tjandra, K. C.; Thordarson, P., Multivalency in Drug Delivery-When Is It Too Much of a Good Thing? *Bioconjug Chem* **2019,** *30* (3), 503-514.

193. Mintzer, M. A.; Dane, E. L.; O'Toole, G. A.; Grinstaff, M. W., Exploiting Dendrimer Multivalency To Combat Emerging and Re-Emerging Infectious Diseases. *Molecular Pharmaceutics* **2012,** *9* (3), 342-354.

194. Pieters, R. J., Intervention with bacterial adhesion by multivalent carbohydrates. *Medicinal Research Reviews* **2007,** *27* (6), 796-816.

195. Kiessling, L. L.; Gestwicki, J. E.; Strong, L. E., Synthetic multivalent ligands in the exploration of cell-surface interactions. *Curr Opin Chem Biol* **2000,** *4* (6), 696-703.

196. Rao, J.; Lahiri, J.; Isaacs, L.; Weis, R. M.; Whitesides, G. M., A Trivalent System from Vancomycin·d-Ala-d-Ala with Higher Affinity Than Avidin·Biotin. *Science* **1998,** *280* (5364), 708.

197. Woller, E. K.; Walter, E. D.; Morgan, J. R.; Singel, D. J.; Cloninger, M. J., Altering the Strength of Lectin Binding Interactions and Controlling the Amount of Lectin Clustering Using Mannose/Hydroxyl-Functionalized Dendrimers. *Journal of the American Chemical Society* **2003,** *125* (29), 8820-8826.

198. Mangold, S. L.; Cloninger, M. J., Binding of monomeric and dimeric Concanavalin A to mannose-functionalized dendrimers. *Organic & Biomolecular Chemistry* **2006,** *4* (12), 2458-2465.

199. Mammen, M.; Choi, S. K.; Whitesides, G. M., Polyvalent Interactions in Biological Systems: Implications for Design and Use of Multivalent Ligands and Inhibitors. *Angew Chem Int Ed Engl* **1998,** *37* (20), 2754-2794.

200. Gestwicki, J. E.; Cairo, C. W.; Strong, L. E.; Oetjen, K. A.; Kiessling, L. L., Influencing Receptor−Ligand Binding Mechanisms with Multivalent Ligand Architecture. *Journal of the American Chemical Society* **2002,** *124* (50), 14922-14933.

201. Bojarová, P.; Křen, V., Sugared biomaterial binding lectins: achievements and perspectives. *Biomaterials Science* **2016,** *4* (8), 1142-1160.

202. Becer, C. R., The Glycopolymer Code: Synthesis of Glycopolymers and Multivalent Carbohydrate–Lectin Interactions. *Macromolecular Rapid Communications* **2012,** *33* (9), 742-752.

203. Roy, R.; Murphy, P. V.; Gabius, H. J., Multivalent Carbohydrate-Lectin Interactions: How Synthetic Chemistry Enables Insights into Nanometric Recognition. *Molecules* **2016,** *21* (5).

204. André, S.; Pieters, R. J.; Vrasidas, I.; Kaltner, H.; Kuwabara, I.; Liu, F. T.; Liskamp, R. M.; Gabius, H. J., Wedgelike glycodendrimers as inhibitors of binding of mammalian galectins to glycoproteins, lactose maxiclusters, and cell surface glycoconjugates. *Chembiochem* **2001,** *2* (11), 822-30.

205. Lavilla, C.; Yilmaz, G.; Uzunova, V.; Napier, R.; Becer, C. R.; Heise, A., Block-Sequence-Specific Glycopolypeptides with Selective Lectin Binding Properties. *Biomacromolecules* **2017,** *18* (6), 1928-1936.

206. Chen, Y.; Lord, M. S.; Piloni, A.; Stenzel, M. H., Correlation between Molecular Weight and Branch Structure of Glycopolymers Stars and Their Binding to Lectins. *Macromolecules* **2015,** *48* (2), 346-357.

207. Hoshino, Y.; Nakamoto, M.; Miura, Y., Control of Protein-Binding Kinetics on Synthetic Polymer Nanoparticles by Tuning Flexibility and Inducing Conformation Changes of Polymer Chains. *Journal of the American Chemical Society* **2012,** *134* (37), 15209-15212.

208. Boden, S.; Wagner, K. G.; Karg, M.; Hartmann, L. Presenting Precision Glycomacromolecules on Gold Nanoparticles for Increased Lectin Binding *Polymers (Basel)* [Online], 2017.

209. J.C, M.-V.; Reyes Fernandez, P.; M.P, M.-R.; Navarro, S.; C, M.; A, S.-O.; Villamón, E.; Piqueras, M.; Grau, E.; Cañete, A.; Castel, V.; Noguera, R.; Ferriz-Martínez, R.; Ic, T.-A.; Blanco-Labra, A.; T, G.-G.; Castro Guillén, J.; Pérez, J. L.; Cruz-Orea, A.; Delgado-Enciso, I., *New approaches in the treatment of cancer*. 2010.

210. Wittmann, V.; Pieters, R. J., Bridging lectin binding sites by multivalent carbohydrates. *Chemical Society Reviews* **2013,** *42* (10), 4492-4503.

211. Bhatia, S.; Camacho, L. C.; Haag, R., Pathogen Inhibition by Multivalent Ligand Architectures. *Journal of the American Chemical Society* **2016,** *138* (28), 8654-8666.

212. Topin, J.; Lelimousin, M.; Arnaud, J.; Audfray, A.; Pérez, S.; Varrot, A.; Imberty, A., The Hidden Conformation of Lewis x, a Human Histo-Blood Group Antigen, Is a Determinant for Recognition by Pathogen Lectins. *ACS Chemical Biology* **2016,** *11* (7), 2011-2020.

213. Abraham, S. N.; Goguen, J. D.; Sun, D.; Klemm, P.; Beachey, E. H., Identification of two ancillary subunits of Escherichia coli type 1 fimbriae by using antibodies against synthetic oligopeptides of fim gene products. *J Bacteriol* **1987,** *169* (12), 5530-5536.

214. Krogfelt, K. A.; Bergmans, H.; Klemm, P., Direct evidence that the FimH protein is the mannose-specific adhesin of Escherichia coli type 1 fimbriae. *Infect Immun* **1990,** *58* (6), 1995-8.

215. Hatton, N. E.; Baumann, C. G.; Fascione, M. A., Developments in Mannose-Based Treatments for Uropathogenic Escherichia coli-Induced Urinary Tract Infections. *Chembiochem* **2021,** *22* (4), 613-629.

216. Hartmann, M.; Lindhorst, T. K., The Bacterial Lectin FimH, a Target for Drug Discovery – Carbohydrate Inhibitors of Type 1 Fimbriae-Mediated Bacterial Adhesion. *European Journal of Organic Chemistry* **2011,** *2011* (20-21), 3583-3609.

217. Sauer, M. M.; Jakob, R. P.; Eras, J.; Baday, S.; Eriş, D.; Navarra, G.; Bernèche, S.; Ernst, B.; Maier, T.; Glockshuber, R., Catch-bond mechanism of the bacterial adhesin FimH. *Nature Communications* **2016,** *7* (1), 10738.

218. Fiege, B.; Rabbani, S.; Preston, R. C.; Jakob, R. P.; Zihlmann, P.; Schwardt, O.; Jiang, X.; Maier, T.; Ernst, B., The Tyrosine Gate of the Bacterial Lectin FimH: A Conformational Analysis by NMR Spectroscopy and X-ray Crystallography. *ChemBioChem* **2015,** *16* (8), 1235-1246.

219. Schönemann, W.; Lindegger, M.; Rabbani, S.; Zihlmann, P.; Schwardt, O.; Ernst, B., 2-C-Branched mannosides as a novel family of FimH antagonists—Synthesis and biological evaluation. *Perspectives in Science* **2017,** *11*, 53-61.

220. Rabbani, S.; Fiege, B.; Eris, D.; Silbermann, M.; Jakob, R. P.; Navarra, G.; Maier, T.; Ernst, B., Conformational switch of the bacterial adhesin FimH in the absence of the regulatory domain: Engineering a minimalistic allosteric system. *J Biol Chem* **2018,** *293* (5), 1835-1849.

221. Sauer, M. M.; Jakob, R. P.; Luber, T.; Canonica, F.; Navarra, G.; Ernst, B.; Unverzagt, C.; Maier, T.; Glockshuber, R., Binding of the Bacterial Adhesin FimH to Its Natural, Multivalent High-Mannose Type Glycan Targets. *J Am Chem Soc* **2019,** *141* (2), 936-944.

222. Mydock-McGrane, L. K.; Hannan, T. J.; Janetka, J. W., Rational design strategies for FimH antagonists: new drugs on the horizon for urinary tract infection and Crohn's disease. *Expert Opin Drug Discov* **2017,** *12* (7), 711-731.

223. Han, Z.; Pinkner, J. S.; Ford, B.; Obermann, R.; Nolan, W.; Wildman, S. A.; Hobbs, D.; Ellenberger, T.; Cusumano, C. K.; Hultgren, S. J.; Janetka, J. W., Structure-Based Drug Design and Optimization of Mannoside Bacterial FimH Antagonists. *Journal of Medicinal Chemistry* **2010,** *53* (12), 4779-4792.

224. Jarvis, C.; Han, Z.; Kalas, V.; Klein, R.; Pinkner, J. S.; Ford, B.; Binkley, J.; Cusumano, C. K.; Cusumano, Z.; Mydock-McGrane, L.; Hultgren, S. J.; Janetka, J. W., Antivirulence Isoquinolone Mannosides: Optimization of the Biaryl Aglycone for FimH Lectin Binding Affinity and Efficacy in the Treatment of Chronic UTI. *ChemMedChem* **2016,** *11* (4), 367-373.

225. Hung, C. S.; Bouckaert, J.; Hung, D.; Pinkner, J.; Widberg, C.; DeFusco, A.; Auguste, C. G.; Strouse, R.; Langermann, S.; Waksman, G.; Hultgren, S. J., Structural basis of tropism of Escherichia coli to the bladder during urinary tract infection. *Mol Microbiol* **2002,** *44* (4), 903-15.

226. Wellens, A.; Garofalo, C.; Nguyen, H.; Van Gerven, N.; Slättegård, R.; Hernalsteens, J.-P.; Wyns, L.; Oscarson, S.; De Greve, H.; Hultgren, S.; Bouckaert, J., Intervening with urinary tract infections using anti-adhesives based on the crystal structure of the FimH-oligomannose-3 complex. *PLoS One* **2008,** *3* (4), e2040-e2040.

227. Wellens, A.; Garofalo, C.; Nguyen, H.; Van Gerven, N.; Slättegård, R.; Hernalsteens, J. P.; Wyns, L.; Oscarson, S.; De Greve, H.; Hultgren, S.; Bouckaert, J., Intervening with urinary tract infections using anti-adhesives based on the crystal structure of the FimH-oligomannose-3 complex. *PLoS One* **2008,** *3* (4), e2040.

228. Mydock-McGrane, L.; Cusumano, Z.; Han, Z.; Binkley, J.; Kostakioti, M.; Hannan, T.; Pinkner, J. S.; Klein, R.; Kalas, V.; Crowley, J.; Rath, N. P.; Hultgren, S. J.; Janetka, J. W., Antivirulence C-Mannosides as Antibiotic-Sparing, Oral Therapeutics for Urinary Tract Infections. *Journal of Medicinal Chemistry* **2016,** *59* (20), 9390-9408.

229. Han, Z.; Pinkner, J. S.; Ford, B.; Chorell, E.; Crowley, J. M.; Cusumano, C. K.; Campbell, S.; Henderson, J. P.; Hultgren, S. J.; Janetka, J. W., Lead Optimization Studies on FimH Antagonists: Discovery of Potent and Orally Bioavailable Ortho-Substituted Biphenyl Mannosides. *Journal of Medicinal Chemistry* **2012,** *55* (8), 3945-3959.

230. Mydock-McGrane, L. K.; Cusumano, Z. T.; Janetka, J. W., Mannose-derived FimH antagonists: a promising anti-virulence therapeutic strategy for urinary tract infections and Crohn's disease. *Expert Opinion on Therapeutic Patents* **2016,** *26* (2), 175-197.

231. Kleeb, S.; Pang, L.; Mayer, K.; Eris, D.; Sigl, A.; Preston, R. C.; Zihlmann, P.; Sharpe, T.; Jakob, R. P.; Abgottspon, D.; Hutter, A. S.; Scharenberg, M.; Jiang, X.; Navarra, G.; Rabbani, S.; Smiesko, M.; Lüdin, N.; Bezençon, J.; Schwardt, O.; Maier, T.; Ernst, B., FimH Antagonists: Bioisosteres To Improve the in Vitro and in Vivo PK/PD Profile. *Journal of Medicinal Chemistry* **2015,** *58* (5), 2221-2239.

232. Bouckaert, J.; Berglund, J.; Schembri, M.; De Genst, E.; Cools, L.; Wuhrer, M.; Hung, C.-S.; Pinkner, J.; Slättegård, R.; Zavialov, A.; Choudhury, D.; Langermann, S.; Hultgren, S. J.; Wyns, L.; Klemm, P.; Oscarson, S.; Knight, S. D.; De Greve, H., Receptor binding studies disclose a novel class of high-affinity inhibitors of the Escherichia coli FimH adhesin. *Molecular Microbiology* **2005,** *55* (2), 441-455.

233. Sperling, O.; Fuchs, A.; Lindhorst, T. K., Evaluation of the carbohydrate recognition domain of the bacterial adhesin FimH: design, synthesis and binding properties of mannoside ligands. *Organic & Biomolecular Chemistry* **2006,** *4* (21), 3913-3922.

234. Jiang, X.; Abgottspon, D.; Kleeb, S.; Rabbani, S.; Scharenberg, M.; Wittwer, M.; Haug, M.; Schwardt, O.; Ernst, B., Antiadhesion Therapy for Urinary Tract Infections—A Balanced PK/PD Profile Proved To Be Key for Success. *Journal of Medicinal Chemistry* **2012,** *55* (10), 4700-4713.

235. Heidecke, C. D.; Lindhorst, T. K., Iterative Synthesis of Spacered Glycodendrons as Oligomannoside Mimetics and Evaluation of Their Antiadhesive Properties. *Chemistry – A European Journal* **2007,** *13* (32), 9056-9067.

236. Dubber, M.; Sperling, O.; Lindhorst, T. K., Oligomannoside mimetics by glycosylation of 'octopus glycosides' and their investigation as inhibitors of type 1 fimbriae-mediated adhesion of Escherichia coli. *Organic & Biomolecular Chemistry* **2006,** *4* (21), 3901-3912.

237. Cecioni, S.; Imberty, A.; Vidal, S., Glycomimetics versus Multivalent Glycoconjugates for the Design of High Affinity Lectin Ligands. *Chemical Reviews* **2015,** *115* (1), 525-561.

238. Bernardi, A.; Jiménez-Barbero, J.; Casnati, A.; De Castro, C.; Darbre, T.; Fieschi, F.; Finne, J.; Funken, H.; Jaeger, K.-E.; Lahmann, M.; Lindhorst, T. K.; Marradi, M.; Messner, P.; Molinaro, A.; Murphy, P. V.; Nativi, C.; Oscarson, S.; Penadés, S.; Peri, F.; Pieters, R. J.; Renaudet, O.; Reymond, J.-L.; Richichi, B.; Rojo, J.; Sansone, F.; Schäffer, C.; Turnbull, W. B.; Velasco-Torrijos, T.; Vidal, S.; Vincent, S.; Wennekes, T.; Zuilhof, H.; Imberty, A., Multivalent glycoconjugates as anti-pathogenic agents. *Chemical Society Reviews* **2013,** *42* (11), 4709-4727.

239. Gouin, S. G.; Wellens, A.; Bouckaert, J.; Kovensky, J., Synthetic multimeric heptyl mannosides as potent antiadhesives of uropathogenic Escherichia coli. *ChemMedChem* **2009,** *4* (5), 749-55.

240. Hoyos, P.; Perona, A.; Juanes, O.; Rumbero, Á.; Hernáiz, M. J., Synthesis of Glycodendrimers with Antiviral and Antibacterial Activity. *Chemistry – A European Journal* **2021,** *27* (28), 7593-7624.

241. Ashton, P. R.; Hounsell, E. F.; Jayaraman, N.; Nilsen, T. M.; Spencer, N.; Stoddart, J. F.; Young, M., Synthesis and Biological Evaluation of α-d-Mannopyranoside-Containing Dendrimers. *The Journal of Organic Chemistry* **1998,** *63* (10), 3429-3437.

242. Roy, R.; Murphy, P. V.; Gabius, H.-J., Multivalent Carbohydrate-Lectin Interactions: How Synthetic Chemistry Enables Insights into Nanometric Recognition. *Molecules* **2016,** *21* (5).

243. Al-Lazikani, B.; Jung, J.; Xiang, Z.; Honig, B., Protein structure prediction. *Curr Opin Chem Biol* **2001,** *5* (1), 51-6.

244. Lindhorst, T. K.; Kötter, S.; Krallmann-Wenzel, U.; Ehlers, S., Trivalent α-D-mannoside clusters as inhibitors of type-1 fimbriae-mediated adhesion of Escherichia coli: structural variation and biotinylation. *Journal of the Chemical Society, Perkin Transactions 1* **2001,** (8), 823-831.

245. Lindhorst, T. K.; Bruegge, K.; Fuchs, A.; Sperling, O., A bivalent glycopeptide to target two putative carbohydrate binding sites on FimH. *Beilstein J Org Chem* **2010,** *6*, 801-809.

246. Thuenauer, R.; Landi, A.; Trefzer, A.; Altmann, S.; Wehrum, S.; Eierhoff, T.; Diedrich, B.; Dengjel, J.; Nyström, A.; Imberty, A.; Römer, W., The Pseudomonas aeruginosa Lectin LecB Causes Integrin Internalization and Inhibits Epithelial Wound Healing. *mBio* **2020,** *11* (2), e03260-19.

247. Lyczak, J. B.; Cannon, C. L.; Pier, G. B., Establishment of Pseudomonas aeruginosa infection: lessons from a versatile opportunist. *Microbes Infect* **2000,** *2* (9), 1051-60.

248. Smith, D. C.; Spooner, R. A.; Watson, P. D.; Murray, J. L.; Hodge, T. W.; Amessou, M.; Johannes, L.; Lord, J. M.; Roberts, L. M., Internalized Pseudomonas exotoxin A can exploit multiple pathways to reach the endoplasmic reticulum. *Traffic* **2006,** *7* (4), 379-93.

249. Vance, R. E.; Rietsch, A.; Mekalanos, J. J., Role of the type III secreted exoenzymes S, T, and Y in systemic spread of Pseudomonas aeruginosa PAO1 in vivo. *Infect Immun* **2005,** *73* (3), 1706-13.

250. Woods, D. E.; Schaffer, M. S.; Rabin, H. R.; Campbell, G. D.; Sokol, P. A., Phenotypic comparison of Pseudomonas aeruginosa strains isolated from a variety of clinical sites. *J Clin Microbiol* **1986,** *24* (2), 260-4.

251. Tielker, D.; Hacker, S.; Loris, R.; Strathmann, M.; Wingender, J.; Wilhelm, S.; Rosenau, F.; Jaeger, K. E., Pseudomonas aeruginosa lectin LecB is located in the outer membrane and is involved in biofilm formation. *Microbiology (Reading)* **2005,** *151* (Pt 5), 1313-1323.

252. Hauck, D.; Joachim, I.; Frommeyer, B.; Varrot, A.; Philipp, B.; Möller, H. M.; Imberty, A.; Exner, T. E.; Titz, A., Discovery of two classes of potent glycomimetic inhibitors of Pseudomonas aeruginosa LecB with distinct binding modes. *ACS chemical biology* **2013,** *8* (8), 1775-1784.

253. Wojtczak, K.; Byrne, J. P., Structural Considerations for Building Synthetic Glycoconjugates as Inhibitors for Pseudomonas aeruginosa Lectins. *ChemMedChem* **2022,** *17* (12), e202200081.

254. Sulák, O.; Cioci, G.; Delia, M.; Lahmann, M.; Varrot, A.; Imberty, A.; Wimmerová, M., A TNF-like trimeric lectin domain from Burkholderia cenocepacia with specificity for fucosylated human histo-blood group antigens. *Structure* **2010,** *18* (1), 59-72.

255. Mitchell, E.; Houles, C.; Sudakevitz, D.; Wimmerova, M.; Gautier, C.; Pérez, S.; Wu, A. M.; Gilboa-Garber, N.; Imberty, A., Structural basis for oligosaccharide-mediated adhesion of Pseudomonas aeruginosa in the lungs of cystic fibrosis patients. *Nature Structural Biology* **2002,** *9* (12), 918-921.

256. Mitchell, E. P.; Sabin, C.; Šnajdrová, L.; Pokorná, M.; Perret, S.; Gautier, C.; Hofr, C.; Gilboa-Garber, N.; Koča, J.; Wimmerová, M.; Imberty, A., High affinity fucose binding of Pseudomonas aeruginosa lectin PA-IIL: 1.0 Å resolution crystal structure of the complex combined with thermodynamics and computational chemistry approaches. *Proteins: Structure, Function, and Bioinformatics* **2005,** *58* (3), 735-746.

257. Gajdos, L.; Blakeley, M. P.; Haertlein, M.; Forsyth, V. T.; Devos, J. M.; Imberty, A., Neutron crystallography reveals novel mechanisms used by Pseudomonas aeruginosa for host-cell binding. *bioRxiv* **2021**, 2021.09.24.461693.

258. Fitchette, A. C.; Cabanes-Macheteau, M.; Marvin, L.; Martin, B.; Satiat-Jeunemaitre, B.; Gomord, V.; Crooks, K.; Lerouge, P.; Faye, L.; Hawes, C., Biosynthesis and immunolocalization of Lewis a-containing N-glycans in the plant cell. *Plant Physiol* **1999,** *121* (2), 333-344.

259. Sommer, R.; Wagner, S.; Rox, K.; Varrot, A.; Hauck, D.; Wamhoff, E.-C.; Schreiber, J.; Ryckmans, T.; Brunner, T.; Rademacher, C.; Hartmann, R. W.; Brönstrup, M.; Imberty, A.; Titz, A., Glycomimetic, Orally Bioavailable LecB Inhibitors Block Biofilm Formation of Pseudomonas aeruginosa. *Journal of the American Chemical Society* **2018,** *140* (7), 2537-2545.

260. Johansson, E. M. V.; Crusz, S. A.; Kolomiets, E.; Buts, L.; Kadam, R. U.; Cacciarini, M.; Bartels, K.-M.; Diggle, S. P.; Cámara, M.; Williams, P.; Loris, R.; Nativi, C.; Rosenau, F.; Jaeger, K.-E.; Darbre,

T.; Reymond, J.-L., Inhibition and Dispersion of Pseudomonas aeruginosa Biofilms by Glycopeptide Dendrimers Targeting the Fucose-Specific Lectin LecB. *Chemistry & Biology* **2008,** *15* (12), 1249-1257.

261. Gilboa-Garber, N.; Mizrahi, L.; Garber, N., Mannose-binding hemagglutinins in extracts of Pseudomonas aeruginosa. *Can J Biochem* **1977,** *55* (9), 975-81.

262. Perret, S.; Sabin, C.; Dumon, C.; Pokorná, M.; Gautier, C.; Galanina, O.; Ilia, S.; Bovin, N.; Nicaise, M.; Desmadril, M.; Gilboa-Garber, N.; Wimmerová, M.; Mitchell, E. P.; Imberty, A., Structural basis for the interaction between human milk oligosaccharides and the bacterial lectin PA-IIL of Pseudomonas aeruginosa. *Biochem J* **2005,** *389* (Pt 2), 325-332.

263. Sabin, C.; Mitchell, E. P.; Pokorná, M.; Gautier, C.; Utille, J. P.; Wimmerová, M.; Imberty, A., Binding of different monosaccharides by lectin PA-IIL from Pseudomonas aeruginosa: thermodynamics data correlated with X-ray structures. *FEBS Lett* **2006,** *580* (3), 982-7.

264. Marotte, K.; Sabin, C.; Préville, C.; Moumé-Pymbock, M.; Wimmerová, M.; Mitchell, E. P.; Imberty, A.; Roy, R., X-ray structures and thermodynamics of the interaction of PA-IIL from Pseudomonas aeruginosa with disaccharide derivatives. *ChemMedChem* **2007,** *2* (9), 1328-1338.

265. Sommer, R.; Wagner, S.; Rox, K.; Varrot, A.; Hauck, D.; Wamhoff, E. C.; Schreiber, J.; Ryckmans, T.; Brunner, T.; Rademacher, C.; Hartmann, R. W.; Brönstrup, M.; Imberty, A.; Titz, A., Glycomimetic, Orally Bioavailable LecB Inhibitors Block Biofilm Formation of Pseudomonas aeruginosa. *J Am Chem Soc* **2018,** *140* (7), 2537-2545.

266. Consoli, G. M. L.; Granata, G.; Cafiso, V.; Stefani, S.; Geraci, C., Multivalent calixarene-based C-fucosyl derivative: a new Pseudomonas aeruginosa biofilm inhibitor. *Tetrahedron Letters* **2011,** *52* (44), 5831-5834.

267. Gerland, B.; Goudot, A.; Pourceau, G.; Meyer, A.; Vidal, S.; Souteyrand, E.; Vasseur, J.-J.; Chevolot, Y.; Morvan, F., Synthesis of Homo- and Heterofunctionalized Glycoclusters and Binding to Pseudomonas aeruginosa Lectins PA-IL and PA-IIL. *The Journal of Organic Chemistry* **2012,** *77* (17), 7620-7626.

268. Baldini, L.; Casnati, A.; Sansone, F.; Ungaro, R., Calixarene-based multivalent ligands. *Chemical Society Reviews* **2007,** *36* (2), 254-266.

269. Cecioni, S.; Lalor, R.; Blanchard, B.; Praly, J.-P.; Imberty, A.; Matthews, S. E.; Vidal, S., Achieving High Affinity towards a Bacterial Lectin through Multivalent Topological Isomers of Calix[4]arene Glycoconjugates. *Chemistry – A European Journal* **2009,** *15* (47), 13232-13240.

270. Morvan, F.; Meyer, A.; Jochum, A.; Sabin, C.; Chevolot, Y.; Imberty, A.; Praly, J. P.; Vasseur, J. J.; Souteyrand, E.; Vidal, S., Fucosylated pentaerythrityl phosphodiester oligomers (PePOs): automated synthesis of DNA-based glycoclusters and binding to Pseudomonas aeruginosa lectin (PA-IIL). *Bioconjug Chem* **2007,** *18* (5), 1637-43.

271. Kolomiets, E.; Swiderska, M. A.; Kadam, R. U.; Johansson, E. M.; Jaeger, K. E.; Darbre, T.; Reymond, J. L., Glycopeptide dendrimers with high affinity for the fucose-binding lectin LecB from Pseudomonas aeruginosa. *ChemMedChem* **2009,** *4* (4), 562-9.

272. Wang, B.; Galliford, C. V.; Low, P. S., Guiding principles in the design of ligand-targeted nanomedicines. *Nanomedicine* **2014,** *9* (2), 313-330.

273. Andresen, T. L.; Jensen, S. S.; Jørgensen, K., Advanced strategies in liposomal cancer therapy: problems and prospects of active and tumor specific drug release. *Prog Lipid Res* **2005,** *44* (1), 68-97.

274. Andresen, T. L.; Jensen, S. S.; Kaasgaard, T.; Jørgensen, K., Triggered activation and release of liposomal prodrugs and drugs in cancer tissue by secretory phospholipase A2. *Curr Drug Deliv* **2005,** *2* (4), 353-62.

275. Allen, T. M.; Cullis, P. R., Drug delivery systems: entering the mainstream. *Science* **2004,** *303* (5665), 1818-22.

276. Pham, T. D. M.; Ziora, Z. M.; Blaskovich, M. A. T., Quinolone antibiotics. *MedChemComm* **2019,** *10* (10), 1719-1739.

277. Cao, X.; Du, X.; Jiao, H.; An, Q.; Chen, R.; Fang, P.; Wang, J.; Yu, B., Carbohydrate-based drugs launched during 2000−2021. *Acta Pharmaceutica Sinica B* **2022,** *12* (10), 3783-3821.

278. Meiers, J.; Zahorska, E.; Röhrig, T.; Hauck, D.; Wagner, S.; Titz, A., Directing Drugs to Bugs: Antibiotic-Carbohydrate Conjugates Targeting Biofilm-Associated Lectins of Pseudomonas aeruginosa. *Journal of Medicinal Chemistry* **2020,** *63* (20), 11707-11724.

279. Milner, S. J.; Carrick, C. T.; Kerr, K. G.; Snelling, A. M.; Thomas, G. H.; Duhme-Klair, A.-K.; Routledge, A., Probing Bacterial Uptake of Glycosylated Ciprofloxacin Conjugates. *ChemBioChem* **2014,** *15* (3), 466-471.

280. Wang, L.; Yang, Y.-X.; Shi, X.; Mignani, S.; Caminade, A.-M.; Majoral, J.-P., Cyclotriphosphazene core-based dendrimers for biomedical applications: an update on recent advances. *Journal of Materials Chemistry B* **2018,** *6* (6), 884-895.

281. Caminade, A.-M.; Majoral, J.-P., Bifunctional Phosphorus Dendrimers and Their Properties. *Molecules* **2016,** *21* (4), 538.

282. Dzmitruk, V.; Apartsin, E.; Ihnatsyeu-Kachan, A.; Abashkin, V.; Shcharbin, D.; Bryszewska, M., Dendrimers Show Promise for siRNA and microRNA Therapeutics. *Pharmaceutics* **2018,** *10* (3), 126.

283. Röckendorf, N.; Lindhorst, T. K., Glucuronic Acid Derivatives as Branching Units for the Synthesis of Glycopeptide Mimetics. *The Journal of Organic Chemistry* **2004,** *69* (13), 4441-4445.

284. Wadouachi, A.; Kovensky, J., Synthesis of Glycosides of Glucuronic, Galacturonic and Mannuronic Acids: An Overview. *Molecules* **2011,** *16* (5), 3933-3968.

285. Roy, R.; Shiao, T. C., Glyconanosynthons as powerful scaffolds and building blocks for the rapid construction of multifaceted, dense and chiral dendrimers. *Chemical Society Reviews* **2015,** *44* (12), 3924-3941.

286. Huang, G.; Huang, H., Application of hyaluronic acid as carriers in drug delivery. *Drug Delivery* **2018,** *25* (1), 766-772.

287. Shipkova, M.; Wieland, E., Glucuronidation in therapeutic drug monitoring. *Clinica Chimica Acta* **2005,** *358* (1), 2-23.

288. Stachulski, A. V.; Harding, J. R.; Lindon, J. C.; Maggs, J. L.; Park, B. K.; Wilson, I. D., Acyl Glucuronides: Biological Activity, Chemical Reactivity, and Chemical Synthesis. *Journal of Medicinal Chemistry* **2006,** *49* (24), 6931-6945.

289. V. Stachulski, A.; V. Jenkins, G., The synthesis of O-glucuronides. *Natural Product Reports* **1998,** *15* (2), 173-186.

290. Yu, B.; Zhang, Y.; Tang, P., Carbohydrate Chemistry in the Total Synthesis of Saponins. *European Journal of Organic Chemistry* **2007,** *2007* (31), 5145-5161.

291. Deng, S.; Yu, B.; Lou, Y.; Hui, Y., First Total Synthesis of an Exceptionally Potent Antitumor Saponin, OSW-1. *The Journal of Organic Chemistry* **1999,** *64* (1), 202-208.

292. Capila, I.; Linhardt, R. J., Heparin–Protein Interactions. *Angewandte Chemie International Edition* **2002,** *41* (3), 390-412.

293. van den Bos, L. J.; Litjens, R. E. J. N.; van den Berg, R. J. B. H. N.; Overkleeft, H. S.; van der Marel, G. A., Preparation of 1-Thio Uronic Acid Lactones and Their Use in Oligosaccharide Synthesis. *Organic Letters* **2005,** *7* (10), 2007-2010.

294. Walther, R.; Rautio, J.; Zelikin, A. N., Prodrugs in medicinal chemistry and enzyme prodrug therapies. *Advanced Drug Delivery Reviews* **2017,** *118*, 65-77.

295. Sato, S.; Ito, Y.; Nukada, T.; Nakahara, Y.; Ogawa, T., Total synthesis of X hapten, III3 Fucα-nLc4 Cer. *Carbohydrate Research* **1987,** *167*, 197-210.

296. Nakahara, Y.; Ogawa, T., A highly efficient, practical, and stereoselective approach to the synthesis of α 1→4 linked galactooligosaccharides. *Tetrahedron Letters* **1987,** *28* (24), 2731-2734.

297. Dhamale, O. P.; Zong, C.; Al-Mafraji, K.; Boons, G.-J., New glucuronic acid donors for the modular synthesis of heparan sulfate oligosaccharides. *Organic & Biomolecular Chemistry* **2014,** *12* (13), 2087-2098.

298. Codée, J. D. C.; Stubba, B.; Schiattarella, M.; Overkleeft, H. S.; van Boeckel, C. A. A.; van Boom, J. H.; van der Marel, G. A., A modular strategy toward the synthesis of heparin-like oligosaccharides using monomeric building blocks in a sequential glycosylation strategy. *Journal of the American Chemical Society* **2005,** *127* (11), 3767-3773.

299. Wadouachi, A.; Kovensky, J., Synthesis of Glycosides of Glucuronic, Galacturonic and Mannuronic Acids: An Overview. *Molecules* **2011,** *16* (5).

300. Li, J.-p., Heparin-Heparansulfate Related GlcA C5-Epimerase. In *Handbook of Glycosyltransferases and Related Genes*, Taniguchi, N.; Honke, K.; Fukuda, M.; Narimatsu, H.; Yamaguchi, Y.; Angata, T., Eds. Springer Japan: Tokyo, 2014; pp 965-975.

301. Kieburg, C.; Sadalapure, K.; Lindhorst, Thisbe K., Glucose-Based AB2-Building Blocks for the Construction of Branched Glycopeptidomimetics. *European Journal of Organic Chemistry* **2000,** *2000* (11), 2035-2040.

302. Allen, J. R.; Danishefsky, S. J., New Applications of the n-Pentenyl Glycoside Method in the Synthesis and Immunoconjugation of Fucosyl GM1: A Highly Tumor-Specific Antigen Associated with Small Cell Lung Carcinoma. *Journal of the American Chemical Society* **1999,** *121* (47), 10875-10882.

303. Hsieh, S.-Y.; Jan, M.-D.; Patkar, L. N.; Chen, C.-T.; Lin, C.-C., Synthesis of a carboxyl linker containing Pk trisaccharide. *Carbohydrate Research* **2005,** *340* (1), 49-57.

304. Guo, J.; Ye, X.-S., Protecting Groups in Carbohydrate Chemistry: Influence on Stereoselectivity of Glycosylations. *Molecules* **2010,** *15* (10), 7235-7265.

305. Mulani, S. K.; Hung, W.-C.; Ingle, A. B.; Shiau, K.-S.; Mong, K.-K. T., Modulating glycosylation with exogenous nucleophiles: an overview. *Organic & Biomolecular Chemistry* **2014,** *12* (8), 1184-1197.

306. Reddy, A.; Ramos-Ondono, J.; Abbey, L.; Velasco-Torrijos, T.; Ziegler, T., 2-Chloroethyl and 2-Azidoethyl 2, 3, 4, 6-tetra-O-acetyl-β-d-gluco-andβ-d-galactopyranosides. In *Carbohydrate Chemistry*, CRC Press: 2017; pp 201-208.

307. Crich, D., En Route to the Transformation of Glycoscience: A Chemist's Perspective on Internal and External Crossroads in Glycochemistry. *Journal of the American Chemical Society* **2021,** *143* (1), 17-34.

308. Goodman, L., Neighboring-group participation in sugars. *Adv Carbohydr Chem Biochem* **1967,** *22*, 109-75.

309. Nukada, T.; Berces, A.; Zgierski, M. Z.; Whitfield, D. M., Exploring the Mechanism of Neighboring Group Assisted Glycosylation Reactions. *Journal of the American Chemical Society* **1998,** *120* (51), 13291-13295.

310. Zemplén, G.; Pacsu, E., Über die Verseifung acetylierter Zucker und verwandter Substanzen. *Berichte der deutschen chemischen Gesellschaft (A and B Series)* **1929,** *62* (6), 1613-1614.

311. Lönn, H., Synthesis of a tri- and a hepta-saccharide which contain α-l-fucopyranosyl groups and are part of the complex type of carbohydrate moiety of glycoproteins. *Carbohydrate Research* **1985,** *139*, 105-113.

312. Hanessian, S.; Lavallee, P., The preparation and synthetic utility of tert-butyldiphenylsilyl ethers. *Canadian Journal of Chemistry* **1975,** *53* (19), 2975-2977.

313. Ogilvie, K. K.; Beaucage, S. L.; Entwistle, D. W., A facile method for the removal of phosphate protecting groups in nucleotide synthesis. *Tetrahedron Letters* **1976,** *17* (16), 1255-1256.

314. Corey, E. J.; Samuelsson, B., One-step conversion of primary alcohols in the carbohydrate series to the corresponding carboxylic tert-butyl esters. *The Journal of Organic Chemistry* **1984,** *49* (24), 4735-4735.

315. Nilsson, M.; Svahn, C.-M.; Westman, J., Synthesis of the methyl glycosides of a tri- and a tetra-saccharide related to heparin and heparan sulphate. *Carbohydrate Research* **1993,** *246* (1), 161-172.

316. Wehner, J. W.; Hartmann, M.; Lindhorst, T. K., Are multivalent cluster glycosides a means of controlling ligand density of glycoarrays? *Carbohydr Res* **2013,** *371*, 22-31.

317. Kašáková, M.; Malinovská, L.; Klejch, T.; Hlaváčková, M.; Dvořáková, H.; Fujdiarová, E.; Rottnerová, Z.; Maťátková, O.; Lhoták, P.; Wimmerová, M.; Moravcová, J., Selectivity of original C-hexopyranosyl calix[4]arene conjugates towards lectins of different origin. *Carbohydr Res* **2018,** *469*, 60-72.

318. Bernardi, A.; Jiménez-Barbero, J.; Casnati, A.; De Castro, C.; Darbre, T.; Fieschi, F.; Finne, J.; Funken, H.; Jaeger, K. E.; Lahmann, M.; Lindhorst, T. K.; Marradi, M.; Messner, P.; Molinaro, A.; Murphy, P. V.; Nativi, C.; Oscarson, S.; Penadés, S.; Peri, F.; Pieters, R. J.; Renaudet, O.; Reymond, J. L.; Richichi, B.; Rojo, J.; Sansone, F.; Schäffer, C.; Turnbull, W. B.; Velasco-Torrijos, T.; Vidal, S.; Vincent, S.; Wennekes, T.; Zuilhof, H.; Imberty, A., Multivalent glycoconjugates as anti-pathogenic agents. *Chem Soc Rev* **2013,** *42* (11), 4709-27.

319. Pieters, R. J., Maximising multivalency effects in protein–carbohydrate interactions. *Organic & Biomolecular Chemistry* **2009,** *7* (10), 2013-2025.

320. Cecioni, S.; Imberty, A.; Vidal, S., Glycomimetics versus multivalent glycoconjugates for the design of high affinity lectin ligands. *Chem Rev* **2015,** *115* (1), 525-61.

321. Reymond, J. L.; Bergmann, M.; Darbre, T., Glycopeptide dendrimers as Pseudomonas aeruginosa biofilm inhibitors. *Chem Soc Rev* **2013,** *42* (11), 4814-22.

322. Marotte, K.; Préville, C.; Sabin, C.; Moumé-Pymbock, M.; Imberty, A.; Roy, R., Synthesis and binding properties of divalent and trivalent clusters of the Lewis a disaccharide moiety to Pseudomonas aeruginosa lectin PA-IIL. *Organic & Biomolecular Chemistry* **2007,** *5* (18), 2953-2961.

323. Deguise, I.; Lagnoux, D.; Roy, R., Synthesis of glycodendrimers containing both fucoside and galactoside residues and their binding properties to Pa-IL and PA-IIL lectins from Pseudomonas aeruginosa. *New Journal of Chemistry* **2007,** *31* (7), 1321-1331.

324. Ernst, B.; Magnani, J. L., From carbohydrate leads to glycomimetic drugs. *Nature Reviews Drug Discovery* **2009,** *8* (8), 661-677.

325. Loris, R.; Tielker, D.; Jaeger, K. E.; Wyns, L., Structural basis of carbohydrate recognition by the lectin LecB from Pseudomonas aeruginosa. *J Mol Biol* **2003,** *331* (4), 861-70.

326. Pertici, F.; de Mol, N. J.; Kemmink, J.; Pieters, R. J., Optimizing Divalent Inhibitors of Pseudomonas aeruginosa Lectin LecA by Using A Rigid Spacer. *Chemistry – A European Journal* **2013,** *19* (50), 16923-16927.

327. Gouin, S. G.; Wellens, A.; Bouckaert, J.; Kovensky, J., Synthetic Multimeric Heptyl Mannosides as Potent Antiadhesives of Uropathogenic Escherichia coli. *ChemMedChem* **2009,** *4* (5), 749-755.

328. Touaibia, M.; Roy, R., First Synthesis of "Majoral-Type" Glycodendrimers Bearing Covalently Bound α-d-Mannopyranoside Residues onto a Hexachlocyclotriphosphazene Core. *The Journal of Organic Chemistry* **2008,** *73* (23), 9292-9302.

329. L'Abbé, G.; Forier, B.; Dehaen, W., A fast double-stage convergent synthesis of dendritc polyethers. *Chemical Communications* **1996,** (18), 2143-2144.

330. Das, A.; Banik, B. K., Versatile thiosugars in medicinal chemistry. In *Green Approaches in Medicinal Chemistry for Sustainable Drug Design*, Elsevier: 2020; pp 549-574.

331. Dere, R. T.; Kumar, A.; Kumar, V.; Zhu, X.; Schmidt, R. R., Synthesis of Glycosylthiols and Reactivity Studies. *The Journal of Organic Chemistry* **2011,** *76* (18), 7539-7545.

332. Dondoni, A., The Emergence of Thiol–Ene Coupling as a Click Process for Materials and Bioorganic Chemistry. *Angewandte Chemie International Edition* **2008,** *47* (47), 8995-8997.

333. Hoyle, C. E.; Lee, T. Y.; Roper, T., Thiol–enes: Chemistry of the past with promise for the future. *Journal of Polymer Science Part A: Polymer Chemistry* **2004,** *42* (21), 5301-5338.

334. Hoyle, C. E.; Lowe, A. B.; Bowman, C. N., Thiol-click chemistry: a multifaceted toolbox for small molecule and polymer synthesis. *Chemical Society reviews* **2010,** *39* (4), 1355-1387.

335. Sharma, R.; Kottari, N.; Chabre, Y. M.; Abbassi, L.; Shiao, T. C.; Roy, R., A highly versatile convergent/divergent "onion peel" synthetic strategy toward potent multivalent glycodendrimers. *Chemical Communications* **2014,** *50* (87), 13300-13303.

336. Kunz, H.; Unverzagt, C., Protecting-Group-Dependent Stability of Intersaccharide Bonds—Synthesis of a Fucosyl-Chitobiose Glycopeptide. *Angewandte Chemie International Edition in English* **1988,** *27* (12), 1697-1699.

337. Jančaříková, G.; Herczeg, M.; Fujdiarová, E.; Houser, J.; Kövér, K. E.; Borbás, A.; Wimmerová, M.; Csávás, M., Synthesis of α-l-Fucopyranoside-Presenting Glycoclusters and Investigation of Their Interaction with Photorhabdus asymbiotica Lectin (PHL). *Chemistry* **2018,** *24* (16), 4055-4068.

338. Prihar, H. S.; Behrman, E. J., Chemical synthesis of β-L-fucopyranosyl phosphate and β-L-rhamnopyranosyl phosphate. *Biochemistry* **1973,** *12* (5), 997-1002.

339. Thai Le, S.; Malinovska, L.; Vašková, M.; Mező, E.; Kelemen, V.; Borbás, A.; Hodek, P.; Wimmerová, M.; Csávás, M., Investigation of the Binding Affinity of a Broad Array of l-Fucosides with Six Fucose-Specific Lectins of Bacterial and Fungal Origin. *Molecules* **2019,** *24* (12), 2262.

340. Roy, B.; Mukhopadhyay, B., Sulfuric acid immobilized on silica: an excellent catalyst for Fischer type glycosylation. *Tetrahedron Letters* **2007,** *48* (22), 3783-3787.

341. Nierengarten, J.-F.; Iehl, J.; Oerthel, V.; Holler, M.; Illescas, B. M.; Muñoz, A.; Martín, N.; Rojo, J.; Sánchez-Navarro, M.; Cecioni, S.; Vidal, S.; Buffet, K.; Durka, M.; Vincent, S. P., Fullerene sugar balls. *Chemical Communications* **2010,** *46* (22), 3860-3862.

342. Guchhait, G.; Misra, A. K., Efficient glycosylation of unprotected sugars using sulfamic acid: A mild eco-friendly catalyst. *Catalysis Communications* **2011,** *14* (1), 52-57.

343. Danishefsky, S. J.; Gervay, J.; Peterson, J. M.; McDonald, F. E.; Koseki, K.; Griffith, D. A.; Oriyama, T.; Marsden, S. P., Application of Glycals to the Synthesis of Oligosaccharides: Convergent Total Syntheses of the Lewis X Trisaccharide Sialyl Lewis X Antigenic Determinant and Higher Congeners. *Journal of the American Chemical Society* **1995,** *117* (7), 1940-1953.

344. Gerbst, A. G.; Grachev, A. A.; Ustyuzhanina, N. E.; Khatuntseva, E. A.; Tsvetkov, D. E.; Usov, A. I.; Shashkov, A. S.; Preobrazhenskaya, M. E.; Ushakova, N. A.; Nifantiev, N. E., The Synthesis and NMR and Conformational Studies of Fucoidan Fragments: VI.1 Fragments with an α-(1 → 2)-Linked Fucobioside Unit. *Russian Journal of Bioorganic Chemistry* **2004,** *30* (2), 137-148.

345. Dejter-Juszynski, M.; Flowers, H. M., Studies on the koenigs-knorr reaction: Part IV: The effect of participating groups on the stereochemistry of disaccharide formation. *Carbohydrate Research* **1973,** *28* (1), 61-74.

346. Demchenko, A. V.; Rousson, E.; Boons, G.-J., Stereoselective 1,2-cis-galactosylation assisted by remote neighboring group participation and solvent effects. *Tetrahedron Letters* **1999,** *40* (36), 6523-6526.

347. Gerbst, A. G.; Ustuzhanina, N. E.; Grachev, A. A.; Khatuntseva, E. A.; Tsvetkov, D. E.; Whitfield, D. M.; Berces, A.; Nifantiev, N. E., SYNTHESIS, NMR, AND CONFORMATIONAL STUDIES OF FUCOIDAN FRAGMENTS. III. EFFECT OF BENZOYL GROUP AT O-3 ON STEREOSELECTIVITY OF GLYCOSYLATION BY 3-O- AND 3,4-DI-O-BENZOYLATED 2-O-BENZYLFUCOSYL BROMIDES. *Journal of Carbohydrate Chemistry* **2001,** *20* (9), 821-831.

348. Malinovská, L.; Thai Le, S.; Herczeg, M.; Vašková, M.; Houser, J.; Fujdiarová, E.; Komárek, J.; Hodek, P.; Borbás, A.; Wimmerová, M.; Csávás, M., Synthesis of β-d-galactopyranoside-Presenting Glycoclusters, Investigation of Their Interactions with Pseudomonas aeruginosa Lectin A (PA-IL) and Evaluation of Their Anti-Adhesion Potential. *Biomolecules* **2019,** *9* (11), 686.

349. Nicolaÿ, R., Synthesis of Well-Defined Polythiol Copolymers by RAFT Polymerization. *Macromolecules* **2012,** *45* (2), 821-827.

350. Le Neindre, M.; Magny, B.; Nicolaÿ, R., Evaluation of thiocarbonyl and thioester moieties as thiol protecting groups for controlled radical polymerization. *Polymer Chemistry* **2013,** *4* (22), 5577-5584.

351. Horton, D.; Wolfrom, M. L., Thiosugars. I. Synthesis of Derivatives of 2-Amino-2-deoxy-1-thio-D-glucose1. *The Journal of Organic Chemistry* **1962,** *27* (5), 1794-1800.

352. Boren, B. C.; Narayan, S.; Rasmussen, L. K.; Zhang, L.; Zhao, H.; Lin, Z.; Jia, G.; Fokin, V. V., Ruthenium-Catalyzed Azide−Alkyne Cycloaddition: Scope and Mechanism. *Journal of the American Chemical Society* **2008,** *130* (28), 8923-8930.

353. Dowlut, M.; Hall, D. G.; Hindsgaul, O., Investigation of Nonspecific Effects of Different Dyes in the Screening of Labeled Carbohydrates against Immobilized Proteins. *The Journal of Organic Chemistry* **2005,** *70* (24), 9809-9813.

354. Norberg, O.; Deng, L.; Yan, M.; Ramström, O., Photo-Click Immobilization of Carbohydrates on Polymeric Surfaces—A Quick Method to Functionalize Surfaces for Biomolecular Recognition Studies. *Bioconjugate Chemistry* **2009,** *20* (12), 2364-2370.

355. Chernyak, A. Y.; Sharma, G. V. M.; Kononov, L. O.; Krishna, P. R.; Levinsky, A. B.; Kochetkov, N. K.; Rama Rao, A. V., 2-Azidoethyl glycosides: glycosides potentially useful for the preparation of neoglycoconjugates. *Carbohydrate Research* **1992,** *223*, 303-309.

356. Bagul, R. S.; Hosseini, M. M.; Shiao, T. C.; Roy, R., "Onion peel" glycodendrimer syntheses using mixed triazine and cyclotriphosphazene scaffolds. *Canadian Journal of Chemistry* **2017,** *95* (9), 975-983.

357. Killops, K. L.; Campos, L. M.; Hawker, C. J., Robust, Efficient, and Orthogonal Synthesis of Dendrimers via Thiol-ene "Click" Chemistry. *Journal of the American Chemical Society* **2008,** *130* (15), 5062-5064.

358. Sinha, A. K.; Equbal, D., Thiol−Ene Reaction: Synthetic Aspects and Mechanistic Studies of an Anti-Markovnikov-Selective Hydrothiolation of Olefins. *Asian Journal of Organic Chemistry* **2019,** *8* (1), 32-47.

359. Skirtenko, N.; Richman, M.; Nitzan, Y.; Gedanken, A.; Rahimipour, S., A facile one-pot sonochemical synthesis of surface-coated mannosyl protein microspheres for detection and killing of bacteria. *Chemical Communications* **2011,** *47* (45), 12277-12279.

360. Campos, L. M.; Killops, K. L.; Sakai, R.; Paulusse, J. M. J.; Damiron, D.; Drockenmuller, E.; Messmore, B. W.; Hawker, C. J., Development of Thermal and Photochemical Strategies for Thiol−Ene Click Polymer Functionalization. *Macromolecules* **2008,** *41* (19), 7063-7070.

361. Staros, J. V.; Bayley, H.; Standring, D. N.; Knowles, J. R., Reduction of aryl azides by thiols: implications for the use of photoaffinity reagents. *Biochem Biophys Res Commun* **1978,** *80* (3), 568-72.

362. Cartwright, I. L.; Hutchinson, D. W.; Armstrong, V. W., The reaction between thiols and 8-azidoadenosine derivatives. *Nucleic Acids Research* **1976,** *3* (9), 2331-2340.

363. Kyba, E. P.; Abramovitch, R. A., Photolysis of alkyl azides. Evidence for a nonnitrene mechanism. *Journal of the American Chemical Society* **1980,** *102* (2), 735-740.

364. Leyva, E.; Platz, M. S.; Persy, G.; Wirz, J., Photochemistry of phenyl azide: the role of singlet and triplet phenylnitrene as transient intermediates. *Journal of the American Chemical Society* **1986,** *108* (13), 3783-3790.

365. Xue, J.; Luk, H. L.; Eswaran, S. V.; Hadad, C. M.; Platz, M. S., Ultrafast infrared and UV-vis studies of the photochemistry of methoxycarbonylphenyl azides in solution. *J Phys Chem A* **2012,** *116* (22), 5325-5336.

366. Kumar, G. S.; Lin, Q., Light-Triggered Click Chemistry. *Chemical Reviews* **2020**.

367. Hill, E.; Shukla, R.; Park, S. S.; Baker, J. R., Synthetic PAMAM–RGD Conjugates Target and Bind To Odontoblast-like MDPC 23 cells and the Predentin in Tooth Organ Cultures. *Bioconjugate Chemistry* **2007,** *18* (6), 1756-1762.

368. Percec, V.; Wilson, D. A.; Leowanawat, P.; Wilson, C. J.; Hughes, A. D.; Kaucher, M. S.; Hammer, D. A.; Levine, D. H.; Kim, A. J.; Bates, F. S.; Davis, K. P.; Lodge, T. P.; Klein, M. L.; DeVane, R. H.; Aqad, E.; Rosen, B. M.; Argintaru, A. O.; Sienkowska, M. J.; Rissanen, K.; Nummelin, S.; Ropponen, J., Self-assembly of Janus dendrimers into uniform dendrimersomes and other complex architectures. *Science* **2010,** *328* (5981), 1009-14.

369. Huang, C.-Y.; Thayer, D. A.; Chang, A. Y.; Best, M. D.; Hoffmann, J.; Head, S.; Wong, C.-H., Carbohydrate microarray for profiling the antibodies interacting with Globo H tumor antigen. *Proceedings of the National Academy of Sciences of the United States of America* **2006,** *103* (1), 15-20.

370. Leffler, J. E.; Temple, R. D., Staudinger reaction between triarylphosphines and azides. Mechanism. *Journal of the American Chemical Society* **1967,** *89* (20), 5235-5246.

371. Lowe, A. B., Thiol-ene "click" reactions and recent applications in polymer and materials synthesis. *Polymer Chemistry* **2010,** *1* (1), 17-36.

372. Griesbaum, K., Problems and Possibilities of the Free-Radical Addition of Thiols to Unsaturated Compounds. *Angewandte Chemie International Edition in English* **1970,** *9* (4), 273-287.

373. Ichikawa, Y.; Ohara, F.; Kotsuki, H.; Nakano, K., A New Approach to the Neoglycopeptides: Synthesis of Urea- and Carbamate-Tethered N-Acetyl-d-glucosamine Amino Acid Conjugates. *Organic Letters* **2006,** *8* (22), 5009-5012.

374. Hanessian, S.; Soma, U.; Dorich, S.; Deschênes-Simard, B., Total Synthesis of (+)-ent-Cyclizidine: Absolute Configurational Confirmation of Antibiotic M146791. *Organic Letters* **2011,** *13* (5), 1048-1051.

375. Chevallier, O. P.; Migaud, M. E., Investigation of acetyl migrations in furanosides. *Beilstein J Org Chem* **2006,** *2*, 14-14.

376. Zeng, Y.; Kong, F., Synthesis of 3,6-Branched β-d-Glucose Oligosaccharides. *Journal of Carbohydrate Chemistry* **2003,** *22* (9), 881-890.

377. Alexander, P.; Krishnamurthy, V. V.; Prisbe, E. J., Synthesis and antiviral activity of pyranosylphosphonic acid nucleotide analogues. *J Med Chem* **1996,** *39* (6), 1321-30.

378. Almant, M.; Moreau, V.; Kovensky, J.; Bouckaert, J.; Gouin, S. G., Clustering of Escherichia coli type-1 fimbrial adhesins by using multimeric heptyl α-D-mannoside probes with a carbohydrate core. *Chemistry* **2011,** *17* (36), 10029-38.

379. Lezerovich, A.; Gros, E. G.; Sproviero, J. F.; Deulofeu, V., Reaction of ammonia with some acetylated and benzoylated monosaccharides: Part XI. Intramolecular migration of O-benzoyl groups in the partial ammonolysis of penta-O-benzoyl-D-glucoses. *Carbohydrate Research* **1967,** *4* (1), 1-6.

380. Goddard-Borger, E. D.; Stick, R. V., An Efficient, Inexpensive, and Shelf-Stable Diazotransfer Reagent: Imidazole-1-sulfonyl Azide Hydrochloride. *Organic Letters* **2007,** *9* (19), 3797-3800.

381. Gironda-Martínez, A.; Neri, D.; Samain, F.; Donckele, E. J., DNA-Compatible Diazo-Transfer Reaction in Aqueous Media Suitable for DNA-Encoded Chemical Library Synthesis. *Organic Letters* **2019,** *21* (23), 9555-9558.

382. Sonousi, A.; Crich, D., Selective Protection of Secondary Amines as the N-Phenyltriazenes. Application to Aminoglycoside Antibiotics. *Organic Letters* **2015,** *17* (16), 4006-4009.

383. Lam, H. Y.; Zhang, Y.; Liu, H.; Xu, J.; Wong, C. T. T.; Xu, C.; Li, X., Total Synthesis of Daptomycin by Cyclization via a Chemoselective Serine Ligation. *Journal of the American Chemical Society* **2013,** *135* (16), 6272-6279.

384. Raushel, J.; Pitram, S. M.; Fokin, V. V., Efficient Synthesis of Sulfonyl Azides from Sulfonamides. *Organic Letters* **2008,** *10* (16), 3385-3388.

385. Pandiakumar, A. K.; Sarma, S. P.; Samuelson, A. G., Mechanistic studies on the diazo transfer reaction. *Tetrahedron Letters* **2014,** *55* (18), 2917-2920.

386. Nyffeler, P. T.; Liang, C. H.; Koeller, K. M.; Wong, C. H., The chemistry of amine-azide interconversion: catalytic diazotransfer and regioselective azide reduction. *J Am Chem Soc* **2002,** *124* (36), 10773-8.

387. Barrientos, Á. G.; de la Fuente, J. M.; Rojas, T. C.; Fernández, A.; Penadés, S., Gold Glyconanoparticles: Synthetic Polyvalent Ligands Mimicking Glycocalyx-Like Surfaces as Tools for Glycobiological Studies. *Chemistry – A European Journal* **2003,** *9* (9), 1909-1921.

388. Miura, Y., Design and synthesis of well-defined glycopolymers for the control of biological functionalities. *Polymer Journal* **2012,** *44* (7), 679-689.

389. Zibarov, A.; Oukhrib, A.; Aujard Catot, J.; Turrin, C.-O.; Caminade, A.-M., AB5 Derivatives of Cyclotriphosphazene for the Synthesis of Dendrons and Their Applications. *Molecules* **2021,** *26* (13).

390. Teasdale, I.; Brüggemann, O., Polyphosphazenes: Multifunctional, Biodegradable Vehicles for Drug and Gene Delivery. *Polymers (Basel)* **2013,** *5* (1), 161-187.

391. Janin, A.; Blais, J. F.; Mercier, G.; Drogui, P., Selective recovery of Cr and Cu in leachate from chromated copper arsenate treated wood using chelating and acidic ion exchange resins. *J Hazard Mater* **2009,** *169* (1-3), 1099-105.

392. Spataro, G.; Malecaze, F.; Turrin, C.-O.; Soler, V.; Duhayon, C.; Elena, P.-P.; Majoral, J.-P.; Caminade, A.-M., Designing dendrimers for ocular drug delivery. *European Journal of Medicinal Chemistry* **2010,** *45* (1), 326-334.

393. Roux, S.; Zékri, E.; Rousseau, B.; Paternostre, M.; Cintrat, J. C.; Fay, N., Elimination and exchange of trifluoroacetate counter-ion from cationic peptides: a critical evaluation of different approaches. *J Pept Sci* **2008,** *14* (3), 354-9.

394. Manzi, A.; Esko, J., Direct chemical analysis of glycoconjugates for carbohydrates. *Curr Protoc Mol Biol* **2001,** *Chapter 17*, Unit17.9.

395. Jayaraman, N., Multivalent ligand presentation as a central concept to study intricate carbohydrate–protein interactions. *Chemical Society Reviews* **2009,** *38* (12), 3463-3483.

396. Deniaud, D.; Julienne, K.; Gouin, S. G., Insights in the rational design of synthetic multivalent glycoconjugates as lectin ligands. *Organic & Biomolecular Chemistry* **2011,** *9* (4), 966-979.

397. Bouillon, C.; Meyer, A.; Vidal, S.; Jochum, A.; Chevolot, Y.; Cloarec, J.-P.; Praly, J.-P.; Vasseur, J.-J.; Morvan, F., Microwave Assisted "Click" Chemistry for the Synthesis of Multiple Labeled-Carbohydrate Oligonucleotides on Solid Support. *The Journal of Organic Chemistry* **2006,** *71* (12), 4700-4702.

398. Chevolot, Y.; Bouillon, C.; Vidal, S.; Morvan, F.; Meyer, A.; Cloarec, J.-P.; Jochum, A.; Praly, J.-P.; Vasseur, J.-J.; Souteyrand, E., DNA-Based Carbohydrate Biochips: A Platform for Surface Glyco-Engineering. *Angewandte Chemie International Edition* **2007,** *46* (14), 2398-2402.

399. Morvan, F.; Meyer, A.; Jochum, A.; Sabin, C.; Chevolot, Y.; Imberty, A.; Praly, J.-P.; Vasseur, J.-J.; Souteyrand, E.; Vidal, S., Fucosylated Pentaerythrityl Phosphodiester Oligomers (PePOs): Automated Synthesis of DNA-Based Glycoclusters and Binding to Pseudomonas aeruginosa Lectin (PA-IIL). *Bioconjugate Chemistry* **2007,** *18* (5), 1637-1643.

400. Nagahori, N.; Nishimura, S.-I., Tailored Glycopolymers: Controlling the Carbohydrate−Protein Interaction Based on Template Effect. *Biomacromolecules* **2001,** *2* (1), 22-24.

401. Tsai, C.-S.; Yu, T.-B.; Chen, C.-T., Gold nanoparticle-based competitive colorimetric assay for detection of protein–protein interactions. *Chemical Communications* **2005,** (34), 4273-4275.

402. Nigudkar, S. S.; Demchenko, A. V., Stereocontrolled 1,2-cis glycosylation as the driving force of progress in synthetic carbohydrate chemistry. *Chemical Science* **2015,** *6* (5), 2687-2704.

403. Otsuka, Y.; Yamamoto, T.; Fukase, K., Syntheses of N-aryl-protected glucosamines and their stereoselectivity in chemical glycosylations. *Tetrahedron Letters* **2017,** *58* (31), 3019-3023.

404. Koto, S.; Hirooka, M.; Yago, K.; Komiya, M.; Shimizu, T.; Kato, K.; Takehara, T.; Ikefuji, A.; Iwasa, A.; Hagino, S.; Sekiya, M.; Nakase, Y.; Zen, S.; Tomonaga, F.; Shimada, S., Benzyl Derivatives

of N-2,4-Dinitrophenyl-D-glucosamine and Their Use for Oligosaccharide Synthesis. *Bulletin of the Chemical Society of Japan* **2000,** *73* (1), 173-183.

405. Bindschädler, P.; Dialer, L. O.; Seeberger, P. H., Synthesis of Differentially Protected Glucosamine Building Blocks and Their Evaluation as Glycosylating Agents. *Journal of Carbohydrate Chemistry* **2009,** *28* (7-8), 395-420.

406. Banoub, J.; Boullanger, P.; Lafont, D., Synthesis of oligosaccharides of 2-amino-2-deoxy sugars. *Chemical Reviews* **1992,** *92* (6), 1167-1195.

407. Lemieux, R. U.; Takeda, T.; Chung, B. Y., Synthesis of 2-Amino-2-deoxy-β-<sc>D</sc>-glucopyranosides. In *Synthetic Methods for Carbohydrates*, AMERICAN CHEMICAL SOCIETY: 1977; Vol. 39, pp 90-115.

408. Alais, J.; Veyrières, A., Syntheses of linear tetra-, hexa-, and octa-saccharide fragments of the i-blood group active poly-(N-acetyl-lactosamine) series. Blockwise methods for the synthesis of repetitive oligosaccharide sequences. *Carbohydr Res* **1990,** *207* (1), 11-31.

409. Schmidt, R. R.; Grundler, G., Synthesis of a Tetrasaccharide of the Core Region of O-Glycoproteins. *Angewandte Chemie International Edition in English* **1983,** *22* (10), 776-777.

410. Veeneman, G. H.; van Boom, J. H., An efficient thioglycoside-mediated formation of α-glycosidic linkages promoted by iodonium dicollidine perchlorate. *Tetrahedron Letters* **1990,** *31* (2), 275-278.

411. Toshima, K.; Tatsuta, K., Recent progress in O-glycosylation methods and its application to natural products synthesis. *Chemical Reviews* **1993,** *93* (4), 1503-1531.

412. Kuyama, H.; Nakahara, Y.; Nukada, T.; Ito, Y.; Nakahara, Y.; Ogawa, T., Stereocontrolled synthesis of chitosan dodecamer. *Carbohydrate Research* **1993,** *243* (1), C1-C7.

413. Pedersen, C. M.; Marinescu, L. G.; Bols, M., Conformationally armed glycosyl donors: reactivity quantification, new donors and one pot reactions. *Chemical Communications* **2008,** (21), 2465-2467.

414. Hsu, C.-H.; Hung, S.-C.; Wu, C.-Y.; Wong, C.-H., Toward Automated Oligosaccharide Synthesis. *Angewandte Chemie International Edition* **2011,** *50* (50), 11872-11923.

415. Dasgupta, F.; Garegg, P. J., Reductive Dephthalimidation: A Mild and Efficient Method for The N-Phthaumido Deprotection During Ougosaccharide Synthesis. *Journal of Carbohydrate Chemistry* **1988,** *7* (3), 701-707.

416. Liao, L.; Auzanneau, F.-I., Glycosylation of N-Acetylglucosamine: Imidate Formation and Unexpected Conformation. *Organic Letters* **2003,** *5* (15), 2607-2610.

417. Marqvorsen, M. H. S.; Pedersen, M. J.; Rasmussen, M. R.; Kristensen, S. K.; Dahl-Lassen, R.; Jensen, H. H., Why Is Direct Glycosylation with N-Acetylglucosamine Donors Such a Poor Reaction and What Can Be Done about It? *The Journal of Organic Chemistry* **2017,** *82* (1), 143-156.

418. Goswami, L. N.; Houston, Z. H.; Sarma, S. J.; Jalisatgi, S. S.; Hawthorne, M. F., Efficient synthesis of diverse heterobifunctionalized clickable oligo(ethylene glycol) linkers: potential applications in bioconjugation and targeted drug delivery. *Org Biomol Chem* **2013,** *11* (7), 1116-26.

419. Lopchuk, J. M.; Fjelbye, K.; Kawamata, Y.; Malins, L. R.; Pan, C.-M.; Gianatassio, R.; Wang, J.; Prieto, L.; Bradow, J.; Brandt, T. A.; Collins, M. R.; Elleraas, J.; Ewanicki, J.; Farrell, W.; Fadeyi, O. O.; Gallego, G. M.; Mousseau, J. J.; Oliver, R.; Sach, N. W.; Smith, J. K.; Spangler, J. E.; Zhu, H.; Zhu, J.; Baran, P. S., Strain-Release Heteroatom Functionalization: Development, Scope, and Stereospecificity. *Journal of the American Chemical Society* **2017,** *139* (8), 3209-3226.

420. Cheng, G.; Wang, X.; Bao, H.; Cheng, C.; Liu, N.; Hu, Y., Total Syntheses of (−)-Hanishin, (−)-Longmide B, and (−)-Longmide B Methyl Ester via a Novel Preparation of N-Substituted Pyrrole-2-Carboxylates. *Organic Letters* **2012,** *14* (4), 1062-1065.

421. Kanie, O.; Crawley, S. C.; Palcic, M. M.; Hindsgaul, O., Acceptor-substrate recognition by N-acetylglucosaminyltransferase-V: Critical role of the 4″-hydroxyl group in β-d-GlcpNAc-(1 → 2)-α-d-Manp(1 → 6)-β-d-Glcp-OR. *Carbohydrate Research* **1993,** *243* (1), 139-164.

422. Nicolaou, K. C.; Shelke, Y. G.; Dherange, B. D.; Kempema, A.; Lin, B.; Gu, C.; Sandoval, J.; Hammond, M.; Aujay, M.; Gavrilyuk, J., Design, Synthesis, and Biological Investigation of Epothilone B Analogues Featuring Lactone, Lactam, and Carbocyclic Macrocycles, Epoxide, Aziridine, and 1,1-Difluorocyclopropane and Other Fluorine Residues. *The Journal of Organic Chemistry* **2020,** *85* (5), 2865-2917.

423. Jung, M. E.; Koch, P., An Efficient Synthesis of the Protected Carbohydrate Moiety of Brasilicardin A. *Organic Letters* **2011,** *13* (14), 3710-3713.

424. Shivatare, S. S.; Chang, S.-H.; Tsai, T.-I.; Ren, C.-T.; Chuang, H.-Y.; Hsu, L.; Lin, C.-W.; Li, S.-T.; Wu, C.-Y.; Wong, C.-H., Efficient Convergent Synthesis of Bi-, Tri-, and Tetra-antennary Complex Type N-Glycans and Their HIV-1 Antigenicity. *Journal of the American Chemical Society* **2013,** *135* (41), 15382-15391.

425. Podilapu, A. R.; Kulkarni, S. S., First Synthesis of Bacillus cereus Ch HF-PS Cell Wall Trisaccharide Repeating Unit. *Organic Letters* **2014,** *16* (16), 4336-4339.

426. Dhakal, B.; Crich, D., Synthesis and Stereocontrolled Equatorially Selective Glycosylation Reactions of a Pseudaminic Acid Donor: Importance of the Side-Chain Conformation and Regioselective Reduction of Azide Protecting Groups. *Journal of the American Chemical Society* **2018,** *140* (44), 15008-15015.

427. Salmain, M.; Vessieres, A.; Butler, I. S.; Jaouen, G., (N-Succinimidyl 4-pentynoate)(hexacarbonyldicobalt): a transition-metal carbonyl complex having similar uses to the Bolton-Hunter reagent. *Bioconjugate Chemistry* **1991,** *2* (1), 13-15.

428. Montalbetti, C. A. G. N.; Falque, V., Amide bond formation and peptide coupling. *Tetrahedron* **2005,** *61* (46), 10827-10852.

429. Frérot, E.; Coste, J.; Pantaloni, A.; Dufour, M.-N.; Jouin, P., PyBOP® and PyBroP: Two reagents for the difficult coupling of the α,α-dialkyl amino acid, Aib. *Tetrahedron* **1991,** *47* (2), 259-270.

430. Hφeg-Jensen, T.; Jakobsen, M. H.; Holm, A., A new method for rapid solution synthesis of shorter peptides by use of PyBOP®. *Tetrahedron Letters* **1991,** *32* (44), 6387-6390.

431. Langer, P.; J. Ince, S.; V. Ley, S., Assembly of dendritic glycoclusters from monomeric mannose building blocks. *Journal of the Chemical Society, Perkin Transactions 1* **1998,** (23), 3913-3916.

432. Lindhorst, Thisbe K.; Dubber, M.; Krallmann-Wenzel, U.; Ehlers, S., Cluster Mannosides as Inhibitors of Type 1 Fimbriae-Mediated Adhesion of Escherichia coli: Pentaerythritol Derivatives as Scaffolds. *European Journal of Organic Chemistry* **2000,** *2000* (11), 2027-2034.

433. Figueredo, A. S.; Zamoner, L. O. B.; Rejzek, M.; Field, R. A.; Carvalho, I., Cluster glycosides and heteroglycoclusters presented in alternative arrangements. *Tetrahedron Letters* **2018,** *59* (50), 4405-4409.

434. Balachandra, C.; Sharma, N. K., Direct/Reversible Amidation of Troponyl Alkylglycinates via Cationic Troponyl Lactones and Mechanistic Insights. *ACS Omega* **2018,** *3* (1), 997-1013.

435. Hayashi, K.; Ichimaru, Y.; Sugiura, K.; Maeda, A.; Harada, Y.; Kojima, Y.; Nakayama, K.; Imai, M., Efficiency of Lithium Cations in Hydrolysis Reactions of Esters in Aqueous Tetrahydrofuran. *Chem Pharm Bull (Tokyo)* **2021,** *69* (6), 581-584.

436. Peters, D. S.; Romesberg, F. E.; Baran, P. S., Scalable Access to Arylomycins via C–H Functionalization Logic. *Journal of the American Chemical Society* **2018,** *140* (6), 2072-2075.

437. Giroux, S.; Corey, E. J., Enantioselective Synthesis of a Simple Benzenoid Analogue of Glycinoeclepin A. *Organic Letters* **2008,** *10* (24), 5617-5619.

438. Sriwilaijaroen, N.; Magesh, S.; Imamura, A.; Ando, H.; Ishida, H.; Sakai, M.; Ishitsubo, E.; Hori, T.; Moriya, S.; Ishikawa, T.; Kuwata, K.; Odagiri, T.; Tashiro, M.; Hiramatsu, H.; Tsukamoto, K.; Miyagi, T.; Tokiwa, H.; Kiso, M.; Suzuki, Y., A Novel Potent and Highly Specific Inhibitor against Influenza Viral N1-N9 Neuraminidases: Insight into Neuraminidase-Inhibitor Interactions. *J Med Chem* **2016,** *59* (10), 4563-77.

439. Trost, B. M.; Stivala, C. E.; Fandrick, D. R.; Hull, K. L.; Huang, A.; Poock, C.; Kalkofen, R., Total Synthesis of (−)-Lasonolide A. *Journal of the American Chemical Society* **2016,** *138* (36), 11690-11701.

440. Baggio, D.; Ananda-Rajah, M. R., Fluoroquinolone antibiotics and adverse events. *Aust Prescr* **2021,** *44* (5), 161-164.

441. Cheng, A. V.; Wuest, W. M., Signed, Sealed, Delivered: Conjugate and Prodrug Strategies as Targeted Delivery Vectors for Antibiotics. *ACS Infect Dis* **2019,** *5* (6), 816-828.

442. Hong, L.; Luo, S. H.; Yu, C. H.; Xie, Y.; Xia, M. Y.; Chen, G. Y.; Peng, Q., Functional Nanomaterials and Their Potential Applications in Antibacterial Therapy. *Pharm Nanotechnol* **2019,** *7* (2), 129-146.

443. Lane, D. D.; Chiu, D. Y.; Su, F. Y.; Srinivasan, S.; Kern, H. B.; Press, O. W.; Stayton, P. S.; Convertine, A. J., Well-defined single polymer nanoparticles for the antibody-targeted delivery of chemotherapeutic agents. *Polymer Chemistry* **2015,** *6* (8), 1286-1299.

444. Svenningsen, S. W.; Frederiksen, R. F.; Counil, C.; Ficker, M.; Leisner, J. J.; Christensen, J. B., Synthesis and Antimicrobial Properties of a Ciprofloxacin and PAMAM-dendrimer Conjugate. *Molecules* **2020,** *25* (6), 1389.

445. Vembu, S.; Pazhamalai, S.; Gopalakrishnan, M., Potential antibacterial activity of triazine dendrimer: Synthesis and controllable drug release properties. *Bioorg Med Chem* **2015,** *23* (15), 4561-4566.

446. Caminade, A.-M.; Turrin, C.-O., Dendrimers for drug delivery. *Journal of Materials Chemistry B* **2014,** *2* (26), 4055-4066.

447. Ji, C.; Miller, M. J., Chemical syntheses and in vitro antibacterial activity of two desferrioxamine B-ciprofloxacin conjugates with potential esterase and phosphatase triggered drug release linkers. *Bioorg Med Chem* **2012,** *20* (12), 3828-36.

448. Zheng, T.; Nolan, E. M., Evaluation of (acyloxy)alkyl ester linkers for antibiotic release from siderophore-antibiotic conjugates. *Bioorg Med Chem Lett* **2015,** *25* (21), 4987-4991.

449. Simplício, A. L.; Clancy, J. M.; Gilmer, J. F., Prodrugs for Amines. *Molecules* **2008,** *13* (3).

450. Zhou, G.-C.; Liu, F.; Wan, J.; Wang, J.; Wang, D.; Wei, P.; Ouyang, P., Design, synthesis and evaluation of a cellular stable and detectable biotinylated fumagillin probe and investigation of cell permeability of fumagillin and its analogs to endothelial and cancer cells. *European Journal of Medicinal Chemistry* **2013,** *70*, 631-639.

451. Li, Z.; Teng, D.; Mao, R.; Wang, X.; Hao, Y.; Wang, X.; Wang, J., Improved Antibacterial Activity of the Marine Peptide N6 against Intracellular Salmonella Typhimurium by Conjugating with the Cell-Penetrating Peptide Tat11 via a Cleavable Linker. *Journal of Medicinal Chemistry* **2018,** *61* (17), 7991-8000.

452. Von Daehne, W.; Frederiksen, E.; Gundersen, E.; Lund, F.; Moerch, P.; Petersen, H. J.; Roholt, K.; Tybring, L.; Godtfredsen, W. O., Acyloxymethyl esters of ampicillin. *Journal of Medicinal Chemistry* **1970,** *13* (4), 607-612.

453. Wolfson, J. S.; Hooper, D. C., Fluoroquinolone antimicrobial agents. *Clin Microbiol Rev* **1989,** *2* (4), 378-424.

454. Hooper, D. C.; Rubinstein, E., *Quinolone antimicrobial agents*. ASM Press Washington, DC: 2003; Vol. 453.

455. Fedorowicz, J.; Sączewski, J., Modifications of quinolones and fluoroquinolones: hybrid compounds and dual-action molecules. *Monatsh Chem* **2018,** *149* (7), 1199-1245.

456. Wencewicz, T. A.; Möllmann, U.; Long, T. E.; Miller, M. J., Is drug release necessary for antimicrobial activity of siderophore-drug conjugates? Syntheses and biological studies of the naturally occurring salmycin "Trojan Horse" antibiotics and synthetic desferridanoxamine-antibiotic conjugates. *Biometals* **2009,** *22* (4), 633-48.

457. Wong, P. T.; Choi, S. K., Mechanisms of Drug Release in Nanotherapeutic Delivery Systems. *Chemical Reviews* **2015,** *115* (9), 3388-3432.

458. Lu, C.; Zhong, W., Synthesis of Propargyl-Terminated Heterobifunctional Poly(ethylene glycol). *Polymers* **2010,** *2* (4).

459. Golkowski, M.; Ziegler, T., The 2-(triphenylsilyl)ethoxycarbonyl-("Tpseoc"-) group: a new silicon-based, fluoride cleavable oxycarbonyl protecting group highly orthogonal to the Boc-, Fmoc- and Cbz-groups. *Molecules (Basel, Switzerland)* **2011,** *16* (6), 4695-4718.

460. Merker, R. L.; Scott, M. J., The Reaction of Alkyl Halides with Carboxylic Acids and Phenols in the Presence of Tertiary Amines. *The Journal of Organic Chemistry* **1961,** *26* (12), 5180-5182.

461. Ghosh, A. K.; Brindisi, M., Organic Carbamates in Drug Design and Medicinal Chemistry. *Journal of Medicinal Chemistry* **2015,** *58* (7), 2895-2940.

462. Yan, L.; Crayton, S. H.; Thawani, J. P.; Amirshaghaghi, A.; Tsourkas, A.; Cheng, Z., A pH-Responsive Drug-Delivery Platform Based on Glycol Chitosan–Coated Liposomes. *Small* **2015,** *11* (37), 4870-4874.

463. Klockgether, J.; Munder, A.; Neugebauer, J.; Davenport, C. F.; Stanke, F.; Larbig, K. D.; Heeb, S.; Schöck, U.; Pohl, T. M.; Wiehlmann, L.; Tümmler, B., Genome diversity of Pseudomonas aeruginosa PAO1 laboratory strains. *J Bacteriol* **2010,** *192* (4), 1113-21.

464. Chapman, J. S.; Georgopapadakou, N. H., Routes of quinolone permeation in Escherichia coli. *Antimicrob Agents Chemother* **1988,** *32* (4), 438-442.

465. Hirai, K.; Aoyama, H.; Irikura, T.; Iyobe, S.; Mitsuhashi, S., Differences in susceptibility to quinolones of outer membrane mutants of Salmonella typhimurium and Escherichia coli. *Antimicrob Agents Chemother* **1986,** *29* (3), 535-538.

466. Nikaido, H., Porins and specific diffusion channels in bacterial outer membranes. *J Biol Chem* **1994,** *269* (6), 3905-8.

467. Chevalier, S.; Bouffartigues, E.; Bodilis, J.; Maillot, O.; Lesouhaitier, O.; Feuilloley, M. G. J.; Orange, N.; Dufour, A.; Cornelis, P., Structure, function and regulation of Pseudomonas aeruginosa porins. *FEMS Microbiol Rev* **2017,** *41* (5), 698-722.

468. Valcourt, D. M.; Dang, M. N.; Scully, M. A.; Day, E. S., Nanoparticle-Mediated Co-Delivery of Notch-1 Antibodies and ABT-737 as a Potent Treatment Strategy for Triple-Negative Breast Cancer. *ACS Nano* **2020,** *14* (3), 3378-3388.

469. Anselmo, A. C.; Mitragotri, S., Nanoparticles in the clinic: An update. *Bioeng Transl Med* **2019,** *4* (3), e10143-e10143.

470. Hoshyar, N.; Gray, S.; Han, H.; Bao, G., The effect of nanoparticle size on in vivo pharmacokinetics and cellular interaction. *Nanomedicine (Lond)* **2016,** *11* (6), 673-92.

471. Rele, S. M.; Cui, W.; Wang, L.; Hou, S.; Barr-Zarse, G.; Tatton, D.; Gnanou, Y.; Esko, J. D.; Chaikof, E. L., Dendrimer-like PEO Glycopolymers Exhibit Anti-Inflammatory Properties. *Journal of the American Chemical Society* **2005,** *127* (29), 10132-10133.

472. Allcock, H. R., Polyphosphazenes: New Polymers with Inorganic Backbone Atoms. *Science* **1976,** *193* (4259), 1214-1219.

473. Gladstone, J. H.; Holmes, J. D., XXVII.—On chlorophosphuret of nitrogen, and its products of decomposition. *Journal of the Chemical Society* **1864,** *17* (0), 225-237.

474. Wilson, A.; Carroll, D. F., 515. Phosphonitrilic derivatives. Part II. The structure of trimeric phosphonitrilic chloride. *Journal of the Chemical Society (Resumed)* **1960,** (0), 2548-2552.

475. Allen, C. W., Regio- and stereochemical control in substitution reactions of cyclophosphazenes. *Chemical Reviews* **1991,** *91* (2), 119-135.

476. Chandrasekhar, V.; Thilagar, P.; Murugesa Pandian, B., Cyclophosphazene-based multi-site coordination ligands. *Coordination Chemistry Reviews* **2007,** *251* (9), 1045-1074.

477. Chandrasekhar, V.; Murugesapandian, B., Phosphorus-Supported Ligands for the Assembly of Multimetal Architectures. *Accounts of Chemical Research* **2009,** *42* (8), 1047-1062.

478. Pasut, G.; Veronese, F. M., Polymer–drug conjugation, recent achievements and general strategies. *Progress in Polymer Science* **2007,** *32* (8), 933-961.

479. Duncan, R.; Vicent, M. J.; Greco, F.; Nicholson, R. I., Polymer–drug conjugates: towards a novel approach for the treatment of endrocine-related cancer. *Endocrine-Related Cancer Endocr Relat Cancer* **2005,** *12* (Supplement_1), S189.

480. Parveen, S.; Sahoo, S. K., Nanomedicine: clinical applications of polyethylene glycol conjugated proteins and drugs. *Clin Pharmacokinet* **2006,** *45* (10), 965-988.

481. Torchilin, V. P., Polymer-coated long-circulating microparticulate pharmaceuticals. *Journal of Microencapsulation* **1998,** *15* (1), 1-19.

482. Petersen, H.; Fechner, P. M.; Fischer, D.; Kissel, T., Synthesis, Characterization, and Biocompatibility of Polyethylenimine-graft-poly(ethylene glycol) Block Copolymers. *Macromolecules* **2002,** *35* (18), 6867-6874.

483. Allcock, H. R., Recent advances in phosphazene (phosphonitrilic) chemistry. *Chemical Reviews* **1972,** *72* (4), 315-356.

484. El Brahmi, N.; Mignani, S. M.; Caron, J.; El Kazzouli, S.; Bousmina, M. M.; Caminade, A.-M.; Cresteil, T.; Majoral, J.-P., Investigations on dendrimer space reveal solid and liquid tumor growth-inhibition by original phosphorus-based dendrimers and the corresponding monomers and dendrons with ethacrynic acid motifs. *Nanoscale* **2015,** *7* (9), 3915-3922.

485. Hayder, M.; Poupot, M.; Baron, M.; Nigon, D.; Turrin, C.-O.; Caminade, A.-M.; Majoral, J.-P.; Eisenberg, R. A.; Fournié, J.-J.; Cantagrel, A.; Poupot, R.; Davignon, J.-L., A phosphorus-based dendrimer targets inflammation and osteoclastogenesis in experimental arthritis. *Science translational medicine* **2011,** *3* (81), 81ra35.

486. Allcock, H. R., Small-molecule phosphazene rings as models for high polymeric chains. *Accounts of Chemical Research* **1979,** *12* (10), 351-358.

487. Chapter 5 - Phosphorus - Nitrogen Compounds. In *Studies in Inorganic Chemistry*, Corbridge, D. E. C., Ed. Elsevier: 1980; Vol. 2, pp 219-276.

488. Chandrasekhar, V.; Krishnamurthy, S. S.; Vasudeva Murthy, A. R.; Shaw, R. A.; Woods, M., Spirocyclic phosphazenes derived from the reaction of N3P3Cl6 and N4P4Cl8 with bifunctional reagents. *Inorganic and Nuclear Chemistry Letters* **1981,** *17* (5), 181-185.

489. Caminade, A.-M., Phosphorus dendrimers for nanomedicine. *Chemical Communications* **2017,** *53* (71), 9830-9838.

490. Morozowich, N. L.; Weikel, A. L.; Nichol, J. L.; Chen, C.; Nair, L. S.; Laurencin, C. T.; Allcock, H. R., Polyphosphazenes Containing Vitamin Substituents: Synthesis, Characterization, and Hydrolytic Sensitivity. *Macromolecules* **2011,** *44* (6), 1355-1364.

491. Arkin, M. R.; Wells, J. A., Small-molecule inhibitors of protein-protein interactions: progressing towards the dream. *Nat Rev Drug Discov* **2004,** *3* (4), 301-17.

492. Sharpless, K. B.; Manetsch, R., In situ click chemistry: a powerful means for lead discovery. *Expert Opin Drug Discov* **2006,** *1* (6), 525-38.

493. Rideout, D.; Calogeropoulou, T.; Jaworski, J.; McCarthy, M., Synergism through direct covalent bonding between agents: A strategy for rational design of chemotherapeutic combinations. *Biopolymers* **1990,** *29* (1), 247-262.

494. Lu, G.; Lam, S.; Burgess, K., An iterative route to "decorated" ethylene glycol-based linkers. *Chemical Communications* **2006,** (15), 1652-1654.

495. Toti, U. S.; Moon, S. H.; Kim, H. Y.; Jun, Y. J.; Kim, B. M.; Park, Y. M.; Jeong, B.; Sohn, Y. S., Thermosensitive and biocompatible cyclotriphosphazene micelles. *Journal of Controlled Release* **2007,** *119* (1), 34-40.

496. Mahou, R.; Wandrey, C., Versatile route to synthesize heterobifunctional poly (ethylene glycol) of variable functionality for subsequent pegylation. *Polymers (Basel)* **2012,** *4* (1), 561-589.

497. Bertozzi, C. R.; Bednarski, M. D., The synthesis of heterobifunctional linkers for the conjugation of ligands to molecular probes. *The Journal of Organic Chemistry* **1991,** *56* (13), 4326-4329.

498. Goswami, L. N.; Houston, Z. H.; Sarma, S. J.; Jalisatgi, S. S.; Hawthorne, M. F., Efficient synthesis of diverse heterobifunctionalized clickable oligo(ethylene glycol) linkers: potential applications in bioconjugation and targeted drug delivery. *Organic & Biomolecular Chemistry* **2013,** *11* (7), 1116-1126.

499. Fazio, F.; Bryan, M. C.; Blixt, O.; Paulson, J. C.; Wong, C.-H., Synthesis of Sugar Arrays in Microtiter Plate. *Journal of the American Chemical Society* **2002,** *124* (48), 14397-14402.

500. Norberg, O.; Deng, L.; Aastrup, T.; Yan, M.; Ramström, O., Photo-Click Immobilization on Quartz Crystal Microbalance Sensors for Selective Carbohydrate−Protein Interaction Analyses. *Analytical Chemistry* **2011,** *83* (3), 1000-1007.

501. Nishizawa, Y., Studies on Organophosphorus Compounds. II. On Phosphite Cuprous Halide Complex Compounds. *Bulletin of the Chemical Society of Japan* **1961,** *34* (8), 1170-1178.

502. McManus, J. B.; Onuska, N. P. R.; Jeffreys, M. S.; Goodwin, N. C.; Nicewicz, D. A., Site-Selective C–H Alkylation of Piperazine Substrates via Organic Photoredox Catalysis. *Organic Letters* **2020,** *22* (2), 679-683.

503. Mishra, R.; Pandey, S.; Trivedi, S.; Pandey, S.; Pandey, P. S., Synthesis and properties of l-valine based chiral long alkyl chain appended 1,2,3-triazolium ionic liquids. *RSC Advances* **2014,** *4* (63), 33478-33488.

504. Mahou, R.; Wandrey, C., Versatile Route to Synthesize Heterobifunctional Poly(ethylene glycol) of Variable Functionality for Subsequent Pegylation. *Polymers (Basel)* **2012,** *4* (1).